Habilitation à diriger des recherches

David Pasdeloup

HABILITATION À DIRIGER DES RECHERCHES

Discipline Sciences de la Vie et de la Santé

Année universitaire : 2018 / 2019

présentée et soutenue publiquement par :

David PASDELOUP

le 23 Avril 2019

JURY :

Mme ARHEL Nathalie	Chargée de Recherche, HDR, CNRS	Université de Montpellier
Mr GAUDIN Yves	Directeur de Recherche, CNRS	CNRS Gif-Sur-Yvette
Mme ROZENBERG Flore	PU-PH	Université Paris 5
Mr TOUZE Antoine	Professeur des Universités	Université de Tours
Mr WODRICH Harald	Directeur de Recherche, INSERM	Université de Bordeaux

Résumé

Les Herpèsvirus sont de larges virus à ADN ubiquitaires dans le monde animal. Leur capacité à se maintenir pendant toute la vie de leur hôte a contribué à leur immense succès évolutif et témoigne de leur profonde adaptation à leur hôte. C'est pourquoi ils font partie des virus dont l'étude peut conduire à une meilleure connaissance des mécanismes fondamentaux qui régissent nos cellules.

Ce document résume quinze ans d'étude que j'ai menées sur les mécanismes moléculaires d'infection par les Herpèsvirus avec un focus particulier sur le virus humain de l'Herpès Simplex de type I (HSV-1). Il couvre plusieurs étapes du cycle de réplication de ce virus telle que l'entrée virale et l'interaction de la capside du virus avec le complexe du pore nucléaire de la cellule, qui résulte dans l'injection du génome viral dans le noyau cellulaire et dans l'initiation de la réplication virale. Je décris ici comment ce mécanisme fait intervenir des protéines cellulaires également impliquées dans l'entrée d'autres virus à ADN, tels que les Adénovirus.

Dans une seconde partie, je développe les études centrées sur la capacité du virus à être mobile dans la cellule. En effet, le virus HSV-1 est un virus neurotrope et infecte donc les neurones. Ces cellules hautement différenciées sont très longues et le virus doit être capable de voyager depuis la périphérie de la cellule vers le noyau où son cycle de réplication débute. Ce voyage peut être long d'une dizaine de centimètres, ce qui constitue une distance très importante pour un virus de 200 nm de diamètre. Pour être transporté efficacement, le virus mobilise la machinerie cellulaire de transport à la fois durant l'entrée virale ainsi que durant la sortie des nouveaux virions. Je mets ici en lumière le rôle d'une protéine cellulaire, la Dystonine, dont le rôle dans le contrôle du transport viral était jusqu'ici inconnu.

Le centrosome est le centre organisateur majeur des microtubules, des fibres cytoplasmiques utilisées par le virus pour son transport intracellulaire. Je décris dans une troisième partie comment l'infection par le virus HSV-1 interfère avec la fonction centrosomale, ce qui résulte en la réorganisation du réseau de microtubules. A l'issue de ces observations, nous avons émis l'hypothèse que cette réorganisation du réseau aide à optimiser la sortie des virions néo-formés.

Dans une quatrième partie, j'aborde la description de l'organisation de l'enveloppe virale par microscopie à super-résolution, une nouvelle méthode d'imagerie qui permet de visualiser en fluorescence des objets à une résolution de l'ordre de 50 nm, au lieu des 200 nm au minimum obtenus en imagerie optique classique. Cette méthode nous a permis d'observer l'organisation différentielle des différentes protéines virales à la surface de virions purifiés et, de façon surprenante, d'observer que cette organisation change une fois que le virus est attaché à une cellule-cible.

Enfin, dans une dernière partie, je décris les projets en cours, portant sur l'étude d'un herpèsvirus de poule, le virus de la maladie de Marek (MDV).

SOMMAIRE

Adresse personnelle
PASDELOUP David
1 Rue St-Michel
37110 Monthodon
France
Né le 23 Septembre 1977
Marié

Adresse professionnelle
Laboratoire de Biologie des Virus Aviaires (BioVA)
Unité UMR1282 ISP
INRA Centre Val-de-Loire
37380 Nouzilly

FORMATION et DIPLOMES

Depuis Sept.2015 : CR1 à l'INRA dans le Laboratoire de Biologie des Virus Aviaires (Direction : Caroline Denesvre) au sein de l'UMR1282 ISP (Direction : Nathalie Winter, Nouzilly, France).

2013-2015 : Attaché Temporaire d'Enseignement et de Recherche (ATER) à la faculté de Pharmacie de l'Université Paris-Sud (Chatenay-Malabry) dans l'équipe d'Audrey Esclatine.

2009-2013 : Post-Doctorat au Laboratoire de Virologie Moléculaire et Structurale (Dir.: Yves Gaudin, CNRS, Gif-Sur-Yvette) dans l'équipe de Marc Labetoulle.

2006-2009 : Post-doctorat au MRC – Virology Unit (Glasgow, Royaume-Uni) dans l'équipe de Frazer J. Rixon.

2002-2005 : Thèse de Doctorat de l'Université Paris VII. Travaux de thèse réalisés au Laboratoire de Virologie Moléculaire et Structurale (Dir.: Felix Rey, CNRS, Gif-Sur-Yvette). Responsable scientifique : Danielle Blondel. Sujet de thèse : La protéine UL25 des alphaherpesvirinae : interactions avec des protéines virales et cellulaires ; implication dans l'interaction des capsides aux pores nucléaires. Autre sujet : Le transport nucléocytoplasmique de la phosphoprotéine du virus de la Rage.

2001-2002 : DEA-Master de Virologie Fondamentale (Université Paris VII, Institut Pasteur), mention Très Bien.

Eté 2000 : Stage de maîtrise effectué à l'unité de Virologie Immunologie Moléculaires (INRA, Jouy-en-Josas). Responsable scientifique : Maria-Isabel THOULOUZE. Sujet : Mise au point d'un système de génétique inverse pour le virus de la septicémie hémorragique virale (VSHV), un rhabdovirus de poisson.

1997 : Baccalauréat Scientifique (Lycée Emilie de Breteuil, Montigny-le-Bretonneux).

VIE SCIENTIFIQUE

- Membre d'un jury de thèse en tant que rapporteur (Thèse Muhammad Bilal Latif, 21 Mars 2016, Université de Liège, Belgique)
- Membre d'un jury de thèse en tant qu'examinateur (Thèse Nicolas Richerioux, 1er Juin 2012, Université de Tours)
- Activités de reviewing régulières (environ 4-6 papiers/an)
- Modérateur de la session « Interaction virus-cellule II » aux XXe Journées Francophones de Virologie (2018)

CO-ENCADREMENT THESES

- **Aurélien Chuard, Université de Tours**
  Co-encadrement avec Caroline Denesvre.
  Thèse débutée en Octobre 2017 sur le sujet « Caractérisation de l'interface hôte-pathogène responsable de l'excrétion d'un herpèsvirus aviaire »
  Soutenance prévue pour fin 2020.

- **Ashley P. Roberts, Université de Glasgow, Royaume-Uni**
  Co-encadrement avec le Dr F.J Rixon.
  Thèse débutée en 2006 et soutenue sous l'intitulé « Investigating the role of the inner tegument proteins in HSV-1 infection" en Septembre 2009.
  Publications associées : #2 et #4 sur la liste de publication.

ENCADREMENT MASTER 2

- **Inès Delhomme**, Université de Tours, Décembre 2016-Mai 2017.
  « Développement de deux systèmes d'analyse permettant l'identification de facteurs de tropisme cutané impliqués dans l'excrétion du virus de Marek »

- **Nolwenn Poccardi**, Université Paris-Sud, Janvier-Juin 2013.
  « Analyse fonctionnelle du rôle de la protéine ORF O du virus HSV-1 ».

- **Massinissa Idres**, Université Paris-Sud, Janvier-Juin 2012.
  « Identification des partenaires cellulaires de la protéine de latence ORF O du virus HSV1 ».

ENCADREMENT MASTER 1 et autres

- **Ines Delhomme**, Master I, Université Tours, 6 semaines, 2016.
- **Etienne Jourdier**, Master I, Ecole Polytechnique, 3 mois en 2007.
- **Marion Duriez,** DEUG, Université Paris XI, 6 semaines en 2005.

ENSEIGNEMENT

- Enseignement de virologie et d'infectiologie dans les Masters suivants :
    - Master 2 « Agents Infectieux – interaction avec leurs hôtes et l'environnement » (A2I), Université de Versailles-St-Quentin (UVSQ, Paris-Saclay)
    - Master 2 « Infectiologie cellulaire et moléculaire, vaccinologie, anticorps thérapeutiques » (ICMVAT, Université de Tours)
    - Master Erasmus Mundus « Infectious Diseases and One Health » (IDOH) (1st Semester, module "Host-pathogens interactions", Université de Tours)
- Enseignement de travaux pratiques et dirigés à des étudiants de Licence 3, Master 1ere et 2e année (ATER, Faculté de Pharmacie de Châtenay-Malabry) (2013-2015).

PUBLICATIONS

(*) indique le "corresponding author"

10. Le transport intracellulaire des Herpesvirus (revue)

D.Pasdeloup

Virologie, Janvier-Février 2016.

Annexe #4

9. Insights into Herpesvirus Tegument Organization from Structural Analyses of the 970 Central Residues of HSV-1 UL36 Protein.

Scrima N, Lepault J, Boulard Y, Pasdeloup D, Bressanelli S, Roche S*.

J.Biol.Chem, Avril 2015, 3;290(14):8820-33

Annexe #3, Citations (Scopus au 19/12/18) : **7**

8. Dystonin/BPAG1 promotes plus-end directed transport of Herpes Simplex Virus 1 capsids on microtubules during entry

M. McElwee, F. Beilstein, M. Labetoulle, F.J. Rixon and D. Pasdeloup*

J.Virology, Octobre 2013, 87(20):11008-18

Publication #5 (Partie II) ; Citations (Scopus au 19/12/18) : **22**

7. Differing effects of Herpes Simplex Virus 1 and Pseudorabies Virus infection on centrosomal function

D.Pasdeloup*, M. Labetoulle and F.J Rixon

J.Virology, Juin 2013, 87(12):7102-12

Publication #6 (Partie III), Citations (Scopus au 19/12/18) : **11**

6. Herpesvirus tegument protein pUL37 interacts with dystonin/BPAG1 to promote capsid transport on microtubules during egress

D. Pasdeloup*, M. McElwee, F. Beilstein, M. Labetoulle and F.J Rixon

J.Virology, Mars 2013, 87(5):2857-67

Publication #4 (Partie II); Citations (Scopus au 19/12/18) : **36**

5. Genetic editing of Herpes Simplex 1 and Epstein Barr herpesvirus genomes by human APOBEC-3 cytidine deaminases in culture and *in vivo*

R.Suspene, M.M. Aynaud, S.Koch, D.Pasdeloup, M.Labetoulle, B.Gaertner, J.P. Vartanian, A. Meyerhans and S.Wain-Hobson*

J.Virology, Août 2011, 85(15):7594-602

Annexe #2, Citations (Scopus au 19/12/18) : **63**

4. The Inner Tegument Protein pUL37 of Herpes Simplex Virus Type 1 Is Involved In Directing Capsids to the *Trans*-Golgi Network for Envelopment

D.Pasdeloup*, F.Beilstein, A.P.E Roberts, M.McElwee, D.McNab and F.J Rixon

J.Gen.Virology, Septembre 2010, 91(Pt 9):2145-51

Publication #3 (Partie I), Citations (Scopus au 19/12/18) : **23**

3. Herpesvirus Capsid Association To The Nuclear Pore Complex And Viral DNA Release Involve The Nucleoporin CAN/Nup214 And The Capsid Protein pUL25

D. Pasdeloup*, D.Blondel, A.L Isidro and F.J Rixon

J.Virology, Juillet 2009, 83(13):6610-23

Publication #1 (Partie I), Citations (Scopus au 19/12/18) : **92**

2. Differing roles of inner tegument proteins pUL36 and pUL37 during entry of Herpes Simplex Virus Type 1 (HSV-1)

A.P.E. Roberts, F. Abaitua, P. O'Hare, D. McNab, F.J. Rixon* and D. Pasdeloup

J.Virology, Janvier 2009, 83(1):105-16

Publication #2 (Partie I), Citations (Scopus au 19/12/18) : **85**

1. Nucleocytoplasmic shuttling of the rabies virus P protein requires a nuclear localization signal and a CRM1-dependent nuclear export signal

Pasdeloup D, Poisson N, Raux H, Gaudin Y, Ruigrok RW, Blondel D*.

Virology, Avril 2005 (10;334(2):284-93.)

Annexe #1 ; Citations (Scopus au 19/12/18) : **64**

ARTICLES EN PREPARATION

1. Dynamic organization of Herpesvirus glycoproteins on the viral membrane revealed by super-resolution microscopy (Publication #7)

F. Beilstein, G.H. Cohen, R.J. Eisenberg, V. Nicolas, A. Esclatine and D.Pasdeloup*

2. The major tegument protein pUL47 of Marek's Disease Virus is necessary for viral horizontal transmission

D.Pasdeloup, K.Guyader, S.Rémy, S.Spatz and C.Denesvre

COMMUNICATIONS ORALES

Orateur de toutes les communications listées ci-dessous.

- **8e Journées HerPas (2018), Tours** : « Rôle des protéines pUL47 et pUL48 dans le tropisme viral et la transmission du virus de la maladie de Marek», D.Pasdeloup, S.Rémy, K.Guyader, C.Denesvre.

- **42e congrès International des Herpesvirus, Gand, Belgique (2017)** : « Super-resolution microscopy reveals various patterns of glycoprotein distribution on the surface of free and cell-bound Herpes Simplex particles », F.Beilstein, V.Nicolas, GH Cohen, RJ Eisenberg, A.Esclatine, D.Pasdeloup

- **5e Journées HerPas (2016), Institut Gustave Roussy, Villejuif**: « Localisation des glycoprotéines virales à la surface des virions de HSV-1»

- **3e Journées HerPas (2014), Institut Pasteur, Paris** : « Le virus Herpès Simplex 1 (HSV-1) modifie l'organisation des microtubules en affectant le centrosome »

- **XVe Journées Francophones de Virologie (2013), Paris, en tant qu'invité** : « Transport des Herpesvirus et interaction avec le réseau de microtubules ».

- **37e congrès International des Herpesvirus, Calgary, Canada (2012)** : "Dystonin/Bpag1 promotes plus-end directed transport of Herpesvirus capsids on microtubules", D.Pasdeloup, M. McElwee, F. Beilstein, M. Labetoulle and F.J Rixon

- **XIVe Journées Francophones de Virologie, Paris, France (2012)** : « La Dystonine est nécessaire au transport microtubules-dépendant de polarité positive de la capside du Virus de l'Herpès Simplex 1», D. Pasdeloup, M. McElwee, F. Beilstein, M. Labetoulle and F.J Rixon

- **33e congrès International des Herpesvirus, Estoril, Portugal (2008)**: "The minor capsid protein pUL25 of α-herpesviruses is an interface between incoming capsids and the nuclear pore complex", D.Pasdeloup, D.Blondel and F.J. Rixon.

- **Xe Journées Francophones de Virologie, Paris, France (2008)** : « Du transport vers l'éjection de l'ADN viral : interaction de la capside des Herpesvirus avec le pore

nucléaire », D.Pasdeloup, D.Blondel, F.J. Rixon

COMMUNICATIONS AFFICHEES

Les communications affichées ayant simultanément fait l'objet de communications orales telles que listées ci-dessus ne sont pas mentionnées ici.

- **Xe Journées Francophones de Virologie, Paris, France (2008) :** « Décapsidation de l'ADN viral de HSV-1 : rôle différentiel des protéines de tégument pUL36 et pUL37 », A. Roberts, F.J. Rixon, D.Pasdeloup

- **Xe Journées Francophones de Virologie, Paris, France (2008) :** « Association du tégument interne de HSV-1 au TGN : conséquence pour l'assemblage des virions » D.Pasdeloup, A.Roberts, F.J. Rixon.

TRAVAUX ET PERSPECTIVES

Introduction

Les activités de recherche poursuivies durant ces quinze années ont été essentiellement centrées sur l'interaction du virus de l'Herpès Simplex 1 (HSV-1) avec son hôte naturel, l'Homme. Par souci de clarté, les travaux effectués durant ma thèse sur le transport nucléocytoplasmique de la protéine P du virus de la Rage (annexe I pour la publication associée) ainsi que les travaux effectués dans le cadre de collaborations (annexes II et III) ne seront pas développés ici.

J'ai eu le rare privilège durant ma carrière de pouvoir emporter avec moi les thématiques de recherche qui m'étaient chères et d'être accueilli dans des laboratoires qui non seulement s'intéressaient à ces thématiques, mais aussi me faisaient confiance pour les mener à bien. Il en résulte une certaine continuité dans mon parcours que je vais essayer de décrire ici.

Bien que les études que j'ai menées ont été essentiellement concentrées sur l'étude de HSV-1, elles ont permis de mettre à jour des relations virus-hôte ou des mécanismes communs ou applicables à d'autres virus. De plus, l'étude des éléments cellulaires nécessaires à la réplication du virus a permis de mettre en avant le rôle inconnu de certaines protéines de l'hôte dans des processus cellulaires.

Les activités de recherche passées peuvent être séparées en trois parties : 1) entrée du virus, interaction de la capside virale avec le pore nucléaire et éjection de l'ADN viral ; 2) rôle du tégument interne lors de l'entrée et la sortie de HSV-1; 3) interférence de l'infection avec les fonctions centrosomales. A cela s'ajoutent les projets en cours : 1) l'analyse de la dynamique des glycoprotéines d'enveloppe à la surface de la particule virale de HSV-1 et 2) la caractérisation de la base moléculaire du tropisme pour la peau du virus de la maladie de Marek.

Après un bref rappel des caractéristiques du virus, chacune de ces parties et les résultats associés seront développés.

Les Herpesviridae

La famille des Herpesviridae comprend de très nombreux virus infectant une très grande partie du monde animal. Classiquement, la famille est séparée en trois sous-familles de virus (α, β et γ–herpesvirinae) sur la base de données biologiques et génétiques. Du fait de la très grande diversité d'animaux affectés par les *Herpesviridae*, cette famille de virus constitue une priorité d'étude à la fois en recherche fondamentale, clinique (humaine) et vétérinaire (bétail, volailles voire poissons et crustacés).

Les Herpesviridae sont des virus particulièrement bien adaptés à leurs hôtes. Cette adaptation se traduit par la capacité de ces virus à s'établir à vie à l'état latent au sein de leur hôte, le plus souvent en absence de signes cliniques particuliers, tout du moins dans un contexte d'immunocompétence.

Les Herpesviridae sont de gros virus enveloppés (~200 nm diamètre) dont le génome est un ADN double-brin linéaire dont la taille varie de 124 kb (Virus de la Varicelle Simienne) à 241 kb (Cytomegalovirus du Chimpanzé)[1]. La particule virale est constituée d'une capside icosaédrique renfermant le génome (voir plus bas), entourée d'une couche de protéines virales typique des Herpesviridae appelée « tégument », qui sépare la capside de l'enveloppe virale.

Les mécanismes fondamentaux d'entrée, de transport, de réplication et, dans une moindre mesure, de bourgeonnement sont globalement communs à tous les *Herpesviridae*, avec cependant de subtiles nuances en fonction du type cellulaire et de la sous-famille de virus.

En règle générale, les données obtenues sur la réplication intracellulaire des *Herpesviridae* proviennent en grande partie des études menées sur des alphaherpesvirus modèles à grande capacité réplicative en laboratoire, tels que le virus humain de l'Herpès Simplex 1 (HSV-1) ou le virus porcin de la Pseudorage (PrV).

Les travaux détaillés ci-dessous se sont essentiellement portés sur HSV-1.

Le Virus de l'Herpès Simplex 1 (HSV-1)

Comme beaucoup d'Herpèsvirus humains, HSV-1 est un virus quasi-ubiquitaire dans la population humaine avec 65 à 90% de la population mondiale selon l'OMS, en fonction des régions. Pourtant, il ne cause pas ou peu d'effets pathogènes.

Le virus entre en latence dans le système nerveux sensitif de son hôte. On définit la latence herpétique de HSV-1 par la présence du génome viral dans les neurones sensitifs (en général le ganglion trijumeau) et l'absence de production de particules infectieuses. Dans de très rares cas le virus peut pénétrer dans le système nerveux central et être la cause d'encéphalites sévères voire mortelles (HSV-1 est la première cause d'encéphalites sporadiques en Occident).

Le virus infecte principalement les cellules épithéliales et neuronales. La capacité à entrer en latence est exclusive aux neurones.

Le génome de HSV-1 est constitué d'une molécule d'ADN double-brin linéaire de 152.261 paires de bases (souche 17+) protégé par une capside icosaédrique (T=16) de 125 nm de diamètre. La capside est séparée de l'enveloppe virale par une couche amorphe de protéines typique des *Herpesviridae* et appelée « tégument » (**Figure 1**). On distingue le tégument « interne », qui est attaché à la capside, du tégument externe, plus proche de l'enveloppe virale. Celle-ci contient une douzaine de glycoprotéines virales différentes.

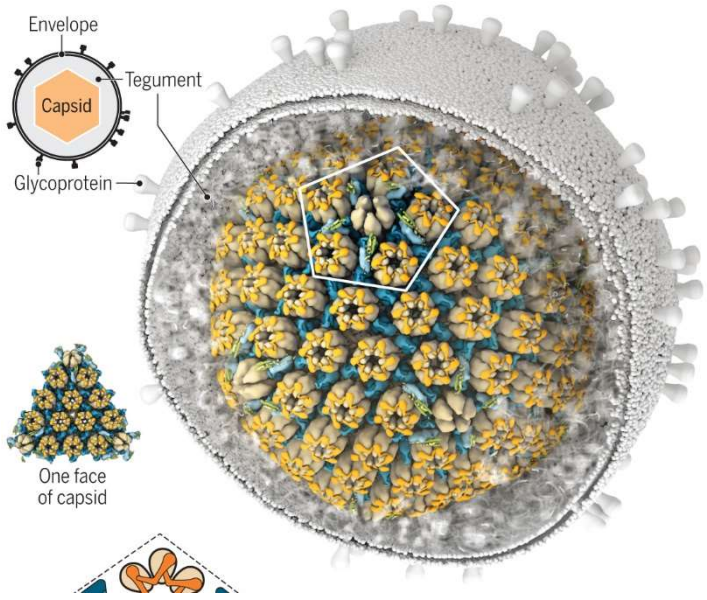

Figure 1. Représentation d'une particule de HSV-1. La capside icosahèdrique, dont la structure est désormais connue à l'échelle atomique, renferme l'ADN viral. Elle est entourée par une couche de protéines amorphe appelée « tégument » qui la sépare de l'enveloppe virale contenant les glycoprotéines. Tiré de Heldwein, Science 2018[2].

Après attachement et fusion (point (i) sur la **Figure 2**) de l'enveloppe virale avec la membrane plasmique, la capside est relâchée dans le cytoplasme de la cellule infectée. Le tégument externe est également relâché dans le cytoplasme tandis que l'essentiel du tégument interne reste attaché à la capside. Le virus ayant un cycle de réplication en grande partie nucléaire, la capside doit atteindre le noyau pour y injecter l'ADN viral et initier le cycle de réplication. Cette phase passe par le transport de la capside de long des microtubules (MTs) (ii) depuis la membrane plasmique jusqu'au noyau en passant par le centrosome (MToC sur **Figure 2**). Une fois au noyau, la capside interagit avec le

complexe du pore nucléaire et injecte l'ADN viral dans le noyau (iii). Le cycle viral lytique commence alors avec la réplication de l'ADN viral et l'assemblage de nouvelles capsides (iv). Une fois que celles-ci ont atteint le cytoplasme (v), elles doivent atteindre les sites d'assemblage (TGN ou endosomes) où se trouvent les protéines de tégument externe et les glycoprotéines (vi). Pour ce faire, elles utilisent encore une fois le réseau de MTs. Une fois les virions assemblés (vii), ils vont être relâchés par exocytose (viii) ou transportés aux extrémités axonales dans le cas de neurones infectés. Là encore, le réseau de MTs sera primordial pour ce transport.

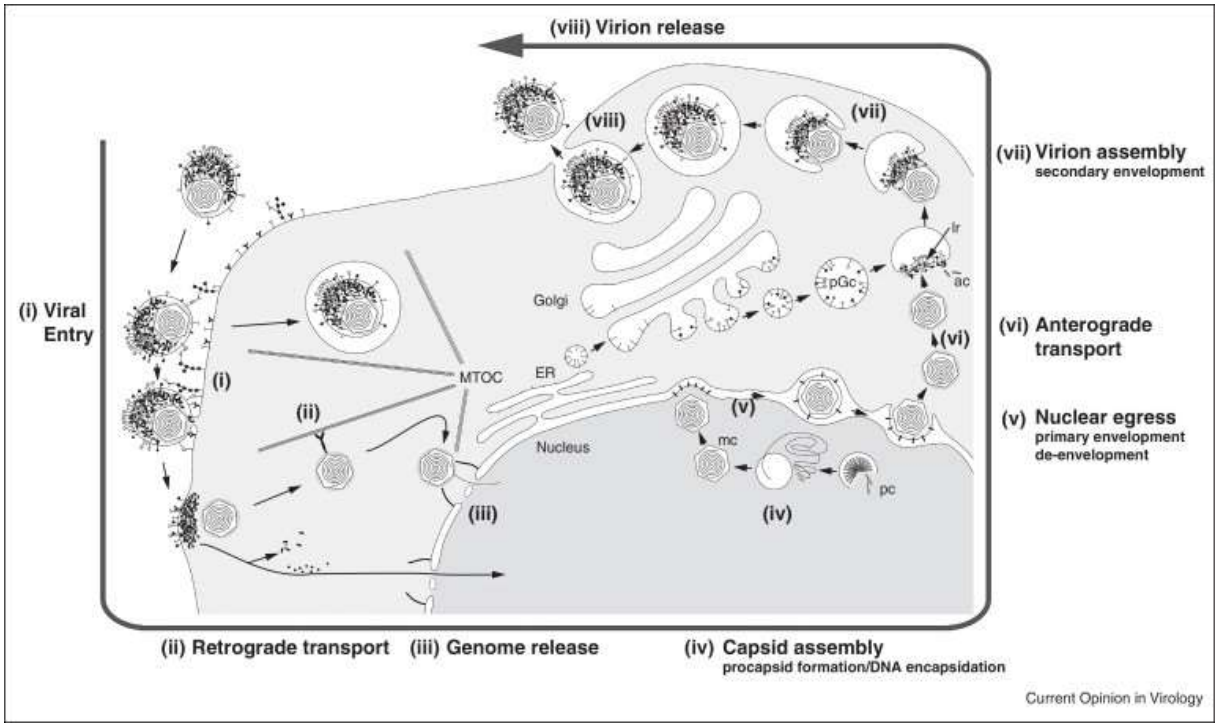

Figure 2. Cycle de réplication lytique des Herpesvirus. Tiré de Mordehai et al.[3]

Mon parcours de recherche peut se calquer sur le cycle viral dans la mesure où j'ai étudié plusieurs aspects de ce cycle, y compris certains aspects structuraux. La figure suivante résume ce parcours avec les publications associées :

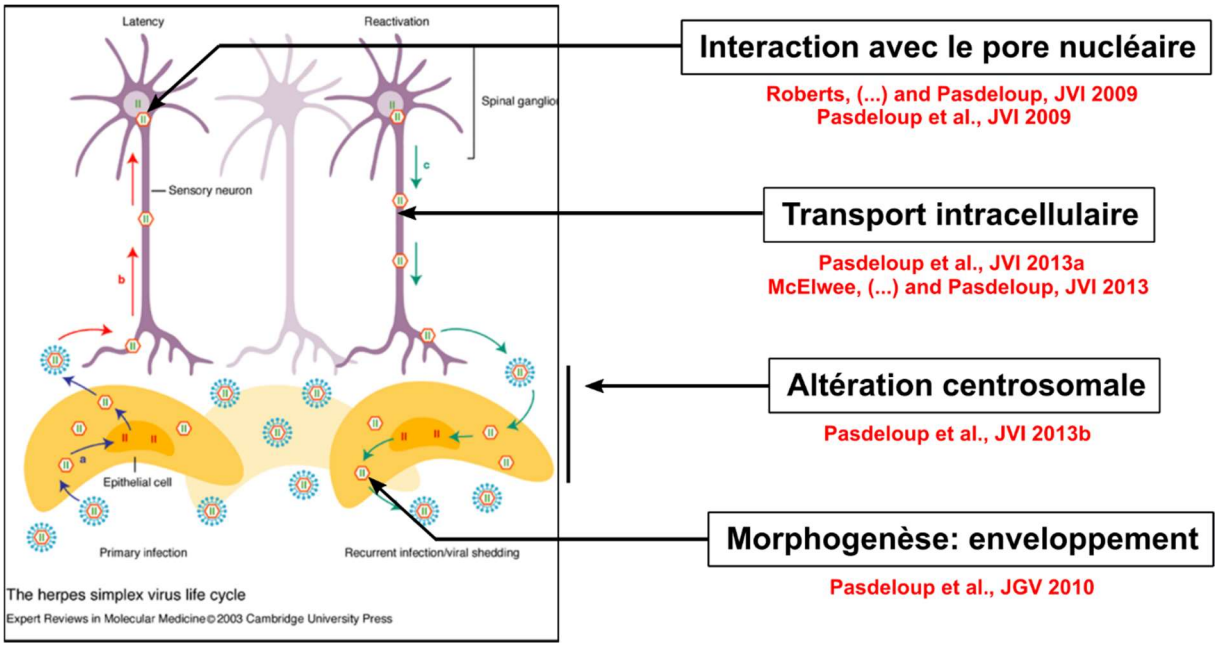

Figure 3. Cycle de vie du virus HSV-1 de la cellule épithéliale au neurone et inversement. Les travaux décrits dans ce manuscrit sont indiqués à droite avec la partie du cycle virale correspondante. La partie I du manuscrit reprend le thème « entrée et interaction avec le pore nucléaire » ainsi que le thème « morphogenèse et enveloppement » ; la partie II reprend la thématique « transport intracellulaire » et la partie III celle de « l'altération centrosomale ». Tiré de Lachmann, 2003[4].

Ce schéma représente la primo-infection (gauche) et la réactivation du virus HSV-1 (droite). Il ne décrit pas le déroulement du cycle viral, mais il permet de voir la relation entre le tropisme épithélial et le tropisme neuronal du virus. On y voit clairement que les types cellulaires naturellement infectés par le virus sont très différents et que leur infection requiert une excellente adaptation du virus, en particulier en ce qui concerne le transport intracellulaire, puisque celui-ci dépend de l'architecture de la cellule, qui diffère énormément entre la cellule épithéliale et la cellule neuronale.

PARTIE I :

Entrée du virus et interaction des capsides avec le complexe du pore nucléaire

Contexte et hypothèse de travail

Mon projet de thèse consistait à caractériser l'interaction entre la protéine pUL25 de virus de la pseudorage (PrV), un alpha-herpesvirus porcin, et deux protéines cellulaires identifiées par crible double-hybride en levures sur une banque d'ADNc d'une lignée cellulaire neuronale de rat: l'importine alpha-7 et Arnt2 (Aryl-Hydrocarbon Receptor Nuclear Translocator 2). pUL25 est une protéine mineure de capside dont le seul rôle connu à l'époque était de maintenir le génome viral dans la capside. En effet, en absence de cette protéine, l'encapsidation du génome viral est impossible et on observe une accumulation de capsides vides dans le noyau[5,6].

Rapidement, nous nous sommes concentrés sur l'interaction avec l'importine α7, pensant qu'elle était impliquée dans la localisation nucléaire de pUL25. En effet, les importines alpha sont des protéines chargées de prendre en charge les protéines à destination du noyau via la reconnaissance d'un signal de localisation nucléaire (NLS), puis de leur faire passer la barrière du complexe du pore nucléaire (NPC)(pour une revue, voir [7]). Nous n'avons pas réussi à mettre en évidence de NLS sur pUL25 et, surtout, l'interaction semblait trop stable pour être une interaction transitoire telle que celle requise pour le passage de la barrière du NPC.

Du fait du rôle de pUL25 dans le maintien du génome viral dans la capside, nous avons pensé que la protéine pourrait être impliquée dans l'éjection de l'ADN viral depuis la capside au niveau du pore nucléaire, et que l'interaction avec l'importine alpha 7 pourrait avoir un rôle dans la prise en charge de la capside par le pore nucléaire et/ou dans la décapsidation. En effet, les importines interagissent avec le pore nucléaire pour permettre la transition des protéines prises en charge à destination du noyau.

Expériences mises en œuvre

Dans un premier temps, j'ai mis au point un système d'interaction des capsides avec des noyaux purifiés *in vitro*, sur la base des résultats de Ojala et collaborateurs[8]. Ces expériences ont montré qu'il était possible d'observer des capsides purifiées fixées de façon stable sur les noyaux (**Figure 4**), et que des anticorps dirigés contre le pore nucléaire ou contre pUL25 inhibait cette interaction (données non publiées). De plus, des capsides purifiées contenant une protéine pUL25 mutée dont la fonction est altérée à température élevée (mutant thermosensible *ts*1249[9]) sont incapables de se fixer aux noyaux à température non-permissive, contrairement à des capsides issues d'un virus WT

(données non publiées, **Figure 4**).

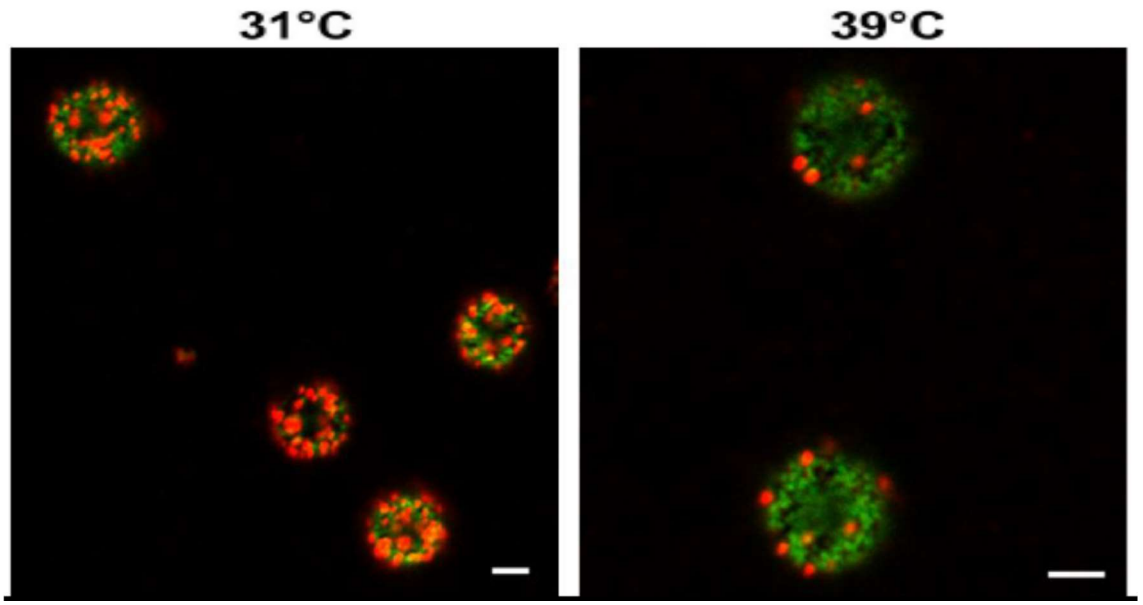

Figure 4. Interaction de capsides B de HSV-1 purifiées avec des noyaux de foie de souris. Des capsides nucléaires B purifiées sur gradient de sucrose et issues du virus ts1249 (mutant thermosensible de pUL25) ont été incubées avec des noyaux de foie de souris purifiés pendant 30 minutes à 31°C (photo de gauche) ou à 39°C (à droite). Les noyaux ont été fixés puis déposés sur des lamelles prétraitées au collagène et mis à adhérer par centrifugation légère. Les capsides ont été marquées avec un anticorps anti-capsides (PTNC, rouge) et les pores nucléaires avec le mAb414 (vert). Les noyaux ont été observés sur un microscope confocal Leica SP4 sur toute leur profondeur (z-stack). Données non publiées. Echelle : 2 µm.

Ces travaux n'ayant pu être achevés dans le cadre de ma thèse, j'ai continué ce projet lors de mon premier post-doctorat au MRC Virology Unit de Glasgow avec Frazer Rixon. Mon arrivée a coïncidé avec celle de Ashley Roberts, un nouvel étudiant en thèse que j'ai co-encadré avec le Dr Rixon. Son projet visait à déterminer le rôle des protéines de tégument interne pUL36 et pUL37 dans l'entrée du virus.

Mes travaux sur pUL25 ont montré que la protéine peut interagir avec deux nucléoporines (des protéines du NPC ou Nup) des filaments cytoplasmiques du NPC: Nup214 et hCG1 (Figure 2 de la publication 1 ou PB1-2)(également appelée NLP1 sur la **Figure 5**).

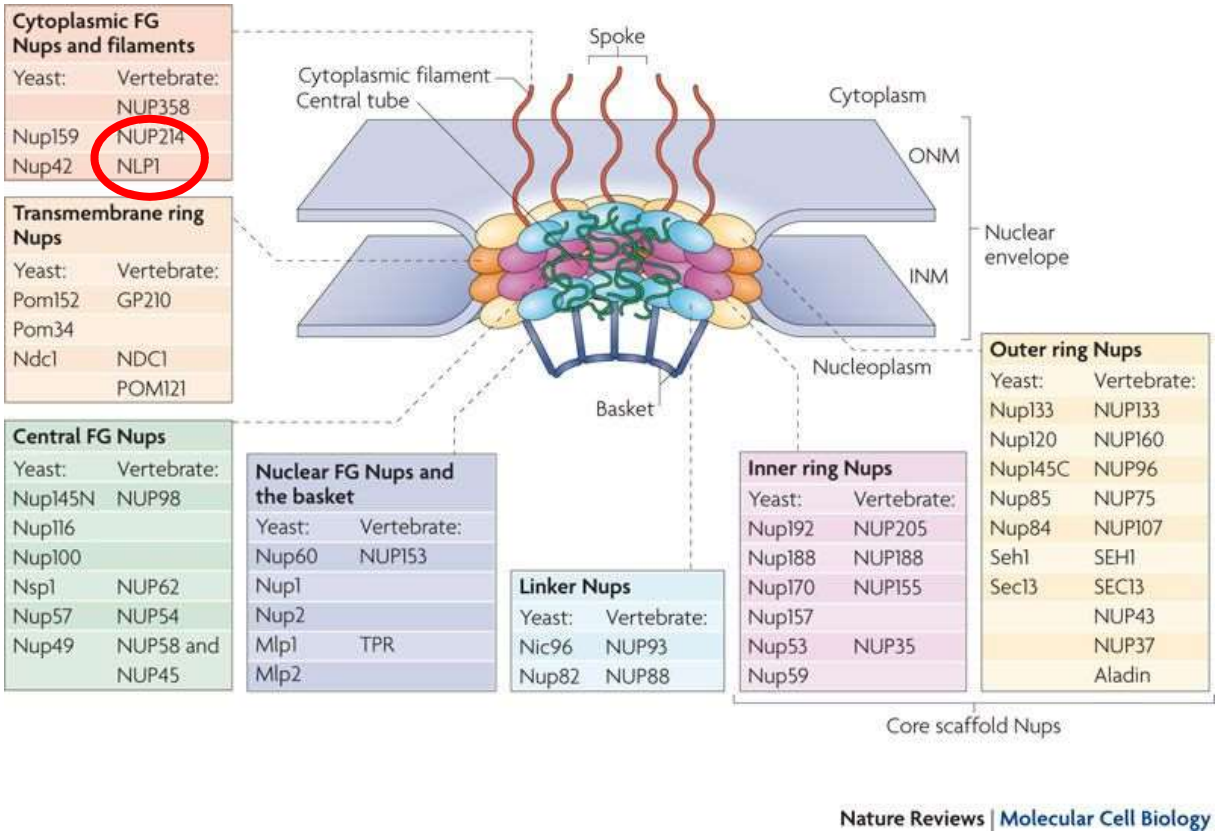

Figure 5. Composition du pore nucléaire. Le NPC est classiquement divisé en trois grandes parties : (i) la partie cytoplasmique avec des nucléoporines (Nups) organisées en filaments. Ces Nups sont logiquement en première ligne pour interagir avec les cargos à destination du noyau ; (ii) la partie transmembranaire et (iii) la partie nucléaire, organisée en forme de « panier ». Les Nups capables d'interagir avec pUL25 sont entourées en rouge. Elles font partie des Nups cytoplasmiques. Nous avons montré que NUP214 est également capable d'interagir avec les capsides durant l'entrée du virus. Tiré de Strambio-de-Castillia et al., 2010[10].

Par ailleurs, nous avons pu établir que les capsides de HSV-1 pouvaient interagir avec CAN/Nup214 durant l'entrée du virus (Figure PB1-1).

Des expériences de shRNA visant Nup214 démontrent que cette Nup est nécessaire à l'entrée du virus, essentiellement à l'éjection de l'ADN viral dans le noyau. Nous avons montré ce dernier point par FISH (Fluorescent In-Situ Hybridisation), qui permet de détecter le génome viral par hybridation d'une sonde fluorescente, et par détection d'une protéine virale associée au génome viral, la protéine ICP4 (Figure PB1-3). Par ailleurs, nous avions démontré que pUL25 interagissait avec la protéine portale pUL6 (Figure PB1-7). Cette protéine forme un canal sur un sommet unique de la capside par lequel l'ADN viral est soit encapsidé, soit éjecté. Cette interaction prouvait donc que pUL25 était bien localisée au point d'éjection de l'ADN viral. De plus, nous avons démontré que pUL25 interagit avec pUL36 via deux domaines d'interaction distincts, l'un constitué des 60 derniers résidus de pUL36,

déjà démontré par une autre équipe[11] et l'autre, plus central et nouveau (Figure PB1-8).

Ashley et moi avons travaillé ensemble sur le rôle de pUL36 et pUL37 dans l'entrée du virus. Ce projet était plutôt ambitieux car les deux protéines forment un complexe essentiel à la réplication du virus en culture de cellules. Par conséquent, il n'est pas possible d'obtenir des virus phénotypiquement dépourvus de l'une ou l'autre de ces protéines, ce qui rend particulièrement difficile l'étude de leur rôle dans l'entrée. Nous avons donc mis au point un système dans lequel le tapis cellulaire était infecté à faible moi (0.01 pfu/cellule) puis les cellules étaient amenées à fusionner artificiellement pour former des cellules polynuclées. Ainsi, nous obtenions des cellules avec plusieurs noyaux (5-15) dans lesquelles seul un ou deux noyaux étaient « infecté(s) », c'est-à-dire produisai(en)t des capsides. Ces capsides étaient ensuite exportées dans le cytoplasme et, si pUL36 ou pUL37 n'avait pas de rôle dans l'entrée, pouvait « infecter » des noyaux « sains », c'est-à-dire éjecter leur ADN viral dans ces noyaux. Nous avons détecté les génomes viraux par FISH et avons observé que tous les noyaux d'une cellule présentaient des signes de réplication du génome viral pour le virus sauvage et pour le virus mutant sans pUL37 (Figure PB2-4). En revanche, seul un noyau par cellule polynuclée était infecté dans le cas du virus ΔUL36. Ces cellules présentaient en outre une forte accumulation de capsides dans le cytoplasme (Figure PB2-5). L'ensemble de ces résultats sont résumés dans la **Figure 6**. Nous en avons conclu que pUL36 mais pas pUL37 était impliquée soit dans l'interaction des capsides avec le NPC et/ou dans l'éjection de l'ADN viral dans le noyau. C'était la première description d'un rôle découplé des deux protéines du complexe. Par la suite, dans la continuité des travaux d'Ashley, nous avons montré que pUL37 était nécessaire à l'initiation de l'enveloppement secondaire des capsides dans le cytoplasme (Publication #3).

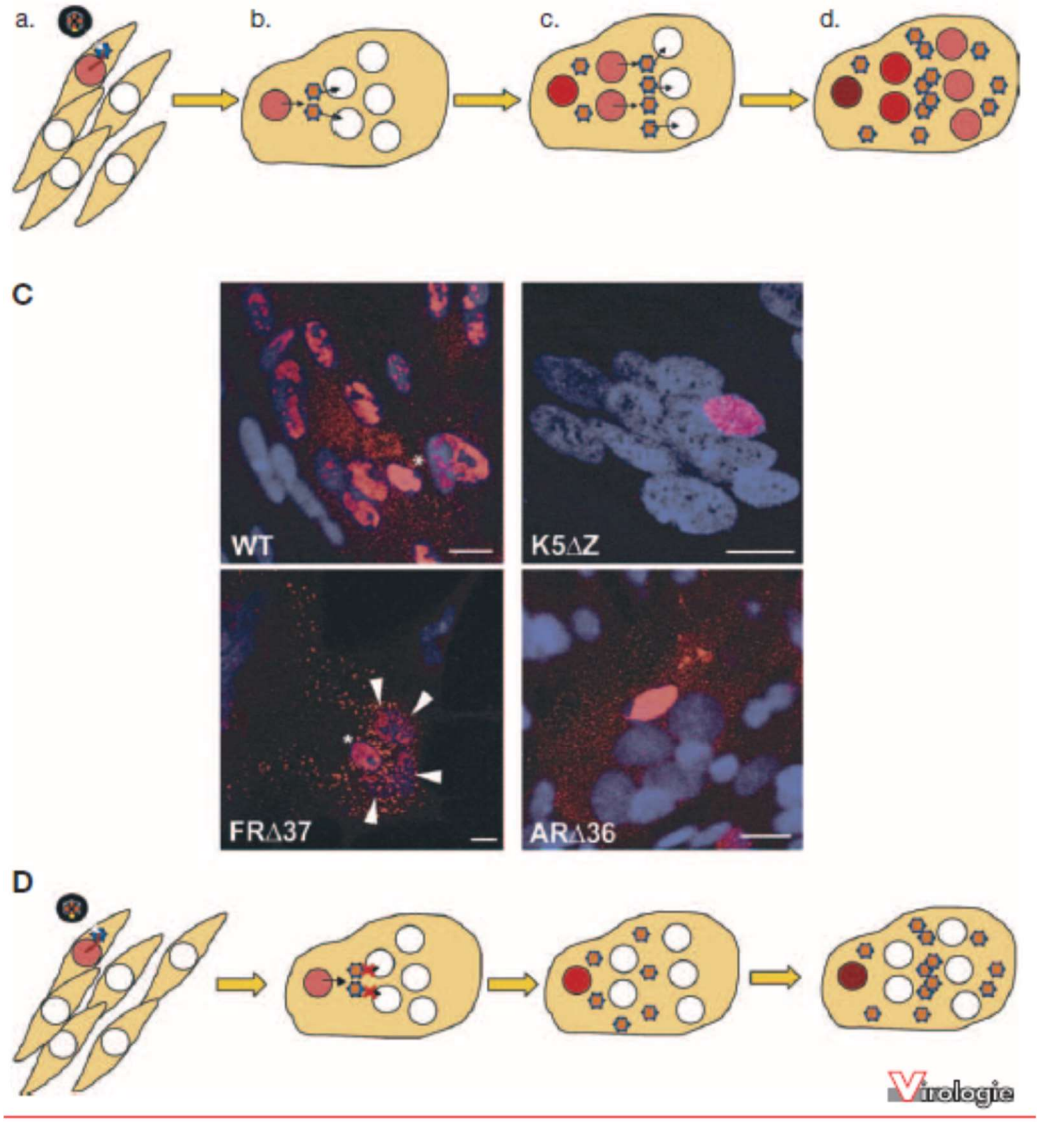

Figure 6. Résumé des résultats obtenus sur le rôle de pUL36 et pUL37 dans l'éjection de l'ADN viral dans le noyau. Haut : schémas expérimental montrant une infection à très faible m.o.i suivie d'une fusion artificielle entre cellules non-infectées et cellules infectées. Ceci conduit à la formation de syncitia avec un nombre très limité de noyaux infectés. Dans le cas où la protéine testée n'est pas nécessaire à l'interaction avec le NPC et/ou à l'éjection de l'ADN viral, les noyaux environnants seront « infectés » par les nouvelles capsides formées à partir du noyau « infecté » en premier lieu. Ce cas de figure était observé pour le virus WT et le virus ne codant pas pour la protéine pUL37 (flèches blanches dans FRΔ37). En revanche, dans le cas d'un virus ne codant pas pour pUL36 (ARΔ36), un seul noyau par syncitium est saturé en ADN viral, tout comme pour le contrôle négatif (K5ΔZ), qui ne code pas pour la protéine majeure de capside VP5. L'ADN viral est détecté par FISH (en rouge) dans les cellules infectées. Notez la présence de nombreux points dans le cytoplasme des cellules infectées par les virus WT, ARΔ36 et FRΔ37, qui représentent des génomes individuels contenus dans les capsides, le cytoplasme des cellules infectées par le virus K5ΔZ ne contenant pas ce type de signal. Tiré de Roberts et al., Virologie 2008.

Répercussion de ces travaux et ce que l'on sait maintenant

La même année où ces travaux ont été publiés, une équipe a montré que pUL36 était impliquée dans l'attachement au NPC et que les nucléoporines Nup214 et Nup358/RanBP2 étaient également impliquées[12]. Le rôle de pUL36 dans l'entrée était suspecté de par l'existence d'un mutant thermosensible de la protéine qui est bloqué durant l'entrée à température non permissive[13-15]. Les travaux du laboratoire de Peter O'Hare ont également souligné le rôle de pUL36 dans l'interaction avec le NPC via la présence de séquences NLS dans la protéine[16].

L'interaction de pUL36 et pUL25 a été observée au niveau structural, et le complexe serait localisé aux sommets (pentons) de la capside[17]. La présence du complexe au niveau du sommet portal reste encore à vérifier mais de récents travaux du laboratoire de D.Bhella (Glasgow) ont montré que pUL25 était très probablement présente au niveau du sommet portal [18]. Par ailleurs, l'équipe de Beate Sodeik a confirmé le rôle de pUL25 dans l'éjection de l'ADN viral[19] ainsi que l'existence de multiples sites d'interaction sur pUL36 avec pUL25[20]. Il reste néanmoins à établir si l'importine α7 a un rôle dans le processus d'import du génome viral.

L'ensemble de ces travaux ont contribué à avoir une image beaucoup plus claire du mécanisme d'attachement des capsides virales au NPC qui a fait l'objet de nombreuses revues[21-25].

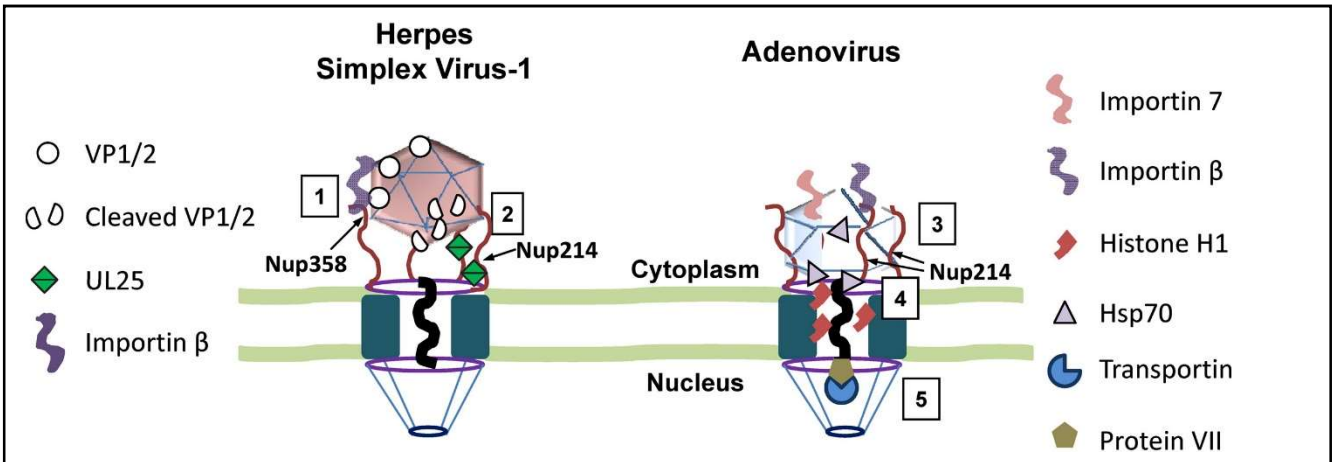

Figure 7. Résumé des connaissances sur la décapsidation de l'ADN des HSV-1 en comparaison avec celle d'un autre virus ADN, l'Adénovirus. VP1/2=pUL36. Tiré de Cohen et al., BBA Mol Cell Research 2011.[21]

Publication #1

Herpesvirus capsid association with the nuclear pore complex and viral DNA release involve the nucleoporin CAN/Nup214 and the capsid protein pUL25.

Pasdeloup D, Blondel D, Isidro AL, Rixon FJ

JOURNAL OF VIROLOGY, July 2009, p. 6610–6623 Vol. 83, No. 13
0022-538X/09/$08.00+0 doi:10.1128/JVI.02655-08

Herpesvirus Capsid Association with the Nuclear Pore Complex and Viral DNA Release Involve the Nucleoporin CAN/Nup214 and the Capsid Protein pUL25▽

David Pasdeloup,[1,2]* Danielle Blondel,[2] Anabela L. Isidro,[2,3] and Frazer J. Rixon[1]

MRC Virology Unit, Church Street, Glasgow G11 5JR, United Kingdom[1]; Laboratoire de Virologie Moléculaire et Structurale, CNRS, Avenue de la Terrasse, 91198 Gif-Sur-Yvette, France[2]; and Instituto de Tecnologia Química e Biológica, Oeiras, Portugal[3]

Received 24 December 2008/Accepted 14 April 2009

After penetrating the host cell, the herpesvirus capsid is transported to the nucleus along the microtubule network and docks to the nuclear pore complex before releasing the viral DNA into the nucleus. The viral and cellular interactions involved in the docking process are poorly characterized. However, the minor capsid protein pUL25 has recently been reported to be involved in viral DNA uncoating. Here we show that herpes simplex virus type 1 (HSV-1) capsids interact with the nucleoporin CAN/Nup214 in infected cells and that RNA silencing of CAN/Nup214 delays the onset of viral DNA replication in the nucleus. We also show that pUL25 interacts with CAN/Nup214 and another nucleoporin, hCG1, and binds to the pUL36 and pUL6 proteins, two other components of the herpesvirus particle that are known to be important for the initiation of infection and viral DNA release. These results identify CAN/Nup214 as being a nuclear receptor for the herpesvirus capsid and pUL25 as being an interface between incoming capsids and the nuclear pore complex and as being a triggering element for viral DNA release into the nucleus.

Many nucleus-replicating viruses have evolved different strategies for delivering their genomes into the nucleus of their host cell through the nuclear pores, which provide the only route of transit across the physical barrier of the nuclear envelope. These strategies depend mainly on the nature of the capsid, which acts both as a protective element for the genome and as a delivery agent (for reviews, see references 21 and 60).

Alphaherpesviruses are large, double-stranded DNA viruses. Their genomes are contained within a 125-nm-diameter capsid that is surrounded sequentially by a thick proteinaceous layer, called the tegument, and a lipid envelope. The herpes simplex virus type 1 (HSV-1) capsid structure has been extensively studied (66) and is a general model for other alphaherpesviruses. It has icosahedral symmetry with the major capsid protein VP5, forming hexamers and pentamers (termed hexons and pentons) at the faces and vertices, respectively, of the icosahedron. There are 150 hexons and 11 pentons per capsid. At one vertex, the penton is replaced by a portal, a structure common to tailed bacteriophages and herpesviruses, through which the viral DNA is encapsidated and released (7, 8). In HSV-1, the portal is a dodecamer of the UL6 gene product, pUL6 (38, 57).

The nuclear pore complex (NPC) is a multiprotein complex that selectively controls the passage of material through the nuclear envelope (for a review, see reference 28). The NPC has three structural components: the nuclear basket, the central framework, which is embedded in the nuclear envelope, and the cytoplasmic filaments. The diameter of the cytoplasmic face is ~125 nm, whereas the central channel is ~60 nm in diameter (3). Its component proteins, termed nucleoporins, perform various roles, being important both in forming a selective gate and in carrying out nucleocytoplasmic transport (41, 55). Several models have been proposed to explain the selectivity of the NPC, all of them involving the phenylalanine-glycine (FG) repeat domains that are present in some nucleoporins (32, 42, 46, 49).

In herpesviruses, transcription, DNA replication, assembly of new capsids, and DNA packaging all take place in the nuclei of infected cells. Infection of new cells is initiated when the virion envelope fuses with the plasma membrane, releasing the tegument and capsid into the cytoplasm. However, the capsid does not itself enter the nucleus but binds to the NPC, where the viral DNA is released and is transferred into the nucleus through the NPC (2, 39, 51, 52). Thus, the binding of the capsid to the NPC is necessary for the initiation of infection. However, the nature of this process and the viral and NPC proteins involved are poorly understood.

Studies have highlighted two herpesvirus structural proteins that are suspected to play roles in the targeting of capsids to the NPC and/or in viral DNA uncoating. The first is the tegument protein pUL36 (also termed VP1/2), the gene product of the UL36 open reading frame (ORF). Tegument proteins have been implicated in the transport of capsids (30, 62), and pUL36 has been shown to be necessary for this transport (31). Furthermore, an HSV-1 temperature-sensitive (*ts*) mutant of UL36, *ts*B7, has been described as being impaired in viral DNA release at nonpermissive temperatures (2), and a recent study has demonstrated that the proteolytic cleavage of pUL36 is required for viral DNA uncoating (24). A second HSV-1 *ts* mutant (*ts*1249) has a phenotype similar to that of *ts*B7 (44). The mutation is in the UL25 gene, which encodes a minor capsid protein, pUL25, that is needed to retain packaged viral DNA within the capsid (34, 53). pUL25 was previously sug-

* Corresponding author. Mailing address: MRC Virology Unit, Institute of Virology, Church Street, Glasgow G11 5JR, United Kingdom. Phone: 44-141-330-4025. Fax: 44-141-337-2236. E-mail: d.pasdeloup@mrcvu.gla.ac.uk.

▽ Published ahead of print on 22 April 2009.

gested to bind as a heterodimer with another minor capsid protein, pUL17, around the capsid vertices (58) and is also known to interact with pUL36 (9).

In the present study, we identified an interaction between HSV-1 capsids and the nucleoporin CAN/Nup214. We further showed that the minor capsid protein pUL25 binds directly to both CAN/Nup214 and a second nucleoporin, hCG1. In addition, we demonstrated the binding of pUL25 to the portal protein pUL6 and the tegument protein pUL36, which both have key roles in viral DNA release (2, 24, 36). Thus, the pUL25 capsid protein appears to play a central role in linking the processes of nuclear pore binding and release of viral DNA.

MATERIALS AND METHODS

Cells and viruses. African green monkey kidney (Vero), 293T, and HeLa cells were grown at 37°C in Dulbecco's modified Eagle medium (DMEM; Invitrogen) supplemented with 10% fetal calf serum. Baby hamster kidney (BHK) cells were grown in Glasgow modified Eagle medium (Invitrogen) supplemented with 10% newborn calf serum and tryptose phosphate broth.

Wild-type (WT) HSV-1 (strain 17^+) and *ts*K/Luci (provided by C. Preston) were propagated on BHK cells infected at 0.01 PFU per cell, and virions were concentrated from supernatant medium by centrifugation at 15,000 × *g* for 2 h. To generate the *ts*K/Luci virus, the β-galactosidase coding region of pMJ102 (23) was replaced by the firefly luciferase coding sequences (with an additional in-frame, C-terminal fusion of chloramphenicol acetyltransferase coding sequences that is irrelevant to the experiments described here). This resulted in a plasmid in which the luciferase coding region was controlled by the HSV-1 immediate-early ICP0 promoter, with the entire construct embedded in the nonessential thymidine kinase (TK) coding region. This plasmid was recombined with genomic DNA of the HSV-1 *ts* mutant *ts*K (15, 43), and TK-negative mutants were isolated as described previously (23, 29). As the *ts*K virus has a *ts* lesion in the ICP4 protein, all experiments using this virus were performed at a permissive temperature (31°C).

The UL37 null mutant of HSV-1 (FRΔUL37) was propagated as described previously (47). vICP4CFP-VP26RFP was made by coinfecting Vero cells with vECFP-ICP4, which expresses the immediate-early protein ICP4 linked to enhanced cyan fluorescent protein (CFP) (19), and vUL35RFP1D1, which was made by fusing monomeric red fluorescent protein (RFP) (Clontech) to the N terminus of the small capsid protein VP26. Progeny virus was collected and serially diluted on fresh cells. Plaques exhibiting both CFP and RFP fluorescence were selected and purified through four rounds of plaque purification.

Antibodies. Rabbit antibody PTNC raised against purified nuclear C capsids recognizes the capsid proteins VP23 and VP26 and the inner tegument protein pUL36 on Western blots. The following antibodies were used. Mouse monoclonal antibody (MAb) DM165 (30) and MAb 4846 (provided by A. Cross, MRC, Glasgow, United Kingdom) against the HSV-1 major capsid protein VP5 and glycoprotein D, respectively, were used. Rabbit antibody NRP14 against respiratory syncytial virus protein N (N_{rsv}) was provided by V. Cowton (35). Rabbit antibody Y11 and MAb F7 against a defined epitope (hemagglutinin [HA]) from influenza virus HA and rabbit antibody A14 against c-myc were obtained from Santa Cruz Biotechnology. MAb 9E10 against c-myc and MAb 414, which recognizes four nuclear pore proteins, were obtained from Sigma and Covance Research, respectively. Alexa Fluor 633-conjugated goat anti-mouse antibody and horseradish peroxidase-conjugated goat anti-mouse antibody were obtained from Molecular Probes and Sigma, respectively.

Plasmids. Vector pCDNA3.1-myc was made by cloning the six-Myc tag sequence, isolated as a BamHI-EcoRI fragment from pCS2-myc (48) (provided by S. Benichou, Institut Cochin, Paris, France), between the BamHI and EcoRI restriction sites of pCDNA3.1 (Invitrogen). Vector pCDNA3.1-HA was made by cloning sequences encoding the HA tag (YPYDVPDYA) between the same restriction sites in pcDNA3.1. pCS2-myc-hCG1 was provided by S. Benichou. pCMV10-HA-UL32 and pECFP-ICP4 were provided by E. Palmer and R. Everett (MRC, Glasgow, United Kingdom), respectively. The HSV-1 UL25 gene was isolated from pCG-UL25 HSV-1 (provided by K. Kaelin, Université Paris) as an EcoRI-XhoI fragment and was subcloned into pCDNA3.1-HA to generate pCDNA3.1-HA UL25. pLexA-UL25 PrV was provided by H. Raux (CNRS, Gif-sur-Yvette, France). The other constructs used were generated by PCR and cloned into pCDNA3.1-myc as described in Table 1.

shRNA. The use of lentiviruses expressing small hairpin RNA (shRNA) was described previously (18). Briefly, 293T cells were cotransfected with three plasmids: (i) pVSV-G, (ii) pCMVDR8.91 (provided by Didier Trono [http://tronolab.com/index.php]), and (iii) pLKO.1Puro-shLuc or pLKO.1Puro-shCAN. The cell supernatant containing recombinant lentivirus was harvested 3 days posttransfection and used to transduce HeLa cells in the presence of hexadimethrine bromide (5 μg/ml polybrene; Sigma). After overnight incubation, the cells were maintained in selective medium containing puromycin (2 μg/ml) for 2 to 3 days before being harvested for Western blot analysis or infected with HSV-1. Silencing of CAN/Nup214 was done by using the 19-nucleotides sequence GAATCA CATCCGCATCAAA. Silencing efficiency was estimated by Western blotting using MAb 414 and quantified using ImageJ software (NIH [http://rsb.info.nih.gov/ij/]) to measure the ratios of Nup358, Nup214, and Nup153 relative to p62, which was used as a loading control. All silencing experiments were carried out in quadruplicate.

Yeast two-hybrid system. The yeast two-hybrid system used in this study was described previously (45). Briefly, the pseudorabies virus (PrV) UL25 ORF was cloned into the EcoRI-BamHI sites of vector pLexA. *Saccharomyces cerevisiae* L40 cells were transformed using lithium acetate, and transformants were selected by their ability to grow on tryptophan-depleted agar plates. These transformants were then transformed with a library of nucleoporin ORFs cloned into a pGAD-based vector (provided by S. Benichou, Institut Cochin, Paris, France) as described previously (27). Double-transformed yeasts were selected on tryptophan- and leucine-depleted agar plates and assayed for β-galactosidase activity.

Plasmid transfection and superinfection. Vero cells grown to 80% confluence on 60-mm plates were transfected with 1.0 μg of a single plasmid DNA or cotransfected with 0.5 μg each of two plasmid DNAs using Lipofectamine 2000 (Invitrogen) according to the manufacturer's instructions. The cells were incubated for 24 h in antibiotic-free DMEM complemented with 10% fetal calf serum and 2 mM glutamine before harvesting. If cells were to be superinfected with FRΔUL37, the transfection mix was removed after 3 h and replaced with fresh medium. After a further 3 h, the cells were infected with 5 PFU/cell, and incubation was continued for 15 h. If cells were to be superinfected with WT HSV-1, the transfection mix was removed after overnight incubation and replaced with fresh medium. The cells were infected with WT HSV-1 at 50 PFU/cell, and incubation was continued for 30 min.

Immunoprecipitation. To prepare extracts for immunoprecipitation, transfected cells were lysed with cytoplasmic protein extraction buffer (CPEB) {50 mM Tris-HCl (pH 8), 150 mM NaCl, 5 mM EDTA, 0.5% IGEPAL [(octylphenoxyl)polyethoxyethano] 630} (Sigma) and protease inhibitors (complete, EDTA free; Roche) for 30 min on ice. Nuclei and cell debris were pelleted at 13,000 × *g* for 2 min. The supernatant was retained (cytoplasmic fraction), and the pellet was resuspended in nuclear protein extraction buffer (20 mM HEPES-KOH [pH 7.9], 420 mM KCl, 20% glycerol, 1 mM EDTA, 2 mM β-mercaptoethanol, and protease inhibitors) for 30 min on ice (33). The nuclear extracts were clarified at 13,000 × *g* for 2 min, and the supernatants from the nuclear and cytoplasmic fractions were pooled to constitute the whole-cell extract. Superinfected cells were lysed with CPEB only, and immunoprecipitation was performed on the cytoplasmic extract. All extracts were mixed with protein A for 30 min at 4°C and centrifuged at 13,000 × *g* for 2 min to eliminate nonspecific binding. A 30-μl sample of the supernatant, constituting 6% of the total extract, was removed before the addition of antibodies for 90 min at 4°C. The immune complexes were collected on protein A-Sepharose beads (Sigma) by incubation for 1 h at 4°C and washed three times in cold CPEB. Proteins were separated by 10% sodium dodecyl sulfate (SDS)-polyacrylamide gel electrophoresis (PAGE) and detected by Western blotting as described previously (47). The immunoprecipitate/cell extract ratio was estimated by quantifying the band of the immunoprecipitated protein and the corresponding band in the cell extract using ImageJ software.

Fluorescence microscopy. For detecting autofluorescent proteins, cells were fixed with 4% paraformaldehyde (PFA), washed three times in phosphate-buffered saline, and mounted directly onto 2.5% 1,4-diazabicyclo[2,2,2]octane (Sigma) in Mowiol (Harco) containing 1 μg/ml 4′,6′-diamidino-2-phenylindole dihydrochloride (DAPI) (Sigma). For immunofluorescent detection, fixed cells were permeabilized with 0.1% Triton X-100 and incubated sequentially with MAb 4846 and Alexa Fluor 633-conjugated goat anti-mouse antibody (90 min for each incubation) before mounting. All samples were examined using a Zeiss LSM 510 Meta confocal microscope using a 63× oil immersion objective and in the multitrack recording mode. For studies of the association between gD and capsids, *z* stacks of whole cells were recorded and assembled for further analysis. Colocalizing signals were extracted from the original image using the histogram colocalization function of the LSM 510 software (version 4). The extracted

TABLE 1. PCR primers used to generate DNA fragments used in interaction studies[e]

Construct (residues)	Template[a]	PCR primer[f]
myc-UL36 (2037–3164)	cos14	CGCGAATTCGATGTGTCCCGAGGCGGCA* CGATCTAGACTAGCCCAGTAACATGCGCAC
myc-UL36 (2037–2572)	cos14	CGCGAATTCGATGTGTCCCGAGGCGGCA* AATTCTAGACTACATGCGAGGGGGGACGGG
myc-UL36 (2037–2504)	cos14	CGCGAATTCGATGTGTCCCGAGGCGGCA* GGATCTAGACTACGGCCGCCCGAGGATAGC
myc-UL36 (2037–2353)	cos14	CGCGAATTCGATGTGTCCCGAGGCGGCA* CGCTCTAGACTAGGGCGCGCCCAGGAGCAC
myc-UL36 (2037–2200)	cos14	CGCGAATTCGATGTGTCCCGAGGCGGCA* GCCTCTAGACGGAGGGCCTCCGGCCG
myc-UL36 (2446–3164)	cos14	GGAGAATTCCATGACCCCGGTCGCGGTG* CGATCTAGACTAGCCCAGTAACATGCGCAC
myc-UL36 (2446–3104)	cos14	GGAGAATTCCATGACCCCGGTCGCGGTG* TGCTCTAGAGGGCGGGGGGCCGAATTG
myc-UL36 (2446–2986)	cos14	GGAGAATTCCATGACCCCGGTCGCGGTG* ATATCTAGAGGGTGCTACATGCCCG
myc-hNup133	pLex12-hs133[b]	CGCGAATTCGGGTACCGGGTCCCGAAGG* TAGCTCGAGTTATATTTGTCCCTGAACATA
myc-hNup50	IMAGE clone 6463796	GAAGCGGCCGCATGGCCAGTGAGGAAGTC TTTTCTAGATCAGGCATCCTTTTTCTCC
myc-hNup54	IMAGE clone 3931652	CTTCTCGAGCATGGCCTTCAATTTTGGG* TGTCTCGAGTCAACTAAAGACACCACC
myc-hCAN Ct	psRET-CAN Ct[c]	CTCGAATTCTGCAGCTGTCACAGCAGCT* GACCTCGAGTCAGCTTCGCCAGCC
myc-UL6 HSV	pAC-UL6 HSV1[d]	GGCGAATTCGACCGCACCACGCTCGCG* GGCTCTAGATCATCGTCGGCCGTC

[a] cos14 is described in reference 12.
[b] Provided by V. Doye (4).
[c] Provided by M. Fornerod (56).
[d] Provided by F. Homa (34).
[e] The PCR primers are listed in pairs, with the forward primer listed first and the reverse primer second. All PCR products were cloned into pCDNA3.1-myc, and the restriction enzyme sites used for cloning are underlined.
[f] * indicates that these primers have a +1 nucleotide after the restriction site to put the gene in frame with the tag.

images were analyzed using the counting and tracking function of the AutDeblur&AutoVisualize software (version 1.4.1; MediaCybernetics).

ICP4-CFP fluorescence in transfected silenced cells was measured 24 h after transfection by fixing the cells with 4% PFA and taking images of nine randomly chosen cells exhibiting CFP fluorescence per condition, using the same gain settings in every case. Quantification was carried out using the profile function of the LSM 510 software.

Luciferase assay. Replicate monolayers of $\sim 10^6$ HeLa cells were infected with 5 PFU/cell of *ts*K/Luci and incubated at 31°C for the times required. Luciferase assays were performed using the luciferase assay system (Promega) according to the manufacturer's instructions, and luciferase activity was assessed using a Glomax 20/20 luminometer (Promega).

Infectious-center experiments. Cells infected with a control lentivirus expressing an shRNA directed against luciferase (shLuc cells) or with a lentivirus expressing a CAN/Nup214-specific shRNA (shCAN cells) were infected with 5 PFU/cell of vICP4CFP-VP26RFP for 1 h at 37°C. The viral inoculum was removed, and the cells were acid washed (0.14 M NaCl, 0.1 M glycine [pH 3]) to remove any residual input virus. The cells were then resuspended by trypsinization and serially diluted in DMEM. The dilutions were mixed with Vero cells in suspension and plated out into six-well dishes in DMEM containing 10% human serum. Once monolayers of adherent cells were formed (6 h later), the medium was replaced with methylcellulose. After incubation at 37°C for 48 h, the cells were stained with Giemsa (VWR), and plaques were counted.

RESULTS

Identification of capsid-binding nucleoporins. Herpesvirus capsids accumulate in the vicinity of nuclear pores before releasing their DNA into the nucleus (39, 52), and it is likely that this process requires interactions between the capsid and proteins of the NPC. Therefore, we exogenously expressed a subset of nucleoporins to examine their potential roles in capsid binding. We selected a set of nucleoporins associated with different parts of the nuclear pore (cytoplasmic face, nucleoplasmic face, and pore membrane) and containing a variety of motifs (Table 2) and cloned them, adding an N-terminal myc tag for detection (Table 1). Because full-length myc-tagged CAN/Nup214 was poorly expressed, we cloned the C-terminal

TABLE 2. Interactions described in this study

Nucleoporin	NPC localization[a]	Motif[b]	Result[f]		
			HSV-1 capsid IP[c]	HSV-1 pUL25 IP[c]	PrV pUL25 yeast[d]
CAN/Nup214[e]	Cyto	FG, Gly, CC, BP, LZ, AH	+	+	+
hNup153	Nuc	FG, Gly, ZF	NT	NT	−
hNup133	Cyto + Nuc	BP, AHR	−	−	NT
hNup54	Cyto + Nuc	FG, Gly, CC	−	−	NT
hNup50	Nuc	FG, RBD	−	−	NT
hCG1	Cyto	FG, ZF, CC	−	+	+[g]
POM121	PM	FG, Gly, TM	NT	NT	−
Nup98	Nuc	FG, Gly	NT	NT	−

[a] Cyto, cytoplasmic face; Nuc, nucleoplasmic face; PM, pore membrane (11).
[b] FG, FG repeats; Gly, glycosylated; RBD, Ran-binding domain; ZF, zinc fingers; CC, coiled coil; LZ, leucine zipper; AH, amphipathic helix; BD, β-propeller; TM, transmembrane helix.
[c] IP, immunoprecipitation. See Fig. 1 and 2 for details.
[d] See Table 3 for details.
[e] Only amino acids 1594 to 2090 (see Fig. 1 and 2 and Table 3 for details).
[f] NT, not tested.
[g] Only amino acids 1 to 380 (see Table 3 for details).

region of the protein, encompassing residues 1594 to 2090 and containing the FG repeat sequences, into pCDNA3.1-myc to produce myc-hCAN Ct. This C-terminal domain was previously shown to bind to the adenovirus capsid (56).

To examine interactions between capsids and nucleoporins, Vero cells were transfected with a plasmid encoding the myc-tagged nucleoporins. After 6 h, the cells were infected with 5 PFU/cell of a UL37 null virus, FRΔUL37, and incubated for a further 15 h. FRΔUL37 has a failure in virion assembly that results in the accumulation of unenveloped capsids in the cytoplasm of infected cells. Recently, it was reported that these capsids retain the ability to deliver their genomes into nuclei, showing that they contain all the functions necessary for interacting with the NPC (47). The accumulation of large numbers of cytoplasmic capsids that are capable of binding to the NPC was expected to enhance the detection of interacting partners. Thus, the cells were lysed, and the cytoplasmic capsids were immunoprecipitated using the antibody PTNC, raised against purified capsids. The immunoprecipitated pellet was analyzed by Western blotting using MAb 9E10 to detect the presence of the myc-tagged nucleoporins. As shown in Fig. 1A, the only protein identified by coimmunoprecipitation with capsids was the C-terminal region of CAN/Nup214 expressed from myc-hCAN Ct.

To rule out the possibility that the nucleoporins were interacting only with newly synthesized proteins rather than assembled capsids in these FRΔUL37-infected cells and to determine whether a similar interaction pattern could be observed during the initial stages of infection, we examined the behavior of incoming capsids following virus infection. Vero cells expressing the selected nucleoporins were infected with 50 PFU/cell of WT HSV-1 and incubated at 37°C for 30 min before undergoing lysis and immunoprecipitation of capsids. Once again, the only protein that coimmunoprecipitated with capsids was myc-hCAN Ct, although the amount of immunoprecipitated capsids was considerably lower than that of the FRΔUL37 capsids (Fig. 1B).

Identification of pUL25-binding nucleoporins. Any specific interaction between capsids and nuclear pore proteins would be expected to involve capsid proteins that have a role in pore binding and DNA release. Two potential candidates, pUL25 and pUL36, have been identified by studying *ts* mutants. pUL36 is a very large tegument protein that also appears to have several functions during virus assembly and infection (2). pUL25 is a minor capsid protein that is required for viral DNA

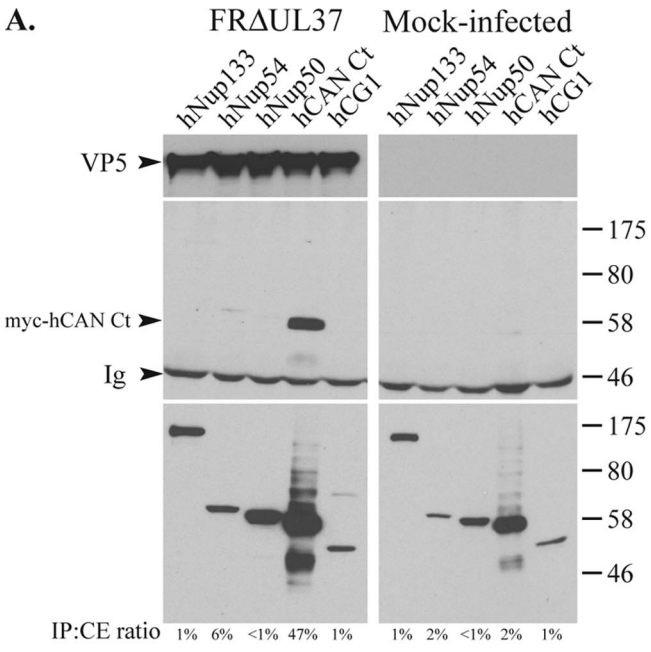

FIG. 1. Interaction of HSV-1 capsids with nucleoporins. (A) Vero cells were transfected with plasmids expressing myc-tagged nucleoporins hNup133, hNup54, hNup50, hCAN Ct, and hCG1 for 6 h before being mock infected or infected with FRΔUL37. Fifteen hours after infection, cells were lysed, and capsids were immunoprecipitated using anti-capsid antibody PTNC. Cell extracts (bottom) and immune complexes (top and middle) were separated by SDS-PAGE and analyzed by Western blotting using anti-VP5 MAb DM165 to reveal the capsids (top) or anti-myc MAb 9E10 to reveal the nucleoporins (middle and bottom). The positions of the VP5 and myc-hCAN Ct bands and of protein size standards are indicated to the left and right, respectively. Ig indicates the immunoglobulin heavy chain. (B) Vero cells were transfected as described above (A) and incubated for 15 h before being mock infected (−) or infected (+) with 50 PFU/cell of WT HSV-1. Thirty minutes after infection, cells were lysed, and capsids were immunoprecipitated using PTNC antibody. Cell extracts (bottom) and immune complexes (top and middle) were separated by SDS-PAGE and analyzed as described above (A). The relative amount of protein present in the immunoprecipitate (IP) is indicated as a percentage of the amount present in the cell extract (CE) (IP:CE ratio).

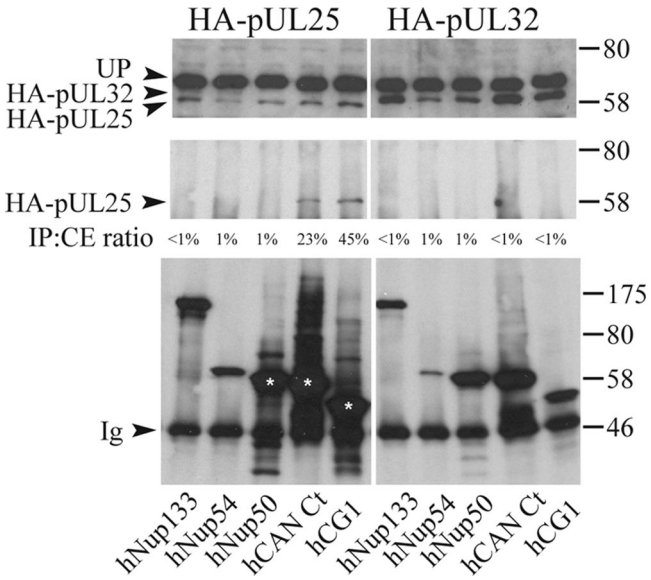

FIG. 2. Interaction of pUL25 with nucleoporins. Vero cells cotransfected with plasmids expressing myc-tagged nucleoporins, as described in the legend of Fig. 1, and either HA-pUL25 or HA-pUL32 were lysed 15 h after transfection. Following immunoprecipitation with anti-myc antibody A14, cell extracts (top) and immune complexes (middle and bottom) were separated by SDS-PAGE and analyzed by Western blotting using anti-HA MAb F7 to reveal the presence of HA-pUL25 (left top and left middle) and HA-pUL32 (right top and right middle). The presence of the nucleoporins in the immunoprecipitate was confirmed by stripping the blots and reprobing with anti-myc MAb 9E10 (bottom). The positions of the HA-pUL25 and HA-pUL32 bands and of protein size standards are indicated to the left and right, respectively. UP indicates an unknown protein in the cell extracts that cross-reacts with anti-HA MAb F7. The relative amount of protein present in the immunoprecipitate (IP) is indicated as a percentage of the amount present in the cell extract (CE) (IP:CE ratio).

release at the nuclear pore (44). The UL25 ORF from HSV-1 with an HA tag inserted at the N terminus was cloned under the control of the human cytomegalovirus immediate-early promoter. Vero cells expressing HA-pUL25 and the different myc-tagged nucleoporins were lysed 15 h after transfection, and coimmunoprecipitations were carried out with myc-specific antibody A14. The immunoprecipitated pellet was analyzed by Western blotting using anti-HA MAb F7 to detect the presence of pUL25 (Fig. 2). HA-pUL25 was detected only in samples containing the C terminus of CAN/Nup214 (hCAN Ct) and hCG1. The specificity of the interaction was confirmed using another, irrelevant, HA-tagged HSV-1 protein, pUL32, which did not interact with any of the nucleoporins tested. The reverse experiment showed that myc-CAN Ct could also be coimmunoprecipitated by pUL25 and not by pUL32 (data not shown).

To provide an independent confirmation of the interaction between pUL25 and the nucleoporins, we used the yeast two-hybrid system. However, as reported previously (26), we observed that the fusion of the LexA domain to the N terminus of the HSV-1 UL25 ORF resulted in an autoactivation of the β-galactosidase reporter gene, making it unsuitable for yeast two-hybrid analyses. Therefore, we used the UL25 gene from a related herpesvirus, PrV, which did not cause autoactivation. The pUL25 proteins from HSV-1 and PrV share a high level of amino acid identity (54%) and have a conserved functional role in virion formation (25). Thus, PrV pUL25 should provide a functional substitute for pUL25 of HSV-1 and would have the additional benefit of demonstrating whether the interaction with CAN Ct is conserved among alphaherpesviruses. LexA-PrV UL25 was screened for interactions against a set of full-length nucleoporins and specific subdomains that had previously been used to identify interactions with the human immunodeficiency virus type 1 (HIV-1) Rev and Vpr proteins (27). In addition, the C-terminal region of CAN/Nup 214 (hCAN Ct) (amino acids 1594 to 2090) used in the immunoprecipitation studies was cloned into pGAD. The results are summarized in Table 3. HIV-1 Rev, which interacts with FG repeat domains, was used as a positive control and indeed gave a positive β-galactosidase signal with all of the FG domain-containing nucleoporins. In contrast, with PrV pUL25, we detected a positive signal only with hCG1 at amino acids 1 to 380 and hCAN Ct (Table 3). In the latter case, the specificity of the interaction could not be tested since yeast cells transformed with hCAN Ct and the LexA control plasmid did not grow. Nevertheless, these results supported the evidence obtained from the coimmunoprecipitation experiments.

In all three types of assays, capsid immunoprecipitation, pUL25 immunoprecipitation, and yeast two-hybrid analyses, the C-terminal region of CAN/Nup214 was detected as a binding partner, with hCG1 also being identified by the latter experiments (Table 2). Therefore, from these results, we conclude that HSV-1 capsids are able to interact with CAN/Nup214 (and possibly with hCG1) and that this interaction is likely to be mediated by pUL25.

Effect of depletion of CAN/Nup214 on early stages of infection. In order to examine its role during HSV-1 infection, we used shRNA technology to deplete CAN/Nup214. To monitor

TABLE 3. Yeast two-hybrid interactions between PrV UL25 and a selection of nucleoporin constructs

Gene (residues)[a]	β-Gal activity[b]		
	HIV-1 Rev[c]	UL25 PrV[c]	LexA alone
CAN/Nup214 (1–256)	−	−	−
CAN/Nup214 (586–1059)	−	−	−
CAN/Nup214 FG	+	−	−
hCAN Ct (CAN/Nup214 Ct) (1594–2090)	NT	+	0
POM121 (73–801)	−	−	−
POM121 FG	+	−	−
Nup98 FG	+	−	−
hCG1 Full length (1–423)	0	0	0
hCG1 (1–380)	+	+	−
hCG1 FG	+	−	−
hCG1 Nt	−	−	−
Nup153 full length	+	−	−
Nup153 Nt	−	−	−

[a] Cloned into vector pGAD, fusing the GAL4-activating domain to the N terminus of the indicated protein. These plasmids were described previously in reference 27, except for hCAN Ct, which contains the C-terminal region of CAN/Nup214, encoding amino acids 1594 to 2090, which was also present in the myc-hCAN Ct plasmid used in the immunoprecipitation studies (Fig. 1 and 2).

[b] − indicates no interaction, + indicates an interaction, and 0 indicates poor yeast growth. NT, not tested.

[c] Cloned into vector pLexA, fusing the LexA domain to the N terminus of the indicated protein.

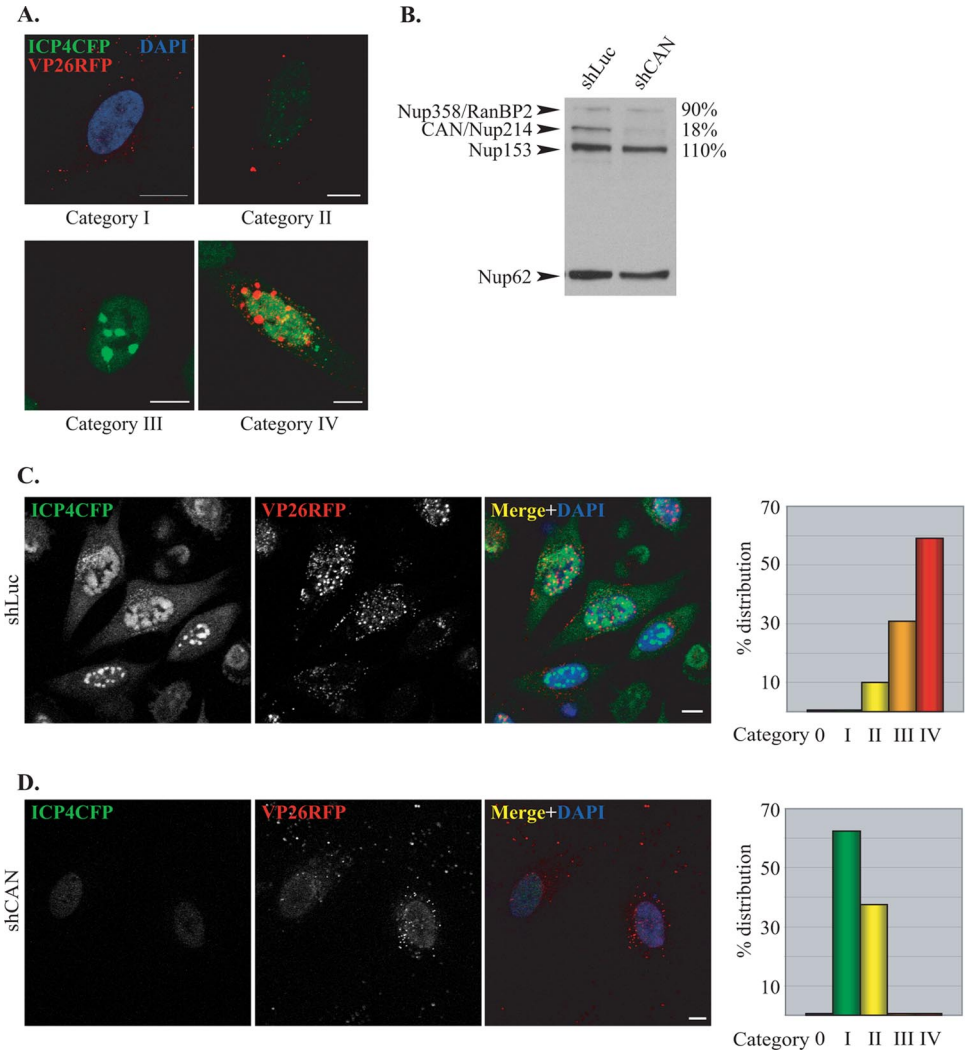

FIG. 3. CAN/Nup214 depletion delays HSV-1 DNA replication. (A) Cells 3 h after infection with vICP4CFP-VP26RFP. Cells were classified into different categories based on the extent of viral DNA replication as determined by ICP4-CFP fluorescence (green). Category 0 comprised cells showing no fluorescence (not shown). The panels show typical examples of cells assigned to category I, with capsids (red) in the cytoplasm but no detectable ICP4-CFP signal. The location of the nucleus is revealed by DAPI staining (blue). Categories II to IV exhibit increasing amounts of ICP4-CFP nuclear fluorescence localized in small (II), large (III), and coalescing (IV) foci. In the latter case, nuclear capsid assembly compartments are visible as VP26RFP foci. Scale bars, 10 μm. (B) Efficiency of CAN/Nup214 silencing. HeLa cells infected with lentiviruses expressing shRNA directed against the luciferase gene (shLuc) or CAN/Nup214 (shCAN) were harvested at 72 h postinfection and analyzed by Western blotting using MAb 414, which recognizes the nucleoporins RanBP2/Nup358, CAN/Nup214, Nup153, and Nup62. Nup62 was used as a loading control, and the relative intensities of the other bands were determined in shCAN and shLuc cells as indicated on the right (shLuc values were set at 100%). (C and D) Representative images from shLuc (C) or shCAN (D) cells infected for 3 h with vICP4CFP-VP26RFP. The pattern of infection was estimated by assessing the proportion of cells belonging to each of the categories shown above (A) as determined from the level of ICP4-CFP expression. A total of 248 randomly selected cells was observed, and the relative number of cells in each category, expressed as a percentage of the total number of cells counted, is shown in the graphs on the right. Scale bars, 10 μm.

the effects of this depletion, we constructed an HSV-1 recombinant virus, vICP4CFP-VP26RFP. This virus has monomeric RFP fused to the VP26 capsid protein and CFP fused to ICP4, an immediate-early HSV-1 protein that associates with virus DNA in the nucleus of infected cells. VP26-RFP could be used to monitor the fate of virus capsids, while ICP4-CFP fluorescence acted as a marker for virus DNA entry into the nucleus (17). Thus, since DNA entry into the nucleus is dependent on the interaction between capsids and the NPC triggering the release of the virus genomes, the efficiency of capsid docking could be monitored as a function of the progress of viral DNA replication. When HeLa cells were infected with this virus, several different patterns of fluorescence were observed at 3 h postinfection (Fig. 3A). These patterns were arbitrarily divided into five categories. Cells in category 0 were uninfected (RFP and CFP minus). Category I had RFP capsids in the cytoplasm but no detectable CFP signal. Category II had cells with small ICP4-CFP foci, indicating the presence of viral DNA in the nucleus. Category III had larger but still-discrete ICP4-CFP foci in the nucleus, indicating early DNA synthesis. In category IV, the foci had started to merge into patches, indicating more-extensive DNA replication, and VP26-RFP was present in some nuclei.

To analyze the effect of the CAN/Nup214 depletion, HeLa cells were infected with a lentivirus expressing a CAN/Nup214-specific shRNA (shCAN) or with a control lentivirus expressing an shRNA directed against luciferase (shLuc). Western blotting with MAb 414, which recognizes the nucleoporins RanBP2/Nup358, CAN/Nup214, Nup153, and p62 (14), confirmed the selective depletion of CAN/Nup214 (Fig. 3B). Thus, there was a reduction in CAN/Nup214 levels of more than 80% in shCAN-infected cells compared to shLuc cells, whereas the levels of the other nucleoporins were not affected. The p62 protein was used as a loading standard since it is a core protein of the NPC, which was previously reported to be unaffected by CAN/Nup214 depletion (5).

To determine the impact of the CAN/Nup214 depletion on early stages of HSV-1 infection, shLuc and shCAN cells were infected with vICP4CFP-VP26RFP, and the ICP4-CFP fluorescence patterns were assessed at 3 h postinfection according to the classification scheme described above. The pattern seen with the shLuc control cells shows the majority of cells (~90%) falling into categories III and IV, indicating that viral DNA had entered the nuclei and was replicating (Fig. 3C). In contrast, cells silenced for CAN/Nup214 exhibited very little ICP4-CFP signal, with virtually all the cells falling into categories I and II (Fig. 3D). The large number of cells in category I (>60%) were at the stage where capsids are present in the cytoplasm, but no ICP4-CFP signal was detectable in the nuclei. The other 40% of the cells were placed into category II, as they displayed weak ICP4-CFP fluorescence. These results show that the depletion of CAN/Nup214 leads to a marked delay in viral DNA entering the nucleus but does not entirely prevent it, since some ICP4-CFP signal could still be detected.

To confirm the effect of the depletion of CAN/Nup214 on the delivery of the viral genome into the nucleus and to provide a quantitative assay, we used another HSV-1 recombinant virus, *ts*K/Luci (provided by C. Preston). This virus is a derivative of the *ts*K virus in which the luciferase coding region was controlled by the HSV-1 immediate-early ICP0 promoter. As shLuc cells would suppress luciferase expression, HeLa cells were infected with a lentivirus encoding an shRNA specific for the GFP gene (shGFP) to act as a control. shCAN- and shGFP-infected cells were infected for 2 h, 3 h, or 7 h with 5 PFU/cell of *ts*K/Luci at 31°C, and their luciferase activities were measured. As shown in Fig. 4, the luciferase levels in shGFP-infected cells was markedly higher than that in shCAN-infected cells, with ~400-times-more activity at 2 h postinfection, ~200-times-more activity at 3 h postinfection, and ~15-times-more activity at 7 h postinfection. This shows that the depletion of CAN/Nup214 has a strong effect at early times postinfection, indicating that an early stage of the viral cycle is affected. Furthermore, the rapid increase in the level of luciferase activity after the initial delay suggests that later functions are not disrupted as a consequence of the CAN/Nup214 depletion. This is the type of behavior that would be expected if the CAN/Nup214 depletion was affecting capsid docking and DNA release, leading to a delay in the entry of the viral genome into the nucleus, but was not inhibiting later replication processes. Thus, these results support the role of CAN/Nup214 in viral DNA release.

Depletion of CAN/Nup214 does not affect virus entry or ICP4 nuclear import. Based on the CAN/Nup214 interaction studies described above, the likely explanation for the delay in the onset of replication is that the depletion of CAN/Nup214 inhibits or alters the binding of capsids to the NPC, which prevents the release of viral DNA. However, two other possibilities need to be considered.

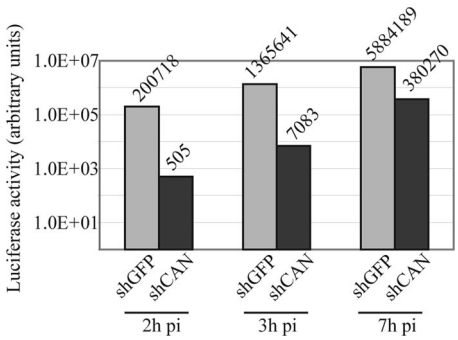

FIG. 4. CAN/Nup214 depletion delays HSV-1 gene expression. HeLa cells infected with lentiviruses expressing shRNA directed against the GFP gene (shGFP) or CAN/Nup214 (shCAN) were infected with 5 PFU/cell of *ts*K/Luci. After incubation at 31°C for 2 h, 3 h, or 7 h, the cells were harvested and processed for luciferase assays. The luciferase activity is indicated on a logarithmic-scaled graph, with the numerical value indicated above each bar. pi, postinfection.

The first possibility is that the cell's susceptibility to HSV-1 infection is reduced as a result of changes in cellular protein expression caused by reduced mRNA export consequent on the CAN/Nup214 depletion. This is unlikely, since it was previously reported that in mammalian cells, mRNA export is barely affected by the CAN/Nup214 depletion (22). However, we compared the efficiencies of virus entry in shLuc and shCAN cells by looking at the breakdown in colocalization between the envelope glycoprotein gD and capsids, which occurs when the virion envelope fuses with the plasma membrane and the capsids are released into the cytosol. For these experiments, shLuc or shCAN cells were infected with vICP4CFP-VP26RFP for 2 h in the presence of cycloheximide, a protein synthesis inhibitor. Capsids were recognized by VP26RFP fluorescence, while gD was identified using gD-specific MAb 4846. As a control, purified vICP4CFP-VP26RFP virions were applied directly onto a glass coverslip. The capsid (VP26RFP) signal colocalized with the gD signal (Fig. 5A) in 93% of the particles (Fig. 5C). Similarly, when membrane fusion was inhibited by adsorbing the virus onto cells for 1 h at 4°C, 88% of capsids were gD positive. In contrast, by 2 h postinfection, at 37°C, 80% of capsids in shLuc cells and 83% of capsids in shCAN cells were gD negative (Fig. 5B and C), thereby indicating that the CAN/Nup214 depletion does not affect the cell's susceptibility to infection.

As a further demonstration that the depletion of CAN did not block the initial stages of virus infection, infectious-center assays were carried out. The numbers of infectious centers produced in shLuc and shCAN cells were comparable, with average titers of 4.9×10^5 PFU/ml in shLuc cells and 4.8×10^5 PFU/ml in shCAN cells (Table 4), thereby confirming that virus entry and replication are not affected by the depletion of CAN, as expected from the results obtained with the *ts*K/Luci virus (Fig. 4).

The second possible explanation for the delay in the appear-

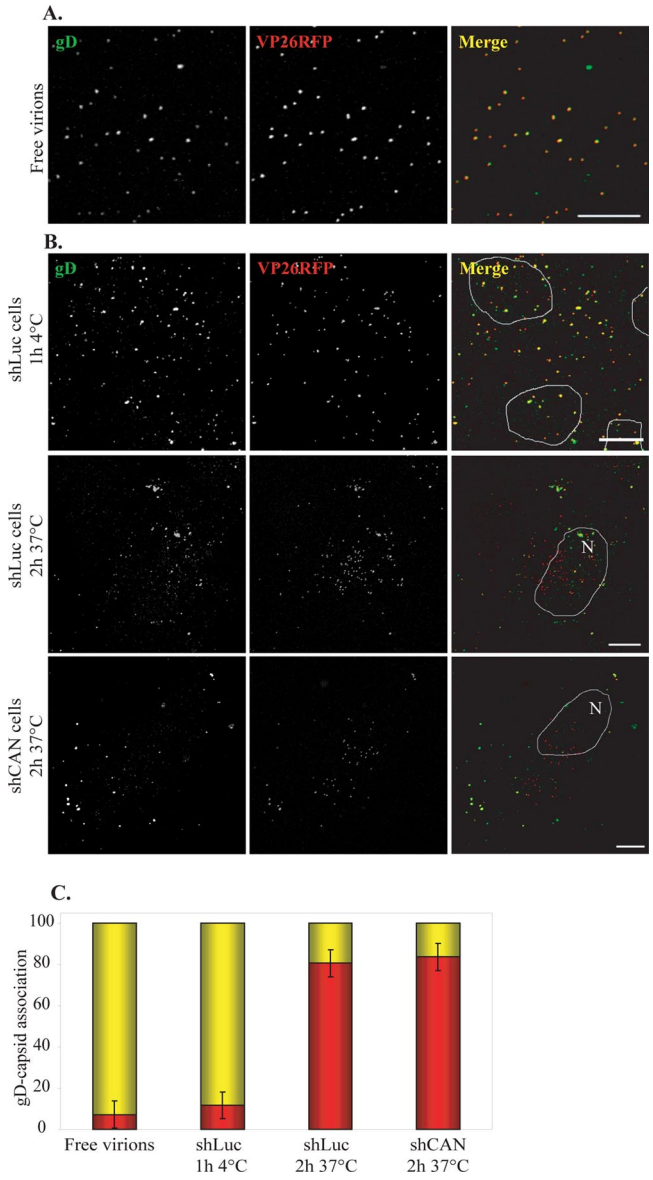

FIG. 5. Effect of CAN/Nup214 depletion on virus entry. (A) vICP4CFP-VP26RFP virions purified on 5-to-15% Ficoll gradients were spread onto collagen-coated glass coverslips, fixed with 4% PFA, and incubated sequentially with anti-gD antibody, MAb 4846, and Alexa Fluor 633-conjugated goat anti-mouse antibody. Capsids and gD were revealed by RFP fluorescence (red) and Alexa Fluor 633 fluorescence (pseudocolored in green), respectively. (B) shLuc (top and middle) and shCAN (bottom) cells (Fig. 3) were incubated with vICP4CFP-VP26RFP virions for 1 h at 4°C (top) or for 2 h at 37°C in the presence of 200 μM cycloheximide (middle and bottom). The cells were fixed, permeabilized, and stained for gD as described above (A). Deconvoluted pictures of *z* stacks are shown. Outlines of nuclei as determined by DAPI staining (not shown) are indicated (N). Scale bars, 10 μm. (C) RFP capsids on randomly chosen cells from the experiment shown above were counted. The presence or absence of gD was assessed by examining colocalization between RFP and Alexa Fluor 633 signals using the colocalization function of the LSM510 software. Results are shown as numbers of gD-positive (yellow) and gD-negative (red) capsids expressed as a percentage of the total number of capsids counted. A total of 1,102 particles were analyzed.

TABLE 4. Titration of infectious centers in shLuc and shCAN cells infected with vICP4CFP-VP26RFP

Cell type	Titer (PFU/ml) in expt:		
	1	2	3
shLuc	4×10^5	4.9×10^5	5.8×10^5
shCAN	4×10^5	5.5×10^5	4.8×10^5

ance of the nuclear ICP4-CFP signal is that the depletion of CAN/Nup214 interferes either with ICP4-CFP production or with its nuclear import. This also appears to be unlikely, since earlier studies showed that the depletion of CAN/Nup214 did not affect nuclear protein import (22, 59). However, to examine the effects of the CAN/Nup214 depletion on the production and transport of ICP4, we carried out experiments that confirmed that the nuclear localization of ICP4-CFP expressed from a transfected plasmid was not affected in shCAN cells (Fig. 6A). Moreover, the fluorescence level of ICP4-CFP appeared to be unchanged in shCAN cells compared to that in shLuc cells, indicating no defect in the expression of the protein in the absence of CAN/Nup214 (Fig. 6B). Thus, we conclude that the delay in infection resulting from the depletion of CAN/Nup214 is compatible with its putative function as part of the NPC docking site for the capsid.

pUL25 as an interface between capsids and the NPC: interaction with pUL6 and pUL36. Binding to the NPC is thought to trigger viral DNA release from capsids. Since we have now demonstrated a potential role for pUL25 in the binding of the capsid to the NPC, we decided to investigate the relationship between pUL25 and two other proteins, pUL6 and pUL36, that are known to have a role in DNA release. The mechanism of release is very poorly understood, but comparison with tailed bacteriophages suggests that the DNA exits through the portal, which is a ring-shaped channel formed by a dodecamer of pUL6 proteins and is located at one vertex of the capsid (7, 8, 38). Also, as mentioned above, pUL36 is important for this process, as a *ts* mutant in UL36 makes particles that are blocked for DNA release at nonpermissive temperatures.

To investigate whether pUL25 interacts with pUL6, Vero cells were cotransfected with plasmids encoding HA-tagged pUL25 (HA-pUL25) and myc-tagged pUL6 (myc-pUL6). Immunoprecipitation was performed with HA antibody Y11 and resulted in the coprecipitation of myc-pUL6 when expressed in the presence of HA-pUL25 but not when expressed with the HA-tagged importin α1 (HA-Imp α1) control (Fig. 7A, lanes 1 and 4). That there was no nonspecific interaction between HA-pUL25 and the myc tag was shown by the failure of the myc-tagged dynamitin control (myc-Dyn) to coprecipitate with HA-pUL25 (Fig. 7A, lane 3). In addition, no myc-pUL6 band was detected when the immunoprecipitation was carried out using a control antibody, NRP14, directed against N_{rsv} (Fig. 7A, lane 2). In the inverse experiment, anti-myc antibody A14 pulled down HA-pUL25 only when coexpressed with myc-pUL6 and not with the unrelated myc-Dyn protein (Fig. 7B, lanes 1 and 3). As described above, there was no interaction between myc-pUL6 and HA-Imp α1 (Fig. 7B, lane 4), and NRP14 did not bring down HA-pUL25 (Fig. 7B, lane 2).

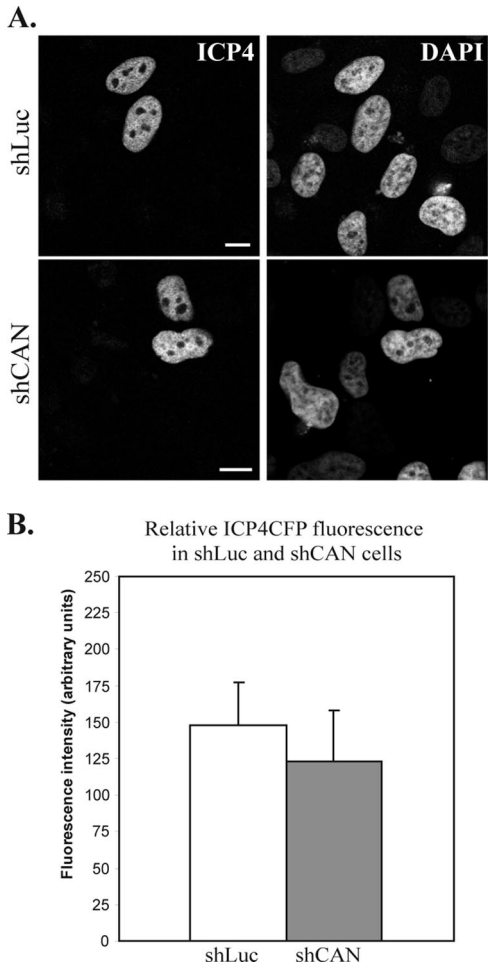

FIG. 6. ICP4-CFP expression and localization in shLuc and shCAN cells. (A) shLuc or shCAN cells were transfected with a plasmid encoding ICP4-CFP. Twenty-four hours later, cells were fixed, and ICP4-CFP localization was assessed by direct CFP fluorescence. Nuclei were counterstained with DAPI. Scale bars, 5 μm. (B) The fluorescence level of nine randomly chosen CFP-positive cells per condition (shLuc or shCAN), imaged using the same acquisition parameters, was quantified on a scale from 0 (no fluorescence) to 250 (saturated fluorescence). The values obtained were averaged and compared on a graph.

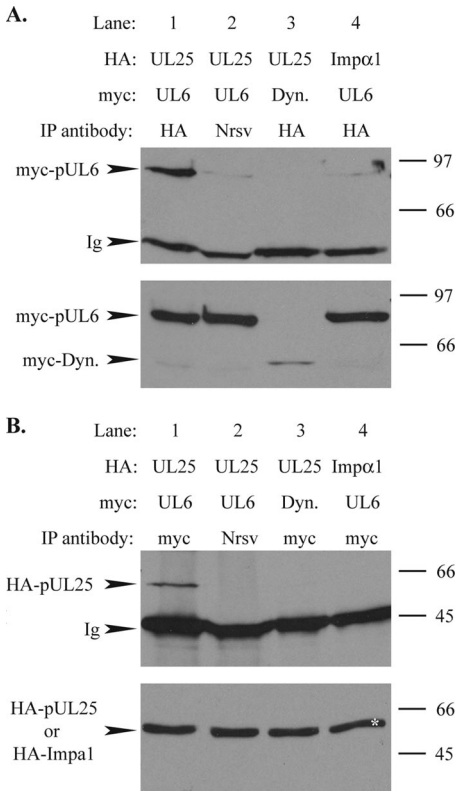

FIG. 7. Interaction between pUL25 and pUL6. Vero cells were cotransfected with plasmids expressing HA-pUL25 (UL25) or HA-importin α1 (Impα1) and myc-pUL6 (UL6) or myc-dynamitin (Dyn.) and harvested 24 h after transfection. (A) Following immunoprecipitation with anti-HA antibody Y11 or an antibody against N_{rsv}, RPN14, cell extracts (bottom) and immune complexes (top) were separated by SDS-PAGE and analyzed by Western blotting using anti-myc MAb 9E10 to reveal the presence of myc-pUL6 and myc-dynamitin. The positions of the myc-pUL6 and myc-dynamitin (myc-Dyn) bands and of protein size standards are indicated to the left and right, respectively. Ig indicates the immunoglobulin heavy chain. (B) Extracts of the transfected cells described above (A) were immunoprecipitated (IP) with anti-myc antibody A14 (myc) or NRP14 (N_{rsv}). Cell extracts (bottom) and immune complexes (top) were separated by SDS-PAGE and analyzed by Western blotting using anti-HA MAb F7 to reveal the presence of HA-pUL25. The positions of the HA-pUL25 band and of protein size standards are indicated to the left and right, respectively. HA-importin α1, which is the same size as HA-pUL25, is marked with an asterisk in lane 4.

Although it cannot be ascertained whether the interaction identified in our system involves the portal structure or monomers of pUL6, these results demonstrate that transiently expressed pUL25 and pUL6 can interact and suggest the possibility of an association between pUL25 and the portal in the virus particle.

The tegument protein pUL36 has also been shown to be implicated in viral DNA uncoating (2, 24), and an interaction between pUL25 and the C terminus of pUL36 was reported previously for both PrV and HSV-1 (9). In order to confirm this interaction in HSV-1, plasmids expressing the last 1,127 or 719 amino acids of pUL36, each fused at its N terminus to a myc tag, were constructed (Table 1). Their products were designated myc-pUL36 2037 and myc-pUL36 2446, respectively, where the number specifies the position of the N-terminal pUL36 residue in the sequence of the full-length, 3,164-amino-acid protein. Both myc-pUL36 2037 and myc-pUL36 2446 were precipitated by HA antibody Y11 when coexpressed with HA-pUL25 (Fig. 8, lanes 1 and 3) but not when expressed on their own (Fig. 8, lanes 2 and 4). Similarly, carrying out the immunoprecipitation with myc antibody A14 resulted in the coimmunoprecipitation of HA-pUL25 when coexpressed with the myc-pUL36 proteins (Fig. 8, lanes 5 and 6) but not when it was expressed alone (Fig. 8, lane 7). As has been frequently observed with pUL36, both myc-pUL36 2037 and myc-pUL36 2446 gave rise to many breakdown products (Fig. 8, bottom, lanes 1 to 4). Interestingly, most of the myc-pUL36 2037 breakdown products coprecipitated with HA-pUL25, whereas those of myc-pUL36 2446 did not (Fig. 8, top, lanes 1 and 3). Since the myc tag is at the N terminus of each construct, all the

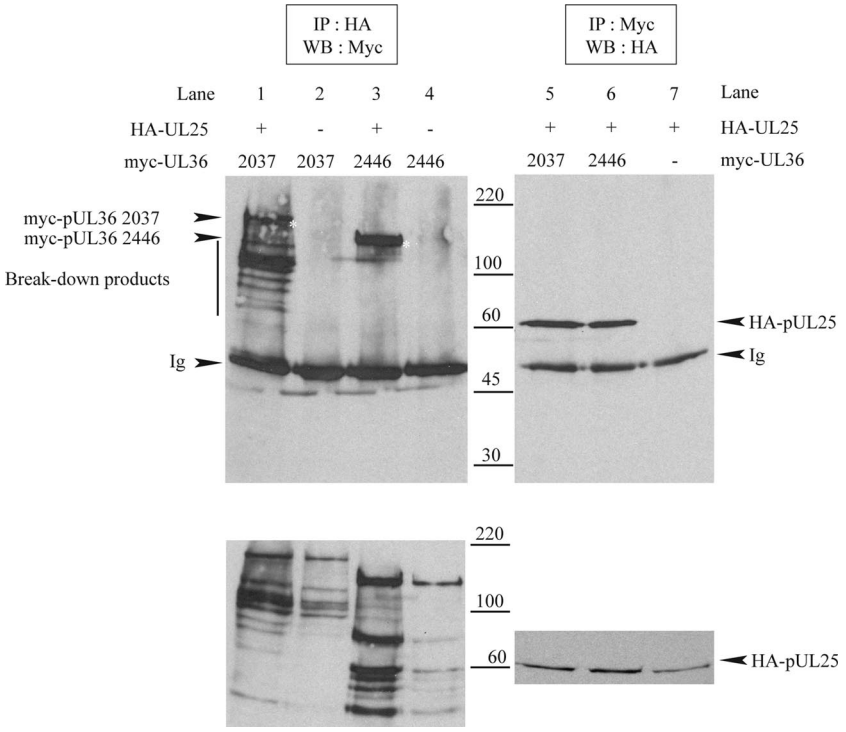

FIG. 8. Interaction between pUL25 and pUL36. Vero cells were cotransfected with plasmids expressing HA-pUL25 and either myc-pUL36 2037 (encoding C-terminal amino acids 2037 to 3164 of pUL36) or myc-pUL36 2446 (encoding C-terminal amino acids 2446 to 3164) and harvested 24 h after transfection. Cell extracts were immunoprecipitated (IP) by anti-HA antibody Y11 (top left) or anti-myc antibody A14 (top right). Cell extracts (bottom) and immune complexes (top) were separated by SDS-PAGE and analyzed by Western blotting (WB) for the presence of myc-tagged pUL36 fragments (left) or HA-pUL25 (right), respectively. The positions of myc-pUL36 bands, HA-pUL25 bands, and protein size standards are indicated to the left, right, and center, respectively. The full-length myc-pUL36 2037 and myc-pUL36 2446 bands are marked with asterisks. Note that breakdown products of the myc-pUL36 fragments are present in both cell extracts and the HA-pUL25 and myc-pUL36 2037 coimmunoprecipitation sample (lane 1) but not in the HA-pUL25 and myc-pUL36 2446 coimmunoprecipitation sample (lane 3). Ig indicates the immunoglobulin heavy chain.

fragments represent C-terminal truncations, suggesting that the deletion of the C terminus of myc-pUL36 2446 caused a loss of binding to pUL25, whereas the deletion of the same part of myc-pUL36 2037 did not. These observations suggested the existence of a second HA-pUL25-binding domain in myc-pUL36 2037 or, alternatively, a multimerization domain on pUL36 that could be indirectly involved in the interaction.

To verify this, we constructed several C-terminal truncations of myc-pUL36 2037 and myc-pUL36 2446 (Fig. 9A) and tested their interactions with HA-pUL25. In the case of myc-pUL36 2446, the deletion of the last 60 amino acids, which removes the previously mapped (9) capsid-binding domain (CBD/pUL25 BDI) (Fig. 9A), was sufficient to prevent the interaction with HA-pUL25 (Fig. 9C, lane 3104). However, with myc-pUL36 2037, the removal of CBD/pUL25 BD I did not block binding since truncations lacking up to 811 residues from the C terminus could still precipitate HA-pUL25 (Fig. 9B, lanes 2572, 2504, and 2353), although deletions lacking a further 153 amino acids could not (Fig. 9B, lane 2200). This surprising result confirms the observations shown in Fig. 8 and demonstrates the existence of a second, independent pUL25-binding domain (pUL25 BD II) (Fig. 9A) located between residues 2037 and 2353 of pUL36.

DISCUSSION

CAN/Nup214 is a nuclear receptor for the herpesvirus capsid. Large nuclear-replicating DNA viruses face the problem of transmitting their genomes into the nucleus. To achieve this, herpesviruses have developed mechanisms for transporting the genome-containing capsid to the nuclear pore, which provides the route through the nuclear membrane. It has long been known that incoming capsids localize to the vicinity of nuclear pores before releasing their DNA. However, the nature of any interaction with the pore and the trigger for DNA release are largely unknown. In this study, we examined interactions between the HSV-1 capsid and selected components of the NPC. Since endogenous nucleoporins are sequestered predominantly in NPCs, we looked at interactions of capsids with uncomplexed proteins by overexpressing selected nucleoporins from plasmids. The set of nucleoporins examined included members from different parts of the NPC. Thus, CAN/Nup214 and hCG1 are associated with the cytoplasmic face; hNup153, hNup50, and hNup98 are components of the nucleoplasmic face; and hNup133 and hNup54 are located on both faces (Table 2). Many NPC proteins contain characteristic FG repeat sequences, which are known to be an important part of the selective gate formed by the pore (for a review, see reference 13). To examine whether they played a role in HSV-1

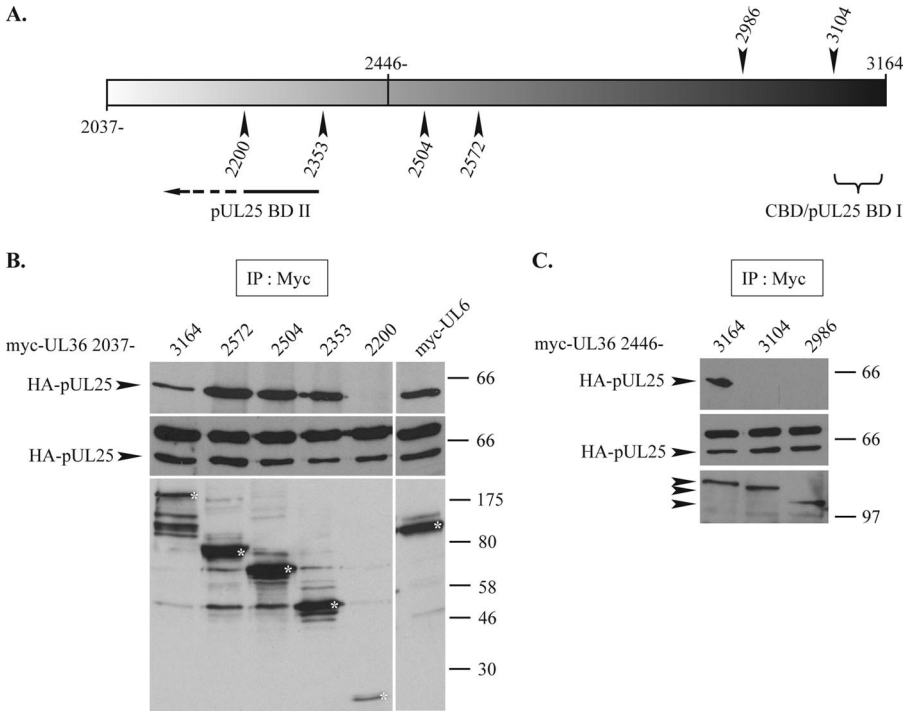

FIG. 9. Mapping of pUL25-binding domains of pUL36. (A) Representation of the pUL36 fragment of amino acids 2037 to 3164. The arrowheads shown above mark the last amino acids encoded by the C-terminal truncations for myc-pUL36 2446, while those below are for myc-pUL36 2037. CBD/pUL25 BD I and pUL25 BD II indicate the pUL25-binding domains (pUL25 BD I is equivalent to the previously mapped capsid-binding domain) (9). (B and C) Interaction of HA-pUL25 with C-terminal truncations of myc-pUL36 2037 and myc-pUL36 2446. Vero cells were cotransfected with plasmids expressing HA-pUL25 and either full-length myc-pUL36 2037 or C-terminal truncations of myc-pUL36 2037 (B) or full-length myc-pUL36 2446 or C-terminal truncations of myc-pUL36 2446 (C), as specified above (A). Twenty-four hours after transfection, the cells were harvested, and extracts were immunoprecipitated (IP) with anti-myc antibody A14. Cell extracts (middle) and immune complexes (top) were separated by SDS-PAGE and analyzed for the presence of HA-pUL25 by Western blotting using anti-HA MAb F7. The immunoprecipitate blots were then stripped and reprobed with anti-myc MAb 9E10 to reveal the presence of the myc-pUL36 truncation products (bottom). The positions of the HA-pUL25 bands and of protein size standards are indicated to the left and right, respectively. Control extracts from cells coexpressing HA-pUL25 and myc-pUL6 were immunoprecipitated using the same procedure. The full-length myc-pUL36 truncation products and the myc-pUL6 band are marked with asterisks.

capsid binding, we included several FG repeat proteins (CAN/Nup214, hNup153, hNup54, hNup50, hCG1, hPOM121, and hNup98). Of the nucleoporins tested, only CAN/Nup214 and hCG1 were identified as being binding partners of pUL25, and only CAN/Nup214 coprecipitated with HSV-1 capsids. Although in our assays the nucleoporins were overexpressed and are unlikely to be incorporated into NPCs, it is interesting that both CAN/Nup214 and hCG1 contain FG repeats, and both are normally localized to the cytoplasmic face of the nuclear pore, where they would be accessible to incoming capsids. Although the precise role of the pUL25-CAN/Nup214 interaction in capsid docking and DNA release is unknown, the functional importance of CAN/Nup214 in these processes was confirmed by shRNA depletion experiments. These experiments showed that reducing the amount of the endogenous protein seriously inhibited the entry of the virus genome into the nucleus. Thus, these studies have identified a likely NPC receptor for HSV-1 capsids.

A recent study has suggested a role for pUL36 and the nucleoporins Nup358/RanBP2 and CAN/Nup214 in the attachment of capsids to the nucleus by syringe-loading and RNA silencing experiments (10). That report demonstrated that antibodies directed against Nup358/RanBP2 had an inhibitory effect on the number of incoming capsids associating with the nucleus, and a similar effect was observed when Nup358/RanBP2 levels were reduced by RNA silencing. Nup358/RanBP2 is a large nucleoporin that is a major component of the NPC cytoplasmic filaments (59, 61, 63, 64) and is therefore appropriately located to act as a receptor for the docking of herpesvirus capsids. A role for CAN/Nup214 in the attachment of capsids to the nucleus was also suggested by RNA silencing experiments, but targeting CAN/Nup214 with an antibody failed to inhibit the capsid-nucleus association. However, it should be noted that the antibody used in this case, QE5, also recognizes other nucleoporins (Nup153 and Nup62) (40) and therefore cannot be considered to be CAN/Nup214 specific. Our silencing data also suggest a role of CAN/Nup214 in nuclear pore binding and/or viral DNA release, in agreement with the results described previously by Copeland et al. (10). However, by using immunoprecipitation to examine capsid-nucleoporin interactions directly, we were able to identify CAN/Nup214 as being a likely docking target for incoming capsids. Interestingly, Nup358/RanBP2 and CAN/Nup214 interact with each other (5) and may therefore constitute a complex that is targeted by herpesvirus capsids.

It is interesting to compare our findings from interactions of

HSV-1 capsids with the NPC with findings from studies of another nuclear-replicating virus. Adenovirus capsids are also transported to nuclear pores. However, unlike the case with herpesviruses, where the capsid retains its integrity and releases its genome through the specialized portal vertex, binding to the NPC triggers capsid disassembly in adenoviruses, resulting in viral DNA uncoating. Despite these very different strategies, it is interesting that adenovirus capsids also interact with CAN/Nup214 and that the same domain is involved in binding to both types of capsid (56). These data show that despite adopting different strategies for uncoating their viral DNA at the NPC, adenovirus and herpesvirus capsids target the same domain of the NPC for binding.

pUL25 acts as an interface between the incoming capsid and the NPC. pUL25 was recently shown to have a role in viral DNA uncoating at the nuclear pore (44). It also has a well-characterized role in stabilizing newly packaged DNA within capsids (34, 53). The crystallographic structure of residues 134 to 580 of pUL25 has been solved and shows a compact, α-helix-rich central core with several solvent-exposed loops, which suggests an ability to interact with a number of different partners (6). Here we demonstrate that pUL25 is able to interact with at least four different proteins, the nucleoporins CAN/Nup214 and hCG1 and the viral proteins pUL6 and pUL36, all of which are likely to be involved in the release of viral DNA at nuclear pores.

The finding that pUL25 binds the C-terminal region of CAN/Nup214 suggests a direct role in capsid binding to the NPC. We also identified a second pUL25-binding nucleoporin, hCG1, although it did not bind to HSV-1 capsids in our assays. It is interesting that CAN/Nup214 and hCG1 share numerous properties. Thus, both are localized on the cytoplasmic side of the NPC (for a review, see reference 50), the yeast homologues of CAN/Nup214 and hCG1 have been shown to act as "modular duplicates" in the NPC architecture in terms of position and fold arrangements (1), and both were previously shown to be involved in the localization of other virus genomes into the nucleus. As mentioned above, adenovirus capsids bind to CAN/Nup214, while the HIV-1 Vpr protein binds hCG1 (27, 56). The pUL25-pUL36 interaction was already known, and a pUL25-binding domain was mapped to the last 60 residues of pUL36 (9). We have confirmed this interaction and identified a second interaction domain between amino acids 2037 and 2353 of pUL36. The independence of these two binding domains indicates that the binding of pUL36 to pUL25 can occur through different mechanisms. The interaction of pUL25 with the portal protein pUL6 has not been described previously but is also compatible with the role of pUL25 in viral DNA packaging and release.

From transport to viral DNA release. Both pUL25 and pUL36 have a role in viral DNA uncoating (2, 44). Since the two proteins interact with each other, it is likely that they form a complex involved in DNA release. pUL36 is an inner tegument protein that is also involved in particle assembly and is essential for cytoplasmic envelopment. It has been demonstrated that pUL36 remains associated with incoming capsids until they reach the nucleus (20, 30). The inner tegument has been shown to promote capsid movement on microtubules (62), and pUL36 has been directly implicated in microtubule-based capsid transport (31). It is likely, therefore, that pUL36 contains the viral receptors for microtubule-linked motors. Altogether, these data strongly suggest a role for the inner tegument, and particularly pUL36, in the transport of capsids toward the nucleus.

pUL6, pUL25, and pUL36 are all associated with the capsid. pUL6 forms the portal that occupies a unique vertex in the capsid shell (7, 8, 38). pUL25 is a minor capsid protein, which preferentially associates with DNA-containing capsids (C capsids) (54). It localizes close to the capsid vertices (37) and has been reported to form part of the additional density seen associated with the vertices in reconstructions of DNA-containing C capsids (58). pUL36 has also been suggested to be on the vertices of capsids present within mature virions (65). The interaction between these two proteins is therefore consistent with their proposed locations on the capsid. In contrast, the interaction of pUL25 and pUL6 described here is not supported by their known spatial arrangements but is consistent with their functions in DNA packaging and release. This suggests the possibility that pUL25 occupies a second position on the capsid in close proximity to the portal.

Given the duality of binding sites of pUL36 for pUL25 and of pUL25 for the capsid (through the pentonal vertices and the portal), we hypothesize that there are two forms of the pUL36-pUL25 complex on the capsid, each with different roles. Thus, penton-associated pUL25-pUL36 would be involved in tegument assembly, envelopment, and egress (16, 47). However, we suggest that pUL25 is also likely to be present at the portal, probably together with pUL36, as a consequence of the interaction between pUL25 and pUL6. In this location, both pUL25 and pUL36 would be suitably positioned to interact with the NPC and trigger the release of the encapsidated DNA through the nuclear pore.

ACKNOWLEDGMENTS

We thank Yves Gaudin and Hélène Raux for helpful advice and Valerie Preston and Duncan McGeoch for critical reading of the manuscript. We also thank David McNab and Marion McElwee for excellent technical assistance. We are very grateful to those listed throughout the text for the provision of reagents.

This work was funded by the MRC (United Kingdom), by the CNRS (France), and by a grant from the French Education and Research Ministry.

REFERENCES

1. **Alber, F., S. Dokudovskaya, L. M. Veenhoff, W. Zhang, J. Kipper, D. Devos, A. Suprapto, O. Karni-Schmidt, R. Williams, B. T. Chait, A. Sali, and M. P. Rout.** 2007. The molecular architecture of the nuclear pore complex. Nature **450:**695–701.
2. **Batterson, W., D. Furlong, and B. Roizman.** 1983. Molecular genetics of herpes simplex virus. VIII. Further characterization of a temperature-sensitive mutant defective in release of viral DNA and in other stages of the viral reproductive cycle. J. Virol. **45:**397–407.
3. **Beck, M., F. Forster, M. Ecke, J. M. Plitzko, F. Melchior, G. Gerisch, W. Baumeister, and O. Medalia.** 2004. Nuclear pore complex structure and dynamics revealed by cryoelectron tomography. Science **306:**1387–1390.
4. **Belgareh, N., G. Rabut, S. W. Bai, M. van Overbeek, J. Beaudouin, N. Daigle, O. V. Zatsepina, F. Pasteau, V. Labas, M. Fromont-Racine, J. Ellenberg, and V. Doye.** 2001. An evolutionarily conserved NPC subcomplex, which redistributes in part to kinetochores in mammalian cells. J. Cell Biol. **154:**1147–1160.
5. **Bernad, R., H. van der Velde, M. Fornerod, and H. Pickersgill.** 2004. Nup358/RanBP2 attaches to the nuclear pore complex via association with Nup88 and Nup214/CAN and plays a supporting role in CRM1-mediated nuclear protein export. Mol. Cell. Biol. **24:**2373–2384.
6. **Bowman, B. R., R. L. Welschhans, H. Jayaram, N. D. Stow, V. G. Preston, and F. A. Quiocho.** 2006. Structural characterization of the UL25 DNA-packaging protein from herpes simplex virus type 1. J. Virol. **80:**2309–2317.

7. **Cardone, G., D. C. Winkler, B. L. Trus, N. Cheng, J. E. Heuser, W. W. Newcomb, J. C. Brown, and A. C. Steven.** 2007. Visualization of the herpes simplex virus portal in situ by cryo-electron tomography. Virology **361:**426–434.
8. **Chang, J. T., M. F. Schmid, F. J. Rixon, and W. Chiu.** 2007. Electron cryotomography reveals the portal in the herpesvirus capsid. J. Virol. **81:** 2065–2068.
9. **Coller, K. E., J. I. Lee, A. Ueda, and G. A. Smith.** 2007. The capsid and tegument of the alphaherpesviruses are linked by an interaction between the UL25 and VP1/2 proteins. J. Virol. **81:**11790–11797.
10. **Copeland, A. M., W. W. Newcomb, and J. C. Brown.** 2009. Herpes simplex virus replication: roles of viral proteins and nucleoporins in capsid-nucleus attachment. J. Virol. **83:**1660–1668.
11. **Cronshaw, J. M., A. N. Krutchinsky, W. Zhang, B. T. Chait, and M. J. Matunis.** 2002. Proteomic analysis of the mammalian nuclear pore complex. J. Cell Biol. **158:**915–927.
12. **Cunningham, C., and A. J. Davison.** 1993. A cosmid-based system for constructing mutants of herpes simplex virus type 1. Virology **197:**116–124.
13. **D'Angelo, M. A., and M. W. Hetzer.** 2008. Structure, dynamics and function of nuclear pore complexes. Trends Cell Biol. **18:**456–466.
14. **Davis, L. I., and G. Blobel.** 1987. Nuclear pore complex contains a family of glycoproteins that includes p62: glycosylation through a previously unidentified cellular pathway. Proc. Natl. Acad. Sci. USA **84:**7552–7556.
15. **Davison, M. J., V. G. Preston, and D. J. McGeoch.** 1984. Determination of the sequence alteration in the DNA of the herpes simplex virus type 1 temperature-sensitive mutant ts K. J. Gen. Virol. **65**(Pt. 5)**:**859–863.
16. **Desai, P. J.** 2000. A null mutation in the UL36 gene of herpes simplex virus type 1 results in accumulation of unenveloped DNA-filled capsids in the cytoplasm of infected cells. J. Virol. **74:**11608–11618.
17. **Everett, R. D., and J. Murray.** 2005. ND10 components relocate to sites associated with herpes simplex virus type 1 nucleoprotein complexes during virus infection. J. Virol. **79:**5078–5089.
18. **Everett, R. D., S. Rechter, P. Papior, N. Tavalai, T. Stamminger, and A. Orr.** 2006. PML contributes to a cellular mechanism of repression of herpes simplex virus type 1 infection that is inactivated by ICP0. J. Virol. **80:**7995–8005.
19. **Everett, R. D., G. Sourvinos, and A. Orr.** 2003. Recruitment of herpes simplex virus type 1 transcriptional regulatory protein ICP4 into foci juxtaposed to ND10 in live, infected cells. J. Virol. **77:**3680–3689.
20. **Granzow, H., B. G. Klupp, and T. C. Mettenleiter.** 2005. Entry of pseudorabies virus: an immunogold-labeling study. J. Virol. **79:**3200–3205.
21. **Greber, U. F., and A. Fassati.** 2003. Nuclear import of viral DNA genomes. Traffic **4:**136–143.
22. **Hutten, S., and R. H. Kehlenbach.** 2006. Nup214 is required for CRM1-dependent nuclear protein export in vivo. Mol. Cell. Biol. **26:**6772–6785.
23. **Jamieson, D. R., L. H. Robinson, J. I. Daksis, M. J. Nicholl, and C. M. Preston.** 1995. Quiescent viral genomes in human fibroblasts after infection with herpes simplex virus type 1 Vmw65 mutants. J. Gen. Virol. **76**(Pt. 6)**:**1417–1431.
24. **Jovasevic, V., L. Liang, and B. Roizman.** 2008. Proteolytic cleavage of VP1-2 is required for release of herpes simplex virus 1 DNA into the nucleus. J. Virol. **82:**3311–3319.
25. **Kuhn, J., T. Leege, B. G. Klupp, H. Granzow, W. Fuchs, and T. C. Mettenleiter.** 2008. Partial functional complementation of a pseudorabies virus UL25 deletion mutant by herpes simplex virus type 1 pUL25 indicates overlapping functions of alphaherpesvirus pUL25 proteins. J. Virol. **82:** 5725–5734.
26. **Lee, J. H., V. Vittone, E. Diefenbach, A. L. Cunningham, and R. J. Diefenbach.** 2008. Identification of structural protein-protein interactions of herpes simplex virus type 1. Virology **378:**347–354.
27. **Le Rouzic, E., A. Mousnier, C. Rustum, F. Stutz, E. Hallberg, C. Dargemont, and S. Benichou.** 2002. Docking of HIV-1 Vpr to the nuclear envelope is mediated by the interaction with the nucleoporin hCG1. J. Biol. Chem. **277:**45091–45098.
28. **Lim, R. Y., and B. Fahrenkrog.** 2006. The nuclear pore complex up close. Curr. Opin. Cell Biol. **18:**342–347.
29. **Lowenstein, P. R., E. E. Morrison, D. Bain, P. Hodge, C. M. Preston, P. Clissold, N. D. Stow, T. A. McKee, and M. G. Castro.** 1994. Use of recombinant vectors derived from herpes simplex virus 1 mutant tsK for short-term expression of transgenes encoding cytoplasmic and membrane anchored proteins in postmitotic polarized cortical neurons and glial cells in vitro. Neuroscience **60:**1059–1077.
30. **Luxton, G. W., S. Haverlock, K. E. Coller, S. E. Antinone, A. Pincetic, and G. A. Smith.** 2005. Targeting of herpesvirus capsid transport in axons is coupled to association with specific sets of tegument proteins. Proc. Natl. Acad. Sci. USA **102:**5832–5837.
31. **Luxton, G. W., J. I. Lee, S. Haverlock-Moyns, J. M. Schober, and G. A. Smith.** 2006. The pseudorabies virus VP1/2 tegument protein is required for intracellular capsid transport. J. Virol. **80:**201–209.
32. **Macara, I. G.** 2001. Transport into and out of the nucleus. Microbiol. Mol. Biol. Rev. **65:**570–594.
33. **McBride, K. M., G. Banninger, C. McDonald, and N. C. Reich.** 2002. Regulated nuclear import of the STAT1 transcription factor by direct binding of importin-alpha. EMBO J. **21:**1754–1763.
34. **McNab, A. R., P. Desai, S. Person, L. L. Roof, D. R. Thomsen, W. W. Newcomb, J. C. Brown, and F. L. Homa.** 1998. The product of the herpes simplex virus type 1 UL25 gene is required for encapsidation but not for cleavage of replicated viral DNA. J. Virol. **72:**1060–1070.
35. **Murray, J., C. Loney, L. B. Murphy, S. Graham, and R. P. Yeo.** 2001. Characterization of monoclonal antibodies raised against recombinant respiratory syncytial virus nucleocapsid (N) protein: identification of a region in the carboxy terminus of N involved in the interaction with P protein. Virology **289:**252–261.
36. **Newcomb, W. W., F. P. Booy, and J. C. Brown.** 2007. Uncoating the herpes simplex virus genome. J. Mol. Biol. **370:**633–642.
37. **Newcomb, W. W., F. L. Homa, and J. C. Brown.** 2006. Herpes simplex virus capsid structure: DNA packaging protein UL25 is located on the external surface of the capsid near the vertices. J. Virol. **80:**6286–6294.
38. **Newcomb, W. W., R. M. Juhas, D. R. Thomsen, F. L. Homa, A. D. Burch, S. K. Weller, and J. C. Brown.** 2001. The UL6 gene product forms the portal for entry of DNA into the herpes simplex virus capsid. J. Virol. **75:**10923–10932.
39. **Ojala, P. M., B. Sodeik, M. W. Ebersold, U. Kutay, and A. Helenius.** 2000. Herpes simplex virus type 1 entry into host cells: reconstitution of capsid binding and uncoating at the nuclear pore complex in vitro. Mol. Cell. Biol. **20:**4922–4931.
40. **Pante, N., R. Bastos, I. McMorrow, B. Burke, and U. Aebi.** 1994. Interactions and three-dimensional localization of a group of nuclear pore complex proteins. J. Cell Biol. **126:**603–617.
41. **Patel, S. S., B. J. Belmont, J. M. Sante, and M. F. Rexach.** 2007. Natively unfolded nucleoporins gate protein diffusion across the nuclear pore complex. Cell **129:**83–96.
42. **Peters, R.** 2005. Translocation through the nuclear pore complex: selectivity and speed by reduction-of-dimensionality. Traffic **6:**421–427.
43. **Preston, C. M.** 1979. Control of herpes simplex virus type 1 mRNA synthesis in cells infected with wild-type virus or the temperature-sensitive mutant *tsK*. J. Virol. **29:**275–284.
44. **Preston, V. G., J. Murray, C. M. Preston, I. M. McDougall, and N. D. Stow.** 2008. The UL25 gene product of herpes simplex virus type 1 is involved in uncoating of the viral genome. J. Virol. **82:**6654–6666.
45. **Raux, H., A. Flamand, and D. Blondel.** 2000. Interaction of the rabies virus P protein with the LC8 dynein light chain. J. Virol. **74:**10212–10216.
46. **Ribbeck, K., and D. Gorlich.** 2001. Kinetic analysis of translocation through nuclear pore complexes. EMBO J. **20:**1320–1330.
47. **Roberts, A. P., F. Abaitua, P. O'Hare, D. McNab, F. J. Rixon, and D. Pasdeloup.** 2009. Differing roles of inner tegument proteins pUL36 and pUL37 during entry of herpes simplex virus type 1. J. Virol. **83:**105–116.
48. **Roth, M. B., A. M. Zahler, and J. A. Stolk.** 1991. A conserved family of nuclear phosphoproteins localized to sites of polymerase II transcription. J. Cell Biol. **115:**587–596.
49. **Rout, M. P., J. D. Aitchison, M. O. Magnasco, and B. T. Chait.** 2003. Virtual gating and nuclear transport: the hole picture. Trends Cell Biol. **13:**622–628.
50. **Schwartz, T. U.** 2005. Modularity within the architecture of the nuclear pore complex. Curr. Opin. Struct. Biol. **15:**221–226.
51. **Shahin, V., W. Hafezi, H. Oberleithner, Y. Ludwig, B. Windoffer, H. Schillers, and J. E. Kuhn.** 2006. The genome of HSV-1 translocates through the nuclear pore as a condensed rod-like structure. J. Cell Sci. **119:**23–30.
52. **Sodeik, B., M. W. Ebersold, and A. Helenius.** 1997. Microtubule-mediated transport of incoming herpes simplex virus 1 capsids to the nucleus. J. Cell Biol. **136:**1007–1021.
53. **Stow, N. D.** 2001. Packaging of genomic and amplicon DNA by the herpes simplex virus type 1 UL25-null mutant KUL25NS. J. Virol. **75:**10755–10765.
54. **Thurlow, J. K., M. Murphy, N. D. Stow, and V. G. Preston.** 2006. Herpes simplex virus type 1 DNA-packaging protein UL17 is required for efficient binding of UL25 to capsids. J. Virol. **80:**2118–2126.
55. **Tran, E. J., and S. R. Wente.** 2006. Dynamic nuclear pore complexes: life on the edge. Cell **125:**1041–1053.
56. **Trotman, L. C., N. Mosberger, M. Fornerod, R. P. Stidwill, and U. F. Greber.** 2001. Import of adenovirus DNA involves the nuclear pore complex receptor CAN/Nup214 and histone H1. Nat. Cell Biol. **3:**1092–1100.
57. **Trus, B. L., N. Cheng, W. W. Newcomb, F. L. Homa, J. C. Brown, and A. C. Steven.** 2004. Structure and polymorphism of the UL6 portal protein of herpes simplex virus type 1. J. Virol. **78:**12668–12671.
58. **Trus, B. L., W. W. Newcomb, N. Cheng, G. Cardone, L. Marekov, F. L. Homa, J. C. Brown, and A. C. Steven.** 2007. Allosteric signaling and a nuclear exit strategy: binding of UL25/UL17 heterodimers to DNA-filled HSV-1 capsids. Mol. Cell **26:**479–489.
59. **Walther, T. C., H. S. Pickersgill, V. C. Cordes, M. W. Goldberg, T. D. Allen, I. W. Mattaj, and M. Fornerod.** 2002. The cytoplasmic filaments of the nuclear pore complex are dispensable for selective nuclear protein import. J. Cell Biol. **158:**63–77.

60. **Whittaker, G. R., M. Kann, and A. Helenius.** 2000. Viral entry into the nucleus. Annu. Rev. Cell Dev. Biol. **16:**627–651.
61. **Wilken, N., J. L. Senecal, U. Scheer, and M. C. Dabauvalle.** 1995. Localization of the Ran-GTP binding protein RanBP2 at the cytoplasmic side of the nuclear pore complex. Eur. J. Cell Biol. **68:**211–219.
62. **Wolfstein, A., C. H. Nagel, K. Radtke, K. Dohner, V. J. Allan, and B. Sodeik.** 2006. The inner tegument promotes herpes simplex virus capsid motility along microtubules in vitro. Traffic **7:**227–237.
63. **Wu, J., M. J. Matunis, D. Kraemer, G. Blobel, and E. Coutavas.** 1995. Nup358, a cytoplasmically exposed nucleoporin with peptide repeats, Ran-GTP binding sites, zinc fingers, a cyclophilin A homologous domain, and a leucine-rich region. J. Biol. Chem. **270:**14209–14213.
64. **Yokoyama, N., N. Hayashi, T. Seki, N. Pante, T. Ohba, K. Nishii, K. Kuma, T. Hayashida, T. Miyata, U. Aebi, et al.** 1995. A giant nucleopore protein that binds Ran/TC4. Nature **376:**184–188.
65. **Zhou, Z. H., D. H. Chen, J. Jakana, F. J. Rixon, and W. Chiu.** 1999. Visualization of tegument-capsid interactions and DNA in intact herpes simplex virus type 1 virions. J. Virol. **73:**3210–3218.
66. **Zhou, Z. H., M. Dougherty, J. Jakana, J. He, F. J. Rixon, and W. Chiu.** 2000. Seeing the herpesvirus capsid at 8.5 Å. Science **288:**877–880.

Publication #2

Differing roles of inner tegument proteins pUL36 and pUL37 during entry of herpes simplex virus type 1.

Roberts AP, Abaitua F, O'Hare P, McNab D, Rixon FJ, Pasdeloup D.

JOURNAL OF VIROLOGY, Jan. 2009, p. 105–116 Vol. 83, No. 1
0022-538X/09/$08.00+0 doi:10.1128/JVI.01032-08

Differing Roles of Inner Tegument Proteins pUL36 and pUL37 during Entry of Herpes Simplex Virus Type 1▽†

Ashley P. E. Roberts,[1] Fernando Abaitua,[2] Peter O'Hare,[2] David McNab,[1] Frazer J. Rixon,[1]* and David Pasdeloup[1]

MRC Virology Unit, Institute of Virology, University of Glasgow, Church Street, Glasgow G11 5JR, United Kingdom,[1] and Marie Curie Research Institute, The Chart, Oxted, Surrey RH8 0TL, United Kingdom[2]

Received 16 May 2008/Accepted 10 October 2008

Studies with herpes simplex virus type 1 (HSV-1) have shown that secondary envelopment and virus release are blocked in mutants deleted for the tegument protein gene UL36 or UL37, leading to the accumulation of DNA-containing capsids in the cytoplasm of infected cells. The failure to assemble infectious virions has meant that the roles of these genes in the initial stages of infection could not be investigated. To circumvent this, cells infected at a low multiplicity were fused to form syncytia, thereby allowing capsids released from infected nuclei access to uninfected nuclei without having to cross a plasma membrane. Visualization of virus DNA replication showed that a UL37-minus mutant was capable of transmitting infection to all the nuclei within a syncytium as efficiently as the wild-type HSV-1 strain 17^+ did, whereas infection by UL36-minus mutants failed to spread. Thus, these inner tegument proteins have differing functions, with pUL36 being essential during both the assembly and uptake stages of infection, while pUL37 is needed for the formation of virions but is not required during the initial stages of infection. Analysis of noninfectious enveloped particles (L-particles) further showed that pUL36 and pUL37 are dependent on each other for incorporation into tegument.

Herpesvirus virions have characteristic structures that combine symmetrical and nonsymmetrical components (22, 45, 58). The viral DNA genome is contained within an icosahedral capsid, a protein layer called the tegument surrounds the capsid, and the virion is bounded by a lipid envelope, which contains numerous glycoprotein spikes. Capsids are robust structures that can be readily purified from infected cells and studied in isolation from the other virion components. They are classified according to their internal composition as A-capsids (empty), B-capsids (containing scaffold), and C-capsids (containing DNA) (19, 23, 42, 50). The symmetry and uniformity of the capsid shell make it amenable to structural analysis, and its composition, structure, and morphogenesis have been studied extensively (23, 50, 59). In contrast, the bulk of the tegument appears to be highly variable, with the numbers of some component proteins differing widely among individual virus particles (7, 11). Compositionally, it is the most complex part of the virion, containing more than 15 viral gene products (23, 36, 50), many of which can be deleted without obviously affecting the virion structure. The tegument is usually described as amorphous, and its structure appears not to be correlated to that of the capsid, except at its inner boundary where a pattern of icosahedrally arranged elements interacting with capsid proteins is evident. These connections are distributed across the entire surface of the capsid in simian and human cytomegaloviruses (6, 53) but are confined to the vertices in herpes simplex virus type 1 (HSV-1) (22, 58).

Capsid assembly and DNA packaging take place in the nuclei of infected cells. The DNA-containing capsids (C-capsids) exit the nucleus by traversing the two layers of the nuclear membrane (36). They become enveloped at the inner leaflet but lose this primary envelope by fusion with the outer leaflet, which releases the capsid into the cytoplasm. Two viral gene products (genes UL31 and UL34) are required for this process (40, 44), but they do not form part of the mature virus particle (18). The US3-encoded protein kinase (pUS3), which is a constituent of tegument, is important for efficient nuclear exit (41, 56), but no tegument protein is known to be essential for capsid exit from the nucleus. The sequence and location of tegument assembly are still poorly understood. It has been reported that the HSV-1 tegument protein, pUL48 (VP16), and the HSV-1 and pseudorabies virus (PrV) pUS3 proteins are associated with primary enveloped capsids in the perinuclear space (21, 38, 41). However, the bulk of the tegument appears to be added in the cytoplasm, following which the mature virion is thought to be formed by envelopment at vesicles of the *trans*-Golgi network.

The products of HSV-1 genes UL36 and UL37 are tegument proteins which are believed to be closely associated with the capsid. The UL36 protein (pUL36) has been proposed as a possible candidate for the tegument protein attached to the vertices of capsids within virions (58), although recently it has been suggested that the proteins encoded by UL17 and UL25 form part of this material (53). There is no direct evidence for the location of the UL37 protein (pUL37) in the tegument, but it is known to interact with pUL36 (25, 37, 55) and has been described as an inner tegument protein. It is not clear where pUL36 and pUL37 become incorporated into virions, although both proteins have been reported as associating with capsids purified from the nuclei of infected cells (5). The putative interaction between pUL36 and the capsid may not entirely

* Corresponding author. Mailing address: MRC Virology Unit, Institute of Virology, University of Glasgow, Church Street, Glasgow G11 5JR, United Kingdom. Phone: 44 141 330 4025. Fax: 44 141 337 2236. E-mail: f.rixon@mrcvu.gla.ac.uk.

† Supplemental material for this article may be found at http://jvi.asm.org/.

▽ Published ahead of print on 29 October 2008.

account for its presence in the virion tegument, as it is also found in L-particles, which resemble virions in size and shape but lack capsids and therefore consist solely of enveloped tegument (52). L-particles are formed both in productive infections and in circumstances where virion assembly is blocked (43). Although pUL36 and pUL37 are components of L-particles (34, 52), studies with PrV mutants have shown that either one is dispensable for L-particle production (17, 26).

Mutational analysis has established that UL36 is essential for virus replication in both HSV-1 (3, 14) and PrV (17). However, although UL37 is essential in HSV-1 (13), deletion of this gene in PrV results in impairment but not abolition of growth (26). The phenotypes of HSV-1 mutants deleted for UL36 and UL37 are similar, and in both cases C-capsids accumulate in the cytoplasm of infected cells. This implies that the proteins are not required for capsid assembly, DNA packaging, or exit from the nucleus but are important for the further addition of tegument and envelope.

As well as being important in virus assembly and egress, UL36 plays a role during the initial phase of infection. Thus, infection of cells at nonpermissive temperatures with an HSV-1 temperature-sensitive mutant of UL36 (tsB7) prevents release of the viral DNA from capsids and causes them to accumulate in the vicinity of nuclear pores (3). No temperature-sensitive mutant has been reported for UL37, and its importance in initiation of infection is unknown. However, both pUL36 and pUL37 remain associated with capsids during transport to the nucleus (20, 29), indicating a possible role for pUL37 at this stage of infection.

In this paper we use deletion mutants with deletions of the UL36 and UL37 genes to study their roles during viral infection. Our studies confirm that neither protein is needed for formation of cytoplasmic C-capsids or for bulk tegument assembly, as evidenced by L-particle formation, making it likely that they act as the link between these two virion compartments. In addition, by examining the spread of infection within syncytia, we show that capsids lacking pUL36 are unable to transmit infection between nuclei, whereas initiating a new infectious cycle does not require pUL37.

MATERIALS AND METHODS

Cell culture. Human fetal foreskin fibroblasts ($HFFF_2$; European Collection of Cell Cultures) were grown in Dulbecco's modified Eagle medium (DMEM) supplemented with 10% fetal bovine serum (Gibco). Baby hamster kidney cells (BHK 21 clone 13; ATCC) were grown in Glasgow modified Eagle medium supplemented with 10% newborn bovine serum (Gibco) and tryptose phosphate broth. Rabbit skin (RS) cells (2) were grown in DMEM supplemented with 10% fetal bovine serum and 1% nonessential amino acids (Gibco).

Cell lines expressing HSV-1 genes. All complementing cell lines were derived from RS cells. Plasmids expressing the appropriate HSV-1 genes (see below) were mixed with pSV2Neo (Clontech) or with pC1-Neo (Promega) and cotransfected by calcium phosphate precipitation (51) into 35-mm dishes of RS cells. Transfected cells were incubated for 24 h at 37°C before subculture into 24-well plates. Cells were overlaid with medium containing 1 mg/ml G418 (Gibco). The selection medium was replaced every 3 days, until colony growth was evident. The drug-resistant colonies were then selected, expanded, and tested for their ability to support growth of the mutant viruses.

(i) UL19. UL19(1) cells were provided by V. Preston (MRC Virology Unit). Briefly, the open reading frame (ORF) of UL19 (residues 40,528 to 36,353 [32]) was isolated from pJN6 (39) as a BglII fragment and cloned into the BamHI site of pApV (27). G418-resistant cell lines produced as described above were tested for their ability to support growth of the UL19 deletion mutant K5ΔZ (12), and one line was selected for further use (V. Preston, personal communication).

(ii) UL36. The expression plasmid pApV (27) was modified using the double-stranded oligonucleotide pApVBstBI generated from the complementary sequences 5′-CTAGAACGGATCCGTCGACTTCGAAC and 5′-GATCGTTCG AAGTCGACGGATCCGTT. pApVBstBI was inserted between the unique XbaI and BamHI sites to produce pApVB. This creates a new BamHI site and introduces a BstBI site between the HSV-1 ICP6 (UL39) promoter and simian virus 40 polyadenylation sequence. The C-terminal ~8,000 nucleotides of the UL36 ORF were isolated from cosmid cos14 (9) as a BamHI fragment (see Fig. S1 in the supplemental material) and cloned into BamHI-digested pApVB to form pApVB36C. pApVB36C was digested with BstBI and religated to give plasmid pApVB36CBs, which has only 32 bp of HSV-1 sequence downstream of the UL36 ORF. The missing N-terminal region of UL36 was generated by PCR using primers UL36_HA_Nterm and UL36CTBamHIF (see Fig. S1 in the supplemental material) and cloned as an XbaI/BamHI fragment into XbaI/BamHI-digested pApVB36CBs to produce pHAUL36. This contains the full-length UL36 ORF (residues 80,540 to 71,016), fused to an influenza virus hemagglutinin (HA) epitope tag inserted at the N terminus. Cell lines generated using pHAUL36 and pSV2Neo (see above) were tested for their ability to complement the growth of the temperature-sensitive mutant tsB7 and the deletion mutant KΔUL36 (14). One line (HAUL36-1) was selected and used for all subsequent experiments.

(iii) UL37. Cell lines expressing UL37 were produced by two methods. Initially, the green fluorescent protein (GFP) vector, GFPemd (Packard), was modified to introduce SpeI sites at the N and C termini of the GFP ORF. The resulting SpeI fragment was cloned into the unique SpeI site located adjacent to the 3′ end of the UL37 ORF (see Fig. S1 in the supplemental material) in plasmid pGX336, which contains the BamHI O fragment (residues 79,441 to 86,980) cloned into pUC118. The resulting plasmid, pGX336GFP, which expresses a pUL37-GFP fusion protein was cotransfected with pSV2neo into RS cells. G418-resistant clones were screened for GFP expression following infection with wild-type (WT) HSV-1. One clone [1.40(2)] was selected and used in the production of the UL37 deletion mutant FRΔUL37 (see below). The plasmid, pGX336GFP, used to produce cell line 1.40(2) contains the UL37 ORF flanked by extensive HSV-1 sequences. To reduce the possibility that recombination with these sequences would rescue the FRΔUL37 mutation (see below), a second pUL37-expressing cell line was produced. The UL37 ORF (residues 84,171 to 80,707) was isolated from pUL373 (33) by BamHI digestion and cloned into BamHI-digested pApV to form pApV-UL373. pApV-UL373 was cotransfected into RS cells with pC1-Neo. G418-resistant clones were screened for their ability to complement the growth of FRΔUL37. One clone (80C02) was selected and used for all subsequent experiments.

Virus mutants. K5ΔZ (minus UL19) and KΔUL36 were provided by P. Desai (12, 14).

(i) UL36. Because the existing mutant, KΔUL36, contained only a partial deletion of the UL36 ORF, a second, complete deletion mutant was made using the HSV-1 bacterial artificial chromosome (BAC) pBAC SR27. In pBAC SR27 (supplied by C. Cunningham [MRC Virology Unit]), loxP recombination sites flank the bacterial maintenance sequences and a Cre recombinase gene, which are inserted between genes US1 and US2. The Cre recombinase is expressed following transfection into mammalian cells and results in the loss of the bacterial sequences (48). The UL36 ORF was removed from pBAC SR27 using a variation on the Lambda RED recombination system (Genebridges, GmbH). PCR was carried out on the supplied rpsL-neo template using primers UL36rm_loxFAS_F and UL36rm_loxFAS_R (see Fig. S1 in the supplemental material). The resulting PCR product contains the neomycin cassette flanked by nested FAS sites and sequences from upstream and downstream of the UL36 ORF. FAS sites are variant loxP sequences that will not undergo heterologous recombination with the archetypal loxP sites present in pBAC SR27 (47). The PCR fragment was recombined into pBAC SR27, and bacterial colonies were selected for neomycin resistance. The resulting BAC (pBAC SR27Δ36-1) has the UL36 ORF replaced by the neomycin cassette. Following transfection into HAUL36-1 cells, Cre recombinase is expressed, which excises both the FAS-flanked neomycin cassette and the loxP-flanked BAC maintenance sequences. Individual virus plaques were picked, and their ability to grow on HAUL36-1 and control RS cells was examined. Deletion of the UL36 ORF was confirmed by PCR and DNA sequencing, and one isolate (ARΔUL36) was selected for further use.

(ii) UL37. pGX336 was digested with ClaI and HpaI, which flank the UL37 ORF (see Fig. S1 in the supplemental material). The ClaI site was rendered blunt ended by treatment with T4 polymerase, and the plasmid was recircularized by ligation to generate pGX336-37minus. The red fluorescent protein (RFP) ORF from pDsRed-Monomer-N1 (Clontech) was isolated as an NheI/XbaI fragment and ligated into SpeI-digested pGX336-37minus to generate

pFRΔUL37. This removes the UL37 ORF apart from the three C-terminal amino acids and places the RFP ORF under the control of the UL37 promoter. pFRΔUL37 was cotransfected with HSV-1 strain 17^+ virion DNA into 1.40(2) cells (see above). Red fluorescent plaques were selected and screened for their differential ability to grow on 1.40(2) cells and parental RS cells. One isolate (FRΔUL37) was selected and grown for further use on 80C02 cells.

Rescuants. The NheI fragment (residues 68,662 to 85,304) containing the UL36 and UL37 sequences was cloned into the XbaI site of pUC19 to generate pUCNhe4. Noncomplementing RS cells transfected with pUCNhe4 were superinfected with 1 PFU of ARΔUL36 or FRΔUL37 per cell. Progeny virus was screened for the ability to grow on RS cells, and one virus from each rescue, designated ARΔUL36R and FRΔUL37R, was selected and grown for further use.

Cell fusion. $HFFF_2$ cells were seeded onto 22-mm square cover glasses in 35-mm culture dishes at 5×10^5 cells per dish and incubated at 37°C overnight. Duplicate plates of cells were infected for 1 h at 37°C with 0.01 PFU of the appropriate virus per cell. One plate from each pair was then overlaid with 2 ml of DMEM supplemented with 10% pooled human serum (Cellect). The second plate was washed twice in serum-free DMEM and then overlaid with 1 ml of 50% polyethylene glycol 1500 (PEG1500) in 75 mM HEPES (pH 8) (Roche) for 1 min at 37°C (28). The PEG solution was removed, and the cells were rinsed three times in DMEM containing 15% dimethyl sulfoxide and three times in DMEM and then overlaid with DMEM containing 10% pooled human serum. Both plates were maintained at 37°C for a further 23 h.

Preparation of fluorescent DNA probe. A pseudolibrary was produced by SacII digestion of a bacmid containing the entire HSV-1 genome and cloning 200- to 500-bp gel-purified fragments into pEGFP-C1 (Clontech). DNA from this pseudolibrary was used as a template for a PCR using Cy3-conjugated pEGFP-C1-specific primers (MWG). PCR products of suitable size (200 to 500 bp) were gel purified and used as a probe for fluorescent in situ hybridization (FISH).

FISH. Cells grown on cover glasses as described above were rinsed twice in phosphate-buffered saline (PBS) and fixed in 95% ethanol and 5% acetic acid at −20°C for 5 min. After fixation, the cells were air dried, rehydrated in PBS, and stored at 4°C until required. To carry out FISH (16), the cover glasses were incubated in hybridization buffer (50% formamide, 10% dextran sulfate, and 4× SSC [1× SSC is 0.15 M NaCl plus 0.015 M sodium citrate]) for 30 min at 37°C and then in probe solution (1 μl HSV-1 probe, 0.5 μl salmon testis DNA [10 mg/ml], 8.5 μl hybridization buffer) for 2 min at 95°C, before they were placed, cell side down, onto glass slides and incubated overnight at 37°C in a humidified hybridization chamber (Camlabs). They were washed twice at 65°C and once at room temperature with 2× SSC and overlaid with PBS before processing for immunofluorescence staining. If cytoplasmic labeling was required, they were then incubated for 30 min in PBS containing 0.5 μg/ml CellMask deep red (Invitrogen) and washed three times in PBS. All cover glasses were mounted in 2.5% 1,4-diazabicyclo[2.2.2]octane (Sigma) in Mowiol (Harco) containing 1 μg/ml 4′,6-diamidino-2-phenylindole dihydrochloride (DAPI) (Sigma). Samples were examined using a Zeiss LSM 510 meta confocal microscope.

Antibodies. The following antibodies were used: mouse monoclonal antibodies (MAbs) E12-E3 raised against the N-terminal 1 to 287 amino acids of pUL36 (1), DM165 against VP5 (31), VP16 (1-21) against pUL48 (Santa Cruz Biotechnology), MCA406 against VP22a (AbD Serotec), and DM1A against α-tubulin (Sigma); rabbit polyclonal antibody M780 against pUL37 (46); AGV031 against pUL49 (15); Alexa Fluor 488-conjugated goat anti-mouse antibody (Molecular Probes); and horseradish peroxidase-conjugated goat anti-mouse and goat anti-rabbit antibodies (Sigma).

Capsid and L-particle preparation. Ten 850-cm^2 roller bottles of BHK cells were infected at 5 PFU/cell with the appropriate virus. Three hours after infection, the cells were washed with 50 ml of PBS twice to remove unbound virus, then overlaid with 40 ml of fresh Glasgow modified Eagle medium supplemented with 10% newborn bovine serum and tryptose phosphate broth, and incubated for a further 21 h at 37°C. The culture medium was removed and retained for isolation of extracellular particles. Infected cells were removed, and nuclear and cytoplasmic fractions were separated by overlaying the monolayers with 25 ml of ice-cold PBS containing 1% IGEPAL [(octylphenoxy)polyethoxyethanol] CA-630 (Sigma) and protease inhibitors (complete, EDTA-free; Roche). Nuclei were harvested by centrifugation at 3,000 rpm for 10 min and resuspended in 30 ml of NTE buffer (0.5 M NaCl, 0.02 M Tris [ph 7.4], 0.01 M EDTA) containing 1% IGEPAL. Both the nuclear and cytoplasmic fractions were disrupted with a Branson sonifier 350 and clarified by centrifugation at 3,000 rpm for 10 min. The supernatants were transferred to fresh tubes, and the capsids were pelleted through 40% (wt/vol) sucrose cushions before being separated on 20 to 50% (wt/vol) sucrose gradients by centrifugation for 1 h at 25,000 rpm on an AH629 rotor (Sorvall).

TABLE 1. Growth of mutant viruses on complementing and noncomplementing cells

Virus	Growth of virus (titer) on:	
	Noncomplementing cells	Complementing cells
WT HSV-1	1.8×10^{10}	1.2×10^{10}
K5ΔZ	$<10^{4a}$	1.6×10^9
FRΔUL37	$<10^{4a}$	1.9×10^9
FRΔUL37R	6.2×10^{10}	9×10^{10}
KΔUL36	$<10^{4a}$	3.1×10^9
ARΔUL36	$<10^{4a}$	2.0×10^9
ARΔUL36R	2.5×10^{10}	2.4×10^{10}

[a] The input virus caused severe cytopathic effects at lower dilutions.

Extracellular particles were purified from the culture medium on 5 to 15% (wt/vol) Ficoll gradients as described previously (52).

Western blot analysis. Protein samples separated by electrophoresis on 10% sodium dodecyl sulfate (SDS)-polyacrylamide gels (SDS-polyacrylamide gel electrophoresis [SDS-PAGE]) were transferred electrophoretically to Hybond ECL membrane (Amersham). Blots were blocked for 30 min with 5% Marvel (Premium Brands) milk powder in 20 mM Tris (pH 8), 0.15 M NaCl, 1% Tween 20 (TBS-Tween) and incubated overnight at 4°C with appropriate antibodies diluted in 1% Marvel milk powder in TBS-Tween. Immunodetection was by enhanced chemiluminescence (ECL; Amersham). Before the blots were reprobed, the bound antibodies were stripped by incubating the membrane at 50°C in 62.5 mM Tris (pH 7), 2% SDS, and 100 mM β-mercaptoethanol for 30 min and washed two times in TBS-Tween.

Electron microscopy. Thirty-five-millimeter dishes of cells were fixed with 2.5% glutaraldehyde and 1% osmium tetroxide. Fixed cells were harvested and pelleted through 1% SeaPlaque agarose (Flowgen). The cell pellets were dehydrated through a graded alcohol series and embedded in Epon 812 resin. Thin sections were cut and examined in a JEOL 1200 EX II electron microscope.

RESULTS

Characterization of UL36 and UL37 mutants. The virus mutants studied in the following experiments were made using a variety of techniques, were generated from different parental strains, and include both complete (FRΔUL37 and ARΔUL36 [strain 17]) and partial (K5ΔZ and KΔUL36 [strain KOS]) gene deletions. Therefore, to compare their phenotypes, the growth characteristics and particle assembly pathways of the mutants were examined. Titration of virus stocks showed that the WT HSV-1 and the rescuants FRΔUL37R and ARΔUL36R grew equally well on complementing and noncomplementing cells and confirmed that all mutations were lethal for virus growth, with reductions in titer of $>10^5$ in each case (Table 1). Since each of the complementing cell lines was generated to contain only the relevant HSV-1 ORF, their ability to complement growth of the mutant viruses implies that no secondary mutations were contributing to the growth defects. This was confirmed by single-step growth analysis on complementing cells, which showed that all the mutant viruses exhibited similar growth patterns and grew to titers equivalent to that of wild-type HSV-1 (Fig. 1).

To determine the effects of the deletions on virus assembly, infected cells were examined by electron microscopy (Fig. 2). No enveloped virions were seen either on the cell surface or in cytoplasmic vacuoles of cells infected with any of the UL36 and UL37 mutants, while large numbers of nonenveloped C-capsids were present in the cytoplasm, confirming that these viruses are defective in envelopment and virus release. In

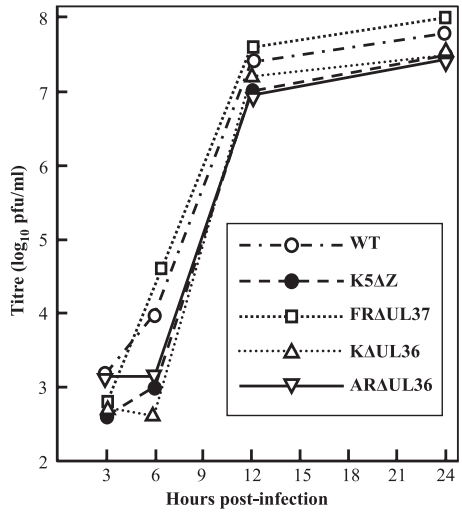

FIG. 1. Single-step virus growth. Replicate 35-mm dishes of complementing RS cells were infected with 10 PFU/cell of HSV-1 strain 17^+ (WT), K5ΔZ, FRΔUL37, KΔUL36, or ARΔUL36 mutant virus. After 1 h at 37°C, the cells were washed at low pH to remove residual input infectivity and overlaid with 2 ml of DMEM, and incubation was continued at 37°C. Wild-type HSV-1 was grown on RS cells in an identical fashion as a control. At 3, 6, 12, and 24 h after infection, the cells were harvested by scraping into the supernatant medium, and the progeny virus was titrated on complementing cells.

FRΔUL37-infected cells, the cytoplasmic C-capsids congregated in large aggregates similar to those seen with the independently derived mutant KΔUL37 (13) and their PrV counterpart, PrV-ΔUL37 (26). The tendency of these capsids to aggregate is indicative of the presence of tegument proteins, which are known to cause clumping of de-enveloped virions (35). However, they lack the densely staining tegument found associated with cytoplasmic PrV capsids when secondary envelopment was blocked by mutations in glycoproteins gE/gI and gM (4). Similar aggregations of cytoplasmic C-capsids were present in the KΔUL36-infected cells. In contrast, no aggregates were seen in ARΔUL36-infected cells with individual C-capsids being distributed throughout the cytoplasm, reproducing the pattern seen with the PrV mutant, PrV-ΔUL36F (17). The distribution of capsids in infected cells was quantified by counting the numbers present in electron microscopic images of randomly selected cell sections (Table 2). This confirmed that C-capsids accumulated in the cytoplasm of FRΔUL37-, KΔUL36-, and ARΔUL36-infected cells, with the majority of the FRΔUL37 and KΔUL36 C-capsids occurring in aggregates.

Sucrose gradient sedimentation was performed to analyze the properties of the mutant capsids. When nuclear extracts were sedimented through sucrose gradients, three bands corresponding to A-, B- and C-capsids were visible in all samples apart from K5ΔZ, which is deleted for the major capsid protein gene (12) and fails to assemble capsids (see Fig. S2A in the supplemental material). When cytoplasmic extracts from the same cells were analyzed, capsid bands were again present in KΔUL36 and ARΔUL36 gradients, but none were seen for WT HSV-1 or FRΔUL37 mutant virus (see Fig. S2B in the supplemental material). To determine the fate of the large number of cytoplasmic capsids present in FRΔUL37-infected cells, nuclear and cytoplasmic fractions from PBS-IGEPAL-treated cells were embedded, sectioned, and examined by electron microscopy (not shown). Very few capsids were found in the cytoplasmic fraction, while large numbers were present in the nuclear fraction, where the expected pattern of A-, B-, and C-capsids was observed inside nuclei. In addition, clusters of C-capsids were present outside the nuclear membrane, indicating that the large aggregations of cytoplasmic capsids seen in Fig. 2 had copelleted with the nuclei.

The differing distributions (aggregated and dispersed, respectively) of KΔUL36 and ARΔUL36 cytoplasmic C-capsids seen in Fig. 2, may reflect differences in the nature of their mutations. Thus, in ARΔUL36, the entire UL36 ORF has been deleted, whereas in KΔUL36 only the central portion has been removed (14), leaving 361 codons at the N terminus (plus a further 42 codons arising from a frameshift) that could encode a truncated form of pUL36. To determine whether this truncated form was expressed, the protein profiles of cells infected with WT HSV-1 or with FRΔUL37, KΔUL36, or ARΔUL36 mutant virus were probed with the pUL36-specific antibody, E12-E3. Western blotting confirmed that pUL36 bands of the expected sizes were present in the WT HSV-1- and FRΔUL37-infected cells, but not in the KΔUL36- or ARΔUL36-infected cells (Fig. 3A). However, the KΔUL36 sample did contain a strong band of the size expected for the residual N-terminal portion of pUL36 present in this mutant (predicted size of 43 kDa). Capsids were prepared from the cytoplasm of KΔUL36-infected cells and purified on sucrose gradients. Western blotting of gradient fractions showed that the 43-kDa protein fragment cosedimented with the capsid bands, confirming its association with KΔUL36 capsids (Fig. 3B). No signal was detected when these blots were probed with antibodies against pUL37 or the outer tegument protein, pUL48 (not shown).

Roles of UL36 and UL37 in the initial stages of virus infection. Since pUL36 and pUL37 are required for assembly of infectious virions, it is not possible to purify virions lacking these proteins in order to examine their behavior during the initial stages of infection. To overcome this limitation, we required a system in which virus could spread without needing to exit from and reenter cells. This is achieved naturally by syncytial viruses, in which the fusion of neighboring cell membranes exposes naïve cells to the contents of an infected cell's cytoplasm. To mimic this situation, we carried out studies in which cells, after infection, were induced to form syncytia by exposure to polyethylene glycol. Typical syncytia under these circumstances contained less than 20 nuclei. Therefore, infection at 0.01 PFU/cell ensured that few syncytia contained more than one initially infected cell. Following infection with the UL36 and UL37 mutants, the nuclear stages of assembly take place as normal, and capsids containing intact viral genomes are released into the cytoplasm. These progeny capsids have access to the other nuclei within the syncytium, and their ability to "infect" them can be determined by looking for replicating viral DNA.

Experiments in BHK and $HFFF_2$ cells gave similar results, and the $HFFF_2$ data are shown here as they produced more clearly delineated syncytia. To examine the spread of infection, monolayers of $HFFF_2$ cells were infected with HSV-1 strain 17^+ (WT) or with K5ΔZ, ARΔUL36, KΔUL36, or FRΔUL37

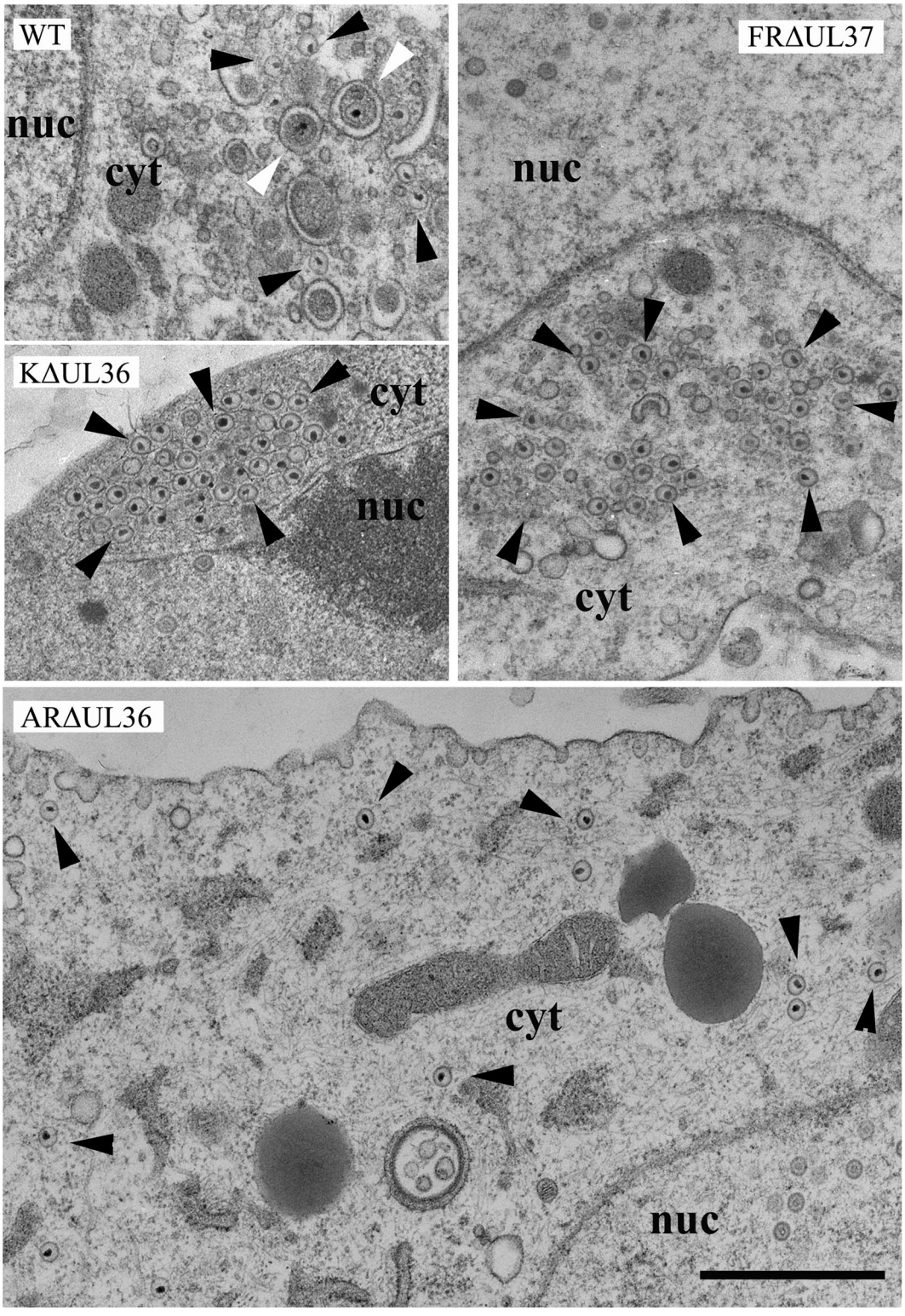

FIG. 2. Cytoplasmic capsids in infected cells. Replicate monolayers of $HFFF_2$ cells were infected with 5 PFU/cell of HSV-1 strain 17^+ (WT) or K5ΔZ, FRΔUL37, KΔUL36, or ARΔUL36 mutant virus. Cells were fixed and prepared for electron microscopy at 24 h postinfection. Both free capsids (black arrowheads) and enveloped virions (white arrowheads) were present in the cytoplasm of WT HSV-1-infected cells. In addition, large numbers of virions were present on the cell surfaces (not shown). KΔUL36 and FRΔUL37 cytoplasmic capsids accumulated in aggregates, while ARΔUL36 capsids were dispersed individually throughout the cytoplasm. No enveloped virions were seen with any of the mutant viruses. Nuclear (nuc) and cytoplasmic (cyt) compartments are labeled. Bar = 1 μm.

TABLE 2. Nuclear and cytoplasmic distribution of capsids in WT and mutant HSV-1-infected cells

Virus and capsid type	Nuclear		Cytoplasmic		
	No. of capids	% of total nuclear capsids	No. of free capids	No. of aggregated capsids	% of total DNA-containing capsids
WT HSV-1					
A	154	17	2		
B	691	76	2		
C	63	7	40		
Virions[a]			217		
FRΔUL37					
A	227	13	2	3	
B	1,380	77	4	21	
C	177	10	39	425	72
KΔUL36					
A	107	14	17	1	
B	586	77	10	2	
C	71	9	149	324	87
ARΔUL36					
A	161	19	13		
B	544	66	68		
C	123	15	276		69

[a] Includes enveloped cytoplasmic and extracellular capsids.

mutant virus (Fig. 4). WT HSV-1 was used as a positive control for spread within syncytia, and K5ΔZ was used as a negative control. After 1 h, the virus inoculum was removed, and the cells were either treated with PEG1500 (Roche) to induce fusion or left untreated. The cells were incubated for a further 23 h to allow time for infection to spread, then they were fixed, and the distribution of viral DNA was analyzed by fluorescent in situ hybridization. Infected nuclei were identified by the presence of fluorescent areas indicating replicating viral DNA. The addition of phosphonoacetic acid (an inhibitor of HSV-1 DNA polymerase) abolished labeling, confirming that the FISH probe was specifically recognizing newly synthesized virus DNA (not shown). Cells were counterstained with DAPI and CellMask deep red to highlight nuclei and cytoplasm, respectively.

Infection of unfused cells with WT virus gave rise to patches of cells with fluorescent nuclei, confirming that the virus was able to spread from an initially infected cell (Fig. 4A). As expected for a spreading infection, the pattern of labeling differed among individual cells, in some cases involving the entire nucleus and in others only localized patches. In contrast, infection of unfused cells with K5ΔZ, KΔUL36, ARΔUL36, or FRΔUL37 mutant virus resulted in only isolated fluorescing cells; the lack of spread to adjacent cells reflecting the inability of these mutants to produce infectious virus particles.

In PEG-treated cells, WT virus had also spread between nuclei, generating labeling patterns within syncytia similar to those seen in unfused cells (Fig. 4B). In contrast, the mutant viruses exhibited a range of labeling patterns. As would be predicted, in K5ΔZ-infected samples, viral DNA was confined to individual nuclei within syncytia, showing that unpackaged viral DNA could not spread between nuclei. In contrast, the FRΔUL37-infected samples contained multiple labeled nuclei. This demonstrates that formation of intact virions is not necessary for the spread of infection within syncytia but that this process can be mediated directly by cytoplasmic C-capsids. In both KΔUL36- and ARΔUL36-infected samples, replicating viral DNA was again confined to individual nuclei, indicating that not all cytoplasmic C-capsids are equally capable of transferring infection between nuclei and suggesting that, unlike pUL37, pUL36 plays an essential role in initiation of infection.

To determine the presence of cytoplasmic labeling, the experiment was repeated but without using CellMask deep red (Fig. 5). Cytoplasmic labeling clearly denoted the positions of extranuclear C-capsids or virions. Thus, fluorescent spots indicative of C-capsids were present in the cytoplasm of the WT HSV-1-, KΔUL36-, ARΔUL36-, and FRΔUL37-infected cells, but none were seen in cells infected with the major capsid protein mutant, K5ΔZ. Furthermore, the cytoplasmic fluorescence patterns confirmed the capsid distributions seen by electron microscopy. Thus, in FRΔUL37-infected cells, much of

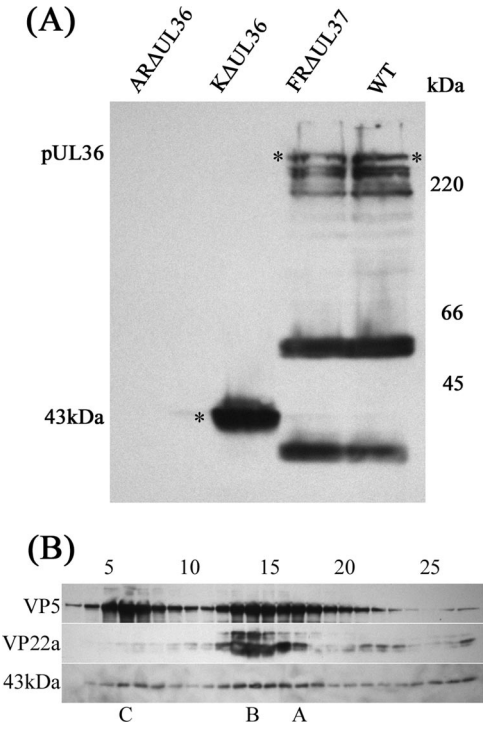

FIG. 3. KΔUL36 protein expression. (A) BHK cells were harvested 24 h after infection with 5 PFU/cell of HSV-1 strain 17^+ (WT) or FRΔUL37, KΔUL36, or ARΔUL36 mutant virus. Proteins were separated by SDS-PAGE, transferred to a nitrocellulose membrane, and probed with MAb E12-E3 directed against pUL36. The positions of full-length pUL36 and the 43-kDa N-terminal fragment (*) are indicated to the left of the gel and in the gel, and the positions of the protein size standards (in kilodaltons) are shown to the right of the gel. (B) Cytoplasmic capsids from KΔUL36-infected cells were separated by sucrose gradient sedimentation (see Fig. S2 in the supplemental material). The gradients were collected from the bottom in 30 equal fractions. Gradient fractions 3 to 27 were resolved by SDS-PAGE and analyzed by Western blotting. Blots were probed sequentially with MAb E12-E3 (anti-pUL36), DM165 (anti-VP5; to show the distribution of all capsid types), and MCA406 (anti-VP22a scaffolding protein; to show the location of B-capsids). The positions at which A-, B-, and C-capsids migrated are indicated below the blots. The positions of gradient fractions 5, 10, 15, 20, and 25 are shown above the blots.

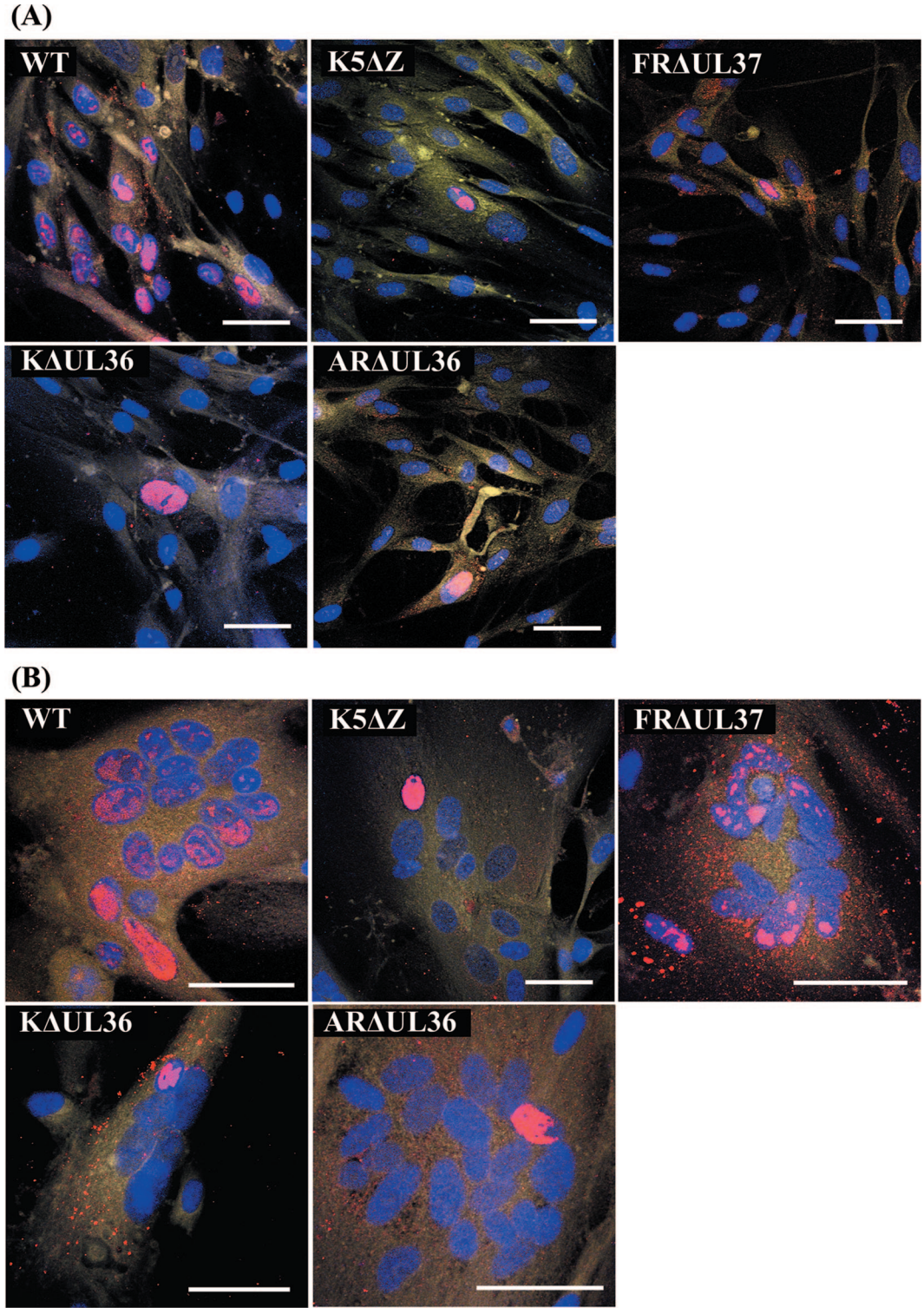

FIG. 4. Spread of virus infection. Replicate monolayers of $HFFF_2$ cells were infected with 0.01 PFU/cell of HSV-1 strain 17^+ (WT) or K5ΔZ, FRΔUL37, KΔUL36, or ARΔUL36 mutant virus. (A) Unfused cells; (B) cells after treatment with PEG and dimethyl sulfoxide at 1 h postinfection to induce syncytium formation. The cells were fixed and labeled at 24 h postinfection. Viral DNA was visualized by FISH using Cy3-labeled probe (red), nuclei were stained with DAPI (blue), and cell cytoplasm was stained with CellMask deep red (yellow). Bars, 50 μm in all panels.

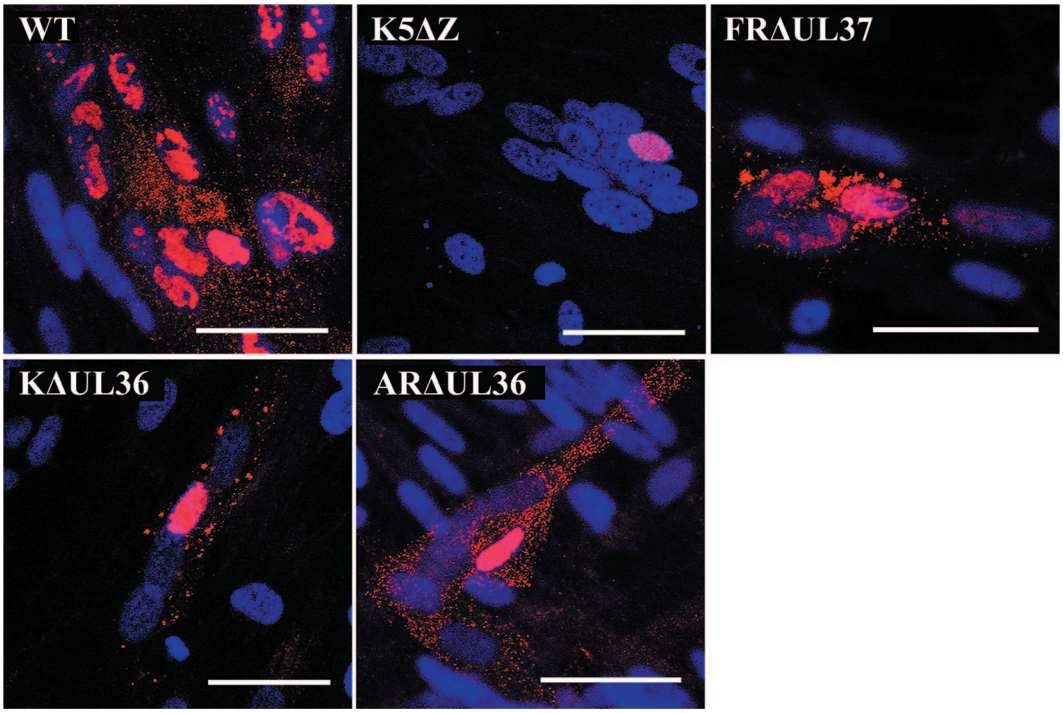

FIG. 5. Capsid distribution in infected syncytia. Replicate monolayers of $HFFF_2$ cells were infected and induced to form syncytia as described in the legend to Fig. 4. Viral DNA was visualized by FISH using Cy3-labeled probe (red), and nuclei were stained with DAPI (blue). Bars, 50 μm in all panels.

the labeling was in large irregular patches corresponding to the capsid aggregates shown in Fig. 2, although widely dispersed individual capsids were also evident. A similar pattern was seen in KΔUL36-infected cells, although the labeled patches were generally smaller than in FRΔUL37-infected cells. However, in ARΔUL36-infected cells, all cytoplasmic labeling was in uniformly distributed, discrete spots. That these patterns of cytoplasmic DNA labeling accurately reflected the distribution of cytoplasmic capsids was confirmed by immunofluorescent labeling using an antibody against the major capsid protein (see Fig. S3 in the supplemental material). The failure of KΔUL36 and ARΔUL36 to "infect" naïve nuclei within syncytia despite the evident ability of their capsids to spread throughout the cytoplasm suggests that the defect is not a result of reduced capsid mobility, while the divergent behaviors of the ΔUL36 and ΔUL37 mutants imply different roles for these two inner tegument proteins in capsid transport and DNA release during virus entry.

Role of microtubules in the spread of infection. To examine the role of microtubules in the spread of virus, cells were treated with nocodazole to depolymerize the microtubule network. Nocodazole was added 3 h after infection, and cells were incubated at 37°C for a further 21 h before being fixed and processed for FISH as before. Disruption of the microtubule network was confirmed by immunofluorescence (Fig. 6).

Nocodazole treatment had no obvious effect on the overall distribution of cytoplasmic capsids with the patterns of spread and aggregation in wild-type and mutant virus-infected syncytia resembling those seen in Fig. 4 and 5. Furthermore, nocodazole treatment of WT HSV-1-infected syncytia did not prevent the spread of infection but reduced its extent, with approximately half the number of labeled nuclei observed in nocodazole-treated syncytia (Fig. 6 and Table 3). This agrees with previous studies on unfused cells, which showed that disruption of microtubules delayed but did not prevent infection (49). A similar result was obtained with FRΔUL37, with nocodazole inhibiting but not abolishing spread within syncytia (Fig. 6 and Table 3). Unsurprisingly, nocodazole treatment had no effect on ARΔUL36 and KΔUL36 infections, which remained confined to individual nuclei (not shown). The disruption of the microtubule network did have any obvious effect on the gross distribution of capsids in infected syncytia, suggesting that extensive movement through the cytoplasm could occur by alternative mechanisms.

Incorporation of pUL36 and pUL37 into L-particles. pUL36 and pUL37 are components of virions and L-particles, and it has been shown for PrV that neither protein is required for L-particle assembly. To analyze tegument assembly in these virus mutants, particles released into infected-cell culture medium were collected and purified by Ficoll gradient sedimentation. All of the mutants gave similar sedimentation profiles with a broad light-scattering band in the position expected for L-particles and a complete absence of the prominent virion band found in WT HSV-1 (see Fig. S4 in the supplemental material). Gradient fractions were resolved by SDS-PAGE, and the distribution of virions and L-particles was determined using an antibody (AGV031) against the abundant tegument protein pUL49 (VP22; Fig. 7A). Interestingly, this appears to show that L-particles produced by the UL36 and UL37 mutants extended higher up the gradients than those of WT or K5ΔZ. The presence of pUL36 (Fig. 7B) and pUL37 (Fig. 7C) was determined by Western blotting with antibodies E12-E3

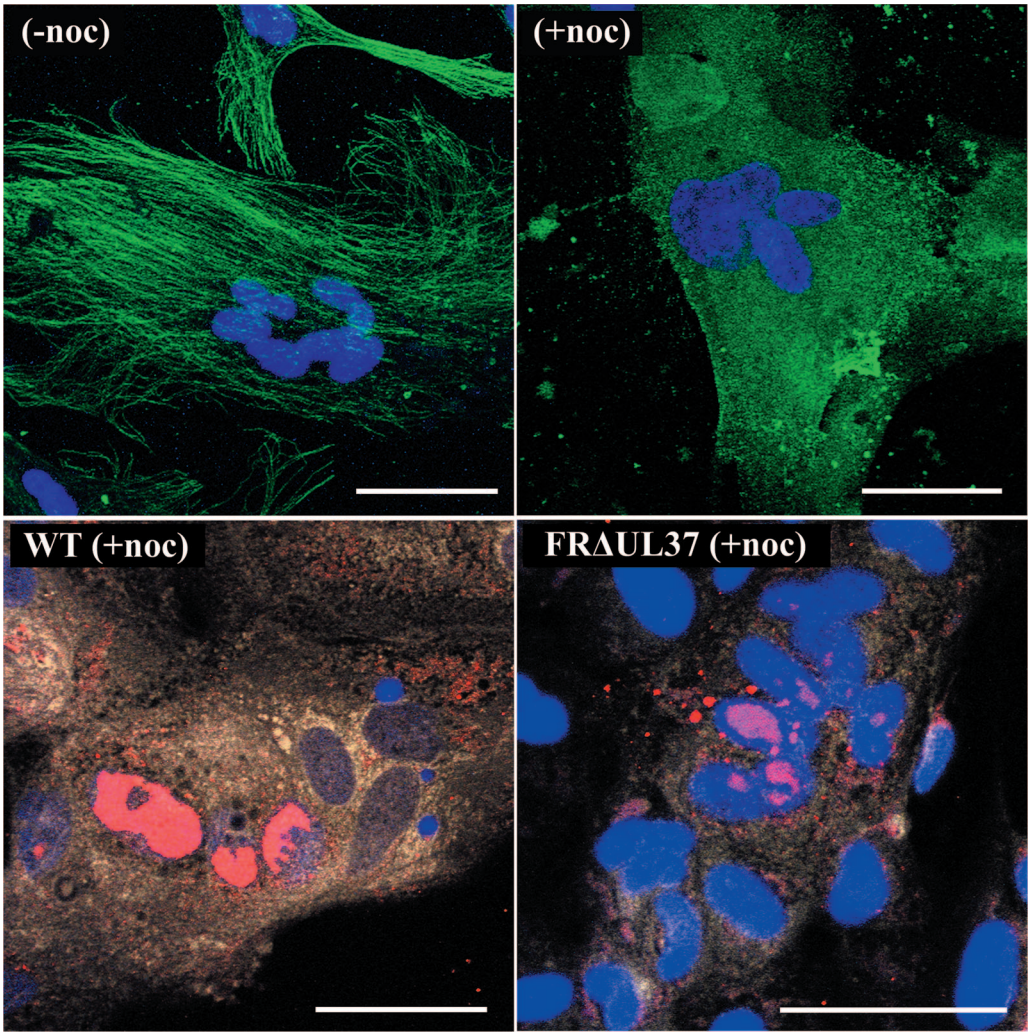

FIG. 6. Effect of nocodazole on spread of virus infection within syncytia. Replicate monolayers of $HFFF_2$ cells were infected with HSV-1 strain 17^+ (WT) or FRΔUL37 mutant virus and induced to form syncytia as described in the legend to Fig. 4. Nocodazole (0.5 μg/ml) was added at 3 h postinfection, and incubation was continued for a further 21 h. For immunofluorescence, cells were fixed (54), and microtubule proteins were identified with MAb DM1A and Alexa Fluor 488-conjugated goat anti-mouse secondary antibody (green). Viral DNA was visualized by FISH using Cy3-labeled probe (red). Nuclei were stained with DAPI (blue) The top panels show that the fibrillar microtubule network seen in uninfected syncytia [no nocodazole (−noc)] is disrupted by the addition of nocodazole (+noc). The bottom panels show the distribution of viral DNA in nocodazole-treated, WT HSV-1- and FRΔUL37-infected syncytia. Bars, 50 μm in all panels.

and M780, respectively. As expected, full-length pUL36 was detected in WT virions and L-particles and in K5ΔZ L-particles, but not in ARΔUL36 or KΔUL36 L-particles. However, the 43-kDa N-terminal fragment (Fig. 7B) of KΔUL36 had a sedimentation profile identical to that of pUL49, indicating that it had been incorporated into L-particles. Interestingly, only traces of pUL36 were detected in FRΔUL37 L-particles despite being present in normal amounts in the infected cells (Fig. 3A). Similarly, pUL37 was also present in WT HSV-1 and K5ΔZ particles and absent from FRΔUL37 L-particles (Fig. 7C). However, it was not detected in either ARΔUL36 or KΔUL36 L-particles, providing further evidence that pUL36 and pUL37 are dependent on one another for incorporation into tegument.

TABLE 3. Percentage of labeled nuclei in WT and mutant HSV-1-infected syncytia[a]

Virus	% of labeled nuclei	
	Not treated with nocodazole	Treated with nocodazole
WT HSV-1	98	46
FRΔUL37	76	32
ARΔUL36	10	13

[a] Only syncytia with at least one labeled nucleus were counted.

DISCUSSION

Previous studies to analyze the properties of HSV-1 and PrV mutants with deletions in the UL36 and UL37 genes have described the effects of the mutations on virion assembly and egress. Thus, UL36 and UL37 in HSV-1 (13, 14) and UL36 in

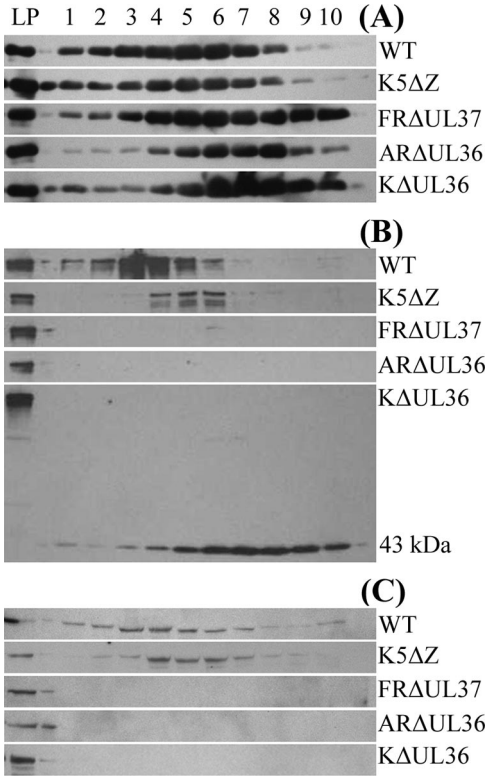

FIG. 7. Protein content of virions and L-particles. Extracellular virions and L-particles from cells infected with HSV-1 strain 17^+ (WT) and L-particles from cells infected with mutant virus K5ΔZ, FRΔUL37, KΔUL36, or ARΔUL36 were separated by Ficoll gradient sedimentation (see Fig. S4 in the supplemental material). The gradients were collected from the bottom in 10 equal fractions. A control sample of HSV-1 strain 17^+ L-particles (LP) was run on each gel. Gradient fractions were resolved by SDS-PAGE and analyzed by Western blotting. Blots were probed sequentially with E12-E3 (anti-pUL36) (B), M780 (anti-pUL37) (C), and AGV031 (anti-pUL49) (A). The position of the 43-kDa N-terminal fragment of pUL36 is indicated in panel B.

PrV (17, 30) are all essential for assembly of infectious virions, while studies in PrV showed that loss of UL37 reduced but did not abolish virus replication (26, 30). The results presented here using independently derived HSV-1 mutants support those of Desai et al. (13, 14) and confirm the phenotypic divergence between the HSV-1 and PrV UL37 mutants. A common feature of all the UL36 and UL37 deletion mutants described so far is that they produce large numbers of nonenveloped C-capsids when they infect noncomplementing cells. However, there are differing accounts of their effects on the nuclear and cytoplasmic distributions of these capsids. In UL37-minus mutants of both HSV-1 and PrV, the C-capsids form large aggregates in the cytoplasm (13, 26) (Fig. 2 and 5). Desai et al. (13) reported that their HSV-1 mutant, KΔUL37, also accumulated large numbers of capsids around the inner surface of the nuclear membrane, which they interpreted as indicating a block on nuclear exit. We did not see intranuclear accumulations with our independently derived HSV-1 mutant, FRΔUL37, although the total number of nuclear capsids was higher than found with WT HSV-1 or either UL36 mutant (Table 2). Furthermore, the ratio of A-, B-, and C-capsids in the nuclei suggested no specific accumulation of C-capsids. To quantify the effect of their mutation on capsid exit from the nucleus, Desai et al. (13) carried out gradient analysis of lysates prepared from nuclear and cytoplasmic fractions of KΔUL37-infected cells which showed that 75% of the DNA-containing capsids were associated with the nuclear fraction. This contrasted with data from our electron micrographs, which showed that the majority (72%) of the DNA-containing capsids were in the cytoplasm (Table 2). In an attempt to resolve this apparent contradiction, we repeated the separation of FRΔUL37-infected cells into nuclear and cytoplasmic fractions and analyzed their capsid content by electron microscopy. The electron microscopy images revealed that most C-capsids were indeed present in the nuclear pellet but were located outside nuclei. This suggests that the preferential association of C-capsids in the nuclear fraction is misleading and results from the large cytoplasmic capsid aggregates, which are a feature of the UL37 deletion mutants, copelleting with the nuclei. Inhibition of nuclear exit has also been reported for a UL37 mutant of PrV (30), although studies on a second PrV mutant (17, 26) produced no evidence of retention of capsids in the nucleus. The reasons for the differing behaviors of these mutations are unknown, but our studies and those of Klupp et al. (26) suggest that the major effect of deleting UL37 is to block secondary envelopment in the cytoplasm and that any role of pUL37 in nuclear exit is minor.

Differing behaviors have also been described for the UL36 mutants. Luxton et al. (30) reported that deletion of UL36 from PrV caused a dramatic reduction in capsid egress from nuclei. They suggested that the absence of such an effect in the HSV-1 mutant KΔUL36 could be due to the incomplete nature of its deletion. However, as shown here, removal of the entire UL36 ORF did not prevent efficient egress of capsids from the nucleus (Fig. 2 and 5; Table 2), nor was this effect observed with a different UL36 mutant of PrV (17). This phenotype therefore is not typical of other UL36 mutants. Another difference in the behavior of UL36 mutants is in their cytoplasmic distributions. Thus, KΔUL36 showed a tendency for capsids to accumulate in cytoplasmic clusters (14) in contrast to the PrV mutant, PrV-ΔUL36F, where capsids were dispersed evenly throughout the cytoplasm (17). However, the results described here for KΔUL36 and our independent HSV-1 mutant, ARΔUL36, show that this apparent difference does not reflect any biological distinction between HSV-1 and PrV but is most likely a consequence of the incomplete deletion in KΔUL36. Western blotting (Fig. 3) confirmed that the 43-kDa N-terminal truncation product of UL36 copurified with cytoplasmic KΔUL36 capsids, although they did not contain either pUL37 or pUL48. Therefore, it appears that this fragment is sufficient to cause their aggregation. The "stickiness" of UL36 has previously been suggested to account for the formation of large capsid aggregates by the UL37-minus mutants (17). Interestingly, the association of the 43-kDa fragment with capsids implies that capsid binding sequences map in this N-terminal region. Since a binding site for the minor capsid protein, pUL25, has recently been mapped to the C-terminal 62 residues of pUL36 (8), it appears that both N- and C-terminal regions of pUL36 interact with capsids.

Perhaps surprisingly in view of their close association with capsids, both pUL36 and pUL37 are found in L-particles, which lack capsids and consist solely of tegument and enve-

lope. It is likely that this reflects the probable function of these proteins as an interface between the capsid and outer tegument and that interaction with one or more of the outer tegument proteins accounts for their presence in L-particles. Indeed, L-particles from cells infected with a PrV, UL48-minus mutant did not contain either pUL36 or pUL37 (17). In view of this, it is interesting that pUL36 and pUL37 were dependent on one another for incorporation into L-particles (Fig. 7), suggesting that they enter L-particles as a complex. If these two proteins must form a complex before interacting with the outer tegument proteins, it would explain why tegument-like material is not detected around pUL36- or pUL37-minus cytoplasmic capsids (Fig. 2) (26). The occurrence of the 43-kDa N-terminal fragment of pUL36 in KΔUL36 L-particles is intriguing. This fragment does not include the region homologous to the pUL37 binding site in PrV (17), although it does overlap with a pUL48 interaction domain in HSV-1 (37). Its presence demonstrates that, unlike the full-length protein, this region of pUL36 can be incorporated into L-particles in the absence of pUL37.

Although the involvement of UL36 and UL37 in virus egress has been well documented, their role in virus entry is less easy to analyze. Studies with an HSV-1 temperature-sensitive mutant of UL36 (tsB7), which showed that capsids migrated to the vicinity of the nuclear pores but failed to release their DNA into the nucleus, provided the first indication that pUL36 functioned during the initial stages of infection (3). This is supported by recent work which showed that protease inhibitors prevented infection (10, 24) and linked their action to inhibition of cleavage of pUL36 on incoming capsids (24). Because UL36 deletion mutants do not form virions, they have not previously been used to study the role of pUL36 in entry. To circumvent this problem, we examined the behavior of the UL36 deletion mutants in artificially induced syncytia, since in the absence of plasma membranes separating neighboring cells, the virus capsids leaving an infected nucleus can gain direct access to uninfected nuclei without needing to undergo envelopment. Under these conditions, the environment of the capsids present in the cytoplasm of these syncytia was broadly equivalent to that of capsids from infecting virions that had undergone a normal fusion event. The failure of UL36 deletion mutants KΔUL36 and ARΔUL36 to infect new nuclei within syncytia despite having ready access to them confirms that pUL36 is involved in the initiation of infection and further strongly suggests that it must be present on the capsids. Therefore, the inhibition of infection seen with tsB7 or in the presence of protease inhibitors is not due to any failure to remove pUL36 from particles but reflects a positive requirement for pUL36 to ensure correct capsid transport and/or DNA release.

As with UL36, UL37 deletion mutants of HSV-1 fail to produce virions, and although UL37 mutants of PrV are viable, they are severely disabled, and it has not been possible to determine whether the small number of virions they produce have reduced specific infectivity (26, 30). Since no temperature-sensitive mutants in UL37 are available, essentially nothing was known of the role of this protein in virus entry. The observation that cytoplasmic capsids produced by FRΔUL37 were able to infect new nuclei clearly showed that pUL37 does not play an essential role in the initiation of infection and that its primary function is in the virion envelopment/release pathway, where it appears to act together with pUL36 as a template for assembly of outer tegument proteins.

The spread of infection within a syncytium will depend on the ability of the mutant virus particles to reach nuclear pores, to interact appropriately with them, and to release the virus genome into the nucleus. The retention of pUL36 and pUL37 on capsids during transport to the nucleus (29) would allow them to function at any or all of these stages. There is considerable evidence both from studies using an in vitro microtubule model (57) and from fluorescence microscopy of live cells (30) that the inner tegument proteins are important for capsid motility. In particular, studies of cells infected with PrV mutants showed that during virus egress pUL36 was absolutely required for processive capsid transport along microtubules, while pUL37 increased its efficiency (30). Furthermore, it was known that intact microtubules were needed to direct incoming capsids to the nuclear membrane (49), raising the possibility that failure of capsids to reach the nuclear pore could explain the block on infection by the UL36 deletion mutants. However, disrupting microtubules with nocodazole did not completely block HSV-1 infection of individual cells (49) and although the rate of spread was decreased, both WT HSV-1 and FRΔUL37 were able to infect naïve nuclei in nocodazole-treated syncytia. In addition, the widespread distribution of ARΔUL36 and KΔUL36 capsids throughout infected syncytia suggests that the uninfected nuclei were not physically inaccessible to them. Therefore, it is highly unlikely that the restriction of infection seen with the UL36 mutants is due solely to inefficient transport, and an additional role in nuclear pore recognition and/or DNA release seems probable.

In conclusion, we have shown that two inner tegument proteins that remain on capsids during the initial stages of infection have differing roles. One, pUL37, is dispensable during the initial stages of virus infection, while the second, pUL36, plays an essential, but as yet undefined, role in DNA release from the capsid and entry into the nucleus. The syncytial infection model should allow further investigation of the role of UL36 in the initial stages of infection.

ACKNOWLEDGMENTS

The HSV-1 bacterial artificial chromosome, pBAC SR27, was provided by C. Cunningham and A. J. Davison. Antibodies M780 and AGV031 were provided by F. Jenkins, (University of Pittsburgh) and G. Elliott (Imperial College), respectively. We thank M. McElwee for excellent technical support and V. Preston and D. McGeoch for critically reading the manuscript.

REFERENCES

1. **Abaitua, F., and P. O'Hare.** 2008. Identification of a highly conserved functional nuclear localization signal within the N-terminal region of herpes simplex virus type 1 VP1-2 tegument protein. J. Virol. **82:**5234–5244.
2. **Baines, J. D., and B. Roizman.** 1991. The open reading frames U_L3, U_L4, U_L10, and U_L16 are dispensable for the replication of herpes simplex virus 1 in cell culture. J. Virol. **65:**938–944.
3. **Batterson, W., D. Furlong, and B. Roizman.** 1983. Molecular genetics of herpes simplex virus. VIII. Further characterization of a temperature-sensitive mutant defective in release of viral DNA and in other stages of the viral reproductive cycle. J. Virol. **45:**397–407.
4. **Brack, A. R., J. M. Dijkstra, H. Granzow, B. G. Klupp, and T. C. Mettenleiter.** 1999. Inhibition of virion maturation by simultaneous deletion of glycoproteins E, I, and M of pseudorabies virus. J. Virol. **73:**5364–5372.
5. **Bucks, M. A., K. J. O'Regan, M. A. Murphy, J. W. Wills, and R. J. Courtney.** 2007. Herpes simplex virus type 1 tegument proteins VP1/2 and UL37 are associated with intranuclear capsids. Virology **361:**316–324.
6. **Chen, D. H., H. Jiang, M. Lee, F. Y. Liu, and Z. H. Zhou.** 1999. Three-

dimensional visualization of tegument/capsid interactions in the intact human cytomegalovirus. Virology **260:**10–16.
7. **Clarke, R. W., N. Monnier, H. T. Li, D. J. Zhou, H. Browne, and D. Klenerman.** 2007. Two-color fluorescence analysis of individual virions determines the distribution of the copy number of proteins in herpes simplex virus particles. Biophys. J. **93:**1329–1337.
8. **Coller, K. E., J. I.-H. Lee, A. Ueda, and G. A. Smith.** 2007. The capsid and tegument of the alphaherpesviruses are linked by an interaction between the UL25 and VP1/2 proteins. J. Virol. **81:**11790–11797.
9. **Cunningham, C., and A. J. Davison.** 1993. A cosmid-based system for constructing mutants of herpes simplex virus type 1. Virology **197:**116–124.
10. **Delboy, M. G., D. G. Roller, and A. V. Nicola.** 2008. Cellular proteasome activity facilitates herpes simplex virus entry at a postpenetration step. J. Virol. **82:**3381–3390.
11. **del Rio, T., T. H. Ch'ng, E. A. Flood, S. P. Gross, and L. W. Enquist.** 2005. Heterogeneity of a fluorescent tegument component in single pseudorabies virus virions and enveloped axonal assemblies. J. Virol. **79:**3903–3919.
12. **Desai, P., N. A. Deluca, J. C. Glorioso, and S. Person.** 1993. Mutations in herpes simplex virus type 1 genes encoding VP5 and VP23 abrogate capsid formation and cleavage of replicated DNA. J. Virol. **67:**1357–1364.
13. **Desai, P., G. L. Sexton, J. M. McCaffery, and S. Person.** 2001. A null mutation in the gene encoding the herpes simplex virus type 1 UL37 polypeptide abrogates virus maturation. J. Virol. **75:**10259–10271.
14. **Desai, P. J.** 2000. A null mutation in the UL36 gene of herpes simplex virus type 1 results in accumulation of unenveloped DNA-filled capsids in the cytoplasm of infected cells. J. Virol. **74:**11608–11618.
15. **Elliott, G., D. O'Reilly, and P. O'Hare.** 1996. Phosphorylation of the herpes simplex virus type-I tegument protein VP22. Virology **226:**140–145.
16. **Everett, R. D., J. Murray, A. Orr, and C. M. Preston.** 2007. Herpes simplex virus type 1 genomes are associated with ND10 nuclear substructures in quiescently infected human fibroblasts. J. Virol. **81:**10991–11004.
17. **Fuchs, W., B. G. Klupp, H. Granzow, and T. C. Mettenleiter.** 2004. Essential function of the pseudorabies virus UL36 gene product is independent of its interaction with the UL37 protein. J. Virol. **78:**11879–11889.
18. **Fuchs, W., B. G. Klupp, H. Granzow, N. Osterrieder, and T. C. Mettenleiter.** 2002. The interacting UL31 and UL34 gene products of pseudorabies virus are involved in egress from the host-cell nucleus and represent components of primary enveloped but not mature virions. J. Virol. **76:**364–378.
19. **Gibson, W., and B. Roizman.** 1972. Proteins specified by herpes simplex virus. VIII. Characterization and composition of multiple capsid forms of subtypes 1 and 2. J. Virol. **10:**1044–1052.
20. **Granzow, H., B. G. Klupp, and T. C. Mettenleiter.** 2005. Entry of pseudorabies virus: an immunogold-labeling study. J. Virol. **79:**3200–3205.
21. **Granzow, H., B. G. Klupp, and T. C. Mettenleiter.** 2004. The pseudorabies virus US3 protein is a component of primary and of mature virions. J. Virol. **78:**1314–1323.
22. **Grunewald, K., P. Desai, D. C. Winkler, J. B. Heymann, D. M. Belnap, W. Baumeister, and A. C. Steven.** 2003. Three-dimensional structure of herpes simplex virus from cryo-electron tomography. Science **302:**1396–1398.
23. **Homa, F. L., and J. C. Brown.** 1997. Capsid assembly and DNA packaging in herpes simplex virus. Rev. Med. Virol. **7:**107–122.
24. **Jovasevic, V., L. Liang, and B. Roizman.** 2008. Proteolytic cleavage of VP1-2 is required for release of herpes simplex virus 1 DNA into the nucleus. J. Virol. **82:**3311–3319.
25. **Klupp, B. G., W. Fuchs, H. Granzow, R. Nixdorf, and T. C. Mettenleiter.** 2002. Pseudorabies virus UL36 tegument protein physically interacts with the UL37 protein. J. Virol. **76:**3065–3071.
26. **Klupp, B. G., H. Granzow, E. Mundt, and T. C. Mettenleiter.** 2001. Pseudorabies virus UL37 gene product is involved in secondary envelopment. J. Virol. **75:**8927–8936.
27. **Lamberti, C., and S. K. Weller.** 1998. The herpes simplex virus type 1 cleavage/packaging protein, UL32, is involved in efficient localization of capsids to replication compartments. J. Virol. **72:**2463–2473.
28. **Lewis, L., and G. Albrechtbuehler.** 1987. Distribution of multiple centrospheres determines migration of BHK syncytia. Cell Motil. Cytoskelet. **7:**282–290.
29. **Luxton, G. W. G., S. Haverlock, K. E. Coller, S. E. Antinone, A. Pincetic, and G. A. Smith.** 2005. Targeting of herpesvirus capsid transport in axons is coupled to association with specific sets of tegument proteins. Proc. Natl. Acad. Sci. USA **102:**5832–5837.
30. **Luxton, G. W. G., J. I. H. Lee, S. Haverlock-Moyns, J. M. Schober, and G. A. Smith.** 2006. The pseudorabies virus VP1/2 tegument protein is required for intracellular capsid transport. J. Virol. **80:**201–209.
31. **McClelland, D. A., J. D. Aitken, D. Bhella, D. McNab, J. Mitchell, S. M. Kelly, N. C. Price, and F. J. Rixon.** 2002. pH reduction as a trigger for dissociation of herpes simplex virus type 1 scaffolds. J. Virol. **76:**7407–7417.
32. **McGeoch, D. J., M. A. Dalrymple, A. J. Davison, A. Dolan, M. C. Frame, D. McNab, L. J. Perry, J. E. Scott, and P. Taylor.** 1988. The complete DNA sequence of the long unique region in the genome of herpes simplex virus type 1. J. Gen. Virol. **69:**1531–1574.
33. **McLauchlan, J.** 1997. The abundance of the herpes simplex virus type 1 UL37 tegument protein in virus particles is closely controlled. J. Gen. Virol. **78:**189–194.
34. **McLauchlan, J., K. Liefkens, and N. D. Stow.** 1994. The herpes simplex virus type 1 UL37 gene-product is a component of virus particles. J. Gen. Virol. **75:**2047–2052.
35. **McLauchlan, J., and F. J. Rixon.** 1992. Characterization of enveloped tegument structures (L-particles) produced by alphaherpesviruses: integrity of the tegument does not depend on the presence of capsid or envelope. J. Gen. Virol. **73:**269–276.
36. **Mettenleiter, T. C.** 2002. Herpesvirus assembly and egress. J. Virol. **76:**1537–1547.
37. **Mijatov, B., A. L. Cunningham, and R. J. Diefenbach.** 2007. Residues F593 and E596 of HSV-1 tegument protein pUL36 (VP1/2) mediate binding of tegument protein pUL37. Virology **368:**26–31.
38. **Naldinho-Souto, R., H. Browne, and T. Minson.** 2006. Herpes simplex virus tegument protein VP16 is a component of primary enveloped virions. J. Virol. **80:**2582–2584.
39. **Nicholson, P., C. Addison, A. M. Cross, J. Kennard, V. G. Preston, and F. J. Rixon.** 1994. Localization of the herpes simplex virus type 1 major capsid protein VP5 to the cell nucleus requires the abundant scaffolding protein VP22a. J. Gen. Virol. **75:**1091–1099.
40. **Reynolds, A. E., B. J. Ryckman, J. D. Baines, Y. P. Zhou, L. Liang, and R. J. Roller.** 2001. U_L31 and U_L34 proteins of herpes simplex virus type 1 form a complex that accumulates at the nuclear rim and is required for envelopment of nucleocapsids. J. Virol. **75:**8803–8817.
41. **Reynolds, A. E., E. G. Wills, R. J. Roller, B. J. Ryckman, and J. D. Baines.** 2002. Ultrastructural localization of the herpes simplex virus type 1 UL31, UL34, and US3 proteins suggests specific roles in primary envelopment and egress of nucleocapsids. J. Virol. **76:**8939–8952.
42. **Rixon, F. J.** 1993. Structure and assembly of herpesviruses. Semin. Virol. **4:**135–144.
43. **Rixon, F. J., C. Addison, and J. McLauchlan.** 1992. Assembly of enveloped tegument structures (L-particles) can occur independently of virion maturation in herpes-simplex virus type 1-infected cells. J. Gen. Virol. **73:**277–284.
44. **Roller, R. J., Y. P. Zhou, R. Schnetzer, J. Ferguson, and D. DeSalvo.** 2000. Herpes simplex virus type 1 U_L34 gene product is required for viral envelopment. J. Virol. **74:**117–129.
45. **Schrag, J. D., B. V. V. Prasad, F. J. Rixon, and W. Chiu.** 1989. Three-dimensional structure of the HSV-1 nucleocapsid. Cell **56:**651–660.
46. **Shelton, L. S., A. G. Albright, W. T. Ruyechan, and F. J. Jenkins.** 1994. Retention of the herpes simplex virus type 1 (HSV-1) UL37 protein on single-stranded DNA columns requires the HSV-1 ICP8 protein. J. Virol. **68:**521–525.
47. **Siegel, R. W., R. Jain, and A. Bradbury.** 2001. Using an in vivo phagemid system to identify non-compatible loxP sequences. FEBS Lett. **499:**147–153.
48. **Smith, G. A., and L. W. Enquist.** 2000. A self-recombining bacterial artificial chromosome and its application for analysis of herpesvirus pathogenesis. Proc. Natl. Acad. Sci. USA **97:**4873–4878.
49. **Sodeik, B., M. W. Ebersold, and A. Helenius.** 1997. Microtubule-mediated transport of incoming herpes simplex virus 1 capsids to the nucleus. J. Cell Biol. **136:**1007–1021.
50. **Steven, A. C., and P. G. Spear.** 1997. Herpesvirus capsid assembly and envelopment, p. 312–351. *In* W. Chiu, R. M. Burnett, and R. Garcea (ed.), Structural biology of viruses. Oxford University Press, Oxford, United Kingdom.
51. **Stow, N. D., and N. M. Wilkie.** 1976. An improved technique for obtaining enhanced infectivity with herpes simplex virus type 1 DNA. J. Gen. Virol. **33:**447–458.
52. **Szilagyi, J. F., and C. Cunningham.** 1991. Identification and characterization of a novel non-infectious herpes simplex virus-related particle. J. Gen. Virol. **72:**661–668.
53. **Trus, B. L., W. W. Newcomb, N. Q. Cheng, G. Cardone, L. Marekov, F. L. Horna, J. C. Brown, and A. C. Steven.** 2007. Allosteric signaling and a nuclear exit strategy: binding of UL25/UL17 heterodimers to DNA-filled HSV-1 capsids. Mol. Cell **26:**479–489.
54. **Vielkind, U., and S. H. Swierenga.** 1989. A simple fixation procedure for immunofluorescent detection of different cytoskeletal components within the same cell. Histochemistry **91:**81–88.
55. **Vittone, V., E. Diefenbach, D. Triffett, M. W. Douglas, A. L. Cunningham, and R. J. Diefenbach.** 2005. Determination of interactions between tegument proteins of herpes simplex virus type 1. J. Virol. **79:**9566–9571.
56. **Wagenaar, F., J. M. A. Pol, B. Peeters, A. L. J. Gielkens, N. Dewind, and T. G. Kimman.** 1995. The US3-encoded protein kinase from pseudorabies virus affects egress of virions from the nucleus. J. Gen. Virol. **76:**1851–1859.
57. **Wolfstein, A., C. H. Nagel, K. Radtke, K. Dohner, V. J. Allan, and B. Sodeik.** 2006. The inner tegument promotes herpes simplex virus capsid motility along microtubules in vitro. Traffic **7:**227–237.
58. **Zhou, Z. H., D. H. Chen, J. Jakana, F. J. Rixon, and W. Chiu.** 1999. Visualization of tegument-capsid interactions and DNA in intact herpes simplex virus type 1 virions. J. Virol. **73:**3210–3218.
59. **Zhou, Z. H., M. Dougherty, J. Jakana, J. He, F. J. Rixon, and W. Chiu.** 2000. Seeing the herpesvirus capsid at 8.5 Å. Science **288:**877–880.

Publication #3

Inner tegument protein pUL37 of herpes simplex virus type 1 is involved in directing capsids to the trans-Golgi network for envelopment.

Pasdeloup D, Beilstein F, Roberts AP, McElwee M, McNab D, Rixon FJ.

Journal of General Virology (2010), **91**, 2145–2151 DOI 10.1099/vir.0.022053-0

Short Communication

Inner tegument protein pUL37 of herpes simplex virus type 1 is involved in directing capsids to the *trans*-Golgi network for envelopment

David Pasdeloup,† Frauke Beilstein,‡ Ashley P. E. Roberts,§ Marion McElwee, David McNab and Frazer J. Rixon

MRC Virology Unit, Institute of Virology, University of Glasgow, Church Street, Glasgow G11 5JR, UK

Correspondence
David Pasdeloup
pasdeloup@vms.cnrs-gif.fr

Received 16 March 2010
Accepted 25 May 2010

Secondary envelopment of herpes simplex virus type 1 has been demonstrated as taking place at the *trans*-Golgi network (TGN). The inner tegument proteins pUL36 and pUL37 and the envelope glycoproteins gD and gE are known to be important for secondary envelopment. We compared the cellular localizations of capsids from a virus mutant lacking the UL37 gene with those of a virus mutant lacking the genes encoding gD and gE. Although wild-type capsids accumulated at the TGN, capsids of the pUL37^{-} mutant were distributed throughout the cytoplasm and showed no association with TGN-derived vesicles. This was in contrast to capsids from a gD^{-}gE^{-} mutant, which accumulated in the vicinity of TGN vesicles, but did not colocalize with them, suggesting that they were transported to the TGN but were unable to undergo envelopment. We conclude that the inner tegument protein pUL37 is required for directing capsids to the TGN, where secondary envelopment occurs.

Morphogenesis of the herpesvirus particle begins when the capsid is formed in the nucleus of an infected cell (Homa & Brown, 1997). The capsid exits the nucleus by budding at the inner nuclear membrane, thus gaining a primary envelope, which then fuses with the outer nuclear membrane, releasing the capsid into the cytosol (Mettenleiter *et al.*, 2006). How the capsid then acquires the bulk of the tegument and undergoes secondary envelopment is not clear. The *trans*-Golgi network (TGN) appears to be an important site of envelopment where glycoproteins and tegument proteins accumulate (Sugimoto *et al.*, 2008; Turcotte *et al.*, 2005). The fact that TGN targeting of these proteins can occur independently of the presence of capsids has been shown directly for several glycoproteins (Turcotte *et al.*, 2005) and is supported by the observation that L-particles, consisting of enveloped tegument, are formed under conditions where capsid formation is blocked (Rixon *et al.*, 1992; Roberts *et al.*, 2009). A number of viral proteins have been implicated in the secondary envelopment process of herpes simplex virus type 1 (HSV-1) or pseudorabies virus, including the glycoproteins gD, gE, gI and gM (Brack *et al.*, 1999; Farnsworth *et al.*, 2003), the envelope protein pUL20 (Baines *et al.*, 1991; Foster *et al.*, 2004) and the tegument proteins pUL48 (Mossman *et al.*, 2000), pUL11 (Baines & Roizman, 1992; Leege *et al.*, 2009), pUL36 and pUL37 (Desai, 2000; Desai *et al.*, 2001; Roberts *et al.*, 2009). The inner tegument proteins pUL36 and pUL37 interact with each other and the interaction is conserved across members of the family *Herpesviridae* (Bechtel & Shenk, 2002; Klupp *et al.*, 2002; Mijatov *et al.*, 2007; Rozen *et al.*, 2008; Uetz *et al.*, 2006; Vittone *et al.*, 2005). Both proteins are components of both infectious virions and L-particles (McLauchlan *et al.*, 1994; Szilagyi & Cunningham, 1991). Their presence in L-particles implies that their interaction with outer tegument proteins does not depend on the presence of capsids. This was confirmed by recent studies showing that pUL37 associates with the TGN of infected cells and that this localization depends on the presence of pUL36, but not of capsids (Desai *et al.*, 2008). Furthermore, studies with deletion mutants have shown that pUL36 and pUL37 are mutually co-dependent for incorporation into L-particles, suggesting that they normally occur as a complex (Roberts *et al.*, 2009). pUL36 has been reported to interact with the outer tegument protein pUL48 (Vittone *et al.*, 2005) and to be important for its incorporation in virions (Ko *et al.*, 2009). pUL48, in turn, binds to several other tegument proteins and glycoproteins, including pUL46, pUL49 and gH (Elliott *et al.*, 1995; Gross *et al.*, 2003; Lee *et al.*, 2008;

†Present address: Laboratoire de Virologie Moléculaire et Structurale, CNRS, Avenue de la Terrasse, 91198 Gif-sur-Yvette, France.

‡Present address: Centre de Recherches Biomédicales des Cordeliers, 15 rue de l'Ecole de Médecine, 75270 Paris cedex 06, France.

§Present address: Centre for Biomolecular Sciences, School of Pharmacy, University of Nottingham, University Park, Nottingham NG7 2RD, UK.

Supplementary methods and references and three supplementary figures are available with the online version of this paper.

Vittone *et al.*, 2005). pUL36 has also been shown to interact with the minor capsid protein pUL25 (Coller *et al.*, 2007; Pasdeloup *et al.*, 2009), and pUL37 has been reported to interact with pUL46 in a yeast two-hybrid assay (Lee *et al.*, 2008). Both pUL36 and pUL37 have essential roles in virion assembly, and virus mutants deleted for either gene accumulate large numbers of unenveloped capsids in the cytoplasm of infected cells (Desai, 2000; Desai *et al.*, 2001; Fuchs *et al.*, 2004; Klupp *et al.*, 2001; Roberts *et al.*, 2009).

Taken together, these observations identify pUL36 and pUL37 as likely candidates to act as a bridge between the capsid and the outer tegument and envelope compartments during virion assembly. Therefore, we compared the behaviour of a UL37-null mutant with that of a gD-/gE-null virus to examine the role of these proteins in targeting capsids to the TGN.

As we wished to observe the behaviour of intracellular capsids and to avoid the poor antibody labelling typically seen with wild-type (WT) HSV-1 capsids, we generated a number of viruses encoding a fluorescently tagged capsid protein. In vVP26GFP, the green fluorescent protein (GFP) fused to the N terminus of the small capsid protein VP26 (Desai & Person, 1998) was recombined into the WT HSV-1 (strain 17+) genome. vVP26GFP was then used to generate the UL37$^-$ virus vFRΔ37-VP26GFP by co-infecting the pUL37-expressing cell line 80C02 with FRΔUL37 (Roberts *et al.*, 2009) and vVP26GFP and selecting plaques exhibiting both GFP fluorescence and a defect in growth on non-complementing rabbit skin (RS) cells.

To screen vFRΔ37-VP26GFP for fusion of GFP to VP26 and for the absence of pUL37, RS cells were infected for 24 h with WT HSV-1, vVP26GFP or vFRΔ37-VP26GFP. The cells were then harvested and analysed by Western blot analysis using GFP-, VP26- and UL37-specific antibodies [see Supplementary Methods (available in JGV Online) for antibody details]. Fig. 1(a) shows that pUL37 is present in WT HSV-1-infected and vVP26GFP-infected cells (lanes 4 and 3, respectively), but is missing from vFRΔ37-VP26GFP-infected cells (lane 2). The VP26-specific antibody recognizes a band of 14 kDa in WT HSV-1-infected cells (lane 4, right), but this band is missing in vFRΔ37-VP26GFP-infected and vVP26GFP-infected cells (lanes 2 and 3, right), where a band of approximately 40–45 kDa is recognized by both VP26- and GFP-specific antibodies. This band is of the approximate size expected for the GFP–VP26 fusion protein (39 kDa).

To compare the growth characteristics of vFRΔ37-VP26GFP, vVP26GFP and WT HSV-1, virus stocks were titrated on complementing and non-complementing cells. This confirmed that the Δ37 mutation was lethal for virus growth, with a reduction in titre of $>10^5$ (Fig. 1c). Single-step growth-curve analysis on the complementing cell line showed that vFRΔ37-VP26GFP grew with similar kinetics to WT HSV-1 and vVP26GFP, but reached a slightly lower titre (around 7 % lower) after 24 h (see Supplementary Fig. S1, available in JGV Online).

The combined absence of glycoproteins gD and gE prevents virus budding and results in accumulation of tegumented, unenveloped capsids in the cytoplasm (Farnsworth *et al.*, 2003). In order to compare this well-characterized phenotype with that observed with vFRΔ37-VP26GFP, we used vgD-gE-VP26RFP, which contains both a red fluorescent protein (RFP)-tagged VP26 and a gD–gE deletion. The vgD-gE-VP26RFP virus was obtained by co-infecting the gD-expressing cell line VD60 with vUL35RFP1D1, a virus containing an RFP-tagged VP26, and the gD$^-$, gE$^-$ virus vRR1097-gEβ (Farnsworth *et al.*, 2003) (see Supplementary Methods for details of virus constructions).

We first characterized these viruses with regard to their growth defect. Titration of virus stocks on complementing (VD60) and non-complementing (Vero) cells confirmed that the deletion of the US6 open reading frame encoding gD was lethal for virus growth, with a reduction in titre of $\geqslant 10^5$ for vgD-gE-VP26RFP (Fig. 1c). The higher background level of vgD-VP26RFP seen on the non-complementing cell line was a result of recombination between the mutant genome and the extensive virus sequences used to make the complementing cell line (Ligas & Johnson, 1988). The protein-expression phenotypes of the virus mutants were examined by infecting non-complementing Vero cells with 5 p.f.u. of WT HSV-1, vRR1097-gEβ, vUL35RFP1D1, vgD-VP26RFP or vgD-gE-VP26RFP per cell and by analysing cell lysates by Western blotting using antibodies against VP26, gD and gE (Fig. 1b). Glycoproteins gD and gE were detected as a pattern of bands, reflecting different states of glycosylation and maturation of the proteins (Cohen *et al.*, 1978). These bands were present in WT HSV-1- and vUL35RFP1D1-infected cells (lanes 1 and 3) and absent from vRR1097-gEβ- and vgD-gE-VP26RFP-infected cells (lanes 2 and 5). As expected, the vgD-VP26RFP-infected cell lysate showed the presence of gE and the absence of gD (lane 4). The fusion of RFP to VP26 was confirmed by the shift in molecular mass of VP26 from approximately 14 kDa in WT HSV-1- and vRR1097-gEβ-infected cells (lanes 1 and 2) to approximately 40 kDa in vUL35RFP1D1-, vgD-VP26RFP- and vgD-gE-VP26RFP-infected cells (lanes 3–5). This experiment confirmed the absence of gD and gE and the fusion of RFP to VP26 in the newly engineered vgD-gE-VP26RFP virus.

To examine the effect of the UL37 and gD–gE mutations on capsid association with the TGN, $HFFF_2$ (human fetal foreskin fibroblasts; European Collection of Cell Cultures) and HeLa cells were infected for 15, 18 or 24 h with 5 p.f.u. of vVP26GFP, vFRΔ37-VP26GFP, vUL35RFP1D1 or vgD-gE-VP26RFP per cell, and stained for the TGN using the anti-TGN46 antibody (Fig. 2) or for the Golgi with the anti-giantin antibody (see Supplementary Fig. S2, available in JGV Online). Similar results were observed at all times post-infection and only the 15 h images are shown. The TGN is disrupted into small vesicles upon infection by HSV-1, as described previously (Campadelli *et al.*, 1993). In all cases, the patterns of association between capsids and TGN vesicles

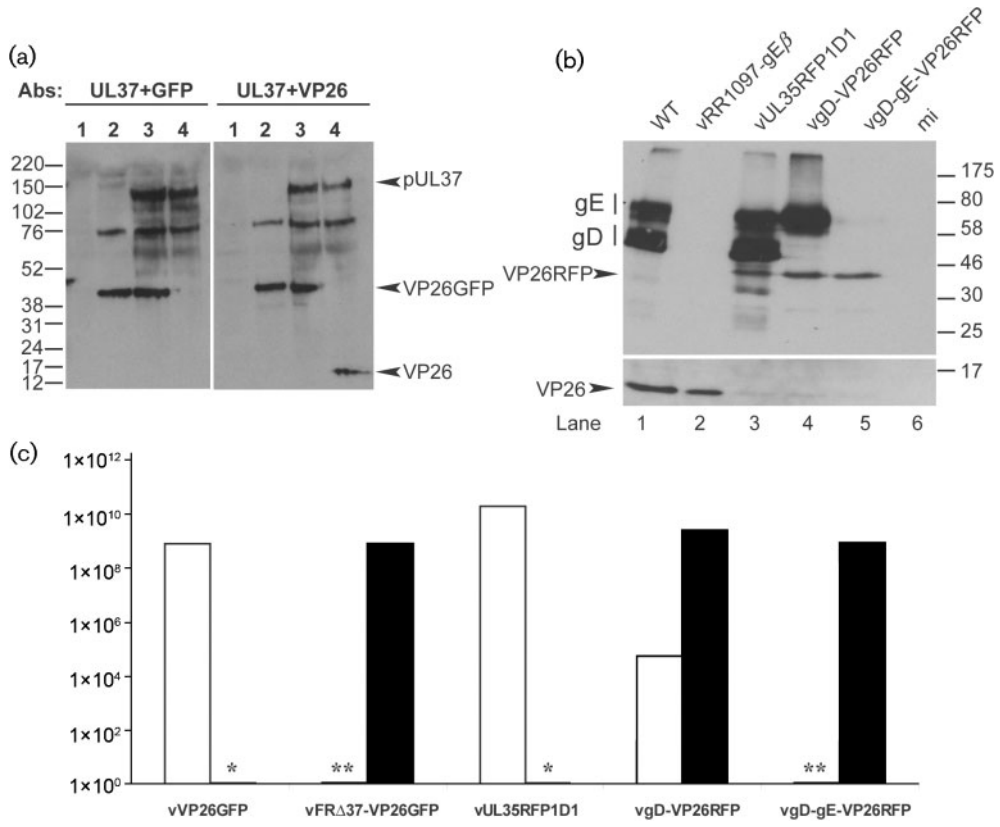

Fig. 1. Characterization of the vFRΔ37-VP26GFP and vgD-gE-VP26RFP viruses. (a) RS cells were mock-infected (lane 1) or infected with 5 p.f.u. of vFRΔ37-VP26GFP (lane 2), vVP26GFP (lane 3) or WT HSV-1 (lane 4) per cell and harvested after 24 h. Proteins were analysed by Western blotting using the pUL37 antibody, together with either the GFP-specific antibody (left panel) or the VP26-specific antibody (right panel). Note that a viral protein migrating at approximately 75 kDa is recognized non-specifically by the pUL37 antibody. Molecular mass markers (in kDa) are indicated to the left of the figure. (b) Vero cells were infected with 5 p.f.u. of WT HSV-1 (lane 1), vRR1097-gEβ (lane 2), vUL35RFP1D1 (lane 3), vgD-VP26RFP (lane 4) or vgD-gE-VP26RFP (lane 5) per cell or were mock-infected (lane 6), and harvested after 24 h. Proteins were analysed by Western blotting using a gD antibody, a gE antibody and a VP26-specific antibody. Molecular mass markers (in kDa) are indicated to the right of the figure. (c) Growth of viruses on complementing (filled bars) and non-complementing (empty bars) cell lines. Concentrated stocks of virus were titrated on RS cells (vVP26GFP), Vero cells (vUL35RFP1D1, vgD-VP26RFP, vgD-gE-VP26RFP), 80C02 cells [a clone of RS cells expressing UL37 (Roberts *et al.*, 2009)] (vFRΔ37-VP26GFP) or VD60 cells [a clone of Vero cells expressing gD (Ligas & Johnson, 1988)] (vgD-VP26RFP, vgD-gE-VP26RFP). *vVP26GFP and vUL35RFP1D1 were not tested on complementing cells. **The titres of vFRΔ37-VP26GFP and vgD-gE-VP26RFP on non-complementing cells were assigned as $<10^3$ because the input virus caused severe cytopathic effects at lower dilutions.

were the same in $HFFF_2$ and HeLa cells. However, while cytoplasmic capsids formed aggregates in vFRΔ37-VP26GFP-infected HFFF2 cells, as described previously for other $UL37^-$ mutants (Desai *et al.*, 2001; Klupp *et al.*, 2001; Roberts *et al.*, 2009), aggregates were not seen in HeLa cells, where their absence made it easier to observe the behaviour of individual capsids. Many of the capsids in the control vVP26GFP- and vUL35RFP1D1-infected cells colocalized with TGN vesicles, although they were also present in other regions of the cytoplasm (Fig. 2a, b). In the case of vgD-gE-VP26RFP, capsids accumulated in clusters adjacent to, but separated from, TGN vesicles (Fig. 2b). The tendency of capsids to aggregate in the absence of gD and gE was described previously for the parental mutant, vRR1097-gEβ (Farnsworth *et al.*, 2003). In contrast to the juxtaposition of capsids and TGN seen with vgD-gE-VP26RFP, vFRΔ37-VP26GFP capsids accumulated throughout the cytoplasm of infected cells, without exhibiting any association with TGN46- or giantin-positive vesicles (Fig. 2a; Supplementary Fig. S2). The differing behaviours of vFRΔ37-VP26GFP and vgD-gE-VP26RFP were not due to capsid aggregation, as vFRΔ37-VP26GFP capsids also failed to associate with TGN in $HFFF_2$ cells, where large aggregates formed readily (Fig. 2d). Quantification of the fluorescence signals confirmed that there was a significant decrease (approx. 90 %) in the level of colocalization of vFRΔ37-VP26GFP and vgD-gE-VP26RFP capsids with TGN, compared with their corresponding controls (Fig. 2c). To

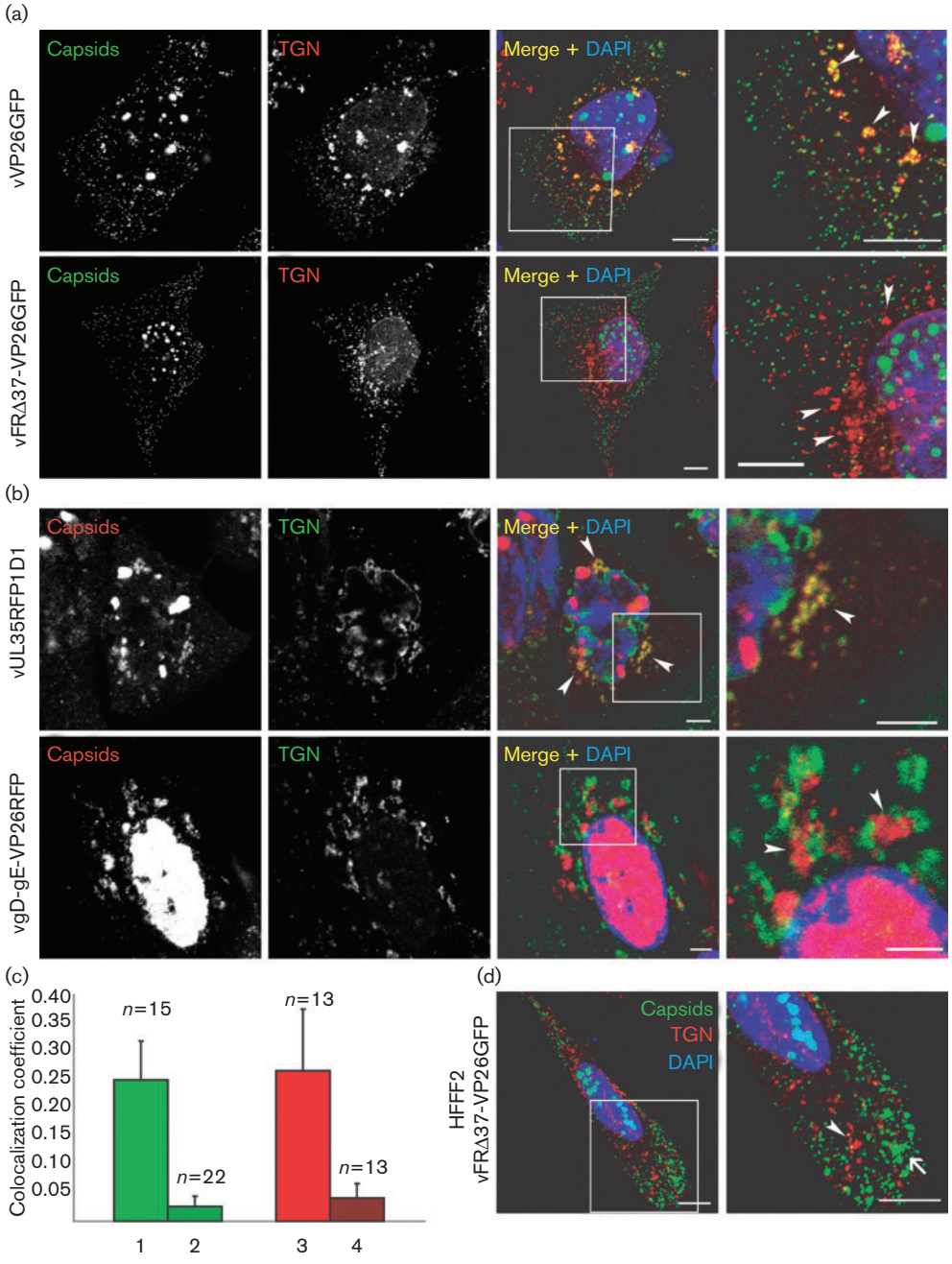

Fig. 2. Association of capsids with the TGN. (a) HeLa cells were infected with 5 p.f.u. of vVP26GFP or vFRΔ37-VP26GFP per cell. At 15 h post-infection, the cells were fixed and stained with anti-TGN46 antibody and a GAR_{568} antibody (red). Capsids were visualized through direct GFP fluorescence (green). Bar, 10 μm. (b) HeLa cells were infected with 5 p.f.u. of vUL35RFP1D1 or vgD-gE-VP26RFP per cell. At 15 h post-infection, cells were fixed and labelled with anti-TGN46 antibody and a GAR_{Cy5} antibody (pseudo-coloured in green). Capsids were visualized through direct RFP fluorescence (red). In all cases, nuclei were stained with DAPI (blue). The boxed regions in the Merge+DAPI images are shown enlarged in the final panel and the positions of some TGN-derived vesicles are indicated by arrowheads. (c) Quantification of the amount of TGN signal that colocalizes with capsid signal for the four different viruses in HeLa cells (1, vVP26GFP; 2, vFRΔ37-VP26GFP; 3, vUL35RFP1D1; 4, vgD-gE-VP26RFP). The numbers of fields of view analysed are indicated above each bar. (d) $HFFF_2$ cells were infected with 5 p.f.u. of vFRΔ37-VP26GFP per cell and labelled as above. A capsid aggregate is indicated by an arrow and a TGN vesicle by an arrowhead. Bars, 5 μm.

confirm that the fluorescent protein tags on VP26 were not influencing the behaviour of capsids, the experiments were repeated using the original untagged versions of the mutants, vFRΔUL37 and vRR1097-gEβ (see Supplementary Fig. S3, available in JGV Online). In agreement with previous results, WT capsids were largely colocalized with TGN vesicles and

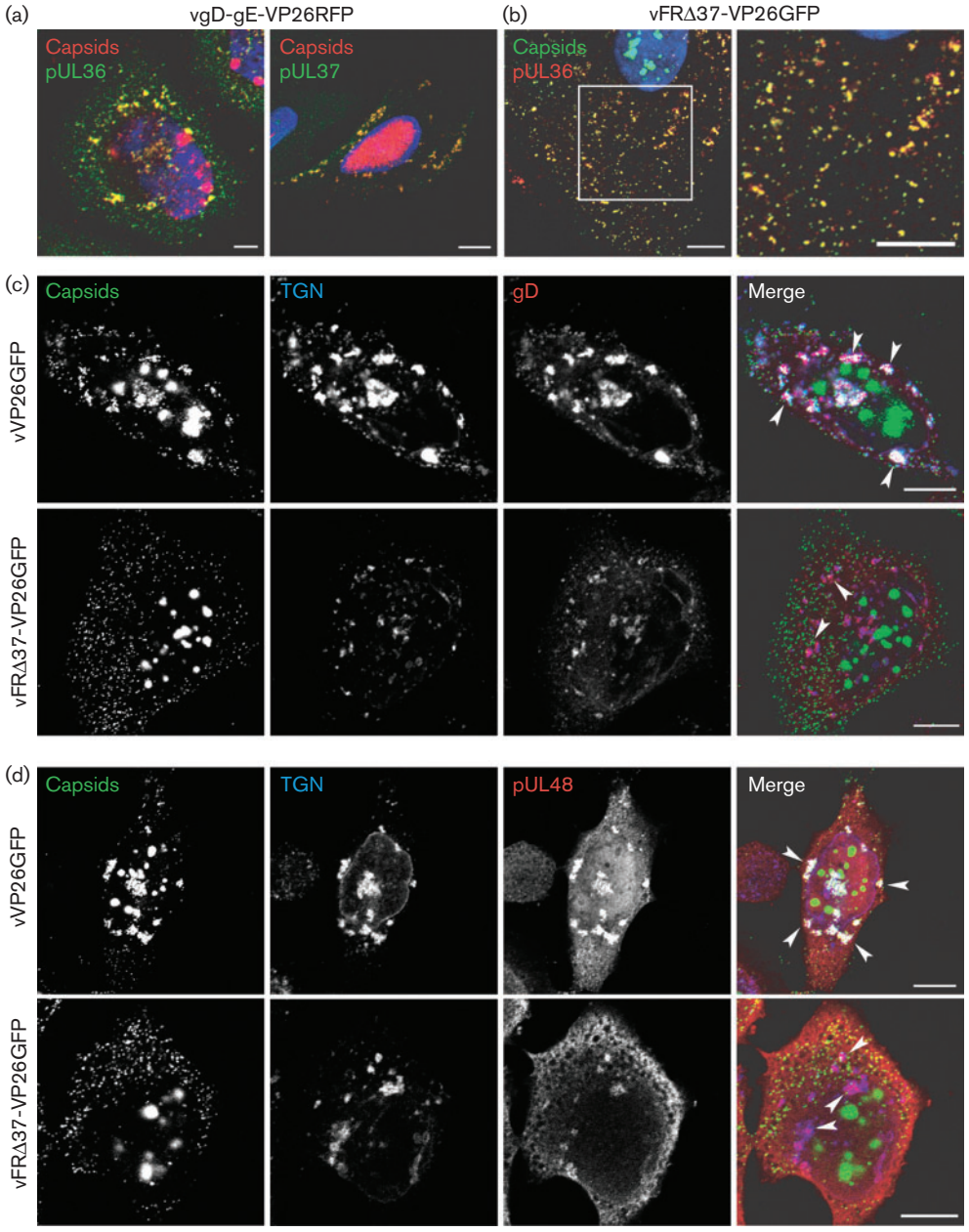

Fig. 3. Effect of UL37 and gD–gE deletions on the localization of glycoproteins and tegument proteins. (a) HeLa cells infected with vgD-gE-VP26RFP for 15 h were fixed and labelled with the anti-pUL36 antibody and a GAM_{633} antibody (pseudo-coloured in green) or were permeabilized with digitonin and labelled with anti-pUL37 antibody and a GAR_{Cy5} antibody (pseudo-coloured in green) under native conditions as described by Copeland *et al.* (2009). Bar, 5 μm. (b) HeLa cells were infected with vFRΔ37-VP26GFP for 15 h, fixed and labelled with anti-pUL36 antibody and a GAR_{568} antibody (red). (c) HeLa cells were infected with 5 p.f.u. of vVP26GFP or vFRΔ37-VP26GFP per cell. At 15 h post-infection, cells were fixed and labelled with TGN46-specific antibody and a GAR_{Cy5} antibody to label the TGN (blue), and with a gD-specific antibody and a GAM_{568} antibody to label gD (red). Capsids were visualized through direct GFP fluorescence (green). (d) Cells were infected and treated as in (c) except that the gD-specific antibody was replaced by pUL48-specific antibody to label pUL48 (red). Arrowheads in (c) and (d) indicate the positions of some TGN-derived vesicles. Bars, 10 μm.

vRR1097-gEβ capsids were aggregated and juxtaposed to TGN vesicles, whereas vFRΔUL37 capsids were widely dispersed and showed no association with the TGN.

As lack of both the inner tegument protein pUL37 and the envelope glycoproteins gD–gE blocked the colocalization of capsids with the TGN, it was important to show that these two classes of structural protein were functioning independently. Immunofluorescence using the anti-UL36 or anti-pUL37 antibody revealed extensive colocalization between pUL36 or pUL37 and vgD-gE-VP26RFP capsid clusters (Fig. 3a). The presence of pUL36 and UL37 implies that the failure of capsids to gain an envelope was a direct result of the absence of the glycoproteins and not due to a block on the association between these capsids and inner tegument proteins. Moreover, we could exclude the possibility that the phenotype observed in vFRΔ37-VP26GFP-infected cells was due to a possible absence of pUL36 on capsids, as vFRΔ37-VP26GFP capsids were stained for pUL36 using the anti-UL36 antibody (Fig. 3b). To examine whether localization of viral glycoproteins to the TGN was affected by the lack of pUL37, vVP26GFP- and vFRΔ37-VP26GFP-infected cells were stained for TGN46 and the glycoprotein gD. In both cases, gD was found on all TGN vesicles (Fig. 3c), either in association with capsids (vVP26GFP-infected cells) or in their absence (vFRΔ37-VP26GFP-infected cells). Similar observations were made with gI and gE (data not shown), demonstrating that pUL37 is not required to direct any of these glycoproteins to the TGN. Similarly, examination of the outer tegument protein pUL48 showed its presence at the TGN in both vVP26GFP- and vFRΔ37-VP26GFP-infected cells (Fig. 3d). Thus, the absence of pUL37 appears to block envelopment by directly preventing the targeting of capsids to the TGN, rather than by interfering with the localization of envelopment-related glycoproteins or outer tegument proteins. It is clear, therefore, that the maturation defects observed in the inner tegument protein and glycoprotein mutants are different in nature, with pUL37 being required to direct capsids to the TGN, and gD and gE being needed for their envelopment once they have arrived there.

The mechanism by which pUL37 helps guide capsids to the TGN is unclear. Directed movement would require the involvement of cellular factors, which might be expected to be recruited to capsids by interacting with pUL37 or with its inner tegument partner, pUL36. However, any such factors remain to be identified. Although our data support a role for pUL37 in directing capsids to the TGN, this does not preclude involvement in later stages of envelopment.

Acknowledgements

We are grateful to the following for providing reagents: F. Jenkins, University of Pittsburgh, PA, USA (pUL37 antibody), D. C. Johnson, Oregon Health and Science University, Portland, OR, USA (vRR1097-gEβ) and Peter O'Hare, Marie Curie Research Institute, Oxted, Surrey, UK (pUL36 antibody). vVP26GFP was generated by V. Preston, MRC Virology Unit, Glasgow, UK, from the VP26-GFP plasmid supplied by P. Desai (John Hopkins University School of Medicine, Baltimore, MD, USA).

References

Baines, J. D. & Roizman, B. (1992). The UL11 gene of herpes simplex virus 1 encodes a function that facilitates nucleocapsid envelopment and egress from cells. *J Virol* **66**, 5168–5174.

Baines, J. D., Ward, P. L., Campadelli-Fiume, G. & Roizman, B. (1991). The UL20 gene of herpes simplex virus 1 encodes a function necessary for viral egress. *J Virol* **65**, 6414–6424.

Bechtel, J. T. & Shenk, T. (2002). Human cytomegalovirus UL47 tegument protein functions after entry and before immediate-early gene expression. *J Virol* **76**, 1043–1050.

Brack, A. R., Dijkstra, J. M., Granzow, H., Klupp, B. G. & Mettenleiter, T. C. (1999). Inhibition of virion maturation by simultaneous deletion of glycoproteins E, I, and M of pseudorabies virus. *J Virol* **73**, 5364–5372.

Campadelli, G., Brandimarti, R., Di Lazzaro, C., Ward, P. L., Roizman, B. & Torrisi, M. R. (1993). Fragmentation and dispersal of Golgi proteins and redistribution of glycoproteins and glycolipids processed through the Golgi apparatus after infection with herpes simplex virus 1. *Proc Natl Acad Sci U S A* **90**, 2798–2802.

Cohen, G. H., Katze, M., Hydrean-Stern, C. & Eisenberg, R. J. (1978). Type-common CP-1 antigen of herpes simplex virus is associated with a 59,000-molecular-weight envelope glycoprotein. *J Virol* **27**, 172–181.

Coller, K. E., Lee, J. I., Ueda, A. & Smith, G. A. (2007). The capsid and tegument of the alphaherpesviruses are linked by an interaction between the UL25 and VP1/2 proteins. *J Virol* **81**, 11790–11797.

Copeland, A. M., Newcomb, W. W. & Brown, J. C. (2009). Herpes simplex virus replication: roles of viral proteins and nucleoporins in capsid-nucleus attachment. *J Virol* **83**, 1660–1668.

Desai, P. J. (2000). A null mutation in the UL36 gene of herpes simplex virus type 1 results in accumulation of unenveloped DNA-filled capsids in the cytoplasm of infected cells. *J Virol* **74**, 11608–11618.

Desai, P. & Person, S. (1998). Incorporation of the green fluorescent protein into the herpes simplex virus type 1 capsid. *J Virol* **72**, 7563–7568.

Desai, P., Sexton, G. L., McCaffery, J. M. & Person, S. (2001). A null mutation in the gene encoding the herpes simplex virus type 1 UL37 polypeptide abrogates virus maturation. *J Virol* **75**, 10259–10271.

Desai, P., Sexton, G. L., Huang, E. & Person, S. (2008). Localization of herpes simplex virus type 1 UL37 in the Golgi complex requires UL36 but not capsid structures. *J Virol* **82**, 11354–11361.

Elliott, G., Mouzakitis, G. & O'Hare, P. (1995). VP16 interacts via its activation domain with VP22, a tegument protein of herpes simplex virus, and is relocated to a novel macromolecular assembly in coexpressing cells. *J Virol* **69**, 7932–7941.

Farnsworth, A., Goldsmith, K. & Johnson, D. C. (2003). Herpes simplex virus glycoproteins gD and gE/gI serve essential but redundant functions during acquisition of the virion envelope in the cytoplasm. *J Virol* **77**, 8481–8494.

Foster, T. P., Melancon, J. M., Baines, J. D. & Kousoulas, K. G. (2004). The herpes simplex virus type 1 UL20 protein modulates membrane fusion events during cytoplasmic virion morphogenesis and virus-induced cell fusion. *J Virol* **78**, 5347–5357.

Fuchs, W., Klupp, B. G., Granzow, H. & Mettenleiter, T. C. (2004). Essential function of the pseudorabies virus UL36 gene product is

independent of its interaction with the UL37 protein. *J Virol* **78**, 11879–11889.

Gross, S. T., Harley, C. A. & Wilson, D. W. (2003). The cytoplasmic tail of herpes simplex virus glycoprotein H binds to the tegument protein VP16 *in vitro* and *in vivo*. *Virology* **317**, 1–12.

Homa, F. L. & Brown, J. C. (1997). Capsid assembly and DNA packaging in herpes simplex virus. *Rev Med Virol* **7**, 107–122.

Klupp, B. G., Granzow, H., Mundt, E. & Mettenleiter, T. C. (2001). Pseudorabies virus UL37 gene product is involved in secondary envelopment. *J Virol* **75**, 8927–8936.

Klupp, B. G., Fuchs, W., Granzow, H., Nixdorf, R. & Mettenleiter, T. C. (2002). Pseudorabies virus UL36 tegument protein physically interacts with the UL37 protein. *J Virol* **76**, 3065–3071.

Ko, D. H., Cunningham, A. L. & Diefenbach, R. J. (2009). The major determinant for addition of tegument protein pUL48 (VP16) to capsids in herpes simplex virus type 1 is the presence of the major tegument protein pUL36 (VP1/2). *J Virol* **84**, 1397–1405.

Lee, J. H., Vittone, V., Diefenbach, E., Cunningham, A. L. & Diefenbach, R. J. (2008). Identification of structural protein–protein interactions of herpes simplex virus type 1. *Virology* **378**, 347–354.

Leege, T., Fuchs, W., Granzow, H., Kopp, M., Klupp, B. G. & Mettenleiter, T. C. (2009). Effects of simultaneous deletion of pUL11 and glycoprotein M on virion maturation of herpes simplex virus type 1. *J Virol* **83**, 896–907.

Ligas, M. W. & Johnson, D. C. (1988). A herpes simplex virus mutant in which glycoprotein D sequences are replaced by β-galactosidase sequences binds to but is unable to penetrate into cells. *J Virol* **62**, 1486–1494.

McLauchlan, J., Liefkens, K. & Stow, N. D. (1994). The herpes simplex virus type 1 UL37 gene product is a component of virus particles. *J Gen Virol* **75**, 2047–2052.

Mettenleiter, T. C., Klupp, B. G. & Granzow, H. (2006). Herpesvirus assembly: a tale of two membranes. *Curr Opin Microbiol* **9**, 423–429.

Mijatov, B., Cunningham, A. L. & Diefenbach, R. J. (2007). Residues F593 and E596 of HSV-1 tegument protein pUL36 (VP1/2) mediate binding of tegument protein pUL37. *Virology* **368**, 26–31.

Mossman, K. L., Sherburne, R., Lavery, C., Duncan, J. & Smiley, J. R. (2000). Evidence that herpes simplex virus VP16 is required for viral egress downstream of the initial envelopment event. *J Virol* **74**, 6287–6299.

Pasdeloup, D., Blondel, D., Isidro, A. L. & Rixon, F. J. (2009). Herpesvirus capsid association with the nuclear pore complex and viral DNA release involve the nucleoporin CAN/Nup214 and the capsid protein pUL25. *J Virol* **83**, 6610–6623.

Rixon, F. J., Addison, C. & McLauchlan, J. (1992). Assembly of enveloped tegument structures (L particles) can occur independently of virion maturation in herpes simplex virus type 1-infected cells. *J Gen Virol* **73**, 277–284.

Roberts, A. P., Abaitua, F., O'Hare, P., McNab, D., Rixon, F. J. & Pasdeloup, D. (2009). Differing roles of inner tegument proteins pUL36 and pUL37 during entry of herpes simplex virus type 1. *J Virol* **83**, 105–116.

Rozen, R., Sathish, N., Li, Y. & Yuan, Y. (2008). Virion-wide protein interactions of Kaposi's sarcoma-associated herpesvirus. *J Virol* **82**, 4742–4750.

Sugimoto, K., Uema, M., Sagara, H., Tanaka, M., Sata, T., Hashimoto, Y. & Kawaguchi, Y. (2008). Simultaneous tracking of capsid, tegument, and envelope protein localization in living cells infected with triply fluorescent herpes simplex virus 1. *J Virol* **82**, 5198–5211.

Szilagyi, J. F. & Cunningham, C. (1991). Identification and characterization of a novel non-infectious herpes simplex virus-related particle. *J Gen Virol* **72**, 661–668.

Turcotte, S., Letellier, J. & Lippe, R. (2005). Herpes simplex virus type 1 capsids transit by the *trans*-Golgi network, where viral glycoproteins accumulate independently of capsid egress. *J Virol* **79**, 8847–8860.

Uetz, P., Dong, Y. A., Zeretzke, C., Atzler, C., Baiker, A., Berger, B., Rajagopala, S. V., Roupelieva, M., Rose, D. & other authors (2006). Herpesviral protein networks and their interaction with the human proteome. *Science* **311**, 239–242.

Vittone, V., Diefenbach, E., Triffett, D., Douglas, M. W., Cunningham, A. L. & Diefenbach, R. J. (2005). Determination of interactions between tegument proteins of herpes simplex virus type 1. *J Virol* **79**, 9566–9571.

PARTIE II :

Transport intracellulaire des capsides de HSV-1 sur le réseau de microtubules

Contexte et hypothèse de travail

La question du transport intracellulaire des virus est une question qui est restée longtemps sous-estimée dans le domaine de la virologie, essentiellement à cause des limites techniques inhérentes à ces études. En effet, afin d'étudier une infection virale en temps réel, il faut pouvoir disposer non seulement de microscopes capables d'enregistrer un nombre continu d'images dans un temps relativement long, mais il faut également posséder les outils de biologie moléculaire qui permettent d'obtenir des virus recombinants viables codant pour des protéines fluorescentes. Lors de mon arrivée au laboratoire de Virologie Moléculaire et Structurale, un microscope à fluorescence équipé d'une chambre d'incubation thermostatée dans un confinement de sécurité L2 était à disposition depuis peu. Par ailleurs, les derniers travaux effectués lors de mon stage post-doctoral à Glasgow portaient sur les protéines de tégument interne pUL36 et pUL37, en continuité directe de l'étude du rôle de ces protéines dans l'entrée du virus. En effet, entre la pénétration de la capside dans la cellule au niveau de la membrane plasmique et son arrivée au pore nucléaire, le virus doit parcourir des distances importantes, surtout dans les neurones où la capside entre généralement via la terminaison axonale. Le réseau de microtubules (MTs) a rapidement été identifié comme le principal réseau du cytosquelette impliqué dans ce transport[26].

Ce n'est qu'à partir de 2006 que les premières expériences de vidéo-microscopie ont permis de montrer que la protéine pUL36 était nécessaire à ce transport[27]. D'autres études ont confirmé que le tégument interne (pUL36 et pUL37) était nécessaire au transport des capsides[28], car des capsides sans ces protéines ne peuvent pas fixer les moteurs moléculaires associés aux MTs[29]. De plus, les capsides avec le tégument interne sont capables de lier les deux types de moteurs moléculaires à la fois[29]. Par ailleurs, durant l'entrée du virus, pUL36 et pUL37 sont les seules protéines de tégument qui restent associées aux capsides[30-32]. Toutefois, si le rôle des deux protéines semblait ne faire aucun doute, aucune interaction n'avait encore été démontrée permettant de comprendre le mécanisme moléculaire de recrutement de la machinerie de transport cellulaire par le tégument interne des capsides du virus.

Expériences mises en œuvre

Alors que les efforts de la plupart des laboratoires se sont concentrés sur pUL36, de loin la meilleure candidate pour le recrutement des moteurs moléculaires, nous nous sommes penchés sur le rôle de sa partenaire, la protéine pUL37. En effet, cette protéine est de taille plus modeste (1123

résidus) que pUL36 (3139 résidus) et est par conséquent d'avantage compatible avec les expériences de double-hybride en levures que nous avions planifié. Notre stratégie était de chercher à mettre en évidence les facteurs cellulaires recrutés par le complexe pour permettre le transport efficace des capsides durant l'entrée virale. Nous avons utilisé la protéine entière pUL37 comme appât contre une banque d'expression de cellules neuronales de rat PC12. Parmi le petit nombre de partenaires ainsi mis en avant, nous avons identifié la protéine Dystonine/BPAG1. A l'époque, cette protéine géante (7393 acides aminés pour la forme la plus longue) n'était connue qu'en tant que cross-linker entre les différents réseaux du cytosquelette. Les autres partenaires étaient alors beaucoup moins bien caractérisés. Surtout, la dystonine avait été décrite comme ayant un rôle dans le transport rétrograde des vésicules neuronales[33] et antérograde de vésicules de sécrétion[34] ce qui nous a décidé à étudier cette interaction de plus près. La dystonine est présente dans les tissus épithéliaux, neuronaux et musculaires sous trois isoformes différentes[35]. Le fragment que nous avons identifié comme étant suffisant pour l'interaction avec pUL37 est une partie du domaine plakine, commun à toutes les isoformes (Figure 1 de la publication 4 ou PB4-1). Nous avons montré par des expériences de shRNA et de vidéo-microscopie que la dystonine était nécessaire au transport vers le pôle positif (+) des MTs, c'est-à-dire vers la périphérie de la cellule durant la sortie, ou vers le noyau durant l'entrée (voir **Figure 8** pour l'orientation du réseau de MTs).

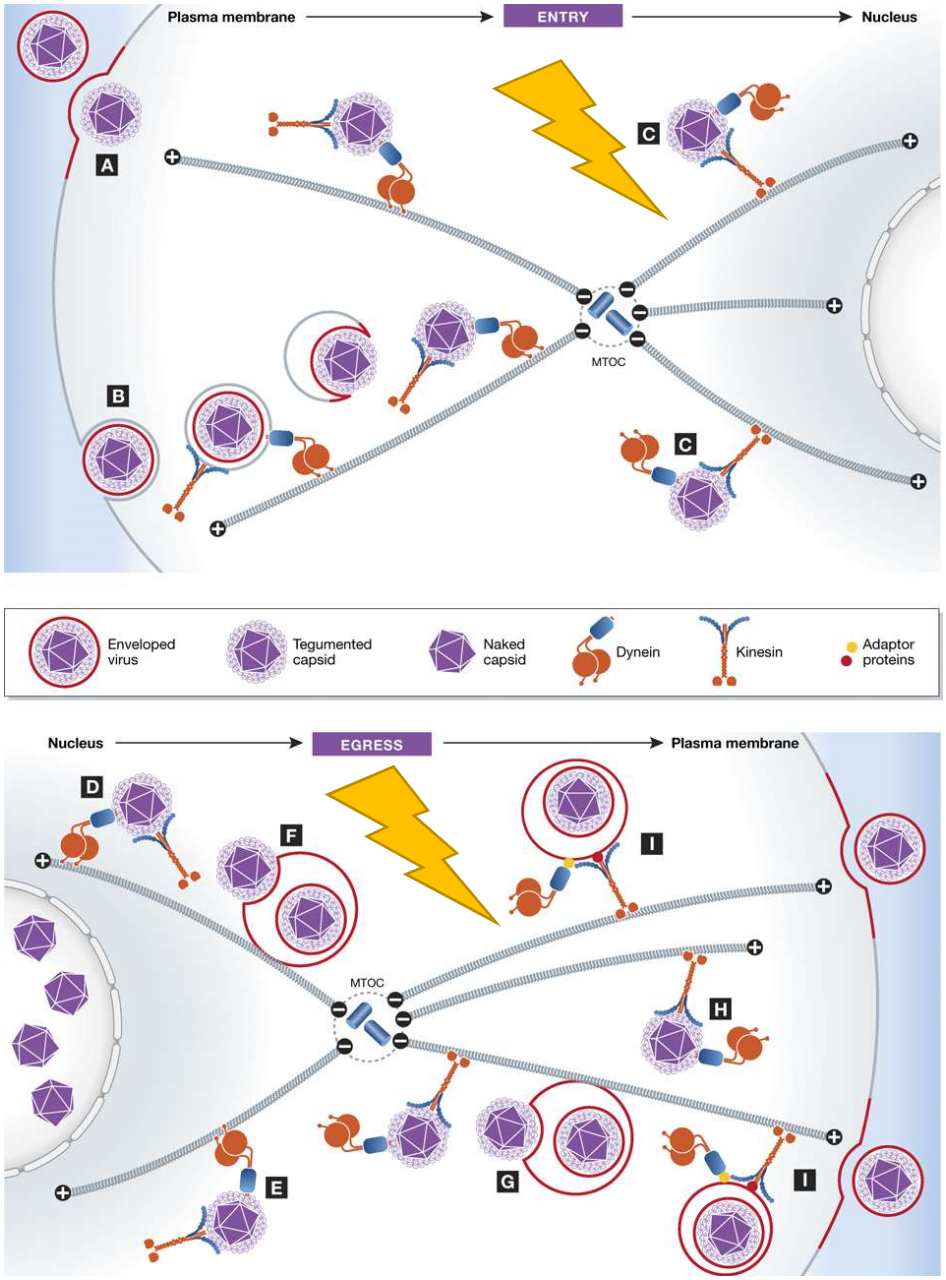

Figure 8. Schéma général du transport intracellulaire d'un virus enveloppé lors de l'entrée (en haut) ou de la sortie virale (en bas). Dans les faits, ce schéma peut s'appliquer à HSV-1, même si le transport lors de la sortie du virus (egress) est différente du fait de l'absence de centrosome fonctionnel dans les cellules infectées (voir partie III). Les flèches jaunes indiquent les processus de transport qui sont altérés chez HSV-1 dans des cellules déplétées en dystonine. Tiré de Dodding & Way, EMBO J 2011.[36].

En effet, en conditions où la protéine est absente ou en très faible quantité, nous avons observé une accumulation de capsides au centrosome (MToC) durant l'entrée (Figure PB5-6). Le transport des capsides depuis la périphérie vers le centrosome était normal (transport vers le pôle (-) des MTs) mais leur redirection depuis le centrosome vers le noyau était altérée (transport vers le pôle (+)) (Figure PB5-7). Lors de la sortie des capsides nouvellement formées du noyau, nous avons observé une

accumulation de capsides cytoplasmiques immobiles (Figure PB4-6). Cette accumulation conduit à la formation de clusters de capsides, un phénotype typiquement observé avec un virus ne codant pas pour la protéine pUL37 (Desai 2001, Klupp 2001). Ainsi, la seule absence d'un partenaire de pUL37 suffit à récapituler l'un des phénotypes majeurs observés chez un virus ΔUL37. Etant donné que le transport vers le pôle (+) des MTs est le principal mode de transport des capsides sortant du noyau, l'ensemble des résultats obtenus nous a conduit à conclure que la dystonine avait un rôle dans la direction du transport des capsides (ici vers le pôle (+)) plutôt qu'un rôle générique dans le transport.

Répercussion de ces travaux et ce que l'on sait maintenant

Nos travaux ainsi que ceux d'autres laboratoires ont permis d'avancer l'idée que les deux protéines pUL36 et pUL37 avaient des rôles distincts et complémentaires dans le transport intracellulaire des capsides. En effet, la même année où nos travaux ont été publiés, l'équipe de G.Smith à Chicago a finalement montré une interaction directe entre pUL36 et des co-facteurs du moteur dynéine, impliqué dans le transport vers le pôle (-) des MTs[37]. pUL36 est donc présentée comme la protéine « effectrice » du transport, celle qui va permettre aux capsides en transit de fixer les moteurs moléculaires (même si aucune interaction fonctionnelle avec les moteurs de type kinésine n'a été démontrée pour l'instant). pUL37, en revanche, ne semble pas capable d'interagir directement avec les moteurs. Nous avons démontré sa capacité à interagir avec un élément présent aux pôles (+) des MTs. Dans les années qui ont suivi ces travaux, le rôle jusqu'alors inconnu ou imprécis de trois partenaires cellulaires de pUL37 obtenus lors de notre crible double-hybride réalisé en 2009 a été élucidé par plusieurs équipes différentes. Ces protéines sont associées soit au centrosome, soit aux pôles (-) des MTs non-centrosomaux (données non publiées). L'ensemble de ces résultats suggère donc que pUL37 serait la protéine « régulatrice » du transport, c'est-à-dire l'élément du complexe qui régulerait quel moteur moléculaire serait lié ou activé par pUL36 et, par conséquent, qui régulerait la direction du transport. Des travaux récents ont confirmé cette théorie[38].

Publication #4

Herpesvirus tegument protein pUL37 interacts with dystonin/BPAG1 to promote capsid transport on microtubules during egress.

Pasdeloup D, McElwee M, Beilstein F, Labetoulle M, Rixon FJ

JVI Journals.ASM.org

Herpesvirus Tegument Protein pUL37 Interacts with Dystonin/BPAG1 To Promote Capsid Transport on Microtubules during Egress

David Pasdeloup,[a,b] Marion McElwee,[b] Frauke Beilstein,[a] Marc Labetoulle,[a] Frazer J. Rixon[b]

Laboratoire de Virologie Moléculaire et Structurale, CNRS, Gif-Sur-Yvette, France[a]; MRC-University of Glasgow Centre for Virus Research, Glasgow, United Kingdom[b]

Herpes simplex virus 1 (HSV-1) is a neurotropic virus that travels long distances through cells using the microtubule network. Its 125-nm-diameter capsid is a large cargo which efficiently recruits molecular motors for movement. Upon entry, capsids reach the centrosome by minus-end-directed transport. From there, they are believed to reach the nucleus by plus-end-directed transport. Plus-end-directed transport is also important during egress, when capsids leave the nucleus to reach the site of envelopment in the cytoplasm. Although capsid interactions with dynein and kinesins have been described *in vitro*, the actual composition of the cellular machinery recruited by herpesviruses for capsid transport in infected cells remains unknown. Here, we identify the spectraplakin protein, dystonin/BPAG1, an important cytoskeleton cross-linker involved in microtubule-based transport, as a binding partner of the HSV-1 protein pUL37, which has been implicated in capsid transport. Viral replication is delayed in dystonin-depleted cells, and, using video microscopy of living infected cells, we show that dystonin depletion strongly inhibits capsid movement in the cytoplasm during egress. This study provides new insights into the cellular requirements for HSV-1 capsid transport and identifies dystonin as a nonmotor protein part of the transport machinery.

Microtubules (MTs) are long, polarized structures made of heterodimers of alpha and beta tubulin. They are nucleated from microtubule organizing centers (MTOCs), the nature of which may differ according to cell type (reviewed in reference 1). The most common MTOC is the centrosome, from where nascent MTs grow by polymerization of tubulin at their plus ends. The minus ends are thought to be anchored and stabilized at the centrosome by specific proteins (2). In general, MTs radiate from the centrosome to the cell periphery.

Microtubule motors such as cytoplasmic dynein or kinesins are involved in trafficking and transport of various cargoes, such as protein complexes, vesicles, or even organelles along microtubules. It has become progressively apparent that motor-cargo interactions are often indirect in nature, with adaptor proteins or lipids linking the molecular motor to its cargo (reviewed in reference 3).

Herpes simplex virus 1 (HSV-1) is a neurotropic human virus, well known for its ability to traffic efficiently within cells, especially sensory neurons (4, 5), using the MT network (6, 7). It is a large, double-stranded DNA virus. The genome is packaged in an icosahedral capsid which is surrounded by tegument, a proteinaceous layer that is characteristic of herpesviruses, and an outer envelope. On entry, capsids migrate from the plasma membrane to the nuclear membrane (retrograde transport), where they release the viral genome into the nucleus. Newly formed capsids exiting the nucleus are assumed to travel from the nucleus to sites of secondary envelopment through plus-end-directed transport (anterograde transport). In neurons, this potentially implies traveling long distances between the cell body and the axon terminus during both entry and egress. Therefore, efficient recruitment of the cellular trafficking machinery is required. HSV-1 tegumented capsids were shown to bind to the molecular motors dynein and kinesin-1 and -2 *in vitro* (8), and the dynein complex was shown to be necessary for capsid transport in infected cells (9). Kinesin-1 is also present on enveloped capsids undergoing anterograde transport in neuronal processes (10). However, although numerous interactions have been described between HSV-1 proteins and molecular motors, as yet, none have been demonstrated as functionally relevant in infected cells, and the actual composition of the cellular transport machinery recruited by herpesvirus capsids remains unknown (5, 11). To date, the best documented viral candidates for a role in capsid transport are the tegument proteins pUL36 and pUL37 (12). Unlike the majority of tegument proteins, these proteins, which interact with each other, have been reported to remain attached, at least in part, to capsids in transit to the nucleus (4, 13). The same is true for the related pseudorabies herpesvirus (PrV) (14, 15). In addition, it was demonstrated that in their absence, intracellular transport of PrV capsids is either severely impaired (pUL37) or totally absent (pUL36) (16, 17).

To unravel cellular factors involved in herpes capsid trafficking, we used pUL37 as bait in a yeast two-hybrid screen and identified the protein dystonin (DST; or BPAG1) as a binding partner. Dystonin is a giant protein which belongs to the conserved spectraplakin superfamily of proteins and, as such, contains numerous spectrin repeats and a plakin domain (reviewed in references 18, 19, and 20). Additionally, it may have an actin-binding domain (AB) and an MT-binding domain (MTBD) (Fig. 1A), depending on the isoform. Four major isoforms have been identified to date, with different cell specificities. Dystonin e (2,611 residues; sizes relate to the murine form of dystonin) is found in epithelial cells, whereas dystonin a (5,379 residues) is predominantly neuronal and dystonin b (7393 residues) is mostly muscular (21). Isoform n refers to the originally described neuronal dystonin (BPAG1n) (22), but it is still unclear whether this isoform is actually pro-

Received 28 September 2012 Accepted 17 December 2012
Published ahead of print 26 December 2012
Address correspondence to David Pasdeloup, pasdeloup@vms.cnrs-gif.fr.
Supplemental material for this article may be found at http://dx.doi.org/10.1128/JVI.02676-12.

doi:10.1128/JVI.02676-12

duced (21). Determining the molecular mechanism of action of dystonin has proved to be challenging, mostly because of its large size and the variety of isoforms. It has been shown to be necessary for stabilizing MTs in neurones (23), and one isoform was reported to be essential for retrograde transport in neuronal cells through its interaction with the $p150^{glued}$ subunit of dynactin, a cofactor of the dynein motor (24). Recently, it was also shown to function during anterograde transport of secretory vesicles (25).

Using live-cell imaging and RNA silencing, we investigated the relevance of the pUL37-dystonin interaction to intracytoplasmic transport of HSV-1 capsids.

MATERIALS AND METHODS

Cells and viruses. African green monkey kidney (Vero), 293T, baby hamster kidney (BHK), and human fetal foreskin fibroblast (HFFF2) cells were grown at 37°C in Dulbecco's modified Eagle medium (DMEM; PAA Laboratories) supplemented with 8% fetal calf serum (FCS). For live-cell microscopy studies, cells were grown on 35-mm MaTek glass-bottomed petri dishes.

Wild-type (WT) HSV-1 (strain 17^+) and vSR27-VP26GFP (where GFP is green fluorescent protein) were propagated on BHK cells infected at 0.01 PFU per cell, and virions were concentrated from supernatant medium by centrifugation at 15,000 × *g* for 2 h.

The UL37-null mutant of HSV-1 (FRΔUL37-VP26GFP) was grown on the complementing cell line 80C02 (26, 27). Cells were infected at 0.01 PFU/cell, and 3 days later virions were concentrated from supernatant medium by centrifugation at 15,000 × *g* for 2 h.

vSR27-VP26GFP was obtained by cotransfecting BHK cells with the SR27 BACmid, containing the full-length genome of HSV-1 17+ (provided by C. Cunningham) and with the plasmid pK26GFP (provided by P. Desai), which encodes a VP26-GFP fusion protein (28). Progeny virus was serially diluted, and a GFP-positive plaque was isolated and grown to high titer.

The vUL35RFP1D1 virus has a wild-type background (17syn+), except that it encodes a VP26 capsid protein fused at its N terminus to the monomeric red fluorescent protein (mRFP) (26).

vUL37GFP-VP26RFP was obtained by coinfecting BHK cells with vUL35RFP1D1 and with vUL37GFP, a virus encoding a fusion of GFP to the C terminus of pUL37 (10). Progeny virus was collected and serially diluted on fresh cells. Plaques exhibiting both GFP and RFP fluorescence were selected and purified through five rounds of plaque purification.

Plasmids. pCDNA3.1-myc and pCDNA3.1-hemagluttinin (HA) vectors were described in reference 29. pHA-UL32 was provided by E. Palmer. UL37 was amplified by PCR from HSV-1 BAC SR27 and cloned into the EcoRI-XbaI sites of pCDNA3.1-HA (pHA-UL37) or the EcoRI-BamHI sites of the pLexA vector (pLexA-UL37), in frame with the respective tag. The pUL37-interacting fragment of dystonin was amplified by PCR from the clone isolated in the yeast two-hybrid screen and cloned into the EcoRI-XbaI sites of pcDNA3.1-myc, yielding pMyc-dystonin. Plasmid pGFP-hEB3 was a kind gift of John Victor Small (Institute of Molecular Biotechnology, Vienna, Austria).

Antibodies. The following antibodies were used. Rabbit antibodies Y11 and monoclonal antibody (MAb) F7 against a defined epitope (HA) from the influenza hemagglutinin and rabbit antibody A14 against c-myc were obtained from Santa Cruz Biotechnology. MAb 9E10 against c-myc, mouse anti-alpha-tubulin clone DM1A, and rabbit polyclonal anti-DST antibody against human were obtained from Sigma. Capsids were visualized using the rabbit PTNC antibody (29). Alexa Fluor 488- or 633-conjugated goat anti-mouse (GAM_{488} or GAM_{633}) antibodies and Alexa Fluor 568-conjugated goat anti-rabbit antibody (GAR_{568}) were obtained from Molecular Probes, and tetramethyl rhodamine isocyanate (TRITC)-conjugated phalloïdin and horseradish peroxidase-conjugated goat anti-mouse antibody were from Sigma.

Fluorescence microscopy. All immunofluorescence with tubulin staining was done as follows. Cells were fixed in a mix of 3.7% formaldehyde and 0.1% Triton X-100 in PEM buffer (100 mM PIPES, 5 mM EGTA, 2 mM $MgCl_2$, pH 6.8) for 5 min at room temperature as described in reference 30. Microtubules were stained using MAb DM1A against alpha-tubulin (Sigma) and GAM_{488} or GAM_{633} antibody (90 min each incubation). Actin fibers were stained using TRITC-phalloidin.

Samples were mounted in ImmuMount (Thermo) containing 1 μg/ml 4′,6-diamidino-2-phenylindole dihydrochloride (DAPI) (Sigma) for DNA staining. All samples were visualized using a Zeiss Axio Observer Z1 microscope using a 63× Plan apochromat oil-immersion objective (numerical aperture [NA] of 1.4; Zeiss).

Live-cell microscopy. HFFF2 cells were infected with 1 PFU/cell of virus for 1 h at room temperature and incubated for 24 h at 37°C before live-cell imaging.

At 37°C, the distance traveled by capsids moving at ~2 μm/s on average is ~1.3 μm in the minimum acquisition window of 600 ms allowed by our equipment. These conditions would allow tracking of only small numbers of capsid moving in a large space. Under normal infection conditions, numerous moving capsids are present in a small space, making it very difficult to identify and track efficiently capsids which have traveled ~1 μm between each frame. Therefore, all live-cell microscopy was recorded at room temperature (~25°C). Under these conditions, capsid motion is slower, allowing more efficient tracking of a greater number of capsids per movie. Movies were recorded at a rate of 1 frame/s for 55 to 60 s, with an average exposure time of 200 ms.

Capsid tracking. Movies were converted to an .avi file format using the AxioVision software (release 4.8.1; Zeiss) and imported into ImageJ (version 1.43u). Capsids were tracked using the Particles Detector&Tracker plug-in (version 1.5) (31). Depending on the quality of each individual movie, detection parameters were set as follows: radius = 3 or 5, cutoff = 3.0 or 0.0, percentile = 0.6 to 1.5%; linking parameters were: link range = 2 and displacement = 10 to 20. Capsid motion was analyzed using the coordinates provided by the software to calculate the distance to origin. Capsid tracking starts as the capsid enters the field of view and stops as it leaves it or when it moves out of focus. The directionality of each trajectory was estimated according to the respective positions of the nucleus and of the plasma membrane (see Fig. 6).

shRNA. The use of lentiviruses expressing short hairpin RNA (shRNA) has been described previously (29, 32). Silencing of dystonin was done by using two different 19-nt-long sequences, GTGTTGAAAGCCA TTTAGA (shDyst1) or GTTGCACAGATTAGAGAGT (shDyst2). These sequences (positions 1897 and 2027, respectively, on the murine open reading frame) correspond to the plakin domain of human and murine dystonin and are specific for all known isoforms of dystonin. They are not conserved within sequences of other known plakin proteins. shControl corresponds to a sequence specific to the luciferase gene (GTGCGTTGC TAGTACCAAC) for all experiments. Silencing efficiency was routinely assessed by real-time reverse transcription (RT)-PCR from total RNA before every experiment. Only cells with a silencing rate of 70% or more were used.

Reverse transcription and real-time PCR analysis. Total RNA was isolated using TRI reagent (Molecular Research Center) according to the manufacturer's protocol. Reverse transcription experiments were performed with 1 μg of total RNA in a total volume of 20 μl using Transcriptor reverse transcriptase (Roche). PCRs were performed in triplicate using a LightCycler capillar machine (Roche). For each reaction, a 1:400 final dilution of the reverse transcription product was used with a 0.4 μM final concentration of each primer in SYBR green I master mixture (Roche). PCR conditions were one step of denaturation (8 min at 95°C) followed by 45 cycles (each cycle consisted of 10 s at 95°C, 10 s at 60°C, and 10 s at 72°C). Gene expression was normalized to expression of GAPDH. The following primers were used for real-time PCR analysis (forward primer listed first and reverse primer second): human dystonin (5′-CCAGCCC GGTTAACTATTGA-3′/5′-TGGCAGAGCTGTAAGATCCA-3′) and

human GAPDH (5′-GAGTCCACTGGCGTCTTCAC-3′/5′-TTCACAC CCATGACGAACAT-3′).

A PCR control was also performed from the same cDNA samples using the following primers: 5′-ACCACAGTCCATGCCATCAC-3′ and 5′-TCCACCACCCTGTTGCTGTA-3′ (GAPDH, forward and reverse, respectively, human and murine), 5′-AGCAAAGGACGCATACTGA C-3′ (dystonin, forward, human only), 5′-AGCAAAGGACGCATGCTG AC-3′ (dystonin, forward, murine only), and 5′-CTTGGCAAATCTGAG CCCCA-3′ (dystonin, reverse, human and murine). The PCR products were run on a 1% agarose gel.

Single-step virus growth. Replicate 35-mm dishes of HFFF2 cells, expressing shControl, shDyst1, or no shRNA, were infected with 5 PFU/cell of HSV-1 strain 17+ (WT). After 1 h at 37°C, the cells were washed at low pH to remove residual input infectivity and overlaid with 1 ml of DMEM, and incubation was continued at 37°C. At 6, 12, 24, and 48 h after infection, the cells were harvested by scraping into the medium and pelleted, and the progeny virus was titrated from the supernatant on Vero cells. For growth in the presence of nocodazole, the drug (10 μM) was added onto the cells 1 h before infection and kept all the time of infection (see "Nocodazole" in Fig. 4B) or not at all and was replaced by dimethyl sulfoxide (DMSO). Viral titers were determined as described above.

Yeast two-hybrid assay. The yeast two-hybrid system used in this study has been described previously (33). L40 yeasts were transformed with pLexA-UL37 HSV1 using lithium acetate, and transformants were selected by their ability to grow on tryptophane-depleted agar plates. These were then transformed with a cDNA library from differentiated PC12 cells cloned in pGAD-GH (kindly provided by H. Raux, VMS, CNRS, Gif-sur-Yvette) and screened as described in reference 33. The control for specificity was the lack of interaction between the putative pUL37-binding proteins and control proteins (lamin and LexA domain alone). A total of 127,000 transformants were obtained, and 27 were positive for specific interaction with pUL37 after screening and control. Liquid β-galactosidase assays were conducted as described in reference 33.

Immunoprecipitation. Coimmunoprecipitations were done as described previously (29), except that only the cytoplasmic fraction was kept for analysis.

Secondary structure prediction. The sequence of pUL37 from HSV-1 strain 17+ (34) was analyzed by two secondary structure prediction algorithms, APSSP2 (http://imtech.res.in/raghava/apssp/) and SOPMA (http://npsa-pbil.ibcp.fr/cgi-bin/npsa_automat.pl? page=npsa_sopma.html) to determine regions of the protein which were predicted to be unfolded. These were used to select suitable positions at which to truncate the protein.

RESULTS

pUL37 interacts with the plakin domain of dystonin. To identify cellular proteins interacting with pUL37, a cDNA library prepared from differentiated PC12 cells, a rat neuronal cell line, was screened by yeast two-hybrid (Y2H) assay using pLexA-UL37 as bait. Out of 127,000 transformants, 27 were positive for interaction as assessed by β-galactosidase staining and growth on selective medium. Among these 27 clones representing 17 different genes, we identified a sequence corresponding to dystonin/BPAG1. This protein was of particular interest for several reasons: (i) its ability to bind MTs (23, 35), (ii) its role in retrograde and anterograde transport (24, 25), and (iii) it is expressed in tissues relevant to infection by HSV-1, namely, epithelial and neuronal cells (21). In particular, dystonin-null mice develop severe sensory nerve degeneration (36), highlighting its role in the natural target cell type of HSV-1, the sensory neuron.

The fragment of dystonin that we isolated from the Y2H screen encompasses residues 526 to 851 on isoform a and represents part of the plakin domain of the protein which is common to all dystonin isoforms (Fig. 1A).

To map the domain of pUL37 that interacts with dystonin, we cloned different truncations of pUL37 as LexA fusions and tested them against the 526-to-851 fragment of dystonin isolated from the Y2H screen (Fig. 1B). The boundaries of each truncation were chosen to be in regions of the protein expected to be unfolded, as determined by secondary structure prediction algorithms. Fragments 517 to 1123, 1 to 899, and 578 to 899 were shown to interact with dystonin in Y2H as assessed by liquid β-galactosidase assay (Fig. 1B). Surprisingly, we were unable to detect any interaction with fragment 517 to 899, while fragment 1 to 899 gave a stronger β-galactosidase signal (around 3-fold higher) than wild-type UL37 or any of the other positive fragments. Presumably, amino acids 517 to 578 fold in such a way as to mask the interaction site or disrupt its folding when present in the 517-to-899 fragment, but this effect is prevented in longer proteins or when these sequences are deleted. No interaction could be observed with fragments shorter than 578 to 899. These results map the dystonin interaction domain between residues 578 and 899 of pUL37.

We attempted to confirm the interaction in mammalian cells by coimmunoprecipitation. Vero cells were cotransfected with pHA-UL37, encoding full-length pUL37 fused to an N-terminal HA tag, and with pMyc-dystonin, encoding the 526-to-851 fragment of dystonin fused to an N-terminal myc tag. As a control, pHA-UL32, encoding a full-length, unrelated herpesviral protein, pUL32, fused to an N-terminal HA tag, was used in place of pHA-UL37. Twenty-four hours after transfection, cells were lysed and pUL37 or pUL32 were immunoprecipitated with an HA-specific antibody. The immunoprecipitates were analyzed by Western blotting using a myc-specific antibody to reveal the presence of myc-dystonin. In pHA-UL37 immunoprecipitates, myc-dystonin could be readily detected, but it was absent from pHA-UL32 immunoprecipitates (Fig. 1C). Similar results were obtained when the converse experiment was carried out. Thus, HA-pUL37 could be immunoprecipitated with myc-dystonin, whereas HA-pUL32 could not (Fig. 1D). These results validate the interaction between pUL37 and dystonin in mammalian cells.

Based on these results, we conclude that pUL37 interacts with the plakin domain of dystonin and that residues 578 to 899 of pUL37 are sufficient for this interaction.

Reduction of dystonin levels in HFFF2 cells and cellular localization of dystonin. In order to identify a possible role for dystonin in the HSV-1 replication cycle, silencing experiments were set up using small-hairpin RNA (shRNA) technology. HFFF2 cells were transduced with lentivirus vectors expressing two different shRNAs against sequences that are common to all known isoforms of human dystonin or with a control lentivirus (henceforward referred to as shDyst1, shDyst2, and shControl cells, respectively). As it proved difficult to detect endogenous dystonin in cells by Western blotting, due to its large size and relatively low abundance, the efficiency of RNA silencing was assessed at the transcript level and by immunofluorescence. RT-PCR assays using a set of universal primers for the known isoforms of dystonin confirmed that dystonin mRNA could be detected in our cell line (Fig. 2A). Upon RNA silencing in HFFF2 cells, the amount of dystonin transcripts decreased by ~80% and ~60% in shDyst1 and shDyst2 cells, respectively, compared to the control, as assessed by quantitative RT-PCR (Fig. 2B).

Using an antibody directed against human dystonin (anti-DST antibody), the protein could be detected in uninfected HFFF2 shControl cells, where it was localized throughout the cytoplasm

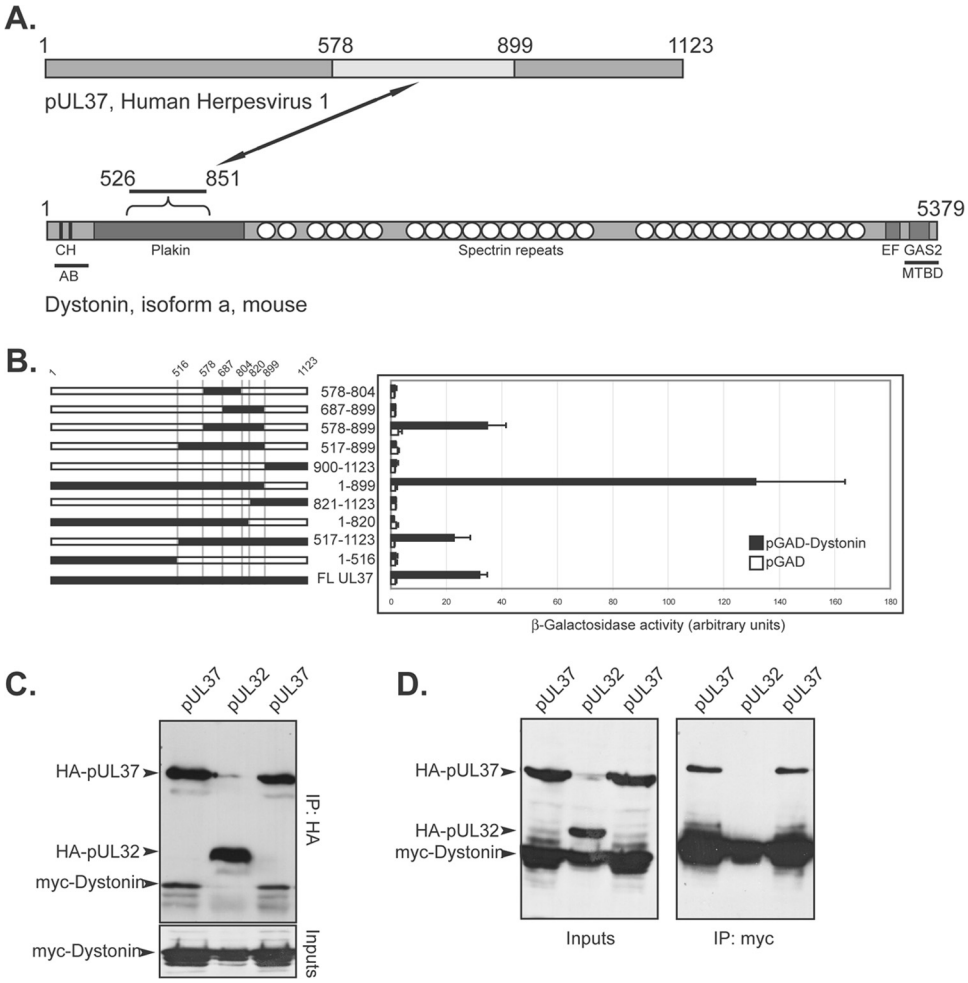

FIG 1 pUL37 interacts with the plakin domain of dystonin. (A) A yeast two-hybrid (Y2H) screen was set up using the LexA-pUL37 HSV-1 construct as bait and a cDNA library isolated from differentiated PC12 cells (rat neuroblastoma) as prey. pUL37 is shown on top, with the domain interacting with dystonin in light gray (residues 578 to 899, see panel B). A simplified domain map of the neuronal isoform of murine dystonin (isoform a) is depicted below pUL37. Note that dystonin is not drawn to scale compared to pUL37 and that although the plakin domain is common to isoforms a, b, and e of dystonin, only isoform a is shown here. CH, calponin homology domains; EF, EF hands; GAS2, GAS2 domain; AB, actin-binding domain; MTBD, MT-binding domain. Based on reference 20. The domain of dystonin interacting with pUL37 (526 to 851) is shown. (B) Different truncations of pUL37 (black lines, left) were fused to the LexA DNA-binding domain and tested for Y2H interaction with pGAD-dystonin, which contains the plakin domain of dystonin obtained from the initial Y2H screen, fused to the GAL4 activation domain (AD). pGAD alone was used as a negative control. The interaction was evaluated by quantification of β-galactosidase activity in liquid yeast cultures by an optical density at 420 nm (OD_{420}) (right). Bars represent standard deviations of the mean. (C, D) Coimmunoprecipitation of HA-pUL37 and myc-dystonin. Vero cells were cotransfected with plasmids coding for HA-pUL37 or HA-pUL32 and the 526-to-851 region of rat dystonin (myc-dystonin) and were lysed 16 h later. Following immunoprecipitation with anti-myc A14 (C) or anti-HA Y11 (D) antibodies, cell extracts (inputs) and immune complexes (IP) were separated by SDS-PAGE and analyzed by Western blotting using anti-HA F7 to reveal the presence of HA-pUL37 and HA-pUL32 and using anti-myc 9E10 to reveal the presence of myc-dystonin. The coimmunoprecipitations between pUL37 and dystonin were carried out in duplicate for each set of conditions.

in spots or short lines, mostly alongside and at the end of MTs (Fig. 3A). In shDyst1 cells, however, no specific fluorescence could be detected, confirming that the silencing was efficient at the protein level (Fig. 3A). As reported previously, the distribution of MTs in shControl cells that had been infected for 16 h was less well organized (37). However, dystonin localization appeared unaffected by infection (Fig. 3B). The localization pattern of dystonin is typical of a protein linked to the plus end of MTs. To check whether this was the case, HFFF2 cells were transfected with a plasmid expressing human end-binding protein 3 (EB3), a plus-end-binding protein (38), fused to GFP. As shown in Fig. 3C, dystonin short lines colocalized with EB3 "comets" at the plus ends of MTs, thereby confirming that dystonin can localize to MT plus ends.

Effect of dystonin reduction on growth of HSV-1. To establish whether reducing the level of dystonin transcripts affected HSV-1 replication, single-step growth analysis of WT HSV-1 was carried out in shDyst1, shControl, or untreated HFFF2 cells. At 6 h, 12 h, 24 h, and 48 h postinfection, cells were scraped into the medium and pelleted. The supernatant was harvested, and the titer of progeny virus was determined on Vero cells (Fig. 4A). This showed that silencing of dystonin led to a significant delay in the production of infectious virus, compared to both the untreated and shControl cells, although by 24 h after infection, the amount of virus produced under all 3 conditions was similar. We compared these growth kinetics with those obtained under conditions where the MT network was disrupted by nocodazole (Fig. 4B).

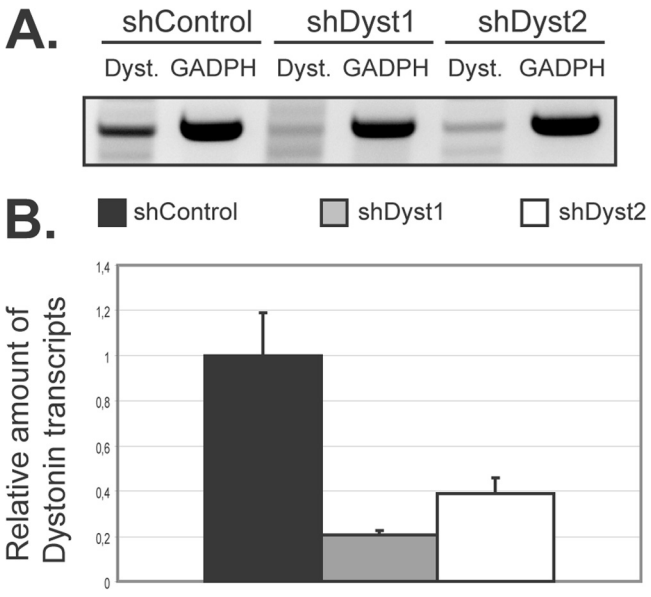

FIG 2 Silencing of dystonin in HFFF2 cells as assessed by quantitative reverse transcription-PCR (qRT-PCR). (A) Dystonin mRNA levels in silenced cells. HFFF2 cells transduced by two different shRNAs targeting dystonin (shDyst1 and shDyst2) or by an irrelevant shRNA (shControl) were lysed 3 days postransduction. RT-PCR was performed on the extracted total mRNA, and the resulting cDNA was used as a template for a PCR using primers specific for the plakin domain of dystonin (Dyst.) or for GAPDH as a loading control. The PCR product was visualized on an agarose gel (A) or quantified by real-time qPCR where shControl transcript levels were defined as 1 (B). GAPDH transcripts were used as a standard for quantification.

The time course of virus production when the MT network was disrupted by nocodazole was very similar to that seen following dystonin depletion. Thus, virus production was delayed but eventually attained equivalent levels to that seen in control cells. Similar behavior has been reported previously for cells treated with nocodazole (37). To show that the delay in infection following dystonin depletion was not a result of nonspecific inhibition of viral gene expression, levels of late protein synthesis were determined by examining the major capsid protein VP5. Western blotting confirmed that VP5 expression at 16 h and 24 h postinfection was unaffected by treatment of cells with shDyst1 (Fig. 4C). These results showed that the effects of reducing the amount of dystonin and disrupting the MT network were similar and suggested a possible involvement of dystonin in virus transport.

Association of capsids with endogenous dystonin in infected cells. The possibility that dystonin is involved in transport during virus egress was examined by looking for association of capsids with endogenous dystonin. HFFF2 cells were infected with 1 PFU/cell of vSR27-VP26GFP or vFRΔ37-VP26GFP for 16 h, and capsid localization relative to dystonin was monitored. As shown in Fig. 5, capsids could be observed colocalizing with dystonin spots in vVP26GFP-infected cells, albeit at low frequency. In contrast, we were unable to see any colocalization between individual capsids and dystonin in cells infected with the UL37-null mutant vFRΔ37-VP26GFP. These data indicate that HSV-1 capsids can recruit dystonin during infection and that this requires pUL37. However, the low frequency of colocalization between dystonin and capsids may indicate that this interaction is transient or intermittent.

Role of dystonin in capsid movement during egress. Given the demonstrated role of dystonin in anterograde transport of vesicles (25), its preferred localization at plus ends of MTs (Fig. 3), and its association with capsids, we postulated that dystonin might be involved in capsid transport during egress. To verify this, shControl and shDyst1 HFFF2 cells were infected at 37°C with 1 PFU/cell of vSR27-VP26GFP (a virus expressing a GFP-tagged capsid protein), and 24 h postinfection, capsid movements in the cytoplasm were monitored by live-cell microscopy. Live-cell imaging was carried out at room temperature (~25°C), because at 37°C the large number of capsids moved too fast to be tracked efficiently, thus limiting both the reliability of the tracking and the number of capsids that could be analyzed (see Materials and Methods). However, the large effect of dystonin depletion on capsid transport as described in Fig. 6 was also observed at 37°C (data not shown). shControl cells contained numerous capsids moving throughout the cytoplasm (Fig. 6A and B; see also Movie S1 in the supplemental material). Movement was both anterograde (away from the nucleus; 50% of capsids) and retrograde (35% of capsids) (Fig. 6J). The average maximum distance to origin (defined as the capsid position at the start of recording) was 5.6 μm, with a peak at more than 19 μm for the duration of the acquisition (around 1 min, Fig. 6A and I). The average maximum speed observed was 0.95 μm/s. This was in sharp contrast with what was seen in shDyst1 cells, where capsids showed no or limited motion (Fig. 6C and D; see also Movie S2 in the supplemental material). The average maximum distance to origin was 0.54 μm (Fig. 6C and I), and the average maximum speed was 0.19 μm/s. The few moving capsids had essentially retrograde movement (Fig. 6J). This behavior was very similar to that observed in cells where the MT network was disrupted by treatment with 10 μM nocodazole (Fig. 6E, F, and I; see also Movie S3 in the supplemental material).

An interesting feature of the shDyst1 cells was that many of the capsids formed small aggregates (arrowheads in Fig. 6D), although this was not the reason for the lack of movement, as tracking was carried out on individual capsids. Capsid aggregation is typically observed in cells infected with a virus lacking the UL37 gene (26, 27, 39, 40). Furthermore, capsid motion was shown to be very limited in cells infected with a UL37-null mutant of PrV (17). Indeed, HFFF2 cells infected with a UL37-null virus (vFRΔ37-VP26GFP) showed very similar behavior to shDyst1 cells infected with the parental virus. Both contained capsid aggregates, while individual capsids displayed essentially no motion (Fig. 6G to J; see also Movie S4 in the supplemental material). This similarity in behavior suggests that the effect of reducing dystonin levels is mimicking the absence of pUL37. This phenotype is different from what was observed in nocodazole-treated HFFF2 cells infected with vSR27-VP26GFP, where capsid motion was also absent, but capsids did not aggregate (Fig. 6E and F).

To determine whether the capsid aggregation and lack of mobility in shDyst1 cells could be caused by lack of pUL37, we checked whether pUL37 was present on capsids in dystonin-depleted cells. shControl or shDyst1 cells were infected for 30 h with vUL37GFP-VP26RFP, a virus with GFP fused to the C terminus of pUL37 and mRFP fused to the N terminus of the capsid protein VP26. As shown in Fig. 7, pUL37 was associated with capsids in both control and dystonin-depleted cells, confirming that the lack of capsid movement in the latter was not due to a lack of pUL37 on these capsids.

These results demonstrate that dystonin has a major role in capsid trafficking during egress.

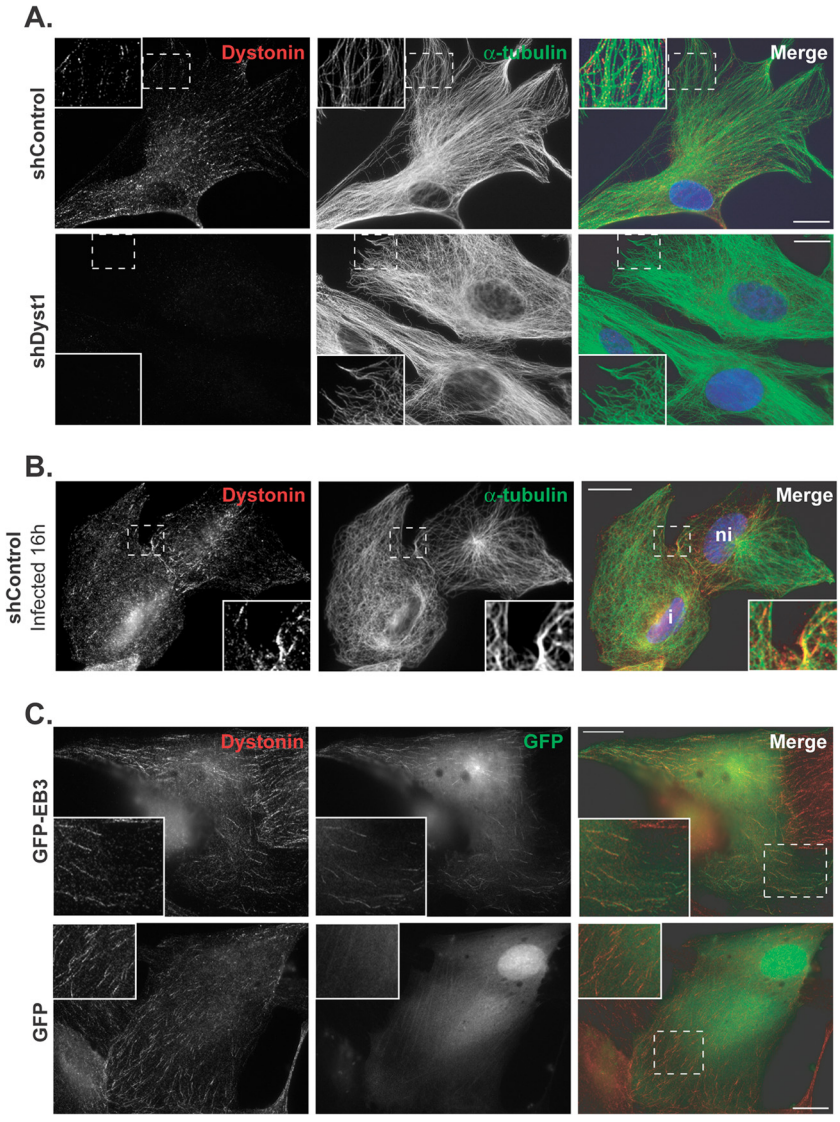

FIG 3 Dystonin localization in HFFF2 cells. (A) shControl or shDyst1 cells were fixed, and the distributions of dystonin (red) and alpha-tubulin (green) were determined using antibodies DST and GAR_{568} and DM1A and GAM_{488}, respectively. Identical exposure times were used to collect images of shControl and shDyst1 cells. (B) shControl cells were infected with vUL35RFP1D1, a virus that encodes a VP26 capsid protein fused to the mRFP. Sixteen hours postinfection, cells were fixed and stained as described above, except that secondary antibodies were GAR_{488} and GAM_{647}. Infected cells (i) were distinguished from noninfected cells (ni) through mRFP fluorescence (not shown). (C) HFFF2 cells were transfected with pGFP-hEB3, which encodes GFP fused to the plus-end-binding protein EB3 or with pEGFP-C1 as a control. Twenty-four hours after transfection, cells were fixed and immunostained for dystonin as described for panel A (red). GFP-EB3 and GFP are visualized through autofluorescence (green). An area from each cell image (dashed box) is enlarged. Scale bars, 20 μm.

Effect of dystonin silencing and of HSV-1 infection on microtubule and actin networks. HSV-1 has been reported to cause reorganization of the MT network at late stages of infection (37). In addition, dystonin can stabilize MTs by cross-linking them to the actin cytoskeleton (23). Therefore, a possible explanation for the effects we observed is that the combination of dystonin silencing and infection by HSV-1 destabilized the cytoskeleton, thereby preventing efficient capsid transport during egress.

To determine whether this was the case, shControl or shDyst1 HFFF2 cells were mock infected or infected with vSR27-VP26GFP for 24 h and then stained to reveal MTs and F-actin. As shown in Fig. 8A, treatment with 10 μM nocodazole for 1 h, which prevents capsid transport (Fig. 6E and I), caused most of the MTs to depolymerize, leaving only a small number of twisted filaments. In contrast, dystonin silencing did not disrupt the MT network in mock-infected cells, but it appeared to result in a denser pattern of MTs at the vicinity of the nucleus than that in shControl cells (Fig. 8B and C). Infection had a noticeable effect on the MT network in both shDyst1 and shControl cells, resulting in a more disorganized, less nuclear-centric arrangement, although the higher density of MTs observed in mock-infected shDyst1 cells was still apparent in infected shDyst1 cells (Fig. 8C).

Therefore, although the combination of dystonin silencing and infection may lead to a local reorganization of the MTs close to the nucleus, it does not cause the disruption of the MT network that is observed in cells treated with nocodazole.

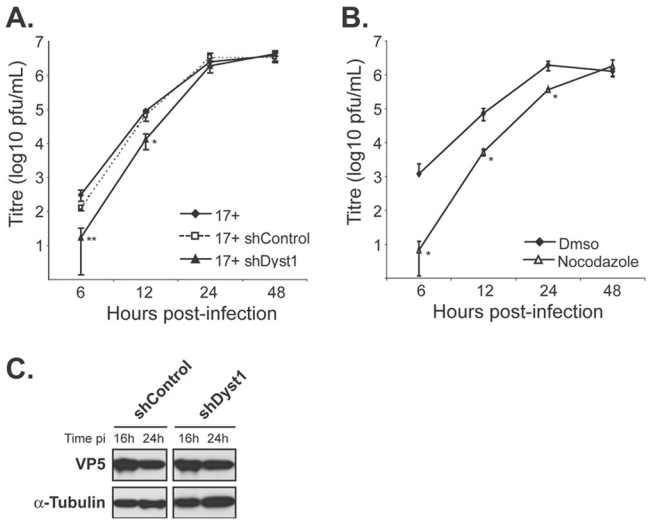

FIG 4 Growth kinetics of HSV-1 in the absence of dystonin or of MTs. Single-step growth curves of HSV-1 WT virus (17+) in control cells or cells silenced for dystonin (A) or in the presence or absence of nocodazole (B). (A) HFFF2 cells were transduced with shControl or shDyst1 shRNAs or untreated before being infected with 5 PFU/cell of HSV-1 17+. One hour after infection, the viral suspension was removed and cells were acid washed. At 6, 12, 24, or 48 h after infection, cells were scraped into the medium and pelleted. The supernatant was harvested and the titer of progeny virus was determined on Vero cells. (B) HFFF2 cells were incubated with 10 μM nocodazole 1 h before infection and all the time of infection (nocodazole) or not at all (DMSO). Infection and titration were done as described for panel A. Experiments were done in triplicate. Error bars indicate standard deviations of the mean (SDM). Asterisks indicate statistical differences with control conditions (17+ in untreated cells in panel A and DMSO condition in panel B) as determined by a paired Student *t* test (*, $P < 0.05$; **, $P < 0.01$). (C) Western blot analysis of lysates obtained from shControl or shDyst1 cells infected with 5 PFU/cell of 17+ for the indicated times (16 h or 24 h pi). The progress of infection was visualized using the DM165 antibody directed against the major capsid protein VP5, and alpha-tubulin levels were monitored as loading controls using the DM1A antibody.

Since dystonin localizes at plus-end tips of MTs (Fig. 3C), we looked at possible effects of dystonin depletion on MT plus-end dynamics. shControl or shDyst1 HFFF2 cells were transfected with a plasmid encoding EB3-GFP, and MT plus ends were tracked by live-cell microscopy (see Movie S5 in the supplemental material). This showed that MT plus-end dynamics were unaffected by dystonin depletion.

In summary, the striking reduction in capsid movement during egress observed in shDyst1 cells (Fig. 6) does not appear to result from disruption of the MT network or from an effect on MT plus-end dynamics.

DISCUSSION

In this paper, our aim was to identify cellular factors that could account for the efficient capsid trafficking seen in HSV-1-infected cells. Although it is clear that microtubules and their associated molecular motors are involved (6, 7, 9), the intermediates between the viral capsid and these motors, if any, were unknown. The inner tegument proteins pUL36 and pUL37 are strongly suspected as having important roles in capsid transport. For example, although pUL37 is dispensable for release of viral DNA into the nucleus of HSV-1-infected cells (27), PrV capsid translocation to the nucleus (16) and capsid trafficking during egress (17) are both impaired in its absence. Furthermore, *in vitro* studies have shown that HSV-1 capsids which are associated with inner tegument proteins bind to dynein, dynactin, and kinesin-1, whereas untegumented capsids do not (8). However, whether capsid transport requires direct interactions between motor proteins and particle components is unknown, and the role such interactions play in transport within infected cells remains to be determined.

The cellularprotein dystonin is an important element in cytoskeleton organization in skin, muscle, and neuron cells. It belongs to the plakin family (18) and, as such, contains a plakin domain, which is common to all known isoforms of dystonin and which, as we show here, is targeted by pUL37. It is possible that pUL37 may bind to other members of the plakin family, such as the closely related protein MACF/ACF7 (41, 42), although we have not examined this. One isoform of dystonin (BPAG1n4) was shown to have a role in retrograde transport in neurons through interactions with the $p150^{glued}$ subunit of dynactin (a cofactor of the dynein motor [24]) and retrolinkin, a component of vesicle membranes (43). More recently, dystonin has also been shown to be involved in anterograde transport of vesicles (25). The identification of dystonin as a binding partner for pUL37 in our Y2H assay therefore suggested a plausible role for this interaction in trafficking of

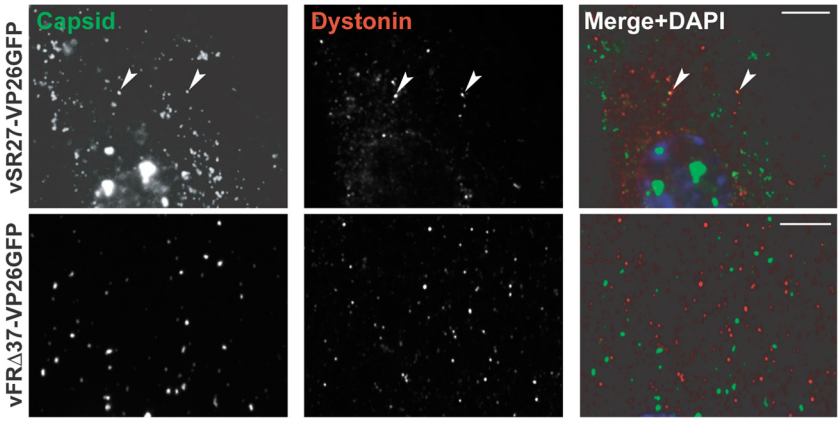

FIG 5 Capsid association with dystonin. HFFF2 cells were infected with 1 PFU/cell of vSR27-VP26GFP or vFRΔ37-VP26GFP. Sixteen hours later, cells were fixed and endogenous dystonin was visualized using specific antibodies DST and GAR_{568} (red). Capsids were visualized through autofluorescence (green). Arrowheads indicate capsids colocalizing with dystonin spots. Scale bars, 5 μm.

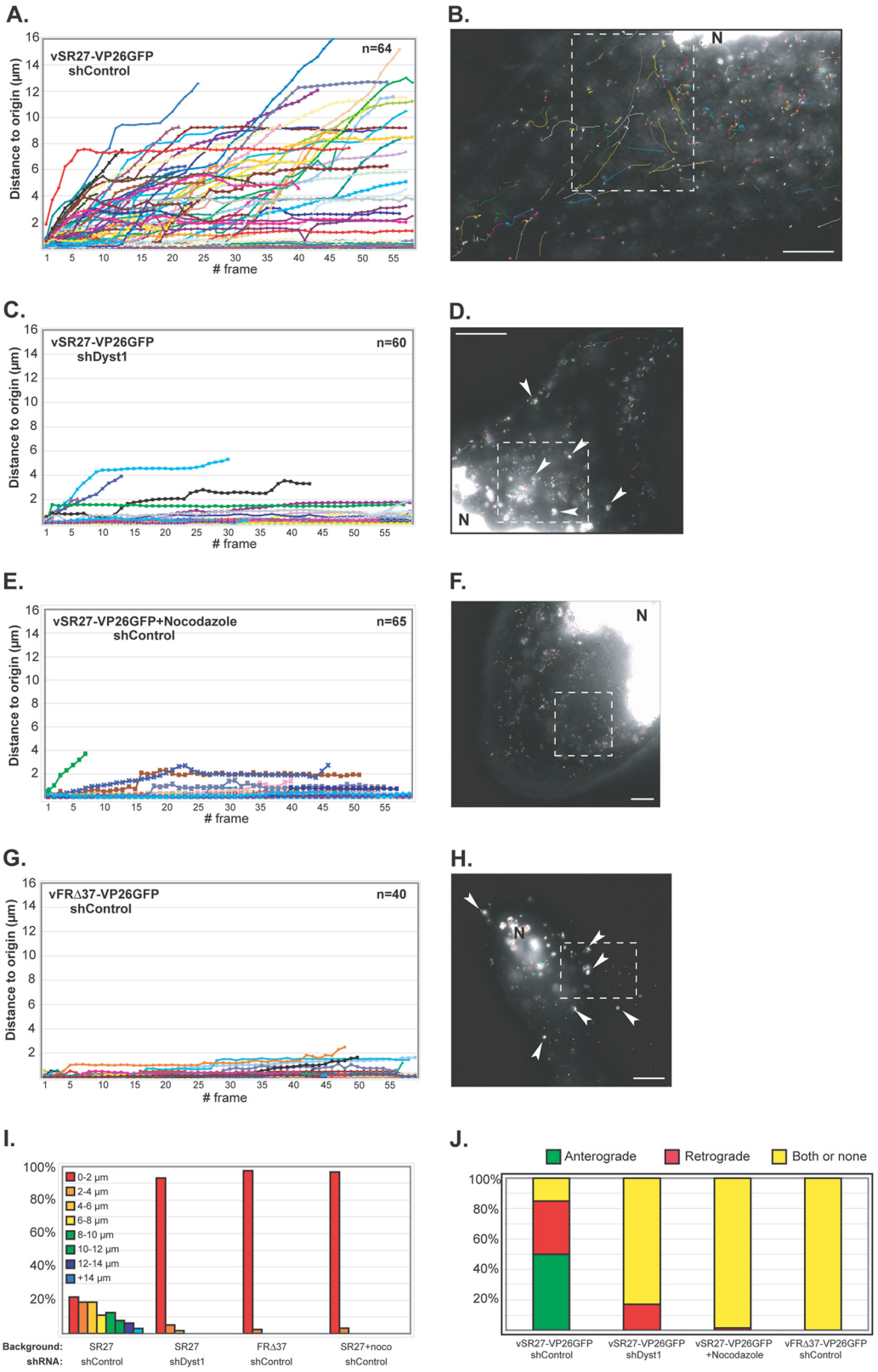

FIG 6 Impact of dystonin reduction on capsid transport during egress. HFFF2 cells transduced with shControl (A and B and E to H) or shDyst1 (C and D) were infected with one PFU/cell of vSR27-VP26GFP (A to F) or vFRΔ37-VP26GFP (G and H). Cytoplasmic capsid movements were monitored by live-cell imaging at 24 h postinfection, at a rate of one frame per second. Results are plotted as the distance to origin (in μm) for every individual capsid for each frame taken (A, C, E, and G). The premature truncation of some lines is due to the capsids moving out of the field of view. The slope of each line indicates capsid speed. A representative cell with all capsid trajectories from one movie per condition is shown (B, D, F, and H). Dashed boxes show the area displayed in the corresponding movie (see Movies S1, S2, S3, and S4, respectively). N, nucleus. Note the absence (B, F) or presence (arrowheads in D, H) of capsid aggregates. (I) Summary of the maximum distances to origin from the data shown in panels A to H as percentages of cells in categories of distance to origin. (J) Every moving capsid was tracked individually, and its directionality was estimated according to positions of the nucleus and the plasma membrane. "Both or none" indicates either a capsid having opposite directionalities within the same run or the absence of clear directionality. Scale bars, 10 μm.

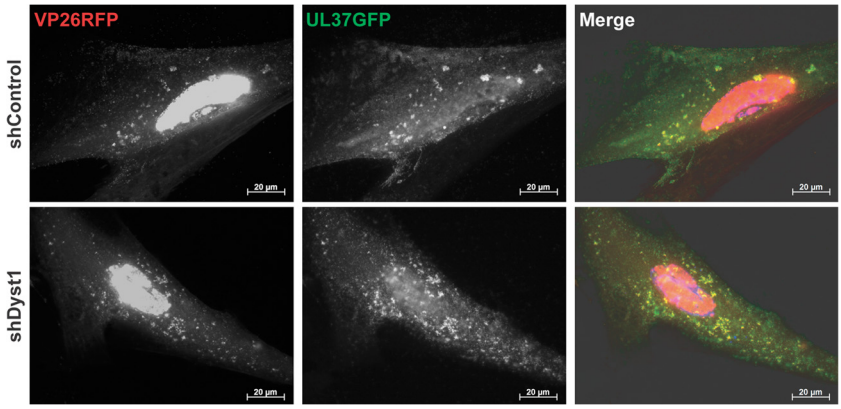

FIG 7 Association of pUL37 to capsids in shControl and shDyst1 cells. shControl or shDyst1 HFFF2 cells were infected with 5 PFU/cell of vUL37GFP-VP26RFP for 30 h before fixation. pUL37 was visualized through direct GFP fluorescence (green) and capsids through direct RFP fluorescence (red). Scale bars, 20 μm.

HSV-1 capsids. Efficient pUL37-dependent transport of capsids is necessary during egress for acquisition of the outer tegument and subsequent envelopment (17, 26, 39, 40), and capsid trafficking during egress was severely inhibited by dystonin shRNA treatment. The consequence for capsid transport of reducing the level of dystonin was equivalent to that seen in the absence of pUL37 or when the MT network was disrupted by the addition of nocodazole (Fig. 6).

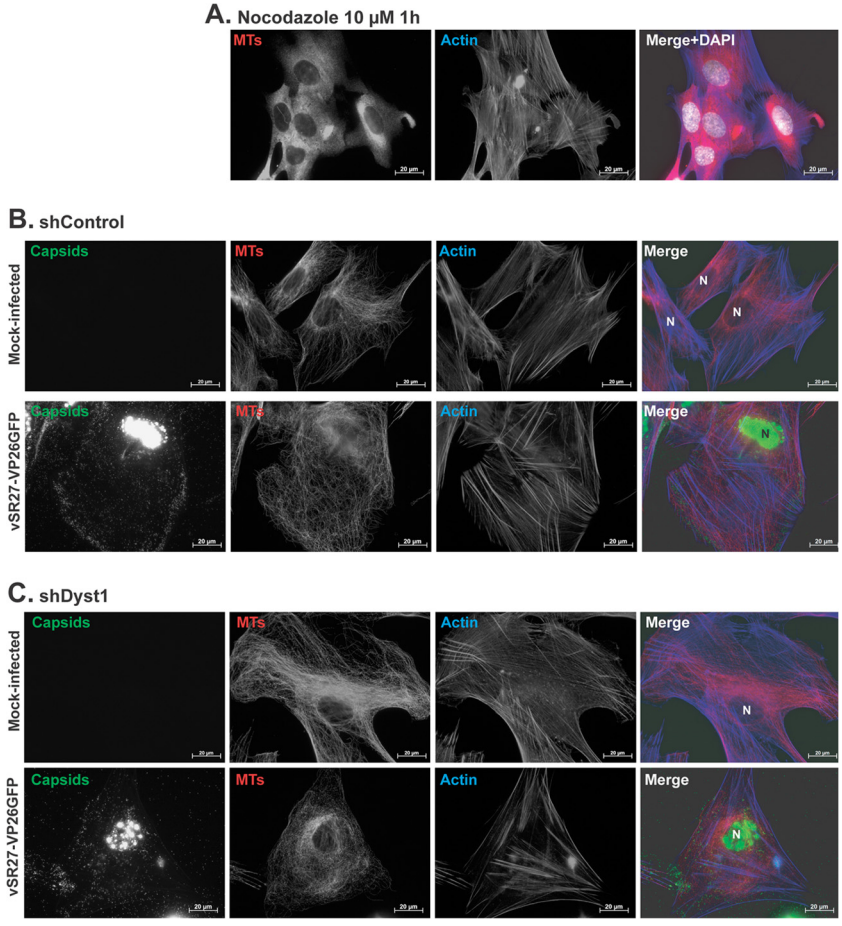

FIG 8 Effect of nocodazole, infection, and dystonin silencing on MT and actin networks. (A) HFFF2 cells were incubated with 10 μM nocodazole for 1 h before being fixed and stained with MAb DM1A against alpha-tubulin and GAM_{488} (pseudocolored in red) and with TRITC-conjugated phalloidin to label actin (blue). Nuclei were visualized with DAPI (white). shControl (B) or shDyst1 HFFF2 (C) cells were either mock infected or infected with 5 PFU/cell of vSR27-VP26GFP. Twenty-four hours later, cells were fixed and stained with MAb DM1A against alpha-tubulin and GAM_{633} (red) and with TRITC-conjugated phalloidin to label actin (blue). Capsids were visible through direct GFP fluorescence (green). N, nucleus. Scale bars, 20 μm.

It is significant that despite the almost total block on capsid movement during virus egress resulting either from depletion of dystonin or from MT disruption, production of infectious virus eventually reached normal levels (Fig. 4). However, in both cases, virus production was delayed. This is consistent with previous studies which have shown that MT transport is important for increasing the efficiency of infection (37) but that alternative transport mechanisms for capsids exist if the MT network is disabled, for example, the actin cytoskeleton (17). It is also possible that some MTs are stabilized by infection and therefore more resistant to nocodazole treatment, as was shown previously (44).

During egress, it is likely that the greater part of capsid movement from the nucleus to the site of secondary envelopment occurs through plus-end-directed transport. Therefore, the inhibition of capsid transport during egress following reduction of dystonin levels (Fig. 6) is probably indicative of a role for the dystonin-pUL37 interaction in plus-end-directed transport. It is notable, therefore, that our analysis of dystonin distribution within cells showed that it preferentially colocalized with the MT plus-end-binding protein, EB3 (Fig. 3). This is consistent with the presence of an SxIP EB1-binding motif (45) in the microtubule-binding domain of dystonin (MTBD in Fig. 1). Interestingly, a recent study demonstrated that Shot (the *Drosophila* orthologue of spectraplakin proteins) also associates with the plus end of MTs through an interaction with the plus-end-binding protein EB1 (46). We are currently investigating whether plus-end-directed transport of capsids is also affected during virus entry.

In the course of this study, the interaction domain of pUL37 with dystonin was mapped to residues 578 to 899 (Fig. 1). We were not able to investigate the importance of the interaction in virus infection by deleting this region, as it is known to be important for the essential interaction of pUL37 with pUL36 (47, 48). Therefore, we attempted to define the interaction domain more accurately by random mutagenesis. However, although we were able to identify residues which abolished the interaction of full-length pUL37 with dystonin (but not with pUL36) in Y2H, these were in regions of the protein important for other interactions, indicating that this portion of pUL37 contains multiple binding sites (data not shown).

A well-described phenotype of UL37-null mutants of HSV-1 and PrV is the aggregation of capsids in the cytoplasm of infected cells (26, 27, 39, 40). This phenotype is very similar to what we observed in dystonin-depleted cells, where aggregation occurred even though pUL37 was present on the capsids (Fig. 7). Therefore, preventing the interaction of pUL37 and dystonin appears to mimic the effect of removing pUL37 altogether, indicating the importance of this interaction for pUL37 function.

The mechanism of action of the pUL37-dystonin interaction remains to be elucidated. Dystonin appears to have several functions in the cell. It has been shown to interact with the MT-associated protein 1 (MAP1) to support MT stability through tubulin acetylation and is also important for maintaining TGN integrity (25). However, we did not observe any obvious defect in MT organization or stability in our shDyst cells (Fig. 8), and although TGN fragmentation occurred in shDyst cells (data not shown), it is also a common consequence of HSV-1 infection (37). Therefore, these effects appear unlikely to be the cause of the defect in capsid transport observed in dystonin-depleted cells. A more intriguing possibility is that dystonin acts as a linker between HSV-1 capsids and molecular motors, as was suggested to be the case with neuronal vesicles (24, 43). By nature, this interaction would be expected to be transient and could explain the low frequency of colocalization observed between capsids and endogenous dystonin in infected cells (Fig. 5). Such a linker role would account for both the effects of dystonin depletion described in this paper and for the properties of UL37-null mutants. Further investigation into the mechanism of action of the pUL37-dystonin interaction would shed light not only on herpesvirus capsid transport but also on the role of dystonin in cellular mechanisms of transport.

ACKNOWLEDGMENTS

We thank Y. Gaudin for critical reading of the manuscript. We are grateful to H. Raux for advice with the yeast two-hybrid screen and the gift of the PC12 cDNA library. We are indebted to P. Desai (John Hopkins University) for the plasmid pK26GFP, to John Victor Small (Institute of Molecular Biotechnology, Vienna, Austria) for pGFP-hEB3, and to the following from the CVR, Glasgow: R. Everett for silencing plasmids, E. Palmer for the plasmid pCMV10-HA-UL32, and V. Preston and C. Cunningham for BACmid SR27.

REFERENCES

1. **Bartolini F, Gundersen GG.** 2006. Generation of noncentrosomal microtubule arrays. J. Cell Sci. **119**:4155–4163.
2. **Bornens M.** 2002. Centrosome composition and microtubule anchoring mechanisms. Curr. Opin. Cell Biol. **14**:25–34.
3. **Caviston JP, Holzbaur EL.** 2006. Microtubule motors at the intersection of trafficking and transport. Trends Cell Biol. **16**:530–537.
4. **Antinone SE, Smith GA.** 2010. Retrograde axon transport of herpes simplex virus and pseudorabies virus: a live-cell comparative analysis. J. Virol. **84**:1504–1512.
5. **Lyman MG, Enquist LW.** 2009. Herpesvirus interactions with the host cytoskeleton. J. Virol. **83**:2058–2066.
6. **Mabit H, Nakano MY, Prank U, Saam B, Dohner K, Sodeik B, Greber UF.** 2002. Intact microtubules support adenovirus and herpes simplex virus infections. J. Virol. **76**:9962–9971.
7. **Sodeik B, Ebersold MW, Helenius A.** 1997. Microtubule-mediated transport of incoming herpes simplex virus 1 capsids to the nucleus. J. Cell Biol. **136**:1007–1021.
8. **Radtke K, Kieneke D, Wolfstein A, Michael K, Steffen W, Scholz T, Karger A, Sodeik B.** 2010. Plus- and minus-end directed microtubule motors bind simultaneously to herpes simplex virus capsids using different inner tegument structures. PLoS Pathog. **6**:e1000991. doi:10.1371/journal.ppat.1000991.
9. **Dohner K, Wolfstein A, Prank U, Echeverri C, Dujardin D, Vallee R, Sodeik B.** 2002. Function of dynein and dynactin in herpes simplex virus capsid transport. Mol. Biol. Cell **13**:2795–2809.
10. **Miranda-Saksena M, Boadle RA, Aggarwal A, Tijono B, Rixon FJ, Diefenbach RJ, Cunningham AL.** 2009. Herpes simplex virus utilizes the large secretory vesicle pathway for anterograde transport of tegument and envelope proteins and for viral exocytosis from growth cones of human fetal axons. J. Virol. **83**:3187–3199.
11. **Dohner K, Nagel CH, Sodeik B.** 2005. Viral stop-and-go along microtubules: taking a ride with dynein and kinesins. Trends Microbiol. **13**:320–327.
12. **Wolfstein A, Nagel CH, Radtke K, Dohner K, Allan VJ, Sodeik B.** 2006. The inner tegument promotes herpes simplex virus capsid motility along microtubules *in vitro*. Traffic **7**:227–237.
13. **Aggarwal A, Miranda-Saksena M, Boadle RA, Kelly BJ, Diefenbach RJ, Alam W, Cunningham AL.** 2012. Ultrastructural visualization of individual tegument protein dissociation during entry of herpes simplex virus 1 into human and rat dorsal root ganglion neurons. J. Virol. **86**:6123–6137.
14. **Granzow H, Klupp BG, Mettenleiter TC.** 2005. Entry of pseudorabies virus: an immunogold-labeling study. J. Virol. **79**:3200–3205.
15. **Luxton GW, Haverlock S, Coller KE, Antinone SE, Pincetic A, Smith GA.** 2005. Targeting of herpesvirus capsid transport in axons is coupled to association with specific sets of tegument proteins. Proc. Natl. Acad. Sci. U. S. A. **102**:5832–5837.

16. **Krautwald M, Fuchs W, Klupp BG, Mettenleiter TC.** 2009. Translocation of incoming pseudorabies virus capsids to the cell nucleus is delayed in the absence of tegument protein pUL37. J. Virol. **83**:3389–3396.
17. **Luxton GW, Lee JI, Haverlock-Moyns S, Schober JM, Smith GA.** 2006. The pseudorabies virus VP1/2 tegument protein is required for intracellular capsid transport. J. Virol. **80**:201–209.
18. **Leung CL, Green KJ, Liem RK.** 2002. Plakins: a family of versatile cytolinker proteins. Trends Cell Biol. **12**:37–45.
19. **Roper K, Gregory SL, Brown NH.** 2002. The 'spectraplakins': cytoskeletal giants with characteristics of both spectrin and plakin families. J. Cell Sci. **115**:4215–4225.
20. **Young KG, Kothary R.** 2007. Dystonin/Bpag1—a link to what? Cell Motil. Cytoskeleton **64**:897–905.
21. **Leung CL, Zheng M, Prater SM, Liem RK.** 2001. The BPAG1 locus: alternative splicing produces multiple isoforms with distinct cytoskeletal linker domains, including predominant isoforms in neurons and muscles. J. Cell Biol. **154**:691–697.
22. **Brown A, Bernier G, Mathieu M, Rossant J, Kothary R.** 1995. The mouse dystonia musculorum gene is a neural isoform of bullous pemphigoid antigen 1. Nat. Genet. **10**:301–306.
23. **Yang Y, Bauer C, Strasser G, Wollman R, Julien JP, Fuchs E.** 1999. Integrators of the cytoskeleton that stabilize microtubules. Cell **98**: 229–238.
24. **Liu JJ, Ding J, Kowal AS, Nardine T, Allen E, Delcroix JD, Wu C, Mobley W, Fuchs E, Yang Y.** 2003. BPAG1n4 is essential for retrograde axonal transport in sensory neurons. J. Cell Biol. **163**:223–229.
25. **Ryan SD, Bhanot K, Ferrier A, De Repentigny Y, Chu A, Blais A, Kothary R.** 2012. Microtubule stability, Golgi organization, and transport flux require dystonin-a2-MAP1B interaction. J. Cell Biol. **196**:727–742.
26. **Pasdeloup D, Beilstein F, Roberts AP, McElwee M, McNab D, Rixon FJ.** 2010. Inner tegument protein pUL37 of herpes simplex virus type 1 is involved in directing capsids to the trans-Golgi network for envelopment. J. Gen. Virol. **91**:2145–2151.
27. **Roberts AP, Abaitua F, O'Hare P, McNab D, Rixon FJ, Pasdeloup D.** 2009. Differing roles of inner tegument proteins pUL36 and pUL37 during entry of herpes simplex virus type 1. J. Virol. **83**:105–116.
28. **Desai P, Person S.** 1998. Incorporation of the green fluorescent protein into the herpes simplex virus type 1 capsid. J. Virol. **72**:7563–7568.
29. **Pasdeloup D, Blondel D, Isidro AL, Rixon FJ.** 2009. Herpesvirus capsid association with the nuclear pore complex and viral DNA release involve the nucleoporin CAN/Nup214 and the capsid protein pUL25. J. Virol. **83**:6610–6623.
30. **Vielkind U, Swierenga SH.** 1989. A simple fixation procedure for immunofluorescent detection of different cytoskeletal components within the same cell. Histochemistry **91**:81–88.
31. **Sbalzarini IF, Koumoutsakos P.** 2005. Feature point tracking and trajectory analysis for video imaging in cell biology. J. Struct. Biol. **151**:182–195.
32. **Everett RD, Rechter S, Papior P, Tavalai N, Stamminger T, Orr A.** 2006. PML contributes to a cellular mechanism of repression of herpes simplex virus type 1 infection that is inactivated by ICP0. J. Virol. **80**:7995–8005.
33. **Raux H, Flamand A, Blondel D.** 2000. Interaction of the rabies virus P protein with the LC8 dynein light chain. J. Virol. **74**:10212–10216.
34. **McGeoch DJ, Dalrymple MA, Davison AJ, Dolan A, Frame MC, McNab D, Perry LJ, Scott JE, Taylor P.** 1988. The complete DNA sequence of the long unique region in the genome of herpes simplex virus type 1. J. Gen. Virol. **69**(Part 7):1531–1574.
35. **Kapur M, Wang W, Maloney MT, Millan I, Lundin VF, Tran TA, Yang Y.** 2012. Calcium tips the balance: a microtubule plus end to lattice binding switch operates in the carboxyl terminus of BPAG1n4. EMBO Rep. **13**:1021–1029.
36. **Guo L, Degenstein L, Dowling J, Yu QC, Wollmann R, Perman B, Fuchs E.** 1995. Gene targeting of BPAG1: abnormalities in mechanical strength and cell migration in stratified epithelia and neurologic degeneration. Cell **81**:233–243.
37. **Avitabile E, Di Gaeta S, Torrisi MR, Ward PL, Roizman B, Campadelli-Fiume G.** 1995. Redistribution of microtubules and Golgi apparatus in herpes simplex virus-infected cells and their role in viral exocytosis. J. Virol. **69**:7472–7482.
38. **Nakagawa H, Koyama K, Murata Y, Morito M, Akiyama T, Nakamura Y.** 2000. EB3, a novel member of the EB1 family preferentially expressed in the central nervous system, binds to a CNS-specific APC homologue. Oncogene **19**:210–216.
39. **Desai P, Sexton GL, McCaffery JM, Person S.** 2001. A null mutation in the gene encoding the herpes simplex virus type 1 UL37 polypeptide abrogates virus maturation. J. Virol. **75**:10259–10271.
40. **Klupp BG, Granzow H, Mundt E, Mettenleiter TC.** 2001. Pseudorabies virus UL37 gene product is involved in secondary envelopment. J. Virol. **75**:8927–8936.
41. **Kodama A, Karakesisoglou I, Wong E, Vaezi A, Fuchs E.** 2003. ACF7: an essential integrator of microtubule dynamics. Cell **115**:343–354.
42. **Leung CL, Sun D, Zheng M, Knowles DR, Liem RK.** 1999. Microtubule actin cross-linking factor (MACF): a hybrid of dystonin and dystrophin that can interact with the actin and microtubule cytoskeletons. J. Cell Biol. **147**:1275–1286.
43. **Liu JJ, Ding J, Wu C, Bhagavatula P, Cui B, Chu S, Mobley WC, Yang Y.** 2007. Retrolinkin, a membrane protein, plays an important role in retrograde axonal transport. Proc. Natl. Acad. Sci. U. S. A. **104**:2223–2228.
44. **Elliott G, O'Hare P.** 1998. Herpes simplex virus type 1 tegument protein VP22 induces the stabilization and hyperacetylation of microtubules. J. Virol. **72**:6448–6455.
45. **Honnappa S, Gouveia SM, Weisbrich A, Damberger FF, Bhavesh NS, Jawhari H, Grigoriev I, van Rijssel FJ, Buey RM, Lawera A, Jelesarov I, Winkler FK, Wuthrich K, Akhmanova A, Steinmetz MO.** 2009. An EB1-binding motif acts as a microtubule tip localization signal. Cell **138**: 366–376.
46. **Alves-Silva J, Sanchez-Soriano N, Beaven R, Klein M, Parkin J, Millard TH, Bellen HJ, Venken KJ, Ballestrem C, Kammerer RA, Prokop A.** 2012. Spectraplakins promote microtubule-mediated axonal growth by functioning as structural microtubule-associated proteins and EB1-dependent +TIPs (tip interacting proteins). J. Neurosci. **32**:9143–9158.
47. **Bucks MA, Murphy MA, O'Regan KJ, Courtney RJ.** 2011. Identification of interaction domains within the UL37 tegument protein of herpes simplex virus type 1. Virology **416**:42–53.
48. **Kelly BJ, Mijatov B, Fraefel C, Cunningham AL, Diefenbach RJ.** 2012. Identification of a single amino acid residue which is critical for the interaction between HSV-1 inner tegument proteins pUL36 and pUL37. Virology **422**:308–316.

Publication #5

Dystonin/BPAG1 promotes plus-end-directed transport of herpes simplex virus 1 capsids on microtubules during entry.

McElwee M, Beilstein F, Labetoulle M, Rixon FJ, Pasdeloup D.

JVI Journals.ASM.org

Dystonin/BPAG1 Promotes Plus-End-Directed Transport of Herpes Simplex Virus 1 Capsids on Microtubules during Entry

Marion McElwee,[a] Frauke Beilstein,[b] Marc Labetoulle,[b] Frazer J. Rixon,[a] David Pasdeloup[a,b]

MRC-University of Glasgow Centre for Virus Research, Glasgow, United Kingdom[a]; Laboratoire de Virologie Moléculaire et Structurale, CNRS, Gif-Sur-Yvette, France[b]

During infection by herpes simplex virus 1 (HSV-1), the viral capsid is transported around the cytoplasm along the microtubule (MT) network. Although molecular motors have been implicated in this process, the composition of the molecular machinery required for efficient directional transport is unknown. We previously showed that dystonin (BPAG1) is recruited to HSV-1 capsids by the capsid-bound tegument protein pUL37 to promote efficient cytoplasmic transport of capsids during egress. Dystonin is a cytoskeleton cross-linker which localizes at MT plus ends and has roles in retrograde and anterograde transport in neurons. In this study, we investigated the role of dystonin during the entry stages of HSV-1 infection. Because of the way in which the MT network is organized, capsids are required to change their direction of motion along the MTs as they travel from the point of entry to the nucleus, where replication takes place. Thus, capsids first travel to the centrosome (the principal microtubule organizing center) by minus-end-directed transport and then switch polarity and travel to the nucleus by plus-end-directed transport. We observed that transport of capsids toward the centrosome was slowed, but not blocked, by dystonin depletion. However, transport of capsids away from the centrosome was significantly impaired, causing them to accumulate in the vicinity of the centrosome and reducing the numbers reaching the nucleus. We conclude that, during entry of HSV-1, dystonin has a specific role in plus-ended transport of capsids from the centrosome to the nucleus.

A successful outcome of infection demands precise control of particle movement around the cell. The cell has a number of transport mechanisms available, but the most important for herpesviruses is the microtubule (MT) network (1, 2), which is the main route of movement between the cell surface, where virus entry and exit take place, and the nucleus, which is the site of virus transcription, DNA replication, and capsid assembly. The MT network is typically organized around one or more microtubule-organizing centers (MTOCs), with the MT minus ends anchored at the MTOC and the plus ends radiating outwards (3). Because of this arrangement, a herpesvirus capsid has to switch polarity in order to travel from the plasma membrane to the nucleus. Thus, the capsids travel from the plasma membrane to the centrosome (the principal MTOC in most cell types) by minus-end-directed transport but must then transfer to another MT to complete its journey by plus-end-directed transport. The direction of transport along MTs is determined by the molecular motors that transport the cargo. These are of two basic types, kinesins and dynein, which carry out plus-end- and minus-end-directed transport, respectively. Association of herpes simplex virus 1 (HSV-1) capsids with molecular motors, such as dynein or kinesins, has been reported *in vitro* (4), and kinesin 3 interaction with the viral membrane protein pUs9 was shown to be important for anterograde transport of pseudorabies virus (PrV) capsids in neurons (5). Two other viral proteins that are known to have important roles in herpesvirus capsid transport are the inner tegument proteins pUL36 and pUL37, two proteins interacting with each other (6) and essential for growth of HSV-1 (7, 8). Unlike most tegument proteins, these two remain attached to the capsid during transport to the nucleus (9–12). pUL36 has been shown to interact with the dynein/dynactin motor complex in transfected cells (13) and is required for active capsid transport and nuclear targeting (14–19). pUL37 was also found to have a role in efficient capsid transport during entry (20) and egress (16, 21). In previous studies, we showed that the MT-binding protein dystonin (BPAG1) is recruited to capsids via pUL37 and is required for efficient transport of HSV-1 capsids during virus egress (22). In this study, we extended our analysis to look at the role of dystonin during virus entry. Live-cell imaging of cells depleted of dystonin showed that dystonin is not required for minus-end-directed transport of capsids from the sites of entry to the centrosome. However, it plays an important role in plus-end-directed transport of capsids from the centrosome to the nucleus.

MATERIALS AND METHODS

Cells and viruses. 293T, baby hamster kidney (BHK), and human fetal foreskin fibroblast 2 (HFFF2) cells were grown at 37°C in Dulbecco's modified Eagle medium (DMEM; PAA Laboratories) supplemented with 8% fetal calf serum (FCS). For live-cell microscopy studies, cells were grown on 35-mm ibidi petri dishes.

Wild-type (WT) HSV-1 (strain 17^+), vSR27-VP26GFP (expressing a green fluorescent protein [GFP]-tagged capsid protein), and tsK/luci (provided by C. Preston) were propagated on BHK cells infected at 0.01 PFU per cell, and virions were concentrated from the medium supernatant by centrifugation at 15,000 × *g* for 2 h. The tsK/luci virus was generated as described earlier (23). As the tsK virus has a temperature-sensitive lesion in the ICP4 protein that is not relevant to our studies, all experiments using this virus were performed at the permissive temperature for this mutant (31°C). vSR27-VP26GFP was generated as described in reference 22.

Antibodies. The following antibodies were used. Mouse anti-alpha-tubulin clone DM1A and mouse anti-gamma-tubulin clone GTU-88 were

Received 14 June 2013 Accepted 26 July 2013

Published ahead of print 31 July 2013

Address correspondence to David Pasdeloup, pasdeloup@vms.cnrs-gif.fr.

Supplemental material for this article may be found at http://dx.doi.org/10.1128/JVI.01633-13.

doi:10.1128/JVI.01633-13

obtained from Sigma. In Fig. 2 and 6, capsids were visualized using the rabbit purified HSV-1 nuclear C capsid (PTNC) antibody (23). Mouse anti-ICP0 11060 antibody was from Santa Cruz Biotechnology. Mouse DM165 antibody against VP5 was described previously (24); mouse monoclonal antibody (MAb) 4846 against glycoprotein D (gD) was a gift of A. Cross (University of Glasgow). Alexa Fluor 488- or Alexa Fluor 568-conjugated goat anti-mouse antibodies (GAM_{488} and GAM_{568}, respectively) and Alexa Fluor 568-conjugated goat anti-rabbit antibody (GAR_{568}) were obtained from Molecular Probes. Goat anti-mouse Dylight680 was obtained from Cell Signaling.

shRNA. The use of lentiviruses expressing short hairpin RNA (shRNA) directed against dystonin has been described previously (23, 25). Silencing of dystonin was done using the sequence GTGTTGAAAGCCA TTTAGA (shDyst). This sequence (position 1897 on the murine open reading frame) corresponds to the plakin domain of human and murine dystonin and is common to all known isoforms of dystonin. It is not conserved within sequences of other known plakin proteins. The control corresponded to an shRNA sequence specific for the luciferase gene (shControl; GTGCGTTGCTAGTACCAAC) for all experiments except the luciferase experiments, where an shRNA construct specific for GFP (shGFP; GAGTACAACTACAACAGCC) was used. Silencing efficiency was routinely assessed by real-time reverse transcription-PCR from total RNA before every experiment, as described in reference 22.

Western blotting and quantification. Cells transduced with the shControl or shDyst1 lentivirus (here referred to as shControl and shDyst cells, respectively) were infected with 5 PFU/cell of HSV-1 WT for 2 h, 4 h, 7 h, 12 h, or 16 h before being harvested and lysed directly with Laemmli buffer. Cell lysates were analyzed by Western blotting using antibodies 11060 and DM165 against ICP0 and VP5, respectively. Antibody DM1A against alpha-tubulin was used as a loading control. Western blots were visualized and quantified using the quantitative near-infrared fluorescent Dylight680-conjugated GAM secondary antibody and an Odyssey Imaging system (LI-COR). Quantification was performed using Image Studio software (version 1.1.7; LI-COR).

Virus penetration assay. shControl and shDyst HFFF2 cells were incubated with gradient-purified vSR27-VP26GFP virions for 1 h at 4°C or for 2 h at 37°C. The cells were then fixed with 4% paraformaldehyde and labeled for gD with MAb 4846 and GAM_{568}. Capsids were visualized through GFP fluorescence, and nuclei were visualized with DAPI (4′,6-diamidino-2-phenylindole). The total numbers of capsids present on randomly chosen cells were determined by counting the number of diffraction-limited green spots, and the proportion having envelopes was determined by colocalization between GFP (capsid) and Alexa Fluor 568 (envelope) signals. Counting was done using the Cell Counter plug-in of ImageJ software (version 1.47m).

Fluorescence microscopy. Immunofluorescence that included tubulin staining was done as follows. Cells were fixed in a mix of 3.7% formaldehyde and 0.1% Triton X-100 in PEM buffer (100 mM PIPES [piperazine-*N*,*N*′-bis(2-ethanesulfonic acid)], 5 mM EGTA, 2 mM $MgCl_2$, pH 6.8) for 5 min at room temperature, as described by Vielkind and Swierenga (26). Microtubules were stained using MAb DM1A against alpha-tubulin (Sigma) and GAM_{568} antibody (90 min for each incubation).

To visualize centrosomes, cells were fixed with −20°C methanol and incubated at −20°C for 5 min. The methanol was removed, and cells were left to dry before being rehydrated with phosphate-buffered saline. Centrosomes were stained using MAb GTU-88 against gamma-tubulin (Sigma) and GAM_{488}. Capsids were stained using the rabbit antibody PTNC (23) and GAR_{568}.

Samples were mounted in ImmuMount mounting agent (Thermo) containing 1 μg/ml DAPI dihydrochloride (Sigma) for DNA staining. All samples were visualized using a Zeiss Axio Observer Z1 microscope with a ×63 Plan-Apochromat oil-immersion objective (numerical aperture, 1.4; Zeiss).

Live-cell microscopy. All live-cell microscopy was done at room temperature (~23°C). Under these conditions, capsid motion is slower, thereby allowing more efficient tracking, as detailed previously (22). Movies were recorded at a rate of 1 frame/s for 55 to 60 s with an average exposure time of 200 ms, except for centrosome-based movies (see Movies S3 and S4 in the supplemental material), where acquisition was for 120 s at a 1-frame/s rate.

Capsid tracking. Capsid tracking was done as described in reference 22. Briefly, movies were imported into ImageJ (version 1.47m). Capsids were tracked using the Particles Detector & Tracker plug-in (version 1.5) (27). Depending on the quality of each individual movie, detection parameters were set as follows: radius, 3 or 5; cutoff, 3.0 or 0.0; percentile, 0.6 to 1.5%. Linking parameters were a link range of 2 and a displacement of 10 to 20. Capsid motion was analyzed using the coordinates provided by the software to calculate the distance to the origin. Capsid tracking starts as the capsid enters the field of view and stops as it leaves it or when it moves out of focus. The directionality of each trajectory was estimated according to the position of the nucleus (see Fig. 5). A capsid which, over the period of the recording, moved away from the cell periphery and toward the nucleus was categorized as having retrograde motion, a capsid that moved away from the nucleus and toward the cell periphery was categorized as having anterograde motion, and capsids with no movement or no clear directionality were categorized as "none or both."

Luciferase assay. Replicate monolayers of HFFF2 cells were infected with 5 PFU/cell of tsK/luci and incubated at 31°C for the times required. Luciferase assays were performed using a luciferase assay system (Promega) according to the manufacturer's instructions. Luciferase activity was assessed on a Glomax 20/20 luminometer (Promega) and normalized to the cell count.

Fluorescence-activated cells sorter (FACS) analysis. shControl or shDyst HFFF2 cells were infected with 5 PFU/cell of WT HSV-1 for 2 h, 4 h, or 6 h at 37°C. They were then harvested, fixed with 4% paraformaldehyde, and permeabilized with 0.1% Triton X-100. Cells were incubated with antibody 11060 against ICP0 and GAM_{488} for 1 h at room temperature and washed three times. Mock-infected shControl cells were similarly treated and were used as negative controls. Data were collected on an Accuri C6 flow cytometer (BD) mounted with a 20-mW 488-nm solid-state blue laser and a 533/30-nm optical filter. Data were analyzed using Accuri C6 software (version 1.0.264.21).

RESULTS

Initiation of infection is delayed in dystonin-depleted cells. Using shRNA technology, we previously demonstrated that the levels of dystonin mRNA could be depleted by up to 80% in cells transduced with the shDyst1 lentivirus (shDyst cells) compared to the level in cells transduced with a control lentivirus (22). In shDyst cells, virus production was significantly delayed compared to that in control cells. Part of this delay could be explained by the severe defect in capsid egress observed in dystonin-depleted cells (22). To determine whether dystonin depletion also affected entry, shGFP (negative control) and shDyst cells were infected with tsK/luci, which encodes a luciferase gene under the control of a viral immediate early promoter. Cells were infected with 5 PFU/cell of tsK/luci for 2 h, 4 h, or 7 h postinfection (p.i.) and luciferase activity was monitored. As shown in Fig. 1, luciferase levels in shDyst cells (192 ± 9) were more than 15-fold lower than those in shGFP cells (3135 ± 230) at 2 h p.i. and corresponded to background levels (138 ± 97). At 4 h p.i., luciferase levels had increased only slightly in shDyst cells (365 ± 20) and were ~330-fold lower than those in shGFP cells (120,639 ± 15,385). At 7 h p.i., luciferase levels in shDyst cells were higher (5,707 ± 1,113) but were still more than 2.5 $\log_{10}$ units lower than those in shGFP cells (1,522,604 ± 8,383). The rate of increase in luciferase levels at between 4 and 7 h p.i. in shDyst cells paralleled that in shGFP cells

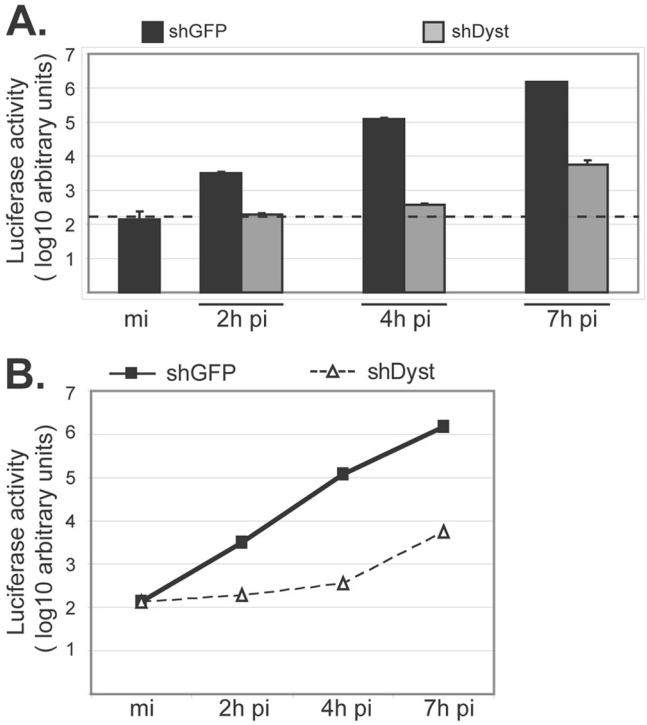

FIG 1 Initiation of HSV-1 replication in dystonin-depleted and control cells. (A) shGFP or shDyst HFFF2 cells were infected with 5 PFU/cell of tsK/luci and incubated for 2 h, 4 h, or 7 h at a permissive temperature (31°C). Cells were then harvested and lysed and luciferase activity was measured. Dashed line, background level. (B) Data shown in panel A are represented as a graph to show the rate of increase in luciferase levels with time after infection. mi, mock infected.

at between 0 and 2 h p.i. (Fig. 1B), suggesting that dystonin depletion affects the initiation of infection and not a later step.

To confirm these results, shControl and shDyst cells were infected with 1 PFU/cell of WT virus, and the levels of expression of the immediate early gene RL2, encoding the protein ICP0, and the late gene UL19, encoding the major capsid protein VP5, were monitored by Western blotting (Fig. 2A). ICP0 could be clearly detected in shControl cells as early as 4 h p.i. and at increasing levels until the latest time (16 h) analyzed. In contrast, ICP0 was first detected in small amounts in shDyst cells at 7 h p.i., and its level then increased rapidly to reach a level similar to that in shControl cells by 16 h. Expression of VP5 presented a similar pattern, although with late gene expression kinetics. Thus, VP5 was present from 7 h p.i. in shControl cells but was first detected at 12 h p.i. in shDyst cells. As with ICP0, the amounts of VP5 in shDyst cells had reached the level of that in shControl cells by 16 h p.i. Similar results were obtained with cells infected with 3 or 5 PFU/cell, but only a very moderate effect was observed with 50 PFU/cell (data not shown).

Immunofluorescence analysis of cells infected with 1 PFU/cell of HSV-1 WT showed behavior similar to that described above, where only ~2% of shDyst cells but nearly half of shControl cells were assessed to be positive for ICP0 by 3 h after infection (Fig. 2B). To quantify this effect, we carried out FACS analysis. ShControl or shDyst cells were mock infected or infected with HSV-1 WT for 2 h, 4 h, or 6 h. Cells were then fixed, permeabilized, stained for ICP0, and analyzed by flow cytometry. At 2 h, ~13% of shControl cells had a detectable amount of ICP0, while at 4 h and 7 h, the percentages had increased to 38% and 47%, respectively. In comparison, ICP0 expression was greatly reduced in shDyst cells, where 0%, 4%, and 7% of cells were ICP0 positive at 2 h, 4 h, and 7 h, respectively (Fig. 3A). In keeping with these results, the fluorescence intensity was also markedly reduced in shDyst cells compared to shControl cells (Fig. 3B).

Taken together, these data provide strong support for a mechanism in which a lack of dystonin delays the onset of virus expression but has no effect on expression once it has started.

Dystonin is dispensable for virus entry into the cell. A possible explanation for the delay in the onset of infection observed in dystonin-depleted cells is a defect in the ability of the virus to enter the cell. To determine whether this was the case, we carried out experiments to examine virus entry at the cell surface, as assessed by the presence of the virion envelope. shControl or shDyst cells were incubated with 5 PFU/cell of vSR27-VP26GFP (expressing a GFP-tagged capsid protein) and then fixed, permeabilized, and stained for glycoprotein D (gD) (Fig. 4A). Intact virions should appear as both GFP- and gD-positive spots, as their envelope and capsid are tightly associated. This was the case when infection was carried out at 4°C, where virus particles can attach to the cell but membrane fusion is inhibited (Fig. 4A). Under these conditions, almost all capsids seen on cells were associated with gD (97% ± 3%) (Fig. 4B). However, in cells infected at 37°C, membrane fusion can occur, leading to dissociation of the capsid and envelope proteins. Under these conditions, 88% of the capsids (±4%) in shControl cells were gD negative, indicating successful viral entry. Similarly, 84% of the capsids (±4%) in shDyst cells were gD negative (Fig. 4). In addition, the absolute numbers of cytosolic capsids per cell were similar in shControl and shDyst cells (Fig. 4C). This clearly demonstrates that entry occurs normally in cells depleted for dystonin.

Capsid transport in dystonin-depleted cells. Given the demonstrated role of dystonin in capsid transport during egress, an obvious early step that might be affected by depletion of dystonin would be the MT-based retrograde transport of capsids from the cell periphery to the nucleus. To test this hypothesis, we monitored infected shControl or shDyst cells by live-cell microscopy. These cells were infected at 37°C with 50 PFU/cell of vSR27-VP26GFP, and capsid movements were monitored by live-cell microscopy at 30 min postinfection. Live-cell imaging was carried out at room temperature (~25°C) because capsids moved too fast to be tracked efficiently at 37°C with our equipment (see Materials and Methods and reference 22).

On initial examination, capsid movement was observed in both shControl and shDyst cells (see Movies S1 and S2 in the supplemental material). This indicated that dystonin silencing did not have as dramatic an influence on overall capsid transport during entry as that seen during egress, when capsid movement was almost completely blocked (22). Capsid movement was measured and plotted as the distance moved from the point of origin at the start of imaging against time (Fig. 5A and C). The capsid velocity (Fig. 5E and F), the maximum distance moved (Fig. 5G), and the direction of movement (Fig. 5H) were also measured. The histogram in Fig. 5H shows the overall direction of capsid movement (retrograde for movement from the cell periphery to the nucleus; anterograde for movement from the nucleus to the cell periphery) rather than the time spent moving in one or the other direction. Analysis of a total of 185 capsid trajectories revealed differences in

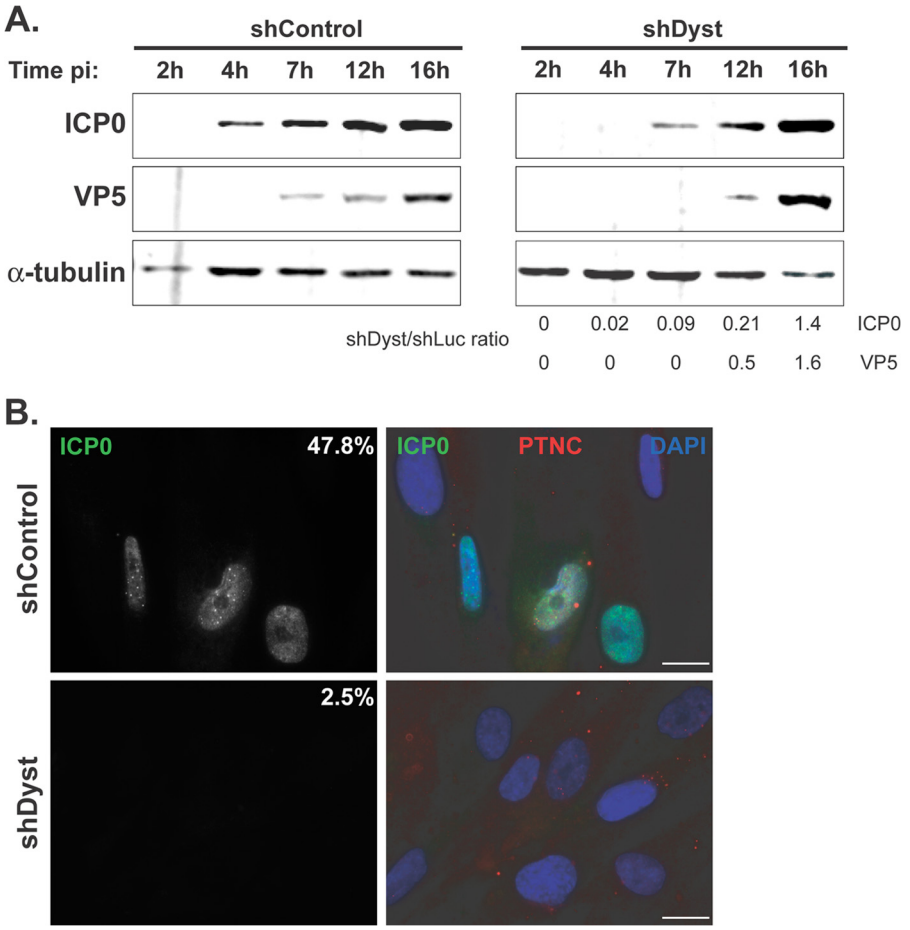

FIG 2 Onset of viral protein production in dystonin-depleted and control cells assessed by Western blotting and immunofluorescence analysis. (A) shControl or shDyst HFFF2 cells were infected with 5 PFU/cell of WT HSV-1. Cells were harvested at 2 h, 4 h, 7 h, 12 h, or 16 h after infection, and the levels of the immediate early protein ICP0 and of the late capsid protein VP5 were monitored using antibodies 11060 and DM165, respectively. Alpha-tubulin was detected using MAb DM1A and was used as a loading control. Protein quantities were normalized to the amount of alpha-tubulin, and the relative levels of ICP0 and VP5 in shDyst and shLuc cells were calculated. (B) ShControl or shDyst HFFF2 cells were infected with 1 PFU/cell of WT HSV-1. At 3 h after infection, the cells were fixed and stained for ICP0 (green) or capsids (red) using antibodies 11060 and PTNC, respectively. The numbers indicate the percentages of cells that were ICP0 positive out of 69 shControl cells and 80 shDyst cells counted.

capsid trafficking between infected shControl and shDyst cells (Fig. 5A and C). Capsid velocities were significantly lower in shDyst cells (average of maxima = 0.5 ± 0.2 μm/s) than in shControl cells (average of maxima = 1.4 ± 0.8 μm/s) (Fig. 5E and F), although the effect was not as great as that seen at late times after infection (22). As a consequence, capsids tended to travel longer distances under control conditions than in shDyst cells (Fig. 5G). However, the direction of motion was similar for the two conditions, with 45% of capsids showing retrograde movement (i.e., from the cell periphery to the nucleus) in shControl cells and 39% showing retrograde movement in shDyst cells (Fig. 5H).

Thus, the overall pattern of capsid transport was not disrupted in dystonin-depleted cells, but the rate of movement was reduced.

Effect of dystonin silencing on nuclear targeting of capsids. Despite the limited effects of dystonin depletion on overall capsid movement at early times of infection (Fig. 5), the observed delay in immediate early gene expression when dystonin levels were reduced (Fig. 1 to 3) suggested that an early, pre-nuclear step was affected. Given the usual close proximity of the centrosome to the nucleus, the majority of capsid movement during entry would be expected to be minus-end directed along the MTs toward the centrosome, with only a small amount of plus-end-directed transport required to reach the nucleus, while the reverse should be true during egress, when plus-end-directed transport would predominate. Therefore, because blocking the limited amount of plus-end-directed transport during entry would explain why capsid transport was less dramatically affected than during egress (22) (Fig. 5), we hypothesized that plus-end-directed transport of capsids was involved. If dystonin is required for plus-end-directed transport, depleting it might be expected to have no effect on capsids moving toward the centrosome but would prevent them from moving away from it, leading to an accumulation of capsids in the vicinity of the centrosome with a concomitant decrease in the number of capsids reaching the nucleus.

To test whether this was the case, shControl or shDyst HFFF2 cells were infected with 25 PFU/cell of WT HSV-1 for 3 h at 37°C in the presence of cycloheximide, an inhibitor of *de novo* protein

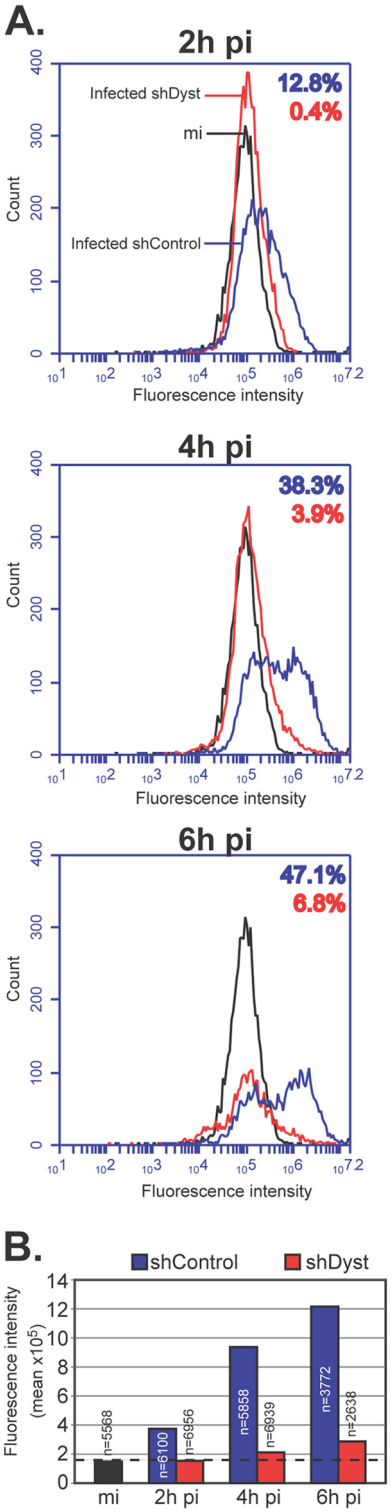

FIG 3 Onset of viral protein production in dystonin-depleted and control cells assessed by FACS analysis. (A) Mock-infected shControl cells or shControl or shDyst HFFF2 cells infected with 5 PFU/cell of WT HSV-1 were harvested at 2 h, 4 h, or 6 h after infection, fixed, permeabilized, and incubated with antibody 11060 against ICP0 and GAM_{488}. Cells were then analyzed by flow cytometry. The numbers of fluorescing cells and their fluorescence intensities were determined for mock-infected shControl cells (black line), infected shControl cells (blue line), or infected shDyst cells (red line). The percentages of the total cell population identified as positive (i.e., above the background level, as defined by the fluorescence intensity of the mock-infected shControl cells) are indicated using the same color coding. (B) Summary of mean fluorescence intensities indicated for panel A. The number of cells analyzed is given for each condition. Dashed line, background level defined by the fluorescence intensity of mock-infected shControl cells.

synthesis commonly used in studies of HSV capsid accumulation at the nucleus (1, 2, 28–31). Addition of cycloheximide increases capsid retention at the nucleus and prevents confusion between input capsids and newly formed nuclear capsids.

Numerous capsids were seen in the area of the nucleus in shControl cells and frequently formed a distinct ring around the nuclear periphery (Fig. 6A). In contrast, capsids never formed rings around the nuclei of shDyst cells, and overall, there were fewer capsids associated with the nuclei. Visual comparison gave the impression that capsids were present at a higher density in the vicinity of the centrosome in shDyst cells (Fig. 6A). To quantify these observations, we compared the number of capsids present over the nuclear area and at the nuclear rim (as estimated by DAPI staining) to the number of capsids present within an area of 9 μm^2 centered on the centrosome (minus any overlapping nuclear area). The number of capsids counted in each region was divided by its area to measure capsid density (number of capsids per μm^2). This showed that in shControl cells ($n = 19$ cells), 0.22 capsid/μm^2 was present in nuclear areas and 0.07 capsid/μm^2 was present in centrosomal areas (Fig. 6B). These proportions were inverted in shDyst cells ($n = 11$ cells), where capsid density was lower in nuclear areas (0.09 capsid/μm^2) than in centrosomal areas (0.24 capsid/μm^2). These results show that reducing the levels of dystonin limits the ability of capsids to reach the nucleus and causes them to concentrate in the vicinity of the centrosome.

Effect of dystonin silencing on capsid trafficking in the vicinity of the centrosome. To directly ascertain the effect of dystonin silencing on plus-end-directed MT transport, capsid trafficking to and from the centrosome was imaged by live-cell microscopy of shControl and shDyst HFFF2 cells infected with 50 PFU/cell of vSR27-VP26GFP. Capsid monitoring started once the centrosome became distinguishable as a result of capsid accumulation in its vicinity (see Movies S3 and S4 in the supplemental material). As early as 45 min after infection, capsids could be seen accumulating close to the nucleus. Subsequent staining of fixed cells for tubulin confirmed that this area of capsid accumulation was an MTOC, most likely the centrosome (arrowhead in Fig. 7A). As can be seen in Movies S3 and S4 in the supplemental material, capsids were clearly moving both toward and away from the MTOC in shControl cells (see Movie S3 in the supplemental material). In contrast, although capsids were also seen moving toward the MTOC in shDyst cells, very few were seen leaving it (see Movie S4 in the supplemental material). To quantify this effect, capsids were classified as trafficking either toward (marked as red lines in Fig. 7B and C) or away from (marked as yellow lines) the MTOC. A total of 1,219 moving capsids and their directions were monitored in shControl cells ($n = 32$ cells) and shDyst cells ($n = 32$ cells). This revealed that in shControl cells, 45% of moving capsids were traveling away from the MTOC, with 55% moving in the opposite direction, whereas in shDyst cells, only 21% of capsids were moving away from the MTOC and 79% were moving

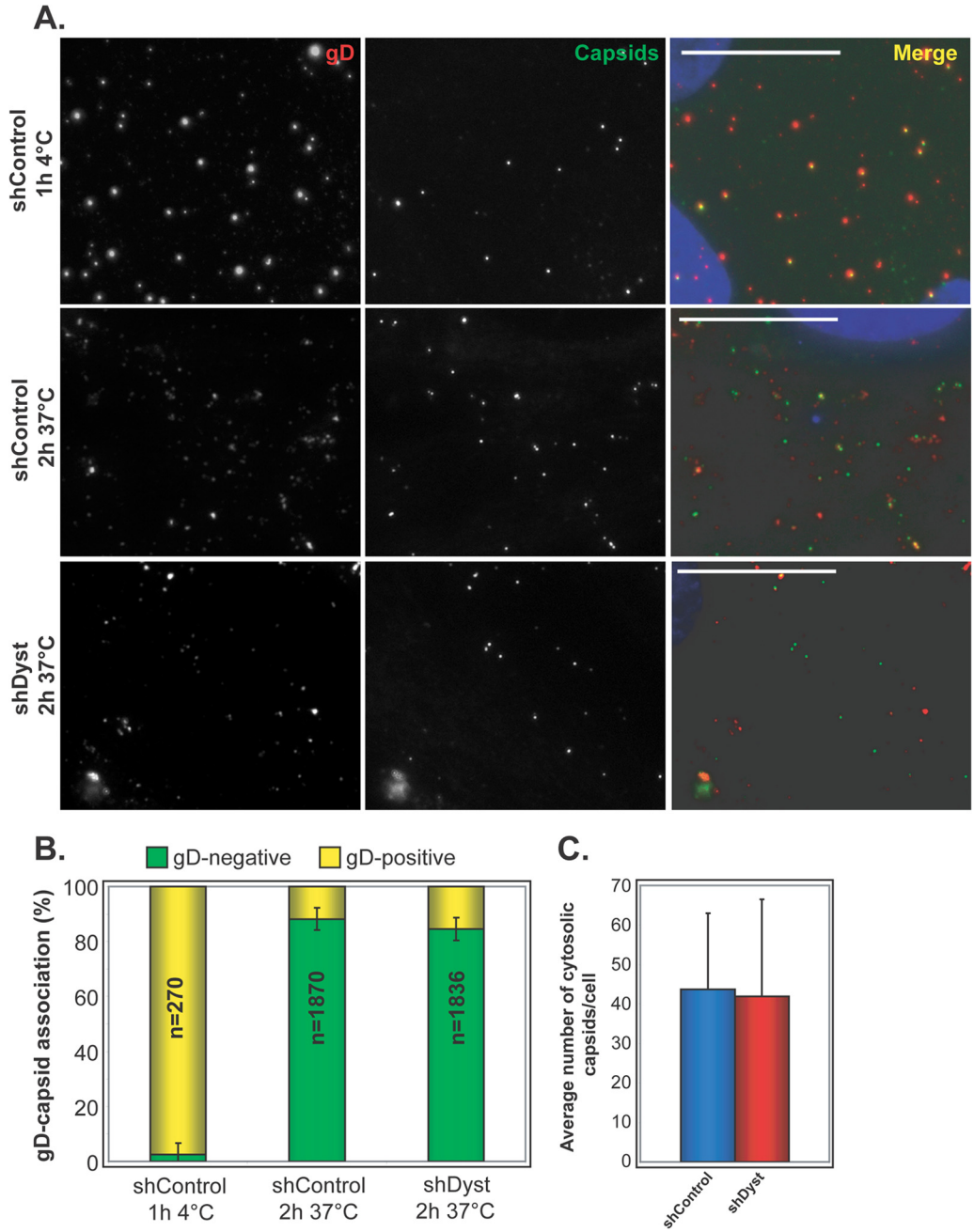

FIG 4 Virus penetration in dystonin-depleted and control cells. (A) shControl and shDyst HFFF2 cells were incubated with vSR27-VP26GFP virions for 1 h at 4°C or for 2 h at 37°C. The cells were fixed and labeled for gD with MAb 4846 and GAM_{568} (red). Capsids were visualized through GFP fluorescence (green). Nuclei were visualized with DAPI (blue). Bars, 20 μm. (B) The total numbers of capsids present on randomly chosen cells from the experiment whose results are shown in panel A were counted, and the proportion having envelopes was determined by colocalization between GFP (capsid) and Alexa Fluor 568 (envelope) signals. Results are shown as the numbers of gD-positive (yellow) and gD-negative (green) capsids expressed as a percentage of the total number of capsids counted. (C) Average number of cytosolic (gD-negative) capsids per cell at 37°C. A total of 270 (ShControl, 4°C), 1,870 (shControl, 37°C), and 1,836 (shDyst, 37°C) particles were analyzed in 27, 43, and 46 cells, respectively.

toward it. As each capsid that moves to the centrosome would subsequently be expected to move away from it, the expected ratio of capsids moving to and from the MTOC would be approximately 50:50. That 45% of capsids were identified as moving away from the MTOC in control cells means that this is the case for 45/55, or 82%, of capsids. This drops to 21/79, or 26.5%, in shDyst cells, which, although not indicative of a complete block, does suggest that a capsid is more likely to become trapped in the vicinity of the centrosome. Therefore, the ability of capsids to be redirected from the MTOC to the nucleus is at least three times less efficient in shDyst cells than in shControl cells.

This supports a role for dystonin in the transport of HSV-1 capsids by plus-end-directed MT transport, which is in accordance with the known functions of pUL37.

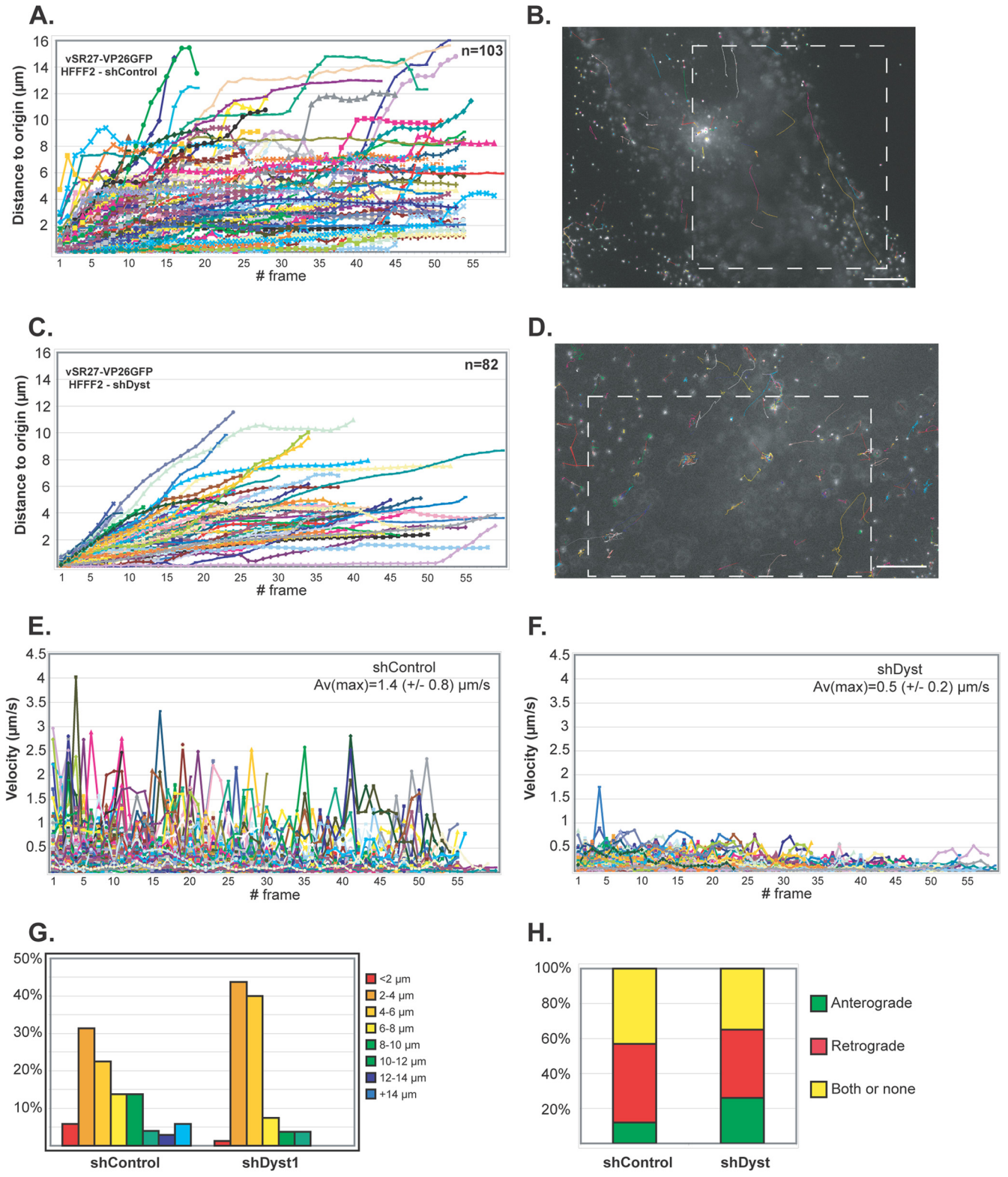

FIG 5 Impact of dystonin reduction on capsid transport during entry. shControl (A, B, and E) or shDyst (C, D, and F) HFFF2 cells were infected with 50 PFU/cell of vSR27-VP26GFP. Starting at 45 min after infection, cytoplasmic capsid movements were monitored by live-cell imaging at a rate of one frame per second. Results for each individual capsid tracked are plotted as the distance to the origin (A and C) or as the velocity (E and F) for each frame. The premature truncation of some lines is due to the capsids moving out of the field of view. A representative cell with all capsid trajectories plotted is shown for each condition (B and D). Dashed boxes, the area displayed in the corresponding movies (see Movies S1 and S2 in the supplemental material, respectively). Bars, 10 µm. (G) Summary of the maximum distances to the origin taken from the data shown in panels A and C as percentages of cells in categories of the distance to the origin. (H) Every moving capsid was tracked individually, and its directionality was estimated according to the position of the nucleus. Results are shown as the percentage of capsids having overall retrograde (away from the cell periphery and toward the nucleus) or anterograde (away from the nucleus and toward the cell periphery) motion. Both or none, either a capsid having opposite directionalities within the same run, a capsid that was not moving, or a capsid where the direction of movement relative to the nucleus could not be categorized.

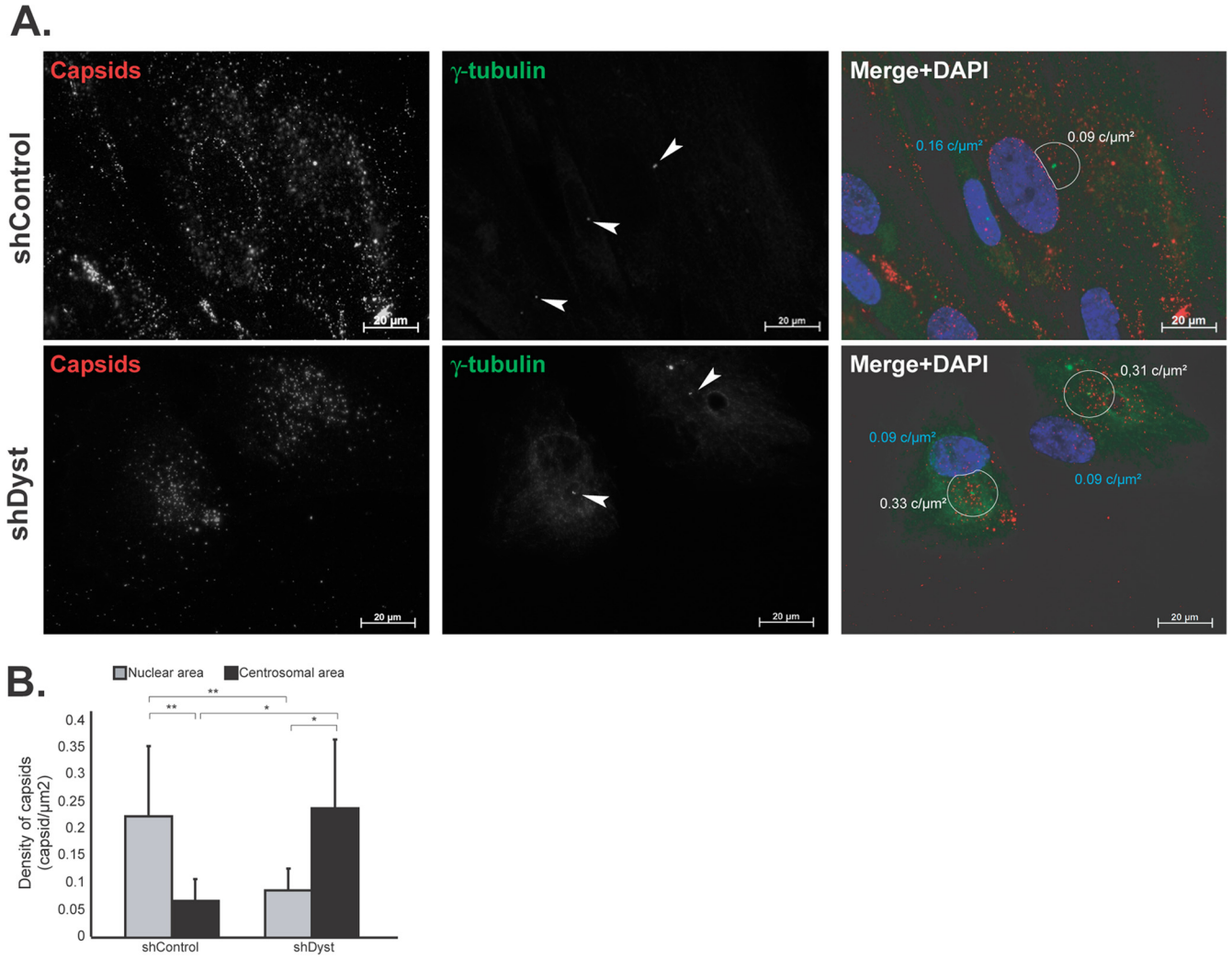

FIG 6 Effect of dystonin silencing on capsid localization during entry. ShControl or shDyst HFFF2 cells were infected with 25 PFU/cell of WT HSV-1 for 3 h at 37°C in the presence of 100 μg/ml cycloheximide before being fixed. (A) Capsids were visualized with the rabbit anticapsid antibody PTNC and GAR_{568} (red), and centrosomes were visualized with MAb GTU-88 against gamma-tubulin and GAM_{488} (green). Nuclei were visualized with DAPI (blue). z-stacks of the whole-cell thickness were collected and are shown here in projection. Arrowheads, centrosomes; white circles, an area of 9 μm^2 centered on the centrosome excluding any overlapping nuclear area. The density of capsids (in number of capsids per μm^2 of surface [c/μm^2]; see below) in each circle is specified. (B) Nuclear capsids (defined as capsids present within the DAPI-labeled area) and centrosomal capsids (defined as capsids present within the area delineated by the white circles) were counted. A total of 2,102 capsids were counted in 19 shControl cells and 1,083 capsids were counted in 11 shDyst cells. The nuclear and centrosomal surface areas were calculated using Zeiss Axiovision software, and the number of capsids per μm^2 of surface (capsid density) was calculated. Asterisks indicate statistical differences (*t* test; *, $P < 0.01$; **, $P = 0.001$).

DISCUSSION

In an earlier paper, we reported that the tegument protein pUL37 of HSV-1 can bind the cellular protein dystonin and that capsids colocalized with endogenous dystonin in infected cells in a UL37-dependent manner (22). Dystonin had previously been suggested to act as a linker between MT motor proteins and their cargoes during retrograde transport (32, 33), to be involved in anterograde transport (34), and to localize to the plus ends of MTs (22, 35). When dystonin expression was inhibited, we observed a dramatic decrease in capsid movement at late times of infection and interpreted this as indicating a role for dystonin in capsid transport during egress. In view of these observations, it was rather surprising that depletion of dystonin did not appear to have a dramatic effect on overall capsid transport during entry, while it strongly delayed the onset of virus expression at high multiplicities of infection (MOIs; 1, 3, or 5 PFU/cell) but not at the very high MOI of 50 PFU/cell (data not shown). However, closer analysis revealed that although transport of capsids to the MTOC was not strongly affected, redirection of capsids from the MTOC to the nucleus was significantly impaired. To make this observation, cells were infected with 50 PFU/cell to have a sufficient number of capsids to track. Under these conditions, the delay in the onset of infection was very moderate (data not shown), which can be explained by the remaining number of capsids that leave from the MTOC in the absence of dystonin (Fig. 7). Since the onset of infection was strongly delayed at an MOI of 1, 3, or 5, it is possible that the ratio of capsids arriving at the MTOC that are redirected to the nucleus is actually much lower under these conditions than that observed in our live-cell experiments.

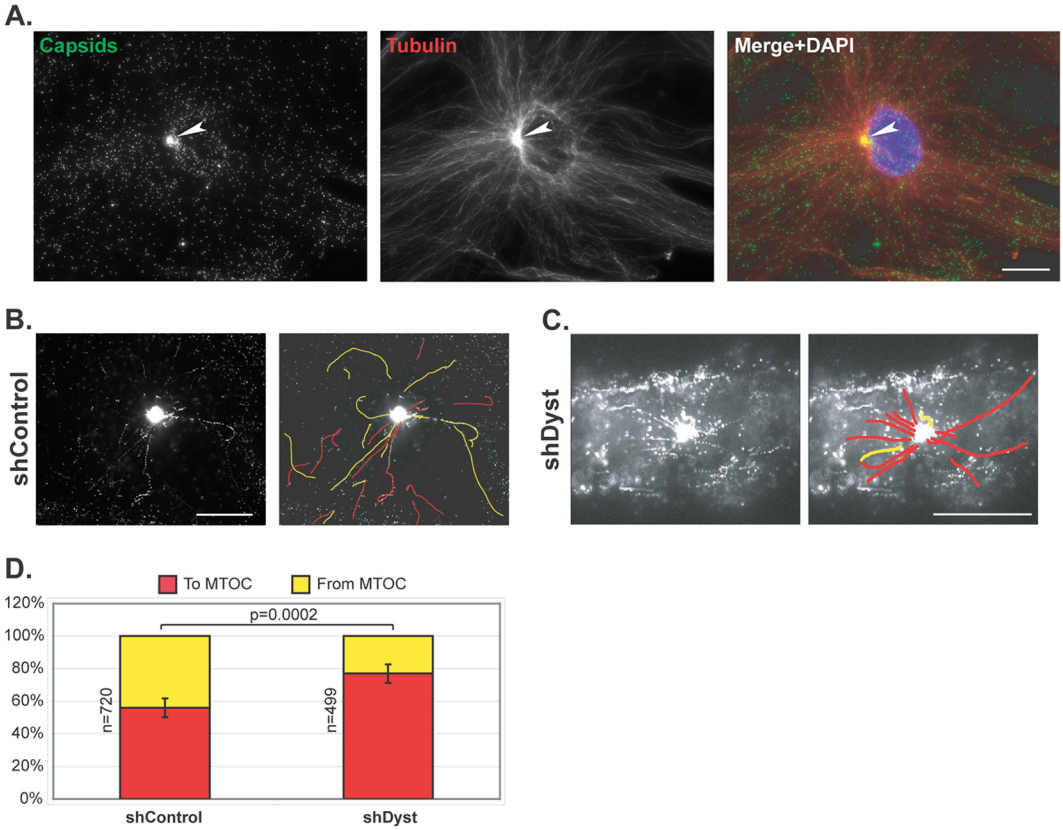

FIG 7 Capsid trafficking in the vicinity of the centrosome. shControl or shDyst HFFF2 cells were infected with 50 PFU/cell of vSR27-VP26GFP at 37°C. (A) shControl cells were fixed at 3 h postinfection and stained for microtubules with an antibody directed against alpha-tubulin and GAM_{568} (red). Capsids were visualized through direct GFP fluorescence (green). White arrowhead, MTOC. Bar, 20 μm. (B, C) shControl or shDyst cells were infected for 45 min at 37°C, and capsid trafficking was monitored by time-lapse microscopy at room temperature (see Movies S3 and S4 in the supplemental material, respectively). Capsid movement was visualized through a maximum-intensity projection of the whole time-lapse stack and interpreted as moving to (red) or from (yellow) the centrosome. (D) A total of 1,219 capsids from 114 different movies were tracked in shControl ($n = 32$) and shDyst ($n = 32$) HFFF2 cells. Their motion relative to the centrosome was determined and plotted as a percentage of the total number of capsids tracked.

The typical perinuclear location of the centrosome ensures that during entry, most of the movement will be between the plasma membrane and the centrosome. This transport involves minus-end-directed motors (13), and although capsid movement was slower in the absence of dystonin, it was not prevented (Fig. 5). However, the shorter distance between the centrosome and the nucleus is expected to be crossed by plus-end-directed transport, and this was strongly impaired in dystonin-depleted cells. Based on these observations, we postulate that the pUL37-dystonin interaction has a specific role in plus-end-directed transport of incoming capsids. Interestingly, although pUL37 is important for efficient nuclear targeting of incoming PrV capsids (20), it is not essential for nuclear binding of HSV-1 capsids and viral DNA release (17). A role in plus-end-directed transport is in accordance with the reported role of its binding partner dystonin in anterograde transport of cellular vesicles (34) and its localization to the plus ends of MTs (22, 35) and provides the first evidence that transport directionality can be conferred on the capsid by recruitment of cellular nonmotor proteins.

It is not clear whether the directional specificity seen during entry would account for the observed behavior during egress. The proximity of the centrosome to the nucleus might seem to imply that outward transport would be predominantly plus ended, given the relatively greater distance between the centrosome and the sites of envelopment. However, there is increasing evidence that functional centrosomes are no longer present in HSV-infected cells by the time that newly formed capsids are entering the cytoplasm (36–38). Capsid transport must therefore be along MTs originating from noncentrosomal sites. The polarity of these MTs is not known, and it remains unclear whether outgoing capsids are directed to the sites of envelopment by plus- or minus-end-directed transport.

Herpesvirus intracellular transport is a complex process that is likely to involve different viral and cellular proteins, depending on the cell type and the stage of the viral cycle. This is of particular relevance in differentiated neurons, a highly asymmetric cell type, where the distances traveled are typically much longer than those in other cells. The state of the capsid during transport from the neuronal cell body to the tip of the axon is still a matter of debate. Two models have been proposed, with one suggesting that capsids are transported to the axon tips for envelopment and the other suggesting that capsids are enveloped in the cell body and mature virions are transported to the axon tips (39). Recent studies have shown that the viral membrane protein pUs9 interacts with kinesin 3 to transport enveloped virions from the cell body to the axonal termi-

nus (5). As for the alternative mechanism, it would be interesting to determine whether the pUL37-dystonin interaction plays any role in transport of unenveloped capsids to the axon tips. The diverse requirements of transporting virus capsids around cells makes it clear that many of the factors involved in the complex intracellular trafficking of herpesviruses, together with the mechanisms associated with them, are still to be unraveled.

Interaction studies have failed to identify a direct interaction between pUL37 and molecular motors (22, 40), as has been done for pUL36 (13) and pUs9 (5). Since pUL36 appears to play a central role in capsid transport along microtubules (16) and given the apparent involvement of the pUL37-dystonin interaction in controlling transport polarity, it seems plausible that pUL37 may act as a regulatory protein modulating the outcome of the interaction between pUL36 and the motor proteins.

ACKNOWLEDGMENTS

We thank Y. Gaudin for his support of this project. We are grateful to C. Preston (CVR, Glasgow, Scotland) for his gift of the tsK/Luci virus and to R. Everett (CVR, Glasgow, Scotland) for his gift of silencing plasmids.

This work was funded by the CNRS and the MRC.

REFERENCES

1. **Mabit H, Nakano MY, Prank U, Saam B, Dohner K, Sodeik B, Greber UF.** 2002. Intact microtubules support adenovirus and herpes simplex virus infections. J. Virol. **76:**9962–9971.
2. **Sodeik B, Ebersold MW, Helenius A.** 1997. Microtubule-mediated transport of incoming herpes simplex virus 1 capsids to the nucleus. J. Cell Biol. **136:**1007–1021.
3. **Bartolini F, Gundersen GG.** 2006. Generation of noncentrosomal microtubule arrays. J. Cell Sci. **119:**4155–4163.
4. **Radtke K, Kieneke D, Wolfstein A, Michael K, Steffen W, Scholz T, Karger A, Sodeik B.** 2010. Plus- and minus-end directed microtubule motors bind simultaneously to herpes simplex virus capsids using different inner tegument structures. PLoS Pathog. **6:**e1000991. doi:10.1371/journal.ppat.1000991.
5. **Kramer T, Greco TM, Taylor MP, Ambrosini AE, Cristea IM, Enquist LW.** 2012. Kinesin-3 mediates axonal sorting and directional transport of alphaherpesvirus particles in neurons. Cell Host Microbe **12:**806–814.
6. **Klupp BG, Fuchs W, Granzow H, Nixdorf R, Mettenleiter TC.** 2002. Pseudorabies virus UL36 tegument protein physically interacts with the UL37 protein. J. Virol. **76:**3065–3071.
7. **Desai P, Sexton GL, McCaffery JM, Person S.** 2001. A null mutation in the gene encoding the herpes simplex virus type 1 UL37 polypeptide abrogates virus maturation. J. Virol. **75:**10259–10271.
8. **Desai PJ.** 2000. A null mutation in the UL36 gene of herpes simplex virus type 1 results in accumulation of unenveloped DNA-filled capsids in the cytoplasm of infected cells. J. Virol. **74:**11608–11618.
9. **Aggarwal A, Miranda-Saksena M, Boadle RA, Kelly BJ, Diefenbach RJ, Alam W, Cunningham AL.** 2012. Ultrastructural visualization of individual tegument protein dissociation during entry of herpes simplex virus 1 into human and rat dorsal root ganglion neurons. J. Virol. **86:**6123–6137.
10. **Antinone SE, Smith GA.** 2010. Retrograde axon transport of herpes simplex virus and pseudorabies virus: a live-cell comparative analysis. J. Virol. **84:**1504–1512.
11. **Granzow H, Klupp BG, Mettenleiter TC.** 2005. Entry of pseudorabies virus: an immunogold-labeling study. J. Virol. **79:**3200–3205.
12. **Luxton GW, Haverlock S, Coller KE, Antinone SE, Pincetic A, Smith GA.** 2005. Targeting of herpesvirus capsid transport in axons is coupled to association with specific sets of tegument proteins. Proc. Natl. Acad. Sci. U. S. A. **102:**5832–5837.
13. **Zaichick SV, Bohannon KP, Hughes A, Sollars PJ, Pickard GE, Smith GA.** 2013. The herpesvirus VP1/2 protein is an effector of dynein-mediated capsid transport and neuroinvasion. Cell Host Microbe **13:**193–203.
14. **Abaitua F, Hollinshead M, Bolstad M, Crump CM, O'Hare P.** 2012. A nuclear localization signal in herpesvirus protein VP1-2 is essential for infection via capsid routing to the nuclear pore. J. Virol. **86:**8998–9014.
15. **Batterson W, Furlong D, Roizman B.** 1983. Molecular genetics of herpes simplex virus. VIII. Further characterization of a temperature-sensitive mutant defective in release of viral DNA and in other stages of the viral reproductive cycle. J. Virol. **45:**397–407.
16. **Luxton GW, Lee JI, Haverlock-Moyns S, Schober JM, Smith GA.** 2006. The pseudorabies virus VP1/2 tegument protein is required for intracellular capsid transport. J. Virol. **80:**201–209.
17. **Roberts AP, Abaitua F, O'Hare P, McNab D, Rixon FJ, Pasdeloup D.** 2009. Differing roles of inner tegument proteins pUL36 and pUL37 during entry of herpes simplex virus type 1. J. Virol. **83:**105–116.
18. **Jovasevic V, Liang L, Roizman B.** 2008. Proteolytic cleavage of VP1-2 is required for release of herpes simplex virus 1 DNA into the nucleus. J. Virol. **82:**3311–3319.
19. **Schipke J, Pohlmann A, Diestel R, Binz A, Rudolph K, Nagel CH, Bauerfeind R, Sodeik B.** 2012. The C terminus of the large tegument protein pUL36 contains multiple capsid binding sites that function differently during assembly and cell entry of herpes simplex virus. J. Virol. **86:**3682–3700.
20. **Krautwald M, Fuchs W, Klupp BG, Mettenleiter TC.** 2009. Translocation of incoming pseudorabies virus capsids to the cell nucleus is delayed in the absence of tegument protein pUL37. J. Virol. **83:**3389–3396.
21. **Sandbaumhuter M, Dohner K, Schipke J, Binz A, Pohlmann A, Sodeik B, Bauerfeind R.** 2013. Cytosolic herpes simplex virus capsids not only require binding inner tegument protein pUL36 but also pUL37 for active transport prior to secondary envelopment. Cell. Microbiol. **15:**248–269.
22. **Pasdeloup D, McElwee M, Beilstein F, Labetoulle M, Rixon FJ.** 2013. Herpesvirus tegument protein pUL37 interacts with dystonin/BPAG1 to promote capsid transport on microtubules during egress. J. Virol. **87:**2857–2867.
23. **Pasdeloup D, Blondel D, Isidro AL, Rixon FJ.** 2009. Herpesvirus capsid association with the nuclear pore complex and viral DNA release involve the nucleoporin CAN/Nup214 and the capsid protein pUL25. J. Virol. **83:**6610–6623.
24. **McClelland DA, Aitken JD, Bhella D, McNab D, Mitchell J, Kelly SM, Price NC, Rixon FJ.** 2002. pH reduction as a trigger for dissociation of herpes simplex virus type 1 scaffolds. J. Virol. **76:**7407–7417.
25. **Everett RD, Rechter S, Papior P, Tavalai N, Stamminger T, Orr A.** 2006. PML contributes to a cellular mechanism of repression of herpes simplex virus type 1 infection that is inactivated by ICP0. J. Virol. **80:**7995–8005.
26. **Vielkind U, Swierenga SH.** 1989. A simple fixation procedure for immunofluorescent detection of different cytoskeletal components within the same cell. Histochemistry **91:**81–88.
27. **Sbalzarini IF, Koumoutsakos P.** 2005. Feature point tracking and trajectory analysis for video imaging in cell biology. J. Struct. Biol. **151:**182–195.
28. **Dohner K, Wolfstein A, Prank U, Echeverri C, Dujardin D, Vallee R, Sodeik B.** 2002. Function of dynein and dynactin in herpes simplex virus capsid transport. Mol. Biol. Cell **13:**2795–2809.
29. **Ojala PM, Sodeik B, Ebersold MW, Kutay U, Helenius A.** 2000. Herpes simplex virus type 1 entry into host cells: reconstitution of capsid binding and uncoating at the nuclear pore complex in vitro. Mol. Cell. Biol. **20:**4922–4931.
30. **Rode K, Dohner K, Binz A, Glass M, Strive T, Bauerfeind R, Sodeik B.** 2011. Uncoupling uncoating of herpes simplex virus genomes from their nuclear import and gene expression. J. Virol. **85:**4271–4283.
31. **Turcotte S, Letellier J, Lippe R.** 2005. Herpes simplex virus type 1 capsids transit by the trans-Golgi network, where viral glycoproteins accumulate independently of capsid egress. J. Virol. **79:**8847–8860.
32. **Liu JJ, Ding J, Kowal AS, Nardine T, Allen E, Delcroix JD, Wu C, Mobley W, Fuchs E, Yang Y.** 2003. BPAG1n4 is essential for retrograde axonal transport in sensory neurons. J. Cell Biol. **163:**223–229.
33. **Liu JJ, Ding J, Wu C, Bhagavatula P, Cui B, Chu S, Mobley WC, Yang Y.** 2007. Retrolinkin, a membrane protein, plays an important role in retrograde axonal transport. Proc. Natl. Acad. Sci. U. S. A. **104:**2223–2228.
34. **Ryan SD, Bhanot K, Ferrier A, De Repentigny Y, Chu A, Blais A, Kothary R.** 2012. Microtubule stability, Golgi organization, and transport flux require dystonin-a2-MAP1B interaction. J. Cell Biol. **196:**727–742.
35. **Kapur M, Wang W, Maloney MT, Millan I, Lundin VF, Tran TA, Yang Y.** 2012. Calcium tips the balance: a microtubule plus end to lattice binding switch operates in the carboxyl terminus of BPAG1n4. EMBO Rep. **13:**1021–1029.
36. **Avitabile E, Di Gaeta S, Torrisi MR, Ward PL, Roizman B, Campadelli-**

Fiume G. 1995. Redistribution of microtubules and Golgi apparatus in herpes simplex virus-infected cells and their role in viral exocytosis. J. Virol. **69:**7472–7482.
37. **Kotsakis A, Pomeranz LE, Blouin A, Blaho JA.** 2001. Microtubule reorganization during herpes simplex virus type 1 infection facilitates the nuclear localization of VP22, a major virion tegument protein. J. Virol. **75:**8697–8711.
38. **Pasdeloup D, Labetoulle M, Rixon FJ.** 2013. Differing effects of herpes simplex virus 1 and pseudorabies virus infection on centrosomal function. J. Virol. **87:**7102–7112.
39. **Johnson DC, Baines JD.** 2011. Herpesviruses remodel host membranes for virus egress. Nat. Rev. Microbiol. **9:**382–394.
40. **Kelly BJ, Diefenbach E, Fraefel C, Diefenbach RJ.** 2012. Identification of host cell proteins which interact with herpes simplex virus type 1 tegument protein pUL37. Biochem. Biophys. Res. Commun. **417:**961–965.

PARTIE III :

Interférence des infections à HSV-1 et PRV sur la fonction centrosomale

Contexte et hypothèse de travail

Le centrosome est le centre organisateur majeur des microtubules (MToC) dans la plupart des types cellulaires. Dans le fibroblaste, le réseau de MTs croît à partir du centrosome en direction de la membrane plasmique. Il est composé de deux centrioles elles-mêmes composées de plusieurs protéines (la plupart regroupées sous des noms tels que CepXXX, pour une revue voir[39]).

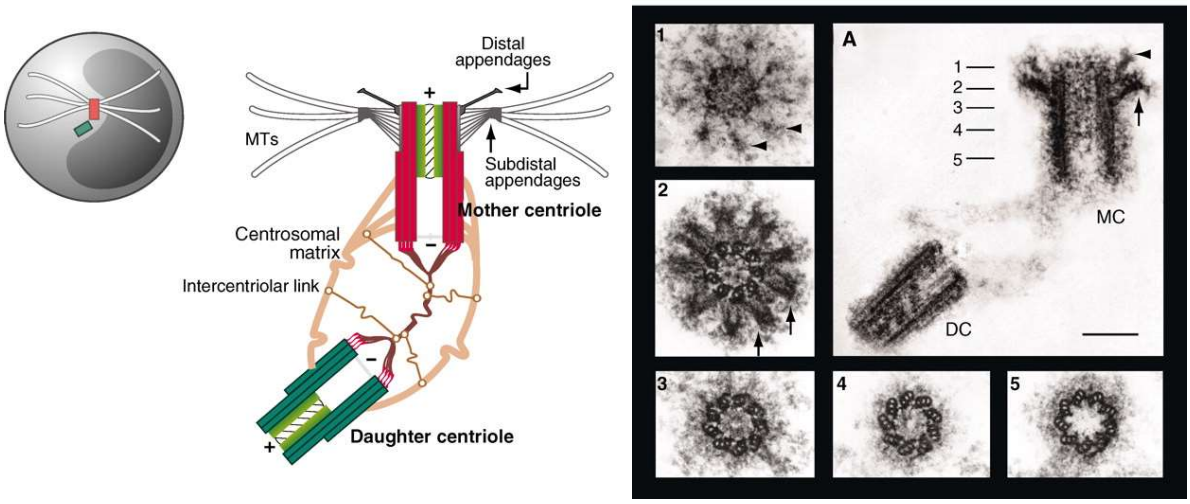

Figure 9. Organisation du centrosome en cellules animales. Le centrosome est formé d'une paire de centrioles, la centriole « mère » (MC) et la centriole « fille » (DC). La centriole mère présente 9 appendices nécessaires à l'ancrage des MTs (en bas sur la photo de microscopie électronique). Tiré de Bornens, Science 2012[40].

Les centrioles stabilisent l'extrémité (-) des MTs. Néanmoins, des MToC alternatifs existent et sont particulièrement importants voire majoritaires dans des types cellulaires très différenciés, tels que la cellule épithéliale ou le neurone (**Figure 10**). Ces deux derniers types cellulaires sont précisément les cibles majeures du virus HSV-1 *in vivo*.

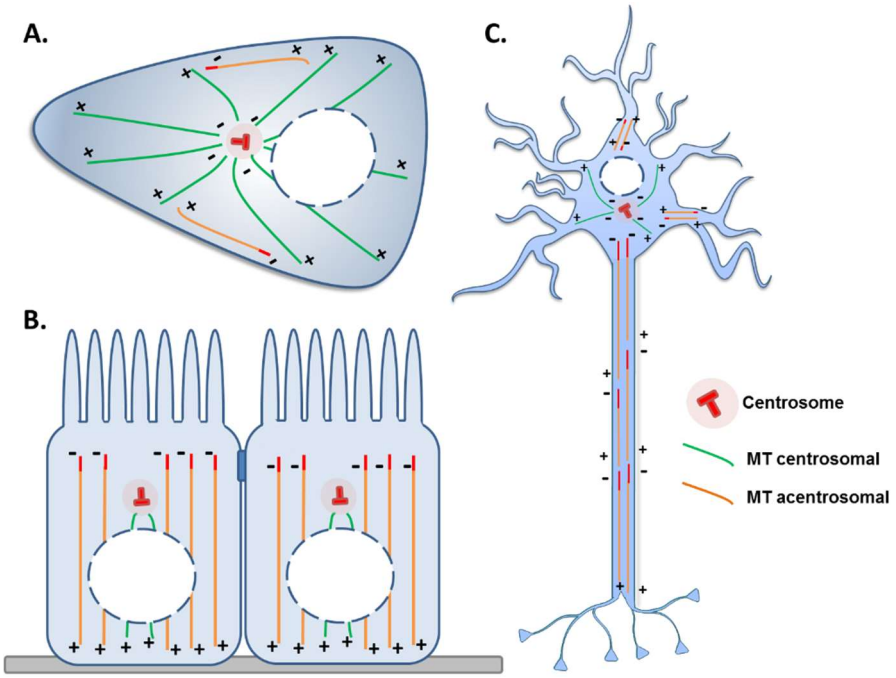

Figure 10. Organisation du réseau de microtubules et importance du centrosome en tant que centre organisateur des MTs dans différents types cellulaires relevants pour l'infection aux Herpesvirus. Le centrosome est le MToC majeur des cellules pas ou faiblement polarisées tels que les fibroblastes (A). Dans ce cas, les MTs non-centrosomaux sont minoritaires et dépendent de MToC alternatifs tels que le Golgi. En revanche, des cellules très polarisées ont un réseau réorganisé selon la fonction de ces cellules. Ainsi, les cellules épithéliales ont leurs MTs orientés selon l'axe baso-apical afin de faciliter le transit des vésicules d'une extrémité à l'autre (B). Dans ce cas, les MTs non-centrosomaux sont majoritaires et le centrosome a un rôle mineur en tant que MToC. Il en va de même pour la cellule neuronale où le réseau est radial dans le corps cellulaire et où le centrosome a un rôle de MToC important, mais pas dans les axones et dendrites, où la stabilité des MTs est assurée par des protéines coiffant et stabilisant l'extrémité (-) des MTs (en rouge) (C). Tiré de Pasdeloup, Virologie 2016.

Par ailleurs, il a été démontré que l'infection à HSV-1 résultait en la modification du réseau de MTs[41,42]. Dans le cadre de notre étude sur le transport de HSV-1 sur le réseau de MTs, nous avons voulu déterminer les causes et conséquences de ces modifications sur le traffic intracellulaire du virus.

Expériences mises en œuvre

Durant notre étude sur le transport intracellulaire des herpèsvirus, nous avons constaté un phénomène étrange : dans les premières heures après infection par HSV-1, le réseau de MT ne semblait plus organisé autour d'un MToC clair. Nous avons alors constaté que le centrosome des cellules n'était plus détectable. Nous avons confirmé cette observation en utilisant différents marqueurs du centrosome pour nous assurer qu'il ne s'agissait pas de la déplétion d'un ou plusieurs éléments du centrosome

plutôt que de la structure elle-même. L'analyse par WB a montré que les niveaux de ces marqueurs étaient inchangés, alors que le centrosome n'était plus détectable dans les cellules 6h post-infection (Figure 1 de la publication 6 ou PB6-1). Nous avons observé ce phénomène dans deux lignées cellulaires différentes (Vero et HFFF). De façon remarquable, le centrosome de cellules Vero ou PK15 (une lignée cellulaire porcine) n'était pas affecté par l'infection par un autre alpha-herpèsvirus modèle, le virus de la pseudorage (PrV) (Figure PB6-2 et 6-3). Nous avons ainsi quantifié que >80% des cellules HFFF infectées par HSV-1 n'avait plus de centrosome détectable à 16h pi (60% en Vero) et jusqu'à 90% à partir de 24h pi (>70% en Vero). En revanche, seules 20% des cellules PK15 infectées par PrV 16h pi ne présentaient pas de centrosome détectable (<5% en Vero) (Figure PB6-4). Nous avons tenté de déterminer quel facteur viral pouvait être la cause de la disparition du centrosome en infectant des cellules HFFF2 avec des virus HSV-1 délétés de l'une ou l'autre des protéines candidates (VP22, ICP0, pUL36, pUL37 et pUL19 pour tester l'influence de la production de nouvelles capsides). Aucune de ces protéines n'était nécessaire à la disparition du centrosome (Figure PB6-5). Nous avons ensuite testé la répercussion fonctionnelle de l'absence de centrosome sur la dynamique des MTs. Pour cela, nous avons traité des cellules HFFF avec du nocodazole à une dose permettant la destruction complète du réseau. La drogue ayant un effet réversible, le réseau est reconstitué dans les dix minutes qui suivent l'élimination de la drogue dans des cellules non-infectées (Figure PB6-6). Dans les cellules infectées par HSV-1, aucune reconstitution du réseau n'est observée jusqu'à une heure après élimination de la drogue (Figure PB6-6, 6-8 et 6-9). Dans les cellules infectées par PrV, le réseau est reconstitué mais plus lentement et il apparait moins dense que dans les cellules non-infectées (Figure PB6-6, 6-7 et 6-9).

A l'issue de ces travaux, nous avons émis l'hypothèse que dans les types cellulaires infectés naturellement par le virus HSV-1 (cellules épithéliales, neurones), le virus réorganise le réseau de MTs en détruisant le centrosome afin de favoriser les MTs non-centrosomaux. Ces MTs sont souvent ancrés au 2^{e} MToC majoritaire des cellules : le réseau de Golgi (*trans*), qui est un site d'assemblage majeur des Herpesvirus. Ainsi, en détruisant le réseau de MTs centrosomal, le virus favoriserait les MTs qui émanent du Golgi, c'est-à-dire l'organelle ciblé par les capsides cytosoliques avant l'enveloppement secondaire, et optimiserait donc le transport noyau -> Golgi en court-circuitant le centrosome.

Répercussion de ces travaux et ce que l'on sait maintenant

Quatre mois après la publication de ces travaux, Naghavi et al. confirment la destruction du

centrosome par l'infection à HSV-1 ainsi que la stabilisation des MTs non-centrosomaux lors de l'infection. Ils mettent en avant le rôle de la protéine virale Us3 et de la protéine cellulaire CLASP (une protéine qui ancre les MTs au Golgi) dans le phénomène de stabilisation des MTs non centrosomaux[43]. Plus récemment, la même équipe a montré que le centrosome perd son rôle de MToC majeur dans les cellules infectées par le cytomégalovirus humain (HCMV) et que le compartiment d'assemblage périnucléaire du virus joue le rôle de MToC alternatif viro-induit[44].

Publication #6

Differing effects of herpes simplex virus 1 and pseudorabies virus infections on centrosomal function.

Pasdeloup D, Labetoulle M, Rixon FJ.

JVI Journals.ASM.org

Differing Effects of Herpes Simplex Virus 1 and Pseudorabies Virus Infections on Centrosomal Function

David Pasdeloup,[a] Marc Labetoulle,[a] Frazer J. Rixon[b]

Laboratoire de Virologie Moléculaire et Structurale, CNRS, Gif-Sur-Yvette, France[a]; MRC-University of Glasgow Centre for Virus Research, Glasgow, United Kingdom[b]

Efficient intracellular transport of the capsid of alphaherpesviruses, such as herpes simplex virus 1 (HSV-1), is known to be dependent upon the microtubule (MT) network. Typically, the MT network radiates from an MT-organizing center (MTOC), which is, in most cases, the centrosome. During herpesvirus egress, it has been assumed that capsids travel first from the nucleus to the centrosome and then from the centrosome to the site of envelopment. Here we report that the centrosome is no longer a primary MTOC in HSV-1-infected cells, but it retains this function in cells infected by another alphaherpesvirus, pseudorabies virus (PrV). As a result, MTs formed at late times after infection with PrV grow from a major, centralized MTOC, while those formed after HSV-1 infection arise from dispersed locations in the cytoplasm, indicating the presence of alternative and minor MTOCs. Thus, loss of the principal MT nucleating center in cells following HSV-1 infection raises questions about the mechanism of HSV-1 capsid egress. It is possible that, rather than passing via the centrosome, capsids may travel directly to the site of envelopment after exiting the nucleus. We suggest that, in HSV-1-infected cells, the disruption of centrosomal functions triggers reorganization of the MT network to favor noncentrosomal MTs and promote efficient viral spread.

The microtubule (MT) network is commonly used for intracellular transport of virus particles (1), including the capsids of alphaherpesviruses such as herpes simplex virus 1 (HSV-1), which infects humans, and pseudorabies virus (PrV), a porcine herpesvirus (2, 3). This is important during entry, when capsids travel from the plasma membrane toward the nucleus, and during egress, when newly formed capsids exit the nucleus and travel toward the sites of envelopment at the *trans*-Golgi network (TGN) (4, 5). The MT network typically nucleates from a microtubule-organizing center (MTOC), which is most commonly the centrosome (6). The minus ends of MTs are embedded in the MTOC, while the highly dynamic plus ends extend throughout the cell. Because of this arrangement, it has been assumed that during entry, herpesvirus capsids travel from the plasma membrane to the centrosome, from which they are redirected to the nucleus, and that during egress, capsids are transported from the nucleus to the centrosome and then from the centrosome to the sites of envelopment (7). However, many viruses, such as adenovirus (8), rotavirus (9, 10), vaccinia virus (11, 12), and African swine fever virus (13), are known to reorganize the MT network and/or affect the centrosome during infection. Likewise, reorganization of the MT network and loss of the MTOC following HSV-1 infection have been reported (14, 15), leaving open the issue of what role the centrosome plays in HSV-1 capsid transport during egress. Although the interaction of capsids with the transport machinery is the subject of intensive research, the role of the centrosome in the process of capsid transport has not been fully evaluated.

In this paper, we investigate the effect of HSV-1 and PrV infections on the centrosome and on MT growth. We show that centrosome function is disrupted in HSV-1-infected cells but not in PrV-infected cells. Repolymerization of MTs following nocodazole treatment begins at the centrosome in mock- and PrV-infected cells, whereas it is absent in HSV-1-infected cells, thereby demonstrating that the centrosome no longer functions as an MTOC in these cells. Finally, EB3 labeling of MT plus ends revealed that whereas MTs no longer arise from a unique MTOC in HSV-1 cells, although they continue to do so in PrV-infected cells, they do still undergo growth, albeit slowly and from multiple locations in the cell.

MATERIALS AND METHODS

Cells and viruses. African green monkey kidney (Vero), porcine kidney cells (PK15), and Human Fetal Foreskin Fibroblast (HFFF2) cells were grown at 37°C in Dulbecco's modified Eagle medium (DMEM; PAA Laboratories) supplemented with 8% fetal calf serum.

The *17syn*+ strain of HSV-1 and the Kaplan strain of PrV were used as wild-type viruses. The ICP0-null virus *dl1403* (16), the UL49-null virus Δ22 (which does not encode VP22 [17]), and the UL19-null virus K5ΔZ (18) were kindly provided by R. Everett (CVR, Glasgow, United Kingdom), G. Elliott (Imperial College, London, United Kingdom), and P. Desai (Johns Hopkins University, Baltimore, MD), respectively. The UL36- and UL37-null viruses ARΔUL36 and FRΔUL37 were described previously (19). To identify HSV-1-infected cells in live-cell microscopy experiments (see below), cells were infected with the vUL35RFP1D1 virus. This virus has a wild-type background (17syn+) except that it encodes a VP26 capsid protein fused to the monomeric Red Fluorescent Protein (mRFP) (20).

Antibodies and reagents. The following antibodies were used: mouse monoclonal antibodies DM1A against alpha-tubulin (Sigma), GTU-88 against gamma-tubulin (Sigma), 11060 against HSV-1 ICP0 (SantaCruz Biotechnology), and DM165 against HSV-1 VP5 (21); rabbit polyclonal antibodies HPA016820 against pericentrin (Sigma), 14C10 against glyceraldehyde-3-phosphate dehydrogenase (GAPDH; Cell Signaling), and PTNC, specific for HSV-1 capsid proteins VP23, VP26, and pUL36 (described in reference 22). Rabbit antibody 1702 directed against PrV capsids and mouse polyclonal antibody a5 against

Received 19 March 2013 Accepted 10 April 2013

Published ahead of print 17 April 2013

Address correspondence to David Pasdeloup, pasdeloup@vms.cnrs-gif.fr.

Supplemental material for this article may be found at http://dx.doi.org/10.1128/JVI.00764-13.

doi:10.1128/JVI.00764-13

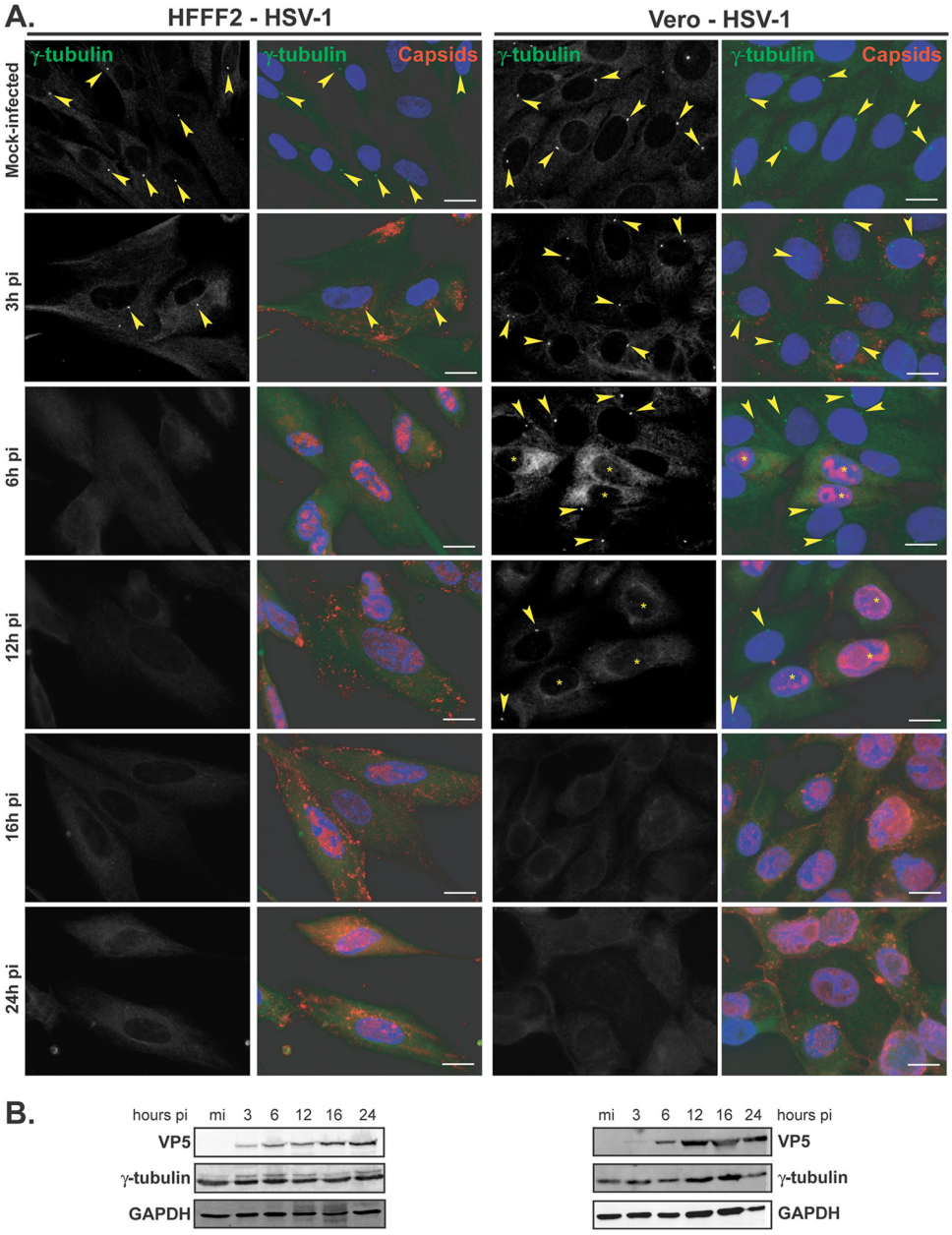

FIG 1 Gamma-tubulin loses centrosomal localization in HFFF2 and Vero cells infected with HSV-1. (A) HFFF2 (left panels) or Vero (right panels) cells were infected with 1 PFU/cell of HSV-1 for the indicated times before fixation. Gamma-tubulin was visualized using mouse monoclonal antibody GTU-88 (green), and infected cells were visualized with the PTNC rabbit antibody (red). The nuclei were counterstained with DAPI. Arrowheads show centrosomal localization of gamma-tubulin. Asterisks indicate infected cells in panels also containing uninfected cells. Bars, 20 μm. (B) Western blot analysis of lysates obtained from cells infected for the indicated times. The progress of infection was visualized using the DM165 antibody directed against the major capsid protein VP5, gamma-tubulin levels were assessed using the GTU-88 antibody, and GAPDH levels were monitored as loading controls.

PrV pUL25 were gifts from K. Kaelin (VMS, Gif-sur-Yvette, France) (23). Secondary antibodies for immunofluorescence were goat anti-mouse or anti-rabbit Alexa 488 or Alexa 568 conjugated (GAM_{488}, GAM_{568}, GAR_{488}, or GAR_{568}) obtained from Molecular Probes. For Western blot analysis, secondary antibodies were goat anti-mouse DyLight680 and anti-rabbit DyLight800 (Cell Signaling). The plasmid pGFP-hEB3 encoding a green fluorescent protein (GFP) fusion of the human EB3 protein was a kind gift of John Victor Small (Institute of Molecular Biotechnology, Vienna, Austria). Nocodazole was obtained from Sigma, resuspended in dimethyl sulfoxide (DMSO) as a stock solution at a concentration of 10 mM, and used at a final concentration of 10 μM.

Nocodazole recovery experiments. Cells were infected with 1 PFU/cell of the appropriate virus for 12 h before being incubated with 10 μM nocodazole for 1 h at 4°C. Cells were washed 2 times with cold DMEM followed by one wash with warm DMEM and then incubated for the indicated time in warm DMEM at 37°C. Cells were then fixed immediately as described below.

Fluorescence microscopy. All immunofluorescence with alpha-tubulin staining was done as follows. Cells were fixed in a mix of 3.7% formaldehyde and 0.1% Triton X-100 in PEM buffer [100 mM piperazine-*N*,*N*′-bis(2-ethanesulfonic acid) (PIPES), 5 mM EGTA, 2 mM $MgCl_2$, pH 6.8] for 5 min at room temperature as described in refer-

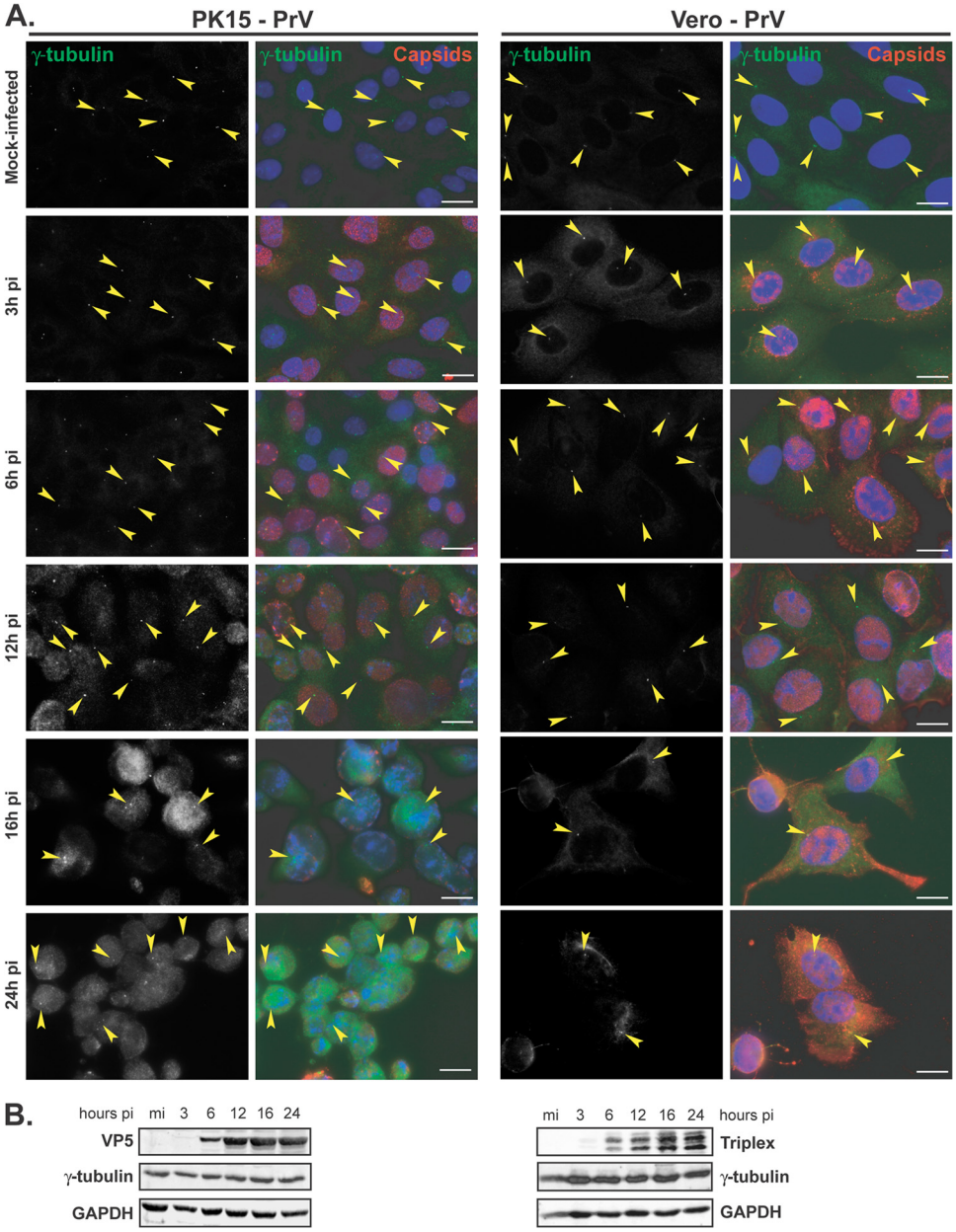

FIG 2 Gamma-tubulin retains centrosomal localization in PK15 and Vero cells infected with PrV. (A) PK15 (left panels) or Vero (right panels) cells were infected with 1 PFU/cell of PrV for the indicated times before fixation. Gamma-tubulin was visualized using mouse monoclonal antibody GTU-88 (green), and infected cells were visualized with the 1702 antibody (red). The nuclei were counterstained with DAPI. Arrowheads show examples of centrosomal localization of gamma-tubulin. Bars, 20 μm. (B) Western blot analysis of lysates obtained from cells infected for the indicated times. The progress of infection was visualized using the anti-capsid 1702 antibody to show either VP5 or the two triplex proteins, gamma-tubulin levels were assessed using the GTU-88 antibody, and GAPDH levels were monitored as loading controls.

ence 24. Microtubules were stained using the alpha-tubulin antibody and GAM_{488}.

To visualize centrosomes, cells were fixed with −20°C methanol and incubated at −20°C for 5 min. Methanol was discarded, and the cells were left to dry before being rehydrated with phosphate-buffered saline (PBS). Centrosomes were stained using the gamma-tubulin antibody and GAM_{488} or with the anti-pericentrin antibody and GAR_{488}. Infected cells were identified using the anti-HSV-1 capsid antibody PTNC or with the anti-PrV capsid antibody 1702 and visualized with GAR_{568}. Alternatively, infected cells were labeled with antibodies against HSV-1 ICP0 or PrV pUL25 and visualized with GAM_{568}. When rabbit antibodies were used, 8% human serum (Sigma) was used to block the virus-encoded Fc-binding sites (25).

Samples were mounted in ImmuMount (Thermo) containing 1 μg/ml 4′,6-diamidino-2-phenylindole dihydrochloride (DAPI) (Sigma) for DNA staining. All samples were visualized using a Zeiss Axio Observer Z1 microscope and a 63× Plan-apochromat oil-immersion objective (Zeiss) (numerical aperture = 1.4).

Live-cell microscopy. Cells were seeded on glass-bottomed petri dishes (MatTek) and transfected with 0.5 μg of pGFP-hEB3 using Lipofectamine 2000 (Invitrogen) following the manufacturer's instructions. At 6 h later, cells were infected with 1 PFU/cell of vUL35RFP1D1 or PrV

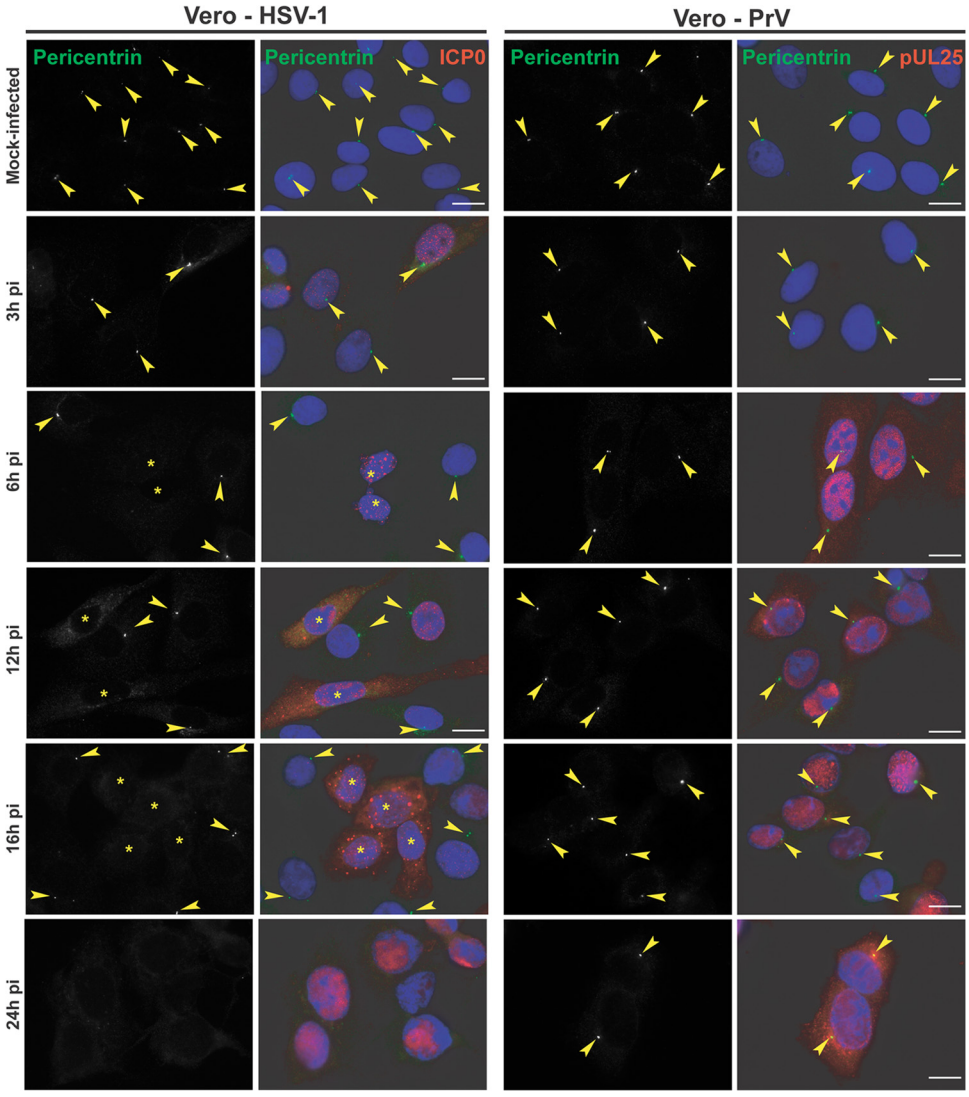

FIG 3 Differential loss of centrosomal localization of pericentrin in Vero cells infected with HSV-1 or PrV. Vero cells were infected with 1 PFU/cell of HSV-1 or PrV for the indicated times before fixation. Pericentrin was visualized using rabbit polyclonal antibody HPA016820 (green), and infected cells were visualized with the mouse antibodies 11060 against HSV-1 ICP0 and a5 against PrV pUL25 (red). The nuclei were counterstained with DAPI. Arrowheads show centrosomal localization of pericentrin. Asterisks indicate infected cells in panels also containing uninfected cells. Bars, 20 μm.

for 12 h. Live-cell recording was done on the same microscope as described above in an incubation chamber with controlled temperature (37°C) and atmosphere (5% CO_2, humidified). Movies of 60 frames were recorded at a rate of 1 frame every 2 s. Infected cells were identified through VP26RFP fluorescence (HSV-1) or subsequent immunostaining (PrV).

EB3 comet tracking. Movies were imported into ImageJ (version 1.43u). EB3 comets were tracked using the Particles Detector&Tracker plug-in (version 1.5 [26]). Depending on the quality of each individual movie, detection parameters were set as Radius = 5, Cutoff = 0.0, and Percentile = 0.1 to 1.8% and linking parameters were Link Range = 2 and Displacement = 10 to 20. Comet motion was analyzed using the coordinates provided by the software to calculate the distance traveled and velocity.

RESULTS

Centrosomal localization of gamma-tubulin is lost in HSV-1- but not in PrV-infected cells. In the course of investigating the fate of the centrosome during HSV-1 infection, HFFF2, a human cell line, or Vero cells, a monkey cell line routinely used for alphaherpesviruses, were mock infected or infected with 1 PFU/cell of HSV-1 for 3 h, 6 h, 12 h, 16 h, and 24 h. The cells were analyzed using an antibody specific for gamma-tubulin, an integral component of the centrosome (27, 28), and infection was monitored using a capsid-directed rabbit antibody (PTNC). Gamma-tubulin staining of mock-infected HFFF2 or Vero cells showed typical centrosomal localization, with fluorescence localized as one or two spots close to the nucleus (arrowheads in Fig. 1A). This localization was lost by 6 h postinfection (pi), after which time no specific labeling of gamma-tubulin was evident. Western blotting showed that overall gamma-tubulin levels were unaffected by HSV-1 infection, thereby demonstrating that the loss of centrosomal fluorescence reflected changes in the distribution of the protein (Fig. 1B). To determine whether the dispersal of gamma-tubulin was a general property of alphaherpesviruses, we repeated the experiment with another virus from this subfamily, namely,

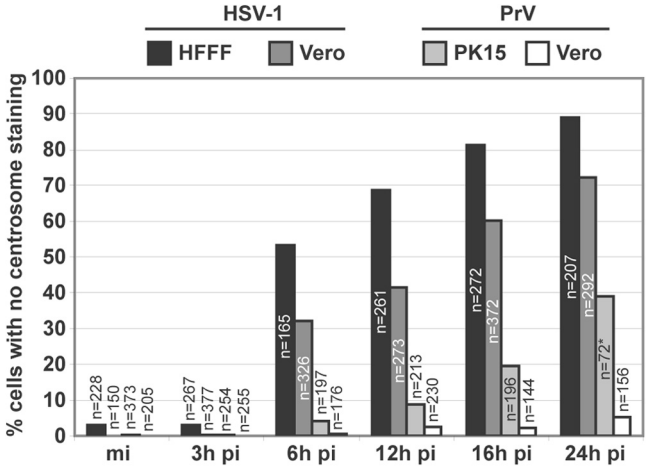

FIG 4 Quantification of centrosomal disruption in different cell lines infected by HSV-1 or PrV. A total number of 5661 cells, mock infected or infected with either HSV-1 or PrV for different times, were analyzed for the presence of the centrosome. Results are expressed as the percentage of cells with no detectable centrosomal gamma-tubulin staining. The asterisk indicates that due to extensive cell loss, fewer cells could be analyzed; most of the cells exhibited strong cytopathic effects.

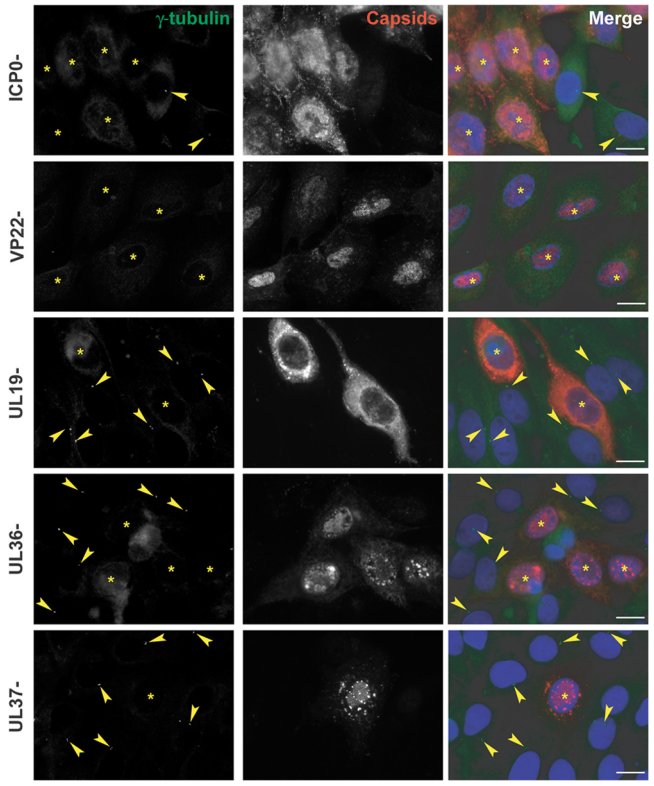

FIG 5 Centrosomal disruption in HFFF2 cells infected with ICP0-, VP22-, UL19-, UL36-, or UL37-null HSV-1 virus. HFFF2 cells were infected with 1 PFU/cell of *dl1403* (ICP0-), Δ22 (VP22-), K5ΔZ (UL19-), ARΔUL36 (UL36-), or FRΔUL37 (UL37-) virus for 16 h before fixation. Centrosomes were visualized by staining for gamma-tubulin using mouse monoclonal antibody GTU-88 (green), and infected cells were visualized with the PTNC antibody (red). The nuclei were counterstained with DAPI. Arrowheads show centrosomes. Asterisks indicate infected cells. Bars, 20 μm.

PrV, a porcine herpesvirus. PK15 cells, a porcine cell line, or Vero cells were mock infected or infected with 1 PFU/cell of PrV, and gamma-tubulin was monitored as described for HSV-1-infected cells. PrV-infected cells were visualized using a PrV-capsid-directed rabbit antibody (1702). In contrast to HSV-1, gamma-tubulin localization was unaffected, at the level of immunocytochemistry, in PrV-infected cells (Fig. 2A), although strong cytopathic effects evident at 16 and 24 h pi made it increasingly difficult to assess localization of gamma-tubulin due to changes in the cell shape and high background fluorescence. As with HSV-1, levels of gamma-tubulin were unchanged over the course of the infection (Fig. 2B).

These results show that gamma-tubulin loses its centrosomal localization in HSV-1-infected cells but not in PrV-infected cells.

Pericentrin centrosomal localization is lost in HSV-1- but not in PrV-infected cells. To determine whether the consequences of HSV-1 infection for gamma-tubulin were indicative of a more widespread effect, we monitored the localization of another centrosomal protein, pericentrin (29). Pericentrin was detected using the rabbit antibody HPA016820, which necessitated the use of mouse antibodies a5, directed against PrV pUL25 (a minor capsid protein [23]), and 11060, directed against HSV-1 ICP0, to monitor the infections. In mock-infected Vero cells, pericentrin localized to the centrosome, as expected, but in HSV-1-infected cells, the pericentrin behavior mimicked that of gamma-tubulin and this localization had disappeared by 6 h postinfection (Fig. 3). Once again, dispersion of the centrosome was not seen in PrV-infected cells, and pericentrin remained localized even at late times after infection.

Thus, these results support the data obtained with gamma-tubulin staining and confirm that the centrosome is altered in HSV-1-infected cells but not in PrV-infected cells.

We quantified the loss of centrosomal markers in HFFF2 or Vero cells infected with HSV-1, and in PK15 or Vero cells infected with PrV, by determining the number of cells lacking detectable gamma-tubulin foci at different times after infection (Fig. 4). This showed that by 6 h pi, more than 50% of HFFF2 and more than 30% of Vero cells infected with HSV-1 had no detectable centrosomes. This number increased with time of infection to reach 89% in HFFF2 cells after 24 h. In contrast, PrV-infected Vero cells showed no significant centrosomal loss throughout the time of infection, while in PK15 cells, only ~20% of cells had lost visible centrosomes by 16 h pi, and this number increased to ~40% at 24 h pi. However, the extensive cytopathic effect evident in PK15 cells from 16 h pi (as shown in Fig. 2A) made it difficult to image these cells and could account for this apparent centrosomal loss. It is clear from these results that the effect of infection on the behavior of these centrosomal markers is much greater in HSV-1-infected cells than in cells infected by PrV, particularly at 6 h and 12 h pi.

ICP0, VP22, capsid formation, and the inner tegument are not necessary for centrosomal disruption. To investigate candidate proteins that might influence centrosome function, we infected HFFF2 cells for 16 h with a range of HSV-1 mutants lacking specific functions. The HSV-1 immediate early protein ICP0 has been reported to dismantle the MTOC-based organization of the MT network (30). Therefore, we checked whether ICP0 was responsible for the loss of gamma-tubulin centrosomal localization using the ICP0-null virus *dl1403* (16). As shown in Fig. 5, centrosomes could not be detected in *dl1403* virus-infected cells, suggesting that ICP0 is not required. The tegument protein VP22

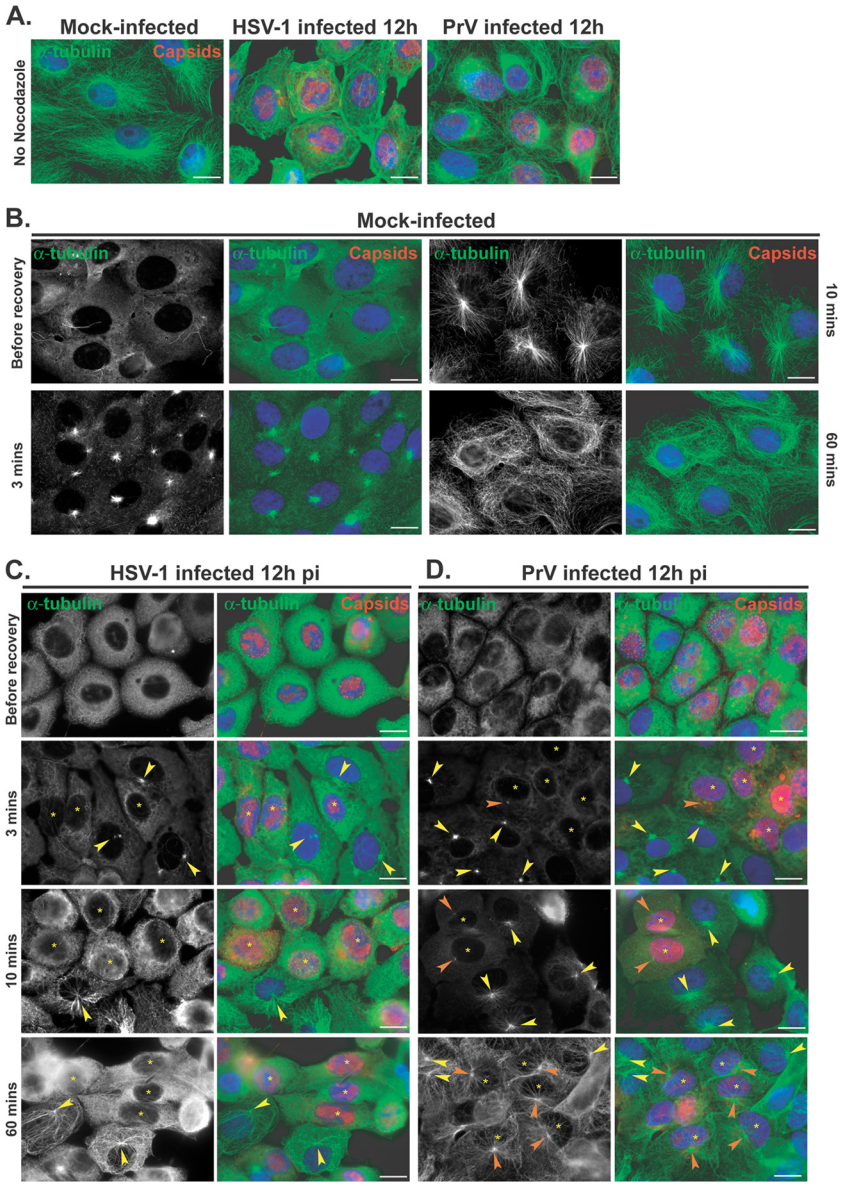

FIG 6 Recovery of nocodazole-disrupted MTs in Vero cells infected with HSV-1 or PrV. (A) Comparison of MT networks in untreated Vero cells that were mock infected or infected with HSV-1 or PrV for 12 h. (B to D) Nocodazole recovery experiments. Vero cells were mock infected (B) or infected with HSV-1 (C) or PrV (D) for 12 h before being treated with 10 μM nocodazole. One hour later, the drug was washed out and cells were fixed after the indicated times. MTs were visualized using a mouse antibody directed against alpha-tubulin (green). HSV-1-infected cells were visualized using the PTNC rabbit antibody and PrV-infected cells using the 1702 rabbit antibody (red). Arrowheads in panels C and D indicate centers of MT growth in infected cells (orange) or uninfected cells (yellow). Asterisks indicate infected cells in panels also containing uninfected cells. Note that MT growth is absent (C) or limited (D) in infected cells compared to uninfected cells. Bars, 20 μm.

(pUL49) was reported to localize to MTs in transfected cells (31) and thus might be expected to influence the centrosome. However, gamma-tubulin dispersion was observed following infection with the VP22-null Δ22 virus (17), thus precluding a role for the protein in the process (Fig. 5). Since a major function of MTs at late times after infection is to transport capsids across the cytoplasm from the nucleus to the sites of envelopment, we examined whether this process might be necessary for centrosome disruption. The inner tegument proteins pUL36 and pUL37 have been shown to be important for capsid transport (32, 33). Therefore, we infected cells with the mutant viruses ARΔUL36 and FRΔUL37 (deleted for UL36 and UL37, respectively [19]). We used the UL19-null mutant, K5ΔZ, which is unable to produce capsids (18), as an additional control. Gamma-tubulin dispersion was observed in cells infected with each of these mutant viruses, which indicates that capsid transport and the inner tegument proteins pUL36 and pUL37 are not involved in changes to the centrosome.

MT recovery after nocodazole washout is impaired in HSV-1- but not in PrV-infected cells. Loss of the centrosome during HSV-1 infection would imply that it no longer functioned as the major MTOC, meaning that MT growth from the centrosome would not occur. To monitor this, nocodazole recovery assays were carried out. Nocodazole is a drug which triggers MT

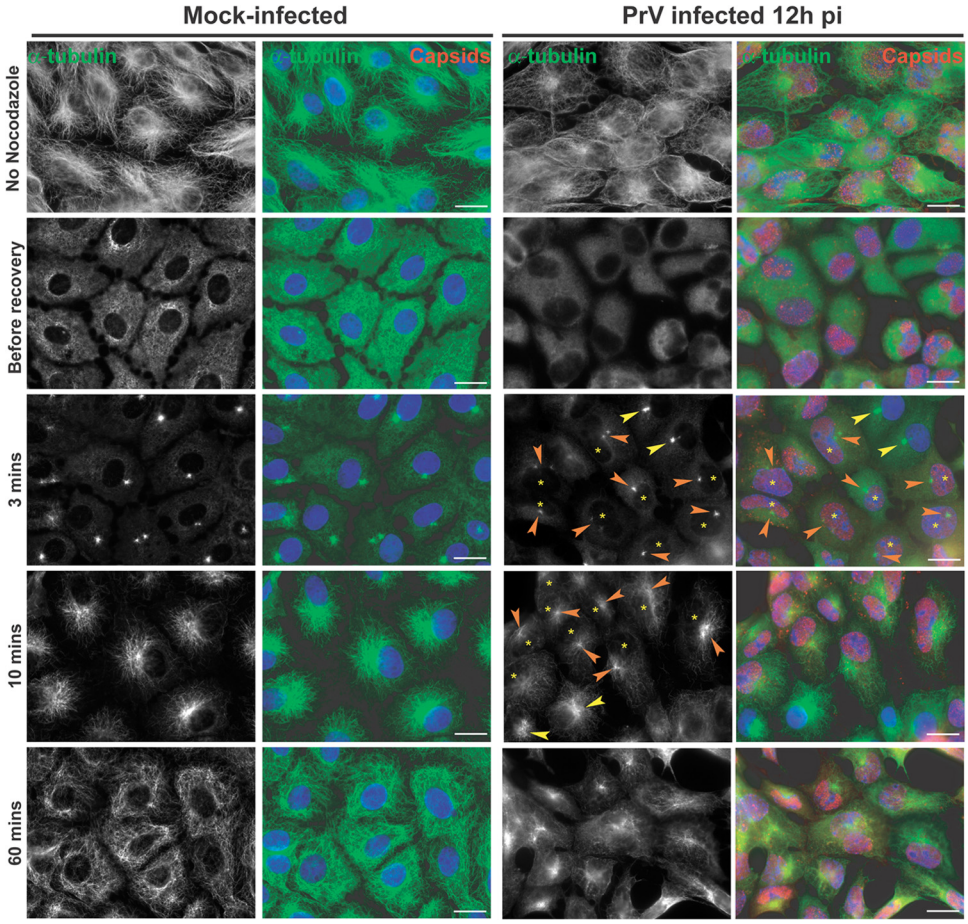

FIG 7 Recovery of nocodazole-disrupted MTs in PK15 cells infected with PrV. PK15 cells were mock infected or infected with PrV for 12 h before being treated with 10 μM nocodazole. One hour later, the drug was washed out and cells were fixed after the indicated time. Immunolabeling was carried out as described for Fig. 6. Arrowheads indicate centers of MT growth in infected cells (orange) or uninfected cells (yellow). Asterisks indicate infected cells in panels also containing uninfected cells. Note that MTs are centrally nucleated in infected cells. Bars, 20 μm.

depolymerization. This effect is reversible, and upon nocodazole washout, MTs polymerize *de novo* from MTOCs, which in most cells are provided by the centrosome. Vero cells were mock infected or infected with 1 PFU/cell of HSV-1 or PrV. In order to observe a significant number of cells with centrosomal disruption while avoiding severe cytopathic effects, infection was carried out for 12 h. Cells were then either fixed directly or incubated with 10 μM nocodazole for 1 h. Then, cells were fixed immediately ("before recovery") or 3, 10, or 60 min after the drug was washed out. As shown in Fig. 6A, the MT network underwent reorganization in cells infected for 12 h in the absence of nocodazole. In both HSV-1- and PrV-infected cells, the MT network was less dense than in mock-infected cells. In PrV-infected cells, MT filaments were usually observed concentrated in a perinuclear area suggestive of the presence of a centrosome whereas most HSV-1-infected cells showed no such organization (Fig. 6A).

Treatment of mock-infected and infected cells with 10 μM nocodazole for 1 h was sufficient to depolymerize the majority of Vero cell MTs (Fig. 6B to D). Three minutes after nocodazole washout, MT polymerization had started in mock-infected cells and was clearly centralized at an MTOC, presumably the centrosome (Fig. 6B). By 10 min, MT recovery was almost complete, with the MTOC organization very evident, and after 1 h the MT network was fully recovered. This contrasted sharply with the behavior in cells infected with HSV-1 for 12 h, where no *de novo* polymerized MT filaments were detected even at 1 h after nocodazole washout (Fig. 6C).

In PrV-infected Vero cells, initiation of MT growth was delayed compared to mock-infected cells, with little visible 3 min after nocodazole washout. By 10 min after washout, MT growth from visible MTOCs had started (Fig. 6D), although it was much more limited than in mock-infected cells. One hour after nocodazole washout, MTOC-based networks of MTs radiated throughout the infected cells, although the growth was less dense than that seen in mock-infected cells (Fig. 6A).

These effects were not limited to Vero cells. In PrV-infected PK15 cells, the same behavior was observed, although the MT repolymerization was more efficient than in infected Vero cells (Fig. 7). Nevertheless, as with the Vero cells, the MT network did not fully recover after 1 h, which suggests that PrV infection has an inhibitory effect on MT polymerization and/or MT stability but not on centrosomal-based nucleation of MTs. Similarly, the influence of HSV-1 infection on MT polymerization was not cell specific, since MTOC-based MT repolymerization following nocodazole treatment and washout was also lacking in HFFF2 cells (Fig. 8).

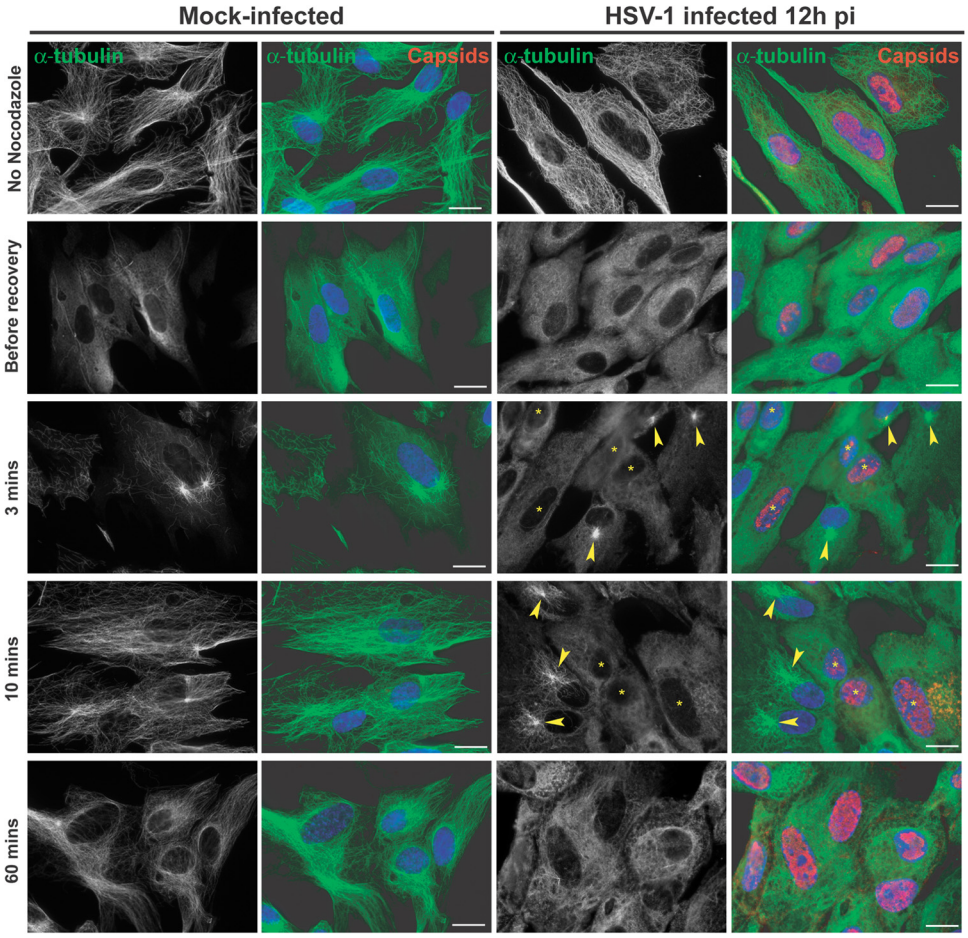

FIG 8 Recovery of nocodazole-disrupted MTs in HFFF2 cells infected with HSV-1. HFFF2 cells were mock infected or infected with HSV-1 for 12 h before being treated with 10 μM nocodazole. One hour later, the drug was washed out and cells fixed after the indicated time. Immunolabeling was carried out as described for Fig. 6. Arrowheads indicate centers of MT growth. Asterisks indicate infected cells in panels also containing uninfected cells. Note the absence of centralized MT growth in infected cells. Bars, 20 μm.

These experiments show that in cells infected by HSV-1, the growth, and possibly the stability, of MTs originating from the centrosome is impaired, thereby indicating that the centrosome is functionally disrupted. This does not appear to be the case for PrV.

Growth of MTs is less efficient and originates from noncentrosomal sites in HSV-1-infected cells. To investigate MT nucleation in HSV-1- and PrV-infected cells, MT dynamics were followed in living cells by tracking the distribution of End-Binding protein 3 (EB3), which predominantly binds to the plus-end tip of growing MTs (34). To illustrate the pattern of MT growth, time-lapse movies were collected and projections of the first 5, 10, 25, and 60 time-lapse frames, covering periods of 10, 20, 50, and 120 s, respectively, were produced (Fig. 9; see also Movies S1 to S4 in the supplemental material). Mock-infected HFFF2 cells expressing EB3 fused to GFP (GFP-EB3) showed strong fluorescence with a typical "comet" shape at the plus-end tip of each growing MT (see Movie S1 in the supplemental material). MT growth was active throughout cells, with most originating at an obvious nucleating center near the nucleus (arrowheads in Fig. 9; see also Movie S1 in the supplemental material). In cells infected with HSV-1 for 12 h, MT growth was very limited. It was mostly localized near the plasma membrane at cell extremities, and no obvious nucleation centers were visible (Fig. 9; see also Movie S2 in the supplemental material). The GFP-EB3 signal was weak and diffuse, and EB3 comets were reduced in number. Specifically, individual comets were almost five times shorter (Fig. 9B) and the rate of MT growth appeared to be ~40% lower than in mock-infected cells (Fig. 9C; see also Movie S2 in the supplemental material). Moreover, the comets in infected cells appear to be less stable, since many of them were observed in only ~7 to 8 consecutive frames before they disappeared, whereas those in mock-infected cells were frequently present throughout the period of observation (more than 30 consecutive frames; Fig. 9D). Similar observations were made at later times after infection, including 16 h and 24 h pi (data not shown).

The dispersed pattern of MT growth and lack of a single focal site support the idea that the centrosome is lost during HSV-1 infection and suggest the possibility that MT growth originates from multiple noncentrosomal nucleating centers throughout the infected cell.

Live-cell experiments were also carried out in PK15 cells. These showed smaller comet tips and shorter runs than HFFF2 cells but had similar comet velocities (Fig. 9B to D). As with HSV-1 in

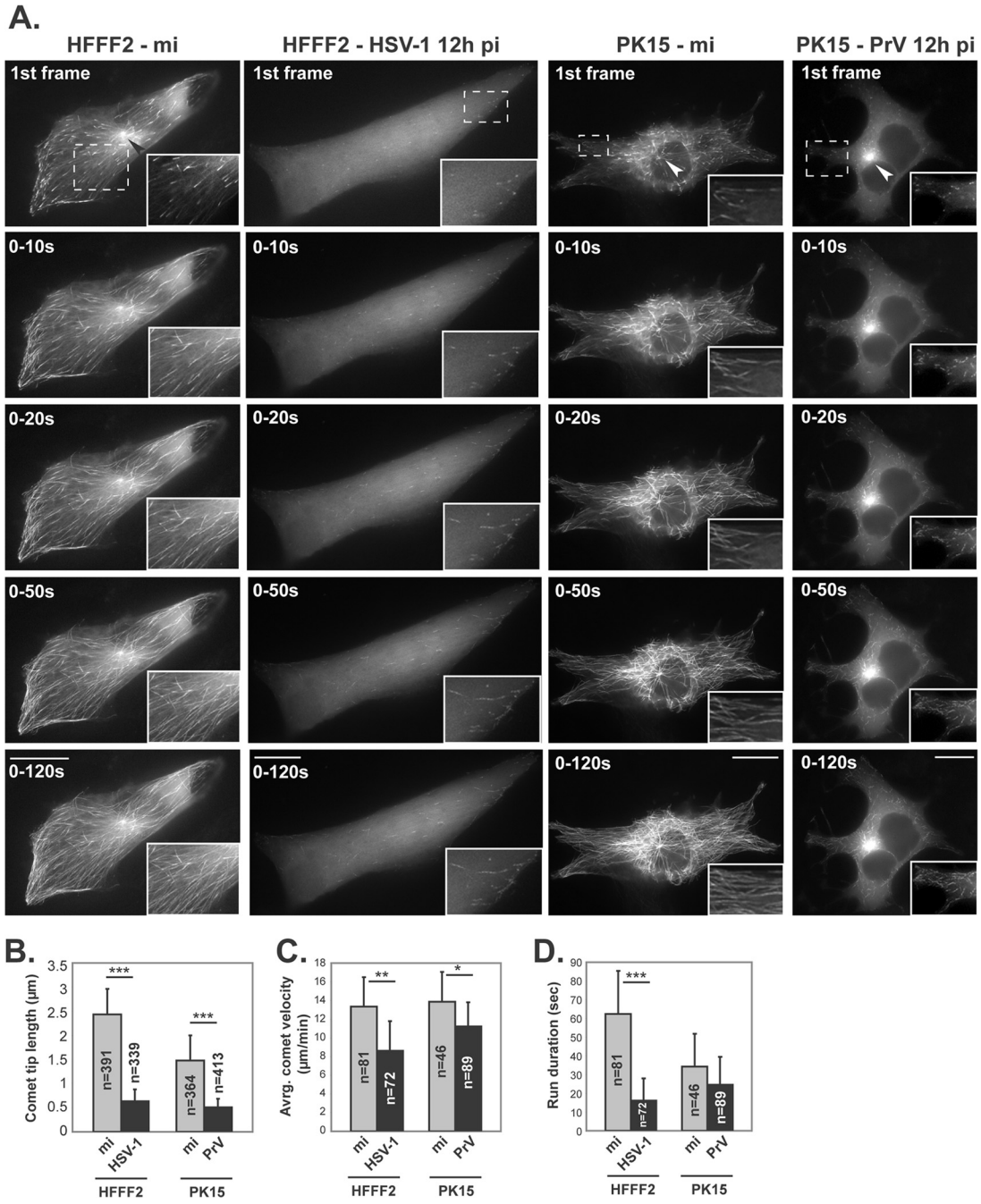

FIG 9 MT growth in living HFFF2 and PK15 cells that were mock infected or infected with HSV-1 or PrV. HFFF2 and PK15 cells were transfected with a plasmid encoding GFP-EB3, a protein that localizes at plus-end tips of MTs. At 6 h later, HFFF2 cells were mock infected (mi) or infected with vUL35RFP1D1 (an HSV-1 virus in which the capsid protein VP26 is fused to the mRFP) and PK15 cells were infected with wild-type PrV. After a further 12 h, GFP-EB3 localization was recorded by live-cell microscopy at a rate of one frame every 2 s. Infected HFFF2 cells were identified by mRFP fluorescence (not shown). Infection of PK15 cells by PrV was subsequently checked by immunostaining for capsids (not shown). (A) Individual panels show cumulative projections of frames obtained over the indicated periods after the start of recording. Arrowheads show MT nucleating centers in the first frame images. An area from each cell image (dashed boxes) is enlarged. To observe MT growth, see Movies S1 and S2 (mock-infected and HSV-1-infected HFFF2 cells, respectively) and Movies S3 and S4 (mock-infected and PrV-infected PK15 cells, respectively) in the supplemental material. Bars, 20 μm. Movies were taken at a rate of 1 frame every 2 s for 120 s and are shown at a rate of 10 frames/s. (B) The length of 730 EB3 comets was measured in single time frames from movies of nine mock-infected (mi) and 10 HSV-1-infected HFFF2 cells. The length of 777 EB3 comets was measured in single time frames from movies of four uninfected and eight PrV-infected PK15 cells. (C and D) A total of 153 (HFFF2) and 135 (PK15) comets were tracked, and their velocity was measured (C) as well as the number of consecutive frames where they could be tracked (run duration) (D). *, $P < 0.05$; **, $P < 0.01$; ***, $P < 0.001$.

HFFF2 cells, infection of PK15 cells by PrV resulted in shorter comet tips than in mock-infected cells. The reduction was less than that seen in HSV-1-infected HFFF2 cells (~3 times shorter compared to ~5 times shorter). However, their length of 0.5 μm (± 0.17) is very similar to that in HSV-infected HFFF2 cells (0.64 μm ± 0.24). In contrast to HSV-1-infected cells, comet velocity was only slightly lower in PrV-infected cells than in mock-infected cells (Fig. 9C), and run duration was not significantly altered (Fig. 9D). As would be expected from the nocodazole washout experiments, MT growth in PrV-infected PK15 cells predominantly originated from a major MTOC, presumably the centrosome (Fig. 9A; see also Movie S4 in the supplemental material). In this respect, PrV-infected cells resemble mock-infected cells and differ from HSV-1-infected cells (see Movie S2 in the supplemental material).

These results show that infection by both HSV-1 and PrV alters MT growth, although to differing degrees, but only infection by HSV-1 disrupts the MTOC function of the centrosome.

DISCUSSION

This paper reports on two main findings. First, the centrosome's function as an MTOC is disrupted in the course of infection by HSV-1 but not by another alphaherpesvirus, PrV. Second, MT dynamics are modified in cells infected with either HSV-1 or PrV, although to different degrees. These observations raise questions regarding egress of alphaherpesviruses and their interactions with the MT network.

The capsids of alphaherpesviruses are known to rely on MTs for transport throughout the cell (3). In particular, MTs have been shown to be important for rapid capsid transport at late stages of infection (32, 35). Since the MT network is typically organized around MTOCs, the most prominent of which is the centrosome, it was reasonably assumed that capsids would have to pass through MTOCs during entry and egress (7). Traversing the centrosome represents an important phase in capsid transport since it would require a change of transport polarity. However, this step and the fate of the centrosome during herpesvirus infection have not been extensively analyzed. One study described loss of the MTOC in Vero cells at 6 h pi and its reformation at 25 h pi (15), while MT reorganization at 6 h pi has also been reported (14). Another study reported that the MT network is disrupted in HSV-1-infected Vero cells, that this requires ICP0, and that tubulin colocalizes into cytoplasmic globular bodies with ICP0 (30). In this paper, we demonstrate using centrosome-specific markers and functional assays that the centrosome ceases to function as the primary MTOC following HSV-1 infection and confirm that the disruption of centrosomal activity starts by 6 h pi. In contrast to Kotsakis and collaborators (15), we did not observe reformation of the centrosome at 24 h pi but were unable to check later times given the extent of the cytopathic effect. Unlike Liu et al. (30), we saw no accumulation of tubulin into globular bodies in HSV-1-infected Vero or HFFF2 cells and we show that deletion of ICP0 did not prevent loss of the centrosome.

As already stated, loss of the centrosomal MTOC function is apparent by about 6 h after HSV-1 infection, which is around the time when capsids start to exit the nucleus and have to be transported across the cytoplasm to the sites of envelopment. It is interesting, therefore, to speculate as to how these changes might affect viral egress. In most cell types, the majority of MT minus ends are embedded in the centrosome and uncapped MT minus ends typically disassemble quickly in the cytoplasm. In the centrosome, MTs nucleate from their minus ends through γ-tubulin ring complexes (or γ-TuRCs), in which γ-tubulin plays a critical role (36). Therefore, it is likely that if the centrosome or its nucleating material is lost as a result of HSV-1 infection (as is suggested by the absence of centrosomal γ-tubulin), the population of MTs with their minus ends anchored at the centrosome will also be lost. However, MTs with free and stable minus ends, independent of the centrosome, are found in some cell lines (37). In addition, there are specialized cell types, such as epithelial and neuronal cells, in which "noncentrosomal" MTOCs have been described as performing the MT-stabilizing role (6, 37, 38). It is not clear whether either of these mechanisms accounts for some or all of the noncentrosomal MTs observed in both Vero and HFFF2 cells infected with HSV-1. However, we did observe growth of noncentrosomal MTs in HFFF2 cells infected with HSV-1 (Fig. 9) and observations in live cells confirmed that MTs were growing from many different points, predominantly localized in the vicinity of the plasma membrane. One noncentrosomal MTOC that has previously been identified is the TGN (39). This suggests the possibility that disruption of the centrosome and destabilization of centrosomal MTs could favor noncentrosomal MTs emanating from alternative MTOCs such as the TGN. Since the TGN is an important site of envelopment for the virus, such noncentrosomal MTs could provide a direct route from the nucleus to the TGN for the many newly formed capsids. The retention of centrosomal organization would suggest that this is not the case for PrV.

In addition to the loss of centrosomal organization in HSV-1-infected cells, live-cell microscopy of MT plus ends in HSV-1-infected cells revealed that the rate and duration of MT growth were also reduced following infection (Fig. 9). Although MTs were observed growing from centrosomal sites in PrV-infected PK15 and Vero cells, the rate and extent of this growth also seemed to be limited compared to mock-infected cells (Fig. 6, 7, and 9). These observations suggest that MT growth is affected in cells infected with either HSV-1 or PrV and that the effects on MT growth may be at least partly independent of those on the centrosome.

HSV-1 is not the only virus reported to have a disruptive effect on the centrosome. Infections by vaccinia virus and African swine fever virus also trigger centrosome loss (12, 13). Moreover, Bystrevskaya and colleagues reported on centriole alteration in dividing human embryo lung fibroblasts (HEL) and Vero cells productively infected with human cytomegalovirus (40). It is therefore plausible that centrosomal disruption is part of a general viral strategy to optimize the MT network in a way that benefits viral egress. How this works is yet to be determined.

In summary, the data presented here suggest that alphaherpesviruses can adopt differing egress strategies and that investigating the role of the centrosome will provide interesting insights into their nature.

ACKNOWLEDGMENTS

We thank Yves Gaudin for critical reading of the manuscript. We are grateful to John Victor Small (Institute of Molecular Biotechnology, Vienna, Austria) for providing the pGFP-hEB3 plasmid, to Karin Kaelin (VMS, Gif-sur-Yvette, France) for antibodies 1702 and a5, to Roger Everett for the *dl1403* virus, to Gillian Elliott (Imperial College, London, United Kingdom) for the Δ22 virus, and to Prashant Desai (John Hopkins University, Baltimore, MD) for the K5ΔZ virus.

This work was supported by funds from the CNRS.

REFERENCES

1. **Greber UF, Way M.** 2006. A superhighway to virus infection. Cell **124**: 741–754.
2. **Mabit H, Nakano MY, Prank U, Saam B, Dohner K, Sodeik B, Greber UF.** 2002. Intact microtubules support adenovirus and herpes simplex virus infections. J. Virol. **76**:9962–9971.
3. **Sodeik B, Ebersold MW, Helenius A.** 1997. Microtubule-mediated transport of incoming herpes simplex virus 1 capsids to the nucleus. J. Cell Biol. **136**:1007–1021.
4. **Harley CA, Dasgupta A, Wilson DW.** 2001. Characterization of herpes simplex virus-containing organelles by subcellular fractionation: role for organelle acidification in assembly of infectious particles. J. Virol. **75**: 1236–1251.
5. **Turcotte S, Letellier J, Lippe R.** 2005. Herpes simplex virus type 1 capsids transit by the trans-Golgi network, where viral glycoproteins accumulate independently of capsid egress. J. Virol. **79**:8847–8860.
6. **Bartolini F, Gundersen GG.** 2006. Generation of noncentrosomal microtubule arrays. J. Cell Sci. **119**:4155–4163.
7. **Radtke K, Dohner K, Sodeik B.** 2006. Viral interactions with the cytoskeleton: a hitchhiker's guide to the cell. Cell Microbiol. **8**:387–400.
8. **Warren JC, Rutkowski A, Cassimeris L.** 2006. Infection with replication-deficient adenovirus induces changes in the dynamic instability of host cell microtubules. Mol. Biol. Cell **17**:3557–3568.
9. **Brunet JP, Jourdan N, Cotte-Laffitte J, Linxe C, Geniteau-Legendre M, Servin A, Quero AM.** 2000. Rotavirus infection induces cytoskeleton disorganization in human intestinal epithelial cells: implication of an increase in intracellular calcium concentration. J. Virol. **74**:10801–10806.
10. **Zambrano JL, Sorondo O, Alcala A, Vizzi E, Diaz Y, Ruiz MC, Michelangeli F, Liprandi F, Ludert JE.** 2012. Rotavirus infection of cells in culture induces activation of RhoA and changes in the actin and tubulin cytoskeleton. PLoS One **7**:e47612. doi:10.1371/journal.pone.0047612.
11. **Arakawa Y, Cordeiro JV, Way M.** 2007. F11L-mediated inhibition of RhoA-mDia signaling stimulates microtubule dynamics during vaccinia virus infection. Cell Host Microbe **1**:213–226.
12. **Ploubidou A, Moreau V, Ashman K, Reckmann I, Gonzalez C, Way M.** 2000. Vaccinia virus infection disrupts microtubule organization and centrosome function. EMBO J. **19**:3932–3944.
13. **Jouvenet N, Wileman T.** 2005. African swine fever virus infection disrupts centrosome assembly and function. J. Gen. Virol. **86**:589–594.
14. **Avitabile E, Di Gaeta S, Torrisi MR, Ward PL, Roizman B, Campadelli-Fiume G.** 1995. Redistribution of microtubules and Golgi apparatus in herpes simplex virus-infected cells and their role in viral exocytosis. J. Virol. **69**:7472–7482.
15. **Kotsakis A, Pomeranz LE, Blouin A, Blaho JA.** 2001. Microtubule reorganization during herpes simplex virus type 1 infection facilitates the nuclear localization of VP22, a major virion tegument protein. J. Virol. **75**:8697–8711.
16. **Stow ND, Stow EC.** 1986. Isolation and characterization of a herpes simplex virus type 1 mutant containing a deletion within the gene encoding the immediate early polypeptide Vmw110. J. Gen. Virol. **67**(Pt 12): 2571–2585.
17. **Elliott G, Hafezi W, Whiteley A, Bernard E.** 2005. Deletion of the herpes simplex virus VP22-encoding gene (UL49) alters the expression, localization, and virion incorporation of ICP0. J. Virol. **79**:9735–9745.
18. **Desai P, DeLuca NA, Glorioso JC, Person S.** 1993. Mutations in herpes simplex virus type 1 genes encoding VP5 and VP23 abrogate capsid formation and cleavage of replicated DNA. J. Virol. **67**:1357–1364.
19. **Roberts AP, Abaitua F, O'Hare P, McNab D, Rixon FJ, Pasdeloup D.** 2009. Differing roles of inner tegument proteins pUL36 and pUL37 during entry of herpes simplex virus type 1. J. Virol. **83**:105–116.
20. **Pasdeloup D, Beilstein F, Roberts AP, McElwee M, McNab D, Rixon FJ.** 2010. Inner tegument protein pUL37 of herpes simplex virus type 1 is involved in directing capsids to the trans-Golgi network for envelopment. J. Gen. Virol. **91**:2145–2151.
21. **McClelland DA, Aitken JD, Bhella D, McNab D, Mitchell J, Kelly SM, Price NC, Rixon FJ.** 2002. pH reduction as a trigger for dissociation of herpes simplex virus type 1 scaffolds. J. Virol. **76**:7407–7417.
22. **Pasdeloup D, Blondel D, Isidro AL, Rixon FJ.** 2009. Herpesvirus capsid association with the nuclear pore complex and viral DNA release involve the nucleoporin CAN/Nup214 and the capsid protein pUL25. J. Virol. **83**:6610–6623.
23. **Kaelin K, Dezelee S, Masse MJ, Bras F, Flamand A.** 2000. The UL25 protein of pseudorabies virus associates with capsids and localizes to the nucleus and to microtubules. J. Virol. **74**:474–482.
24. **Vielkind U, Swierenga SH.** 1989. A simple fixation procedure for immunofluorescent detection of different cytoskeletal components within the same cell. Histochemistry **91**:81–88.
25. **Baucke RB, Spear PG.** 1979. Membrane proteins specified by herpes simplex viruses. V. Identification of an Fc-binding glycoprotein. J. Virol. **32**:779–789.
26. **Sbalzarini IF, Koumoutsakos P.** 2005. Feature point tracking and trajectory analysis for video imaging in cell biology. J. Struct. Biol. **151**:182–195.
27. **Stearns T, Evans L, Kirschner M.** 1991. Gamma-tubulin is a highly conserved component of the centrosome. Cell **65**:825–836.
28. **Zheng Y, Jung MK, Oakley BR.** 1991. Gamma-tubulin is present in Drosophila melanogaster and Homo sapiens and is associated with the centrosome. Cell **65**:817–823.
29. **Doxsey SJ, Stein P, Evans L, Calarco PD, Kirschner M.** 1994. Pericentrin, a highly conserved centrosome protein involved in microtubule organization. Cell **76**:639–650.
30. **Liu M, Schmidt EE, Halford WP.** 2010. ICP0 dismantles microtubule networks in herpes simplex virus-infected cells. PLoS One **5**:e10975. doi: 10.1371/journal.pone.0010975.
31. **Elliott G, O'Hare P.** 1998. Herpes simplex virus type 1 tegument protein VP22 induces the stabilization and hyperacetylation of microtubules. J. Virol. **72**:6448–6455.
32. **Luxton GW, Lee JI, Haverlock-Moyns S, Schober JM, Smith GA.** 2006. The pseudorabies virus VP1/2 tegument protein is required for intracellular capsid transport. J. Virol. **80**:201–209.
33. **Wolfstein A, Nagel CH, Radtke K, Dohner K, Allan VJ, Sodeik B.** 2006. The inner tegument promotes herpes simplex virus capsid motility along microtubules in vitro. Traffic **7**:227–237.
34. **Nakagawa H, Koyama K, Murata Y, Morito M, Akiyama T, Nakamura Y.** 2000. EB3, a novel member of the EB1 family preferentially expressed in the central nervous system, binds to a CNS-specific APC homologue. Oncogene **19**:210–216.
35. **Pasdeloup D, McElwee M, Beilstein F, Labetoulle M, Rixon FJ.** 2013. Herpesvirus tegument protein pUL37 interacts with dystonin/BPAG1 to promote capsid transport on microtubules during egress. J. Virol. **87**: 2857–2867.
36. **Kollman JM, Merdes A, Mourey L, Agard DA.** 2011. Microtubule nucleation by gamma-tubulin complexes. Nat. Rev. Mol. Cell Biol. **12**: 709–721.
37. **Dammermann A, Desai A, Oegema K.** 2003. The minus end in sight. Curr. Biol. **13**:R614–R624.
38. **Döhner K, Nagel CH, Sodeik B.** 2005. Viral stop-and-go along microtubules: taking a ride with dynein and kinesins. Trends Microbiol. **13**:320–327.
39. **Efimov A, Kharitonov A, Efimova N, Loncarek J, Miller PM, Andreyeva N, Gleeson P, Galjart N, Maia AR, McLeod IX, Yates JR, III, Maiato H, Khodjakov A, Akhmanova A, Kaverina I.** 2007. Asymmetric CLASP-dependent nucleation of noncentrosomal microtubules at the trans-Golgi network. Dev. Cell **12**:917–930.
40. **Bystrevskaya VB, Lobova TV, Smirnov VN, Makarova NE, Kushch AA.** 1997. Centrosome injury in cells infected with human cytomegalovirus. J. Struct. Biol. **120**:52–60.

PARTIE IV :

Analyse de la distribution des glycoprotéines d'enveloppe du virus HSV-1 par microscopie à « super-résolution »

Contexte et hypothèse de travail

Les Herpesvirus codent pour un nombre variable de différentes glycoprotéines d'enveloppe. Dans le cas du virus HSV-1, on en dénombre 11[45] auxquelles peuvent s'ajouter d'autres protéines d'enveloppe. Malgré une certaine variabilité dans le nombre des protéines d'enveloppe entre les différentes sous-familles d'Herpesviridae, il est maintenant bien établi que le « cœur » de protéines nécessaires au mécanisme de fusion consiste en la protéine gB ainsi que de l'hétérodimère gH/gL dont les structures cristallographiques ont été publiées[46,47]. Dans le cas de HSV-1, la protéine d'attachement gD est également requise pour l'activation de la fusion[45]. Cette protéine permet l'attachement du virus aux cellules via l'interaction avec ses récepteurs, tels que HVEM (Herpes Virus Entry Mediator) ou Nectin-1[48,49]. En amont de cet attachement, la protéine gC est impliquée dans le « pré-attachement » ou adsorption du virus aux cellules. Cette protéine, non-essentielle en culture de cellules, intéragit avec les héparanes sulfates[50] ou le récepteur MARCO[51] afin de permettre une meilleure adsorption du virus sur les cellules en amont de l'interaction spécifique de gD avec ses récepteurs.

Ainsi, le modèle d'entrée de HSV-1 peut-être ainsi résumé[45] :

(1) adsorption (gC) -> (2) attachement aux récepteurs (gD) et activation de gD -> (3) activation de gH/gL par gD activée -> (4) activation de gB par gH/gL activée -> fusion des membranes virales et cellulaires.

Contrairement à de nombreux virus n'ayant qu'une ou deux glycoprotéines d'enveloppe, la densité de protéines différentes à la surface du virus rend difficile l'identification ainsi que l'analyse du nombre et, surtout, de la localisation de chaque type de glycoprotéine sur la particule virale. La microscopie électronique par tomographie a permis de montrer que la densité de glycoprotéines à la surface du virus n'est pas homogène[52,53]. Cette densité semble être fonction de la position de la capside dans le virion. Cette position dépend de la maturation de la particule virale. En effet, Newcomb et al. ont montré que la capside était présente au centre du virion dans les particules nouvellement produites, mais que cette localisation centrale changeait au cours du temps pour une localisation asymétrique telle qu'observée dans des particules virales purifiées observées par cryo-tomographie (**Figure 11**)[54].

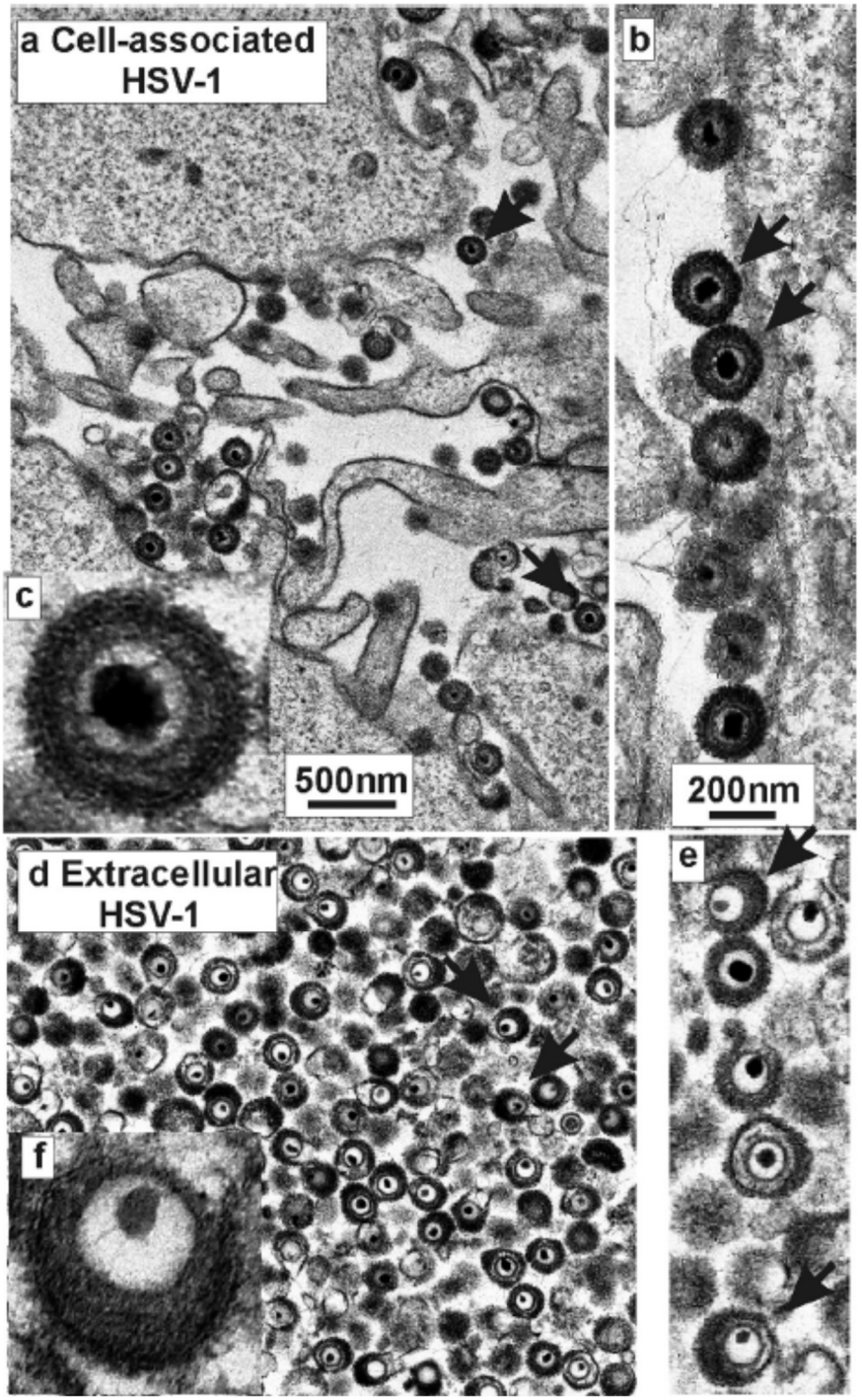

Figure 11. Comparaison entre l'ultrastructure de virions « immatures » (ici marqués « cell-associated ») et « matures » (ici marqués « extracellular »). Les virions associés aux cellules sont des virions qui ne sont pas encore libérés de la cellule. Les virions extra-cellulaires ont été purifiés à partir de surnageant de cellules infectées. La position asymétrique de la capside dans les virions extra-cellulaire est marquée par rapport aux virions immatures. Cet arrangement est similaire à celui décrit par cryo-electron-tomographie[52]. Tiré de Newcomb et al, JVI 2009[54].

Ainsi, il semble que des changements structuraux se produisent au cours de la maturation de la particule virale, ce qui conduirait à une distribution asymétrique de la capside dans le virion et, par conséquent, à une modification de la distribution des glycoprotéines sur l'enveloppe du virus.

Quel avantage pour le virus ? L'hypothèse la plus attractive tient à l'existence du sommet « portal » sur la capside (voir section I)[55] :

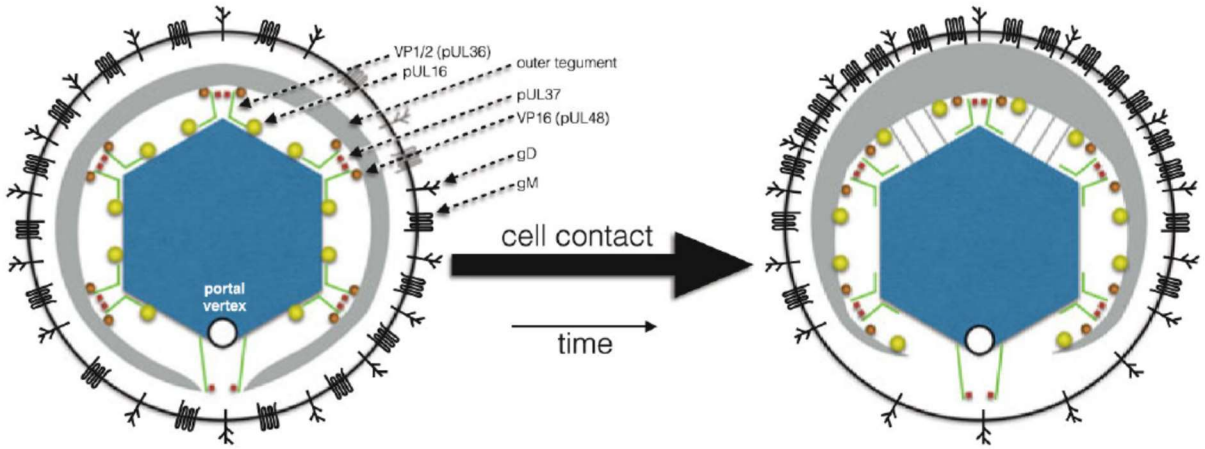

Figure 12. Modèle de réarrangement du tégument et des glycoprotéines d'enveloppe dans la particule virale en fonction du temps ou du contact avec la cellule. Selon ce modèle, la particule virale « immature » serait symétriquement arrangée (à gauche). La maturation de la particule et/ou son contact avec la cellule enclencherait un réarrangement du tégument et une distribution asymétrique dans la particule virale, avec une couche de tégument mince à proximité du sommet portal et une couche plus dense au pôle opposé (à droite). Le tégument étant lié aux glycoprotéines d'enveloppe, la redistribution du tégument entrainerait la redistribution d'au moins une partie des glycoprotéines d'enveloppe telles que gD et gM ici schématisées. gM est une glycoprotéine dont le rôle est actuellement suggéré comme inhibiteur de la liaison du virion aux récepteurs. Dans ce modèle, la protéine gD, qui lie le récepteur, serait relocalisée au niveau du sommet portal, à un pôle où gM serait absente. Ceci favoriserait l'attachement de la particule virale via le pôle proche du sommet portal et permettrait de pré-orienter la particule avant même l'entrée de la cellule. Ce type de pré-orientation peut être primordial pour que la capside puisse présenter le sommet portal au NPC pour l'éjection de l'ADN viral dans le noyau durant l'entrée. Une réorganisation post-contact aurait quant à elle l'avantage de regrouper les protéines du complexe gH/gL et gB autour de gD au point de contact des membranes pour leur activation et une optimisation de la fusion. Tiré de Smith, Adv Anat Embryol Cell Biol 2017[55].

Selon ce modèle résumé en **Figure 12**, le pôle proximal du virion où la capside est la plus proche de l'enveloppe, correspondrait à l'endroit de la capside où se situe le sommet portal. Ce serait au niveau de ce pôle que se trouverait une densité plus importante de protéines d'enveloppe impliquées dans l'attachement et/ou la fusion.

Le but des expériences décrites ici a été de déterminer la localisation sur la particule virale de 4 glycoprotéines ou complexes importants pour l'attachement et la fusion à savoir gC, gD, gH/gL et gB, et ce soit sur des particules virales libres, soit sur des particules virales attachées aux cellules.

Expériences mises en œuvre

Afin de pouvoir observer spécifiquement ces protéines à une résolution permettant de les visualiser *in situ* dans la particule virale, nous avons utilisé la microscopie à « super-résolution », plus spécifiquement la microscopie STED (Stimulated Emission-Depletion). Cette technique permet de s'affranchir de la limite naturelle de résolution de la lumière (typiquement 200 nm pour une longueur d'onde de 488 nm) et d'obtenir des résolutions de l'ordre de 50 nm, ce qui permet de visualiser des sous-structures virales au sein d'une particule dont la taille moyenne est de 200 nm. En collaboration avec Gary Cohen et Roselyn Eisenberg (Université de Pennsylvanie, USA) qui nous ont fourni des anticorps spécifiques de nos protéines d'intérêt (un monoclonal et un polyclonal pour chaque protéine), nous avons marqué chaque glycoprotéine sur des particules virales purifiées (fournies par Marion McElwee, CVR, Université de Glasgow, UK) attachées à des lamelles de verre ou attachées à des cellules. Dans ce dernier cas, les particules virales ont été déposées sur des cellules HFFF2 ou HeLa et incubées à 4°C pour permettre l'attachement des virions aux cellules sans permettre de fusion membranaire, ce qui pourrait modifier la localisation des protéines virales. Nous avons ainsi observé en microscopie STED que les protéines pouvaient être observées soit comme des anneaux soit comme des points. Nous interprétons ces localisations comme la distribution homogène autour de la particule virale (anneaux) ou une distribution ponctuelle (points) (Figure 1 de la publication 7 ou PB7-1). Les points pouvaient être observés soit uniques soit multiples (2-4) pour une particule. La quantification de la distribution des glycoprotéines en fonction de ces localisations a montré que toutes les protéines localisaient essentiellement en anneaux sur les particules virales libres, à l'exception notable de gD, dont la localisation était majoritairement sous forme de points et ce avec les deux anticorps utilisés (Figure PB7-2). Sur les particules virales attachées aux cellules, la localisation de toutes les glycoprotéines était sous forme d'anneaux, y compris gD. Cela indique que soit la distribution de gD sur le virion change au contact de la cellule, soit que seule la portion de virions ayant gD distribué en anneaux est capable de s'attacher aux cellules. Dans ce dernier cas de figure, cela indiquerait que les particules virales ayant gD en anneaux sont les particules matures, par opposition aux particules virales ayant gD distribuée sous forme ponctuelle.

Comme nous l'avons vu et à l'exception de gD, l'ensemble des glycoprotéines sont essentiellement distribuées en anneaux tant sur les virions libres que sur les virions attachés aux cellules. Toutefois, les images obtenues avec les virions attachés aux cellules semblaient indiquer que le diamètre de ces anneaux était différent de celui des particules libres. Pour nous en assurer, nous

avons quantifié le diamètre des anneaux des particules libres et nous l'avons comparé à celui des particules attachées aux cellules. Nous avons ainsi observé une réduction d'environ 20% du diamètre des anneaux des particules attachées aux cellules par rapport aux particules libres (Figure PB7-3). Sachant que le STED n'est pas résolutif en z, nous faisons l'hypothèse que la réduction de diamètre observée est due à une relocalisation des protéines depuis l'ensemble de la surface de la particule vers un pôle unique de la particule (Figure PB7-5A).

Enfin, nous avons pu réaliser des observations STED avec deux fluorochromes différents afin d'évaluer si les protéines d'enveloppe étaient regroupées en un locus fonctionnel après liaison aux cellules. Dans un premier temps, nous avons analysé la proportion de virions qui étaient effectivement double-marqués dans toutes les combinaisons possibles avec les anticorps dont nous disposions. Nous avons ainsi remarqué un co-marquage globalement efficace (>90%) sauf dans le cas du marquage de gC. En effet, ce marquage a montré que 15% de nos particules ne contenaient que gC (ou plutôt étaient négatives pour gD, gH/gL et gB) (Figure PB7-4A). Par ailleurs, nous avons remarqué que le co-marquage gC/gD était particulièrement inefficace. Or il a été démontré que les deux protéines étaient proches sur l'enveloppe virale[56,57]. Ainsi, une hypothèse pour expliquer un co-marquage faible de gC et gD est que les deux protéines sont physiquement proches sur l'enveloppe et que leur marquage est mutuellement exclusif, probablement à cause de l'encombrement stérique de la fixation d'un anticorps spécifique sur l'une des deux protéines qui empêcherait la fixation du second anticorps.

Le co-marquage sur les particules virales libres montre une faible colocalisation des glycoprotéines entre elles en général, ce qui n'est pas très surprenant à cette résolution (Figure PB7-4B). Néanmoins, une colocalisation partielle ou totale pouvait être observée entre gD et gC (ce qui renforce l'idée d'une proximité entre les deux molécules sur l'enveloppe virale) et gB et gH/gL. L'absence de colocalisation entre gD et gB sur les particules libres est particulièrement bien illustrée dans le cas où les assemblages ponctiformes de gD ne colocalisent pas avec les anneaux de gB. En effet, ces anneaux sont rarement complets et, fait surprenant, les points de gD sont fréquemment observés à l'endroit des anneaux où le marquage de gB est le moins dense. Ainsi, sur les particules virales libres, il semble y avoir deux groupes physiquement distincts sur la membrane virale : les paires gD/gC (protéines d'attachement) et gB/gH-gL (fusion).

Conclusions

Les observations obtenues en STED sur la localisation des glycoproteines d'enveloppe nous ont apporté beaucoup d'informations et presqu'autant de questions.

Il semble clair que la localisation de gD sur les particules virales libres est différentes des autres protéines d'enveloppe que nous avons analysé dans cette étude. Il est clair aussi que les particules attachées aux cellules ont gD redistribuée autour de la particule virale. Il reste à établir si ce changement de localisation précède ou suit l'attachement aux cellules. L'hypothèse que nous privilégions est plutôt que gD est relocalisée autour de la particule virale une fois celle-ci « mature ». Cette configuration faciliterait l'attachement aux cellules, ce qui expliquerait la sur-représentation des particules attachées aux cellules avec gD autour de la particule. Ce cas de figure a été décrit par analyse STED pour HIV-1, où les auteurs ont montré que le regroupement de la protéine Env sur la particule virale était dépendant de la maturation de la particule virale et *nécessaire à un attachement efficace aux cellules*[58].

L'analyse en deux couleurs des différentes protéines montre que les protéines d'attachement et celles de fusion forment probablement des entités physiquement distinctes sur les membranes, même si la résolution du STED reste insuffisante pour l'établir très clairement. Il nous reste à déterminer ce qu'il en est des particules virales attachées aux cellules. Enfin, le point le plus difficile à interpréter est celui de la réduction du diamètre des anneaux de protéines sur les particules attachées aux cellules par rapport aux particules libres. L'explication que nous avançons à ce stade est une relocalisation des protéines sur un pôle de la particule virale au lieu d'un agencement homogène sur l'ensemble de la particule. Ainsi, dans la limite du plan confocal, le diamètre serait réduit à celui de la base de la particule virale Figure PB7-5A). Nous avons tenté de vérifier cette hypothèse en réalisant une série d'images en z mais la puissance du laser de déplétion en STED provoque un photo-blanchissement tel qu'il n'est pas possible d'enchaîner plus de 4-5 prises de vue sur un fluorophore aussi stable que l'Oregon Green 488.

Nous n'avons pas analysé la localisation de gM car nous n'avons pas trouvé d'anticorps qui soient suffisamment fiables pour l'analyse par STED. Il reste que l'analyse par double-marquage de gD et gM pourrait confirmer ou infirmer certains aspects du modèle de Smith.

Publication #7

Version telle que soumise à PNAS

Dynamic organization of Herpesvirus glycoproteins on the viral membrane revealed by super-resolution microscopy

Beilstein F, Cohen G.H, Eisenberg R.J, Nicolas V, Esclatine A, Pasdeloup D

Dynamic organization of Herpesvirus glycoproteins on the viral membrane revealed by super-resolution microscopy

Frauke Beilstein[1], Gary H. Cohen[2], Roselyn J. Eisenberg[3], Valérie Nicolas[4], Audrey Esclatine[5] and David Pasdeloup[5,6]*

(1) Laboratory of Molecular Virology, INTS, CNRS INSERM U1134, Paris, France

(2) Department of Microbiology, School of Dental Medicine, University of Pennsylvania, Philadelphia, Pennsylvania, USA

(3) Department of Pathobiology, School of Veterinary Medicine, University of Pennsylvania, Philadelphia, Pennsylvania, USA

(4) IPSIT, University of Paris-Sud, Châtenay-Malabry, France

(5) Laboratory "Virulence and latency of Herpesviruses", I2BC, University of Paris-Sud – Faculty of Pharmacy, Gif sur Yvette – France

(6) Laboratory of Biology of Avian Viruses, UMR1282 ISP, INRA Centre Val-de-Loire, Nouzilly, France

*Corresponding author: Mailing address: Laboratoire de Biologie des Virus Aviaires, UMR1282 ISP, INRA Centre Val-de-Loire, 37380 Nouzilly, France.

Phone : 00 332 47 42 77 52

E-mail: david.pasdeloup@inra.fr

Running title : HSV-1 glycoproteins dynamic organization

Abstract

The processes of cell attachment and membrane fusion of Herpesviruses involve many different membrane glycoproteins. Viral proteins gC and gD bind to cellular receptors. Upon binding, gD activates the gH/gL complex which in turn activates gB to trigger membrane fusion. Thus, these proteins must be located at the point of contact between cellular and viral membranes to interact and allow fusion. Using super-resolution microscopy, we show that gB, gH/gL and most of gC are distributed all around purified cell-free virions. In contrast, gD and a subset of gC involved in cell binding localize essentially as clusters. Remarkably, we observe that all glycoproteins regroup to form an identical pattern upon cell binding. This redistribution of glycoproteins upon cell attachment could contribute to optimize membrane fusion by regrouping and activating gB and gH/gL at the points of contact between cellular and viral membranes, where gD interacts with its receptors.

Keywords : herpesvirus / glycoprotein / super-resolution microscopy / receptor

Herpesviruses encode a complex variety of different glycoproteins some of whose functions remain unclear. For Herpes Simplex Virus 1 (HSV-1), the core set of proteins required for attachment and entry are gD, gH, gL and gB. gD interacts with receptors such as HVEM (Herpesvirus Entry Mediator) and Nectin-1 (1-3), and activates the gH/gL complex and gB to trigger membrane fusion (4, 5). Thus, these proteins must be spatially close to allow this chain of activations. In particular, the interaction of gB and gH/gL is required for fusion (6, 7). In addition to these proteins, glycoprotein gC engages heparan sulfates to facilitate viral particle attachment prior to the binding of gD to its specific receptors (8). gC is non-essential in cell culture since binding to heparan sulfates can also be mediated by gB (9). In the absence of precise data, it has generally been assumed that glycoproteins are randomly distributed over the viral envelope, although an uneven distribution at distinct poles of the particles have been suggested (10). Observation of the actual organization of a selected glycoprotein on the viral membrane has been possible so far only by immuno-electron microscopy (immuno-EM) (11) and fluorescence microscopy. Although the latter allows for the analysis of a great number of particles, it is limited by the diffraction limit of light to a resolution of around 200 nm, which is roughly the size of the HSV-1 virion. Immuno-EM allows the visualization of specific protein types on the particle but uses conditions of sample preparation which can alter antigenic properties of the protein. In addition, the number of particles which can be reliably analyzed by immuno-EM often limits the strength of the interpretation. Super-resolution fluorescence microscopy (or nanoscopy) is a new and powerful tool which allows the visualization of the organization of a specific glycoprotein at the surface of viral particles. It combines the advantage of using specific antibodies to target a given protein on a large number of particles with an achievable resolution compatible with the identification of sub-structures within the viral particle (12-14). Here we used stimulated emission-depletion (STED) microscopy to analyze the organization of gC, gD, gB and gH/gL at the surface of HSV-1 particles with a

lateral resolution of 60 nm. We describe and characterize the patterns of glycoprotein organization at the surface of both free and cell-bound virions. We observed that specific glycoprotein types have different distributions on the viral particle, and further showed that their distributions change between free and cell-bound particles. Moreover, dual-color STED microscopy revealed that receptor-binding proteins gC and gD on one hand, and fusion-triggering proteins gB and gH/gL on the other, are preferentially located close together. Our results raise the possibility that the reorganization of glycoproteins at the surface of the herpesvirus particle following receptor binding, acts as a trigger for membrane fusion by regrouping gD, gH/gL and gB.

Results

Comparative observation of glycoprotein distributions at the surface of viral particles by super-resolution and conventional fluorescence microscopy

HSV-1 virions (unmodified 17+ strain) purified on a Ficoll gradient and attached to glass coverslips were visualized using conventional confocal microscopy with or without a gated STED (gSTED) set-up (see Methods for details). Virions labelled with monoclonal antibody (mAb) LP11 directed against gH/gL and observed in diffraction-limited mode showed an overall picture consisting of spots that were uniformly round, large in size (average of 454 +/- 50 nm, n=67) and varying in fluorescence intensity (Figure 1A, Confocal). When the gSTED set-up was applied, the large uniform spots resolved to show more varied and better defined features (Figure 1A, gSTED). These features could be further refined by applying a noise-filtering algorithm (Figure 1A, gSTED Noise-filtered). The features observed consisted essentially of single, double or multiple spots, or rings of glycoproteins (Figure 1B), features which were previously impossible to visualize by conventional methods of fluorescence microscopy. We interpret the single spots as a single glycoprotein or a group of glycoproteins

localized together in a single location (Figure 1C). Rings are most likely several glycoproteins or group of glycoproteins distributed all around the viral membrane surrounding the virion and visualized as a ring in a confocal section (our STED set-up is not resolutive in z)

As shown in Figure 1B, each distinct type of localization was indiscernible by conventional confocal microscopy. The resolution obtained with our gSTED set-up was estimated by FWHM (Full Width at Half-Maximum) analysis on immune complexes at 60 nm on average (n=6) (Supplementary Figure 1). We thus conclude that individual virions may have differing distribution of glycoproteins at their surface, and we investigated whether these features were also observed with other glycoproteins.

Glycoprotein patterns at the surface of free and cell-attached virions

The patterns of distribution of glycoproteins gC, gD, gH/gL and gB were determined on unmodified WT virions which were either free or cell-attached. We used untagged WT viruses to ensure that glycoprotein distribution was not influenced by the presence of a tag. Cell-attached virions were obtained by adding purified virions on human fibroblasts for 30 minutes at 4°C to allow cell attachment while preventing membrane fusion. Cells were then washed, fixed and stained using one monoclonal (mAb) and one polyclonal (pAb) antibody for each glycoprotein. A total of 8,313 particles were imaged by gSTED and analysed. This revealed that the distribution of glycoproteins gB and gH/gL on free and cell-bound virions was essentially a ring-like distribution for 60% or more of observed particles (Figure 2). This result was consistent between polyclonal and monoclonal antibodies and was similar for cell-bound virions. In contrast, receptor-binding glycoproteins gD and gC showed different patterns. gD displayed no more than ~40% of ring-like distribution on free virions whatever the antibody used, indicating that the glycoprotein is preferentially organized as single or multiple spots on the viral membrane. However, there was a significant increase in the proportion of cell-attached

particles labelled for gD that displayed ring-like localization when compared to free virions: 73% as opposed to 40% for pAb R8 and 94% as opposed to 36% for mAb MC23. Labelling of particles containing a fluorescent capsid with gD-specific mAb MC23 confirmed that gD labelling was specific to viral particles (data not shown). These results suggest either that cell binding triggered a reorganization of gD at the surface of cell-bound virions, or that the subpopulation of virions with ring-like distribution of gD is more competent for cell binding. Polyclonal antibody R47 against gC showed a distribution of the glycoprotein similar to the one observed with gB or gH/gL on free and cell-bound virions with 72% and 67% of rings respectively. However, labelling of gC with monoclonal antibody IC8 showed a strong spotty localization of the protein, essentially composed of single spots (72%). We interpret this apparent contradiction to the detection by mAb IC8 of a subpopulation of gC that is localized at a specific position in the membrane, unlike the totality of gC molecules detected by pAb R47, which are spread evenly around the particle. This interpretation is supported by the failure of mAb IC8 to detect gC on cell-attached particles, in contrast to R47, possibly because this mAb recognizes an epitope of gC involved in receptor interaction.

Rings size of glycoproteins on free and cell-attached particles

Although no obvious change in the profile of localization was observed for gB and gH/gL, subjective comparison of images suggested that the ring diameters differed between free and cell-bound particles. To determine the extent of any differences, we measured the diameter of 1,512 rings observed with different glycoproteins with free or cell-bound virions. The average diameters measured are shown in Figure 3A and representative pictures with illustrative intensity profiles are shown in Figure 3B. The average diameter of rings of free virions as shown by labelling with polyclonal antibodies was similar between gB, gH/gL and gD at 300, 307 and 291 nm respectively. Interestingly, there was a decrease of ~20% in the

average ring diameter between free virions and cell-attached virions labelled with the same antibodies at 240, 248 and 257 nm respectively. Decreases were also observed with monoclonal antibodies against gB (-12%: from 270 nm to 243 nm) and gD (-21% : from 295 nm to 233 nm). Of note, no equivalent decrease was seen with mAb LP11 against gH/gL, which showed a non-significant increase of 5% from 263 to 278 nm between free and cell-bound particles instead. The diameter of 263 nm for free particles is close to the diameter (248 nm) of cell-bound particles labelled with pAb R137, which recognizes the same protein. This indicates that LP11-positive glycoproteins might already be localized at the viral surface of free virions in a comparable way as is R137+ gH/gL after cell binding.

There was no significant change in the ring diameter of gC between free and cell-bound particles with 313 and 318 nm respectively.

Dual color STED microscopy

In order to determine the relative localization of one glycoprotein to another, we proceeded to dual-color gSTED microscopy using the same sets of antibodies as above and combining a polyclonal antibody directed against one glycoprotein with a monoclonal antibody against a second.

For each pair of antibodies, we first quantified the number of particles that were singly or doubly labelled (Figure 4A). In most cases, when labelling for gC was excluded, more than 90% of particles were dual-labelled. In the case of gC-labelled particles, 22% to 34% of particles stained with a polyclonal antibody against gD, gB or gH/gL and with mAb IC8 against gC had no gC signal (lanes x-xii, red bars). These numbers were different when dual-labelling was reverse (lanes i, vii and v, green bars). For instance, dual-labelling with IC8 and R68 (gB) showed that 34% of particles were gB+/gC- (lane xi, red bar), whereas dual-labelling with pAb R47 (gC) and mAb SS63 (gB) showed that only 8% of particles were gB+/gC- (lane vii, green

bar). This illustrates that IC8 does not label all gC+ particles. Moreover, labelling using gC-specific polyclonal antibody R47 showed that 14 and 18% of particles were labelled for gC only and not for gB or gH/gL respectively (lanes vii and v). This was even more significant for particles labelled with gD mAb MC23 since 36% of them were gC+ and gD- (lane i). These findings were not dependent on the antibody used as when gC was labelled using mAb IC8 and the other glycoproteins were labelled with their respective polyclonal antibody, numbers of particles labelled with gC only were similar: 12% (gC+/gB-, lane xi), 16% (gC+/gH/gL-, lane xii) and 30% (gC+/gD-, lane x). This suggests that a significant number of particles (roughly around 15%), which are presumably defective, contain gC but none of the other glycoproteins tested. Notably, the fraction of particles that labelled only for gC was twice as great in gD co-labelled particles as for other glycoproteins (red bar in lane i and green bar in lane x). If 15% of particles contain only gC, this means that the remaining 15% of gC+/gD- particles are gB+/gH-gL+/gD-. However, we only observed 4.3% of gH-gL+/gD- particles (lane iv, green bar) and 5.5% of gB+/gD- (lane ix, green bar) when gD was labelled with pAb R8. Therefore, the most likely explanation for the existence of the high number of gC+/gD- particles is that co-labelling with their respective antibodies, mAb or pAb, is mutually inefficient.

We then analyzed the localization in free virions of each glycoprotein relative to the others (Figure 4B). As expected, gB and gH/gL were found predominantly as complete rings, which resulted in overlapping signals (lanes vi and viii). Moreover, when single spots of both glycoproteins were found, they were often in close proximity to each other, indicating that the two proteins are close together on the viral membrane. gD was more frequently found as discrete spots rather than as rings and, surprisingly, these spots rarely overlapped with rings of gB or gH/gL and were often found in areas where the gB or gH/gL signals were the weakest (lanes ii, iii, iv and ix). We made similar observations for epitope IC8 of gC which localizes

overwhelmingly as spots (lanes xi and xii). In contrast, spots of gD and gC were often observed as close or colocalizing (lane i).

Although interpretation of dual-color STED is limited because of the small size of the virion and the resolution limit of 60 nm with our set-up, we conclude that gB and gH/gL are more likely to be localized close together than either is to gD or gC. Moreover, a fraction of gD molecules seem to be sufficiently close to gC to display colocalization in our set-up.

Discussion

It was first established by cryo electron tomography (cryo-ET) that the virion of HSV-1 has an asymmetrical architecture with the capsid close to the viral membrane at one pole and separated from the opposite side of the membrane by ~35 nm of tegument (15). This intriguing feature has been confirmed by other groups using either conventional electron microscopy (16), cryo-ET with no imposed symmetry (17) or ensemble mapping of fluorescently tagged viruses (18). The polarity created by this structural asymmetry is essentially visible through the eccentricity of the capsid within the particle. Moreover, it is time dependent which is indicative of a possible maturation of the virion over time (16). In addition, differing densities of glycoprotein spikes have also been observed at the surface of viral particles, suggesting that glycoprotein distribution is uneven (15). Interestingly, cryo-ET analysis of cell-bound viruses showed that particles were bound to the cell through the capsid proximal pole of the viral membrane, which had a lower density of glycoprotein spikes than the opposite pole (or distal pole) (10).

Here, using super-resolution fluorescence microscopy, we made two observations which could relate to a polar organization of some glycoproteins on free and cell-attached particles.

First observation concerns gC and gD. Although pAb R47 staining showed that gC was distributed essentially around the viral particles (free or cell-attached) as for gB or gH/gL,

214 labelling with mAb IC8 revealed a strong spotty localization on free particles which could
215 represent a cluster of one or several proteins at one pole of the virion. This signal was lost on
216 cell-bound particles, suggesting that the IC8 epitope is involved in binding of heparan sulfates.
217 Given the differing pattern of total gC (as seen with R47) and IC8-positive gC, we infer that
218 the IC8 epitope, involved in receptor binding, is accessible only on a subpopulation of gC.
219 Therefore, there could be at least two antigenically different populations of gC on the surface
220 of purified particles. Interestingly, dual-color labelling of particles showed that a significant
221 proportion (around 15%) of gC-positive particles were gD-negative (Figure 4A). On dual-
222 labelled particles, spots of gC and spots of gD could be seen either very close to each other or
223 overlapping (Figure 4B). This is in line with previous reports showing that gC and gD can be
224 cross-linked on virions (19) and that accessibility of gD to neutralizing antibodies could be
225 enhanced when gC was mutated (20).

226 Second observation regarding the possible polar distribution of glycoproteins is the
227 apparent "constriction" of rings of gB, gH/gL and gD upon cell-attachment. We quantified this
228 change of diameter to around 20% on average (Figure 3). We exclude the possibility that this
229 is caused by a general change of diameter of the whole viral particle since the diameter of gC
230 rings remained unchanged upon cell binding. Instead, we suggest that this constriction could
231 represent a regrouping of glycoproteins at one pole of the virion, as was proposed in earlier
232 studies (10, 21) and as is illustrated in Figure 5A. Thus, rings are considered to represent 2D
233 projections of a confocal slice containing the virions (STED is not resolutive in z with our set-
234 up) where the glycoproteins would be evenly distributed around the particle. In the case where
235 proteins would be regrouped on one pole rather than all around the particle, the same 2D
236 projection would be expected to show a ring of smaller diameter. Although we have no evidence
237 yet showing that poles of gB and gH/gL or clusters of gC labelled by IC8 are actually at the
238 same position on the virion, they could be spatially related because (i) the IC8 epitope is

undetectable on cell-bound particles, suggesting that this epitope is engaged with receptors, hence located at a pole of the virion which is in contact with the cellular membrane; and (ii) regrouping of gB, gH/gL or gD is observed only on cell-bound particles, showing that it is related to receptor binding. Moreover, the interaction between gB and gH/gL is necessary for the process of membrane fusion and is triggered by gD activation upon receptor binding (6, 7, 22).

Although the change in ring diameters of gB, gH/gL or gD upon cell attachment is relatively obvious (Figure 3), the marked difference between the distribution pattern of gD at the surface of free virions and that of cell-attached virions is probably the most remarkable illustration that the localization of glycoproteins at the viral membrane is dynamic upon cell contact. We observed that only 40% of free particles have a ring-like distribution of gD when labelled with pAb R8 (36% with mAb MC23), as opposed to >60% for other glycoproteins. We excluded the possibility that the presence of spots rather than rings was due to under-labelling of samples because all antibodies, representing multiple epitopes within the same glycoprotein, were used at the same dilution. In conditions of under-labelling, antibodies with the lowest concentration would be expected to give more single spots than antibodies which are the most concentrated. As illustrated in Supplementary Figure 2, this was not what was observed, since (i) the most concentrated antibody (IC8, 8.6 mg/mL) was the antibody giving the largest number of particles with single spots (72%, see Figure 3); (ii) gD antibodies MC23 and R8 gave similar pattern of localization despite the fact that R8 is 5.4 times more concentrated than MC23 and (iii) MC23 showed 94% of rings on cell-bound viral particles despite being the least concentrated antibody of our stock (1.2 mg/mL). An additional argument for the specificity of the single or multiple spots of gD comes from dual-labelling of particles which showed that at least 90% of particles labelled with either antibody against gD were also co-labelled for another glycoprotein (gC excepted) (Figure 4). Finally, we also verified that gD labelling with mAb

MC23 was specific using a recombinant virus with a fluorescently tagged capsid (data not shown).

This clustered localization of gD on the membrane was not reported in previous studies of the viral structure at high resolution. Using STORM (Stochastic Optical Reconstruction Microscopy), another method of super-resolution microscopy, Laine and collaborators reported on the ring-like distribution of gD on purified particles using mAb LP2 (23), which binds an epitope very close to the one recognized by MC23 used in our study (24, 25). They did not report gD as being present in single spots possibly because the authors assumed a spherical distribution of gD from the start, and focused on determining the parameters of those spheres in a model-imposed reconstruction. Using diffraction-limited fluorescence microscopy, Bohannon et al. used an elegant system where the centroid of fluorescence was determined by Gaussian fitting to model the relative position of fluorescently tagged proteins of recombinant pseudorabies virus (PrV) virions (18). This showed that gD localization on free virions was not eccentric on the basis that the average displacement of fluorescence from the capsid was less or equal to the one expected from the asymmetric organization of the particle (15 +/- 5 nm). In the case of the double or multiple spots of gD that we observed, the average displacement would be expected to be low as well when spots are radially distributed from the center of the particle (which was observed frequently as visible in Figures 1 and 3) and thus have a barycenter close to the one of a whole envelope distribution of gD. Considering that the total of free particles we observed with double or multiple spots or rings of gD equals 74% to 88% of the particles, our results are not incompatible with those of Bohannon et al. Other possible explanations include (i) the absence of clusters of gD on PrV membranes as opposed to HSV-1; (ii) the GFP fusion on gD hinders with its distribution and/or (iii) the transition of gD from the clustered state to the evenly distributed state (as described below) is faster on PrV than on HSV-1 membranes.

There are several possible scenarios which can account for the difference of localization of gD at the surface of free and cell-bound particles, as illustrated in Figure 5B. Contrary to particles with gD all around the membrane (lane i), particles with clusters of gD could be defective particles which cannot bind to cells and are therefore lost in our cell-binding assays (lane ii). Alternatively, these particles could undergo a structural change resulting in gD being redistributed at one pole of the virion, before (iii) or without (iv) a possible intermediate "matured" state. It is conceivable that a maturation mechanism occurs for Herpesviruses, since the symmetry of the particle was reported to change upon time, with nascent particles being symmetrical as opposed to released, presumably "matured" particles, which were essentially asymmetrical (16). Interestingly, viral particle maturation has been reported for glycoprotein Env of HIV-1 (26). Using STED microscopy, the authors observed clustering of Env proteins at the surface of viral particles which was dependent on particle maturation. Immature particles displayed glycoproteins which were organized as multiple spots or in a ring-shape, whereas mature particles had a single cluster of glycoproteins.

It remains to be clearly established how herpesvirus virion asymmetry and the polarization of glycoprotein distribution are related in time. Cryo-ET showed that virions bind to the plasma membrane preferentially through the capsid-proximal pole of the particle, where the density of glycoproteins was lower than on the opposite side (10). The authors suggested that the glycoproteins involved on the proximal pole were entry-related as opposed to those on the distal pole. Our results show that gB, gH/gL and gD are indeed concentrated at the likely point of contact between viral and cellular membranes but only after binding to the cell. It would be of interest to determine how regulatory glycoproteins which are known to inhibit fusion, such as gM (27, 28), are localized relatively to gB and others on purified virions.

Unravelling the molecular mechanism controlling glycoprotein organization of herpesviruses would be challenging, partly because of the great complexity of herpesviruses

particles, which contain more than 12 different membrane proteins. Nevertheless, it is likely that some tegument proteins, interacting with cytoplasmic tails of glycoproteins, could be involved in such a maturation process, as was suggested previously (21). For instance, tegument protein VP22 interacts with gD (29) and gE/gI (30) and VP16 interacts with gH (31).

Altogether, these results shed new light on glycoprotein distribution at the surface of viral particles showing that this distribution is dynamic and that different populations of a given protein may exist within the particle, possibly with differing roles. Super-resolution microscopy is thus expected to contribute significantly to our understanding of the in-depth composition of large viruses and the dynamics of their structures.

Methods

Cells and viruses

Human Fetal Foreskin Fibroblasts (HFFF2) cells were grown at 37°C in Dulbecco's modified Eagle medium (DMEM; Gibco) supplemented with 8% fetal calf serum.

The HSV-1 strain used in this study is the 17+ strain. High-quality virions were purified and separated from L-particles on Ficoll gradients(32) and were generously provided by Marion McElwee and Frazer Rixon (University of Glasgow, UK).

Antibodies

All monoclonal and polyclonal antibodies used in this study are listed in supplementary Figure 2. Secondary antibodies used were goat anti-mouse or goat anti-rabbit conjugated with either Oregon Green 488 or AlexaFluor 532 (ThermoScientific).

Sample preparation for gSTED microscopy

A suspension of purified WT 17+ virions was layered on type #1.5 coverslips with thickness of 0.17 mm (Zeiss) in 6-well plates and incubated for 30 minutes at RT. Coverslips were washed three times with PBS and fixed with 4% paraformaldehyde. Samples were incubated with 0.2% fish gelatin (Sigma) and 5% goat serum to saturate non-specific binding sites. Glycoprotein labelling was carried out by incubating the fixed particles with primary antibodies at a dilution of 1/100 for 1h at RT. Secondary labelling was performed by incubating the samples with secondary antibodies at a dilution of 1/50 for 1h at RT followed by three washes in PBS. Samples were then mounted with Prolong Gold (Life Technologies) and cured before imaging. High concentrations of antibodies were necessary to obtain a signal strong enough for gSTED imaging.

For observation of cell-attached virions, HFFF2 cells were seeded on sterile type #1.5 coverslips with thickness of 0.17 mm (Zeiss) 24h before incubation with 50 pfu (plaque-forming units) per cell of WT virions for 1h at 4°C. Unbound virus was washed off with PBS (three washes) and cells were fixed and processed as described above.

gSTED microscopy and noise-filtering

gSTED microscopy was carried out on a Leica TCS SP8 confocal microscope equipped with a white light laser (WLL operating at 70% of its nominal power), a hybrid detector, a 592 nm depletion laser and a gating system. Observations were made using a HC PL APO 100X oil-immersion objective (N.A=1.4). Visualization of Oregon Green 488-labelled particles was done with an excitation wavelength of 495 nm at a power of 8%. The detection window of the AOBS (Acousto-Optical Beam Splitter) was set at 508-570 nm with a time-gated detection window of 2 to 6 ns. Detection was using a Hybrid Detector (HyD) with an unmodified gain of 100%. Depletion was obtained with a power of 78% on the 592 nm depletion laser. Visualization of AlexaFluor 532-labelled particles was with an excitation wavelength of 532 nm at a power of

20%. The detection window of the AOBS (Acousto-Optical Beam Splitter) was set at 548-573 nm with a gated detection window of 1 to 4.5 ns. Detection was using a Hybrid detector with a reduced gain of 61%. Depletion was obtained with a power of 15% on the 592 nm depletion laser.

Noise-filtering was done using Huygens software (Scientific Volume Imaging) with the following parameters: an excitation fill factor of 1.2, a saturation factor of 45 and an immunity fraction set to 1%. Background level was defined according to the quality of each image independently. Noise-filtered pictures were used only for illustration purposes and not for quantifications.

Quantification and statistics

All quantifications were performed on raw pictures to avoid any potential flaw introduced by the noise-filtering procedure. Dual labelling was assessed using the Leica LAS AF lite software. Glycoprotein distribution was quantified manually using ImageJ software on a total of 8,313 particles (Figure 2). A Pearson's chi-squared test was used to determine whether the profiles of distribution were statistically different between free and cell-bound virions. As the p-value indicates the likelihood of a correlation, a p-value > 0.05 was considered as representing a statistically significant difference. Ring diameters shown on Figure 3 were measured manually from edge to edge on 1,512 particles using the Leica LAS AF lite software. The possible difference between the diameters of free and cell-bound viruses was tested by a unpaired student's *t* test with a significance threshold set at $p<0.01$ (significance level : 1%), after the Gaussian distribution of the values was verified by a Shapiro-Wilk test for $p>0.05$.

Acknowledgments

We are indebted to Frazer Rixon and Marion McElwee (University of Glasgow, UK) for the gift of purified virions and for reviewing the manuscript. We are grateful to Yves Gaudin for fruitful discussions and for critical reading of the manuscript. We also thank Caroline Denesvre for her comments and for her support of this work.

Conflict of interest

The authors declare no conflict of interest.

References

1. Geraghty RJ, Krummenacher C, Cohen GH, Eisenberg RJ, & Spear PG (1998) Entry of alphaherpesviruses mediated by poliovirus receptor-related protein 1 and poliovirus receptor. *Science* 280(5369):1618-1620.
2. Krummenacher C, *et al.* (2004) Comparative usage of herpesvirus entry mediator A and nectin-1 by laboratory strains and clinical isolates of herpes simplex virus. *Virology* 322(2):286-299.
3. Montgomery RI, Warner MS, Lum BJ, & Spear PG (1996) Herpes simplex virus-1 entry into cells mediated by a novel member of the TNF/NGF receptor family. *Cell* 87(3):427-436.
4. Eisenberg RJ, *et al.* (2012) Herpes virus fusion and entry: a story with many characters. *Viruses* 4(5):800-832.
5. Heldwein EE & Krummenacher C (2008) Entry of herpesviruses into mammalian cells. *Cell Mol Life Sci* 65(11):1653-1668.
6. Atanasiu D, *et al.* (2007) Bimolecular complementation reveals that glycoproteins gB and gH/gL of herpes simplex virus interact with each other during cell fusion. *Proc Natl Acad Sci U S A* 104(47):18718-18723.
7. Atanasiu D, *et al.* (2010) Bimolecular complementation defines functional regions of Herpes simplex virus gB that are involved with gH/gL as a necessary step leading to cell fusion. *J Virol* 84(8):3825-3834.
8. Herold BC, WuDunn D, Soltys N, & Spear PG (1991) Glycoprotein C of herpes simplex virus type 1 plays a principal role in the adsorption of virus to cells and in infectivity. *J Virol* 65(3):1090-1098.
9. Herold BC, Visalli RJ, Susmarski N, Brandt CR, & Spear PG (1994) Glycoprotein C-independent binding of herpes simplex virus to cells requires cell surface heparan sulphate and glycoprotein B. *J Gen Virol* 75 (Pt 6):1211-1222.
10. Maurer UE, Sodeik B, & Grunewald K (2008) Native 3D intermediates of membrane fusion in herpes simplex virus 1 entry. *Proc Natl Acad Sci U S A* 105(30):10559-10564.
11. Stannard LM, Fuller AO, & Spear PG (1987) Herpes simplex virus glycoproteins associated with different morphological entities projecting from the virion envelope. *J Gen Virol* 68 (Pt 3):715-725.
12. Grove J (2014) Super-resolution microscopy: a virus' eye view of the cell. *Viruses* 6(3):1365-1378.
13. Sahl SJ, Hell SW, & Jakobs S (2017) Fluorescence nanoscopy in cell biology. *Nat Rev Mol Cell Biol* 18(11):685-701.

14. Witte R, Andriasyan V, Georgi F, Yakimovich A, & Greber UF (2018) Concepts in Light Microscopy of Viruses. *Viruses* 10(4).
15. Grunewald K, *et al.* (2003) Three-dimensional structure of herpes simplex virus from cryo-electron tomography. *Science* 302(5649):1396-1398.
16. Newcomb WW & Brown JC (2009) Time-dependent transformation of the herpesvirus tegument. *J Virol* 83(16):8082-8089.
17. Schmid MF, *et al.* (2012) A tail-like assembly at the portal vertex in intact herpes simplex type-1 virions. *PLoS Pathog* 8(10):e1002961.
18. Bohannon KP, Jun Y, Gross SP, & Smith GA (2013) Differential protein partitioning within the herpesvirus tegument and envelope underlies a complex and variable virion architecture. *Proc Natl Acad Sci U S A* 110(17):E1613-1620.
19. Handler CG, Eisenberg RJ, & Cohen GH (1996) Oligomeric structure of glycoproteins in herpes simplex virus type 1. *J Virol* 70(9):6067-6070.
20. Hook LM, Huang J, Jiang M, Hodinka R, & Friedman HM (2008) Blocking antibody access to neutralizing domains on glycoproteins involved in entry as a novel mechanism of immune evasion by herpes simplex virus type 1 glycoproteins C and E. *J Virol* 82(14):6935-6941.
21. Meckes DG, Jr. & Wills JW (2008) Structural rearrangement within an enveloped virus upon binding to the host cell. *J Virol* 82(21):10429-10435.
22. Campadelli-Fiume G, Menotti L, Avitabile E, & Gianni T (2012) Viral and cellular contributions to herpes simplex virus entry into the cell. *Curr Opin Virol* 2(1):28-36.
23. Laine RF, *et al.* (2015) Structural analysis of herpes simplex virus by optical super-resolution imaging. *Nat Commun* 6:5980.
24. Cairns TM, *et al.* (2017) Global sensing of the antigenic structure of herpes simplex virus gD using high-throughput array-based SPR imaging. *PLoS Pathog* 13(6):e1006430.
25. Lazear E, *et al.* (2012) Antibody-induced conformational changes in herpes simplex virus glycoprotein gD reveal new targets for virus neutralization. *J Virol* 86(3):1563-1576.
26. Chojnacki J, *et al.* (2012) Maturation-dependent HIV-1 surface protein redistribution revealed by fluorescence nanoscopy. *Science* 338(6106):524-528.
27. Klupp BG, Nixdorf R, & Mettenleiter TC (2000) Pseudorabies virus glycoprotein M inhibits membrane fusion. *J Virol* 74(15):6760-6768.
28. Koyano S, Mar EC, Stamey FR, & Inoue N (2003) Glycoproteins M and N of human herpesvirus 8 form a complex and inhibit cell fusion. *J Gen Virol* 84(Pt 6):1485-1491.
29. Chi JH, Harley CA, Mukhopadhyay A, & Wilson DW (2005) The cytoplasmic tail of herpes simplex virus envelope glycoprotein D binds to the tegument protein VP22 and to capsids. *J Gen Virol* 86(Pt 2):253-261.
30. Maringer K, Stylianou J, & Elliott G (2012) A network of protein interactions around the herpes simplex virus tegument protein VP22. *J Virol* 86(23):12971-12982.
31. Gross ST, Harley CA, & Wilson DW (2003) The cytoplasmic tail of Herpes simplex virus glycoprotein H binds to the tegument protein VP16 in vitro and in vivo. *Virology* 317(1):1-12.
32. Szilagyi JF & Cunningham C (1991) Identification and characterization of a novel non-infectious herpes simplex virus-related particle. *J Gen Virol* 72 (Pt 3):661-668.

Figure legends

Figure 1. gSTED reveals various features of glycoprotein organization at the surface of viral particles.

(A) Purified WT 17+ virions were attached onto a glass coverslip and labelled with mAb LP11 against gH/gL and an Oregon green 488-labelled secondary antibody. Images were acquired using the diffraction-limited confocal mode or with a gated STED set-up (gSTED). Images could be further processed for noise-filtering using Huygens software algorithms. Scale bars : 500 nm. (B) Different patterns of glycoprotein organization were observed in the gSTED mode, which were undistinguishable in the confocal mode. From top to bottom these were: single, double, and multiple spots, and rings. Three of the patterns correspond to particles boxed in (A). The single spot image is of a particle labelled with gC-specific mAb IC8. Each different pattern is shown in the confocal and in the gSTED mode with corresponding noise-filtered images. Arrows delineate the line (400 nm long) used for profile analysis of normalized intensity. The blue line and the orange line in the graph correspond to the intensity profile observed in the confocal and in the gSTED mode respectively. Analysis was carried out on raw, unprocessed images. Scale bars: 100 nm. (C) Schematic illustration of the different patterns described in (B). The number of proteins per cluster (one or more) is unknown.

Figure 2. Free and cell-bound particles may display different glycoprotein patterns

Particles attached to cells (+) or attached to coverslips (-),were imaged using gSTED and the localization of glycoproteins gB, gH/gL, gD and gC was assessed by using a monoclonal (mAb) and a polyclonal antibody (pAb) recognizing each glycoprotein. Localization was categorized as single (blue), double (green) or multiple spots (yellow) or rings (red), as described in Figure 1. No IC8-positive signal could be observed on cell-attached particles. A Pearson's chi-squared test was used to determine whether the profile of distribution of one glycoprotein was statistically different between free and cell-bound virions. The p-value

indicates the likelihood of a correlation, therefore a p-value > 0.05 was considered as indicating a statistically significant difference between the two sets. ns : $p<0.05$, ** : $p>0.1$, *** : $p > 0.5$.

Figure 3. The diameter of labelled rings may differ between glycoproteins and between free and cell-attached viral particles

(A) The diameter of 1,512 rings observed on raw, unmodified pictures obtained in gSTED mode was measured and compared according to the type of glycoprotein labeled and whether the particles were bound to cells or not. Statistical differences were measured using an unpaired student's t-test after the Gaussian distribution of values was verified using a Shapiro-Wilk normality test. ns : $p >0.01$, *** : $p<0.0001$ (B) Representative noise-filtered pictures of glycoprotein distribution on the surface of free or cell-bound viral particles, as observed in gSTED mode, for all antibodies available (Supplementary Figure 2). The intensity profile of one particle per field along a 400 nm-long line delineated by two arrows is shown above each picture. Blue line: confocal profile; orange line: gSTED profile. The intensity profile was always determined on unmodified raw images. The peak-to-peak distance is indicated for every graph to illustrate the potential difference in ring size. No specific signal could be observed with the IC8 antibody on cell-bound particles. Scale bars : 500 nm.

Figure 4. Relative positions of glycoproteins on free virus particles as revealed by dual-color gSTED

(A) Purified free particles were double-labelled with twelve different pairs of antibodies. In each case, the percentage of particles labelled with mAb only is shown in green, the

520 percentage of particles labelled with pAb only is shown in red and the percentage of double-
521 labelled particles is shown in yellow. (B) For every pair of antibodies, representative noise-
522 filtered gSTED pictures are shown. The images on the left show more commonly observed
523 patterns while those on the right are less commonly observed. mAb staining is pseudo-colored
524 in green and pAb staining is pseudo-colored in magenta. All pictures are 700 x 700 nm.

525

526 **Figure 5. Proposed interpretations of the different configurations revealed by gSTED**

527 (A) Illustration of the "constriction" of rings observed with gB, gD and gH/gL upon cell
528 binding. A pool of glycoproteins evenly distributed on the whole surface of the virion sphere
529 is expected to have a larger diameter when projected (300 nm in average observed on free
530 particles) than a pool of glycoproteins concentrated at a pole of the sphere (250 nm in average
531 for cell-bound particles). Note: our STED set-up is not resolutive in z. (B) Two populations of
532 gD-positive particles are observed on free virions: particles with rings (i) and particles with
533 spots (ii-iv). However, cell-bound particles exclusively display rings with a constricted
534 diameter. We illustrate several scenarios to account for this observation: (ii) released virions
535 with patches of glycoprotein would represent "immature" particles which are not competent
536 for cell-binding as opposed to particles with even distribution of gD (i); (iii) upon maturation,
537 gD is distributed all-round the particle which then becomes competent for binding. As for
538 other glycoproteins, gD is then concentrated at a given pole upon binding to the cell. A direct
539 switch from particles with clusters of gD to the cell-bound form exhibiting constricted rings
540 cannot be excluded (iv). The number of glycoproteins shown in clusters of gD is only
541 illustrative. Pictures embedded in lane (iii) are noise-filtered images from particles labelled
542 with mAb MC23. Scale bars: 200 nm.

Supplementary Figure 1. Determination of the gSTED resolution by FWHM analysis. (A) Free virions were attached to glass coverslips and incubated with mAb IC8 against gC or irrelevant anti-GFP monoclonal antibodies and Oregon-green 488-conjugated secondary antibodies. The nonspecific signal consisting essentially of immune complexes was then imaged using the diffraction limited confocal mode, or the gSTED set-up using the same conditions as those described for imaging of glycoproteins. Scale bar: 2 µm. (B) Enlargement of the particles boxed in A and the corresponding intensity profiles shown along a line of 400 nm. Note the difference in profile observed in gSTED mode between the gC labelled particle and the nonspecific labelling. To determine the resolution of the gSTED set-up, the full-width at half maximum (FWHM) was calculated for six different particles one of which is illustrated here. The average of FWHM was 60 nm (52 nm here).

Supplementary Figure 2. Summary of all antibodies used in this study and the corresponding patterns of glycoprotein distribution as described in Figure 2. Color-coding is identical as that of Figure 2: red: rings; yellow : multiple spots; green: double spots and blue : single spots.

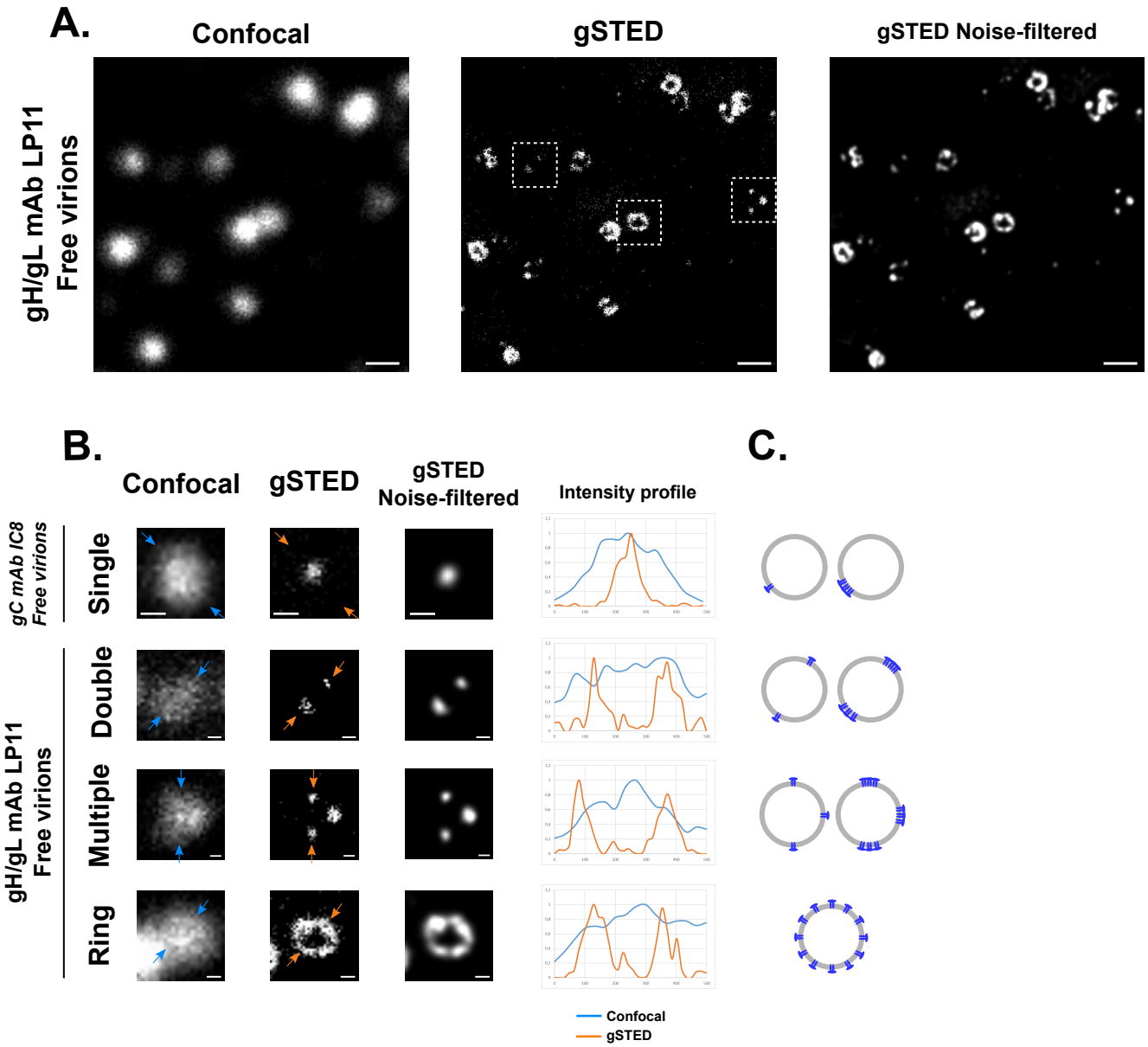
A.
Confocal
gSTED
gSTED Noise-filtered
gH/gL mAb LP11
Free virions
B.
Confocal
gSTED
gSTED
Noise-filtered
Intensity profile
C.
gC mAb IC8
Free virions
Single
gH/gL mAb LP11
Free virions
Double
Multiple
Ring
Confocal
gSTED

Figure 1

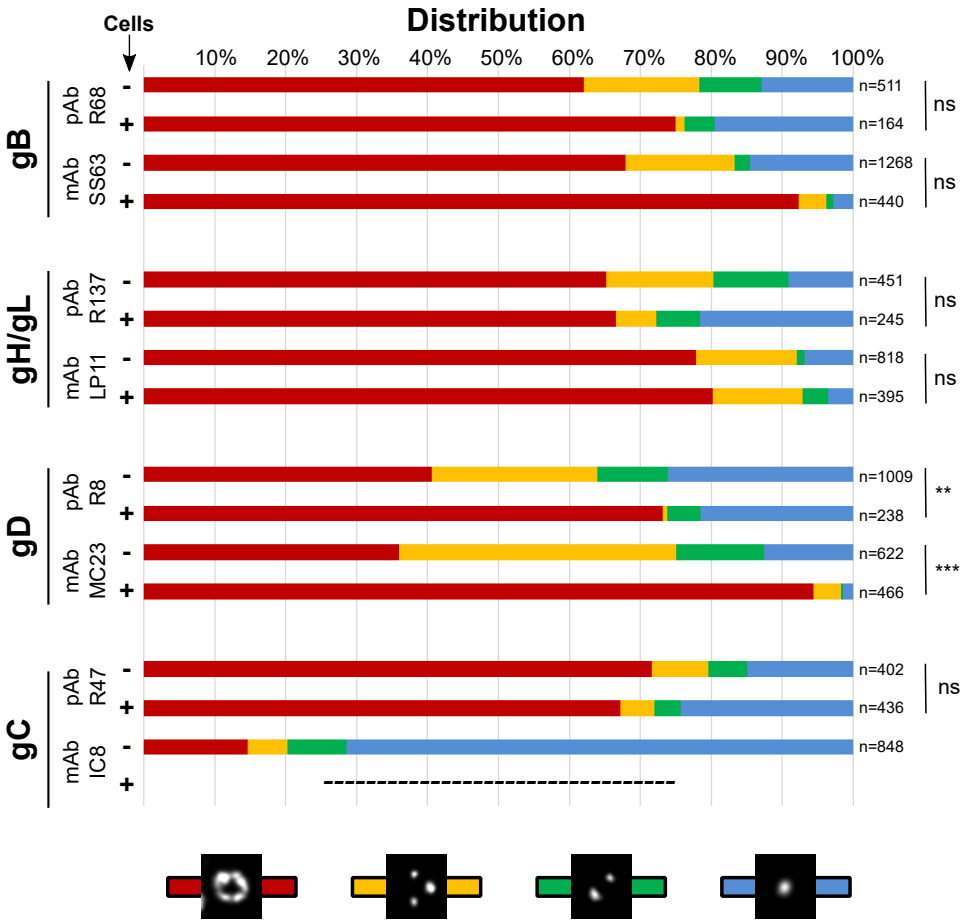
Cells
Distribution
10%
20%
30%
40%
50%
60%
70%
80%
90%
100%
gB
pAb R68
mAb SS63
gH/gL
pAb R137
mAb LP11
gD
pAb R8
mAb MC23
gC
pAb R47
mAb IC8
n=511
n=164
n=1268
n=440
n=451
n=245
n=818
n=395
n=1009
n=238
n=622
n=466
n=402
n=436
n=848
ns
**
***

Figure 2

Figure 3

A.

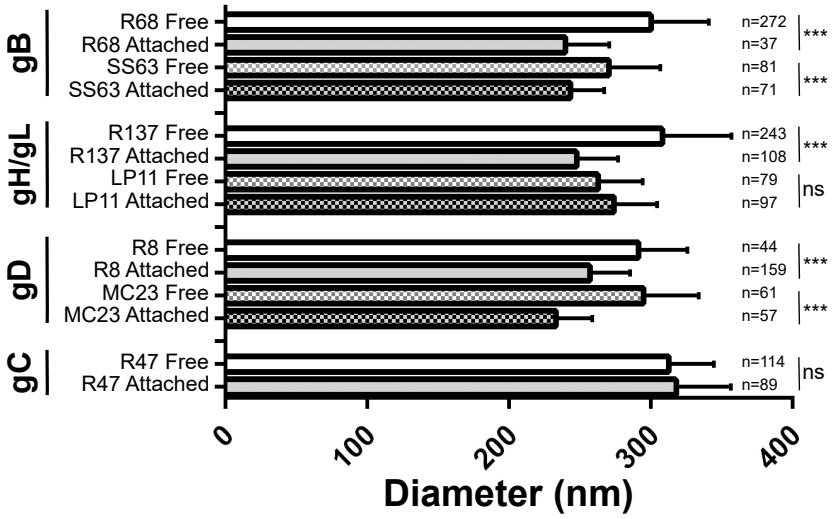
gB
R68 Free
R68 Attached
SS63 Free
SS63 Attached
gH/gL
R137 Free
R137 Attached
LP11 Free
LP11 Attached
gD
R8 Free
R8 Attached
MC23 Free
MC23 Attached
gC
R47 Free
R47 Attached
n=272
n=37
***
n=81
n=71
***
n=243
n=108
***
n=79
n=97
ns
n=44
n=159
***
n=61
n=57
***
n=114
n=89
ns
0
100
200
300
400
Diameter (nm)

B.

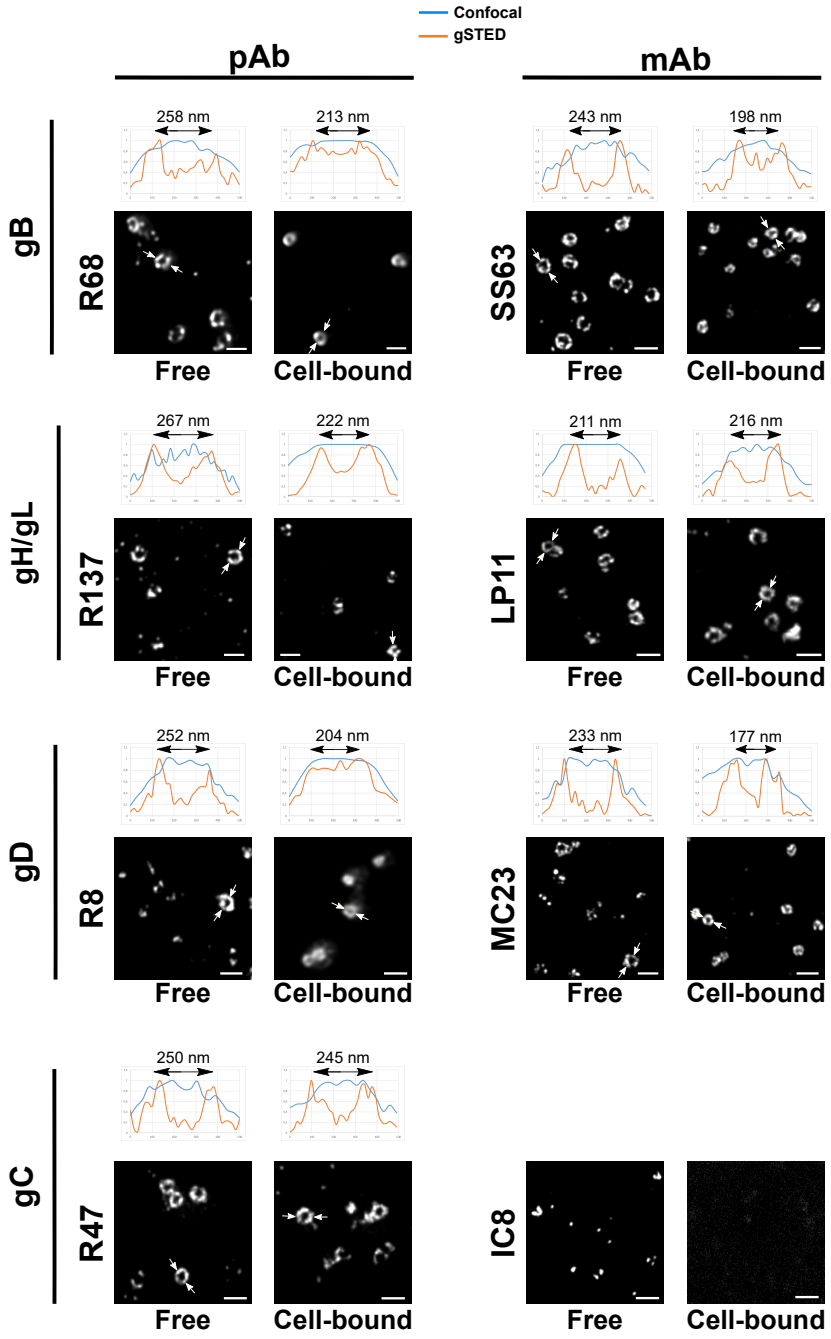
Confocal
gSTED
pAb
mAb
gB
R68
SS63
gH/gL
R137
LP11
gD
R8
MC23
gC
R47
IC8
258 nm
213 nm
243 nm
198 nm
267 nm
222 nm
211 nm
216 nm
252 nm
204 nm
233 nm
177 nm
250 nm
245 nm
Free
Cell-bound

Figure 4

A.

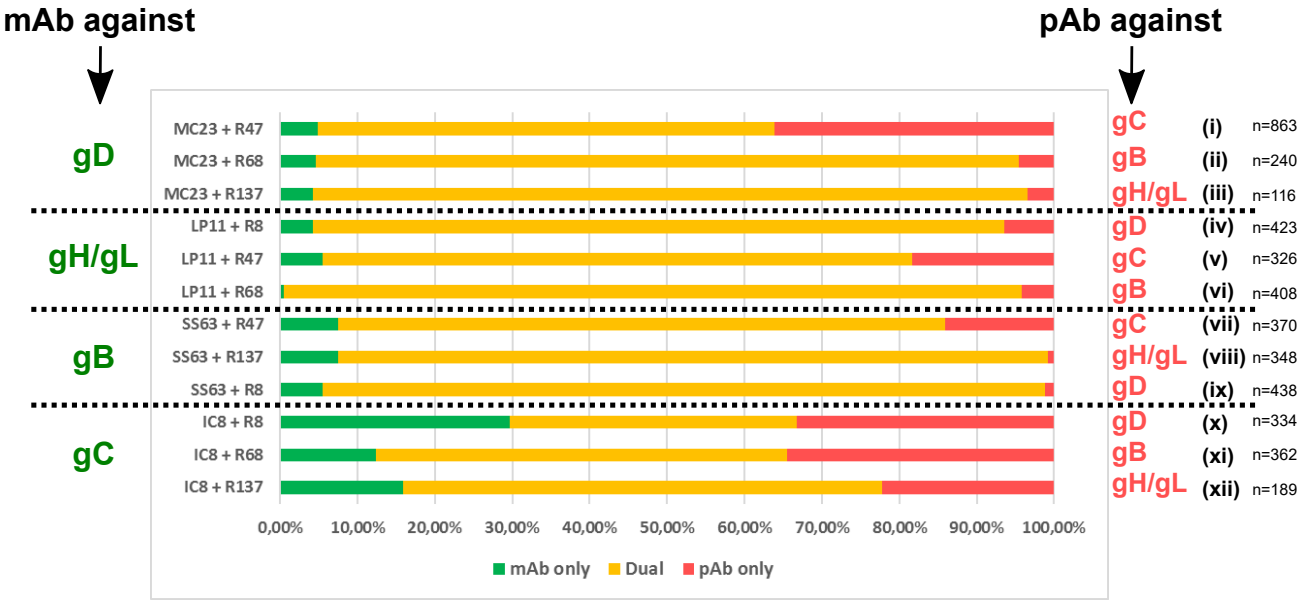
mAb against
pAb against
gD
gH/gL
gB
gC
MC23 + R47
MC23 + R68
MC23 + R137
LP11 + R8
LP11 + R47
LP11 + R68
SS63 + R47
SS63 + R137
SS63 + R8
IC8 + R8
IC8 + R68
IC8 + R137
gC (i) n=863
gB (ii) n=240
gH/gL (iii) n=116
gD (iv) n=423
gC (v) n=326
gB (vi) n=408
gC (vii) n=370
gH/gL (viii) n=348
gD (ix) n=438
gD (x) n=334
gB (xi) n=362
gH/gL (xii) n=189
0,00% 10,00% 20,00% 30,00% 40,00% 50,00% 60,00% 70,00% 80,00% 90,00% 100,00%
mAb only
Dual
pAb only

B.

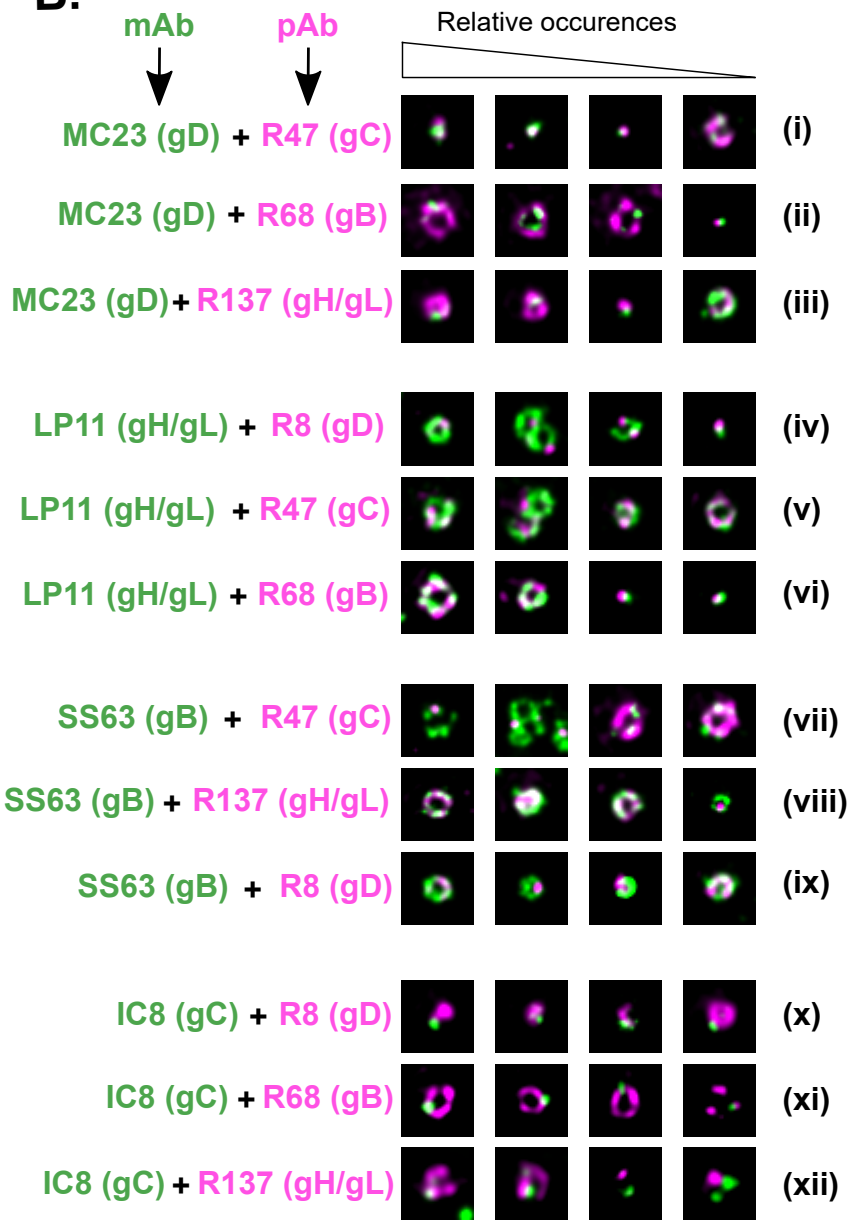
mAb
pAb
Relative occurences
MC23 (gD) + R47 (gC) (i)
MC23 (gD) + R68 (gB) (ii)
MC23 (gD) + R137 (gH/gL) (iii)
LP11 (gH/gL) + R8 (gD) (iv)
LP11 (gH/gL) + R47 (gC) (v)
LP11 (gH/gL) + R68 (gB) (vi)
SS63 (gB) + R47 (gC) (vii)
SS63 (gB) + R137 (gH/gL) (viii)
SS63 (gB) + R8 (gD) (ix)
IC8 (gC) + R8 (gD) (x)
IC8 (gC) + R68 (gB) (xi)
IC8 (gC) + R137 (gH/gL) (xii)

Figure 5

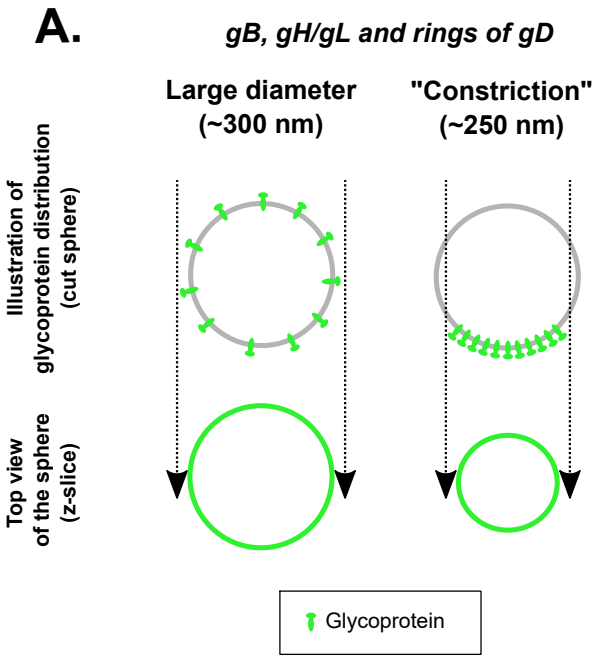
A.
gB, gH/gL and rings of gD
Large diameter
(~300 nm)
"Constriction"
(~250 nm)
Illustration of glycoprotein distribution (cut sphere)
Top view of the sphere (z-slice)
Glycoprotein

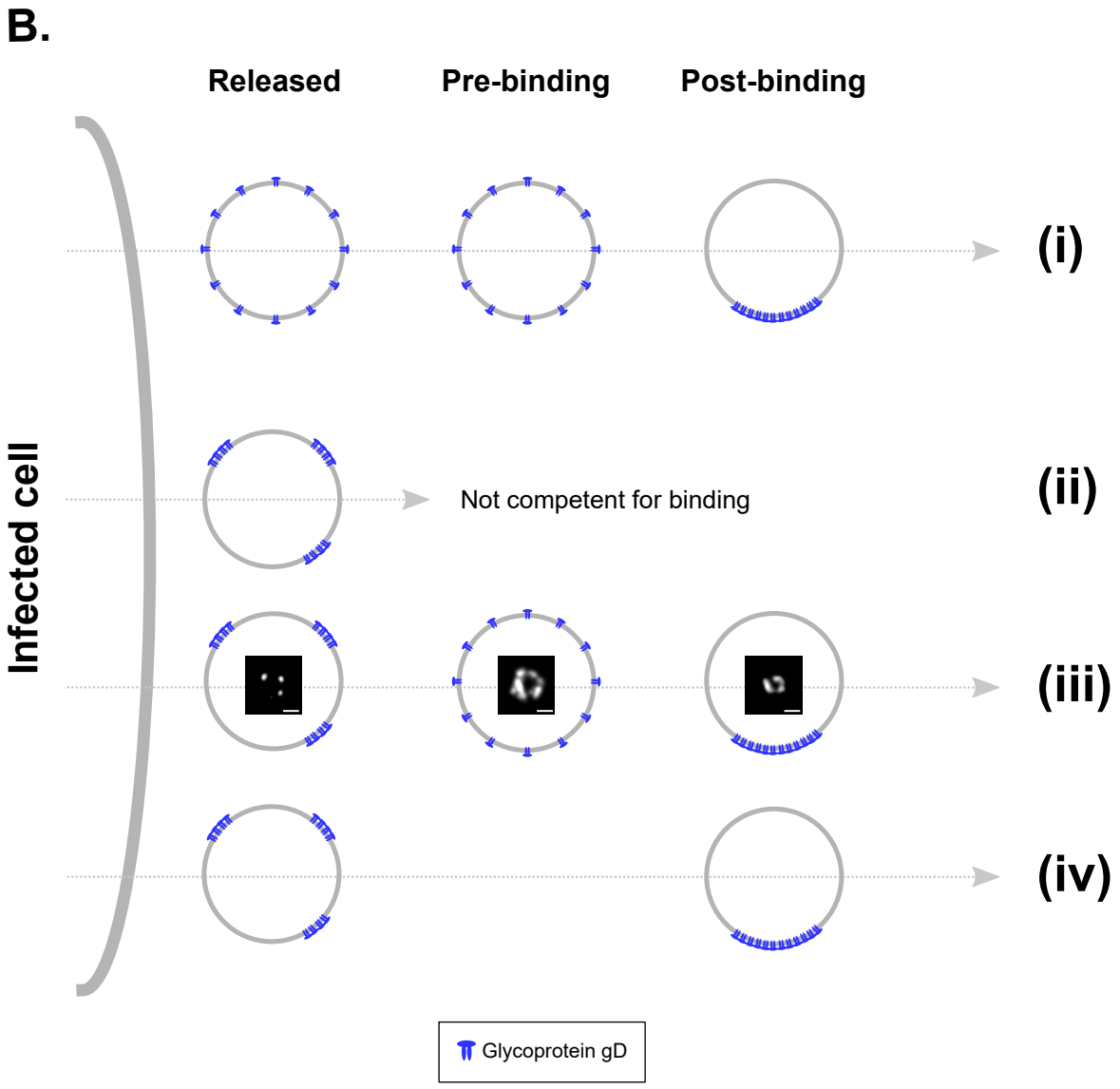
B.
Released
Pre-binding
Post-binding
Infected cell
(i)
(ii)
Not competent for binding
(iii)
(iv)
Glycoprotein gD

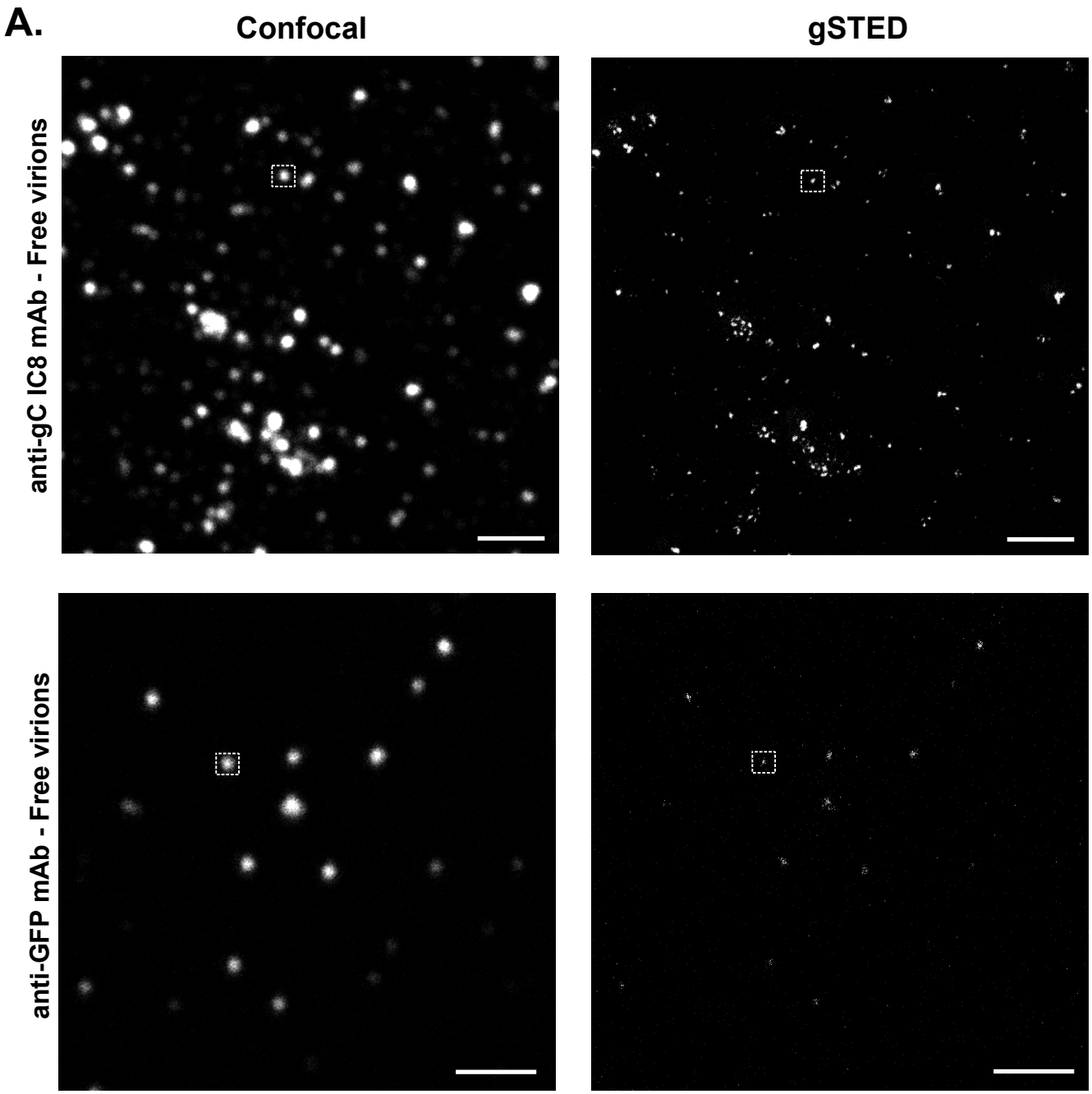

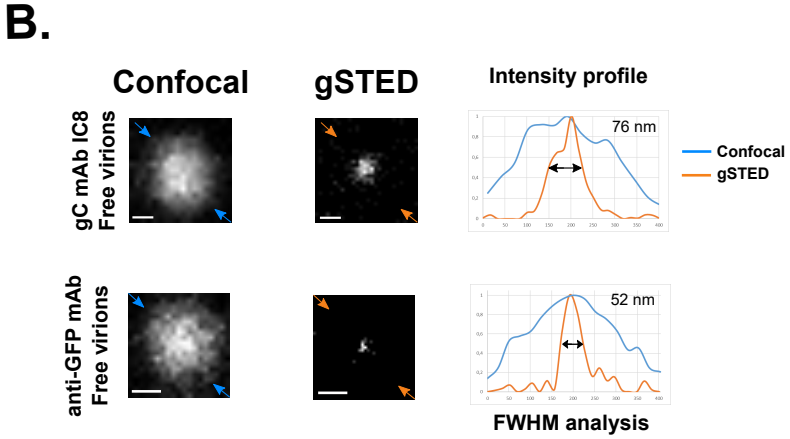

Supp. Figure 1

Supp. Figure 2

Target	Name	Type	Concentration	Distribution	
				Free virions	Attached
gB	SS63	mAb	2,5 mg/mL		
	R68	pAb	8,3 mg/mL		
gH/gL	LP11	mAb	3,7 mg/mL		
	R137	pAb	5 mg/mL		
gD	MC23	mAb	1,2 mg/mL		
	R8	pAb	6,5 mg/mL		
gC	IC8	mAb	8,6 mg/mL		
	R47	pAb	ND		

PARTIE V :

Identification des facteurs viraux et cellulaires impliqués dans la transmission du virus de la maladie de Marek et dans son tropisme cutané

Contexte et hypothèse de travail

Je conduis actuellement ce projet avec Caroline Denesvre et Aurélien Chuard au sein du laboratoire de biologie des virus aviaires (BioVA) de l'UMR Infectiologie & Santé Publique (ISP) de l'INRA de Nouzilly.

Le virus de la maladie de Marek (MDV) est un alpha-herpèsvirus très atypique sur de nombreux points. C'est un virus tumorigène de la poule très contagieux qui se propage via inhalation de poussières contaminées par des squames de peau infectés. Le virus infecte les lymphocytes B et T, ces derniers étant la cible principale du virus où il s'établit à l'état latent. Durant la latence, le génome viral est intégré au génome cellulaire au niveau des télomères et quelques protéines sont produites, dont certaines sont oncogènes, afin de maintenir les cellules en vie. Une sous-population de lymphocytes T ainsi infectés seront à l'origine de lymphomes qui conduisent à la mort de l'animal. Depuis les années 70, il existe plusieurs vaccins permettant d'empêcher la mort des animaux. Toutefois, les animaux vaccinés peuvent être infectés par les virus WT circulants et les excrètent. Ainsi, la vaccination ne permet pas d'éradiquer le virus. Du fait de sa circulation continue et de la protection des animaux contre sa mortalité, le virus continue d'évoluer et des souches de virulence croissante apparaissent[59] (**Figure 13**) avec la possibilité d'apparition de souches pour lesquelles le

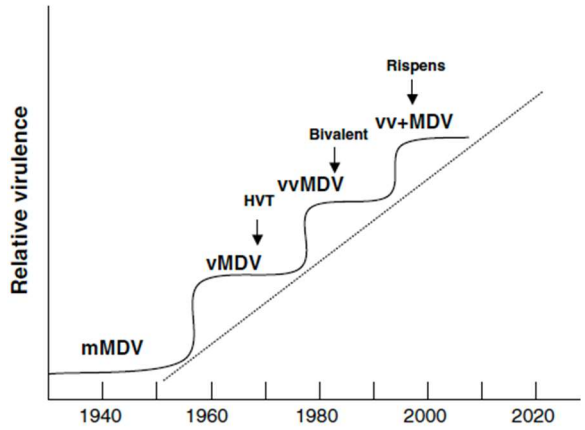

Figure 13. Evolution relative de la virulence des différentes souches ayant emergées au cours des 70 dernières années avec indication de l'introduction des différents vaccins (HVT, Bivalent et « Rispens »). Les pathotypes de MDV sont indiqués par la lettre précédant le MDV : m=mild, v=virulent, vv= very virulent et vv+. Tiré de Nair, 2005[60].

vaccin serait inefficace. Par ailleurs, le MDV est un virus très fortement associé aux cellules et il n'existe à l'heure actuelle aucune méthode *in vitro* permettant d'obtenir des particules virales libres. De plus, en l'absence de lignée cellulaire capable d'offrir une réplication virale efficace, les cellules primaires de

peau d'embryon de poulet continuent d'être utilisées pour la réplication du virus. Ainsi, les formes vaccinales actuellement utilisées se présentent essentiellement sous forme de cellules primaires infectées, ce qui est coûteux et peut avoir des conséquences sur la stabilité du vaccin (conservation et transport en azote liquide).

Au laboratoire, nous tentons de mettre au point un vaccin de nouvelle génération qui soit cultivable sur une lignée cellulaire, qui ne soit pas excrété dans l'environnement par les animaux vaccinés et qui empêche la circulation des souches pathogènes WT. Un tel vaccin serait plus efficace, plus économique et devrait permettre à terme d'éradiquer le virus. Pour répondre à l'ensemble de ces défis, nous nous concentrons sur le tropisme du virus pour la peau. En effet, c'est dans la peau, et plus particulièrement dans l'épithélium du follicule plumeux (EFP, **Figure 14**), que le virus est répliqué le plus efficacement et sous une forme complète et libre[61].

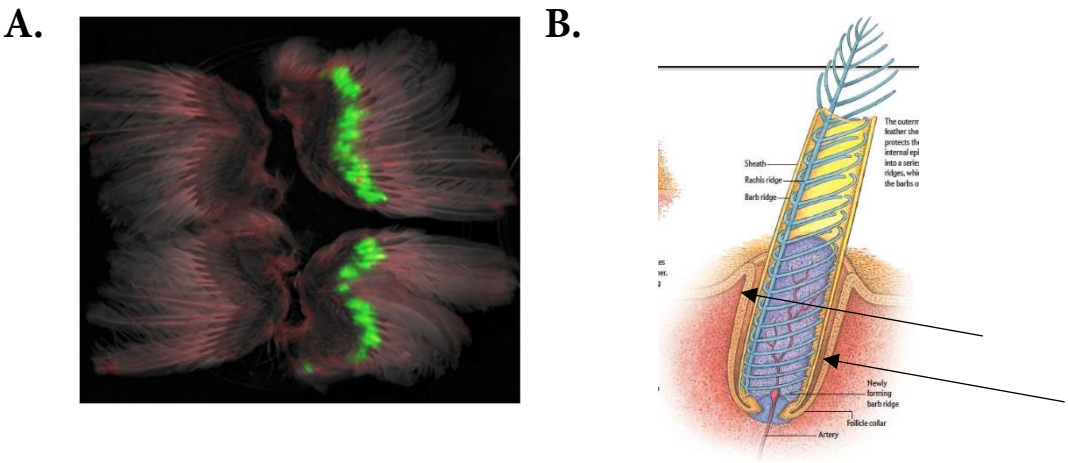

Figure 14. Site de réplication du virus à la base de la plume. (A) Des ailes issues d'une poule non-infectée (à gauche) ou infectée avec un virus MDV RB1B codant pour une cassette GFP (à droite) sont visualisées à l'aide de l'imageur IVIS Spectrum. La réplication virale, marquée en vert, est très localisée à la base des plumes sur ces images. Données non publiées. (B) Représentation schématique d'une plume et de l'EFP à sa base. Les flèches montrent la localisation de l'épithélium du follicule où se déroule la réplication virale. Tiré de P.J Wynne, Scientific American 2014.

Nous cherchons à déterminer la base moléculaire responsable de cette spécificité tissulaire afin (i) de pouvoir mettre au point une lignée cellulaire contenant les facteurs requis pour la multiplication efficace du virus et son excrétion et (ii) d'identifier les cibles permettant de produire un vaccin conférant une immunité complète contre le virus.

Projet

Le projet s'articule autour de plusieurs axes complémentaires :

- identification des protéines virales importantes pour le tropisme pour la peau de MDV et sa réplication dans ce tissu ;
- identification des protéines cellulaires spécifiques de l'EFP permettant une réplication plus efficace du virus dans ce tissu.

Une hypothèse sur laquelle nous travaillons est que la ou les protéines virales importantes pour la réplication dans la peau sont des facteurs d'assemblage qui manquent dans les autres tissus, ce qui pourrait expliquer la forte réplication du virus dans la peau par opposition aux autres tissus ou à la culture cellulaire.

L'observation au microscope électronique de cellules en culture infectées par MDV montre plusieurs caractéristiques très atypiques pour un alpha-herpesvirus[62] :

a) le nombre de capsides dans le noyau est faible mais il représente la majorité des capsides observables (90% chez MDV, de l'ordre de 20% chez HSV-1);

b) le nombre de capsides dans le cytoplasme est très faible (9% chez MDV, de l'ordre de 30% chez HSV-1)

c) les capsides cytoplasmiques de MDV peuvent être de chacun des trois types A (vide), B (intermédiaire d'assemblage) et C (complète avec le génome viral). Les types A et B sont normalement exclusivement nucléaires.

d) les capsides cytoplasmiques ne présentent pas de traces de tégument et les virions complets et enveloppés sont très rares (0.5% contre environ 20% chez HSV-1).

Ces observations conduisent aux hypothèses correspondantes suivantes :

a) transcription des gènes tardifs faible ou dérégulée. Protéines potentiellement impliquées : ICP4, ICP27 (il n'existe pas de ICP0 chez MDV)

b) export nucléaire des capsides inefficace. Protéines potentiellement impliquées : pUL31, pUL34, pUs3, pUL36, pUL47

c) mauvais contrôle-qualité des capsides en sortie du noyau. Protéines potentiellement impliquées : aucune connue à ce jour, mais les protéines listées en b) sont des candidats naturels auxquels l'on peut ajouter pUL25, connue comme essentielle pour la reconnaissance des capsides C par le complexe

d'export des capsides nucléaires[63,64].

d) faible tégumentation ou tégumentation incomplète. Protéines potentiellement impliquées : pUL36, pUL37, pUL47, pUL48, pUL46, pUL49.

Nous avons concentré nos efforts sur les protéines suivantes : pUL47, pUL48, pUL36 et pUL51.

La protéine pUL36 est une protéine de tégument fortement associée à la capside. Elle est nécessaire à la réplication de tous les herpesviridae. Elle est nécessaire pour l'initiation de la tégumentation car c'est la première protéine de tégument à interagir avec les capsides nues[29,65]. De plus, des formes tronquées de la protéine existent qui faciliteraient l'export des capsides nucléaires chez PrV[66]. Ainsi, l'absence d'une protéine pUL36 fonctionnelle dans les cellules « non-productives » de MDV expliquerait un export des capsides nucléaires médiocre et une tégumentation (et l'enveloppement qui s'ensuit) inexistante ou très inefficace.

pUL47, pUL48 et pUL51 sont des protéines de tégument externe[67,68]. Alors que pUL47 et pUL48 sont abondantes dans le tégument, pUL51 est une protéine mineure. Néanmoins, les trois protéines ont une fonction en commun : ce sont des facteurs connus de tropisme cutané chez le Virus de la Varicelle et du Zona[69,70], un alpha-herpesvirus qui partage de nombreux points communs avec MDV (excepté l'aspect tumorigène de MDV et le neurotropisme de VZV). pUL51 est également incriminée dans l'enveloppement secondaire de VZV dans des cellules neuronales[71]. Par ailleurs, pUL47 et pUL48 sont fortement exprimées dans la peau des animaux infectés par MDV alors qu'elles sont faiblement détectables dans les lymphocytes et en culture de cellules primaires[72,73].

Premiers résultats

Nous avons construit des virus recombinants ne codant pas pour pUL47 ou pour pUL48 (pUL51 est une protéine essentielle chez MDV). Nous avons ainsi montré que les deux protéines ne sont pas nécessaires pour la réplication du virus dans la peau des animaux infectés et son excrétion. En revanche, nous avons observé que pUL47 est nécessaire à la transmission horizontale du virus (manuscrit en préparation).

La recherche de protéines cellulaires importantes pour la réplication du virus dans l'EFP dépend, dans notre approche, de l'utilisation d'un facteur viral impliqué.

Afin de déterminer ces protéines cellulaires, nous avons retenu deux approches complémentaires. La première repose sur le double-hybride en levures. Pour ce système, il a fallu mettre au point des

banques de cDNA inédites chez la poule provenant du thymus (source de lymphocytes T qui sont la cible du virus et où il s'établit en latence) ou de la pulpe de plumes (source de tissu dermique et épidermique de l'EFP). Ces banques sont en cours d'utilisation afin de déterminer des partenaires cellulaires de pUL47 et pUL51, préférentiellement spécifiques à l'EFP.

La seconde approche repose sur l'isolement des complexes protéiques *in vivo,* c'est-à-dire dans l'EFP d'animaux infectés. Pour cela, nous avons mis au point des virus recombinants porteurs d'une étiquette de purification en tandem telles que TAP (domaine protéine A + domaine de liaison à la calmoduline) ou S-HA (étiquette Strep-tag liant la streptavidine + épitope HA) sur les protéines pUL47 ou pUL51.

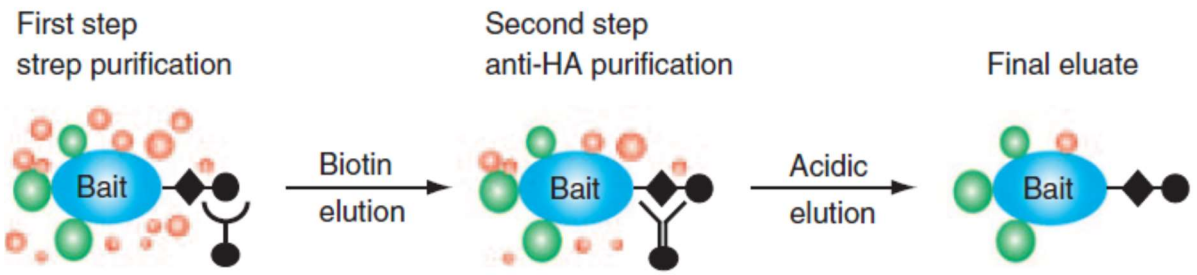

Figure 15. Description du système de purification en tandem S-HA. Les complexes protéiques sont retenus sur une colonne de Strep-Tactin via leur domaine Strep-tag (7 aa, rond) puis élués avec de la biotine. Les complexes ainsi purifiés sont soumis à une seconde étape de purification par fixation sur une colonne d'affinité via l'épitope HA (8aa, losange). Les complexes protéiques sont élués par lavage acide et leur composition analysée par spectrométrie de masse.

Des animaux ont été inoculés avec un virus UL47-TAP, UL51-TAP ou UL51-SHA. Trois semaines plus tard, une fois la réplication virale dans les plumes bien établies, les animaux ont été sacrifiés et des plumes et de la peau ont été prélevées afin de procéder à l'extraction des complexes protéiques.

L'approche TAP n'a toutefois pas aboutie car le rendement de purification de pUL47 avec cette étiquette n'était pas satisfaisant aussi bien *in vitro* qu'*in vivo*. La fusion de TAP à pUL51 a considérablement atténué le virus et n'a pas permis d'isoler suffisamment de tissus infectés à partir des animaux. Nous avons donc retenu l'étiquette S-HA pour une purification des complexes protéiques associés à pUL51. Les premiers résultats montrent un meilleur rendement mais la purification des complexes à partir de ces tissus requiert encore quelques étapes d'optimisation qui sont en cours.

Perspectives

L'ensemble des résultats attendus de ce projet devraient nous permettre de mettre à jour la base moléculaire de la spécificité de l'EFP dans la sécrétion du virus dans l'environnement. L'identification d'une ou plusieurs protéines cellulaires impliquées dans l'assemblage efficace du virus pourrait en outre conduire à la mise au point d'une lignée cellulaire enfin capable de produire du virus extracellulaire, en mimant ce qui se produit naturellement dans l'EFP. Une telle lignée aurait des répercussions importantes car l'incapacité actuelle d'obtenir du virus abondamment produit et extracellulaire est un frein important pour la production de vaccins ainsi que pour la recherche fondamentale sur ce virus. En effet, MDV est un excellent modèle d'étude des Herpesvirus car les virus de cette famille sont fortement adaptés à leur hôte et MDV est un des rares Herpèsvirus à pouvoir être étudié sur l'ensemble de son cycle de vie, incluant son hôte naturel.

Références bibliographiques

1 McGeoch, D. J., Rixon, F. J. & Davison, A. J. Topics in herpesvirus genomics and evolution. *Virus Res* **117**, 90-104 (2006).
2 Heldwein, E. E. Up close with herpesviruses. *Science* **360**, 34-35, doi:10.1126/science.aat3990 (2018).
3 Zeev-Ben-Mordehai, T., Hagen, C. & Grunewald, K. A cool hybrid approach to the herpesvirus 'life' cycle. *Curr Opin Virol* **5**, 42-49, doi:10.1016/j.coviro.2014.01.008 (2014).
4 Lachmann, R. Herpes simplex virus latency. *Expert Rev Mol Med* **5**, 1-14, doi:doi:10.1017/S1462399403006975 (2003).
5 McNab, A. R. *et al.* The product of the herpes simplex virus type 1 UL25 gene is required for encapsidation but not for cleavage of replicated viral DNA. *J Virol* **72**, 1060-1070 (1998).
6 Stow, N. D. Packaging of genomic and amplicon DNA by the herpes simplex virus type 1 UL25-null mutant KUL25NS. *J Virol* **75**, 10755-10765, doi:10.1128/JVI.75.22.10755-10765.2001 (2001).
7 Miyamoto, Y., Yamada, K. & Yoneda, Y. Importin alpha: a key molecule in nuclear transport and non-transport functions. *J Biochem* **160**, 69-75, doi:10.1093/jb/mvw036 (2016).
8 Ojala, P. M., Sodeik, B., Ebersold, M. W., Kutay, U. & Helenius, A. Herpes simplex virus type 1 entry into host cells: reconstitution of capsid binding and uncoating at the nuclear pore complex in vitro. *Mol Cell Biol* **20**, 4922-4931 (2000).
9 Preston, V. G., Murray, J., Preston, C. M., McDougall, I. M. & Stow, N. D. The UL25 gene product of herpes simplex virus type 1 is involved in uncoating of the viral genome. *J Virol* **82**, 6654-6666, doi:10.1128/JVI.00257-08 (2008).
10 Strambio-De-Castillia, C., Niepel, M. & Rout, M. P. The nuclear pore complex: bridging nuclear transport and gene regulation. *Nat Rev Mol Cell Biol* **11**, 490-501, doi:10.1038/nrm2928 (2010).
11 Coller, K. E., Lee, J. I., Ueda, A. & Smith, G. A. The capsid and tegument of the alphaherpesviruses are linked by an interaction between the UL25 and VP1/2 proteins. *J Virol* **81**, 11790-11797, doi:10.1128/JVI.01113-07 (2007).
12 Copeland, A. M., Newcomb, W. W. & Brown, J. C. Herpes simplex virus replication: roles of viral proteins and nucleoporins in capsid-nucleus attachment. *J Virol* **83**, 1660-1668, doi:10.1128/JVI.01139-08 (2009).
13 Abaitua, F., Daikoku, T., Crump, C. M., Bolstad, M. & O'Hare, P. A single mutation responsible for temperature-sensitive entry and assembly defects in the VP1-2 protein of herpes simplex virus. *J Virol* **85**, 2024-2036, doi:10.1128/JVI.01895-10 (2011).
14 Abaitua, F., Souto, R. N., Browne, H., Daikoku, T. & O'Hare, P. Characterization of the herpes simplex virus (HSV)-1 tegument protein VP1-2 during infection with the HSV temperature-sensitive mutant tsB7. *J Gen Virol* **90**, 2353-2363, doi:10.1099/vir.0.012492-0 (2009).
15 Batterson, W., Furlong, D. & Roizman, B. Molecular genetics of herpes simplex virus. VIII. further characterization of a temperature-sensitive mutant defective in release of viral DNA and in other stages of the viral reproductive cycle. *J Virol* **45**, 397-407 (1983).
16 Abaitua, F., Hollinshead, M., Bolstad, M., Crump, C. M. & O'Hare, P. A Nuclear localization signal in herpesvirus protein VP1-2 is essential for infection via capsid routing to the nuclear pore. *J Virol* **86**, 8998-9014, doi:10.1128/JVI.01209-12 (2012).
17 Dai, X. & Zhou, Z. H. Structure of the herpes simplex virus 1 capsid with associated tegument protein complexes. *Science* **360**, doi:10.1126/science.aao7298 (2018).
18 McElwee, M., Vijayakrishnan, S., Rixon, F. & Bhella, D. Structure of the herpes simplex virus portal-vertex. *PLoS Biol* **16**, e2006191, doi:10.1371/journal.pbio.2006191 (2018).
19 Rode, K. *et al.* Uncoupling uncoating of herpes simplex virus genomes from their nuclear import and gene expression. *J Virol* **85**, 4271-4283, doi:10.1128/JVI.02067-10 (2011).
20 Schipke, J. *et al.* The C terminus of the large tegument protein pUL36 contains multiple capsid binding sites that function differently during assembly and cell entry of herpes simplex virus. *J Virol* **86**, 3682-3700, doi:10.1128/JVI.06432-11 (2012).
21 Cohen, S., Au, S. & Pante, N. How viruses access the nucleus. *Biochim Biophys Acta* **1813**, 1634-1645, doi:10.1016/j.bbamcr.2010.12.009 (2011).
22 Fay, N. & Pante, N. Nuclear entry of DNA viruses. *Front Microbiol* **6**, 467, doi:10.3389/fmicb.2015.00467 (2015).
23 Flatt, J. W. & Greber, U. F. Viral mechanisms for docking and delivering at nuclear pore complexes. *Semin Cell Dev Biol* **68**, 59-71, doi:10.1016/j.semcdb.2017.05.008 (2017).
24 Kobiler, O., Drayman, N., Butin-Israeli, V. & Oppenheim, A. Virus strategies for passing the nuclear envelope barrier. *Nucleus* **3**, 526-539, doi:10.4161/nucl.21979 (2012).
25 Le Sage, V. & Mouland, A. J. Viral subversion of the nuclear pore complex. *Viruses* **5**, 2019-2042, doi:10.3390/v5082019 (2013).
26 Sodeik, B., Ebersold, M. W. & Helenius, A. Microtubule-mediated transport of incoming herpes simplex virus 1 capsids to the nucleus. *J Cell Biol* **136**, 1007-1021 (1997).
27 Luxton, G. W., Lee, J. I., Haverlock-Moyns, S., Schober, J. M. & Smith, G. A. The pseudorabies virus VP1/2 tegument protein is required for intracellular capsid transport. *J Virol* **80**, 201-209, doi:10.1128/JVI.80.1.201-209.2006 (2006).

28 Wolfstein, A. *et al.* The inner tegument promotes herpes simplex virus capsid motility along microtubules in vitro. *Traffic* **7**, 227-237, doi:10.1111/j.1600-0854.2005.00379.x (2006).
29 Radtke, K. *et al.* Plus- and minus-end directed microtubule motors bind simultaneously to herpes simplex virus capsids using different inner tegument structures. *PLoS Pathog* **6**, e1000991 (2010).
30 Antinone, S. E. & Smith, G. A. Retrograde axon transport of herpes simplex virus and pseudorabies virus: a live-cell comparative analysis. *J Virol* **84**, 1504-1512 (2010).
31 Granzow, H., Klupp, B. G. & Mettenleiter, T. C. Entry of pseudorabies virus: an immunogold-labeling study. *J Virol* **79**, 3200-3205, doi:10.1128/JVI.79.5.3200-3205.2005 (2005).
32 Luxton, G. W. *et al.* Targeting of herpesvirus capsid transport in axons is coupled to association with specific sets of tegument proteins. *Proc Natl Acad Sci U S A* **102**, 5832-5837 (2005).
33 Liu, J. J. *et al.* BPAG1n4 is essential for retrograde axonal transport in sensory neurons. *J Cell Biol* **163**, 223-229, doi:10.1083/jcb.200306075 (2003).
34 Ryan, S. D. *et al.* Microtubule stability, Golgi organization, and transport flux require dystonin-a2-MAP1B interaction. *J Cell Biol* **196**, 727-742, doi:10.1083/jcb.201107096 (2012).
35 Leung, C. L., Liem, R. K., Parry, D. A. & Green, K. J. The plakin family. *J Cell Sci* **114**, 3409-3410 (2001).
36 Dodding, M. P. & Way, M. Coupling viruses to dynein and kinesin-1. *EMBO J* **30**, 3527-3539, doi:10.1038/emboj.2011.283 (2011).
37 Zaichick, S. V. *et al.* The herpesvirus VP1/2 protein is an effector of dynein-mediated capsid transport and neuroinvasion. *Cell Host Microbe* **13**, 193-203, doi:10.1016/j.chom.2013.01.009 (2013).
38 Richards, A. L. *et al.* The pUL37 tegument protein guides alpha-herpesvirus retrograde axonal transport to promote neuroinvasion. *PLoS Pathog* **13**, e1006741, doi:10.1371/journal.ppat.1006741 (2017).
39 Kumar, A., Rajendran, V., Sethumadhavan, R. & Purohit, R. CEP proteins: the knights of centrosome dynasty. *Protoplasma* **250**, 965-983, doi:10.1007/s00709-013-0488-9 (2013).
40 Bornens, M. The centrosome in cells and organisms. *Science* **335**, 422-426, doi:10.1126/science.1209037 (2012).
41 Avitabile, E. *et al.* Redistribution of microtubules and Golgi apparatus in herpes simplex virus-infected cells and their role in viral exocytosis. *J Virol* **69**, 7472-7482 (1995).
42 Kotsakis, A., Pomeranz, L. E., Blouin, A. & Blaho, J. A. Microtubule reorganization during herpes simplex virus type 1 infection facilitates the nuclear localization of VP22, a major virion tegument protein. *J Virol* **75**, 8697-8711 (2001).
43 Naghavi, M. H., Gundersen, G. G. & Walsh, D. Plus-end tracking proteins, CLASPs, and a viral Akt mimic regulate herpesvirus-induced stable microtubule formation and virus spread. *Proc Natl Acad Sci U S A* **110**, 18268-18273, doi:10.1073/pnas.1310760110 (2013).
44 Procter, D. J. *et al.* The HCMV Assembly Compartment Is a Dynamic Golgi-Derived MTOC that Controls Nuclear Rotation and Virus Spread. *Dev Cell* **45**, 83-100 e107, doi:10.1016/j.devcel.2018.03.010 (2018).
45 Eisenberg, R. J. *et al.* Herpes virus fusion and entry: a story with many characters. *Viruses* **4**, 800-832, doi:10.3390/v4050800 (2012).
46 Chowdary, T. K. *et al.* Crystal structure of the conserved herpesvirus fusion regulator complex gH-gL. *Nat Struct Mol Biol* **17**, 882-888, doi:10.1038/nsmb.1837 (2010).
47 Heldwein, E. E. *et al.* Crystal structure of glycoprotein B from herpes simplex virus 1. *Science* **313**, 217-220, doi:10.1126/science.1126548 (2006).
48 Krummenacher, C. *et al.* Herpes simplex virus glycoprotein D can bind to poliovirus receptor-related protein 1 or herpesvirus entry mediator, two structurally unrelated mediators of virus entry. *J Virol* **72**, 7064-7074 (1998).
49 Montgomery, R. I., Warner, M. S., Lum, B. J. & Spear, P. G. Herpes simplex virus-1 entry into cells mediated by a novel member of the TNF/NGF receptor family. *Cell* **87**, 427-436 (1996).
50 Herold, B. C., WuDunn, D., Soltys, N. & Spear, P. G. Glycoprotein C of herpes simplex virus type 1 plays a principal role in the adsorption of virus to cells and in infectivity. *J Virol* **65**, 1090-1098 (1991).
51 MacLeod, D. T., Nakatsuji, T., Yamasaki, K., Kobzik, L. & Gallo, R. L. HSV-1 exploits the innate immune scavenger receptor MARCO to enhance epithelial adsorption and infection. *Nat Commun* **4**, 1963, doi:10.1038/ncomms2963 (2013).
52 Grunewald, K. *et al.* Three-dimensional structure of herpes simplex virus from cryo-electron tomography. *Science* **302**, 1396-1398 (2003).
53 Maurer, U. E., Sodeik, B. & Grunewald, K. Native 3D intermediates of membrane fusion in herpes simplex virus 1 entry. *Proc Natl Acad Sci U S A* **105**, 10559-10564, doi:10.1073/pnas.0801674105 (2008).
54 Newcomb, W. W. & Brown, J. C. Time-dependent transformation of the herpesvirus tegument. *J Virol* **83**, 8082-8089, doi:10.1128/JVI.00777-09 (2009).
55 Smith, G. A. Assembly and Egress of an Alphaherpesvirus Clockwork. *Adv Anat Embryol Cell Biol* **223**, 171-193, doi:10.1007/978-3-319-53168-7_8 (2017).
56 Handler, C. G., Eisenberg, R. J. & Cohen, G. H. Oligomeric structure of glycoproteins in herpes simplex virus type 1. *J Virol* **70**, 6067-6070 (1996).

57 Hook, L. M., Huang, J., Jiang, M., Hodinka, R. & Friedman, H. M. Blocking antibody access to neutralizing domains on glycoproteins involved in entry as a novel mechanism of immune evasion by herpes simplex virus type 1 glycoproteins C and E. *J Virol* **82**, 6935-6941, doi:10.1128/JVI.02599-07 (2008).
58 Chojnacki, J. *et al.* Maturation-dependent HIV-1 surface protein redistribution revealed by fluorescence nanoscopy. *Science* **338**, 524-528, doi:10.1126/science.1226359 (2012).
59 Read, A. F. *et al.* Imperfect Vaccination Can Enhance the Transmission of Highly Virulent Pathogens. *PLoS Biol* **13**, e1002198, doi:10.1371/journal.pbio.1002198 (2015).
60 Nair, V. Evolution of Marek's disease -- a paradigm for incessant race between the pathogen and the host. *Vet J* **170**, 175-183, doi:10.1016/j.tvjl.2004.05.009 (2005).
61 Calnek, B. W., Adldinger, H. K. & Kahn, D. E. Feather follicle epithelium: a source of enveloped and infectious cell-free herpesvirus from Marek's disease. *Avian Dis* **14**, 219-233 (1970).
62 Denesvre, C. *et al.* Morphogenesis of a highly replicative EGFPVP22 recombinant Marek's disease virus in cell culture. *J Virol* **81**, 12348-12359, doi:10.1128/JVI.01177-07 (2007).
63 Klupp, B. G., Granzow, H., Keil, G. M. & Mettenleiter, T. C. The capsid-associated UL25 protein of the alphaherpesvirus pseudorabies virus is nonessential for cleavage and encapsidation of genomic DNA but is required for nuclear egress of capsids. *J Virol* **80**, 6235-6246, doi:10.1128/JVI.02662-05 (2006).
64 Trus, B. L. *et al.* Allosteric signaling and a nuclear exit strategy: binding of UL25/UL17 heterodimers to DNA-Filled HSV-1 capsids. *Mol Cell* **26**, 479-489, doi:10.1016/j.molcel.2007.04.010 (2007).
65 Henaff, D., Remillard-Labrosse, G., Loret, S. & Lippe, R. Analysis of the early steps of herpes simplex virus 1 capsid tegumentation. *J Virol* **87**, 4895-4906, doi:10.1128/JVI.03292-12 (2013).
66 Leelawong, M., Lee, J. I. & Smith, G. A. Nuclear egress of pseudorabies virus capsids is enhanced by a subspecies of the large tegument protein that is lost upon cytoplasmic maturation. *J Virol* **86**, 6303-6314, doi:10.1128/JVI.07051-11 (2012).
67 Loret, S., Guay, G. & Lippe, R. Comprehensive characterization of extracellular herpes simplex virus type 1 virions. *J Virol* **82**, 8605-8618, doi:10.1128/JVI.00904-08 (2008).
68 Russell, T., Bleasdale, B., Hollinshead, M. & Elliott, G. Qualitative Differences in Capsidless L-Particles Released as a By-Product of Bovine Herpesvirus 1 and Herpes Simplex Virus 1 Infections. *J Virol* **92**, doi:10.1128/JVI.01259-18 (2018).
69 Che, X. *et al.* Functions of the ORF9-to-ORF12 gene cluster in varicella-zoster virus replication and in the pathogenesis of skin infection. *J Virol* **82**, 5825-5834, doi:10.1128/JVI.00303-08 (2008).
70 Zhang, Z. *et al.* Genome-wide mutagenesis reveals that ORF7 is a novel VZV skin-tropic factor. *PLoS Pathog* **6**, e1000971, doi:10.1371/journal.ppat.1000971 (2010).
71 Jiang, H. F. *et al.* ORF7 of Varicella-Zoster Virus Is Required for Viral Cytoplasmic Envelopment in Differentiated Neuronal Cells. *J Virol* **91**, doi:10.1128/JVI.00127-17 (2017).
72 Jarosinski, K. W., Arndt, S., Kaufer, B. B. & Osterrieder, N. Fluorescently tagged pUL47 of Marek's disease virus reveals differential tissue expression of the tegument protein in vivo. *J Virol* **86**, 2428-2436, doi:10.1128/JVI.06719-11 (2012).
73 Jarosinski, K. W. & Vautherot, J. F. Differential expression of Marek's disease virus (MDV) late proteins during in vitro and in situ replication: role for pUL47 in regulation of the MDV UL46-UL49 gene locus. *Virology* **484**, 213-226, doi:10.1016/j.virol.2015.06.012 (2015).

ANNEXES

Annexe #1

Nucleocytoplasmic shuttling of the rabies virus P protein requires a nuclear localization signal and a CRM1-dependent nuclear export signal.

Pasdeloup D, Poisson N, Raux H, Gaudin Y, Ruigrok RW, Blondel D

Available online at www.sciencedirect.com

SCIENCE DIRECT

Virology 334 (2005) 284–293

VIROLOGY

www.elsevier.com/locate/yviro

Nucleocytoplasmic shuttling of the rabies virus P protein requires a nuclear localization signal and a CRM1-dependent nuclear export signal

David Pasdeloup[a,1], Nicolas Poisson[a,1], Hélène Raux[a], Yves Gaudin[a], Rob W.H. Ruigrok[b], Danielle Blondel[a,*]

[a]*Unité Mixte de Virologie Moléculaire et Structurale UMR2472 CNRS, UMR1157 INRA, 91198 Gif sur Yvette Cedex, France*
[b]*Laboratoire de Virologie Moléculaire et Structurale, FRE 2854 CNRS-UJF, c/o EMBL, BP 181, 38042 Grenoble Cedex 9, France*

Received 22 December 2004; returned to author for revision 31 January 2005; accepted 7 February 2005

Abstract

Rabies virus P protein is a co-factor of the viral RNA polymerase. It has been shown previously that P mRNA directs the synthesis of four N-terminally truncated P products P2, P3, P4, and P5 due to translational initiation by a leaky scanning mechanism at internal Met codons. Whereas P and P2 are located in the cytoplasm, P3, P4, and P5 are found in the nucleus. Here, we have analyzed the molecular basis of the subcellular localization of these proteins. Using deletion mutants fused to GFP protein, we show the presence of a nuclear localization signal (NLS) in the C-terminal part of P (172–297). This domain contains a short lysine-rich stretch (^{211}**KKYK**^{214}) located in close proximity with arginine 260 as revealed by the crystal structure of P. We demonstrate the critical role of lysine 214 and arginine 260 in NLS activity. In the presence of Leptomycin B, P is retained in the nucleus indicating that it contains a CRM1-dependent nuclear export signal (NES). The subcellular distribution of P deletion mutants indicates that the domain responsible for export is the amino-terminal part of the protein. The use of fusion proteins that have amino terminal fragments of P fused to β-galactosidase containing the NLS of SV40 T antigen allows us to identify a NES between residues 49 and 58. The localization of NLS and NES determines the cellular distribution of the P gene products.

Keywords: Rabies virus; P protein; Nuclear import; Nuclear export

Introduction

Eucaryotic cells possess a double nuclear membrane, containing multiple nuclear pores that regulate bi-directional transport of macromolecules that is critically required for the maintenance of normal cell physiology.

Transport proceeds through the nuclear pore complex (NPC), a 125 MDa macromolecular assembly of 50–100 polypeptides that are frequently termed nucleoporins. The NPC spans the nuclear membrane and creates an aqueous channel allowing passive diffusion of globular proteins of up to approximately 50 kDa. Translocation across the NPC into the nucleoplasm or into the cytoplasm is mediated by importins and exportins, respectively, which interact with cargo molecules, the Ran GTPase, and proteins of the NPC. Cargo molecules have localization signals that allow their interaction with importins and exportins. The classical nuclear localization signal (NLS) comprises one or two short stretches of basic amino acids. Examples are the simian virus 40 (SV40) T antigen NLS (PKKKRKV) (Kalderon et al., 1984) or the cellular nucleoplasmin protein NLS (KRPAATKKAGQAKKK) (Robbins et al., 1991). These sequences are recognized in the cytoplasm by importin α which forms a stable heterodimeric complex with the importin β (Kohler et al., 1999). Importin β mediates the interaction of the importin α–β complex with the NPC and Ran GTPase. The complex translocates into the nucleus where importin α and β receptors dissociate from the cargo and shuttle back into the cytoplasm. The cycle is controlled by a Ran GTP gradient across the nuclear

* Corresponding author. Fax: +33 1 69 82 43 08.
E-mail address: danielle.blondel@vms.cnrs-gif.fr (D. Blondel).
[1] These authors contributed equally to this work.

0042-6822/$ - see front matter © 2005 Elsevier Inc. All rights reserved.
doi:10.1016/j.virol.2005.02.005

envelope. Low levels of Ran GTP in the cytoplasm allow the binding of importins to their cargoes, whereas high levels of Ran GTP in the nucleus induce their dissociation (Gorlich and Mattaj, 1996; Gorlich et al., 1995; Nigg, 1997). More recently, many other NLSs have been identified that do not conform to the classical NLS consensus motif with respect to size and/or highly basic character. Some of them are non-conventional importin α-interacting domains. This is the case of the influenza virus nucleoprotein (Wang et al., 1997), and the Borna disease virus p10 protein (Wolff et al., 2002).

The nuclear export of proteins and RNA is also a signal-dependent process mediated by soluble receptors called exportins. The best-characterized nuclear export signal (NESs) was first described in the HIV-Rev protein and then identified in an increasing number of proteins (Fischer et al., 1995). These leucine-rich NESs are recognized by the CRM1 nuclear export receptor. Leptomycin B (LMB) binds to the central domain of CRM1 to disrupt its interaction with the NES and provides a useful reagent for studying CRM1-mediated nuclear export (Fornerod et al., 1997; Nishi et al., 1994).

Rabies virus replicates in the host cell cytoplasm. It has a linear, non-segmented, single-strand RNA genome of negative polarity. The ribonucleoprotein (RNP) contains the RNA genome tightly encapsidated by the viral nucleoprotein (N) and the RNA polymerase complex which consists of the large protein (L) and its cofactor, the phosphoprotein (P). Both L and P are involved in transcription and replication. A positive-stranded leader RNA and five mRNAs are synthesized during transcription. The replication process yields nucleocapsids containing full-length antisense genome RNA, which in turn serves as a template for the synthesis of sense genome RNA.

Like the VSV P protein, the rabies virus P protein is a non-catalytic cofactor and a regulatory protein: it associates with the L protein in the polymerase complex and interacts with both soluble and genome-associated N proteins. The P protein contains two N protein-binding sites: one located in the amino-terminal part and the other in the carboxy terminal region (Chenik et al., 1994; Fu et al., 1994; Jacob et al., 2001). The major L-binding site resides within the first 19 residues of P (Chenik et al., 1998). The rabies virus P protein is phosphorylated by two kinases: the unique cellular protein kinase, RVPK (rabies virus protein kinase), and protein kinase C (Gupta et al., 2000). Both kinases phosphorylate specific sites on the P protein, leading to the formation of different phosphorylated forms of the P protein with different motilities in SDS–PAGE (Gupta et al., 2000). In addition, four other amino-terminally truncated products (P2, P3, P4, and P5) translated from P mRNA have been found in the purified virus, in infected cells and in cells transfected with a plasmid encoding the complete P protein. These shorter proteins are translated from internal in-frame AUG initiation codons by a leaky scanning mechanism (Chenik et al., 1995). Whereas P and P2 are located in the cytoplasm, P3–P5 are found mostly in the nucleus. The nuclear products of the P gene have been shown to interact with PML nuclear bodies that could be involved in a cellular defense mechanism against viral infection (Blondel et al., 2002).

In this study, we have analyzed the nuclear shuttling of the products of the rabies virus P gene. We show that the complete P has one NLS and one CRM1-dependent NES. The presence of these signals determines the intracellular localization of P and its products (P2–P5).

Results

The short P3 protein is conserved throughout the Lyssavirus genus

We have previously shown that the rabies CVS strain P mRNA directs the synthesis of four N-terminally truncated P products P2, P3, P4, and P5 due to translational initiation by a leaky scanning mechanism at internal Met codons 20, 53, 69, and 83, respectively (Chenik et al., 1995). Whereas P and P2 are located in the cytoplasm, P3, P4, and P5 are found mostly in the nucleus. Since Met 53 is conserved in the P protein of the most divergent lyssaviruses genotype, GT3 (Badrane et al., 2001), we analyzed first whether P3 was synthesized from Mokola P mRNA and then looked at its subcellular localization. For this, we constructed a plasmid containing the P gene of Mokola with the nucleotide sequence context of the first initiation codon of P mRNA.

Cells were infected with VTF7-3 recombinant vaccinia virus and were transfected with the plasmid encoding the P protein of Mokola (P_{Mok}) under the control of the T7 RNA polymerase promoter. Proteins present in cell extract were analyzed by immunoblotting with a mouse polyclonal anti-P antibody. As shown in Fig. 1A, the $P3_{Mok}$ protein that comigrated with the truncated $P\Delta N52_{Mok}$ protein initiated from the third AUG codons was also expressed from the Mokola P gene. In order to examine the intracellular localization of $P3_{Mok}$ in intact cells, the plasmid $pP\Delta N52_{Mok}$-GFP (encoding P3 fused to GFP) was transfected as described previously. Analysis by confocal microscopy shows that $P3_{Mok}$-GFP is found mainly in the nucleus and showed a distinct speckled nuclear localization similar to that of P3-GFP of the CVS strain (Figs. 1B and 3). This observation provides support for the conservation of the P3 protein and for its nuclear localization throughout the genus.

The difference in cellular localization of P and P3 suggests that there must be targeting information located either within P or P3 to account for their distinctive distributions. A conformational change resulting from truncation of the 52 first residues of P protein might reveal new targeting information within P3. Alternatively the lack of these 52 residues might remove a nuclear export signal

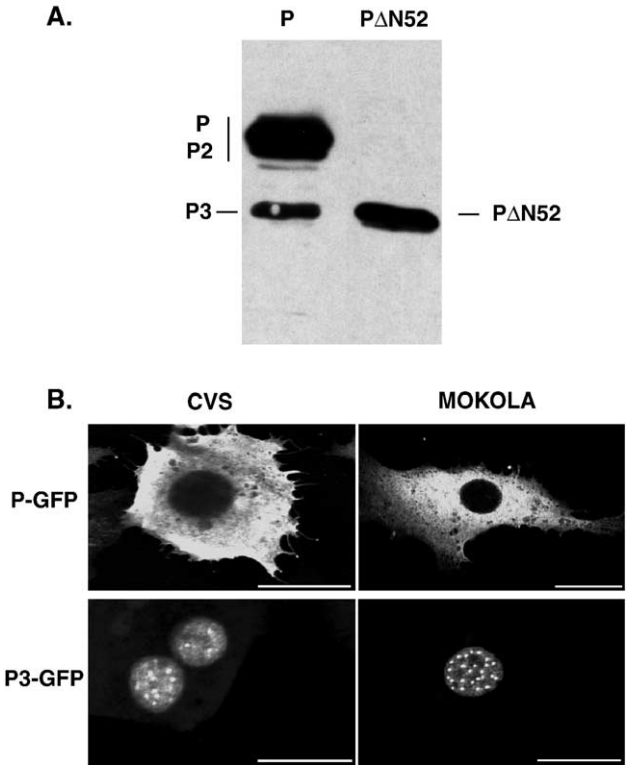

Fig. 1. P3 is expressed from P mRNA of Mokola and is nuclear. (A) BSR cells were infected with VTF7-3 and transfected with plasmids encoding P Mokola for 24 h. Cell extracts were analyzed by Western blotting. The blot was immunostained with the polyclonal anti-P antibody and visualized by the ECL system. (B) Immunostaining of P and P3 in transfected cells. Cells were transfected with plasmids encoding P-GFP or P3-GFP from Mokola or from CVS. After fixation, cells were analyzed for GFP expression by confocal fluorescence microscopy. The scale bars correspond to 20 μm.

that is dominant over nuclear targeting in the context of the complete P protein.

Nuclear localization of P3 requires the presence of a nuclear targeting sequence located between the residues 173–297

The localization of P3 within the nucleus suggested the presence of an NLS but a sequence resembling a classical motif could not be identified. To identify sequence(s) within the P protein that could function as an NLS, N-terminal and C-terminal truncations of P were fused to GFP (Fig. 2A). In contrast to the previous constructs encoding P_{Mok}, sequences upstream the AUG initiation codon have been converted to a Kozak consensus site to further increase the translation efficiency preventing downstream scanning. These truncated P proteins were expressed efficiently in BSR cells with the vaccinia T7 system and migrated as proteins of the expected molecular sizes (data not shown). Protein localization was determined by confocal microscopy (Fig. 2B). In contrast to GFP alone, which was distributed diffusely in both the cytoplasm and the nucleus, the proteins P3-GFP accumulated in the nucleus as P3. This result indicated that the nuclear targeting activity of P is located between residues 52–297. More extended deletions of 83, 138, and 172 amino acids from the amino-terminal part of P had a weak effect upon nuclear localization and these truncated proteins were predominantly nuclear. In contrast a C-terminal truncation of 125 residues abrogated the nuclear localization of the GFP fusion protein.

These findings indicate that the *carboxyl*-terminal part of P from 173 to 297 contains an active NLS.

Identification of the P residues required for nuclear localization

As mentioned above, P protein does not possess an obvious polybasic NLS sequence. However, inspection of the carboxy terminal part of P reveals a motif with a high proportion of basic residues (^{211}**KK**Y**K**^{214}) that is conserved in the seven different genotypes of lyssavirus. Moreover, the crystal structure of the C-terminal domain (186–297) of the P protein reveals that this lysine-rich motif lies on a surface exposed loop in close proximity to arginine 260, another basic residue (Mavrakis et al., 2004).

Mutational analysis of P3-GFP was performed in order to evaluate the role of this motif on nuclear import activity (Fig. 3). Upon transfection, mutated protein P3(^{211}**AA**YK^{214}-R^{260})-GFP exhibited a diffuse staining pattern in the nucleus indicating that this protein was efficiently imported into the nucleus. In contrast, cells expressing the protein P3(^{211}KKY**A**^{214}-R^{260})-GFP presented different staining patterns: an even fluorescence distribution between the nucleus and the cytoplasm or a cytoplasmic staining with few dots in the cytoplasm. The presence of cytoplasmic dots observed with the alanine substitution of lysine 214 could be the result of misfolding or altered stability of P3. However, when a negative aspartic acid residue was substituted to lysine 214, the localization of the protein P3(^{211}KKY**D**^{214}-R^{260})-GFP appeared diffuse in the cytoplasm without any granular staining. This finding indicates that the cytoplasmic localization of the mutants is not an artefact due to protein aggregation. Thus, a substitution of lysine residue at position 214 was sufficient to reduce the nuclear localization of P3-GFP whereas substitutions of the lysine residues at position 211 and 212 have little effect upon nuclear localization. In order to investigate the contribution of the arginine residue 260 in the nuclear import, we constructed the plasmid encoding P3(^{211}KKYK^{214}-**A**^{260})-GFP. This mutant protein exhibited a predominantly cytoplasmic and diffuse distribution indicating that the arginine residue also contributed efficiently to nuclear import activity. When both substitutions of lysine at position 214 and arginine in position 260 by alanine were introduced in the P3 sequence, the corresponding protein P3(^{211}KKY**A**^{214}-**A**^{260})-GFP was completely excluded from the nucleus. As expected, an aspartic acid substitution of lysine 214 associated with the alanine substitution on the arginine 260 also abolished nuclear import. These results

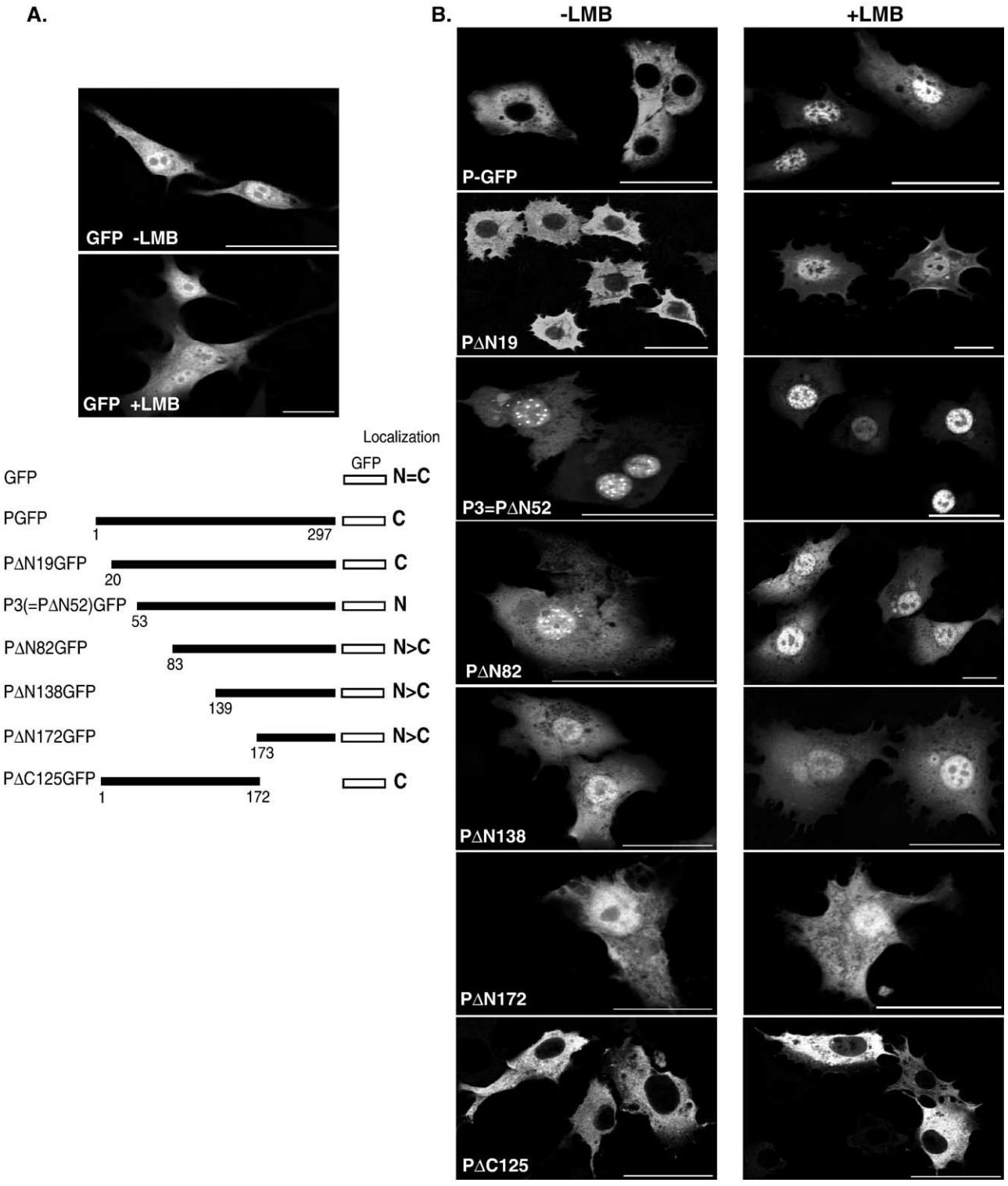

Fig. 2. Identification of an NLS in the P protein. (A) Construction of plasmids encoding truncated P protein fused to GFP. In this schematic representation, dark bars represent the protein product of each deleted gene with amino acid positions indicated. These mutants fused to GFP were expressed in BSR cells with the vaccinia T7 system as described in Material and methods. An immunofluorescence analysis was performed and the intracellular localization of these mutants in the cytoplasm (C) or in the nucleus (N) is summarized. (B) Cells were transfected with plasmids encoding truncated P proteins and incubated in the absence (−LMB) or presence of leptomycin B (+ LMB) at a final concentration of 20 nM during the time of transfection (6 h). After fixation, cells were analyzed for GFP expression by confocal fluorescence microscopy. GFP protein localization was also shown as control in the upper left panel. Representative results for a large number of cells examined in independent experiments are shown. The scale bars correspond to 40 μm.

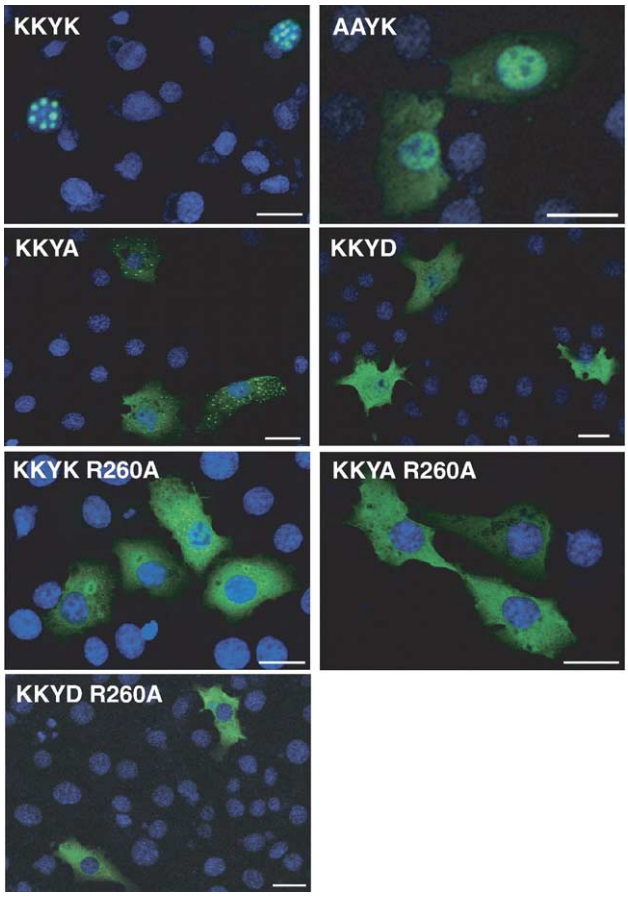

Fig. 3. Delineation of the residues involved in the NLS activity. Site-directed mutagenesis was performed on the motif ^{211}KKYK^{214}R^{260} of the plasmid encoding P3 protein fused to GFP as described in Material and methods. Cells were transfected with plasmids encoding P3(^{211}KKYK^{214}R^{260}), P3(^{211}**AA**YK^{214}R^{260}), P3(^{211}KKY**A**^{214}R^{260}), P3(^{211}KKY**D**^{214}R^{260}), P3(^{211}KKYK^{214}**A**^{260}), P3(^{211}KKY**A**^{214}**A**^{260}), and P3(^{211}KKY**D**^{214}**A**^{260}). Six hours after transfection, cells were fixed, stained with DAPI, and analyzed for GFP expression by confocal fluorescence microscopy. The scale bars correspond to 20 μm.

indicate that K214 and R260 are essential in the P3 nuclear activity and part of a conformational NLS.

Identification of a CRM1-dependent nuclear export signal (NES) within the P sequence

As the complete P protein contains the NLS motif but is cytoplasmic, its nuclear exclusion could be explained by the presence of a nuclear export activity. To determine whether there is a CRM1-dependent NES in P, cells expressing P-GFP were treated with LMB (20 nM), a specific inhibitor of nuclear export. Although P-GFP was cytoplasmic in untreated cells, its distribution was sensitive to LMB with retention of GFP fluorescence in the nucleus indicating that part of P protein was trapped in the nucleus (Figs. 2B and 4). LMB had no effect on the localization of GFP (Fig. 2A). Besides demonstrating the presence of CRM1-dependent NES within the P protein, this finding also indicates the nuclear entry of the complete P protein. To map the putative export signal, we analyzed the subcellular distribution of P deletion mutants fused to GFP and expressed in cells in the presence or absence of LMB (Figs. 2B and 4).

The localization of the amino-terminal deleted PΔN19-GFP protein was sensitive to the addition of LMB which resulted in a significant increase in the nuclear retention of the protein (Fig. 2B). In contrast, the localizations of others P constructs were all insensitive to LMB but for different reasons. As expected the nuclear localization of PΔN52 (P3-GFP) was unchanged in the presence of LMB. For shorter amino-terminal truncated P proteins (PΔN82, PΔN138, PΔN172) which are located in both cytoplasm and nucleus, LMB has no effect indicating the absence of a NES between residues 83–297 (Fig. 4). The fact that the carboxy terminal truncated P protein PΔC125 remained cytoplasmic in the presence of LMB confirms the absence of an NLS between residues 1–172. All these results show that a NES is located in the first 83 residues of P.

CRM1-dependent NESs are characterized by leucine-rich sequences (**L**XXX**L**XX**L**X**L**) although large hydrophobic amino acids (V, M, I) may be substituted to leucine. The examination of the first 83 residues of P revealed two stretches of amino acid residues similar to the characterized hydrophobic rich NES-like sequences (Fig. 5A). They were located between residues 11 and 20, 49, and 58.

In order to address whether the N-terminal domain confers nuclear export to a protein normally restricted to the nucleus, a chimerical protein with residues 6–60 of P fused to β-galactosidase carrying the SV40 T antigen NLS motif was expressed in transfected cells in the presence or absence of LMB (Figs. 5B and C). As expected NLS-β gal (used as a control) was exclusively nuclear. The fusion protein (NLS $P_{6–60}$-β gal) was excluded from the nucleus in the absence of LMB and its localization was sensitive to LMB (Fig. 5B). This result confirms that the domain 6–60 confers nuclear export ability to the fusion protein and contains at least one NES.

To determine more closely which motif is important for the nuclear export, we transferred two distinct fragments of the amino-terminal part of P ($P_{6–44}$, $P_{45–60}$) to the β-galactosidase carrying the SV40 T antigen NLS motif (Figs. 5B and C). The cells expressing the fusion protein NLS-$P_{6–44}$-βgal displayed a predominantly nuclear localization, which was unchanged in LMB treated cells. In contrast, the chimerical protein NLS-$P_{45–60}$-βgal was predominantly localized in the cytoplasm of untreated cells and the LMB treatment induced its accumulation in the nucleus. These findings are consistent with the presence of one functional NES between residues 49–58.

Since the first methionine of P3 (PΔN52) is located inside the NES sequence, P3 does not contain the intact NES. This probably explains the nuclear localization of P3. We then constructed the fusion protein PΔN44-GFP containing 9 more residues than P3-GFP in order to reconstitute the NES (Fig. 6A). In contrast to the original nuclear profile of P3, the completion of the NES to P3-GFP

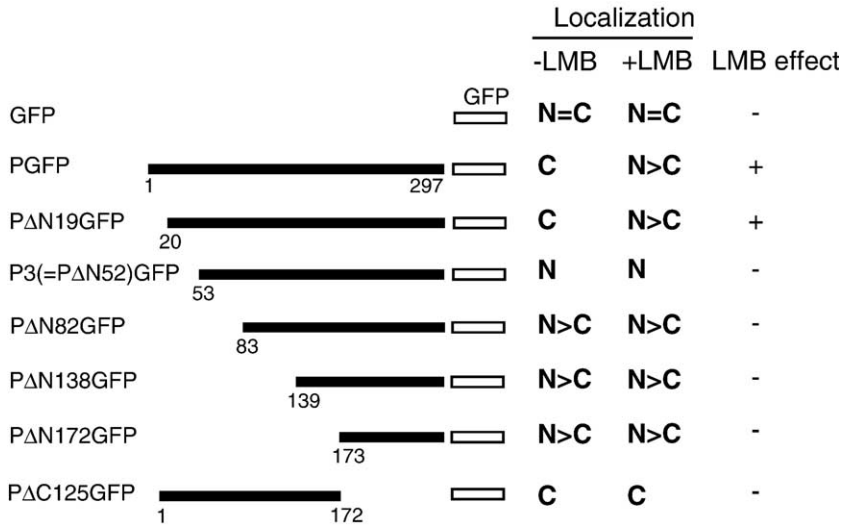

Fig. 4. Detection of the nuclear export signals in the N-terminal part of P. The localization of the truncated P proteins shown in Figs. 2A and B was compared in the absence (−LMB) or presence (+ LMB). The proteins were predominantly cytoplasmic (C), nuclear (N), or evenly distributed in cytoplasm and nucleus (N = C). From these results, the effect of LMB on the intracellular distribution of these truncated P proteins was summarized.

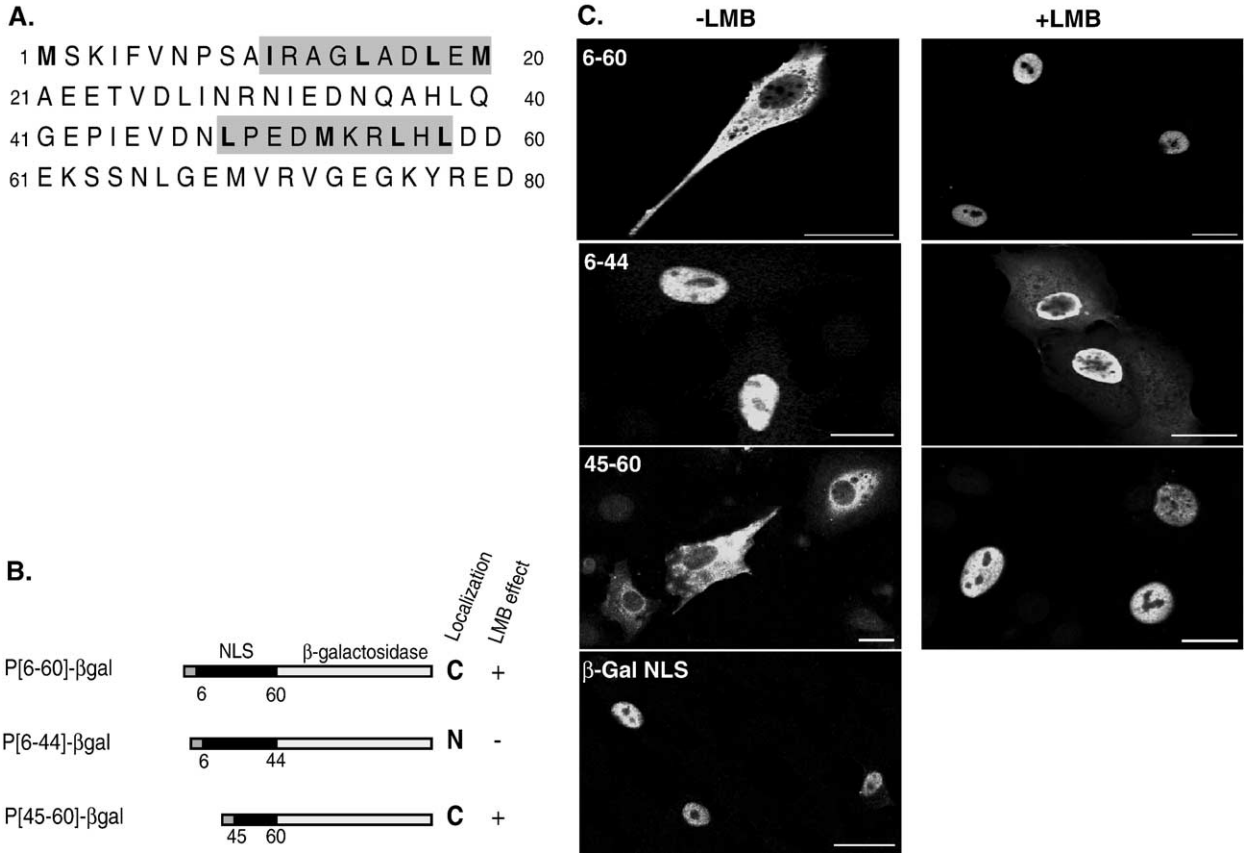

Fig. 5. Identification of a functional NES in the N-terminal part of P. (A) Examination of the N-terminal part of the sequence of P (1–83) revealed two stretches of amino acids residues similar to the characterized leucine-rich sequences NES sequence (**L**XXX**L**XX**L**X**L**), V, M, I may replaced leucine. These sequences were located between amino acids 11 and 20, 49, and 58 (gray boxes). (B) Different domains of the N-terminal part of P containing the putative NES (6–60, 6–44, 45–60, dark bars) were fused to the β-galactosidase (white bars) carrying the SV40 T antigen NLS motif (gray bars). The intracellular localization of these mutants in the cytoplasm (C) or in the nucleus (N) and the effect of LMB are summarized. (C) The plasmids described above were transfected into BSR cells. After 24 h, cells were incubated in the absence or presence of LMB at a final concentration of 20 nM for 2 h. After fixation, cells were permeabilized and were immunostained using the mouse monoclonal anti-β galactosidase followed by incubation with Alexa Fluor 488-conjugated goat anti-mouse IgG. The scale bars correspond to 20 μm.

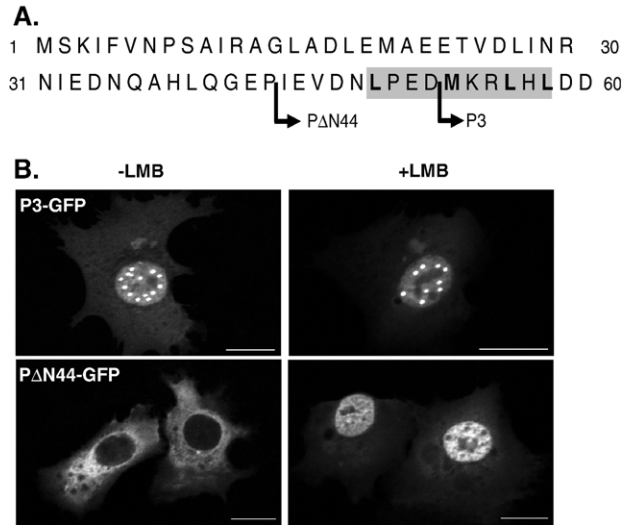

Fig. 6. NES is missing in the P3 protein. (A) The first methionine (bold) of P3 is located inside the NES (gray box). A fusion protein PΔN44-GFP containing 9 more residues than P3-GFP was constructed in order to reconstitute the NES. (B) PΔN44-GFP was expressed in BSR cells treated (right) or not (left) with LMB (as described in Fig. 2). After fixation, the cells were analyzed for GFP expression by confocal fluorescence microscopy. The scale bars correspond to 16 μm.

resulted in the redistribution of the protein to the cytoplasm (Fig. 6B). As expected, the protein PΔN44-GFP was sensitive to the LMB treatment. This result shows that the nuclear localization of P3 is due to the absence of the NES.

Discussion

In this report, we describe that rabies virus P protein is a nucleocytoplasmic shuttling protein that contains a nuclear localization signal (NLS) located in the C-terminal part and a nuclear export signals (NES) located in the N-terminal part of the protein. Although we have not demonstrated a direct interaction of the P protein with a karyopherin, the motif that mediates nuclear import (^{211}KKY**K**^{214} and **R**^{260}) is a cluster of basic residues exposed on the surface as shown from the recently solved crystal structure of the carboxy terminal domain of the P protein (Mavrakis et al., 2004). Therefore, this basic patch probably constitutes a conformational NLS which is conserved in the seven different genotypes of lyssavirus. The same situation exists for M1 protein of Influenza virus that has a positively charged patch on the surface of its N-terminal domain that functions as NLS (Arzt et al., 2001; Ye et al., 1995).

The nuclear export signal of rabies P protein at positions 49–58 is canonical with a high leucine content and is absolutely conserved throughout the lyssavirus genus.

In the light of these results, both P and the small P products P2–P5 contain the NLS but P and P2 are excluded from the nucleus because they contain the NES. It appears that NES counteracts the nuclear import of P to remove P from the nucleus. However, the inhibition of CRM1-dependent export by LMB does not result in a complete nuclear retention of P in the nucleus. Therefore, it is also possible that only a fraction of P goes in the nucleus.

Our data suggest that the intracellular localization of the products of the P gene is tightly regulated. The fact that we have also identified P3 from Mokola virus, the most divergent lyssaviruses genotype, and that its localization is also nuclear, suggests that this regulation is probably conserved throughout the lyssavirus genus. However, the interplay between NLS and NES sequences may only be part of the complexity of the cellular localization of P. Other control mechanisms such as phosphorylation, oligomerization, or interaction with viral or cellular partners may influence the localization of the P products.

It has been shown that phosphorylation or dephosphorylation in the vicinity of an NLS or NES may play a role in the intracellular distribution of proteins (Jans and Hubner, 1996). Rabies virus P proteins are phosphorylated (Gupta et al., 2000; Tuffereau et al., 1985) and the position of one of the phosphorylation sites (S210) is right next to the NLS on the surface of the protein (Mavrakis et al., 2004). Therefore, phosphorylation of P proteins could have an effect on nuclear import as it has been shown for nuclear import of the T-antigen (Hubner et al., 1997). Alternatively, oligomerization of P products could also play a role in their localization. Indeed, P and small P products contain the oligomerization domain which is most probably located between the residues 93 and 130 (Gigant et al., 2000; Jacob et al., 2001) and form oligomers although it is not clear whether these are trimers or tetramers (Gigant et al., 2000; Mavrakis et al., 2003).

In infected cells, the interaction of P with viral partners such as the polymerase L and the N protein may also contribute to the regulation of nucleocytoplasmic shuttling of the P protein. Interestingly the motif ^{211}KKYK^{214}, which is part of the NLS motif, is also required for the interaction with the N-RNA (Jacob et al., 2001; Mavrakis et al., 2004). Therefore, the nuclear import activity of P may be blocked by the direct binding of N to P. Finally, interaction with cellular partners may contribute to the localization of the P gene products. P protein has been shown to interact with the dynein light chain LC8, a cellular factor implicated in retrograde axonal transport that mediates the RNP transport along the neuronal axons (Jacob et al., 2000; Raux et al., 2000). In addition, the nuclear P3 protein has been shown to interact with PML nuclear bodies (Blondel et al., 2002). This could explain why P3 is the only small P protein that shows punctuate staining in nuclei of transfected cells. However, formation of nuclear dots does not require PML since the same localization exists in PML−/− cells (Blondel et al., 2002). The nature of these nuclear structures is still unknown but could be due to specific interaction of P3 (but not P4 and P5) with nuclear proteins, which may retain P3 in such structures. Such an interaction could involve the first residues of P3 corresponding to amino acids 53–67 of P and explain that P3 is more nuclear than shorter P products.

In regards to the role of the nuclear products of the P gene, it has been proposed that P3 via its interaction with PML may overcome the antiviral response of the infected cells (Blondel et al., 2002). Interaction of viral proteins with nuclear proteins is not restricted to viruses that replicate in the nucleus. Many RNA viruses whose replication strictly takes place in the cytoplasm use the nucleus or nuclear components in order to facilitate replication and/or alter host cell function and inhibit antiviral responses (Hiscox, 2003).

The presence of nuclear import and export signals on P protein insures representation of complete or truncated P proteins in the two cellular compartments. This contributes to an increase in the number of various P forms already observed as oligomeric or phosphorylated forms and which perform diversified functions in the virus life cycle.

Materials and methods

Cell cultures, antibodies, and leptomycin B (LMB) treatment

BSR cells, cloned from BHK 21 (baby hamster kidney), were grown at 37 °C in DMEM supplemented with 10% fetal calf serum (FCS). The mouse polyclonal anti-P antibody has been described previously (Raux et al., 1997). The monoclonal anti-β galactosidase antibody was bought from Promega and used as described by the manufacturer. LMB (Sigma) was added to culture medium to a final concentration of 20 nM.

Plasmid constructions

pMC.P encoding the wild-type P of the CVS has been described previously (Chenik et al., 1994). The constructs pP-GFP, pP△N19-GFP, pP△N52-GFP, pP△N82-GFP, pP△N138-GFP, and pP△N172-GFP have been described previously (Blondel et al., 2002). The plasmid pP△C125-GFP was generated by PCR using reverse primers to delete the last 375 nucleotides of P. Amplified cDNA was cut with *AgE*1 and *Eco*R1 and used to replace the P gene *AgE*1/*Eco*R1—excised from the plasmid pCDNA1 encoding P-GFP.

The plasmid pCMV-NLS.βgal containing the SV40 T antigen NLS into plasmid pCMVβ has been described elsewhere (Hiriart et al., 2003) and was a generous gift from Dr. E. Manet (from the Unité de Virologie Humaine, U412 INSERM-ENS Lyon). Different fragments of P (6–60, 6–44, and 45–60) were amplified by PCR using, respectively, the sets of oligonucleotides (5′CCGAGATCTGTTAATAGTGCA3′, 5′CCGAGATCTATCGTCCAGGTG3′; 5′CCGAGATCTGTTAATAGTGCA3′, 5′CCGAGATCTTTCTATGGGTTC3′; 5′CCGAGATCTGAAGTGGACAAC3′, 5′CCGAGATCTATCGTCCAGGTG3′). The amplified double-stranded cDNAs were digested with *bgl*II and inserted downstream of the SV40 T antigen NLS into a *bgl*II site of pCMVNLS βgal.

Site-directed mutagenesis

A two-step PCR-based site-directed mutagenesis approach was used to generate amino acid substitutions in pP-GFP. In a first step, two overlapping PCR fragments were amplified from pP-GFP with primer combinations specific of the mutation (1 and 2) as described in Table 1. In a second step, aliquots of the two PCR products were mixed, annealed, and used as template for a second round of amplification with P- or P3-specific forward primers (5′GCCGAATTCATGAGCAAGATCTTT3′, 5′GCCGAATTCATGAAGCGACTTCAC3′) and GFP-specific reverse primer (5′GCCTCTAGATTACTTGTACAGCTC 3′) in order to amplify the whole mutation containing gene. The products of this second reaction were digested with *Eco*RI/*Xba*I and used to replace the *Eco*RI/*Xba*I excised P-GFP. By using this strategy, we obtained the constructs encoding mutated P or P3 in fusion with GFP with one or two amino acid substitutions (in boldface) in the motif ^{211}KKYK^{214} associated or not with one amino acid R^{260} substitution: pP or pP3(^{211}KKY**A**^{214}-R^{260}), pP or pP3(^{211}KKY**D**^{214}-R^{260}), pP or pP3(^{211}**AA**YK^{214}-R^{260}), pP or pP3(^{211}KKYK^{214}-

Table1
Primers used for the first step of the two-step mutagenesis PCR products

Construction	Sense (1) and antisense (2) primer for the first PCR step	Template
pP(^{211}KKY**A**^{214}-R^{260})	(1) 5′ CCAAGAAGTAC**GCG**TTTCCCTCCCGA 3′	
pP3(^{211}KKY**A**^{214}-R^{260})	(2) 5′ TCGGAGGGAAA**CGC**GTACTTCTTGG 3′	pP-GFP
pP(^{211}KKY**D**^{214}-R^{260})	(1) 5′ CCAAGAAGTAC**GAC**TTTCCCTCCCGA 3′	
pP3(^{211}KKY**D**^{214}-R^{260})	(2) 5′ TCGGGAGGGAAA**GTC**GTACTTCTTGG 3′	pP-GFP
pP(^{211}**AA**YK^{214}-R^{260})	(1) 5′ GAAAGCTTTTCC**GCGGCG**TACAAGTTTCCCTCCCGA 3′	
pP3(^{211}**AA**YK^{214}-R^{260})	(2) 5′ TCGGGAGGGAAACTTGTA**CGCCGC**GGAAAAGCTTTC 3′	pP-GFP
pP(^{211}KKYK^{214}-**A**^{260})		pP-GFP
pP3(^{211}KKYK^{214}-**A**^{260})		pP-GFP
pP(^{211}KKY**A**^{214}-**A**^{260})	(1) 5′ AAAATCCCCCT**GGC**GTGCGTACTGGGA 3′	pP (^{211}KKY**A**^{214}-R^{260})
pP3(^{211}KKY**A**^{214}-**A**^{260})	(2) 5′ TCCCAGTACGCAC**GCC**AGGGGGATTTT 3′	pP3 (^{211}KKY**A**^{214}-R^{260})
pP(^{211}KKY**D**^{214}-**A**^{260})		pP (^{211}KKY**D**^{214}-R^{260})
pP3(^{211}KKY**D**^{214}-**A**^{260})		pP3 (^{211}KKY**D**^{214}-R^{260})

$\mathbf{A}^{260}$, pP or pP3(^{211}KKYK$\mathbf{A}^{214}$-$\mathbf{A}^{260}$), and pP or pP3(^{211}KKYK$\mathbf{D}^{214}$-$\mathbf{A}^{260}$).

Plasmid transfections

BSR cells were grown on sterile glass cover slips in 6 well plates and were transfected (Parker and Stark, 1979). After 24 h at 37 °C cells were prepared for immunofluorescence staining.

In some experiments, proteins were transiently expressed by using the vaccinia T7 expression system according to the method of Fuerst et al. (1986). Briefly, BSR cells were infected with VTF7-3 at a multiplicity of infection of 5 PFU per cell. After 1 h of adsorption the cells were transfected with 2 μg of plasmid and were incubated for 6 h at 37 °C.

Immunofluorescence staining and confocal microscopy

Cells were fixed in 4% paraformaldehyde for 15 min at 4 °C and permeabilized for 5 min with 0.1% Triton X-100 in PBS. GFP distribution was analyzed directly after fixation. The intracellular distribution of β-galactosidase constructions was analyzed by immunostaining using the anti-β-galactosidase antibody at a dilution of 1/1000 and the corresponding anti-mouse IgG antibody conjugated to Alexa Fluor 488 (Molecular Probes). The cells were mounted in mounting medium containing 4,6-diamidino-2-phenylindole (DAPI) to stain nuclei.

Confocal laser microscopy was performed on a Leica SP2 microscope (40× oil-immersion objective) using ultraviolet excitation at 351 nm (DAPI) and/or blue laser excitation at 488 nm (Alexa 488, GFP) in simultaneous recording mode.

Western blot analysis

Cells were washed and re-suspended in PBS, lysed in hot Laemmli sample buffer, and boiled for 5 min. About 20 μg of protein was analyzed on a 10% SDS–PAGE gel and transferred onto a nitrocellulose membrane. The proteins were blocked on the membranes with 10% skimmed milk in TBS for 2 h and incubated overnight at 4 °C with the rabbit polyclonal anti-P antibody. The blots were then washed extensively in TBS–Tween and incubated for 1 h with the peroxidase-coupled secondary antibodies (Amersham). The blots were revealed by chemoluminescence (ECL, Amersham).

Acknowledgments

We acknowledge Dr. E. Manet (from the Unité de Virologie Humaine, U412 INSERM-ENS Lyon) for the plasmid pCMV-NLS.βgal. We would like to thank C. Maheu for technical assistance.

References

Arzt, S., Baudin, F., Barge, A., Timmins, P., Burmeister, W., Ruigrok, R.W.H., 2001. Combined results from solution studies on intact influenza virus M1 protein and from a new crystal form of its N-terminal domain show that M1 is an elongated monomer. Virology 279, 439–446.

Badrane, H., Bahloul, C., Perrin, P., Tordo, N., 2001. Evidence of two Lyssavirus phylogroups with distinct pathogenicity and immunogenicity. J. Virol. 75, 3268–3276.

Blondel, D., Regad, T., Poisson, N., Pavie, B., Harper, F., Pandolfi, P.P., De The, H., Chelbi-Alix, M.K., 2002. Rabies virus P and small P products interact directly with PML and reorganize PML nuclear bodies. Oncogene 21, 7957–7970.

Chenik, M., Chebli, K., Gaudin, Y., Blondel, D., 1994. In vivo interaction of Rabies virus phosphoprotein (P) and nucleoprotein (N): existence of two N-binding sites on P protein. J. Gen. Virol. 75, 2889–2896.

Chenik, M., Chebli, K., Blondel, D., 1995. Translation initiation at alternate in-frame AUG codons in the rabies virus phosphoprotein mRNA is mediated by a ribosomal leaky scanning mechanism. J. Virol. 69, 707–712.

Chenik, M., Schnell, M., Conzelmann, K.K., Blondel, D., 1998. Mapping the interacting domains between the rabies virus polymerase and phosphoprotein. J. Virol. 72, 1925–1930.

Fischer, U., Huber, J., Boelens, W.C., Mattaj, I.W., Luhrmann, R., 1995. The HIV-1 Rev activation domain is a nuclear export signal that accesses an export pathway used by specific cellular RNAs. Cell 82, 475–483.

Fornerod, M., Ohno, M., Yoshida, M., Mattaj, I.W., 1997. CRM1 is an export receptor for leucine-rich nuclear export signals. Cell 90, 1051–1060.

Fu, Z.F., Zheng, Y., Wunner, W.H., Koprowski, H., Dietzschold, B., 1994. Both the N- and the C-terminal domains of the nominal phosphoprotein of Rabies virus are involved in binding to the nucleoprotein. Virology 200, 590–597.

Fuerst, R.T., Niles, E.G., Studier, F.W., Moss, B., 1986. Eukaryotic transient-expression system based on recombinant vaccinia virus that synthesizes bacteriophage T7 RNA polymerase. Proc. Natl. Acad. Sci. U.S.A. 83, 8122–8126.

Gigant, B., Iseni, F., Gaudin, Y., Knossow, M., Blondel, D., 2000. Neither phosphorylation nor the amino-terminal part of Rabies virus phosphoprotein is required for its oligomerization. J. Gen. Virol. 81, 1757–1761.

Gorlich, D., Mattaj, I.W., 1996. Nucleocytoplasmic transport. Science 271, 1513–1518.

Gorlich, D., Kostka, S., Kraft, R., Dingwall, C., Laskey, R.A., Hartmann, E., Prehn, S., 1995. Two different subunits of importin cooperate to recognize nuclear localization signals and bind them to the nuclear envelope. Curr. Biol. 5, 383–392.

Gupta, AK., Blondel, D., Ghoudhary, S., Banerjee, A.K., 2000. The phosphoprotein of Rabies virus is phosphorylated by a unique cellular protein kinase and specific isomers of protein kinase C. J. Virol. 74, 91–98.

Hiriart, E., Farjot, G., Gruffat, H., Nguyen, M.V., Sergeant, A., Manet, E., 2003. A novel nuclear export signal and a REF interaction domain both promote mRNA export by the Epstein–Barr virus EB2 protein. J. Biol. Chem. 278, 335–342.

Hiscox, J.A., 2003. The interaction of animal cytoplasmic RNA viruses with the nucleus to facilitate replication. Virus Res. 95, 13–22.

Hubner, S., Xiao, C.Y., Jans, D.A., 1997. The protein kinase CK2 site (Ser111/112) enhances recognition of the simian virus 40 large T-antigen nuclear localization sequence by importin. J. Biol. Chem. 272, 17191–17195.

Jacob, Y., Badrane, H., Ceccaldi, P.E., Tordo, N., 2000. Cytoplasmic dynein LC8 interacts with lyssavirus phosphoprotein. J. Virol. 74, 10217–10222.

Jacob, Y., Real, E., Tordo, N., 2001. Functional interaction map of lyssavirus phosphoprotein: identification of the minimal transcription domains. J. Virol. 75, 9613–9622.

Jans, D.A., Hubner, S., 1996. Regulation of protein transport to the nucleus: central role of phosphorylation. Physiol. Rev. 76, 651–685.

Kalderon, D., Richardson, W.D., Markham, A.F., Smith, A.E., 1984. Sequence requirements for nuclear location of simian virus 40 large-T antigen. Nature 311, 33–38.

Kohler, M., Speck, C., Christiansen, M., Bischoff, F.R., Prehn, S., Haller, H., Gorlich, D., Hartmann, E., 1999. Evidence for distinct substrate specificities of importin alpha family members in nuclear protein import. Mol. Cell. Biol. 19, 7782–7791.

Mavrakis, M., Iseni, F., Mazza, C., Schoehn, G., Ebel, C., Gentzel, M., Franz, T., Ruigrok, R.W.H., 2003. Isolation and characterisation of the rabies virus N°-P complex produced in insect cells. Virology 305, 406–414.

Mavrakis, M., McCarthy, A., Roche, S., Blondel, D., Ruigrok, R.W., 2004. Structure and function of the C-terminal domain of the polymerase cofactor of rabies virus. J. Mol. Biol. 343, 819–831.

Nishi, K., Yoshida, M., Fujiwara, D., Nishikawa, M., Horinouchi, S., Beppu, T., 1994. Leptomycin B targets a regulatory cascade of crm1, a fission yeast nuclear protein, involved in control of higher order chromosome structure and gene expression. J. Biol. Chem. 269, 6320–6324.

Nigg, E.A., 1997. Nucleocytoplasmic transport: signals, mechanisms and regulation. Nature 386, 779–787.

Parker, B.A., Stark, G.R., 1979. Regulation of simian virus 40 transcription: sensitive analysis of the RNA species present early in infections by virus or viral DNA. J. Virol. 31, 360–369.

Raux, H., Iseni, F., Lafay, F., Blondel, D., 1997. Mapping of monoclonal antibody epitopes of the Rabies virus P protein. J. Gen. Virol. 78, 119–124.

Raux, H., Flamand, A., Blondel, D., 2000. Interaction of the rabies virus P protein with the LC8 dynein light chain. J. Virol. 74, 10212–10216.

Robbins, J., Dilworth, S.M., Laskey, R.A., Dingwall, C., 1991. Two interdependent basic domains in nucleoplasmin nuclear targeting sequence: identification of a class of bipartite nuclear targeting sequence. Cell 64, 615–623.

Tuffereau, C., Fisher, S., Flamand, A., 1985. Phosphorylation of the N and M1 proteins of rabies virus. J. Gen. Virol. 66, 2285–2289.

Wang, P., Palese, P., O'Neill, R.E., 1997. The NPI-1/NPI-3 (karyopherin alpha) binding site on the influenza a virus nucleoprotein NP is a nonconventional nuclear localization signal. J. Virol. 71, 1850–1856.

Wolff, T., Unterstab, G., Heins, G., Richt, J.A., Kann, M., 2002. Characterization of an unusual importin alpha binding motif in the Borna disease virus p10 protein that directs nuclear import. J. Biol. Chem. 277, 12151–12157.

Ye, Z., Robinson, D., Wagner, R.R., 1995. Nucleus-targeting domain of the matrix protein (M1) of influenza virus. J. Virol. 69, 1964–1970.

Annexe #2

Genetic editing of herpes simplex virus 1 and Epstein-Barr herpesvirus genomes by human APOBEC3 cytidine deaminases in culture and in vivo.

Suspène R, Aynaud MM, Koch S, Pasdeloup D, Labetoulle M, Gaertner B, Vartanian JP, Meyerhans A, Wain-Hobson S.

JOURNAL OF VIROLOGY, Aug. 2011, p. 7594–7602 Vol. 85, No. 15
0022-538X/11/$12.00 doi:10.1128/JVI.00290-11

Genetic Editing of Herpes Simplex Virus 1 and Epstein-Barr Herpesvirus Genomes by Human APOBEC3 Cytidine Deaminases in Culture and *In Vivo*▽†

Rodolphe Suspène,[1,2] Marie-Ming Aynaud,[1] Stefanie Koch,[2] David Pasdeloup,[3] Marc Labetoulle,[3] Barbara Gaertner,[2] Jean-Pierre Vartanian,[1] Andreas Meyerhans,[2,4] and Simon Wain-Hobson[1]*

Molecular Retrovirology Unit, Institut Pasteur, CNRS URA 3015, 28 Rue du Dr. Roux, 75724 Paris Cedex 15, France[1]; Department of Virology, Saarland University, 66421 Homburg, Germany[2]; Laboratoire de Virologie Moléculaire et Structurale, CNRS UPR 3296, 91198 Gif-sur-Yvette, France[3]; and ICREA Infection Biology Lab, Department of Experimental and Health Sciences, University Pompeu Fabra, 08003 Barcelona, Spain[4]

Received 9 February 2011/Accepted 16 May 2011

Human APOBEC3 cytidine deaminases target and edit single-stranded DNA, which can be of viral, mitochondrial, or nuclear origin. Retrovirus genomes, such as human immunodeficiency virus (HIV) genomes deficient in the *vif* gene and the hepatitis B virus genome, are particularly vulnerable. The genomes of some DNA viruses, such as human papillomaviruses, can be edited *in vivo* and in transfection experiments. Accordingly, herpesviruses should be no exception. This is indeed the case for herpes simplex virus 1 (HSV-1) in tissue culture, where APOBEC3C (A3C) overexpression can reduce virus titers and the particle/PFU ratio ~10-fold. Nonetheless, A3A, A3G, and AICDA can edit what is presumably a small fraction of HSV genomes in an experimental setting without seriously impacting the viral titer. Hyperediting was found in HSV genomes recovered from 4/8 uncultured buccal lesions. The phenomenon is not restricted to HSV, since hyperedited Epstein-Barr virus (EBV) genomes were readily recovered from 4/5 established cell lines, indicating that episomes are vulnerable to editing. These findings suggest that the widely expressed A3C cytidine deaminase can function as a restriction factor for some human herpesviruses. That the *A3C* gene is not induced by type I interferons begs the question whether some herpesviruses encode A3C antagonists.

The seven-gene human *APOBEC3* (*A3*) cytidine deaminase locus came to the fore with the identification of APOBEC3G (A3G) as the interaction partner of the human immunodeficiency virus (HIV) Vif protein (8, 16, 26, 29, 30, 43, 57). These enzymes belong to a larger group that can edit nucleic acids, of which activation-induced cytidine deaminase (AICDA), responsible for class switch recombination and somatic hypermutation of rearranged immunoglobulin V region genes, is perhaps the most widely known (11). All functional A3 enzymes show specificity for single-stranded DNA (ssDNA). Since the reaction product is uridine (dU), A3 activity results in DNA peppered by C → U substitutions, referred to as hypermutants. Editing can range from a few cytidine targets to over 80% (2, 3, 8, 16, 26, 29, 30, 49, 54). To a good first approximation, all A3 enzymes preferentially edit ssDNA when the edited base is 5′ flanked by thymidine or cytidine, i.e., TpC and CpC. In contrast, AICDA prefers GpC and ApC (2, 3, 9, 17, 27, 39, 49, 54).

Since the HIV-encoded Vif protein protects its genome from the mutagenic effects of A3G, HIV hypermutants are associated with a defective or deleterious *vif* background (43). In contrast, hepatitis B virus (HBV) DNA is particularly susceptible to genetic editing by at least two A3 enzymes *in vivo* (54), perhaps because its small genome does not encode interferon or A3 antagonists. Double-stranded DNA (dsDNA) is prone to editing during replication or transcription when it is partially single-stranded. Human papillomavirus genomes are vulnerable to APOBEC3 editing *in vivo* and in transfection experiments (53). In contrast, vaccinia virus, which replicates in the cytoplasm, is apparently resistant to A3G (22).

Given their very large genomes, between 124 and 241 kb (32), herpesviruses, which replicate in the nucleus, might be particularly sensitive to A3 deamination, since even low levels of deamination, say, <0.1%, would introduce several hundred mutations per genome. The seven *A3* genes are expressed in a very wide variety of cell types, with some of the genes, notably human *APOBEC3A* and *APOBEC3G* (*A3A* and *A3G*), being strongly upregulated by type I interferons (IFNs) (5, 21, 40, 44, 55). Yet since herpes simplex virus (HSV) replication is comparatively resistant to IFN signaling and IFN-mediated responses in tissue culture (13, 34, 35, 41), they may not function as restriction factors. In contrast, *APOBEC3C* (*A3C*) is not only the most abundantly expressed of all *A3* genes across a wide range of tissues and cells but also is insensitive to IFN (19). It can edit transfected human papillomavirus (HPV) DNA and mitochondrial DNA (mtDNA) (46, 53). Hence, it is plausible that *A3C* has posed a particular problem for primate herpesviruses. Here it is shown that HSV-1 is particularly vulnerable to the editing effects of APOBEC3C both in tissue culture and *in vivo*. Equally, Epstein-Barr virus (EBV) genomes in EBV-transformed oligoclonal B-cell lines can be edited by at least one APOBEC3 enzyme.

* Corresponding author. Mailing address: CNRS URA 3015, 28 Rue du Dr. Roux, 75724 Paris Cedex 15, France. Phone: 33 1 45 68 88 21. Fax: 33 1 45 68 88 74. E-mail: simon.wain-hobson@pasteur.fr.

† Supplemental material for this article may be found at http://jvi.asm.org/.

▽ Published ahead of print on 1 June 2011.

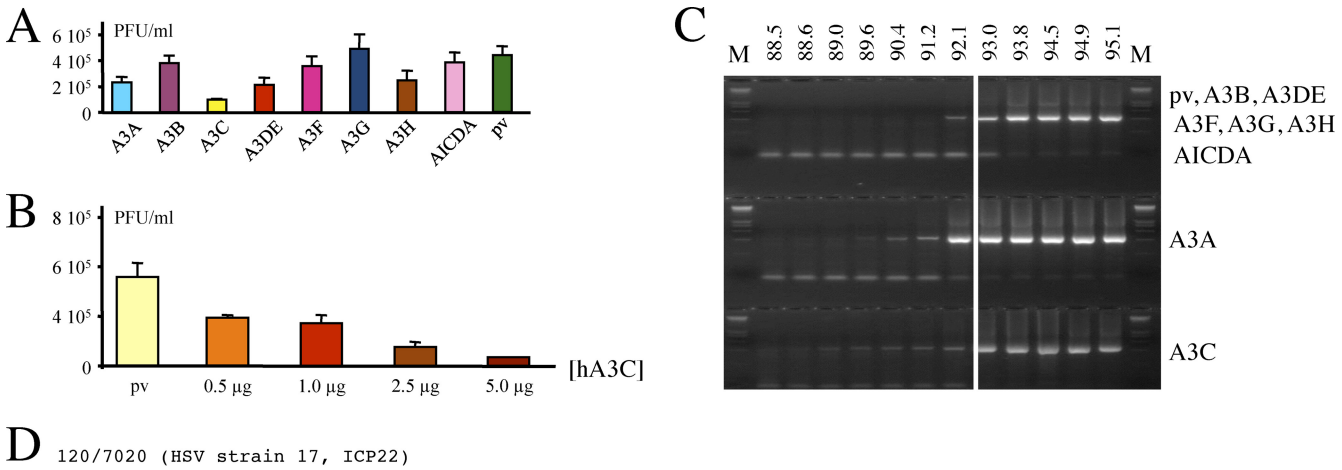

D

```
120/7020 (HSV strain 17, ICP22)
•
CATCTGGGTCGCCCGGCCCAACGGGGGCCGGGGGTTGGGTCTGGCTCATCTTGAGAGCCACGGGGGGGGAACCACCCTCCGCCCAGAGACTCGGGCGATGG
.....................................................................AAAAAA..............................
......A.............................A.....................AAAA..............................
.....AAA..A.....................AA...A.....................A.....................................
.....................................A.....................AAAAAA..................A...........A.
...T.....................................T.....................................................T.........
.....................................................................................................
T.....................................................................................................

                                                                                    320/6825
                                                                                    •
TCGTACCCGGGACTCAACGGGTTACCGGATTACGGGGACTGTCGGTCACGGTCCCGCCGGTTCTTCGATGTGCCACACCCAAGGATGCGTTGGGGGTGAT   # % mut
..A..............AAA.....AA.....................A.........AA.....................................A..   24 16.6%
..A..............A.............AAAA............A.................A..A.A.............A..........A..   25 17.2%
........A.................AA.......A.......A.............T..A.....................G..A....A....A.A.A..   29 20.0%
..A.......A........AA.....AA.....................A..............................AA.......AAA...A..   31 21.4%

.....................................................T...................T......T...........................    9  6.9%
.....................................................T.......T.............TT.....................    12  9.2%
.............T.........TT.................T..............T.......T.............T.....................    15 11.5%
```

FIG. 1. Several human A3 enzymes may restrict HSV-1 replication and edit the genome. (A) Transfection of HeLa cells by 2.5 μg of plasmid DNA followed by HSV-1 infection. pv, empty vector. Titers are the means for triplicate experiments. (B) Dose-response relationship of supernatant titers as a function of A3C DNA concentration. The DNA concentration was maintained constant with the plasmid vector. (C) 3DPCR of HSV-1 DNA for all DNA transfections. The denaturation temperature (T_d) is given across the top; M, molecular weight markers. The HSV-1 sequence between the primers is 410 bp in length. The white vertical bar indicates the minimal T_d (93 to 93.8°C) for cloned wild-type HSV-1 DNA. Bands to lower temperature can be taken as *prima facie* evidence of cytidine deamination. (D) A selection of A3-edited HSV-1 genomes from the HeLa + pv transfection. For clarity, only 200 bp of the 410-bp *ICP22* sequence are shown, while differences are scored with respect to the reference sequence (G → A, n = 25, 10,250 bp; C → T, n = 9, 3,690 bp). The positions in the HSV-1 strain 17 sequence are also given. To the right of each sequence is the total number of C → T transitions on the plus or minus (shown as G → A transitions) strand.

MATERIALS AND METHODS

Cell culture and transfection. HeLa cells and Vero cells were maintained in Dulbecco's modified Eagle's medium (DMEM) supplemented with 10% fetal calf serum, 100 units/ml penicillin, and 100 μg/ml streptomycin (PAA) at 37°C in 5% CO_2. The EBV cell lines were maintained in RPMI supplemented with 10% fetal calf serum, 100 U/ml penicillin, and 100 μg/ml streptomycin (PAA). QT6 cells were maintained in Ham's medium supplemented with 100 U/ml penicillin, 2 mM glutamine, 5% tryptose phosphate, 1% chicken serum, and 10% fetal calf serum. HSV-1 strain 17 was grown in HeLa cells. Two days postinfection, supernatants were recovered and treated with 40 U of Turbo DNase (Ambion) for 30 min at 37°C and frozen at −80°C. Infections were carried out on 6×10^5 QT6 cells in 6-well plates at a multiplicity of infection (MOI) of 1. QT6 supernatants were treated with 40 U of Turbo DNase as described above.

For transfection, 5×10^4 HeLa cells were seeded in 24-well tissue culture plates and incubated for 24 h. Transfections were performed using Lipofectamine 2000 (Invitrogen) or jetPRIME. Briefly, HeLa cells were transfected with equal amounts (2.5 μg) of the individual expression plasmids in duplicate. Controls were performed in parallel without APOBECs. An enhanced green fluorescent protein (EGFP) expression plasmid was transfected in parallel, and the transfection efficiency was determined via flow cytometry: transfection efficiencies were ~70%. Transfection medium was changed after 3 h, and transfected cells were incubated for 24 h and infected with HSV-1 (MOI = 1) for 90 min. After 48 h of incubation, the virus-containing supernatants were collected after centrifugation and stored at −80°C. Western blotting was performed as described previously (46).

Plaque assay. Vero cells (7.5×10^4) were seeded in 24-well tissue culture plates and incubated for 24 h. The confluent cell monolayer was inoculated with serial virus dilutions in DMEM for 90 min and then overlaid with methylcellulose, incubated for 48 h, and washed with phosphate-buffered saline solution (PBS). Plaques were counted manually after fixing and staining with crystal violet.

Particle/PFU ratios. Particle counts of viral supernatants were determined by mixing the supernatants with a preparation of 250-nm-diameter biotin-conjugated latex beads (Sigma) of known concentration. The mixture was then adsorbed onto glass coverslips for 1 h at room temperature and fixed with methanol. Samples were labeled using the mouse VP5-specific monoclonal antibody (DM165) (31) to label capsids or the rabbit polyclonal PTNC antibody (37) to label whole virions and L particles. Secondary antibodies used were goat anti-mouse Alexa 488 and goat anti-rabbit Alexa 568 conjugated antibodies (Molecular Probes). Latex beads were stained using Alexa 633-conjugated streptavidin (Molecular Probes). The relative number of virus particles was estimated according to the number of counted latex beads.

PCR. DNAs were extracted using an Epicentre kit. The HSV-1 *ICP22* gene primers were as follows: 5′ OUT, CGACGCGGGCCCGAGCRTATRCTY YAT; 3′ OUT, GGAAATGGCGGACACCTTCCTGGAYAYYAT; 5′ IN, CT CGTAGTAGACCCRAATCTCCACATT; 3′ IN, GCCGACGTACGCGATGA GATYAAT.

The outer and inner fragments were 880 and 461 bp, respectively. The first reaction involved standard amplification. Reaction parameters were as follows: 95°C for 7 min, followed by 42 cycles (each consisting of 95°C for 1 min, 60°C for 30 s, and 72°C for 3 min), and finally 20 min at 72°C. Differential amplification occurred in the second round (using 1 μl of the first-round reaction as input) by using an Eppendorf gradient Mastercycler S thermal cycler programmed to generate a 6°C gradient in the denaturation temperature. The reaction parameters were 89 to 95°C for 5 min, followed by 42 cycles (each consisting of 89 to 95°C for 1 min, 55°C for 30 s, and 72°C for 2 min), and finally 10 min at 72°C.

For HSV *ICP0*, the primers were as follows: 5′ OUT and IN, 5′ TTGCGCA ATTGCATCCARRTTTTCAT; 3′ OUT, 5′ GAGGGGGAACTCGTGGGTG YTGATT; 3′ IN, 5′ GGACAGCACGGACAYGGAAYTGTT.

The outer and inner fragments were, respectively, 420 bp and 217 bp without primers. The conditions were as for *ICP22*, except for a 63°C annealing step for first-round PCR and an 8°C gradient at the denaturation temperature. The differential DNA denaturation PCR (3DPCR) reaction parameters were 87 to 95°C for 5 min, followed by 42 cycles (each consisting of 87 to 95°C for 1 min, 63°C for 30 s, and 72°C for 2 min), and finally 10 min at 72°C.

For HSV *ICP8*, the primers were as follows: 5′ OUT, 5′ CAAAGCCCAAG ACGGCAACCACCATCAA; 3′ OUT, 5′ CTGGCTGGCTTCGAAGGCCGT GAAYGTA; 5′ IN, 5′ CACCTGGACCCCAGCACCCAGRCCCCAA; 3′ IN, 5′ GCTAAAATCCGGCATGAACAGCTGYAA.

The outer and inner fragments were, respectively, 810 bp and 263 bp without primers. The conditions were as for *ICP22* except for a 65°C annealing step for first-round PCR and an 8°C gradient in the denaturation temperature. The reaction parameters were 87 to 95°C for 5 min, followed by 42 cycles (each consisting of 87 to 95°C for 1 min, 62°C for 30 s, and 72°C for 2 min), and finally 10 min at 72°C.

The EBV *EBNA-1* gene primers were as follows: 5′ OUT, GTAGCATCTCT GTCTGGTGACCTTGAA; 3′ OUT, TTTTGGGGTCTCCGGACACCATCT CTA; 5′ IN, AGGCCTGGCTTGAGGCTCAGGACGCAA; 3′ IN, GACATG ATTCACACTAAAAGAGATCAA.

The outer and inner fragments were 567 and 254 bp, respectively. The first reaction involved standard amplification. The reaction parameters were 95°C for 7 min, followed by 42 cycles (each consisting of 95°C for 1 min, 60°C for 30 s, and 72°C for 3 min), and finally 20 min at 72°C. Differential amplification occurred in the second round (using 1 μl from the first-round reaction as input) by using a 10°C gradient in the denaturation temperature. The reaction parameters were 80 to 90°C for 5 min, followed by 42 cycles (each consisting of 80 to 90°C for 1 min, 60°C for 30 s, and 72°C for 2 min), and finally 10 min at 72°C.

The EBV *EBNA-2* gene primers were as follows: 5′ OUT, 5′ TAACGTGCA AGACGCTAAACTTAACCAA; 3′ OUT, 5′ AGCCTCGGTTGTGACAGAG GTGACAA; 5′ IN, 5′ TGTGTTTTGCTTTATCTGCCGCCATCA; 3′ IN, 5′ CGTCATATCCTAGCGGATCCCTATCAA.

The outer and inner fragments were, respectively, 907 bp and 345 bp without primers. The conditions were as for *EBNA-1* except for a 62°C annealing step for first-round PCR. For the 3DPCR, reaction parameters were 80 to 90°C for 5 min, followed by 42 cycles (each consisting of 80 to 90°C for 1 min, 63°C for 30 s, and 72°C for 2 min), and finally 10 min at 72°C. PCR products were cloned into the pCR2.1 Topo cloning vector (Invitrogen). Sequencing was outsourced to GATC.

RESULTS

A3C restricts HSV replication. To explore the hypothesis that A3 enzymes may impact HSV-1 replication, HeLa cells were transfected by a variety of human cytidine deaminases, including AICDA. Twenty-four hours posttransfection, the cells were infected with HSV-1 at a MOI of 1 and allowed to grow for a further 48 h, after which titers of virus supernatants were determined on Vero cells. A3C reduced HSV titers by ~4-fold (Fig. 1A), in keeping with transfection frequencies of ~70%. The other deaminases had no significant impact compared to controls. A titration was performed with increasing amounts of *A3C*, using a plasmid vector to provide for a constant DNA concentration. A dose-response relationship was obtained (Fig. 1B).

	Sample	mean titre PFU / ml	Complete particles /ml	Complete particles / PFU
A	HeLa mock	$8.4\ 10^6$	$1.2\ 10^8$	14
	HeLa + vector	$4.2\ 10^6$	$4.7\ 10^7$	11
	HeLa + A3C	$2.8\ 10^5$	$3.4\ 10^7$	121
	HeLa + A3G	$1.3\ 10^6$	$3.6\ 10^7$	28
B	HeLa + vector	$6.0\ 10^6$	$1.2\ 10^8$	20
	HeLa + A3C*	$1.4\ 10^6$	$3.3\ 10^7$	24
C	HeLa + si control	$3.2\ 10^7$	$1.9\ 10^8$	6
	HeLa + siA3C	$2.9\ 10^7$	$6.6\ 10^7$	2

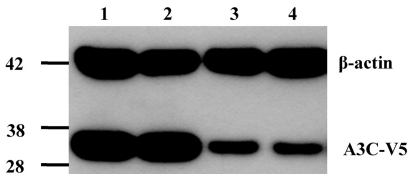

FIG. 2. A3C levels can impact particle/PFU ratios for HSV-1. (A) Impact of active *A3* constructs. (B) Impact of the *A3C* C957S inactive mutant. (C) Impact of A3C siRNA. (D) Western blot of V5-tagged A3C and β-actin loading control for uninfected HeLa cells at 48 h; lanes 1 and 2, 400 ng A3C-V5 tag plus 1 μg siRNA control; lanes 3 and 4, 400 ng A3C-V5 tag plus 1 μg siA3C RNA. Molecular mass markers (in kDa) are shown to the left.

Another measure of HSV infectivity is the particle/PFU ratio, which is typically of the order of 10 to 100 for herpesviruses (12). When HSV was grown on *A3C*-transfected HeLa cells the ratio was increased ~10-fold (Fig. 2A), indicating a higher number of defective particles in this population. In contrast, A3G failed to seriously impact the ratio. The vector transfection control yielded a titer comparable to that of virus from mock-transfected HeLa cells. An A3C catalytic mutant (C97S) yielded a particle/PFU ratio comparable to that of the plasmid vector control (Fig. 2B), while transfection of a small interfering RNA (siRNA) to A3C lowered the particle/PFU ratio compared to that of the siRNA control (Fig. 2C). Since the majority of cells were lysed at 48 h, the efficiency of siRNA knockdown was determined with uninfected cells. At 48 h, there was substantial knockdown of A3C-V5 as shown by Western blotting (Fig. 2D).

Total DNA was extracted and analyzed by 3DPCR, which is a derivative of PCR that allows selective amplification of AT-rich DNA amid excess normal DNA (48). It exploits the lower denaturation temperature (T_d) of AT-rich DNA by carrying out PCR with a T_d gradient. If the lowest positive T_d at which DNA is recovered is lower than that of the control, this can be considered *prima facie* evidence of recovery of AT-rich variants. Since the product of APOBEC3 editing of ssDNA is uridine, which base pairs as thymidine and is readily copied by

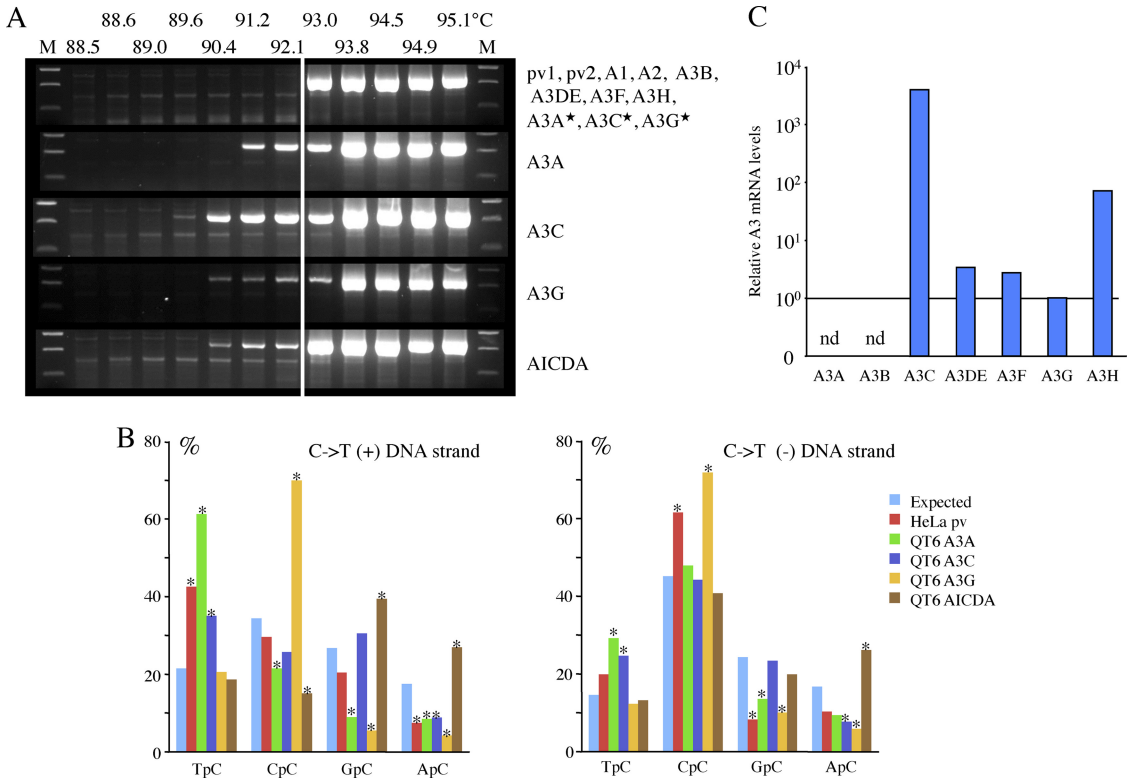

FIG. 3. Four human cytidine deaminases can hyperedit HSV-1 genomes. (A) Agarose gels of *ICP22* 3DPCR DNA products from HSV-1-infected quail QT6 cells expressing various *A3* genes. The annotation is as for Fig. 1C. Stars indicate A3A, A3C, and A3G catalytic mutants. (B) 5′ dinucleotide context associated with editing on the plus and minus strands. Asterisks denote significant deviations from the expected values (χ^2 test, $P < 0.05$) (QT6 + A3A, G → A, $n = 24$, 9,840 bp; C → T, $n = 31$, 12,710 bp; QT6 + A3C, G → A, $n = 50$, 20,500 bp; C → T, $n = 78$, 31,980 bp; QT6 + A3G, G → A, $n = 32$, 13,120 bp; C → T, $n = 8$, 3,280 bp; QT6 + AID, G → A, $n = 9$, 3,690 bp; C → T, $n = 24$, 9,840 bp). (C) TaqMan transcriptome analysis of the seven *A3* genes from HeLa cells. The levels have been normalized to those of *A3G* (horizontal bar). nd, not detected.

Taq polymerase, it is understandable that 3DPCR has proven immensely useful in analyzing A3 editing (5, 36, 38, 44, 46–48, 51, 53, 54).

We chose the *ICP22* immediate-early gene, which encodes a transcription factor involved in regulation of the viral cycle. As can be seen from Fig. 1C, HSV-1 DNA was recovered at denaturation temperatures down to 88.5°C for A3C and 89.6°C for A3A. Since the lowest denaturation temperature for cloned reference HSV-1 is ~93 to 93.8°C (indicated by a white vertical line in Fig. 1C), recovery of HSV-1 DNA at lower temperatures is evidence of AT-rich variants. However, hyperedited HSV-1 DNA was obtained even for the HeLa plasmid vector (pv) transfection control (Fig. 1C). A sequence analysis of 3DPCR products derived from the pv sample with a T_d of 92.1°C revealed hyperedited HSV genomes (Fig. 1D), with both DNA strands being vulnerable. The mean level of editing was 13% per clone, with a range of 1 to 23% ($n = 25$).

To overcome this endogenous editing background from HeLa cells, HSV-1 was passaged four times on the quail QT6 cell line (HSV-1/QT6). The avian lineage does not encode any *A3* genes and has been shown not to give an endogenous editing background when stocks of HIV or HBV are made following transfection (17, 38, 54). DNase treatment of the supernatant was performed each time in order to reduce passive transfer of contaminating edited DNA. As expected, HSV-1/QT6 stock virus failed to give a background signal for editing (Fig. 3A, top). Accordingly, QT6 cells were transfected by human cytidine deaminases and subsequently infected by HSV-1/QT6 virus for 48 h.

When total cell DNAs were examined by 3DPCR, AT-rich DNA was identified from the AICDA, A3A, A3C, and A3G transfections but not from the others (Fig. 3A). Not surprisingly, three A3 catalytic site mutants (A3A C105S, A3C C97S, and A3G C281S) failed to edit HSV-1 genomes. Judging by the lowest denaturation temperature (89.6°C) and band intensities, A3C impacted the HSV-1 genome more severely than the others (Fig. 3A). Sequence analysis of cloned 3DPCR products revealed extensive editing, with mean mutation frequencies of ~23% for the plus strand and between 23 and 42% for the minus strand. For A3A, A3C, and A3G, the minus strand was systematically more heavily edited than the plus strand, whereas for AICDA, the means were comparable (Table 1). Dinucleotide context analysis showed that editing was biased in favor of TpC for A3A and A3C, CpC for A3G, and GpC and ApC for AICDA (Fig. 3B), all of which have been previously noted for other virus genomes (2, 3, 7, 10, 14, 17, 28, 45, 51–54, 56). There was good concordance between the editing biases on both HSV-1 DNA strands (Fig. 3B). With these reference sets, the hyperedited sequences derived from the HeLa stock virus could be examined (Fig. 3B). While the overlap wasn't

TABLE 1. Essential statistics for HSV-1 and EBV edited genomes

Virus (T_d, °C)	Deaminase, cell line, and/or sample	Hyperediting	No. of sequences	Mean mut./seq.[a]	% GC → AT	% other
HSV-1 (91.1–92.1)	A3A/QT6	C → T	31	30	93.7	6.3
		G → A	24	61	96.7	3.3
	A3C/QT6	C → T	78	32	96.2	3.8
		G → A	50	46	96.9	3.1
	A3G/QT6	C → T	8	32	95.1	4.9
		G → A	32	56	96.4	3.6
	AICDA/QT6	C → T	24	32	95.6	4.4
		G → A	10	34	92.9	7.1
HSV-1 (92.1)	HeLa	C → T	9	14	93.4	6.6
		G → A	26	22	94.5	5.5
HSV-1 (90.4–92.1)	P9	C → T	21	25	91.2	8.8
	P9	G → A	94	36	96.3	3.7
HSV-1 (93.8–94.9)	P1		39	2	36.1	63.9
	P5		250	3	64.7	35.3
	P6		186	2	64.2	35.8
	P8		29	4	64.2	35.8
	P9		134	2	50.2	49.8
	P11		30	3	29.8	70.2
	P13		29	5	70.5	29.5
	P14		28	6	77.6	22.4
EBV (82.5–89.8)	EBV-blast P1	G → A	54	17.5	96.8	3.2
	EBV-blast P2	G → A	31	21.6	97.9	2.1
	EBV-blast P3	G → A	32	22.1	97.8	2.2
	EBV-blast Z	G → A	99	19.2	97.5	2.5

[a] Mean number of mutations per sequence.

perfect, there was similarity with the patterns for both A3A and A3C editing. A TaqMan transcriptome analysis (40) of the 7 *A3* genes in HeLa cells was performed. Since *A3A* levels were not detected while *A3C* levels were far higher than those for any other *A3* gene (Fig. 3C), it is most likely that HSV-1 editing is due predominantly to A3C. To establish an overall hypermutant editing frequency, we performed a limiting dilution (cf. reference 47) of the first-round products, followed by PCR at 95°C and in-parallel 3DPCR at 92.1°C. This yielded a differential hypermutant frequency of $\sim 10^{-3}$. Since 3DPCR tends to underestimate lightly edited DNA, this represents an underestimation (54).

Is A3 editing of the HSV-1 genome physiologically relevant? To address this question, we analyzed total DNA extracted directly from several HSV-1-associated lesions, notably pharyngeal washes and labial swabs. Fourteen samples were analyzed, the underlying pathologies ranging from prior liver transplantation to cancer. Using a nested PCR/3DPCR approach, eight samples scored positive for HSV-1 *ICP22* DNA. The results were variable, with the last denaturation temperature ranging from 89.6 to 93.8°C (Fig. 4A). Since the lowest T_d for cloned HSV-1 from QT6 cells is ~93 to 93.8°C, samples P5, P6, and P9 apparently include hyperedited HSV-1 genomes. Sequencing of cloned 3DPCR DNA revealed extensively hypermutated sequences for P5 and P9, although only for P9 was an extensive group of hypermutated sequences recovered, with up to 52 targets edited on both strands (Fig. 4B). Dinucleotide contexts associated with P9 editing, from greatest to least association, were TpC, CpC, and RpC (Fig. 4C), typical of editing by A3 deaminases and highly comparable to that observed for HeLa derived stock (Fig. 3B). Limiting dilution of first-round products for patient 9 yielded a hypermutant frequency of $\sim 10^{-4}$.

To see if there were lightly edited HSV-1 sequences, 3DPCR products in the 93 to 94.5°C temperature range were cloned and sequenced. Numerous sequences encoded 1 to 10 transitions (Fig. 4D). Those with 1 to 4 C → T transitions showed no dinucleotide bias and probably reflect the AT-rich end of the HSV mutant spectrum (Fig. 4C). Furthermore, since the dominant PCR-related mutations are AT → GC, the majority cannot be ascribed to PCR error (15, 33). In contrast, those with 5 or more monotonous C → T transitions in either strand showed the same dinucleotide biases as hypermutated genomes from P9 (Fig. 4C), indicating that they do indeed reflect A3 editing. Accordingly, A3-edited HSV genomes were recovered from 4/8 samples (P5, P6, P9, and P14), albeit to different degrees. Finally, to ascertain whether other regions of the HSV-1 genome could be edited *in vivo*, the *ICP0* and *ICP8* genes were analyzed from patient 5 and 9 DNA, respectively. Hypermutated sequences were readily recovered (see Fig. S1A and B in the supplemental material), indicating that most probably all parts of the HSV-1 genome are vulnerable to editing.

Since hypermutated HSV genomes are physiologically relevant, we were interested in whether other herpesvirus genomes were also susceptible to A3 editing. Since the A3C gene is highly expressed in leukocytes (40, 46), we tested whether Epstein-Barr virus (EBV) genomes from transformed peripheral blood mononuclear cell lines were vulnerable. In such cell lines, EBV is found in its latent form with little transcription,

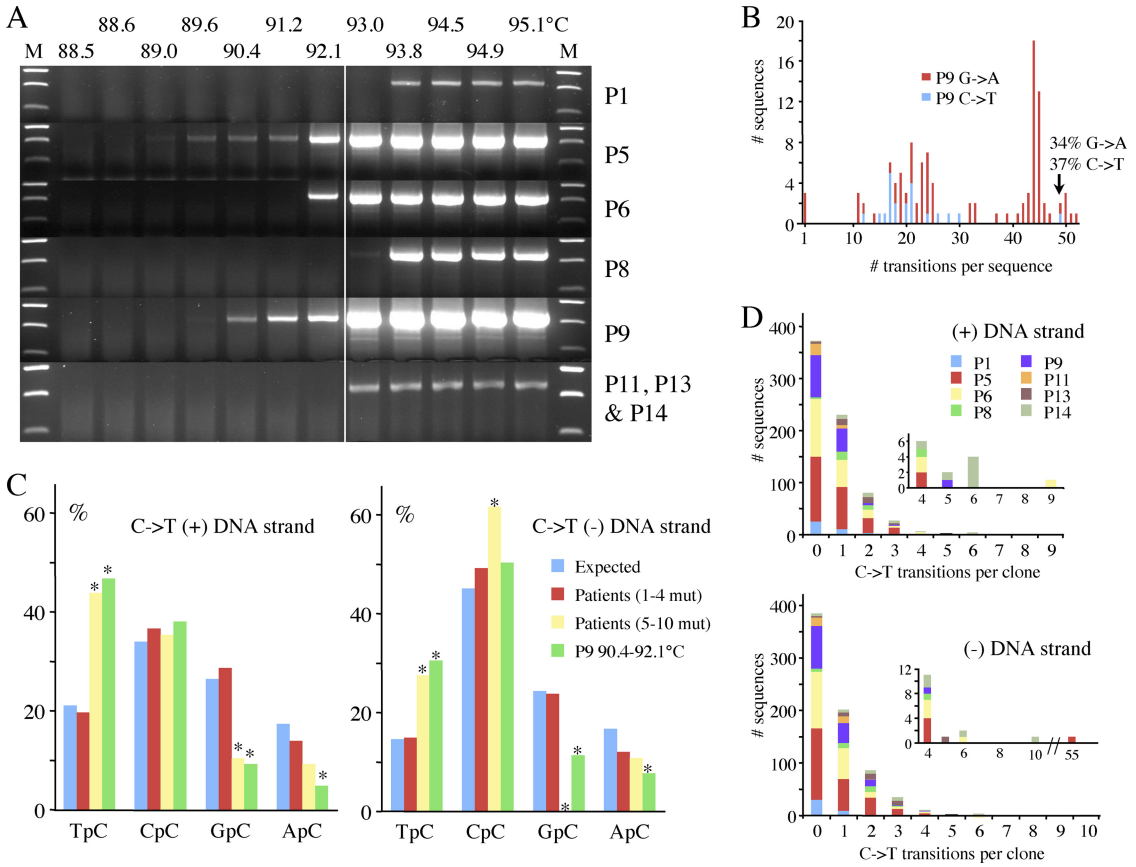

FIG. 4. HSV-1 genomes can be edited *in vivo*. (A) Agarose gels of *ICP22* 3DPCR DNA products from total DNA derived from pharyngeal washes or labial swabs. The annotation is as for Fig. 1C. (B) Frequency distribution of A3-edited HSV-1 sequences from patient P9. Since the cytidine composition of the two strands varies (32% plus strand; 35% minus strand), the % editing differs slightly (P9 G → A, $n = 88$, 36,080 bp; C → T, $n = 21$, 8,610 bp). (C) 5′ dinucleotide context associated with editing on the plus and minus strands for the collection of sequences from patient P9 (T_d = 90.4 to 92.1°C). Asterisks denote significant deviations form the expected values (χ^2 test, $P < 0.05$). Also shown are sequences derived at a higher T_d (93.8 to 94.5°C) with 1 to 4 C → T transitions or 5 to 10 transitions pooled from all patients [Patients (1–4 mut.), $n = 713$, 292,330 bp; Patients (5–10 mut.), $n = 10$, 4,100 bp; P9, G → A, $n = 94$, 38,540 bp; C → T, $n = 21$, 8,610 bp]. (D) Frequency distribution of sequences derived at 93.8 to 94.5°C from all eight patients for both strands. The insets expand the region covering 4 to 55 bp.

although EBNA-1 is transcribed (18). Using a nested PCR/3DPCR approach, we amplified part of the *EBNA-1* gene from total DNA. Four of five EBV$^+$ cell lines (P1, P2, P3, and Z) (Fig. 5A) proved positive for edited EBV DNA given that the reference denaturation temperature for the segment is 86.7°C, far lower than that for HSV-1, reflecting a lower GC content (EBV *EBNA-1*, 54%; HSV-1 *ICP22*, 67%). Cloning and sequencing of the 3DPCR products revealed extensive cytidine editing (Fig. 5B), ranging from 10 to 53% (Fig. 5C). To ascertain whether other regions of the EBV genome could be edited *in vivo*, the *EBNA-2* gene from patient Z was analyzed. Hypermutated sequences were readily recovered (see Fig. S1C in the supplemental material), indicating that most probably all parts of the EBV genome are vulnerable to editing.

The dinucleotide context associated with editing, in order of greatest to least, was CpC, TpC, and RpC, typical of A3G editing (Fig. 5D). A PCR/3DPCR limiting dilution analysis of Z DNA yielded a hypermutant frequency of $\sim 10^{-3}$ (95°C versus 85.3°C). An APOBEC3 transcriptome analysis of these cell lines showed that *A3C* was the most abundantly expressed gene, almost a log more than *A3G*, with *A3A* being the least expressed (46).

DISCUSSION

Like other viral DNA genomes, those of some human herpesviruses are vulnerable to APOBEC3 editing. For HSV-1, A3C appears to be an important restriction factor and can impact both the titer and particle/PFU ratio. The relevance of the experimental findings is confirmed by the recovery of A3-edited genomes in uncultured samples (Fig. 4). HSV-1 is relatively insensitive to type I interferons, which should help protect it from the A3 enzymes whose genes are upregulated by them. However, since *A3C* expression is essentially insensitive to alpha IFN (IFN-α), the present findings raise the question as to whether HSV-1 encodes an A3C antagonist, given that it is sensitive to overexpression of *A3C* (Fig. 1A and B), or whether productive replication occurs in $A3C^{neg}$ or $A3C^{low}$ cells. Certainly, *A3C* siRNA knockdown shows that replication is sensitive to

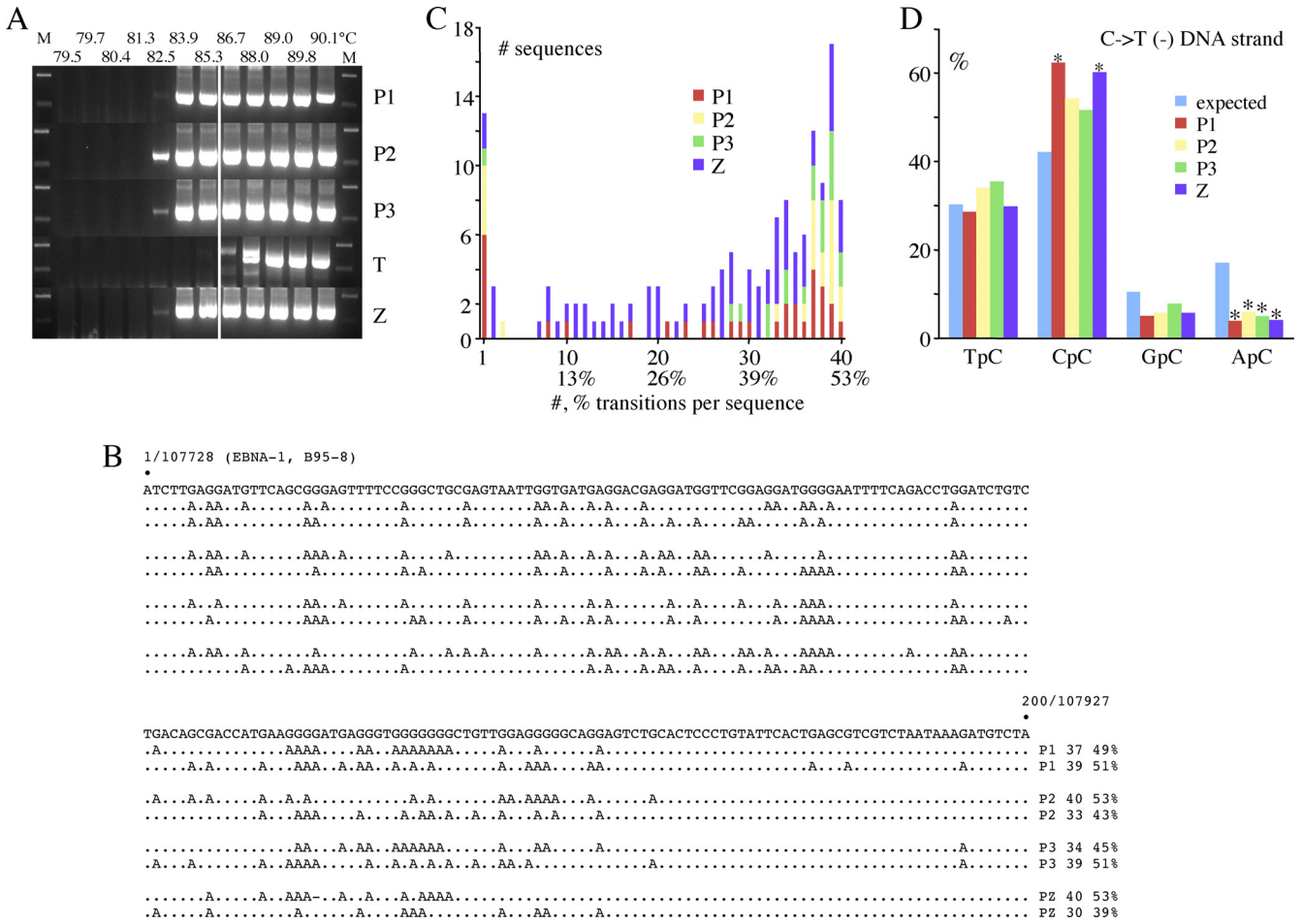

FIG. 5. Hyperediting of EBV genomes in EBV-immortalized human B cell lines. (A) Agarose gels of EBNA-1 3DPCR DNA products from total DNA derived from five EBV-immortalized human B cell lines. The annotation is as for Fig. 1C. The P1 to -3 lines are all *ung*$^{-/-}$; Z is *AICDA*$^{-/-}$, while T is an EBV-cell line from a normal patient without any known leukocyte defect. (B) A selection of hyperedited sequences from P1 to -3 and Z. To the right are the number and % of cytidine residues edited. Plus-strand hypermutants were not always recovered and hence were excluded from analyses. (C) Frequency distribution of A3-edited EBV sequences from four EBV-transformed cell lines. Only minus-strand editing was identified (P1, $n = 32$, 6,400 bp; P2, $n = 21$, 4,200 bp; P3, $n = 19$, 3,800 bp; Z, $n = 72$, 14,400 bp). (D) 5′ dinucleotide context associated with minus-strand editing. Asterisks denote significant deviations from the expected values (χ^2 test, $P < 0.05$).

the expression levels in HeLa cells (Fig. 2C). In short, does HSV editing *in vivo* reflect A3 restriction of genomes defective for the antagonist, analogous to HIV/simian immunodeficiency virus (SIV) hypermutants on a Δ*vif* background (4, 8, 16, 26, 29, 30, 42, 43, 57), or replication in *A3C*$^{neg/low}$ cells, analogous to HBV infection in cirrhosis, since this virus does not encode any known IFN-α or A3 antagonist (54)? With this in mind, it would be particularly interesting to determine A3C expression in sensory neurons, particularly since *A3* levels are generally low in uninfected brain (40). However, since B cells express high levels of *A3* genes yet are propitious for EBV replication, simple correlations with bulk transcription levels may not be reliable. Given that A3C is expressed in a wide range of different cells and tissues and is invariably the most highly expressed of all the seven human *A3* genes, variability in expression levels might perhaps account for part of the variability in plaque titers and particle/PFU ratios as a function of different cell lines. For example, varicella-zoster virus grown on a human melanoma cell line shows one of the highest particle/PFU ratios for any virus (6). However, for herpesviruses other factors can impinge on the particle/PFU ratio (1).

Highly edited genomes are clearly defective. Indeed, if A3 editing of *ICP22* is representative of the whole genome, ~40% editing of cytidine targets in the plus or minus strands translates into >20,000 C → T transitions per genome. Even lightly edited *ICP22* DNA with 5 edits/410 bp translates into ~1,860 substitutions per genome, which is far above the average mutation rate for DNA genomes, and so these too must be defective. Indeed, even a log lower amount of editing would also result in defective genomes. Presumably the vast majority of A3-edited HSV-1 genomes must be defective. Given this and a 68.3% GC content (20), it is unlikely that A3 editing contributes to HSV evolution. In a comparison of HSV-1 genomes, GC → AT transitions slightly outnumbered AT → GC transitions (50). However, when normalized to base composition, AT → GC transitions were more frequent, which again suggests that A3C activity

does not impact HSV genome evolution. A3C presumably accesses replicating HSV DNA in the nucleus. That it impacts the particle/PFU ratio suggests that the lesions are in the packaged genomes, whether as dG-dU base pairs or as incorrectly repaired derivatives.

An interesting feature of the A3 editing described here is that while both strands are edited, we invariably recover more minus-strand than plus-strand hypermutants (G → A as opposed to C → T) (Table 1). Furthermore, the degree of editing was usually greater for the minus-strand than for the plus-strand hypermutants. This feature also shows up for mtDNA and nuclear DNA editing and for the A3-edited HPV hypermutants (46, 53). The variety among such genomes and amplification primers suggests that it is not an artifact but reflects some feature associated with A3 editing. As the minus strand is transcribed, some degree of protection by the transcription complex is clearly irrelevant.

Since A3 editing of the herpesvirus genomes occurs for HSV-1 and EBV genomes in their lytic and latent forms, respectively, it is possible that some of the other six human herpesviruses may be vulnerable too. The three EBV cell lines P1, P2, and P3 were deficient in the human uracil *N*-glycosylase (UNG), which we have shown to be an important component in the dynamics of A3-initiated catabolism of DNA: suppression of UNG activity resulted in higher frequencies of edited DNA (46). Yet in the present context, UNG was not crucial to detection of A3-edited EBV genomes since recovery of such genomes from the EBV^+ Z cell line (*ung*$^+$ yet *AICDA*$^{-/-}$) was comparable, while the EBV^+ line "T," an EBV cell line from a donor without any known genetic defect, failed to yield hyperedited EBV DNA (Fig. 5A). Both HSV-1 and EBV encode divergent UNG enzymes that are able to excise uridine from DNA and are found at the replication fork. They are clearly orthologous to mammalian UNGs (23). Whether these viral UNG enzymes have any impact on detection of A3-edited genomes needs to be established.

The *A3* gene locus appears with the emergence of placental mammals, and while it is generally bounded by the *cbx6* and *cbx7* genes, there is considerable variation (24). For example, the rat and mouse genomes encode a single *A3* gene, the cow genome two, cats three/four, and horses five/six, while the primate lineage encodes seven *A3* genes, six of which are functional (24, 25). Since many of these genes are phylogenically grouped with *A3C*, it is possible that they could represent yet another cross-species barrier, particularly in the sense of herpesvirus transmission to an animal with a more complex *A3* locus. Since herpesviruses may go back 300 million to 400 million years, while the initial single gene *A3* locus arose ~125 million years ago, cytidine deamination would seem to be a relatively recent restriction factor.

In conclusion, at least two human herpesviruses are vulnerable to A3 editing, a physiologically relevant observation. The findings extend the list of genomes which are vulnerable: retroviral (3, 10, 14, 16, 26, 28–30, 43), adeno-associated (7), human papillomavirus (53), human mitochondrial, and nuclear genomes (46), as well as transfected plasmid DNA (44). It appears a plausible working hypothesis that yet more DNA viruses are restricted by A3 enzymes.

ACKNOWLEDGMENTS

We thank Martina Fuss for excellent technical assistance and Frazer Rixon, MRC Virology Unit, Glasgow, United Kingdom, for the DM165 antibody.

R.S. was supported by an EMBO long-term fellowship and a postdoctoral fellowship from l'Association pour la Recherche sur le Cancer (ARC). M.-M.A. is supported by a graduate fellowship from La Ligue contre le Cancer. This work was supported by grants from the Institut Pasteur, CNRS, and HOMFOR and the Spanish Ministry of Science and Innovation (SAF2010-21336). The Molecular Retrovirology Unit is an Equipe Labelise par la Ligue contre le Cancer.

REFERENCES

1. **Ace, C. I., T. A. McKee, J. M. Ryan, J. M. Cameron, and C. M. Preston.** 1989. Construction and characterization of a herpes simplex virus type 1 mutant unable to transinduce immediate-early gene expression. J. Virol. **63:**2260–2269.
2. **Beale, R. C., et al.** 2004. Comparison of the differential context-dependence of DNA deamination by APOBEC enzymes: correlation with mutation spectra in vivo. J. Mol. Biol. **337:**585–596.
3. **Bishop, K. N., et al.** 2004. Cytidine deamination of retroviral DNA by diverse APOBEC proteins. Curr. Biol. **14:**1392–1396.
4. **Bogerd, H. P., B. P. Doehle, H. L. Wiegand, and B. R. Cullen.** 2004. A single amino acid difference in the host APOBEC3G protein controls the primate species specificity of HIV type 1 virion infectivity factor. Proc. Natl. Acad. Sci. U. S. A. **101:**3770–3774.
5. **Bonvin, M., et al.** 2006. Interferon-inducible expression of APOBEC3 editing enzymes in human hepatocytes and inhibition of hepatitis B virus replication. Hepatology **43:**1364–1374.
6. **Carpenter, J. E., E. P. Henderson, and C. Grose.** 2009. Enumeration of an extremely high particle-to-PFU ratio for varicella-zoster virus. J. Virol. **83:**6917–6921.
7. **Chen, H., et al.** 2006. APOBEC3A is a potent inhibitor of adeno-associated virus and retrotransposons. Curr. Biol. **16:**480–485.
8. **Conticello, S. G., R. S. Harris, and M. S. Neuberger.** 2003. The Vif protein of HIV triggers degradation of the human antiretroviral DNA deaminase APOBEC3G. Curr. Biol. **13:**2009–2013.
9. **Conticello, S. G., C. J. Thomas, S. K. Petersen-Mahrt, and M. S. Neuberger.** 2005. Evolution of the AID/APOBEC family of polynucleotide (deoxy) cytidine deaminases. Mol. Biol. Evol. **22:**367–377.
10. **Delebecque, F., et al.** 2006. Restriction of foamy viruses by APOBEC cytidine deaminases. J. Virol. **80:**605–614.
11. **Di Noia, J. M., and M. S. Neuberger.** 2007. Molecular mechanisms of antibody somatic hypermutation. Annu. Rev. Biochem. **76:**1–22.
12. **Dohner, K., K. Radtke, S. Schmidt, and B. Sodeik.** 2006. Eclipse phase of herpes simplex virus type 1 infection: efficient dynein-mediated capsid transport without the small capsid protein VP26. J. Virol. **80:**8211–8224.
13. **Eidson, K. M., W. E. Hobbs, B. J. Manning, P. Carlson, and N. A. DeLuca.** 2002. Expression of herpes simplex virus ICP0 inhibits the induction of interferon-stimulated genes by viral infection. J. Virol. **76:**2180–2191.
14. **Esnault, C., et al.** 2005. APOBEC3G cytidine deaminase inhibits retrotransposition of endogenous retroviruses. Nature **433:**430–433.
15. **Goodenow, M., et al.** 1989. HIV-1 isolates are rapidly evolving quasispecies: evidence for viral mixtures and preferred nucleotide substitutions. J. Acquir. Immune Defic. Syndr. **2:**344–352.
16. **Harris, R. S., et al.** 2003. DNA deamination mediates innate immunity to retroviral infection. Cell **113:**803–809.
17. **Henry, M., et al.** 2009. Genetic editing of HBV DNA by monodomain human APOBEC3 cytidine deaminases and the recombinant nature of APOBEC3G. PLoS One **4:**e4277.
18. **Imai, K., et al.** 2003. Human uracil-DNA glycosylase deficiency associated with profoundly impaired immunoglobulin class-switch recombination. Nat. Immunol. **4:**1023–1028.
19. **Jarmuz, A., et al.** 2002. An anthropoid-specific locus of orphan C to U RNA-editing enzymes on chromosome 22. Genomics **79:**285–296.
20. **Karlin, S., E. S. Mocarski, and G. A. Schachtel.** 1994. Molecular evolution of herpesviruses: genomic and protein sequence comparisons. J. Virol. **68:**1886–1902.
21. **Koning, F. A., et al.** 2009. Defining APOBEC3 expression patterns in human tissues and hematopoietic cell subsets. J. Virol. **83:**9474–9485.
22. **Kremer, M., et al.** 2006. Vaccinia virus replication is not affected by APOBEC3 family members. Virol. J. **3:**86.
23. **Krusong, K., E. P. Carpenter, S. R. Bellamy, R. Savva, and G. S. Baldwin.** 2006. A comparative study of uracil-DNA glycosylases from human and herpes simplex virus type 1. J. Biol. Chem. **281:**4983–4992.
24. **LaRue, R. S., et al.** 2009. Guidelines for naming non-primate APOBEC3 genes and proteins. J. Virol. **83:**494–497.
25. **LaRue, R. S., et al.** 2008. The artiodactyl APOBEC3 innate immune repertoire shows evidence for a multi-functional domain organization that existed in the ancestor of placental mammals. BMC Mol. Biol. **9:**104.

26. **Lecossier, D., F. Bouchonnet, F. Clavel, and A. J. Hance.** 2003. Hypermutation of HIV-1 DNA in the absence of the Vif protein. Science **300:**1112.
27. **Liddament, M. T., W. L. Brown, A. J. Schumacher, and R. S. Harris.** 2004. APOBEC3F properties and hypermutation preferences indicate activity against HIV-1 in vivo. Curr. Biol. **14:**1385–1391.
28. **Mahieux, R., et al.** 2005. Extensive editing of a small fraction of human T-cell leukemia virus type 1 genomes by four APOBEC3 cytidine deaminases. J. Gen. Virol. **86:**2489–2494.
29. **Mangeat, B., et al.** 2003. Broad antiretroviral defence by human APOBEC3G through lethal editing of nascent reverse transcripts. Nature **424:**99–103.
30. **Mariani, R., et al.** 2003. Species-specific exclusion of APOBEC3G from HIV-1 virions by Vif. Cell **114:**21–31.
31. **McClelland, D. A., et al.** 2002. pH reduction as a trigger for dissociation of herpes simplex virus type 1 scaffolds. J. Virol. **76:**7407–7417.
32. **McGeoch, D. J., F. J. Rixon, and A. J. Davison.** 2006. Topics in herpesvirus genomics and evolution. Virus Res. **117:**90–104.
33. **Meyerhans, A., et al.** 1989. Temporal fluctuations in HIV quasispecies in vivo are not reflected by sequential HIV isolations. Cell **58:**901–910.
34. **Mossman, K. L., H. A. Saffran, and J. R. Smiley.** 2000. Herpes simplex virus ICP0 mutants are hypersensitive to interferon. J. Virol. **74:**2052–2056.
35. **Nicholl, M. J., L. H. Robinson, and C. M. Preston.** 2000. Activation of cellular interferon-responsive genes after infection of human cells with herpes simplex virus type 1. J. Gen. Virol. **81:**2215–2218.
36. **Noguchi, C., et al.** 2009. G-to-A hypermutation in hepatitis B virus (HBV) and clinical course of patients with chronic HBV infection. J. Infect. Dis. **199:**1599–1607.
37. **Pasdeloup, D., D. Blondel, A. L. Isidro, and F. J. Rixon.** 2009. Herpesvirus capsid association with the nuclear pore complex and viral DNA release involve the nucleoporin CAN/Nup214 and the capsid protein pUL25. J. Virol. **83:**6610–6623.
38. **Petit, V., et al.** 2009. Murine APOBEC1 is a powerful mutator of retroviral and cellular RNA in vitro and in vivo. J. Mol. Biol. **385:**65–78.
39. **Pham, P., R. Bransteitter, J. Petruska, and M. F. Goodman.** 2003. Processive AID-catalysed cytosine deamination on single-stranded DNA simulates somatic hypermutation. Nature **424:**103–107.
40. **Refsland, E. W., et al.** 2010. Quantitative profiling of the full APOBEC3 mRNA repertoire in lymphocytes and tissues: implications for HIV-1 restriction. Nucleic Acids Res. **38:**4274–4284.
41. **Sainz, B., Jr., and W. P. Halford.** 2002. Alpha/beta interferon and gamma interferon synergize to inhibit the replication of herpes simplex virus type 1. J. Virol. **76:**11541–11550.
42. **Schrofelbauer, B., D. Chen, and N. R. Landau.** 2004. A single amino acid of APOBEC3G controls its species-specific interaction with virion infectivity factor (Vif). Proc. Natl. Acad. Sci. U. S. A. **101:**3927–3932.
43. **Sheehy, A. M., N. C. Gaddis, J. D. Choi, and M. H. Malim.** 2002. Isolation of a human gene that inhibits HIV-1 infection and is suppressed by the viral Vif protein. Nature **418:**646–650.
44. **Stenglein, M. D., M. B. Burns, M. Li, J. Lengyel, and R. S. Harris.** 2010. APOBEC3 proteins mediate the clearance of foreign DNA from human cells. Nat. Struct. Mol. Biol. **17:**222–229.
45. **Stenglein, M. D., and R. S. Harris.** 2006. APOBEC3B and APOBEC3F inhibit L1 retrotransposition by a DNA deamination-independent mechanism. J. Biol. Chem. **281:**16837–16841.
46. **Suspène, R., et al.** 2011. Somatic hypermutation of human mitochondrial and nuclear DNA by APOBEC3 cytidine deaminases, a pathway for DNA catabolism. Proc. Natl. Acad. Sci. U. S. A. **108:**4858–4863.
47. **Suspène, R., et al.** 2005. Extensive editing of both hepatitis B virus DNA strands by APOBEC3 cytidine deaminases in vitro and in vivo. Proc. Natl. Acad. Sci. U. S. A. **102:**8321–8326.
48. **Suspène, R., M. Henry, S. Guillot, S. Wain-Hobson, and J. P. Vartanian.** 2005. Recovery of APOBEC3-edited human immunodeficiency virus G → A hypermutants by differential DNA denaturation PCR. J. Gen. Virol. **86:**125–129.
49. **Suspène, R., et al.** 2004. APOBEC3G is a single-stranded DNA cytidine deaminase and functions independently of HIV reverse transcriptase. Nucleic Acids Res. **32:**2421–2429.
50. **Szpara, M. L., L. Parsons, and L. W. Enquist.** 2010. Sequence variability in clinical and laboratory isolates of herpes simplex virus 1 reveals new mutations. J. Virol. **84:**5303–5313.
51. **Tsuge, M., et al.** 2010. G to A hypermutation of TT virus. Virus Res. **149:**211–216.
52. **Turelli, P., B. Mangeat, S. Jost, S. Vianin, and D. Trono.** 2004. Inhibition of hepatitis B virus replication by APOBEC3G. Science **303:**1829.
53. **Vartanian, J. P., D. Guetard, M. Henry, and S. Wain-Hobson.** 2008. Evidence for editing of human papillomavirus DNA by APOBEC3 in benign and precancerous lesions. Science **320:**230–233.
54. **Vartanian, J. P., et al.** 2010. Massive APOBEC3 editing of hepatitis B viral DNA in cirrhosis. PLoS Pathog. **6:**e1000928.
55. **Wang, F. X., J. Huang, H. Zhang, and X. Ma.** 2008. APOBEC3G upregulation by alpha interferon restricts human immunodeficiency virus type 1 infection in human peripheral plasmacytoid dendritic cells. J. Gen. Virol. **89:**722–730.
56. **Wiegand, H. L., B. P. Doehle, H. P. Bogerd, and B. R. Cullen.** 2004. A second human antiretroviral factor, APOBEC3F, is suppressed by the HIV-1 and HIV-2 Vif proteins. EMBO J. **23:**2451–2458.
57. **Zhang, H., et al.** 2003. The cytidine deaminase CEM15 induces hypermutation in newly synthesized HIV-1 DNA. Nature **424:**94–98.

Annexe #3

Insights into herpesvirus tegument organization from structural analyses of the 970 central residues of HSV-1 UL36 protein.

Scrima N, Lepault J, Boulard Y, Pasdeloup D, Bressanelli S, Roche S.

THE JOURNAL OF BIOLOGICAL CHEMISTRY VOL. 290, NO. 14, pp. 8820–8833, April 3, 2015

Insights into Herpesvirus Tegument Organization from Structural Analyses of the 970 Central Residues of HSV-1 UL36 Protein

Received for publication, September 22, 2014, and in revised form, February 3, 2015 Published, JBC Papers in Press, February 12, 2015, DOI 10.1074/jbc.M114.612838

Nathalie Scrima[‡], Jean Lepault[‡], Yves Boulard[‡§], David Pasdeloup[¶], Stéphane Bressanelli[‡1], and Stéphane Roche[‡2]

From the [‡]Institute for Integrative Biology of the Cell (I2BC), 1 Avenue de la Terrasse, 91198 Gif-sur-Yvette, the [§]Institute of Biology and Technologies of Saclay, Commissariat à l'Energie Atomique, 91191 Gif-sur-Yvette, and the [¶]Faculté de Pharmacie, INSERM UMR 984, 5 Rue J. B. Clément, 92290 Châtenay-Malabry, France

Background: UL36 is a large multifunctional protein that is conserved across herpesviridae.
Results: The 970 central residues of UL36 have been analyzed by several biophysical and structural methods.
Conclusion: These UL36 residues constitute an elongated fiber that is able to form monomers and dimers.
Significance: This provides a framework for understanding how UL36 fulfills its functions.

The tegument of all herpesviruses contains a capsid-bound large protein that is essential for multiple viral processes, including capsid transport, decapsidation at the nuclear pore complex, particle assembly, and secondary envelopment, through mechanisms that are still incompletely understood. We report here a structural characterization of the central 970 residues of this protein for herpes simplex virus type 1 (HSV-1 UL36, 3164 residues). This large fragment is essentially a 34-nm-long monomeric fiber. The crystal structure of its C terminus shows an elongated domain-swapped dimer. Modeling and molecular dynamics simulations give a likely molecular organization for the monomeric form and extend our findings to alphaherpesvirinae. Hence, we propose that an essential feature of UL36 is the existence in its central region of a stalk capable of connecting capsid and membrane across the tegument and that the ability to switch between monomeric and dimeric forms may help UL36 fulfill its multiple functions.

Herpesviruses, such as herpes simplex virus type 1 (HSV-1), share a common four-layer organization. Their double-stranded DNA genome is contained within a T = 16 icosahedral capsid, surrounded by an intermediate proteinaceous tegument and finally an external lipid envelope. The tegument is asymmetric with a minimal thickness of 15 nm and a maximal thickness of 50 nm in extracellular virions. It is subdivided in an "inner" tegument that is tightly bound to the capsid and an "outer" tegument that is connected to the viral envelope (1–4). The HSV-1 tegument is made of more than 20 proteins. Three of them, US3, UL36, and UL37, have been identified as inner tegument proteins according to their localization during fractionation of viral particles and to their association with capsids or membranes during particle assembly and disassembly (5–8). Two of them, UL36 and UL37, form a complex of unknown stoichiometry (9, 10).

The essential tegument protein UL36 is tightly bound to the capsid vertices through an interaction with the vertices' specific component UL25 (11–13). UL36 is involved in several processes during the virus cycle. After fusion of the viral membrane with the plasma membrane during herpesvirus entry, most of the viral tegument is detached, whereas UL36 is one of the few proteins that remain associated with the capsid (14). UL36 together with UL37 play an essential role during entry. It is necessary for capsid transport toward the nucleus during the entry phase and toward the final viral particle assembly sites during egress. Both transports are abolished in the absence of UL36, and they are strongly impaired in the absence of UL37(15–18). Viral capsids are transported along the microtubule network, and several cellular proteins are recruited to this end, including molecular motors kinesin 1 and 2, dynein, and its dynactin cofactor as well as the dystonin/BPAG1, a cross-linker of cytoskeleton elements (14, 18–20).

Besides capsid transport, UL36 is required for capsid routing at the nuclear pore complex (21) and subsequent uncoating (22–24). In contrast, UL37 is not required for this final step (24). The docking process also involves the capsid protein UL25 that is able to bind the cellular nucleoporins CAN/Nup214 and HCG1 (13). These nucleoporins are localized on the cytoplasmic side of the nuclear pore complex and could thus act as a nuclear receptor for the capsid. Finally, an antibody directed against Nup358, a component of the cytoplasmic fibrils of the nuclear pore complex, is also able to block this association. Although several proteins involved in this process have been identified, the detailed mechanisms triggering the DNA ejection and the precise role of UL36 are still unknown (22).

Finally, UL36 has been involved in the last stages of viral assembly. A null mutation in the *UL36* gene leads to an accumulation of unenveloped DNA-filled capsids in the cytoplasm and a massive production of defective "light particles" lacking capsid, thus suggesting that UL36 is necessary for associating the preassembled outer viral layers to the capsids (25, 26). The outer tegument protein UL48 has been shown to interact with

The atomic coordinates and structure factors (codes 4TT0 and 4TT1) have been deposited in the Protein Data Bank (http://wwpdb.org/).

[1] To whom correspondence may be addressed. E-mail: stephane.bressanelli@vms.cnrs-gif.fr.
[2] To whom correspondence may be addressed. E-mail: stephane.roche@vms.cnrs-gif.fr.

UL36 (10, 27). However, disrupting this interaction reduces the incorporation of UL48 in viral particles, but it is not sufficient for preventing the formation of viral particles, thus suggesting that other unidentified direct or indirect interactions between UL36 and outer tegument proteins might be involved (28). Recently, the disruption of interactions between UL37 and the envelope proteins gK and UL20 has been shown to impair secondary envelopment (29). The absence of UL36 would thus abolish the recruitment of UL37 and, as a consequence, of the viral envelope as well.

In addition to these roles in the virus cycle, UL36 has a deubiquitinase domain that is active on both Lys-48 and Lys-63 ubiquitinylations (30, 31). It is able to deubiquitinylate several substrates, including TRAF3 and UL36 itself (32, 33).

Despite the large amount of available functional data, the way by which UL36 fulfills its functions is still elusive. The large size of the protein (336 kDa) and the scarcity of structural data are hindering the study of these mechanisms. Fibrous structures extending radially from the capsid vertices are observed in "T36" capsids, *i.e.* capsids with the inner tegument still bound, but it is unclear whether these fibers are made of UL36, UL37, or both proteins (3). Except for the human cytomegalovirus N-terminal deubiquitinase domain (34), no high resolution data are available for any herpesvirus UL36 proteins, and the structural domains of the protein have not been identified. *In silico* analyses suggest the presence of several coiled coil motifs between amino acids 980 and 1740. Here, we were able to produce in a recombinant system a large fragment (residues 760–1733) of UL36 containing almost one-third of the protein, including these putative coiled coils. Biophysical analyses establish that this central part of UL36 forms a monomeric fiber sufficiently extended to bridge the capsid and membrane. We solved the atomic structure of the C-terminal part of this fiber that surprisingly crystallized as a domain-swapped antiparallel dimer. Molecular dynamics simulations explain how a transition from a monomeric to a dimeric state could occur. Homology modeling suggests that these properties are conserved among alphaherpesvirinae. We discuss what roles extended monomeric and antiparallel dimeric forms of UL36 could have in the virus cycle.

EXPERIMENTAL PROCEDURES

Sequence Analyses—The protein sequence alignments of HSV-1, HSV-2, PRV,[3] VZV, GHV-2, and CHV-1 UL36 were performed using ClustalW and were displayed with ESPRIPT. The coiled coils were predicted with PCOILS. The secondary structure predictions were performed using SOPMA.

Cloning, Expression, and Purification of UL36 Fragments—Amino acids 1600–1733 and 760–1733 of strain 17 HSV-1 UL36 (accession number FJ593289.1) were cloned between the BamHI and EcoRI restriction sites of the pGEX-6P1 (GE-Healthcare) expression vector, resulting in fusions of these fragments with an N-terminal cleavable glutathione *S*-transferase. Both fragments were produced in *Escherichia coli* BL21 (DE3) cells (Stratagene). Freshly transformed cells were incubated overnight in 5 ml of LB supplemented by ampicillin at 37 °C. These cultures were diluted in 1 liter of LB supplemented by 50 μg/ml ampicillin and grown at 37 °C up to an absorbance of 0.6. The temperature was then lowered to 18°, and the protein expression was induced by the addition of 1 mM isopropyl β-D-thiogalactopyranoside. Cells were harvested 16 h after induction.

Cells expressing construct 760–1733 were pelleted by centrifugation at 5000 × *g* for 20 min in a JLA9.1,000 rotor (Beckman Coulter). The pellet was resuspended in 50 mM HEPES, pH 7.0, 500 mM NaCl, 10% glycerol, 1 mM DTT supplemented by a tablet of EDTA-free "Complete" protease inhibitor mixture tablet (Roche Diagnostics) and lysed by sonication at 4 °C. The lysate was then centrifuged at 4 °C for 5 min at 2700 × *g*. The supernatant was recovered and centrifuged at 4 °C for 30 min at 48,000 × *g* in a JA25.50 rotor (Beckman Coulter). The soluble lysate was loaded on Protino glutathione-agarose 4B beads (Macherey Nagel). The column was washed with 20 volumes of 20 mM HEPES, pH 7.0, 200 mM NaCl, 1 mM DTT and eluted with 20 mM HEPES, pH 7.0, 200 mM NaCl, 1 mM DTT, 20 mM glutathione. The GST tag was then removed by the addition of 120 μg of PreScission protease for 150 min at 20 °C. The fragment was then purified by size exclusion chromatography on a Superose 6 10/300 GL pre-equilibrated in 20 mM HEPES, pH 7.0, 200 mM NaCl, 1 mM DTT. Finally, it was loaded again on glutathione beads, and the flow-through containing the fragment of interest was concentrated to 1 mg/ml and stored at −80 °C.

Similarly, cells expressing construct 1600–1733 were lysed in 50 mM HEPES, pH 7.0, 500 mM NaCl, 1 mM DTT supplemented by a tablet of EDTA-free Complete protease inhibitor mixture tablet. After two successive centrifugations at 2700 × *g* for 5 min then 48,000 × *g* for 30 min, the soluble lysate was loaded on a GSTrap FF affinity column (GE Healthcare). The column was washed with 20 volumes of 20 mM HEPES, pH 7.0, 200 mM NaCl and eluted with 20 mM HEPES, pH 7.0, 200 mM NaCl, 20 mM glutathione. After removal of the GST tag by the addition of 50 μg of PreScission protease for 2 h at 20 °C, the protein was purified on a Superdex 200 10/300 GL column and finally loaded on a second GSTrap FF column. The flow-through containing the fragment of interest was concentrated to 1 mg/ml and flash-frozen in liquid nitrogen.

SEC-MALLS Measurements—The experiments were performed with a Wyatt Technology instrument (mini DAWN TREOS + QELS + OPTILab T-rEX) coupled to a Shimadzu HPLC system. For all samples, 30 μl of samples were used. Fragment 1600–1733 in a 20 mM HEPES, pH 7.0, 500 mM NaCl buffer was injected at an initial concentration of 2 mg/ml in a KW-803 column. Fragment 760–1733 in a 20 mM HEPES, pH 7.0, 200 mM NaCl, 1 mM DTT buffer was injected at an initial concentration of 2 mg/ml in a Biosec-3 column.

Analytical Ultracentrifugation—Sedimentation velocity and equilibrium analyses were performed at 20 °C using an An-60Ti rotor in an XLA70 Beckman Coulter centrifuge. For sedimentation velocity, 360 μl of a 5 μM or 9.4 μM solution of the fragment 760–1733 in 20 mM HEPES, pH 7.0, 200 mM NaCl, 1 mM DTT were introduced in a cuvette with a 12-mm optical path-

[3] The abbreviations used are: PRV, pseudorabies virus; r.m.s.d., root mean square deviation; SEC-MALLS, multi-angle laser light scattering; VZV, varicella zoster virus.

way and centrifuged at 40,000 rpm (116,370 × *g*). A_{280} measurements were performed each 5 min. The results were analyzed by SEDFIT. For equilibrium analyses, 110 μl of a 3.3, 5.4, or 8.6 μM solution of the fragment 760–1733 in 20 mM HEPES, pH 7.0, 200 mM NaCl, 1 mM DTT was introduced in a cuvette with a 12-mm pathway and centrifuged successively at 8200, 9800, and 14,200 rpm (corresponding to 4890 × *g*, 6985 × *g*, and 14,665 × *g*). The results were analyzed using SEDPHAT.

Electron Microscopy—The purified 760–1733 fragment was diluted to 0.1 mg/ml in 2 mM HEPES, pH 7, 20 mM NaCl, 50 mM ammonium acetate. The sample was then adsorbed onto air-glow discharge carbon-coated grids and stained with sodium phospho-tungstic acid adjusted to the sample, pH 7.5. The images were recorded in an electron microscope (model CM12; Philips) operated at 80 kV, with a nominal magnification of 35,000. The length and width of the objects were measured using ImageJ.

Crystallization, Structure Determination, and Analysis—The 1600–1733 fragment was concentrated to 5 mg/ml. Crystals were grown by vapor diffusion at 20 °C in hanging drops using 0.1 μl of protein and 0.1 μl of the well solution containing 0.2 M $(NH_4)_2HPO_4$, 20% PEG 3350 (native dataset), or 100 mM HEPES, pH 7.5, and 2 M ammonium formate (KI soak dataset). In both cases, small hexagonal crystals grew within 1–4 days and were harvested 2 weeks later. The native crystals were flash-cooled in 0.2 M $(NH_4)_2HPO_4$, 20% PEG 3350, 20% glycerol, although the derivative crystals were incubated for 10 min in HEPES, pH 7.5, 1 M ammonium formate, 0.8 M potassium iodide, 25% glycerol before flash-freezing.

A native dataset was collected at 100 K on a single crystal at the PROXIMA 1 beamline at the Soleil synchrotron. A highly redundant iodine SAD dataset was collected at 100 K on a single crystal at a wavelength of 1.90745 Å at the ID23-1 beamline of the European Synchrotron Radiation Facility. Both datasets were processed using the XDS package (35) and were found to belong to the same crystal form despite the different crystallization conditions. SIRAS phasing was not attempted due to nonisomorphism. The structure was solved by SAD phasing with the KI soak dataset. SHELXD (36) could localize eight iodine atoms per asymmetric unit. After density modification using SHELXE, interpretable density maps were obtained, initially to 2.8 Å resolution. The structure was refined and analyzed using the PHENIX (37) and CCP4 (38) suites and built using COOT (39). Phenix.autobuild was able to place about 50% of the amino acids in the initial map. Despite significant data anisotropy, we gradually extended refinement resolution for subsequent refinement and building, following the current best practice (40). Thus, we included data according to $CC_{1/2}$ and validated this choice by comparing CC(work) and CC(free) to CC* (Table 1). Coordinates were refined for the two 1600–1733 molecules in the asymmetric unit with local NCS restraints. TLS and individual B-factors were refined with three TLS groups as follows: residues 1628–1723 of both molecules, residues 1595–1627 of molecule B and residues 1597–1627 of molecule A (residues N-terminal to 1600 represent the residual affinity tag). In later stages of refinement, all iodine ions were identified in log-likelihood gradient maps. The asymmetric unit contains 42 iodine atoms (23 with occupancy of at least 50%). The final refined protein model was used as the starting point for refinement against the native dataset keeping the same test set. After rigid body refinement, the same refinement protocol was used as for the KI soak. There is additional weak density in the KI soak that could be ascribed to residues 1724–1725 stabilized by an iodine ion site. We did not include these residues in the final models as no density is apparent in the native dataset. The KI soak (respectively native) models have no Ramachandran outliers, and 98% (respectively, 97%) of residues are in the favored region of the Ramachandran plot. CC* (40) is 0.86 (respectively 0.91) in the highest resolution shell. Crystal packing and interfaces were analyzed with PISA (41) and the NOX-class server (42). Structure visualization was performed and structural figures made with PyMOL. Atomic coordinates and structure factors have been deposited to the RCSB Protein Data Bank under accession number 4TT0 (potassium iodide derivative) and 4TT1 (native crystals).

Tryptophan Fluorescence—The fragment 1600–1733 was diluted to 100 μg/ml in 20 mM HEPES, pH 7, 200 mM NaCl. Identical spectra obtained with other buffers ranging from pH 6 to pH 8 and from 20 mM to 1 M NaCl were also tested. Emission spectra were recorded at 25 °C on a PerkinElmer Life Sciences LS50B fluorimeter. Excitation was performed at 290 nm (slit width 2.5 nm), and the emission was measured between 310 and 400 nm (slit width 2.5 nm) at a speed of 60 nm per min. The displayed spectrum is the average of 10 spectra.

Modeling and Molecular Dynamics Simulations—A putative folded-back 1600–1723 monomer was modeled by including residues 1600–1675 from one crystallographic molecule (chain B) and residues 1680–1723 of the other (chain A). The four intervening residues 1676–1679 were added so as to be stereochemically reasonable. Homology modeling was performed with program MODELLER (43) release 9.14 with default parameters using the alignments shown in Fig. 5*A*. Molecular dynamics simulations of a crystallographic monomer (residues 1600–1722 of chain B) of the modeled folded-back monomer and of homology models corresponding to HSV-1 UL36 residues 1632–1723 were performed using the AMBER 9 program suite (44) with the Parm99SB force field. Hydrogen atoms were added, and proteins were neutralized with 2–4 Na^+ cations and immersed in an explicit TIP3P water box with a solvation shell at least 12 Å-deep using the LEaP program. The systems were then minimized and used to initiate molecular dynamics. All simulations were performed in the isothermal isobaric ensemble (p = 1 atm, T = 300 K), regulated with the Berendsen barostat and thermostat (45), using periodic boundary conditions and Ewald sums for treating long range electrostatic interactions (46). The hydrogen atoms were constrained to the equilibrium bond length using the SHAKE algorithm (47). A 2-fs time step for the integration of Newton's equations was used. The nonbonded cutoff radius of 10 Å was used. For targeted molecular dynamics simulations, the starting and target systems were built so as to be chemically identical (same protein residues, same number of water molecules). Targeted molecular dynamics adds an additional term to the energy function as shown in Equation 1,

$$E(t) = {}^1/_2 k_{\text{force}} \cdot N_{\text{atom}} (\text{r.m.s.d.}_t - \text{r.m.s.d.}_0)^2 \qquad \text{(Eq. 1)}$$

where k_{force} corresponds to the force constant applied during the simulation (kcal/mol·Å^2); N is the number of atoms; r.m.s.d. is the mass weighted root mean square deviation of the positions of protein Cα atoms at time t from the corresponding positions in the target structure. r.m.s.d.$_0$ is the target r.m.s.d. that was set to 0 here. All simulations were run with the SANDER module of the AMBER package.

RESULTS

Biophysical Characterization of UL36 Fragments—The boundaries of the structural domains of UL36 are so far unknown. Sequence analysis software predicts that several segments of UL36 (981–1035, 1292–1328, 1503–1532, 1586–1613, and 1710–1737) organize as coiled coils. All of them are localized within a 760-amino acid segment, suggesting it could correspond to a structural element. Consistent with this, we were able to express and purify a fragment of UL36 composed of residues 760–1733 in *E. coli* (Fig. 1*A*) containing these predicted coiled coil regions. The C-terminal part of this fragment 1600–1733 containing the last two repeats of a predicted helix-turn-helix motif could also be produced (Fig. 1*A*).

Coiled coils can be made of helices belonging to a single polypeptide, but they frequently constitute oligomerization regions. To check for a possible oligomerization, these fragments were analyzed by size exclusion chromatography associated with SEC-MALLS. Although 1600–1733 was less well behaved than 760–1733 and was not recovered quantitatively in SEC, it eluted as a single monomeric species (12.8 ± 0.2 kDa for an expected 14.8 kDa calculated from the fragment sequence) at an effective concentration of 30 μg/ml (Fig. 1*B*, *top*). At 70 μg/ml 760–1733 also eluted as a monomeric species (101.4 ± 0.2 kDa and 100.0 ± 0.1 kDa in two independent experiments for an expected 104.6 kDa) (Fig. 1*B*, *bottom*), but a minor form could also be detected, which in some preparations was in sufficient quantity for its mass to be accurately determined (Fig. 1*B*, *bottom, purple curve*). This mass of 217.3 ± 0.4 kDa is consistent with that of a dimer. The observation of distinct peaks shows that the conversion between monomeric and dimeric 760–1733 is not possible or is at least slower than the characteristic time scale of the experiment. Analytical ultracentrifugation (sedimentation equilibrium and sedimentation velocity) was performed at much higher protein concentrations for 760–1733. Sedimentation equilibrium experiments show that 760–1733 is still a monomer at least up to a concentration of 0.90 mg/ml (Fig. 1*C*).

Given that the inner tegument has been described as fibrous (3), there is a possibility that some or all of these fragments could be elongated. To characterize this, this fragment was analyzed by sedimentation velocity (Fig. 1*D*). A monomodal distribution corresponding to a 3.3 S species ($s_{20,w}$ = 3.5) was observed, and taking into account that 760–1733 is monomeric, it means that this fragment has a f/f_0 ratio of 2.3. This very high value can only be explained by an extremely elongated shape and is typically observed with fibrous proteins.

Because of its large size, fragment 760–1733 could be directly observed by negative staining electron microscopy, which confirms that it is an elongated fiber (Fig. 2, *A–D*). The length distribution of fibers is bimodal with a main population at 33.7 ± 5.5 nm and a minor population at 59.7 ± 2.3 nm, whereas the width distribution is monomodal with a single population at 2.9 ± 0.4 nm (Fig. 2*E*). Additionally, the shorter fibers were sometimes associated via one of their ends, thus constituting "V"-shaped objects (Fig. 2*D*).

The fibers are surprisingly straight for objects with such a large length to width ratio. Only a minority of fibers display one or two kinks separated with straight segments, suggesting that the fragment is made of several rods separated by a discrete number of articulations. At least in the conditions in which the observations were performed, the most extended conformation was dominant.

Crystal Structure of Fragment 1600–1733—To get more detailed information on this fiber, crystallization of the different fragments was undertaken. It was possible to determine the crystal structure of fragment 1600–1733 that crystallized in several different conditions. The two that allowed useful data collection yielded the same crystal form with almost superimposable asymmetric units despite a substantial difference in cell parameters (Table 1 and see under "Experimental Procedures"). The high resolution cutoffs of the two models were validated according to Diederichs and Karplus (40). The asymmetric unit contains two molecules, and residues 1600–1723 could be built for both. The two molecules are very similar, being almost identical over residues 1628–1723 and differing only in different bends of their N-terminal helices at residues 1624–1627. Additional amino acids left over from cleavage of the purification tag could also be observed at the N termini, extending the N-terminal helix of molecule B by five residues (*i.e.* all the residues left from the tag despite their sequence GPLGS having no helical propensity). In accordance to the biophysical analyses, each molecule appears as an elongated fiber about 120 Å long and with a maximal width between α carbons of ~15 Å. Each molecule is constituted by two repeats of a long helix-turn-antiparallel short helix motif, A-B and C-D (Fig. 3*A*). The intrachain contacts are extremely scarce and limited to two short regions. The first region involves residues 1633–1672, including the C-terminal part of helix A, the entire helix B, and the N-terminal part of helix C. This region organizes as a short three-helix bundle. The second region is constituted by the C-terminal part of helix C and the totality of helix D as well as β-like contacts in loop CD. Surprisingly, there is a cluster of exposed hydrophobic residues in both regions (Fig. 3*C*). The first one involves Leu-1636, Leu-1639, Leu-1640, Val-1642, Val-1643, Pro-1646, Ile-1662, and Leu-1669, whereas the second one involves Val-1684, Trp-1686, Leu-1687, Phe-1694, Leu-1709, Leu-1710, and Leu-1720. These hydrophobic residues are strongly conserved through alphaherpesviruses, suggesting that these surfaces have a structural and/or functional role (Fig. 3*B*).

Extended contacts are observed between the two molecules in the asymmetric unit (Fig. 4*A*). The two molecules are wrapped around each other, and they adopt an overall boomerang shape with the N terminus at the extremity and the C terminus in the center. This makes up an extremely elongated dimer with a length of 158 Å and a maximal width of 24 Å. The dimerization involves the formation of a long antiparallel coiled coil between the two C helices. Moreover, the two exposed

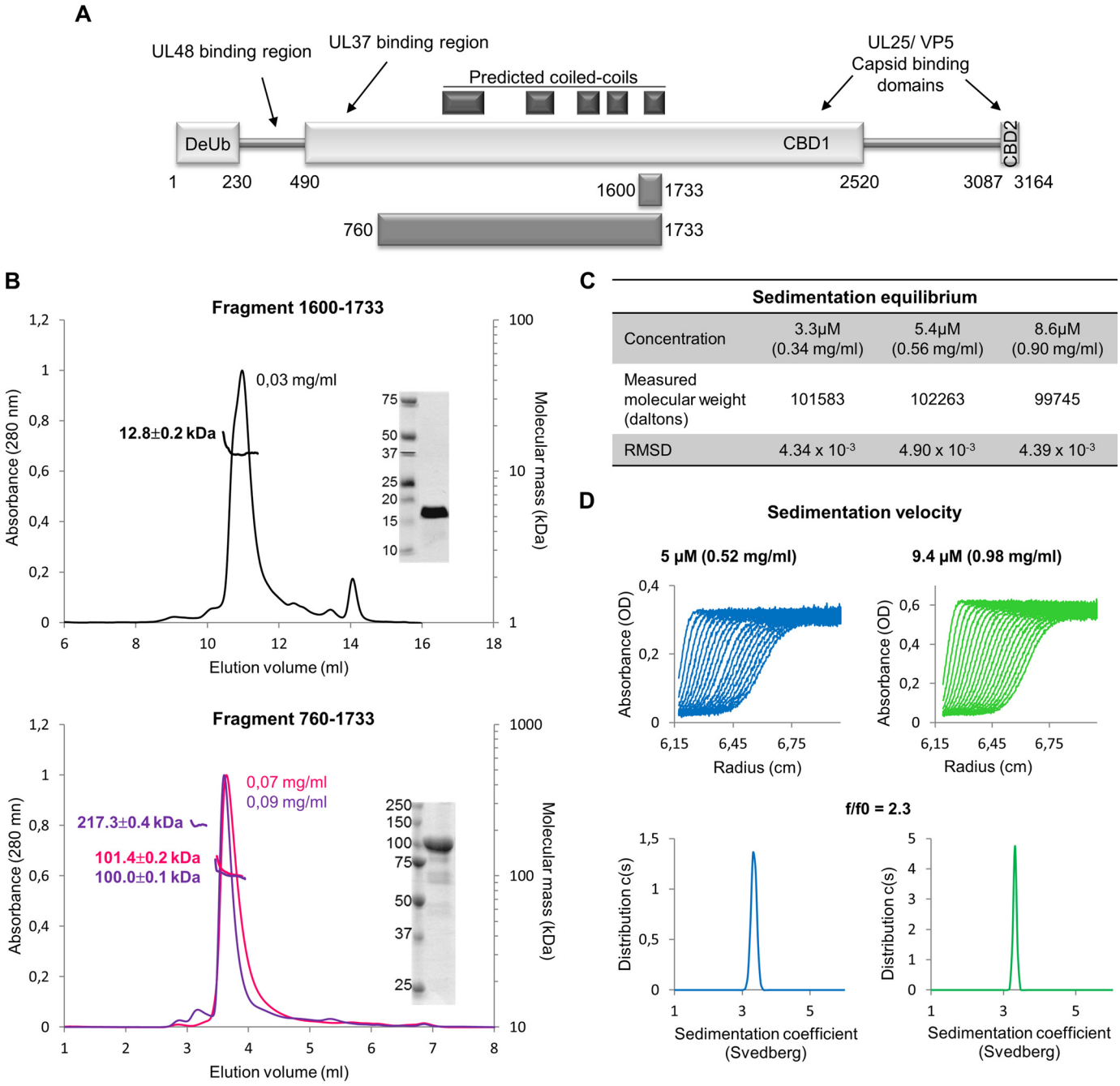

FIGURE 1. **Oligomeric status and shape of HSV-1 UL36 fragments in solution.** *A,* all secondary structure prediction servers predict the presence of three regions with a high propensity to form α-helices and β-strands (*rectangles*) and two large segments with a higher probability to be random coils (thin stretches 230–490 and 1520–3087). Reported interaction regions and predicted coiled coils are indicated. Two fragments, 1600–1733 and 760–1733, have been used in this work. *B,* SEC-MALLS analyses of fragments 1600–1733 (*top*) and 760–1733 (*bottom*). Two independent experiments are presented for fragment 760–1733. The protein concentrations at the peak are indicated. *Insets,* 4 μg of the purified proteins used in SEC-MALLS were analyzed by 16% (1600–1733) or 14% (760–1733) SDS-PAGE with Coomassie staining. *C,* molecular weight of fragment 760–1733 derived from sedimentation equilibrium ultracentrifugation at 3.3, 5.4, and 8.6 μM. *D,* sedimentation velocity experiment of fragment 760–1733 at 5 and 9.4 μM. The experimental curves obtained during a centrifugation at 40,000 rpm in an An-60Ti rotor (*top*) and the fitted data obtained after analyses by Sedfit (*bottom*) are represented.

hydrophobic surfaces of one monomer are now interacting with those of the other, thus constituting two new five-helix bundles involving helices A, B, and C of one monomer and helices C and D of the other monomer. The highly conserved Trp-1686 that would be completely exposed in the isolated monomer is now buried in a pocket of the other molecule (visible on Fig. 3*B*). It is engaged in multiple interchain hydrophobic contacts with Leu-1640, Val-1643, Val-1645, Pro-1646, Val-1649, Val-1666, and Leu-1669. The NH of the indole group is also involved in an intermolecular hydrogen bond with the carbonyl of Leu-1640 (Fig. 4*C*).

The NOXclass server (42) reports 2140 Å^2 of buried surface per molecule for this dimeric interface, accounting for 20% of the accessible surface. Taking into account the amino acid composition of the interface, the server assigns a 99.99% probability that the crystallographic dimer is biologically relevant. How-

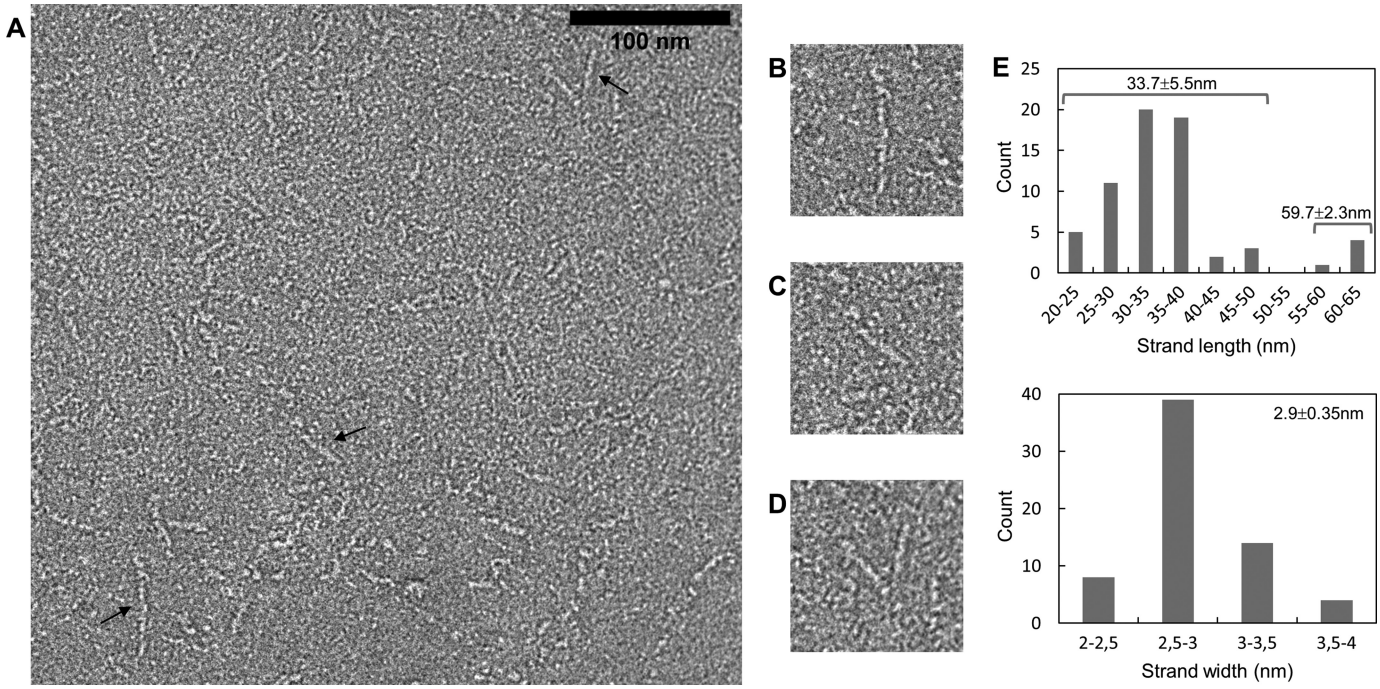

FIGURE 2. **Electron microscopy of fragment 760–1733.** *A–D,* negative staining observation. The *scale bar* for *A* has a length of 100 nm. Several different morphologies are observed. Objects indicated by a *black arrow* are enlarged in *B–D*. *E,* histograms of the measured lengths (*top*) and widths (*bottom*) of the fibers.

TABLE 1

Data collection and refinement statistics

Statistics for the highest resolution shell are shown in parentheses.

	Iodine derivative (SAD phasing) (4TT0)	Native (4TT1)
Resolution range (Å)	48.04–2.599 (2.692–2.599)	38.32–2.75 (2.848–2.75)
Space group	P 61 2 2	P 61 2 2
Unit cell *a, b, c*	110.939, 110.939, 154.93	110.217 110.217 159.939 90 90 120
α, β, γ	90, 90, 120	
Total reflections	208,952 (19,540)	198,088 (17,771)
Unique reflections	17,958 (1,728)	15,528 (1,500)
Multiplicity	11.6 (11.3)	12.8 (11.8)
Completeness (%)	99.97 (99.77)	99.94 (99.60)
Mean $I/\sigma(I)$	14.53 (1.80)	21.00 (1.59)
Wilson B-factor	48.76	76.69
R-merge	0.1792 (1.185)	0.09051 (1.604)
R-pim	0.053 (0.379)	0.026 (0.484)
CC1/2	0.997 (0.577)	1 (0.697)
R-work	0.1853 (0.2858)	0.1950 (0.3598)
R-free	0.2452 (0.3598)	0.2431 (0.4095)
CC*	0.999 (0.855)	1 (0.906)
CC(work)	0.950 (0.749)	0.973 (0.731)
CC(free)	0.926 (0.466)	0.945 (0.564)
No. of non-hydrogen atoms	2014	1942
Macromolecules	1941	1923
Ligands	42	10
Water	31	9
Protein residues	256	253
r.m.s. (bonds)	0.008	0.009
r.m.s. (angles)	0.97	1.14
Ramachandran favored (%)	98	97
Ramachandran allowed (%)	2	3
Ramachandran outliers (%)	0	0
Clashscore	6.57	3.34
Average B-factor	59.90	98.70
Macromolecules	59.70	98.50
Ligands	81.60	142.80
Solvent	42.90	91.20

ever, dimers can be either obligate or nonobligate, *i.e.* the dimer can be stable or it can be in equilibrium with monomers. Here, the calculated probability that it constitutes an obligate dimer is only 89.6%. Thus, the dimer might be a transient species, sensitive to external parameters.

In addition to this major interface, the PISA program (41) predicts no other contact in the crystals to be stable in solution. The second and third most prominent crystal contacts (burying 880 and 520 Å^2 per molecule, respectively) involve antiparallel coiled coils between helices A of two molecules B

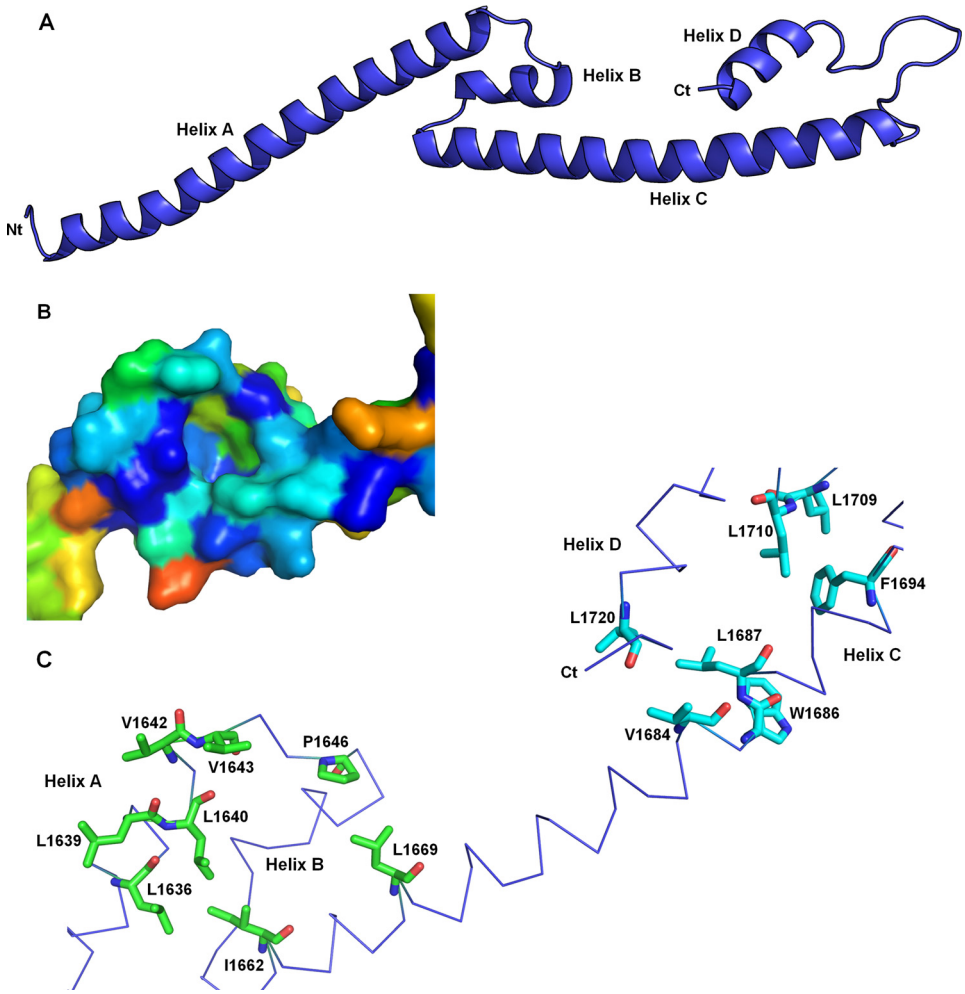

FIGURE 3. **Architecture of a single molecule of fragment 1600–1733.** *A,* four helices termed A, B, C, and D are observed in the crystal structure of fragment 1600–1733. The N-terminal extremity is on the left end, and the C terminus is on the right end. *B,* surface representation of the A-B-C three-helix bundle using the same orientation as in *C*. Residues are colored according to their conservation according to server Consurf from *blue* (fully conserved residues) to *red* (least conserved residues). The sequence alignment used by Consurf contained 136 representative sequences of alphaherpesvirus UL36. *C,* trace representation of residues 1636–1720. Two clusters of conserved and exposed hydrophobic residues are displayed as *sticks*. Residues buried in the dimer interface are colored by atom type (*red,* oxygen; *blue,* nitrogen; carbons, *green* and *cyan* in either hydrophobic patch).

and two molecules A, respectively. The contacts involving helices A are not identical in these two coiled coils, as there is one helical turn shift between the two. The larger buried surface for molecule B is due in part to additional contacts between helices A and C involving the N-terminal extremity of the fragment, including the residues stemming from the purification tag.

The crystallographic data strongly suggest that fragment 1600–1733 is dimeric, whereas the biophysical tools could only detect a monomer in solution. It could suggest that the crystallographic dimer is artifactual; however, it was crystallized under at least two highly different conditions, suggesting that this species is present in the preparation. The high concentration encountered during the crystallization process has then shifted the equilibrium toward this dimeric species. The structure of the main monomeric species is thus still unknown.

Many hydrophobic residues are exposed in the crystallographic monomer, although they are buried in the dimer where they constitute the hydrophobic core of an intermolecular structural domain. It is thus unlikely that the crystallographic monomer is the solution monomer without at least a major structural reorganization. To check for this hypothesis, we decided to take advantage of Trp-1686 that is the single tryptophan in the fragment. In the crystallographic monomer it is highly exposed, although it is completely buried in the dimer in a hydrophobic environment, except for the hydrogen bond between the NH of the side chain of Trp-1686 and the carbonyl of Leu-1640. A tryptophan fluorescence emission spectrum displays a maximum at a wavelength of 338 nm for fragment 1600–1733 (Fig. 4*B*) independently of the pH (between 6 and 8) and of the salt concentration (between 20 mM and 1 M NaCl). This is not consistent with a fully exposed tryptophan but is fully compatible with the environment observed in the dimer (48). Thus, the tryptophan in the solution monomer is similarly buried as in the crystallographic dimer.

The DALI server was used to detect whether the crystallographic and the model folded-back monomers were homologous to other proteins in the Protein Data Bank. The highest Z-score obtained for the crystallographic protomer corresponded to the copper-sensitive operon regulator (Z = 5.2).

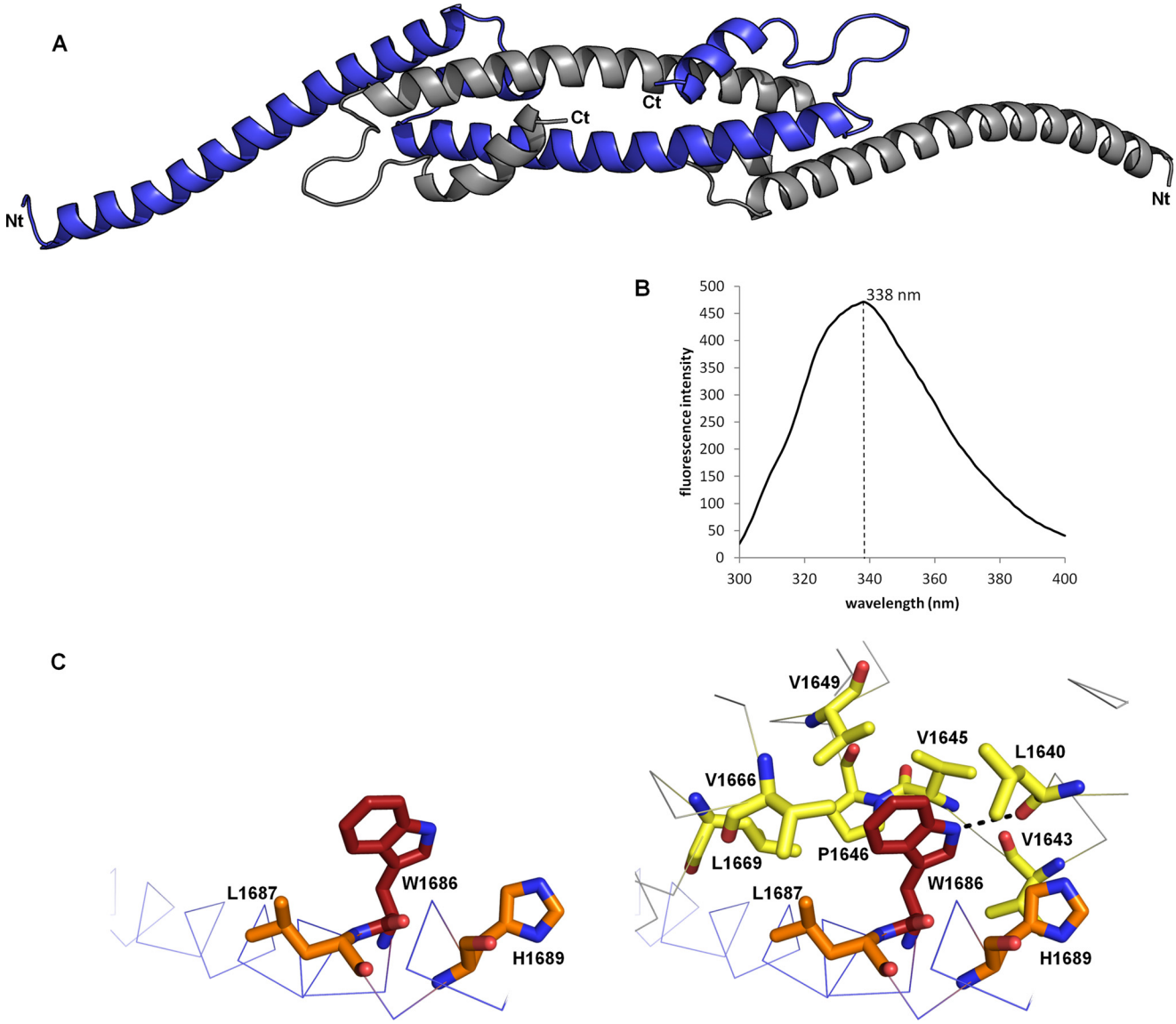

FIGURE 4. **Dimeric structure of fragment 1600–1733.** *A,* architecture of the crystallographic dimer. One monomer is colored in *blue* and the other one in *gray*. *B,* tryptophan fluorescence emission spectrum of fragment 1600–1733. The maximal emission was observed at a wavelength of 338 nm. The spectrum was recorded in a 50 mM Tris, pH 8, 200 mM NaCl buffer. Spectra with a maximum emission at 338 nm were recorded in all the tested buffers, including (50 mM Tris, pH 8, 20 mM to 1 M NaCl), (50 mM HEPES, pH 7, 200 mM NaCl), and (50 mM MES, pH 6, 200 mM NaCl). *C,* environment of tryptophan 1686 in the crystallographic monomer (*left*) and dimer (*right*). The residues with a side chain less than 4.5 Å away from the indole group of W1686_A (*red*) are represented as *orange* (chain A) or *yellow* (chain B) *sticks*. The interchain hydrogen bond between the nitrogen of the indole group of W1686_A and the carbonyl of L1640_B is displayed on the *right*.

However, a detailed analysis reveals that the homology only extends to helix A, which suggests that it is not relevant. Higher Z-scores were obtained for the model folded-back bulge, including the histone-lysine *N*-methyltransferase MLL (3LQH, Z = 6.6), the general control of amino acid synthesis protein 5 GCN5 (3D7C, Z = 6.2), and the human transcription intermediary factor 1α (1YYN, Z = 5.8). All these proteins belong to the bromodomain family. This domain only contains four helices, whereas fragment 1600–1733 has five helices. However, MLL displays an additional segment at the expected position for helix D of fragment 1600–1733, suggesting that the 1600–1733 belongs to this family.

Modeling of the UL36 1600–1733 Monomer and Molecular Dynamics Simulations—The contacts between both monomers involve the two five-helix bundles, but there is a break in the contacts between helices C at their center close to the non-crystallographic 2-fold axis. The last interchain contact on either side of the break involves a salt bridge between Arg-1677 and Asp-1680. However, this region is not strictly conserved; Arg-1677 may be replaced by a lysine in gallid herpesvirus 2 (GHV-2), an alanine in cercopithecine herpesvirus 1 (CHV-1), and a proline in PRV. An even more severe mutation is observed in varicella zoster virus where a glycine is inserted (Fig. 5*A*). These mutations are hardly compatible with a continuous helix C extending from residue 1659 to residue 1696, but it is compatible with two smaller helices separated by a short linker around residue 1677. Taken together, these data suggest that these residues are not necessarily folded as a helix turn as it is the case in the crystal structure and could constitute a conformational switch.

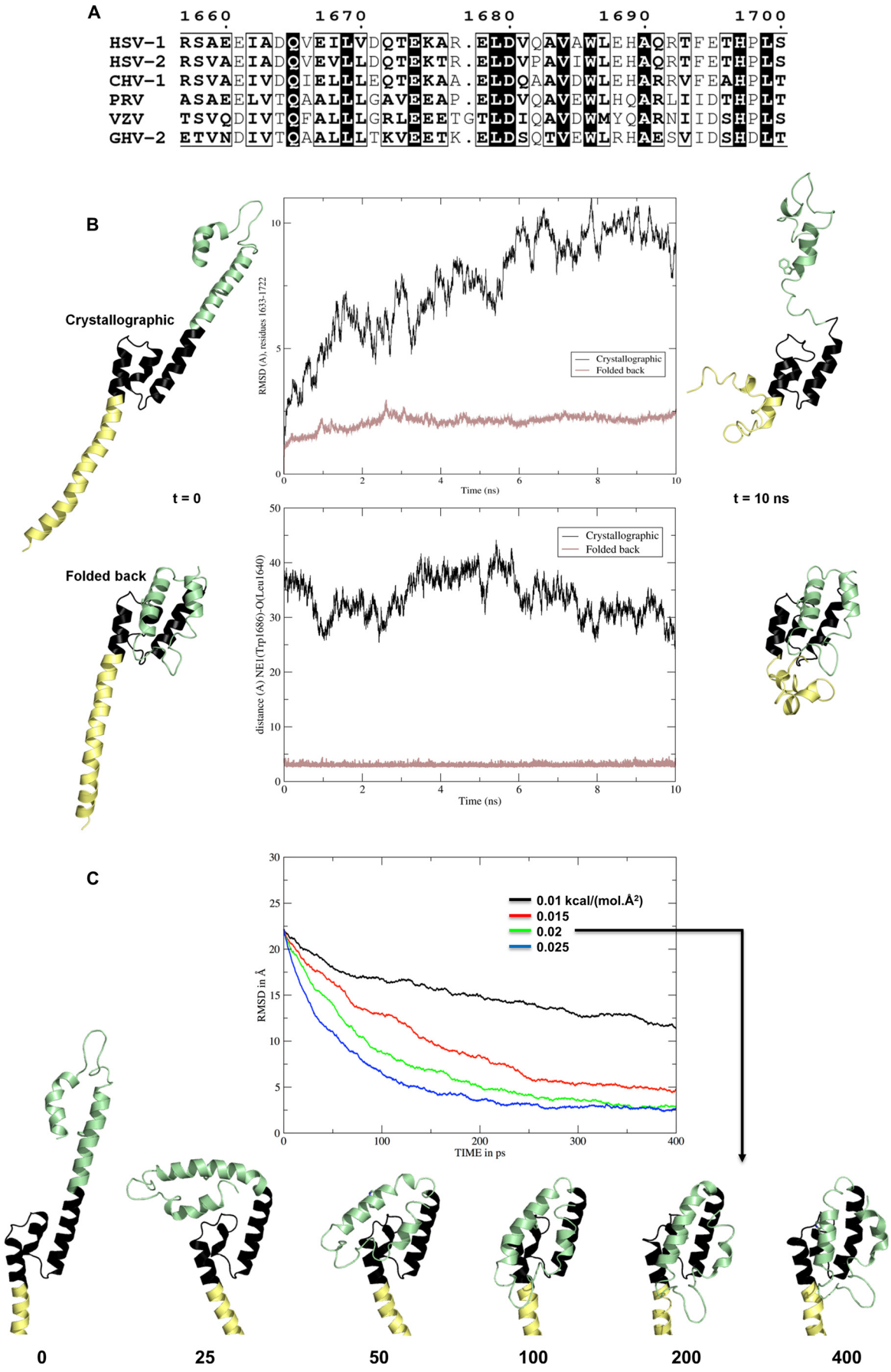

A chimera constituted by residues 1600–1675 of molecule A and 1680–1733 of molecule B would be geometrically possible while explaining the otherwise discordant results. Indeed, residues 1675 of one chain and 1680 of the other chain are sufficiently close (11 Å between their Cα) for the intervening residues 1676 and 1679 to loop between them. The chimera would be monomeric in solution, given that there would not be any interchain contact anymore. Trp-1686 would still be buried as indicated by the tryptophan fluorescence analysis. Under this conformation, fragment 1600–1733 would have a lollipop shape with the N terminus of helix A constituting the stalk and a five-helix bundle made of the C terminus of helix A, the two parts of former helix C and helices B and D, constituting the bulge (Fig. 5*B*, *bottom left*).

To test this hypothesis, we performed all atom molecular dynamics simulations in explicit solvent of such a folded-back lollipop model. In parallel, we also simulated the dynamics of the isolated extended crystallographic molecule. The small central three-helix bundle 1633–1670 (in *black* on Fig. 5*B*) is quite stable whether in the extended or folded-back molecule. After 10 ns of simulation, it is little changed in both and thus still displays the hydrophobic patch that is prominent in the crystallographic dimer interaction, including the Trp-1686 pocket (Figs. 3*B* and 4*C*). In contrast, the N-terminal helix A upstream of Leu-1633 (in *yellow* on Fig. 5*B*) breaks up in both simulations. This is consistent with its observed static flexibility in the two crystallographic molecules (see above). The major difference between the two simulations lies in the C-terminal part downstream of residue 1673 (*green* on Fig. 5*B*). The starting helix C of the extended molecule breaks at residues 1673–1685, whereas the folded-back molecule remains stable over the whole C terminus. Thus, the r.m.s.d. of all atoms for residues 1633–1722 quickly stabilizes at a value below 2.5 Å for the latter molecule, although it rises above 10 Å and has not converged after 10 ns for the extended crystallographic molecule (Fig. 5*B*, *top center*). Similarly, Trp-1686 remains buried and in hydrogen bonding distance of Leu-1640 throughout the simulation for the folded-back molecule, whereas it goes from 38 Å to below 25 Å for the extended molecule and has not yet stabilized after 10 ns. These results confirm that the crystallographic molecule is not the 1600–1733 solution monomer, whereasthe folded-back molecule could be. They further highlight residues 1633–1670 and to a lesser extent 1686–1720 as folding units capable of forming together a stable five-helix bundle. In contrast, the middle of helix C (residues 1673–1685) and the N terminus of helix A (residues 1600–1633) are clearly not stable in solution in the absence of stabilizing contacts. To establish whether extended and folded-back monomers can spontaneously interconvert, we performed targeted molecular dynamics simulations between the two conformations, starting from one and taking the other as the target. Even a very weak force of 0.02 kcal/(mol·Å^2) is sufficient to guide conversion toward the folded-back conformation (Fig. 5*C*). Conversion back from the folded-back conformation is also readily accomplished, although at slightly higher force constant values (data not shown). This indicates that there is no large energy barrier between the observed and hypothesized conformations. Finally the energies of the two chemically identical systems are $-2.474{,}1\ 10^5$ kcal/mol (extended) and $-2.483{,}5\ 10^5$ kcal/mol (folded back). These small differences are consistent with an equilibrium, and one favoring the folded-back conformation.

Finally, we further probed the interconversion hypothesis and sought to extend our results to other alphaherpesviruses by producing homology models taking HSV-1 UL36 residues 1632–1723 as template for HSV-2, PRV, VZV, and the avian alphaherpesvirus GHV-2 (Fig. 6*A*). The extended models (Fig. 6*A*, *top*) illustrate that a straight helix C is indeed not to be found in PRV and VZV and also not in HSV-2 (despite 84% sequence identity) due to the HSV-2 Q1682P substitution (Fig. 5*A*). Molecular dynamics simulations of these extended molecules show the same features as described for the crystallographic HSV-1 monomer, namely instability of helix C and stability of the two helix bundles on either side. In contrast, the folded-back monomer can be modeled with little deviation from the HSV-1 template (Fig. 6*A*, *bottom*). The largest difference is found in PRV, in which a two-residue deletion prevents straight modeling of helix B either for the extended or folded-back monomer (Fig. 6*A*). As exemplified by the case of GHV-2 (despite only 35% sequence identity to HSV-1 UL36 fragment 1632–1723), the modeled structures are stable over 10 ns of simulation in each case. The conserved counterpart of Trp-1686 is inserted into a hydrophobic pocket with its hydrogen bond to the counterpart of Leu-1640 maintained throughout the simulation (Fig. 6*B*). In the case of PRV, only the pocket as modeled is not complete, although it is completely closed and stable in the other three cases.

DISCUSSION

The structural data presented in this study reveal that a fragment of HSV-1 UL36 comprising residues 760–1733 adopts a very elongated conformation. The major species is a stalk conformation with a length of 34 nm and a width of 2.9 nm. A smaller subpopulation of 760–1733 appeared to be even longer with an average length of 60 nm. It could either reveal a conformational change between an extended 60-nm monomeric species and a 34-nm hairpin conformation or a rare dimerization of two 34-nm monomeric fragments via one of their extremities. No significant width difference could be measured between the 34- and 60-nm species, arguing in favor of the second hypothesis.

FIGURE 5. **Stability of crystallographic and folded-back models of fragment 1600–1733 and interconversion between them.** *A,* sequence conservation in alphaherpesviruses for helix C (residues 1659–1696 in the crystal structure of 1600–1733). *B,* molecular dynamics simulations for a crystallographic molecule and a putative monomer folded back at residues 1676–1679. Both systems were neutralized, hydrated in explicit solvent, and minimized. Protein structures are displayed as ribbons at the beginning (*left*) and the end (*right*) of the 10-ns production time. They are aligned on the stable central three-helix bundle (residues 1633–1675, colored *black*). Residues N-terminal to 1633–1675 are colored *pale yellow,* and the C-terminal residues are colored *pale green*, including Trp-1686, whose side chain is displayed as *sticks*. *Middle panels,* change over time for the crystallographic molecule (*black lines*) and the folded-back model (*salmon lines*) of the r.m.s.d. for all atoms in residues 1633–1722 (*top*) and of the distance between Trp-1686 Nϵ and Leu-1640 O (*bottom*). *C,* targeted molecular dynamics simulations between the observed and modeled conformers. *Top,* all atom r.m.s.d. between the simulated, initially extended molecule and the folded-back target for four values of the force constant a·Å^2). The time points are indicated *below* the structures.

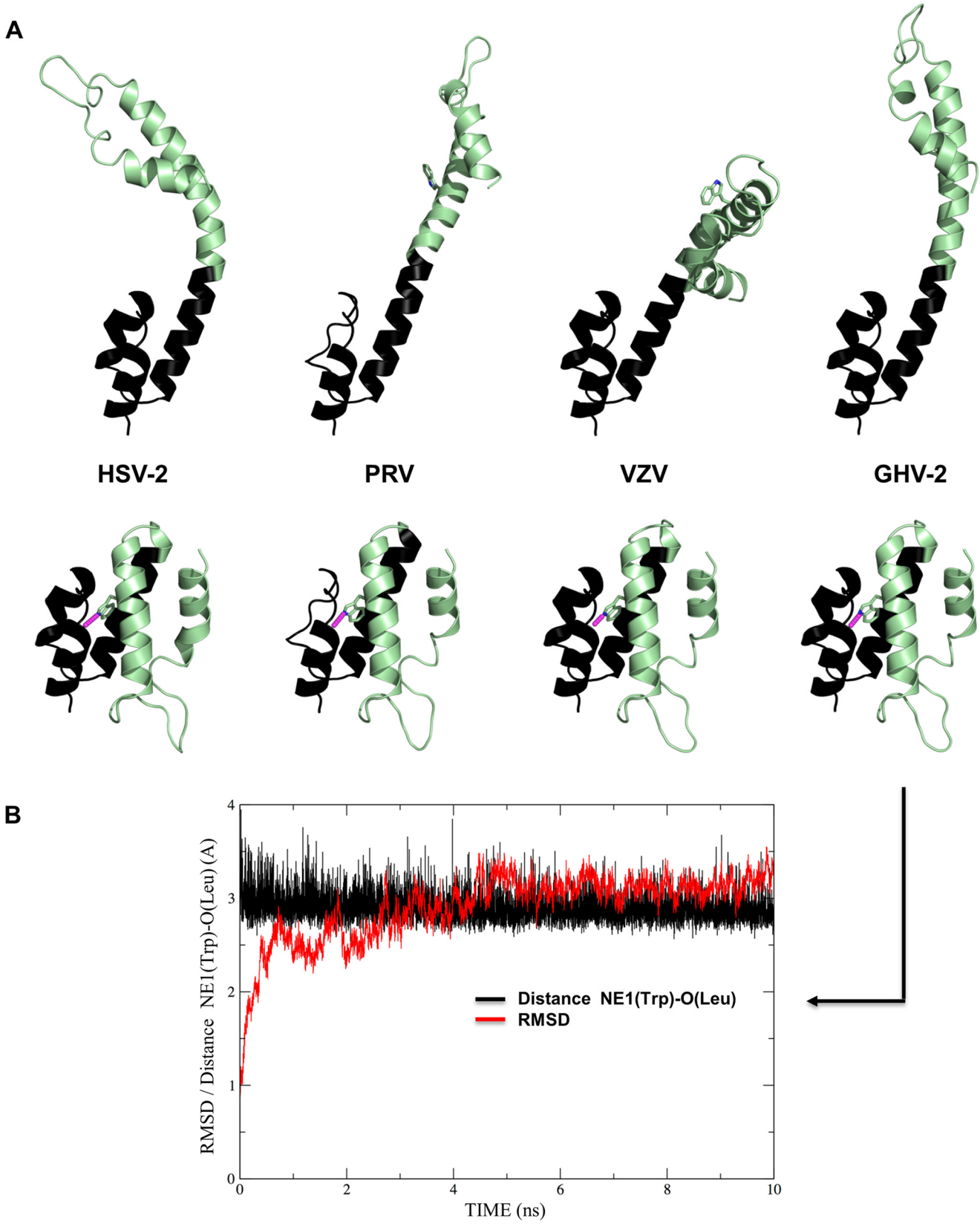

FIGURE 6. **Homology modeling taking residues 1632–1723 of HSV-1 UL36 as templates for other alphaherpesviruses.** *A,* models for HSV-2, VZV, PRV, and GHV-2. *Top,* based on the crystallographic molecule, only the avian GHV-2 fragment can be modeled in a similar conformation. *Bottom,* in contrast, models are readily generated that closely match the folded-back monomer for all viruses. The single tryptophan finds a hydrophobic pocket and hydrogen bonds (displayed in *magenta*) to the same leucine as in the HSV-1 template. *B,* stability of this hydrogen bond and r.m.s.d. for all atoms in a 10-ns molecular dynamics simulation for GHV-2 folded-back monomer.

The measured lengths for UL36 residues 760–1733 have to be compared with the dimensions of the elongated tufts detected at the surface of T36 particles (3). The width of fragment 760–1733 observed by electron microscopy and the width of the five helix bundle in the folded-back model of fragment 1600–1733 are close to the main peak of the distribution (2.9 nm). Moreover, the 760–1733 fragment has a length of 34 nm, whereas the tuft distribution shows three main peaks at 28, 45, and 67.8 nm. Thus, the similar width is compatible with the 760–1733 fragment constituting a major part of the T36 tufts. However, the significantly larger lengths measured for the T36 tufts suggest that the 760–1733 cannot be their sole constituent and that it must also contain other parts of UL36 or UL37. Interestingly, secondary structure predictions suggest that the region between residues 520 and 1920 is a succession of helices separated by short loops, implying that the entire 520–1920 part of UL36 could constitute a very long stalk in the middle of the protein.

The presence of this stalk would divide the entire protein in three main regions. The N-terminal part of the protein contains the deubiquitinase domain, the binding sites to the outer tegument protein UL48 (27) and UL37 (49) and an essential nuclear localization signal (50). The C terminus of UL36 contains the two capsid-binding sites. The intermediate fiber would provide a long stalk between the two extremities. Although the amino acid conservation in the stalk of UL36 is significantly lower than in other parts of UL36 such as the deubiquitinase domain and the capsid-binding sites, it has to be noted that the length of sequence is conserved across all three families of herpesviruses, suggesting that a precise length for UL36 could be an essential property of the protein.

Unexpectedly, the 1600–1733 fragment exists under at least two different conformations, a main monomeric and a minority dimeric species that could be crystallized. Molecular dynamics simulations show that the folded-back monomer is stable at least at the 10-ns scale. In contrast, the intervening region is unstable in the crystallographic monomer, but the 1633–1720 five-helix bundle of the folded-back monomer does not undergo any large rearrangement. Moreover, the folded-back monomer is in agreement with the different analyses in solution, which strongly suggests that it is the main species in solution. Of note, this organization still makes a very extended molecule (80 Å long over 122 residues) while strengthening its local structure, in accordance with the observed stiffness of fragment 760–1733.

In addition to a possible role during assembly, these elongated fibers could be involved in the other main functions of UL36, including capsid transport. Molecular motors typically contain a long arm connecting the motor and cargo-binding domains, thus limiting hindrance between a possible large cargo and the cytoskeleton. Given that UL36 cross-links the viral capsids to kinesin motors, the presence of this stalk could further increase the distance between the capsid and the microtubule, depending on the location of the UL36 kinesin-binding motif. However, in the case of PRV, the complex dynein binding motif of UL36 is bipartite and involves both the first 1285 amino acids of UL36 (corresponding to residues 1–1610 of HSV-1 UL36) and the large C-terminal proline-rich domain, thus suggesting that capsid transport is possible if the molecular motor binding domains are in the C terminus of UL36 (20).

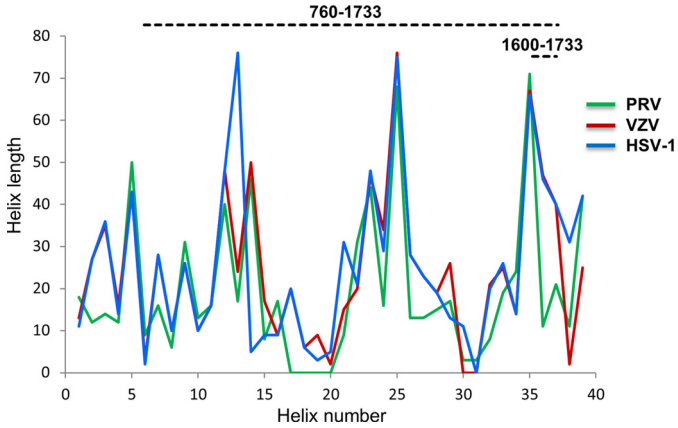

FIGURE 7. **Secondary structure of the central stalk is strongly constrained across alphaherpesvirinae.** The secondary structures of fragments 584–1836 of HSV-1 (*blue*), 522–1708 of VZV (*red*), and 398–1419 of PRV (*green*) UL36 were predicted using SOPMA. Plotted are the predicted lengths of successive helices (numbered 1–39 from N to C terminus) in these fragments. Three insertions are plotted as helices of length 0 in viruses where they are not present (helices 17–20 in PRV, helix 31 in HSV-1, and helices 30–31 in VZV). The HSV-1 and VZV curves are superimposed between helix numbers 4 and 12.

Finally, the thermosensitive HSV-1 UL36 Y1453H mutation (51, 52) is worth reconsidering in the light of our high resolution structural data. This single mutation is sufficient for decreasing the virus production by 5 logs in plaque formation and induces a complex phenotype. During the entry phases, an accumulation of capsid at the nuclear pore is observed, but the viral genome is not efficiently released, and the production of viral proteins is reduced, suggesting that the transport phase has not been altered but that the DNA ejection into the nucleus is impaired. An additional defect in the later stages of the virus cycle is also present (51, 52). At least one and possibly more essential functions of UL36 have thus been altered in a temperature-dependent manner by this single mutation. If the UL36 stalk indeed contains strengthening nodes along its length similar to the one we modeled around Trp-1686, a substitution such as Y1453H could lead to destabilization of one such node, thus inducing a temperature-dependent loss of stiffness. As a consequence, the relative positions of the two extremities of the multifunctional UL36 would be affected, thus inducing a complex thermosensitive phenotype.

The data presented here are probably relevant across all alphaherpesviruses. Sequence conservation is sufficient for accurate homology modeling even to avian alphaherpesviruses based on our crystal structure for residues 1632–1723. Such modeling shows that the two halves of the bulge are complementary across alphaherpesviruses, arguing for a functional interface underlying monomeric folding, dimeric interface, or both. Despite overall low amino acid conservation in other parts of the 760–1733 segment, it is striking that UL36 proteins from all alphaherpesviruses are all predicted to contain a long segment with a high α-helical content in their central part. Moreover, despite fairly low sequence identity, the sizes and order of the predicted helices seem to be strongly constrained, suggesting that the fiber-like structural element presented here

could be an essential feature conserved among all alphaherpesviruses (Fig. 7). It is likely that this fiber is also present in other herpesviruses, but the amino acid conservation in this region is not sufficient for performing reliable sequence alignments. However, the presence of multiple amphipathic helices with a characteristic 4-3-4 spacing of hydrophobic residues is predicted in UL36 from all three families of herpesviruses over a 1000–1200-amino acid-long segment corresponding to residues 760–1733 of UL36 HSV-1. This suggests that this fiber is a strongly conserved element even if its amino acid sequence is much less constrained. Interestingly, it has been recently shown that the homologous protein in the human cytomegalovirus also has a fibrous shape (53). There could thus be a strong evolutionary pressure for maintaining a precise organization of the protein with a central fiber bridging capsid binding elements at the C-terminal end and membrane-interacting elements at the N-terminal end.

Acknowledgments—We are grateful to the ESRF and SOLEIL Synchrotron facilities for allocation of beamtime and especially to Beatriz Guimaraes for help in data collection. We thank Malika Ouldali for help in electron microscopy imaging. We thank Paloma Fernandez-Varela, Christophe Velours, and Karine Madiona of the Structural and Proteomic Biology pole of the IMAGIF integrated platform for the SEC-MALLS and analytical ultracentrifugation experiments. We acknowledge Ines Gallay of the core platform "Cristallisation et Determination de la Structure 3D" (IBBMC, Paris Sud) for crystallization of the 1600–1733 fragment. We also acknowledge Thibaut Leger and Camille Gracia of the "Plateforme Protéomique Structurale et Fonctionnelle/Spectrométrie de Masse de l'Institut Jacques-Monod" for the mass spectrometry analysis of fragments 760–1733 and 1600–1733.

REFERENCES

1. Chen, D. H., Jiang, H., Lee, M., Liu, F., and Zhou, Z. H. (1999) Three-dimensional visualization of tegument/capsid interactions in the intact human cytomegalovirus. *Virology* **260,** 10–16
2. Grünewald, K., Desai, P., Winkler, D. C., Heymann, J. B., Belnap, D. M., Baumeister, W., and Steven, A. C. (2003) Three-dimensional structure of herpes simplex virus from cryo-electron tomography. *Science* **302,** 1396–1398
3. Newcomb, W. W., and Brown, J. C. (2010) Structure and capsid association of the herpesvirus large tegument protein UL36. *J. Virol.* **84,** 9408–9414
4. Zhou, Z. H., Chen, D. H., Jakana, J., Rixon, F. J., and Chiu, W. (1999) Visualization of tegument-capsid interactions and DNA in intact herpes simplex virus type 1 Virions. *J. Virol.* **73,** 3210–3218
5. Aggarwal, A., Miranda-Saksena, M., Boadle, R. A., Kelly, B. J., Diefenbach, R. J., Alam, W., and Cunningham, A. L. (2012) Ultrastructural visualization of individual tegument protein dissociation during entry of herpes simplex virus 1 into human and rat dorsal root ganglion neurons. *J. Virol.* **86,** 6123–6137
6. Antinone, S. E., Zaichick, S. V., and Smith, G. A. (2010) Resolving the assembly state of herpes simplex virus during axon transport by live-cell imaging. *J. Virol.* **84,** 13019–13030
7. Granzow, H., Klupp, B. G., and Mettenleiter, T. C. (2005) Entry of pseudorabies virus: an immunogold-labeling study. *J. Virol.* **79,** 3200–3205
8. Luxton, G. W., Haverlock, S., Coller, K. E., Antinone, S. E., Pincetic, A., and Smith, G. A. (2005) Targeting of herpesvirus capsid transport in axons is coupled to association with specific sets of tegument proteins. *Proc. Natl. Acad. Sci. U.S.A.* **102,** 5832–5837
9. Klupp, B. G., Fuchs, W., Granzow, H., Nixdorf, R., and Mettenleiter, T. C. (2002) Pseudorabies virus UL36 tegument protein physically interacts with the UL37 protein. *J. Virol.* **76,** 3065–3071
10. Vittone, V., Diefenbach, E., Triffett, D., Douglas, M. W., Cunningham, A. L., and Diefenbach, R. J. (2005) Determination of interactions between tegument proteins of herpes simplex virus type 1. *J. Virol.* **79,** 9566–9571
11. Coller, K. E., Lee, J. I., Ueda, A., and Smith, G. A. (2007) The capsid and tegument of the alphaherpesviruses are linked by an interaction between the UL25 and VP1/2 proteins. *J. Virol.* **81,** 11790–11797
12. Lee, J. I., Luxton, G. W., and Smith, G. A. (2006) Identification of an essential domain in the herpesvirus VP1/2 tegument protein: the carboxy terminus directs incorporation into capsid assemblons. *J. Virol.* **80,** 12086–12094
13. Pasdeloup, D., Blondel, D., Isidro, A. L., and Rixon, F. J. (2009) Herpesvirus capsid association with the nuclear pore complex and viral DNA release involve the nucleoporin CAN/Nup214 and the Capsid protein pUL25. *J. Virol.* **83,** 6610–6623
14. Radtke, K., Kieneke, D., Wolfstein, A., Michael, K., Steffen, W., Scholz, T., Karger, A., and Sodeik, B. (2010) Plus- and minus-end directed microtubule motors bind simultaneously to herpes simplex virus capsids using different inner tegument structures. *PLoS Pathog.* **6,** e1000991
15. Luxton, G. W., Lee, J. I., Haverlock-Moyns, S., Schober, J. M., and Smith, G. A. (2006) The pseudorabies virus VP1/2 tegument protein is required for intracellular capsid transport. *J. Virol.* **80,** 201–209
16. Pasdeloup, D., Labetoulle, M., and Rixon, F. J. (2013) Differing effects of herpes simplex virus 1 and pseudorabies virus infections on centrosomal function. *J. Virol.* **87,** 7102–7112
17. Sandbaumhüter, M., Döhner, K., Schipke, J., Binz, A., Pohlmann, A., Sodeik, B., and Bauerfeind, R. (2013) Cytosolic herpes simplex virus capsids not only require binding inner tegument protein pUL36 but also pUL37 for active transport prior to secondary envelopment. *Cell. Microbiol.* **15,** 248–269
18. McElwee, M., Beilstein, F., Labetoulle, M., Rixon, F. J., and Pasdeloup, D. (2013) Dystonin/BPAG1 promotes plus-end-directed transport of herpes simplex virus 1 capsids on microtubules during entry. *J. Virol.* **87,** 11008–11018
19. Pasdeloup, D., McElwee, M., Beilstein, F., Labetoulle, M., and Rixon, F. J. (2013) Herpesvirus tegument protein pUL37 interacts with dystonin/BPAG1 to promote capsid transport on microtubules during egress. *J. Virol.* **87,** 2857–2867
20. Zaichick, S. V., Bohannon, K. P., Hughes, A., Sollars, P. J., Pickard, G. E., and Smith, G. A. (2013) The herpesvirus VP1/2 protein is an effector of dynein-mediated capsid transport and neuroinvasion. *Cell Host Microbe* **13,** 193–203
21. Abaitua, F., Hollinshead, M., Bolstad, M., Crump, C. M., and O'Hare, P. (2012) A nuclear localization signal in herpesvirus protein VP1–2 is essential for infection via capsid routing to the nuclear pore. *J. Virol.* **86,** 8998–9014
22. Copeland, A. M., Newcomb, W. W., and Brown, J. C. (2009) Herpes simplex virus replication: roles of viral proteins and nucleoporins in capsid-nucleus attachment. *J. Virol.* **83,** 1660–1668
23. Jovasevic, V., Liang, L., and Roizman, B. (2008) Proteolytic cleavage of VP1–2 is required for release of herpes simplex virus 1 DNA into the nucleus. *J. Virol.* **82,** 3311–3319
24. Roberts, A. P., Abaitua, F., O'Hare, P., McNab, D., Rixon, F. J., and Pasdeloup, D. (2009) Differing roles of inner tegument proteins pUL36 and pUL37 during entry of herpes simplex virus type 1. *J. Virol.* **83,** 105–116
25. Desai, P. J. (2000) A null mutation in the UL36 gene of herpes simplex virus type 1 results in accumulation of unenveloped DNA-filled capsids in the cytoplasm of infected cells. *J. Virol.* **74,** 11608–11618
26. Fuchs, W., Klupp, B. G., Granzow, H., and Mettenleiter, T. C. (2004) Essential function of the pseudorabies virus UL36 gene product is independent of its interaction with the UL37 protein. *J. Virol.* **78,** 11879–11889
27. Ko, D. H., Cunningham, A. L., and Diefenbach, R. J. (2010) The major determinant for addition of tegument protein pUL48 (VP16) to capsids in herpes simplex virus type 1 is the presence of the major tegument protein pUL36 (VP1/2). *J. Virol.* **84,** 1397–1405
28. Svobodova, S., Bell, S., and Crump, C. M. (2012) Analysis of the interaction

between the essential herpes simplex virus 1 tegument proteins VP16 and VP1/2. *J. Virol.* **86,** 473–483
29. Jambunathan, N., Chouljenko, D., Desai, P., Charles, A.-S., Subramanian, R., Chouljenko, V. N., and Kousoulas, K. G. (2014) Herpes simplex virus 1 protein UL37 interacts with viral glycoprotein gK and membrane protein UL20 and functions in cytoplasmic virion envelopment. *J. Virol.* **88,** 5927–5935
30. Kattenhorn, L. M., Korbel, G. A., Kessler, B. M., Spooner, E., and Ploegh, H. L. (2005) A deubiquitinating enzyme encoded by HSV-1 belongs to a family of cysteine proteases that is conserved across the family herpesviridae. *Mol. Cell* **19,** 547–557
31. Schlieker, C., Korbel, G. A., Kattenhorn, L. M., and Ploegh, H. L. (2005) A deubiquitinating activity is conserved in the large tegument protein of the herpesviridae. *J. Virol.* **79,** 15582–15585
32. Bolstad, M., Abaitua, F., Crump, C. M., and O'Hare, P. (2011) Autocatalytic activity of the ubiquitin-specific protease domain of herpes simplex virus 1 VP1–2. *J. Virol.* **85,** 8738–8751
33. Wang, S., Wang, K., Li, J., and Zheng, C. (2013) Herpes simplex virus 1 ubiquitin-specific protease UL36 inhibits β interferon production by deubiquitinating TRAF3. *J. Virol.* **87,** 11851–11860
34. Schlieker, C., Weihofen, W. A., Frijns, E., Kattenhorn, L. M., Gaudet, R., and Ploegh, H. L. (2007) Structure of a herpesvirus-encoded cysteine protease reveals a unique class of deubiquitinating enzymes. *Mol. Cell* **25,** 677–687
35. Kabsch, W. (2010) XDS. *Acta Crystallogr. D Biol. Crystallogr.* **66,** 125–132
36. Sheldrick, G. M. (2008) A short history of SHELX. *Acta Crystallogr. A* **64,** 112–122
37. Adams, P. D., Afonine, P. V., Bunkóczi, G., Chen, V. B., Davis, I. W., Echols, N., Headd, J. J., Hung, L.-W., Kapral, G. J., Grosse-Kunstleve, R. W., McCoy, A. J., Moriarty, N. W., Oeffner, R., Read, R. J., Richardson, D. C., *et al.* (2010) PHENIX: a comprehensive Python-based system for macromolecular structure solution. *Acta Crystallogr. D Biol. Crystallogr.* **66,** 213–221
38. Collaborative Computational Project No. 4 (1994) The CCP4 suite: programs for protein crystallography. *Acta Crystallogr. D Biol. Crystallogr.* **50,** 760–763
39. Emsley, P., Lohkamp, B., Scott, W. G., and Cowtan, K. (2010) Features and development of Coot. *Acta Crystallogr. D Biol. Crystallogr.* **66,** 486–501
40. Diederichs, K., and Karplus, P. A. (2013) Better models by discarding data? *Acta Crystallogr. D Biol. Crystallogr.* **69,** 1215–1222
41. Krissinel, E., and Henrick, K. (2007) Inference of macromolecular assemblies from crystalline state. *J. Mol. Biol.* **372,** 774–797
42. Zhu, H., Domingues, F. S., Sommer, I., and Lengauer, T. (2006) NOXclass: prediction of protein-protein interaction types. *BMC Bioinformatics* **7,** 27
43. Sali, A., and Blundell, T. L. (1993) Comparative protein modelling by satisfaction of spatial restraints. *J. Mol. Biol.* **234,** 779–815
44. Case, D. A., Cheatham, T. E., 3rd, Darden, T., Gohlke, H., Luo, R., Merz, K. M., Jr., Onufriev, A., Simmerling, C., Wang, B., and Woods, R. J. (2005) The Amber biomolecular simulation programs. *J. Comput. Chem.* **26,** 1668–1688
45. Berendsen, H. J., Postma, J. P., Gunsteren, W. F. van DiNola, A., and Haak, J. R. (1984) Molecular dynamics with coupling to an external bath. *J. Chem. Phys.* **81,** 3684–3690
46. Darden, T., York, D., and Pedersen, L. (1993) Particle mesh Ewald: An *N*·log(*N*) method for Ewald sums in large systems. *J. Chem. Phys.* **98,** 10089–10092
47. Ryckaert, J.-P., Ciccotti, G., and Berendsen, H. J. (1977) Numerical integration of the cartesian equations of motion of a system with constraints: molecular dynamics of *n*-alkanes. *J. Comput. Phys.* **23,** 327–341
48. Shen, C., Menon, R., Das, D., Bansal, N., Nahar, N., Guduru, N., Jaegle, S., Peckham, J., and Reshetnyak, Y. K. (2008) The protein fluorescence and structural toolkit: Database and programs for the analysis of protein fluorescence and structural data. *Proteins* **71,** 1744–1754
49. Mijatov, B., Cunningham, A. L., and Diefenbach, R. J. (2007) Residues F593 and E596 of HSV-1 tegument protein pUL36 (VP1/2) mediate binding of tegument protein pUL37. *Virology* **368,** 26–31
50. Abaitua, F., and O'Hare, P. (2008) Identification of a highly conserved, functional nuclear localization signal within the N-terminal region of herpes simplex virus type 1 VP1–2 tegument protein. *J. Virol.* **82,** 5234–5244
51. Abaitua, F., Souto, R. N., Browne, H., Daikoku, T., and O'Hare, P. (2009) Characterization of the herpes simplex virus (HSV)-1 tegument protein VP1–2 during infection with the HSV temperature-sensitive mutant tsB7. *J. Gen. Virol.* **90,** 2353–2363
52. Abaitua, F., Daikoku, T., Crump, C. M., Bolstad, M., and O'Hare, P. (2011) A single mutation responsible for temperature-sensitive entry and assembly defects in the VP1–2 protein of herpes simplex virus. *J. Virol.* **85,** 2024–2036
53. Tullman, J. A., Harmon, M.-E., Delannoy, M., and Gibson, W. (2014) Recovery of an HMWP/hmwBP (pUL48/pUL47) complex from virions of human cytomegalovirus: subunit interactions, oligomer composition, deubiquitylase activity. *J. Virol.* **88,** 8256–8267

Annexe #4

Le transport intracellulaire des Herpèsvirus (revue)

David Pasdeloup

Virologie 2016, 20 (1) : 38-46

Le transport intracellulaire des herpèsvirus

David Pasdeloup

ISP 1282, Centre Inra de Tours,
équipe biologie des virus aviaires,
37380 Nouzilly, France
<david.pasdeloup@tours.inra.fr>

Résumé. Le transport intracellulaire des virus est un processus important du cycle viral de par l'encombrement important du cytoplasme et des distances importantes à couvrir entre les différents organelles nécessaires au cycle viral. Ce transport est actif, régulé et passe par le recrutement de la machinerie cellulaire. La problématique du transport est particulièrement importante pour les alpha-herpèsvirus neurotropes dont la capside de grosse taille doit parcourir de grandes distances dans des types cellulaires très spécialisés et topologiquement très différents tels que les neurones et les cellules épithéliales. Cette revue vise à résumer les données accumulées sur les 15 dernières années concernant le transport intracellulaire de ces virus qui font partie des mieux caractérisés dans ce domaine grâce à leur manipulation génétique aisée et leur très grande efficacité de recrutement de la machinerie cellulaire de transport.

Mots clés : centrosome, microtubules, moteur moléculaire, capside, herpesvirus, dystonine, transport

Abstract. Intracellular trafficking of viruses is a vital part of the viral life cycle because of the density of the cytosol and of important distances between organelles necessary for viral replication. Viral transport is active, regulated and requires the host machinery. Transport issues are particularly important for neurotropic alpha-herpesviruses whose large capsids travel through large distances in highly specialized cells such as neurons or epithelial cells. In this review, I will summarize the knowledge accumulated for the last 15 years on the intracellular trafficking of these viruses. In this fairly recent field of research, they are among the best described because they are easily genetically modified and also because they recruit the cellular transport machinery very efficiently.

Key words: centrosome, microtubules, molecular motor, capsid, herpesvirus, dystonin, transport

Les virus voyagent abondamment dans la cellule hôte, depuis leur entrée jusqu'à la sortie de nouvelles particules. Parfois, ce transport se fait passivement quand le virus est incorporé dans une structure cellulaire (telle une vésicule d'endocytose ou d'exocytose), elle-même déplacée dans la cellule. Il existe cependant un transport « actif » dans lequel la particule virale elle-même est prise en charge par la cellule pour atteindre le compartiment cellulaire d'intérêt. Ce transport se fait généralement à l'aide du cytosquelette cellulaire par le recrutement des moteurs moléculaires appropriés.

Les herpèsvirus sont parmi les virus les mieux étudiés pour les mécanismes de transport intracellulaire, car ils constituent des cargos bien caractérisés, faciles à suivre et qu'ils sont capables de recruter la machinerie de transport cellulaire très efficacement.

Dans cette revue, nous allons résumer les récentes avancées obtenues dans le domaine du transport intracellulaire des herpèsvirus, c'est-à-dire comment le virus mobilise les ressources cellulaires qui lui permettent de voyager efficacement et rapidement sur de longues distances. Les données présentées ici concernent les apha-herpèsvirus qui sont les mieux caractérisés de la famille dans ce domaine.

Le réseau de microtubules et les moteurs moléculaires associés

Le laboratoire de Helenius a été le premier à démontrer que les herpèsvirus utilisent principalement le réseau de microtubules (MT) [1].

Tirés à part : D. Pasdeloup

doi:10.1684/vir.2016.0630

Pour citer cet article : Pasdeloup D. Le transport intracellulaire des herpèsvirus. *Virologie* 2016; 20(1) : 38-46 doi:10.1684/vir.2016.0630

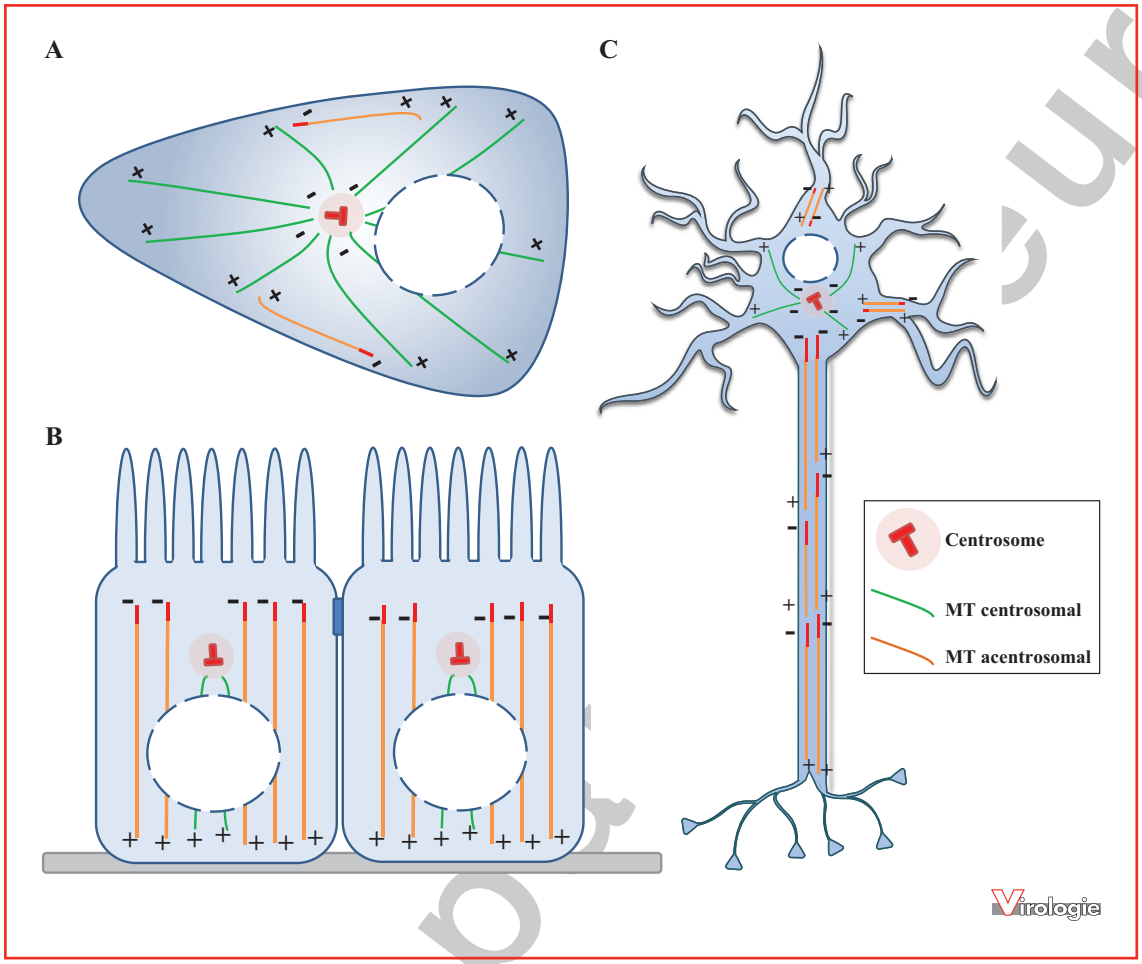

Figure 1. Organisation du réseau de microtubules (MT) dans différents types cellulaires. L'organisation du réseau de MT est schématisée dans des cellules non différenciées **(A)**, des cellules épithéliales polarisées **(B)** ou dans des neurones **(C)**. Les MT dont la nucléation et la stabilité dépendent du centrosome (MT centrosomaux) sont dépeints en vert. Les MT non centrosomaux sont en orange, avec leur extrémité (–) stabilisée par des protéines de liaison au pôle (–) en rouge.

Les MT sont des structures polarisées creuses de 25 nm de diamètre composées d'hétérodimères d'α et de β-tubuline. On distingue l'extrémité positive (+) du MT qui est dynamique, c'est-à-dire où la polymérisation ou la dépolymérisation du MT a essentiellement lieu [2], contrairement à l'extrémité négative (–) qui, dans la cellule, est généralement stabilisée par une structure telle que le centrosome ou certains complexes protéiques non centrosomaux [3]. Le centrosome est le principal centre nucléateur de MT (CNMT) dans la plupart des cellules, c'est-à-dire la structure à partir de laquelle le réseau de MT est polymérisé. Le réseau de MT centrosomal typique se présente donc comme un réseau radial, qui émane du centrosome qui se trouve généralement à proximité du noyau *(figure 1)*. Néanmoins, dans des types cellulaires très différenciés dont la topologie requiert une organisation des MT différente (comme les neurones ou certaines cellules épithéliales), il existe des CNMT « alternatifs », tels que le réseau *trans*-Golgi [4, 5].

Le transport de molécules le long de ce réseau, qu'il s'agisse de complexes protéiques ou de vésicules (également appelés « cargos » de façon plus générique), est coordonné par deux classes de complexes :

– les moteurs moléculaires, qui assurent le mouvement directionnel sur les MT ;
– les adaptateurs, qui font le lien entre le cargo et un moteur moléculaire.

Les moteurs moléculaires associés aux MT sont classiquement découpés en deux grandes superfamilles : les dynéines et les kinésines. La dynéine dite cytoplasmique (par opposition à la dynéine « axonémale ») est la plus importante pour

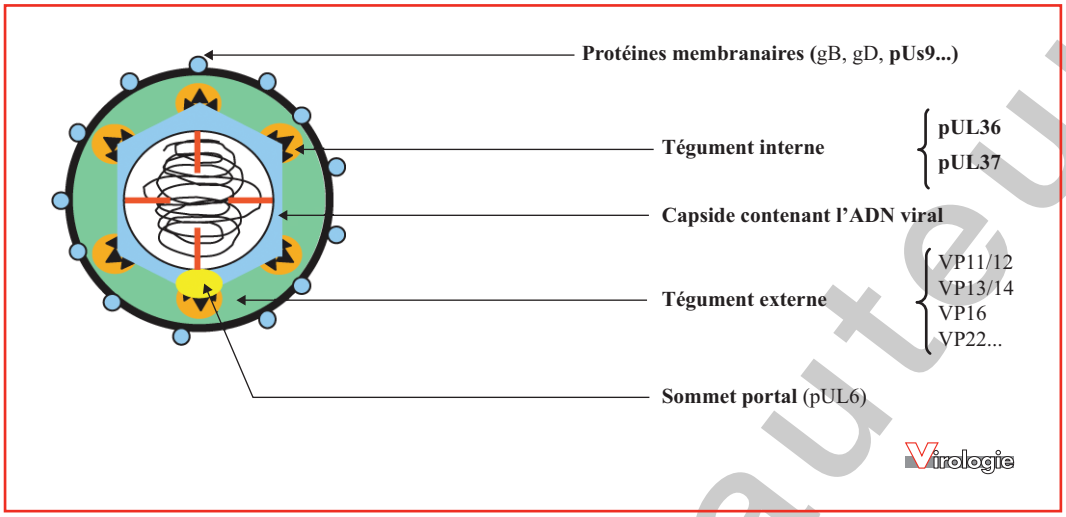

Figure 2. Organisation de la particule virale. Les virions des herpèsvirus sont tous organisés autour de trois structures : la capside icosaédrique qui protège le génome viral qui y entre et en sort à travers le sommet portal (jaune) ; la membrane virale qui contient les glycoprotéines et, entre les deux, le tégument, une couche de protéines spécifique aux herpèsvirus. On distingue deux types de tégument ; le tégument interne (orange) est associé aux capsides, tandis que le tégument externe (vert) est associé à l'enveloppe virale.

le transport. Elle consiste en un complexe multiprotéique de grande taille (environ 1,5 MDa) qui assure le transport du pôle (+) vers le pôle (−) du MT.

La superfamille des kinésines est plus large et plus complexe. Elle regroupe des moteurs qui, sauf exception, assurent le transport du pôle (−) vers le pôle (+) du MT. Il existe des kinésines qui sont dépendantes du type cellulaire.

À l'interface entre le moteur moléculaire et le cargo se trouvent des molécules adaptatrices dont le rôle est de reconnaître le moteur et/ou le cargo. Il s'agit le plus souvent de complexes multiprotéiques, même s'il existe des protéines uniques qui jouent ce rôle. Les protéines Rab et les protéines BiCaudal font partie de tels complexes. La Huntingtine (dont la mutation conduit à la maladie de Huntington) sert d'adaptateur unique entre les vésicules neuronales et les complexes dynéine ou kinésine [6-8]. Selon son état de phosphorylation, elle permet de favoriser l'interaction avec la dynéine ou la kinésine et a donc un rôle déterminant pour coordonner la direction du transport des vésicules [9].

Bien souvent lors d'études sur le transport intracellulaire des virus, les recherches se concentrent sur la nature des protéines virales impliquées et sur les moteurs moléculaires recrutés par ces protéines. Néanmoins, comme tout cargo cellulaire, les virus doivent pouvoir exercer un contrôle étroit sur la direction de leur transport. La nature des mécanismes impliqués dans la régulation de la direction du transport par un cargo, comme illustré par l'étude sur la Huntingtine, demeure encore aujourd'hui un sujet d'étude en plein essor. L'étude du transport des virus, en tant que cargo atypique, permet de mettre en lumière une partie de ces mécanismes. Parmi les virus particulièrement étudiés dans ce domaine, les alpha-herpèsvirus neurotropes tels que l'*Herpes simplex* de type 1 (HSV-1) et le virus de la pseudorage (PrV) font partie des références. En effet, ces virus ont une grosse capside icosaédrique (125 nm) bien caractérisée [10] qui recrute très efficacement la machinerie de transport cellulaire et peut se déplacer très rapidement dans la cellule (~2 µm/s) [11]. Surtout, cette capside peut être facilement visualisée par fluorescence et les outils génétiques disponibles pour ces virus permettent de manipuler n'importe quelle protéine virale à loisir, tant que les altérations n'affectent pas la viabilité virale.

Problématique du transport des particules virales durant l'entrée

La particule virale des herpèsvirus est relativement complexe *(figure 2)*. Elle consiste essentiellement en trois éléments :

- la capside icosaédrique contenant le génome viral ;
- l'enveloppe virale contenant les glycoprotéines ; et
- entre les deux, le tégument.

Le tégument est une couche de protéine amorphe typique des herpèsvirus. On distingue le tégument « interne », attaché aux sommets de la capside, du tégument « externe », attaché à l'enveloppe virale.

Le cycle de réplication des herpèsvirus est en partie nucléaire. Durant l'entrée de ces virus, la capside doit donc atteindre le noyau depuis la membrane plasmique où elle est relâchée, en utilisant le réseau de MT. Dans une cellule

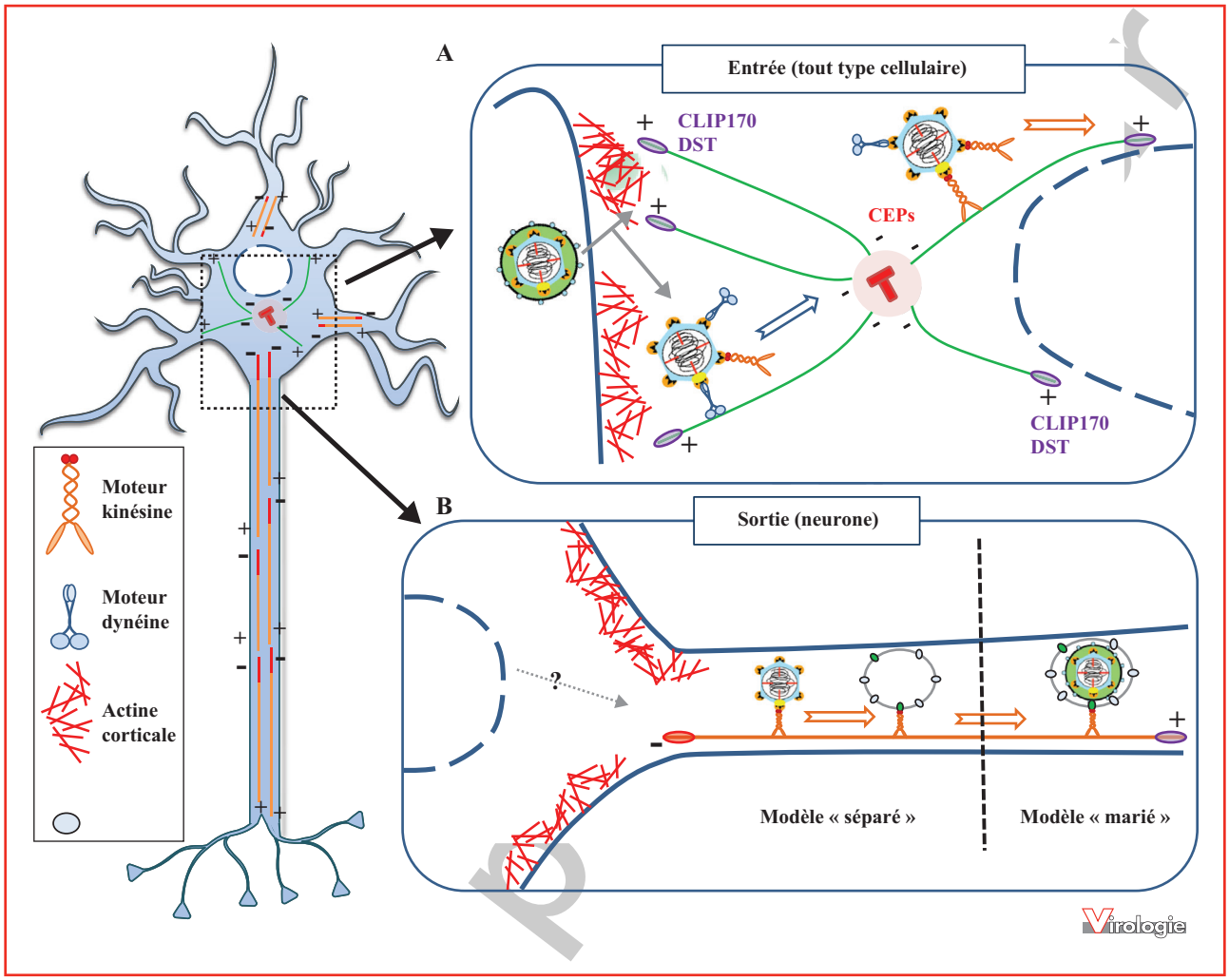

Figure 3. Problématiques du changement de polarité du transport durant l'entrée et de la nature de la particule virale pendant la sortie. Après fusion de l'enveloppe virale avec la membrane plasmique, le tégument externe est relâché dans le cytoplasme tandis que la capside associée au tégument interne (pUL36/pUL37) est rapidement prise en charge par les moteurs moléculaires. Cet engagement semble être médié par les protéines de pôle (+) des MT, comme CLIP170. Le transport rétrograde commence par une phase de transport vers le centrosome (donc vers le pôle (−)) *via* l'interaction de pUL36 avec des éléments du moteur dynéine. Une fois au centrosome, la polarité du transport doit être inversée et les capsides sont redirigées vers le noyau par un transport vers le pôle (+) des MT grâce au moteur kinésine. Cette phase du transport rétrograde, de fait plus courte et plus difficile à visualiser à cause de la proximité du centrosome au noyau, semble néanmoins impliquer la protéine dystonine (DST) puisqu'en son absence, les capsides sont peu efficacement redirigées vers le noyau et s'accumulent aux alentours du centrosome. Une fois la capside au noyau, il n'a pas été établi comment elle passe du MT au pore nucléaire. Une possibilité est que son transport soit médié par le réseau d'actine périnucléaire, comme il a été décrit pour VIH-1 [47]. La sortie virale est plus difficile à cerner dans les neurones, puisque deux modes d'assemblage sont possibles. Dans le modèle « séparé », les capsides migrent du noyau vers la terminaison axonale par transport antérograde vers le pôle (+) des MT. Ce transport est probablement assuré par les mêmes facteurs viraux et cellulaires que ceux décrit durant l'entrée, à savoir pUL36/pUL37 et le moteur kinésine respectivement. Les vésicules contenant des protéines virales membranaires sont également transportées par les kinésines, mais ce transport serait assuré par la protéine membranaire virale pUs9 (en vert) qui peut interagir avec la kinésine 3. Dans ce modèle, l'assemblage final des particules virales se ferait dans la terminaison axonale où les capsides et les vésicules se retrouvent. Dans le modèle « marié », les particules virales enveloppées et en transit dans des vésicules sont transportées *via* l'interaction pUs9/kinésine 3 comme décrit plus haut. Le transit des capsides du noyau vers les axones n'est pas clair puisqu'il n'est pas établi si le centrosome est perdu durant la réplication virale dans ces cellules, comme il a été décrit pour des types cellulaires non neuronaux [41, 48].

faiblement différenciée de type fibroblaste, ce réseau est organisé autour du CNMT principal, à savoir le centrosome, et présente donc une organisation radiale [12] *(figure 1)*. Cela implique que les MT ont leur extrémité (−) stable attachée au centrosome, tandis que l'extrémité (+) est projetée vers la membrane plasmique et vers le noyau. Dans une telle configuration, la capside doit transiter vers le centrosome *via* un transport vers le pôle (−) puis, une fois au centrosome, la polarité du transport doit être inversée pour que la capside soit re-routée depuis le centrosome vers le noyau *via* un transport vers le pôle (+). En d'autres termes, le transport rétrograde en fibroblastes est un transport en deux temps *(figure 3)*.

En cellules neuronales, la topologie du réseau est grossièrement identique dans le corps cellulaire du neurone, mais elle est différente dans l'axone ou les dendrites. Dans l'axone, les MT sont parallèles les uns aux autres et sont tous orientés de façon identique, à savoir l'extrémité (−) vers le corps cellulaire et l'extrémité (+) vers la terminaison axonale. Cette organisation est vitale pour le bon acheminement du flux de vésicules neuronales. Dans l'hypothèse où le virus infecte le neurone *via* sa terminaison axonale, il est donc attendu que le transport rétrograde soit ici aussi en deux temps :

– un transport vers le pôle (−) des MT axonaux puis vers le centrosome une fois dans le corps cellulaire ;

– un transport vers le pôle (+) du centrosome vers le noyau.

Une question importante qui découle de ces observations est de savoir comment la capside (et par extension de nombreux cargos cellulaires) est re-routée efficacement d'un compartiment cellulaire à un autre ?

À la recherche des protéines virales responsables du transport des capsides

Les moteurs moléculaires dynéine et kinésine sont nécessaires au transport de la capside des herpèsvirus [13-15]. Par conséquent, la ou les protéines virales impliquées dans le déplacement des particules virales doivent interagir, directement ou non, avec ces moteurs. Le génome des alpha-herpèsvirus code pour plus de 70 protéines, ce qui rend l'identification des candidats plus compliquée. Un certain nombre de protéines virales a été décrit comme interagissant avec des composants de moteurs moléculaires. Ainsi, les protéines de capside VP5 (protéine majeure de capside) et VP26 (petite protéine de capside présente sur les hexons) ont été parmi les candidats pressentis. VP5 a été décrite comme interagissant avec la sous-unité LC8 de la dynéine par Pepscan [16] et VP26 comme interagissant avec les composants RP3 et Tctex1 de la dynéine en double-hybride [17]. Néanmoins, les résultats obtenus pour VP5 n'ont jamais été confirmés en cellules infectées, tandis que ceux décrits pour VP26 ont été contredits dans deux études différentes, sur deux alpha-herpèsvirus différents [18, 19]. De plus, la capside virale étant généralement recouverte d'une couche de tégument une fois dans le cytoplasme, aussi bien durant l'entrée que la sortie virale, il est difficile d'imaginer comment les moteurs moléculaires peuvent avoir accès aux protéines de capside. Les protéines pUs11 et pUL56 ont également été décrites comme interagissant avec un moteur moléculaire. pUs11 interagirait avec la chaîne lourde de la kinésine conventionnelle [13] mais les données sur le rôle de cette interaction dans le transport des capsides sont manquantes. De plus, la présence de pUs11 dans la particule virale reste controversée [20, 21]. Quant à pUL56, son interaction avec le moteur kinésine KIF1A n'a été démontrée qu'*in vitro*, et n'a jamais été validée fonctionnellement [22].

Place du tégument viral dans le recrutement des moteurs moléculaires durant l'entrée

Les données les plus fiables quant à l'identité des protéines virales impliquées dans le transport sont apparues en 2005-2006. Dans un premier temps, les équipes de Greg Smith et de Thomas Mettenleiter ont montré en parallèle chez PrV que lors de l'entrée du virus, le tégument externe (VP22, VP16 ou VP13/14 par exemple) était perdu alors que le tégument interne (pUL36 et pUL37) était conservé sur les capsides en transit vers le noyau [23, 24]. Cela excluait pour la première fois un rôle du tégument externe dans le transport durant l'entrée virale tout en désignant le tégument interne comme candidat valable. Ces résultats ont été confirmés plus tard chez HSV-1 [25]. En 2006, une étude *in vitro* de l'équipe de Beate Sodeik montrait chez HSV-1 que le tégument interne était nécessaire à l'association de particules virales à des MT purifiés et à leur mouvement dans un système acellulaire [26] dans lequel les vitesses étaient néanmoins bien inférieures à celles observées en cellules infectées. Ces résultats rendaient les protéines pUL36 et pUL37 plus crédibles encore comme acteurs majeurs dans le transport viral. Le même laboratoire allait plus loin en 2010, montrant que les capsides de HSV-1 uniquement associées au tégument interne étaient capables de s'associer aux deux types de moteurs moléculaires à la fois (kinésines et dynéine) *in vitro* [27]. pUL36 et pUL37 sont les principales constituantes du tégument interne. Elles forment un complexe et sont essentielles à la réplication virale. De plus, elles sont indispensables au transport intracellulaire des capsides de HSV-1 et PrV [28-30]. Néanmoins, aucune interaction entre ces deux protéines et des moteurs moléculaires n'a été mise à jour jusqu'à récemment. Zaichick *et al*.

[31] ont finalement démontré en 2013 qu'un fragment de pUL36 riche en proline (UL36PRD), bien que non essentiel à la fonction de la protéine ou à la réplication virale en culture de cellules, était capable de lier le complexe dynéine-dynactine [31]. Cette étude, bien que confirmant que pUL36 semble être la protéine virale responsable du recrutement des moteurs, n'a montré qu'un impact limité du fragment UL36PRD incriminé sur le transport. En effet, la vidéo-microscopie de cellules infectées par un virus mutant dans lequel UL36PRD a été délété montre un effet très modéré de la mutation sur le transport général des capsides. *In vivo*, les auteurs ont montré que ce virus avait des capacités de neuro-invasion réduites et une virulence diminuée.

Ces résultats étaient parmi les premiers montrant une interaction entre une protéine d'un herpèsvirus et une protéine cellulaire impliquée dans le transport qui ait été validée fonctionnellement en cellules infectées. Ils ont permis de confirmer certaines hypothèses sur le recrutement de moteurs moléculaires par pUL36, mais n'ont pas vraiment permis de mettre à jour l'essentiel du mécanisme puisque le transport viral *per se* n'est pas aboli par l'absence du domaine UL36PRD.

Relation entre les protéines non moteurs associées aux MT et le transport directionnel

Les capsides de HSV-1 sont capables de lier les deux types de moteurs moléculaires à la fois [27]. Par conséquent, une hypothèse pour expliquer la dualité de polarité du transport des capsides est que les capsides sont attachées aux deux types de moteurs et que ceux-ci sont engagés dans une compétition (*tug-of-war* en anglais) pour dominer la direction du transport des capsides. Cette hypothèse explique un phénomène couramment observé en culture de cellules infectées : la bidirectionnalité constante des capsides. En effet, dans ces systèmes, il est fréquent d'observer des capsides amorcer un type de transport (par exemple de la membrane plasmique vers le noyau), puis stationner un moment avant de rebrousser chemin, s'arrêter à nouveau, puis repartir dans le sens initial. Néanmoins, cette hypothèse n'explique pas pourquoi le mouvement net s'effectue toujours dans un sens avant de subir une inversion une fois le centrosome atteint. S'il doit y avoir une régulation, elle peut exister à un niveau supérieur, à savoir avec des marqueurs de polarité des MT, telles que des protéines cellulaires non moteurs spécifiques de ces pôles.

Une telle protéine, la dystonine, a été identifiée récemment au laboratoire [32]. Cette protéine géante (entre 2 600 et 7 400 résidus selon les isoformes) est en effet spécifique de l'extrémité (+) des MT et a été montrée comme interagissant spécifiquement avec pUL37. Son rôle a initialement été associé à une fonction de stabilisation du réseau de MT en interconnectant les différents réseaux du cytosquelette en neurones [33]. D'autres études ont finalement complété ce tableau en décrivant une implication de la dystonine dans le transport rétrograde [34] et antérograde [35]. Nous avons démontré que dans des cellules dépourvues de dystonine, les capsides de HSV-1 pouvaient atteindre le centrosome de fibroblastes normalement mais étaient peu efficacement redirigées vers le noyau, indiquant un défaut dans le *switch* de polarité du transport (−) (vers le centrosome) vers (+) (vers le noyau) [36]. Ceci illustre pour la première fois le rôle de protéines non moteurs associées aux MT dans la régulation de la direction du transport des capsides. Il est possible que des mécanismes similaires soient à la base de la régulation de la direction du transport de cargos cellulaires et que d'autres protéines non moteurs soient impliquées dans des mécanismes similaires.

Récemment, il a été montré que l'initiation du transport des capsides juste après leur libération dans le cytoplasme nécessite la présence d'une protéine spécifique de l'extrémité (+) des MT, la protéine CLIP170 [37]. En l'absence de cette protéine, les capsides sont incapables d'atteindre le noyau et restent en périphérie de la cellule. En revanche, le mécanisme moléculaire à la base de la reconnaissance de CLIP170 par la capside n'est pas connu.

Transport des capsides durant la sortie virale

Durant la sortie virale, la problématique des protéines virales impliquées est plus complexe. En effet, selon le type cellulaire infecté, la nature des particules virales transportées change.

En fibroblastes, les capsides nouvellement assemblées dans le noyau arrivent « nues » dans le cytoplasme et sont rapidement tégumentées. L'hypothèse prédominant actuellement est que ce sont les capsides associées aux protéines de tégument interne pUL36 et pUL37 (ou prétégumentées) qui vont être transportées vers les sites d'enveloppement secondaire où elles acquièrent la seconde couche de tégument (le tégument externe) qui les lie aux sites d'enveloppement associés aux glycoprotéines virales. Selon cette hypothèse, les capsides en transit depuis le noyau vers les sites d'enveloppement sont dépendantes à nouveau du complexe pUL36–pUL37 pour leur transport *(figure 3)*. Ceci a été confirmé par les premières études sur des mutants ne codant pas pour l'une ou l'autre protéine [24, 28, 30, 32] montrant à la fois une absence de transport de ces capsides, mais également une absence d'enveloppement secondaire, déjà connue auparavant

[38-40]. Notre laboratoire a également montré que le partenaire de pUL37 dystonine était également nécessaire au transport des capsides durant la sortie virale en fibroblaste, confirmant le rôle de cette protéine non moteur dans la fonction de pUL37 dans le mouvement intracellulaire des capsides [32].

En cellules neuronales, la nature des particules virales sortantes est moins claire et encore sujette à de nombreux débats dans la communauté. Ces débats reposent essentiellement sur l'état d'enveloppement des particules virales transportées, opposant le modèle « marié » au modèle « séparé » *(figure 3)*. Dans le modèle « séparé », les capsides peuvent être tégumentées dans le corps cellulaire puis transportées vers la terminaison axonale où elles seront enveloppées et excrétées. Dans ce cas, le processus de transport est essentiellement comparable à ce qui est décrit en fibroblastes et donc dépendant du complexe pUL36–pUL37. En revanche, si les capsides sont tégumentées et enveloppées dans le corps cellulaire de la même façon qu'en fibroblastes puis transportées vers la terminaison axonale pour y être relâchées (modèle « marié »), cela exclut *de facto* un rôle des protéines de tégument telles que pUL36 et pUL37. Alors que des études ultra-structurales récentes semblent favoriser le modèle « séparé » [42, 43], des résultats du laboratoire d'Enquist ont montré que la protéine pUs9, une protéine virale membranaire, était nécessaire au transport antérograde des particules virales depuis le corps cellulaire vers la terminaison axonale [15]. Dans cette étude, les auteurs ont montré que pUs9 de PrV interagit avec la kinésine 3, un moteur moléculaire particulièrement présent en neurones. Ils ont observé que les capsides en cours de transport étaient associées avec la kinésine 3 par vidéomicroscopie en temps réel et ont démontré que l'interaction avec pUs9 était nécessaire à ce transport. Ces résultats impliquent que pUs9 est présente sur les vésicules de sécrétion contenant les particules virales, ainsi qu'une prépondérance du modèle « marié » puisque pUs9 n'a de rôle que dans le cas du transport de capsides enveloppées. Une étude récente a néanmoins nuancé ces conclusions en démontrant que le rôle de pUs9 était essentiellement de diriger les capsides vers la voie de transport axonale et que la protéine n'avait pas un rôle direct dans le transport antérograde [44].

Ces résultats contradictoires mettent en lumière l'importance des mécanismes d'engagement dans une voie de transport ou dans une autre. En effet, lors d'études du transport viral, les paramètres de vitesse et de mobilité sont souvent les seuls à être pris en compte alors que des paramètres tout aussi vitaux mais plus subtils, tels que la direction du transport ou la régularité des parcours, sont souvent négligés. La problématique de la régulation de la direction du transport est pourtant une question cruciale, particulièrement dans les cellules polarisées.

La problématique particulière du transport des herpèsvirus en cellules polarisées

Les cellules naturellement infectées par les herpèsvirus neurotropes tels que HSV-1 et PrV sont des cellules très polarisées, comme les neurones sensitifs ou les cellules de l'épithélium buccal. Par conséquent, la coordination de la direction du transport est essentielle à une infection réussie. Alors que les éléments cellulaires et viraux impliqués dans le transport commencent à être mieux définis, la régulation du processus reste très floue.

Les études du transport de la capside des herpèsvirus s'accordent néanmoins sur la fonction essentielle du complexe pUL36 et pUL37, même si les mécanismes sont encore loin d'être élucidés.

Une hypothèse particulièrement séduisante sur le fonctionnement de ce duo consiste à attribuer le rôle « effecteur » du transport à pUL36 *via* le recrutement des moteurs moléculaires, comme le suggère l'étude de Zaichick *et al*. [31], tandis que pUL37 exercerait le rôle de « régulateur » de la direction du transport (vers le pôle (+) ou (−) des MT) en fonction des partenaires cellulaires rencontrés. Cette dernière idée est illustrée par les résultats décrits avec le partenaire dystonine de pUL37, puisqu'en l'absence de cette protéine du pôle (+), le transport vers les pôles (+) des MT est affecté à la fois durant l'entrée et la sortie du virus [32, 36]. Si cette hypothèse est correcte, pUL37 devrait interagir également avec des protéines du pôle (−) des MT pour coordonner le transport vers ces pôles. Ces partenaires restent à identifier.

Conclusion

Les virus sont d'excellents marqueurs du système cellulaire de transport car ce sont des cargos, en général facilement manipulables génétiquement, capables de le détourner et donc permettant son étude. L'étude du cycle de vie cellulaire des virus en temps réel a été rendue possible sur les 15 dernières années par la multiplication des techniques d'imagerie efficaces en milieu confiné, conjuguées aux progrès considérables effectués dans le domaine de la manipulation génétique des virus et la disponibilité de nombreuses molécules fluorescentes. Par conséquent, l'étude du transport intracellulaire des virus est relativement récente et en expansion. L'apparition naissante de techniques de microscopie à super-résolution en temps réel (telles que le sSTED ou PA NL-SIM) [45, 46] devrait permettre de franchir un cap supplémentaire dans l'observation et la compréhension des interactions virus–hôtes impliquées dans le transport des virus.

Remerciements. Je remercie Laetitia Trapp-Fragnet pour son aide pour la *figure 1*.

Liens d'intérêts : l'auteur déclare ne pas avoir de lien d'intérêt en rapport avec cet article.

Références

1. Sodeik B, Ebersold MW, Helenius A. Microtubule-mediated transport of incoming Herpes simplex virus 1 capsids to the nucleus. *J Cell Biol* 1997 ; 136 : 1007-21.

2. Howard J, Hyman AA. Dynamics and mechanics of the microtubule plus-end. *Nature* 2003 ; 422 : 753-8.

3. Dammermann A, Desai A, Oegema K. The minus-end in sight. *Curr Biol* 2003 ; 13 : R614-24.

4. Chabin-Brion K, Marceiller J, Perez F, *et al*. The Golgi complex is a microtubule-organizing organelle. *Mol Biol Cell* 2001 ; 12 : 2047-60.

5. Efimov A, Kharitonov A, Efimova N, *et al*. Asymmetric CLASP-dependent nucleation of noncentrosomal microtubules at the trans-Golgi network. *Dev Cell* 2007 ; 12 : 917-30.

6. Engelender S, Sharp AH, Colomer V, *et al*. Huntingtin-associated protein 1 (HAP1) interacts with the p150Glued subunit of dynactin. *Hum Mol Genet* 1997 ; 6 : 2205-12.

7. Li SH, Gutekunst CA, Hersch SM, Li XJ. Interaction of Huntingtin-associated protein with dynactin P150Glued. *J Neurosci* 1998 ; 18 : 1261-9.

8. McGuire JR, Rong J, Li SH, Li XJ. Interaction of Huntingtin-associated protein-1 with kinesin light chain: implications in intracellular trafficking in neurons. *J Biol Chem* 2006 ; 281 : 3552-9.

9. Colin E, Zala D, Liot G, *et al*. Huntingtin phosphorylation acts as a molecular switch for anterograde/retrograde transport in neurons. *EMBO J* 2008 ; 27 : 2124-34.

10. Zhou ZH, Dougherty M, Jakana J, He J, Rixon FJ, Chiu W. Seeing the Herpesvirus capsid at 8.5 A. *Science* 2000 ; 288 : 877-80.

11. Smith GA, Enquist LW. Break ins and break outs: viral interactions with the cytoskeleton of mammalian cells. *Annu Rev Cell Dev Biol* 2002 ; 18 : 135-61.

12. Bartolini F, Gundersen GG. Generation of noncentrosomal microtubule arrays. *J Cell Sci* 2006 ; 119 : 4155-63.

13. Diefenbach RJ, Miranda-Saksena M, Diefenbach E, *et al*. Herpes simplex virus tegument protein Us11 interacts with conventional kinesin heavy chain. *J Virol* 2002 ; 76 : 3282-91.

14. Dohner K, Wolfstein A, Prank U, *et al*. Function of dynein and dynactin in Herpes simplex virus capsid transport. *Mol Biol Cell* 2002 ; 13 : 2795-809.

15. Kramer T, Greco TM, Taylor MP, Ambrosini AE, Cristea IM, Enquist LW. Kinesin-3 mediates axonal sorting and directional transport of alphaherpesvirus particles in neurons. *Cell Host Microbe* 2012 ; 12 : 806-14.

16. Martinez-Moreno M, Navarro-Lerida I, Roncal F, *et al*. Recognition of novel viral sequences that associate with the dynein light chain LC8 identified through a Pepscan technique. *FEBS Lett* 2003 ; 544 : 262-7.

17. Douglas MW, Diefenbach RJ, Homa FL, *et al*. Herpes simplex virus type 1 capsid protein VP26 interacts with dynein light chains RP3 and Tctex1 and plays a role in retrograde cellular transport. *J Biol Chem* 2004 ; 279 : 28522-30.

18. Antinone SE, Shubeita GT, Coller KE, *et al*. The Herpesvirus capsid surface protein, VP26, and the majority of the tegument proteins are dispensable for capsid transport toward the nucleus. *J Virol* 2006 ; 80 : 5494-8.

19. Dohner K, Radtke K, Schmidt S, Sodeik B. Eclipse phase of Herpes simplex virus type 1 infection: efficient dynein-mediated capsid transport without the small capsid protein VP26. *J Virol* 2006 ; 80 : 8211-24.

20. Loret S, Guay G, Lippe R. Comprehensive characterization of extracellular Herpes simplex virus type 1 virions. *J Virol* 2008 ; 82 ; 8605-18.

21. Roller RJ, Roizman B. The Herpes simplex virus 1 RNA binding protein Us11 is a virion component and associates with ribosomal 60S subunits. *J Virol* 1992 ; 66 : 3624-32.

22. Koshizuka T, Kawaguchi Y, Nishiyama Y. Herpes simplex virus type 2 membrane protein UL56 associates with the kinesin motor protein KIF1A. *J Gen Virol* 2005 ; 86 : 527-33.

23. Granzow H, Klupp BG, Mettenleiter TC. Entry of pseudorabies virus: an immunogold-labeling study. *J Virol* 2005 ; 79 : 3200-5.

24. Luxton GW, Haverlock S, Coller KE, Antinone SE, Pincetic A, Smith GA. Targeting of Herpesvirus capsid transport in axons is coupled to association with specific sets of tegument proteins. *Proc Natl Acad Sci U S A* 2005 ; 102 : 5832-7.

25. Antinone SE, Zaichick SV, Smith GA. Resolving the assembly state of Herpes simplex virus during axon transport by live-cell imaging. *J Virol* 2010 ; 84 : 13019-30.

26. Wolfstein A, Nagel CH, Radtke K, Dohner K, Allan VJ, Sodeik B. The inner tegument promotes Herpes simplex virus capsid motility along microtubules *in vitro*. *Traffic* 2006 ; 7 : 227-37.

27. Radtke K, Kieneke D, Wolfstein A, *et al*. Plus- and minus-end directed microtubule motors bind simultaneously to Herpes simplex virus capsids using different inner tegument structures. *PLoS Pathog* 2010 ; 6 : e1000991.

28. Krautwald M, Fuchs W, Klupp BG, Mettenleiter TC. Translocation of incoming pseudorabies virus capsids to the cell nucleus is delayed in the absence of tegument protein pUL37. *J Virol* 2009 ; 83 : 3389-96.

29. Luxton GW, Lee JI, Haverlock-Moyns S, Schober JM, Smith GA. The pseudorabies virus VP1/2 tegument protein is required for intracellular capsid transport. *J Virol* 2006 ; 80 : 201-9.

30. Sandbaumhuter M, Dohner K, Schipke J, *et al*. Cytosolic Herpes simplex virus capsids not only require binding inner tegument protein pUL36 but also pUL37 for active transport prior to secondary envelopment. *Cell Microbiol* 2013 ; 15 : 248-69.

31. Zaichick SV, Bohannon KP, Hughes A, Sollars PJ, Pickard GE, Smith GA. The Herpesvirus VP1/2 protein is an effector of dynein-mediated capsid transport and neuroinvasion. *Cell Host Microbe* 2013 ; 13 : 193-203.

32. Pasdeloup D, McElwee M, Beilstein F, Labetoulle M, Rixon FJ. Herpesvirus tegument protein pUL37 interacts with dystonin/BPAG1 to promote capsid transport on microtubules during egress. *J Virol* 2013 ; 87 : 2857-67.

33. Yang Y, Bauer C, Strasser G, Wollman R, Julien JP, Fuchs E. Integrators of the cytoskeleton that stabilize microtubules. *Cell* 1999 ; 98 : 229-38.

34. Liu JJ, Ding J, Kowal AS, *et al*. BPAG1n4 is essential for retrograde axonal transport in sensory neurons. *J Cell Biol* 2003 ; 163 : 223-9.

35. Ryan SD, Bhanot K, Ferrier A, *et al*. Microtubule stability, Golgi organization, and transport flux require dystonin-a2-MAP1B interaction. *J Cell Biol* 2012 ; 196 : 727-42.

36. McElwee M, Beilstein F, Labetoulle M, Rixon FJ, Pasdeloup D. Dystonin/BPAG1 promotes plus-end-directed transport of Herpes simplex virus 1 capsids on microtubules during entry. *J Virol* 2013 ; 87 : 11008-18.

37. Jovasevic V, Naghavi MH, Walsh D. Microtubule plus-end-associated CLIP-170 initiates HSV-1 retrograde transport in primary human cells. *J Cell Biol* 2015 ; 211 : 323-37.

38. Desai P, Sexton GL, McCaffery JM, Person S. A null mutation in the gene encoding the Herpes simplex virus type 1 UL37 polypeptide abrogates virus maturation. *J Virol* 2001 ; 75 : 10259-71.

39. Desai PJ. A null mutation in the UL36 gene of Herpes simplex virus type 1 results in accumulation of unenveloped DNA-filled capsids in the cytoplasm of infected cells. *J Virol* 2000 ; 74 : 11608-18.

40. Fuchs W, Klupp BG, Granzow H, Mettenleiter TC. Essential function of the pseudorabies virus UL36 gene product is independent of its interaction with the UL37 protein. *J Virol* 2004 ; 78 : 11879-89.

41. Pasdeloup D, Labetoulle M, Rixon FJ. Differing effects of Herpes simplex virus 1 and pseudorabies virus infections on centrosomal function. *J Virol* 2013 ; 87 : 7102-12.

42. Ibiricu I, Huiskonen JT, Dohner K, Bradke F, Sodeik B, Grunewald K. Cryo-electron tomography of Herpes simplex virus during axonal transport and secondary envelopment in primary neurons. *PLoS Pathog* 2011 ; 7 : e1002406.

43. Saksena MM, Wakisaka H, Tijono B, *et al*. Herpes simplex virus type 1 accumulation, envelopment, and exit in growth cones and varicosities in mid-distal regions of axons. *J Virol* 2006 ; 80 : 3592-606.

44. Daniel GR, Sollars PJ, Pickard GE, Smith GA. Pseudorabies virus fast axonal transport occurs by a pUS9-independent mechanism. *J Virol* 2015 ; 89 : 8088-91.

45. Li D, Shao L, Chen BC, *et al*. ADVANCED IMAGING. Extended-resolution structured illumination imaging of endocytic and cytoskeletal dynamics. *Science* 2015 ; 349 : aab3500.

46. Schneider J, Zahn J, Maglione M, *et al*. Ultrafast, temporally stochastic STED nanoscopy of millisecond dynamics. *Nat Methods* 2015 ; 12 : 827-30.

47. Arhel N, Genovesio A, Kim KA, *et al*. Quantitative four-dimensional tracking of cytoplasmic and nuclear HIV-1 complexes. *Nat Methods* 2006 ; 3 : 817-24.

48. Naghavi MH, Gundersen GG, Walsh D. Plus-end tracking proteins, CLASPs, and a viral Akt mimic regulate Herpesvirus-induced stable microtubule formation and virus spread. *Proc Natl Acad Sci U S A* 2013 ; 110 : 18268-73.